FLOCCULATION in NATURAL and ENGINEERED ENVIRONMENTAL SYSTEMS

FLOCCULATION in NATURAL and ENGINEERED ENVIRONMENTAL SYSTEMS

Edited by
Ian G. Droppo • Gary G. Leppard
Steven N. Liss • Timothy G. Milligan

CRC PRESS

Boca Raton London New York Washington, D.C.

Library of Congress Cataloging-in-Publication Data

Flocculation in natural and engineered
environmental systems/edited by Ian G. Droppo . . . [et al.].
p. cm.
Includes bibliographical references and index.
ISBN 1-56670-615-7 (alk. paper)
1. Flocculation. 2. Water—Purification. I. Droppo, Ian G.

QD547.F584 2004
628.1'622—dc22

2004056933

Visit the CRC Press Web site at www.crcpress.com

International Standard Book Number 1-56670-615-7
Library of Congress Card Number 2004056933
Printed in the United States of America 1 2 3 4 5 6 7 8 9 0
Printed on acid-free paper

Preface

In the history of environmental science, there has probably been no greater struggle than the attempt to control the impact of the sediment and solids generated by nature and human influence (including industrial processing) on the terrestrial and aquatic environment and on socioeconomics in general. Untold billions of dollars are spent each year on dredging to maintain navigation channels and harbors. Further costs are added by the need to treat these sediments prior to disposal because of high levels of contamination resulting from anthropogenic impacts on the environment. Significant financial burdens arise as a result of the need to remove solids during drinking water and wastewater treatment processes, a necessity for sustainable development, and the protection of human and aquatic health. It is now well established that the majority of particles within natural (freshwater and saltwater) systems are present in a flocculated form (i.e., flocs), and that the formation of flocs is essential for the effective performance of engineering processes such as biological wastewater treatment.

Flocculation is the process of aggregating smaller particles together to form larger composite particles via various physical, chemical, and biological interactions. These larger composite particles behave differently in terms of their physical (e.g., transport, settling), chemical (e.g., contaminant uptake and transformation), and biological (e.g., community structure activities and metabolism) behavior relative to their constituent individual particles due to differences in size, shape, porosity, density, and compositional characteristics. Given these significant behavioral differences between flocs per se and their individual component parts, flocculation influences a wide array of environmental phenomena related to sediment–water and sediment–sediment interactions. A few of these include sediment and contaminant transport in various aquatic ecosystems, remediation of contaminated bed sediments, contaminated bed sediment stability, and habitat destruction resulting from sedimentation (e.g., coral reef, salmon spawning grounds, mollusk habitat degradation). These concerns, coupled with the ubiquitous nature of flocs within natural and engineered systems and the potential to influence floc properties to control better the environmental and engineering processes, have generated an increased emphasis on floc research.

The traditional disciplines within saltwater, freshwater, and engineering research have, however, remained somewhat mutually exclusive in their approach to the study of flocculation processes. This reality is facilitated by differences in external variables (e.g., environmental conditions), focus driven research, and discipline bias. Regardless of differences in discipline or approach, there is great scope and utility for the sharing of information between scientists who work in these three floc environments. Often methods used in one environment can, and should, be used in another to further our understanding of flocculation processes. While new developments in

genomics, nanotechnology, sampling, and modeling permit increasingly revealing investigations into floc structure, processes, and impact, there is still a fundamental lack of knowledge related to many aspects of the flocculation process.

In light of the importance of flocculation within natural and engineered systems, an international workshop was held on September 4 and 5, 2003, at the Canada Centre for Inland Waters, Burlington, Ontario, Canada. The workshop brought together academics and government scientists from around the globe to address the critical issue of sediment flocculation within freshwater, saltwater, and engineered systems. During the workshop, participants representing these three environments presented their research findings. Three focus areas were used to structure the workshop: (a) modeling, (b) physicochemical, and (c) biological aspects of flocculation. Following individual presentations, the participants were divided up into three working groups to address assigned topics in the focus areas. Each focus group contained researchers from the freshwater, saltwater, and engineered systems to ensure a cross-communication of ideas between environments and to facilitate an understanding of the unifying principles of flocculation. Participants ranged from geographers/geomorphologists who investigate flocculation as it relates to sediment source, transport, and fate within river systems, sedimentologists interested in flocculation's influence within depositional environments, biologists focusing on the biopolymeric matrices and microbial consortia of flocs, oceanographers investigating sediment transport and delivery within estuaries and open ocean environments, and wastewater engineers/biologists interested in floc behavior within engineered systems.

The peer-reviewed 20 chapters that comprise this text are organized by their environment of investigation. The final chapter identifies the unifying principles that were discussed within the workshop focus groups and from the preceding chapters. The text provides a unique perspective in that it integrates the natural sciences and engineering fields as they relate to the central phenomenon of flocculation. We hope that the array of information provided in this book will be valuable to all those interested in flocculation issues within any environment.

Ian G. Droppo
Gary G. Leppard
Steven N. Liss
Timothy G. Milligan

Acknowledgments

The workshop and this resultant text would not have been made possible without the generous support of our sponsors. We would like to thank the National Water Research Institute of Environment Canada, the Department of Fisheries and Oceans, the Wastewater Technology Centre of Environment Canada, the Brockhouse Institute for Materials Research of McMaster University, Ryerson University, and the International Association for Sediment Water Science for their support. The editors are particularly grateful to the Natural Sciences and Engineering Research Council of Canada for their funding support related to research on flocculation.

Each chapter has been peer reviewed by two or three reviewers consistent with the standards set for international scientific journals. We would like to thank these reviewers for their efforts in this regard.

Finally, we would like to thank the National Water Research Institute of Environment Canada for hosting the workshop and John Lawrence, Michel Beland, and John Preston for their support. The efforts of Elizabeth Wendel, Meenu Pall, Dianne Crabtree, Allana Manto, Quintin Rochfort, Christina Jaskot, and Brian Trapp of Environment Canada leading up to, during, and following the workshop are gratefully acknowledged.

About the Editors

Ian G. Droppo is a research scientist with the National Water Research Institute of Environment Canada and is the current elected vice president of the International Association for Sediment Water Science. Dr. Droppo holds adjunct professorships at McMaster University, School of Geography and Earth Sciences and at the State University of New York, College at Buffalo, Department of Geography and Planning. He holds undergraduate and M.Sc. degrees in physical geography from McMaster University, Canada and a Ph.D. in physical geography from the University of Exeter, United Kingdom. He was a recent recipient of Leverhulme International Visiting Fellowship held at the University of Exeter in the United Kingdom. Dr. Droppo's research interests center around sediment dynamics within natural and engineered systems with particular emphasis on flocculation processes. He has applied this knowledge in multiple environments including urban stormwater management, remediation of contaminated bed sediments, contaminated bed sediment stability, and in the source, fate, and effect of sediments and associated contaminants within numerous aquatic environments. His research is supported by awards from Environment Canada, the Natural Sciences and Engineering Research Council of Canada, and a range of industrial partners. He has given many invited lectures and seminars at international conferences, workshops, and universities and has taught many sediment chemistry monitoring courses in developing countries. Dr. Droppo has carried out collaborative research in Canada, United States of America, United Kingdom, Japan, Mexico, Australia and Thailand leading to over 85 peer-reviewed journal publications, book chapters, and technical reports.

Gary G. Leppard is an environmental biochemist and microbiologist who studies the roles of natural and engineered aquatic aggregates (flocs, biofilms) in the transport and fate of contaminants. In concert with these activities, he develops electron-optical means to analyze the colloidal structure of natural dispersing agents and the flocs of water treatment tanks. He joined the staff of the National Water Research Institute of Environment Canada at Burlington (ON) in 1975, as a research scientist. While also holding a professorship at McMaster University and membership in the Brockhouse Institute for Materials Research (Hamilton, ON), he is a Fellow of the International Union of Pure and Applied Chemistry and a Consulting Fellow of the World Innovation Foundation. In sequence, he was an invited scientist at the University of Paris (France), the University of Milan (Italy), Laval University (Quebec City), the National Research Council of Canada (Ottawa), the University of Geneva (Switzerland), the University of Vienna (Austria), and the Rudjer Boskovic Institute (Croatia).

Dr. Leppard received degrees in several fields of biology and biological chemistry from the University of Saskatchewan (Saskatoon, SK) and from Yale University (New Haven, CT, United States). A Ph.D. in cell biology, with a specialization in electron-optical methods, was received from Yale in 1968. Research interests then extended into biogeochemistry, wastewater treatment, materials science, and the activities of natural microbial consortia. His interdisciplinary research has led to awards from the North Atlantic Treaty Organization, the Commission of the European Communities, and the RITE innovative technology organization in Japan, as well as a role on the editorial board of the Encyclopedia of Analytical Science. Current scientific interests focus on the control, by nanoscale phenomena, of macroscale effects in aquatic environments. These interests are coupled to the development of technology for commercial use, and include environmental projects for synchrotron laboratories.

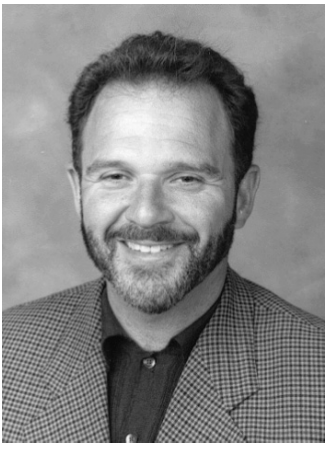

Steven N. Liss is a professor of applied microbiology in the Department of Chemistry and Biology at Ryerson University and is the Associate Dean (Research, Development and Science Programs) for the Faculty of Engineering and Applied Science. Dr. Liss holds adjunct professorships at the University of Toronto in the Departments of Chemical Engineering and Applied Chemistry and Civil Engineering. Dr. Liss holds an undergraduate degree in microbiology and immunology from the University of Western Ontario (1980) and graduate degrees in applied microbiology from the University of Saskatchewan (M.Sc, 1983; Ph.D., 1987). Dr. Liss currently leads research projects on the microbiology of wastewater treatment, water wells, and environmental biotechnology. His research is supported by awards from the Natural Sciences and Engineering Research Council of Canada, the National Centres of Excellence, Ontario Centres of Excellence, Environment Canada, Canada Foundation for Innovation (CFI), and a wide range of industry partners. Specific research activities include microbial floc architecture in engineered and natural systems, microbial ecology, water quality, filamentous microorganisms and bulking problems, biofouling and microbial-based tools for studying, and monitoring biological treatment systems including DNA microarrays. His laboratory has developed expertise related to the physicochemical properties of microbial structures, their composition and structure, and the application of advanced optical microscopy in studying microbial structures and physiology. His research in wastewater microbiology led to the Ryerson Distinguished Research Award in 1998. Dr. Liss has supervised 32 graduate students at the masters and Ph.D. levels. He is the author and co-author of over 100 peer-reviewed journal publications, book chapters, conference presentations, and technical reports.

Timothy G. Milligan is a researcher with the Marine Environmental Sciences Division, Fisheries and Oceans Canada. As head of the Particle Dynamics Laboratory at the Bedford Institute of Oceanography he leads the group's research into the behavior of fine particulate material in aquatic environments. He received his B.Sc in geology and M.Sc in oceanography from Dalhousie University and has been involved with flocs for over 30 years. While his initial contact was in pulp mill effluent, it was the time spent with the late Dr. Kate Kranck, a pioneer in flocculation studies in the marine environment, that gave him his love of mud. Areas of interest include the mechanisms governing the loss of sediment from river plumes, the effect of flocculation on the transport and fate of contaminants, and environmental impacts of offshore oil and gas and aquaculture. Mr. Milligan has led research projects in a wide range of geographical areas, from the Amazon to the Canadian Arctic. While his work concentrates mainly on the marine environment, the fate of terrestrially derived sediments and associated contaminants has led him into the study of fluvial transport as well. Mr. Milligan has been involved in many international ventures, several of which have received funding from the U.S. Office of Naval Research. His work combines *in situ* techniques with process-based parameterization of the size distributions of the component grains in suspended and bottom sediment to better understand the fate of mud in both marine and freshwater systems. Over 80 peer-reviewed primary publications, book chapters, and technical reports have been produced from this work.

Contributors

D. Grant Allen
Department of Chemical Engineering and Applied Chemistry
Pulp & Paper Centre
University of Toronto
Toronto, Ontario, Canada

Joseph F. Atkinson
Department of Civil, Structural and Environmental Engineering
State University at Buffalo
Buffalo, New York, U.S.A.

Adrian B. Burd
Department of Marine Sciences
University of Georgia
Athens, Georgia, U.S.A.

Rajat K. Chakraborti
Department of Civil, Structural and Environmental Engineering
State University at Buffalo
Buffalo, New York, U.S.A.

Holger Daims
Department of Microbial Ecology
Institute for Ecology and Conservation Biology
University of Vienna
Vienna, Austria

Patrick J. Dickhudt
University of Maryland Center for Environmental Science
Horn Point Laboratory
Cambridge, Maryland, U.S.A.

Ian G. Droppo
National Water Research Institute
Environment Canada
Burlington, Ontario, Canada

Ramin Farnood
Department of Chemical Engineering and Applied Chemistry
University of Toronto
Toronto, Ontario, Canada

Carl T. Friedrichs
Virginia Institute of Marine Science
College of William and Mary
Gloucester Point, Virginia, U.S.A.

David D. Fugate
Virginia Institute of Marine Science
College of William and Mary
Gloucester Point, Virginia, U.S.A.

Jean-Francois Gaillard
Department of Civil and Environmental Engineering
Northwestern University
Evanston, Illinois, U.S.A.

Gill G. Geesey
Department of Microbiology
Montana State University
Bozeman, Montana, U.S.A.

Adam P. Hitchcock
Brockhouse Institute for Materials Research
McMaster University
Hamilton, Ontario, Canada

George A. Jackson
Department of Oceanography
Texas A&M University
College Station, Texas, U.S.A.

Bommanna G. Krishnappan
National Water Research Institute
Environment Canada
Burlington, Ontario, Canada

John R. Lawrence
National Water Research Institute
Environment Canada
Saskatoon, Saskatchewan, Canada

Anne A. Lazarides
MEMS Department
Pratt School of Engineering
Duke University
Durham, North Carolina, U.S.A.

Gary G. Leppard
National Water Research Institute
Environment Canada
Burlington, Ontario, Canada

B.Q. Liao
Department of Chemical Engineering
Lakehead University
Thunder Bay, Ontario, Canada

Steven N. Liss
Department of Chemistry and Biology
Faculty of Engineering and Applied Science
Ryerson University
Toronto, Ontario, Canada

Bruce E. Logan
Department of Civil and Environmental Engineering
COE Environmental Institute
The Pennsylvania State University
University Park, Pennsylvania
U.S.A.

Jiri Marsalek
National Water Research Institute
Environment Canada
Burlington, Ontario, Canada

Timothy G. Milligan
Habitat Ecology Section
Bedford Institute of Oceanography
Dartmouth, Nova Scotia, Canada

Fernando Morgan-Sagastume
Department of Chemical Engineering and Applied Chemistry,
Pulp & Paper Centre
University of Toronto
Toronto, Ontario, Canada

Thomas R. Neu
Department of River Ecology Magdeburg
UFZ Centre for Environmental Research
Leipzig-Halle, Germany

Ellen L. Petticrew
Department of Geography
University of Northern British Columbia
Prince George, British Columbia
Canada

John M. Phillips
Environment Agency
Blandford Forum
Dorset, U.K.

Alain Reinhardt
Analytical and Biophysical Environmental Chemistry
University of Geneva
Geneva, Switzerland

Heidi Romine
Virginia Institute of Marine Science
College of William and Mary
Gloucester Point, Virginia, U.S.A.

Laura Rubiano-Gomez
University of Maryland Center for Environmental Science
Horn Point Laboratory
Cambridge, Maryland, U.S.A.

Lawrence P. Sanford
University of Maryland Center for Environmental Science
Horn Point Laboratory
Cambridge, Maryland, U.S.A.

Peter H. Santschi
Laboratory for Oceanographic and Environmental Research
Department of Oceanography
Texas A&M University
Galveston, Texas, U.S.A.

Steven E. Suttles
University of Maryland Center for Environmental Science
Horn Point Laboratory
Cambridge, Maryland, U.S.A.

Laurenz Thomsen
School of Engineering and Science
International University Bremen
Bremen, Germany

John E. VanBenschoten
Department of Civil, Structural and Environmental Engineering
State University of New York at Buffalo
Buffalo, New York, U.S.A.

Fintan Van Ommen Kloeke
Department of Microbiology
Montana State University
Bozeman, Montana, U.S.A.

Desmond E. Walling
Department of Geography
University of Exeter
Exeter, Devon, U.K.

Kevin J. Wilkinson
Analytical and Biophysical Environmental Chemistry
University of Geneva
Geneva, Switzerland

Johan C. Winterwerp
W.L. Delft Hydraulics
Delft, The Netherlands

Marissa Yates
University of Maryland Center for Environmental Science
Horn Point Laboratory
Cambridge, Maryland, U.S.A.

Contents

1 Methods for Analyzing Floc Properties

Steven N. Liss, Timothy G. Milligan, Ian G. Droppo, and Gary G. Leppard

CONTENTS

1.1 INTRODUCTION

The function–structure relationships of flocs are important to environmental scientists, microbiologists, and engineers. Ultimately, their goals include being able to solve practical problems more effectively, and to provide better information for modeling ecological processes and contaminant transport in aquatic environments and in the operation of engineered systems (e.g., wastewater and drinking water). Methods and analytical tools play a critical role in floc research and in achieving these goals. These are intended to do one of two things: (i) to provide descriptive and quantitative information that may lead to a fuller understanding of flocculation and (ii) to have tools that may be applied to the management of floc processes in engineered and environmental systems.

At present, few standard methods with good reproducibility are available, although several physical, chemical, and microbiological measurement and analytical techniques have been developed. Earlier reviews give a comprehensive review of the methods and techniques for the measurement of physical characteristics for activated sludge[1] and an overview of the principles, methods, and applications of particle size analysis in primarily saltwater systems.[2] Eisma et al.[3] and Dyer et al.[4]

1-56670-615-7/05/$0.00+$1.50

conducted a comparative study in the Elbe estuary to evaluate several different *in situ* methods for determining floc size and settling velocity. More recently, several entries in the *Encyclopaedia of Environmental Microbiology*[5] provide overviews of methods, particularly advanced optical microscopy and molecular tools applied to the study of microbial structures including flocs.[6] Common to all these reviews is the wide range of methods employed to determine some of the most basic of parameters that describe flocs in the environment.

In engineered systems, advances have been achieved primarily in studying floc properties (ecology, structure, and physicochemical characteristics) of individual flocs from full-scale systems and from laboratory-scale reactors that were run under well-controlled conditions. In contrast, studies in the marine and freshwater environments have concentrated on bulk properties such as gross morphology, size, and settling velocity in samples collected with an emphasis on *in situ* measurements. One reason for the difference between measurements in the natural environment and engineered systems is the availability of flocs and the ease with which they can be sampled intact. Those involved with studying natural systems have tended to focus on the gross properties and behavior of floc. Engineered systems are suited to detailed examination of surface properties and molecular determinants in floc behavior.

In this chapter, we present an overview of the principal methods presently being used in engineered, freshwater, and marine systems. Some aspects of the methods presented can be applied to both natural and engineered systems. Our goal is to provide an insight into the work being carried out in the different aquatic environments so that researchers can consider adapting the techniques presented to their respective fields.

1.1.1 Floc Size

Floc size is a widely measured floc characteristic. Floc size influences properties such as mass transfer (transport and settling),[7] biomass separation, and sludge dewatering.[8–10] Flocs are generally observed as two-dimensional (2D) projections, and there is no simple means of specifying size or shape.[11] However, flocs are highly irregular in shape, porous, and three-dimensional. Equivalent spherical diameter (ESD), frequently calculated from the two-dimensional area, is often used to characterize floc size due to its simplicity and its application in Stokes' law.[11–13] Bache et al.[11] defined the effective diameter as the geometric mean $\sqrt{(d_{\min} * d_{\max})}$ based on the maximum ($d_{\max}$) and minimum ($d_{\min}$) dimensions across the 2D floc image. Barbusinski and Koscielniak[14] and Li and Ganczarczyk[15] described floc size based on the average floc diameter defined as one half of the sum of the longest and shortest dimensions of the flocs measured.

Flocs in suspension are found over a range of sizes that describe a continuous distribution. Several standard parameters are available to describe floc size distributions. Median (d_{50}), upper quartile (d_{25}), and mode have all been used to describe the size distribution of flocs in suspension.[13,16,17] Due to the open architecture and poorly defined association of particles within a floc, researchers use fractal geometry to describe floc structure.[18–23] Depending on the nature and the sizing technique employed, there is no evidence to show which definition is the best representation of floc size. However, researchers should be clear in their definition of floc size when reporting results.

In general flocs range in size from a few microns to a few millimeters when measured by ESD. One exception is large assemblages of diatoms or other biologically derived material. Sometimes referred to as marine snow to differentiate it from more inorganic rich flocs, these patches of aggregated organic material can reach ESDs many orders of magnitude larger than what could be considered normal flocs. When marine snow becomes buoyant during decomposition, as was observed in the Adriatic Sea during the mucilage phenomenon, "floc size" can exceed 1 m.[24–27]

Many methods and instruments have been developed in the past to measure floc size distributions in natural and engineered systems. One of the earliest methods was the Coulter Counter, which determined the size distribution of particles in suspension. This method was popular in the marine environment as the electrolyte concentration in seawater permitted samples to be analyzed without alteration. However, stresses applied during the counting process can disrupt flocs which raises the issue that this method may be of little value for estimating floc size.[28,29]

The determination of floc size has relied primarily on imaging of flocs followed by image analysis to ascertain the parameters describing the size distribution.[12,30,31] Both microscopic observations and photographic techniques[13,32–35] have been used. *In situ* photography of flocs, although relatively easy to employ, does not allow measurement of very small flocs due to resolution limits. Often these systems can only image down from 50 to 100 μm, although a 10 : 1 camera system with a resolution of 10 μm has been developed.[36,37] Recent advances in digital photography should improve the resolution of *in situ* camera systems. The main advantage of these instruments is their ability to measure floc size with minimal disturbance to the natural stress environment of the flocs. However, they were developed for the natural environment, and may be difficult to apply in an engineered system as they are limited by the concentration of particles in suspension.

Microscopic methods usually incorporate a camera and computerized digitizer to provide images for analysis. The increased resolution of microscopic systems allows for accurate, reproducible, and relatively fast estimates of floc morphological parameters. Specialized techniques such as confocal microscopy and electron microscopy (discussed in detail later in the chapter) allow the internal structure of flocs to be examined. The obvious drawback for microscopic analysis is the requirement to remove flocs from their natural environment and the associated instrument costs.

Common to both photographic and microscopic methods is the requirement to conduct image processing and analysis on the captured image to determine floc size and other descriptive parameters. Image processing and analysis comprises several steps.[38] Different algorithms are applied to the digital image to improve the quality of the image and to separate a floc from its background. Each area of coherent pixels with values within a selected range of threshold values is then used to calculate the different parameters used to describe floc size. There are differing views on the number of pixels required to define a particle with values ranging from 3 to 35 pixels.[39,40] Several different image analysis systems are available on the market but all are based on the same principles for manipulating a matrix of pixel values. Clear explanations of the methods employed in the analysis are critical for understanding how descriptive parameters such as ESD are generated.

Laser based sizing instruments are now being widely used to determine floc size *in situ*.[41,42] Two different laser techniques have been used, focused beam reflectance measurement (FBRM) and laser diffraction. FBRM instruments (modified ParTec) employ a rotating laser beam to determine the size of particles in the sensing zone.[41] When the laser encounters a particle, the beam is reflected for the period of time it takes to traverse the particle. Using the angular velocity of the beam and the duration of the reflected laser pulse, the length of the intersecting particle chord is determined. A chord correction algorithm is then used to determine the size distribution of the particles in suspension. FBRM instruments were designed for process control and are not easily adapted to studies in natural systems. However, they do have the advantage of working at higher concentrations than instruments that rely on light transmission.[41]

Laser diffraction instruments were first used by Bale and Morris,[43] who modified a Malvern particle size analyzer (Malvern Instruments, U.K.) for underwater use. Since then purpose-designed laser diffraction systems have become available, notably the LISST (Sequoia Scientific Inc., WA, United States) and the CILAS (CILAS, France). Laser diffraction instruments are based on the scattering of laser light by particles as the beam transits a known sample zone. The scattering angle is determined by the size of the particle with the scattering angle being small for large particles and large for small particles.[42] A series of concentric ring detectors sense the amount of light they are receiving. Using the Mie or Fraunhofer theory of scattering for spheres, these values can then be inverted to yield the particle size distribution.[42]

Floc size has also been inferred from the settling behavior of flocculated suspensions.[4,44] Settling column methods in general measure the equivalent hydraulic diameter of particles in suspension rather than the actual physical size of the suspended particles. Floc size is expressed in terms of the diameter of a sphere with the density of quartz, settling at the same speed as the particle in question.[45]

1.1.2 Sample Handling and Stabilization

In situ measurement of floc size is clearly preferable due to the fragile nature of flocs. Sample handling may break up existing flocs or promote formation of larger flocs during storage.[46] Gibbs and Konwar[47] showed that common sampling methods disrupt flocs. Critical to any work with flocs outside their natural environment is sample handling and preparation. The need for microscopic examination of flocs and for laboratory experiments with natural flocs has led to the development of new techniques for removing flocs from their ambient conditions with minimal change in floc size or structure. Considerable efforts have been given to overcome perturbation that may be associated with sampling and specimen preparation.

For floc size measurements not performed *in situ*, samples are collected in bulk suspension and transported to the laboratory for sizing. Essential to this first step is minimizing the stress applied to the flocs during sampling. Droppo and Ongley[12] employed traditional laboratory-used plankton chambers within fluvial systems. By using the plankton chamber as both the sampling and analytical chamber for image analysis, potential perturbations are minimized. Depending on the sizing methods, further floc sampling might be required. Some size measurements using

image analysis systems or microscopic observation require subsampling of flocs onto microscope slides. This is normally done using a pipette for which the opening has to be wide enough (2 to 3 mm) to prevent floc breakage and disaggregation.[48]

Floc stabilization prior to further sample handling has been shown to be effective in preserving floc structural characteristics. Droppo et al.[49,50] described a method of utilizing low melting point agarose to physically stabilize microbial flocs before analysis. This technique was found to have no significant effects on floc size distributions. Ganczarczyk et al.[51] used a similar approach in physically stabilizing microbial flocs. Optically clear polyacrylamide gels have been used in marine sediment traps to capture flocs intact for later processing.[52]

1.2 FLOC SETTLING VELOCITY

Settling velocity measurements of flocs are important for studying the fate of sediments within natural systems and for the evaluation of solids removal from treated effluents and in the estimation of floc wet density. Floc settling velocity has been found to increase with increasing floc size[53–57] but not necessarily in accordance with Stokes' law. Floc settling under gravity has been reported to be affected by a wide range of factors including the shape and settling orientation of flocs being measured. The effect of fluid drag force on the settling velocity of a nonspherical particle is larger than that on a spherical particle.[58,59] The fastest settling rate is for particles of spherical shape, followed by that of cylindrical, needle-like, and disc-like shape.[58] Floc settling velocity may be affected by the settling orientations of the flocs because the drag force depends on the floc area facing the settling direction.[53] Fluid flow through the internal structure of flocs may also be important, as this would reduce hydrodynamic resistance and increase settling velocity.[15] Zahid and Ganczarczyk[54] stated that the computation of settling velocity by Stokes' law from the size and density measurements has to consider the effect of floc permeability. This, however, is in contradiction to the usual way of calculating wet density of flocs from the size–settling velocity measurements. The effect of floc permeability on settling velocity is considered negligible.[55,60] To complicate this picture from the floc structure viewpoint, Liss et al.[61] showed that the channels that appeared to be open by conventional optical microscopy (COM) and confocal laser scanning microscopy (CLSM) were in many instances filled with extracellular polymeric substance (EPS) fibrils that could be seen only by transmission electron microscopy (TEM).

Floc settling velocity is most commonly determined by measuring the distance traveled by a floc over a known time using multiple exposure photographic and video imaging.[34,35,53,57,62,63] These techniques are effective in measuring floc size and settling velocity within the resolution limits of the imaging method used. Klimpel et al.[60] used a cinematographic technique to measure larger flocs ($>100\ \mu$m), and the multiple exposure technique to measure smaller flocs ($<100\ \mu$m). Droppo et al.[57] developed a videographic technique to measure floc settling velocity. This technique involves using a stereoscopic microscope or $1\times$ tellecentric lens and a video camera to capture images of settling floc in a column filled with a medium similar to the native environment of the samples. A small quantity ($\sim$1 ml) of floc samples is introduced

at the top of the column. A sufficient travel distance is allowed for flocs to reach terminal velocity. Settling images of flocs are then recorded on a VCR as they pass though the focal plane of the microscope. These images are then analyzed using a computer imaging software for size and settling velocity.

Similar video imaging techniques have been developed to examine floc size–settling velocity relationships *in situ* in marine and freshwater environments.[36,37] All are based on video imaging of settling flocs within a stilled water column. Missing, however, from most studies has been an accurate estimation of floc density. A new instrument called INSSECT (IN situ Size and SEttling Column Tripod) has been designed to measure all the variables that, at present, are thought to influence the flux of fine-grained sediment to the bottom.[52] Comprising a rotating sediment trap and settling column, the rotating tripod is equipped with video and still camera systems, current meters, and polyacrylamide gels to capture settling flocs.

There is no simple equation relating the settling velocity of flocs to their size. Stokes' law or modified Stokes' law best describes the settling velocity of particles that approach a perfect sphere. Despite the limitations, estimations of other floc properties (e.g., density) derived from Stokes' law have proven useful in floc research. Stokes' law is defined as follows:

$$v = \frac{1}{18}\frac{g \cdot d^2(\rho_f - \rho_w)}{\mu} \tag{1.1}$$

where v is the terminal settling velocity, ρ_f the wet density of particle, ρ_w the density of water (assume settling in water), g the gravitational constant, μ the viscosity of water (assume settling in water), and d the diameter of particle.

Li and Ganczarczyk[53] used a power function of the form, $v = AL^n$, and a linear function, $v = A + BL$, to correlate floc settling velocity (v) with its longest dimension as a characteristic size (L), where A, B, and n are the equation coefficients determined experimentally. The power function is considered to be a better way to describe the relationship because the power function predicts that the velocity will be zero when floc size approaches zero while the linear function does not. However, the measured settling velocities can yield coefficients lower than that predicted by Stokes' law ($n = 2$).[54,55,64] The power law coefficients (n) calculated from the power function generally have ranged from 0.55 to 0.88. The number of flocs measured in these studies were as low as 21 and as high as 343. Lee et al.[56] managed to measure a total of 1385 flocs for settling velocity and size determinations and reported a power coefficient of 0.7 to 0.8. A modified linear model incorporating the floc settling shape factor was found to improve the correlation coefficient (R^2) of the linear relationship.[64]

In the marine environment, settling velocities of flocs have been inferred from clearance rates in enclosed sedimentation tubes.[4,44] Commonly, open-ended tubes are submerged horizontally to permit free flow of particles in suspension and then closed, rotated to 90°, and retrieved. Subsamples are removed from the tube at set intervals during settling and the settling velocity is determined from the change in concentration with time.[44] Settling velocities calculated from clearance rates were found to be an order of magnitude less than those determined *in situ* using camera techniques during the Elbe Estuary intercalibration program.[4] However, the ease of

use and the direct application of the results for determining vertical sediment flux have made settling columns a common instrument for nearshore studies.

In short, floc settling in any environment is not only highly related to size, but also related to floc shape and density. While Stokes' law gives a reasonable approximation, the relationship between floc size and settling velocity is best described by a power law equation with the value of the exponent close to 1. Recent advances in digital imaging and image analysis and the ability to collect ancillary data have led to better understanding of the size–settling velocity relationship for flocculated suspensions.[52]

1.3 FLOC DENSITY AND POROSITY

Floc density and porosity are two important floc characteristics in evaluating floc behavior. Along with floc size and shape, floc density plays a strong role in influencing settling velocity with concomitant transport and industrial efficiency implications. As the porosity of a floc has consistently been shown to be negatively correlated to density,[7] it too is an important parameter for floc behavioral assessment. Density is usually derived from the settling velocity–size measurements using Stokes' law or modified Stokes' law.[34,35,53–57,60,65] The validity of this approach has been questioned because it usually assumes spherical flocs and the settling velocity and size relationship do not follow Stokes' law. Zahid and Ganczarczyk[54] stated that there were a number of uncertainties involved in the density calculation from Stokes' law, therefore the approach was regarded only as an approximation. Lee et al.[56] also supported this approach since it provides at least qualitatively valid density estimation.

The following equation is often used to calculate floc porosity from density:[53]

$$\varepsilon = \frac{\rho_s - \rho_f}{\rho_s - \rho_w} \tag{1.2}$$

where ρ_s and ρ_f are the dried floc density (1.34 to 1.69 g/cm^3) and wet floc density, respectively, and ρ_w is the liquid density.

Andreadakis[66] made use of interference microscopy for floc density determination and used the above equation to calculate floc porosity. Density determinations for aggregates are usually based upon observations of terminal velocity, although a method based upon a series of sucrose solutions of incremented densities has been presented by Lagvankar and Gemmell.[67] Ozturgut and Lavelle[59] employed a linear-density stratified column which allows flocs to settle to their isopycnic levels to measure low density but settleable wastewater effluent flocs. Dammel and Schroeder[68] used a similar density gradient centrifugation technique, which allows the flocs to settle in a fluid of continuous increasing density until the flocs become stationary, to measure the density of activated sludge flocs. This technique, however, does not measure floc size concurrently with its density, thus, a size and density relationship might not be established easily. In addition, the ionic strength of the suspension medium and the nature of the medium itself have to be compatible and nontoxic with the biological flocs.

A variety of floc density models have been proposed. Magara et al.[34] proposed the following floc effective density (ρ_e) model based on Stokes' law,

$$\rho_e = \rho_f - \rho_w = 0.003698 \cdot \mu_w v d^{-2} \tag{1.3}$$

where ρ_f and ρ_w are the floc density and liquid density, respectively (g/cm^3), μ_w is the liquid viscosity (g/cm^3 sec^{-1}), v is the floc settling velocity (cm/s) and d is the floc ESD (cm). Tambo and Watanabe[35] suggest a model based on Stokes' law for effective floc density and size:

$$\rho_e = \rho_f - \rho_w = \frac{34\mu_w v}{g d_f^2} \tag{1.4}$$

assuming a drag coefficient of $45/Re$ and a floc sphericity of 0.8. Andreadakis[66] suggested that the floc density (ρ_f) is a function of its size (d),

$$\rho_f = 1 + 0.30\, d^{-0.82} \tag{1.5}$$

assuming a dried sludge density of 1.34 g/cm^3. Glasgow and Hsu[65] developed an empirical equation for kaolin–polymer aggregate to relate its density (ρ) to diameter (d) and pH,

$$\rho = 1.05 \cdot d^{(-0.0038\text{pH}+0.00716)} \tag{1.6}$$

assuming a sphericity of 1.0.

Zahid and Ganczarczyk[54] plotted effective density as a function of average diameter on a logarithmic scale and developed the following equation for the floc effective density and the average diameter (D),

$$\rho_e = \frac{0.005}{D^{1.21}} \tag{1.7}$$

where the two constants, 1.21 and 0.005, represent the slope of the straight line and the effective density of a 1.0 mm diameter particle, respectively. Accordingly, the size–porosity function was expressed as:

$$\varepsilon = 1.0 - \frac{0.007}{D^{1.21}} \tag{1.8}$$

Mikkelsen and Perjrup[69] presented a method for determining effective floc density and calculated settling velocity in coastal marine environments using data collected by a LISST. Assuming that floc fraction and the amount of material in suspension that is found in flocs is high then the effective floc density is equal to the total suspended mass divided by the total volume concentration of the flocs.

Although there are many empirical models available for the estimation of floc density and porosity, none of them can be considered as a universal model. This is

simply because all these models were developed from their specific conditions such as the type of natural or engineered system, the type of microorganisms, the hydrodynamic conditions, and the experimental techniques used. Therefore, floc density and porosity must be experimentally determined in all situations. New instrumentation is now available that can determine the size–settling velocity relationship of flocs in suspension, determine the mass of the flocs, and capture them for microscopic analysis.[52] With these advances, it should be possible to determine densities in natural environments *in situ*.

1.3.1 Floc Structure: Correlative Microscopy

Leppard[70] defined correlative microscopy (CM) as a strategy of using multiple microscopic techniques which can include conventional optical microscopy (COM), confocal laser scanning microscopy (CLSM), and transmission electron microscopy (TEM), and allow one to detect, assess, and minimize artifacts that might arise from using one technique only. CM has been successfully used by Liss et al.[61] with a minimal perturbation approach in studying natural and engineered flocs. A recent minimal perturbation approach[49,50] involves the use of sample stabilization in low melting point agarose and a fourfold multi-preparatory technique. The use of a fourfold multiple preparatory technique and CM has revealed how to maintain the structural integrity of the samples through the stabilization, staining, and washing procedures. The use of only one microscopic technique can bias or limit the information acquired because of the artifacts that arise in specific sample preparations and the resolution constraint associated with a particular technique.

The use of COM is the most common microscopic approach in the analysis of external gross-scale floc structure.[12,14,31,57,71,72] High resolution TEM is often used to investigate the fine structure of natural and engineered flocs, especially in the study of EPS distribution within floc structure.[26,27,72–75] This is generally done by stabilizing samples in a fixing agent such as glutaraldehyde, then embedding in Spurr resin or alternatively a fixation and embedding in Nanoplast; an ultrathin section is then obtained from the embedded sample by slicing with an ultramicrotome and a diamond knife. This ultrathin section (50 to 100 nm) is then placed on a copper grid for further staining (e.g., uranyl acetate) to give better contrast, although at TEM resolution, fibrils, bacterial cells, and other components of floc are visible. TEM can be used in conjunction with energy dispersive spectroscopy (EDS) to detect metal accumulation and to give element abundance in EPS.[61,76] The thickness constraint of ultrathin sections (50 to 100 nm or less) in the preparation of TEM images has restricted the floc sample volume, which has a diameter as large as 1 mm, that can be examined at high resolution due to the consideration of cost and time. COM and CLSM images are useful in indicating the number of TEM sections required to be collected for determining the representative images of flocs.[61]

Nanoplast resin is particularly effective as a stabilization medium since it is a hydrophilic melamine embedding resin that holds the fibrillar EPS in native three-dimensional disposition. Nanoplast omits the solvent dehydration stage, and it forms cross-linkages between matrix colloids prior to structural water loss at the end of the embedding process. Measurements of the dimensions of colloidal matrix material

and their 3-D disposition are realistic. Nanoplast has been recently shown to be useful for stabilizing sediment biofilms and the EPS matrix of these structures for observation by CLSM.[77] The environmental scanning electron microscope (ESEM) permits observations of fully hydrated samples but there have been no published reports to date that describe microbial flocs using ESEM, except a few reports using ESEM information as an aid for interpreting other observations.[76]

CLSM is one of the most recent microscopic techniques used to study flocs and has been shown to be a useful technique in bridging the resolution gap between COM and TEM.[23,61] Images are scanned with a laser beam and collected in a point-by-point fashion by a photodetector system.[78] These collected images are stored in the computer memory for further image processing and analysis. The advantages of CLSM over conventional light microscopy include the reduction of image blurring caused by light scattering, with a concomitant increase in effective resolution. CLSM also allows the examination of a thick specimen such as animal tissue and biological flocs by scanning a series of planar images ($X-Y$ plane) along a vertical axis (Z) one at a time. These series of planar images can be reconstructed in a computer imaging analysis system into a 3D image of the sample.[21–23,61] Floc in excess of 500 μm can be visualized by CLSM. Two photon, or multiphoton laser scanning microscopy (2P-LSM) permits examination of floc and films approaching 1mm in thickness while minimizing photobleaching and phototoxicity. A particularly useful feature of CLSM and 2P-LSM is that these can be used in combination with a variety of fluorescent molecular probes to study the spatial distribution of extracellular polysaccharides, cell viability, pH gradient, proteins, RNA, lipids, and other components of floc nondestructively.[77,79] These techniques are increasingly being adapted by researchers to further our understanding of flocs and the relationship between structure, ecology, and the physicochemical properties of flocs and films.[23]

Other advanced microscopic methods including Raman confocal microspectroscopy can potentially provide insights into the chemical composition of microbial cells and the heterogeneity associated with spatial distribution associated with structure and the conditions of growth.[80,81] Atomic force microscopy (AFM) has emerged as a tool that can provide detailed information on topography of microbial surfaces as well as probing surface properties.[82,83] Through the interaction of the AFM tip and the microbial surface, attractive and repulsive forces can be explored (see Chapter 16). Functionalizing the tip with molecular specific probes is a further advance that permits more detailed examination of molecular interactions. Synchrotron-based scanning transmission x-ray microscopy (STXM) has recently been used correlatively with TEM and CLSM on a riverine biofilm to gain high resolution information on the three-dimensional distribution of specific classes of extracellular polymers.[84]

1.3.2 Extracellular Polymeric Substances

In aqueous environments, bacteria may invest a substantial amount (>70%) of their carbon and energy in the production of extracellular polymeric substances,[77,85] indicating an important role of EPS in the functioning of microbial communities and the structures they form. Over the past 20 years, studies have emphasized the composition

of the EPS based on analyses of whole sludge or the extracted EPS. More recently, investigators are beginning to focus on detailed investigation of the surface properties and EPS through direct examination, by microscopy, of the whole biopolymeric material rather than the extracted EPS as has been done previously[86] (see Chapter 6).

EPS can be classified as capsular EPS (bound) and slime EPS (soluble). The bound EPS is attached tightly to the exterior cell wall, while the soluble EPS is the loosely attached or unattached 'slime' material that can be washed away by centrifugation.[87,88] In order to analyze the composition of bound EPS without inducing cell lysis, a variety of extraction methods have been developed. Brown and Lester[89] have compared bacterial EPS extraction methods from other sources including chemical methods such as ammonium hydroxide, sodium hydroxide, EDTA, sulfuric acid, and boiling benzene. Mechanical extraction methods such as high-speed centrifugation, ultrasonication, and boiling or autoclaving were also investigated. The influence of various separation and extraction processes, on the constituents and quantities of EPS being extracted, has been reviewed recently, along with a comparison of the analytical measures in common use.[90]

Cation exchange resin (CER), utilizing both a mechanical and chemical means of extraction, has been found to be effective in terms of minimal cell lysis and nondisruptive effects on the EPS.[91,92] This extraction method removes divalent cations such as Ca^{2+} and Mg^{2+} from the EPS matrix and replaces them with monovalent cations. By removing the divalent cations the EPS becomes less stable thereby allowing the EPS to separate from the cellular material. Subsequent to capsular EPS extraction, proteins,[93] carbohydrates,[94] acidic polysaccharides,[95] and DNA can be measured.

Although quantitative estimations of EPS in microbial structures have been traditionally accomplished through extraction and chemical methods, fluorescent probes are suitable for estimating EPS *in situ*. In the past, Calcofluor White M2R was used to measure exopolysaccharide production in single bacterial strains such as *Azospirillum*, *Pseudomonas aeruginosa*, and *Klebsiella pneumoniae*.[96,97] Similarly, congo red was employed for general light microscopy staining of polysaccharides.[98] More recently, researchers have begun to use fluorescently labeled lectins as a method to probe the spatial relationships of EPS within thick heterogeneous microbial structures.[99–102] Lectins are a large group of glycoproteins that bind to specific carbohydrates. They are prevalent in nature and are present in plants, bacteria, animals, and humans.[103] Plant lectins have been used as both specific and general stains to estimate EPS, as well as to characterize the EPS left on surfaces after the removal of microbes.[99–101,104]

1.4 SURFACE CHARGE AND HYDROPHOBICITY

As reviewed by Liss,[6] methods used in the past to determine microbial surface charge include attachment to charge-modified polystyrene, fluorescent probe ion exchange resin, and electrophoretic mobility. At present, the most common and reproducible method to determine surface charge density of microbial aggregates is by a colloid titration.[105,106] Mikkelsen[107] recently compared surface charge determinations of sewage sludge by various methods in order to identify applications and limitations

of the colloid titration method for analysis that tends to yield widely ranging values amongst different studies. The colloid titration method was found to be limited to conditions of low reactant doses and valid for charge determination of extracellular polymeric substances primarily. For determining whole floc or sludge surface charge, estimates from zeta potential titrations may be more reliable than that determined from colloid titration.

Numerous methods have been reported in the literature for determining hydrophobic interactions of cells and have been summarized by Liss.[6] These include methods that measure actual binding to a hydrophobic ligand such as microbial adhesion to hydrocarbons (MATH) and those giving an estimate of an overall surface property, such as salt aggregation test (SAT) and contact angle measurement (CAM) of dry cell layers.

The MATH method is a simple method to rapidly quantify cell surface hydrophobicity.[108,109] This method is based on the partitioning of cells possessing hydrophobic surface characteristics at the interface of a biphasic hydrocarbon–-aqueous system after brief mixing. The relative hydrophobicity is calculated from:

$$H = 100(1 - a/A), \tag{1.9}$$

where a is the absorbance of the aqueous layer after phase separation, and A is the initial absorbance of the aqueous phase at 400 nm before mixing with hydrocarbons. Attention must be given to the possibility that cell clumping may occur during the assay, which can result in a huge reduction in absorbance. Changes in the initial cell density can also affect the measurement.

Contact angle measurement is one of the most common techniques for the measurement of hydrophobicity of bacterial cell surfaces and flocs because the surface free energy of these cells can be estimated from the measurement (see Chapter 19). Although different apparatus may be used, all the measurements involve the preparation of a thin bacterial lawn through the vacuum filtration of a bacterial suspension and the determination of sessile drop contact angles on the bacterial lawn, either by using a telegoniometer or by projecting a magnified image system. The application of axisymmetric drop shape analysis (ADSA) may overcome some of the problems inherent in contact angle measurements on biological cells.[110,111]

Salt aggregation test is based on subjecting cells to increasing concentrations of salting-out agents (e.g., ammonium sulfate).[112] The order in which cells are aggregated and settled is a measure of their surface hydrophobicity. The most hydrophobic cells are aggregated first at a low salt concentration. All tests are compared to the reaction at the highest molarity of salt (positive control). Bacterial suspensions mixed with a 0.002 M sodium phosphate (pH 6.8) are used as a negative control. A drop of methylene blue can be added to enhance the visualization of the aggregates.[113] Urbain et al.[114] used this method to study the internal hydrophobicity of sludge flocs. Limitations of SAT include the fact that many hydrophobic bacterial cells will clump in the absence of any added ammonium sulfate, and that it provides only a qualitative estimation of the relative rank of hydrophobicity. Electrostatic interactions may affect the results of SAT more than other hydrophobic measurement techniques.[109]

1.5 MICROBIAL ECOLOGY

The identification and *in situ* detection of microorganisms within activated sludge flocs using DNA probes have been reported for the subclasses of proteobacteria,[115] Gram-negative filamentous bacteria,[116] *Acinetobacter* spp.,[117] and nitrifying bacteria, ammonia- and nitrite-oxidizing bacteria.[118–121] Probes have been found to be effective in monitoring shifts in nutrient amended activated sludge samples and avoid biases associated with culture dependent methods.

Nucleotide probes are also being used in multimethod approaches to the analysis of marine snow. Grossart and Simon[122] studied the bacterial colonization and microbial decomposition of lake snow with rRNA-targeted fluorescent oligonucleotide probes, used in conjunction with standard limnological parameters and measures of hydrolytic enzyme activities, bacterial production and growth rates, and changes in floc composition during aging and sinking. The flocs were shown to be hotspots of enhanced microbial activity, with the microbial community dominated by β-Proteobacteria. The overall results suggested that lake snow and activated sludge flocs have similar functions in their aquatic ecosystems. A review and comparative analysis of the microbial ecology of flocs from many ecosystems have been published recently by Simon et al.,[123] who consider marine, lacustrine, riverine, and estuarine environments. They describe methodology and reference it in considerable detail, and they conclude that the significance of bacteria in aggregation processes is much greater than previously estimated.

A variety of approaches permitting correlation of structure–function relationships with respect to specific metabolic and biogeochemical processes associated with flocs are available. Carbon-substrate oxidation patterns or phenotypic fingerprinting based on commercially available BIOLOG microplates allow for simultaneous testing of 95 separate carbon substrates producing patterns of metabolic response based on the reduction of tetrazolium dye as an indicator of sole carbon utilization.[124] Brock and Brock[125] introduced microautoradiography (MAR) as a tool for looking at the activities of individual microorganisms in their natural habitats. This technique has been used since to address many important ecological questions regarding bacterial activities in natural aquatic systems.[126–129] MAR is a method that can be used to investigate the ability to assimilate organic or inorganic compounds by natural bacterial populations as well as assessing their abilities to be active under different operating conditions; for example, like the aerobic, anoxic, or anaerobic conditions encountered in some activated sludge systems.[130–132] Radiolabeled (^{3}H, ^{14}C, ^{35}S, or ^{33}P) substrates are used and can become associated with cells or biological structures of interest either as a result of adsorption or active uptake. After coating cells with a photographic emulsion and following an appropriate time of exposure, uptake is indicated by deposition of silver grains on the surface of radioactive cells.

Recently, direct combination of fluorescent *in situ* hybridization (FISH) and MAR for simultaneous *in situ* identification and determination of substrate uptake patterns of individual microbial cells within complex microbial community has been applied to activated sludge.[131–135] In the protocols used, an additional step of FISH prior to the 4′,6-diamino-2-phenylindole (DAPI) stain, which is used to obtain total cell counts,[115,130,136,137] and the MAR developing steps, is

incorporated. This combination permits simultaneous *in situ* detection of DAPI signals, probe-conferred fluorescence, and silver grain formation (which indicates the presence of radioactive compounds within the fixed cells) at a single cell level. The technique has been used to examine the identity of unknown bacteria which carry out specific processes, including their roles in organic substrate uptake and biological phosphate removal.[130,131] Some filamentous bacteria from activated sludge have been studied with these techniques, and their roles in the uptake of several organic substrates determined.[133,134]

1.6 CONCLUSION

Recent advances in both microscopic and photographic imaging techniques have led to a much greater understanding of floc behavior and floc structure. While the emphasis in the three different environments (saltwater, freshwater, and engineered systems) differs, new techniques in each discipline present an opportunity to advance our understanding of flocs. Very significant advances have been made in the study of floc properties in engineered systems, whereas the emphasis in natural systems has been on determining bulk properties that control the transport of sediment. Methods for dissecting flocs microscopically and understanding microbial systems and processes at a molecular level are relatively new to the marine and freshwater studies and offer an exciting new area of study provided floc sampling methods can advance at the same time.

REFERENCES

1. Li, D.-H. and Ganczarczyk, J.J. 1986. Physical characteristics of activated sludge flocs. *CRC Crit. Rev. in Environ. Contr.* 17: 53–87.
2. Syvitski, J.P.M. 1991. *Principles, Methods, and Applications of Particle Size Analysis*. Cambridge University Press, Melbourne, Australia.
3. Eisma, D., Bale, A.J., Dearnaley, M.P., Fennessey, M.J., Van Leussen, W., Maldiney, M.A., Pfieffer, A., and Wells, J.T. 1996. Intercomparison of in situ suspended matter (floc) size measurements. *J. Sea Res.* 36: 3–14.
4. Dyer, K.R., Cornelisse, J., Dearnlaley, M.P., Fennessey, M.J., Jones, S.E., Kappenberg, J., McCane, I.N., Perjrup, M., Puls, W., Van Leusse, W., and Wolfstein, K. 1996. A comparison of in situ techniques for estuarine floc settling velocity measurements. *J. Sea Res.* 36: 15–29.
5. Bitton, G. (ed.). 2002. *The Encyclopaedia of Environmental Microbiology*. Volumes 1–6, John Wiley and Sons, New York.
6. Liss, S.N. 2002. Microbial flocs suspended biofilms in *The Encyclopaedia of Environmental Microbiology*. G. Bitton (ed.). Volume 4, John Wiley and Sons, New York, pp. 2000–2012.
7. Droppo, I.G. 2001. Rethinking what constitutes suspended sediment. *Hydrol. Proc.* 15: 1551–1564.
8. Li, D.-H. and Ganczarczyk, J.J. 1993. Factors affecting dispersion of activated sludge flocs. *Water Environ. Res.* 65: 258–263.
9. Bruss, J.H., Nielsen, P.H., and Keiding, K. 1992. On the stability of activated sludge flocs with implications to dewatering. *Water Res.* 26(12): 1597–1604.

10. Mikkelsen, L.H., Gotfredsen, A.K., Agerbæk, M.A., Nielsen, P.H., and Keiding, K. 1996. Effects of colloidal stability on clarification and dewatering of activated sludge. *Water Sci. Technol.* 34: 449–457.
11. Bache, D.H., Hossain, M.D., Al-Ani, S.H., and Jackson, P.J. 1991. Optimum coagulation conditions for a colored water in terms of floc size, density and strength. *Water Supply.* 29: 93–102.
12. Droppo, I.G. and Ongley, E.D. 1992. The state of suspended sediment in the freshwater fluvial environment: A method of analysis. *Water Res.* 26: 65–72.
13. Milligan, T.G. 1996. In situ particle (floc) size measurements with the Benthos 373 plankton silhouette camera, *J. Sea Res.* 36(1–2): 93–100.
14. Barbusinski, K. and Koscielniak, H. 1995. Influence of substrate loading intensity on floc size in sludge process. *Water Res.* 29: 1703–1710.
15. Li, D.-H. and Ganczarczyk, J.J. 1988. Flow through activated sludge flocs. *Water Res.* 22: 789–792.
16. Hill, P.S., Milligan, T.G., and Geyer, W.R. 2000. Controls on effective settling velocity in the Eel River flood plume. *Cont. Shelf Res.* 20: 2095–2111.
17. Fox, J.M., Hill, P.S., Milligan, T.G., and Boldrin, A. 2004. Flocculation and sedimentation on the Po River delta. *Mar. Geol.* 203: 95–107.
18. Glasgow, L.A. 1989. Effects of the physiochemical environment on floc properties. *Chem. Eng. Prog.* Aug: 51–55.
19. Logan, B.E. and Wilkinson, D.B. 1991. Fractal dimensions and porosities of *Zooglea ramigera* and *Saccharomyces cerevisiae* aggregates. *Biotech. Bioeng.* 38: 389–396.
20. Námer, J. and Ganczarczyk, J.J. 1994. Fractal dimension and shape factors of digested sludge particle aggregates. *Water Poll. Res. J. Can.* 29: 441–455.
21. Thill, A., Veerapaneni, S., Simon, B., Weisner, M., Bottero, J.Y., and Snidaro, D. 1998. Determination of structure of aggregates by confocal scanning laser microscopy. *J. Colloid Interface Sci.* 204: 347–362.
22. Thill, A., Wagner, M., and Bottero, J.Y. 1999. Confocal scanning laser microscopy as a tool for the determination of 3D floc structure. *J. Colloid Interface Sci.* 220: 465–467.
23. Schmid, M., Thill, A., Purkhold, U., Walcher, M., Bottero, J.Y., Gineset, P., Nielsen, P.H., Weurtz, S., and Wagner, M. 2003. Characterization of activated sludge flocs by confocal laser scanning microscopy and image analysis. *Water Res.* 37: 2043–2052.
24. Alldredge, A.L. and Silver, M.W. 1988. Characteristics, dynamics and significance of marine snow. *Prog. Oceanogr.* 20: 41–82.
25. Heissenberger, A., Leppard, G.G., and Herndl, G.J. 1996. Relationship between the intracellular integrity and the morphology of the capsular envelope in attached and free-living marine bacteria. *Appl. Environ. Microbiol.* 62: 4521–4528.
26. Heissenberger, A., Leppard, G.G., and Herndl, G.J. 1996. Ultrastructure of marine snow II. Microbiological considerations. *Mar. Ecol. Prog. Ser.* 135: 299–308.
27. Leppard, G.G., Heissenberger, A., and Herndl, G.J. 1996. Ultrastructure of marine snow. I. Transmission electron microscopy methodology. *Mar. Ecol. Prog. Ser.* 135: 289–298.
28. Gibbs, R.J. 1982. Floc stability during Coulter counter sizer analysis. *J. Sedimen. Petrol.* 52: 657–660.
29. Milligan, T.G. and Kranck, K. 1991. Electro-resistance particle size analysers in *Theory, Methods and Applications of Particle Size Analysis*. J.P. Syvitski (ed.), Cambridge University Press, New York, 109–118.

30. Glasgow, L.A., Pollock, R.J., and Barkley, W.A. 1983. Particle size reduction by breakage in biological wastewater treatment. *Biotech. Bioeng.* 25: 901–918.
31. Li, D.H. and Ganczarczyk, J.J. 1986. Application of image analysis system for activated sludge flocs. *Water Poll. Res. J. Canada* 21: 130–140.
32. Sezgin, M., Jenkins, D., and Parker, D.S. 1978. A unified theory of filamentous activated sludge bulking. *J. Water Pollu. Control Fed.* 50(2): 362–381.
33. Pipes, W.O. 1979. Bulking, deflocculation and pinpoint floc. *J. Water Pollut. Control Fed.* 51: 62–70.
34. Magara, Y., Nambu, S., and Utowsa, K. 1976. Biochemical and physical properties of activated sludge on settling characteristics. *Water Res.* 10: 71–77.
35. Tambo, N. and Watanabe, Y. 1979. Physical characteristics of floc I — the focal density function and aluminum floc. *Water Res.* 13: 409–419.
36. Eisma, D. and Kalf, J. 1996. In situ particle (floc) size measurement with the NIOZ in situ camera system. *J. Sea Res.* 36(1–2): 49–53.
37. Eisma, D., Schuhmacher, T., Boekel, H., van Heerwaarden, J., Franken, H., Laan, M., Vaars, A., Eijgenraam, F., and Kalf, J. 1996. A camera and image-analysis system for in situ observation of flocs in natural waters. *Netherlands J. Sea Res.* 27: 43–56.
38. Russ, J.C. 1994. *The Image Processing Handbook*, 2nd Ed. CRC Press, Boca Raton, FL.
39. Fennessy, M.J., Dyer, K.R., Huntley, D.A., and Bale, A.J. 1997. Estimation of settling flux spectra in estuaries using INSSEV, in *Cohesive Sediments*, N. Burt, R. Parker and J. Watts, (eds.), John Wiley & Sons, pp. 87–104.
40. Van der Lee, W.T.B. 2000. Temporal variation of floc size and settling velocity in the Dollard estuary. *Cont. Shelf Res.* 20: 1495–1511.
41. Phillips, J.M. and Walling, D.E. 1995. An assessment of the effects of sample collection, storage and resuspension on the representativeness of measurements of the effective particle size distribution of fluvial suspended sediments. *Water Res.* 29: 2498–2508.
42. Agrawal, Y.C. and Pottsmith, H.C. 2000. Instruments for particle size and settling velocity observations in sediment transport. *Mar. Geol.* 168: 89–114.
43. Bale, A.J. and Morris, A.W. 1987. In situ measurement of particle size in estuarine waters. *Estuar. Coast. Shelf Sci.* 24: 253–263.
44. Owen, M.W. 1976. Determination of the settling velocities of cohesive muds. *Report No IT 161*. Hydraulics Research Station Wallingford, UK.
45. Matthews, M.D. 1991. The effect of pre-treatment on size analysis in *Principles, Methods and Application of Particle Size Analysis*, J.P.M. Syvitski (ed.), Cambridge University Press.
46. Phillips, J.M. and Walling, D.E. 1998. Calibration of a Par-Tec 200 laser back-scatter probe for in situ sizing of fluvial suspended sediment. *Hydrological Proc.* 12: 221–231.
47. Gibbs, R.J. and Konwar, L. 1983. Disruption of mineral flocs using Niskin bottles. *Environ. Sci. Technol.* 17: 374–375.
48. Gibbs, R.J. and Konwar, L. 1982. Effects of pipetting on mineral flocs. *Environ. Sci. Technol.* 16: 119–121.
49. Droppo, I.G., Flannigan, D.T., Leppard, G.G., Jaskot, C., and Liss, S.N. 1996. Floc stabilization for multiple microscopic techniques. *Appl. Environ. Microbiol.* 62: 3508–3515.

50. Droppo, I.G., Flannigan, D.T., Leppard, G.G., and Liss, S.N. 1996. Microbial floc stabilization and preparation for structural analysis by correlative microscopy. *Water Sci. Technol.* 34: 155–162.
51. Ganczarczyk, J.J., Zahid, W.M., and Li, D.H. 1992. Physical stabilization and embedding of microbial aggregates for light microscopy studies. *Water Res.* 26: 1695–1699.
52. Mikkelsen, O.A., Milligan, T.G., Hill, P.S., and Moffat, D. 2004. INSSECT-An instrumented platform for investigating floc properties close to the boundary layer. *Limnol. Oceanogr. Methods 2*: 226–236.
53. Li, D.H. and Ganczarczyk, J.J. 1987. Stroboscopic determination of settling velocity, size, porosity of activated sludge flocs. *Water Res.* 21: 257–262.
54. Zahid, W.M. and Ganczarczyk, J.J. 1990. Suspended solids in biological filter effluents. *Water Res.* 24: 215–220.
55. Námer, J. and Ganczarczyk, J.J. 1993. Settling properties of digested sludge particle aggregates. *Water Res.* 27: 1285–1294.
56. Lee, D.J., Chen, G.W., Liao, C.Y., and Hsieh, C.C. 1996. On the free-settling test for estimating activated sludge floc density. *Water Res.* 30: 541–550.
57. Droppo, I.G., Leppard, G.G., Flannigan, D.T., and Liss, S.N. 1997. The freshwater floc: A functional relationship of water and organic and inorganic floc constituents affecting suspended sediment properties. *Water Air Soil Pollut.* 99: 43–54.
58. Lerman, A. 1979. *Geochemical Processes: Water and Sediment Environment*, Wiley, New York.
59. Ozturgut, E.O. and Lavelle, J.W. 1984. A new method for wet density and settling velocity determination for a waste water effluent. *Environ. Sci. Technol.* 18: 947–952.
60. Klimpel, R.C., Dirican, C., and Hogg, R. 1986. Measurement of agglomerate density in flocculated fine particle suspensions. *Particulate Sci. Technol.* 4: 45–59.
61. Liss, S.N., Droppo, I.G., Flannigan, D.T., and Leppard, G.G. 1996. Floc architecture in wastewater and natural riverine systems. *Environ. Sci. Technol.* 30: 680–686.
62. Fennessy, M.J., Dyer, K.R., and Huntley, D.A. 1994. INSSEV: An instrument to measure the size and settling velocity of flocs in situ. *Mar. Geol.* 117: 107–117.
63. Sternberg, R.W., Berhane, I., and Ogston, A.S. 1999. Measurement of size and settling velocity of suspended aggregates on the northern California continental shelf. *Mar. Geol.* 154: 43–53.
64. Ganczarczyk, J.J. 1994. Microbial aggregates in wastewater treatment. *Water Sci. Technol.* 30: 87–95.
65. Glasgow, L.A. and Hsu, J.-P. 1984. Floc characteristics in water and wastewater treatment. *Particulate Sci. Technol.* 2: 285–303.
66. Andreadakis, A.D. 1993. Physical and chemical properties of activated sludge flocs. *Water Res.* 27(12): 1707–1714.
67. Lagvankar, A.L. and Gemmell, R.S. 1968. A size-density relationship in flocs. *J. AWWA.* 60: 1050–1056.
68. Dammel, E.E. and Schroeder, E.D. 1991. Density of activated sludge solids. *Water Res.* 25: 841–846.
69. Mikkelsen, O.A. and Perjrup, M. 2001. The use of a LISST-100 laser particle sizer for in-situ estimates of floc size, density and settling velocity. *Geo-Mar. Lett.* 29: 187–195.
70. Leppard, G.G. 1992. Evaluation of electron microscope techniques for the description of aquatic colloids in *Environmental Particles.* Vol. 1, Lewis Publishers, Boca Raton, FL, pp. 231–289.

71. Chao, A.C. and Keinath, T.M. 1979. Influence of process loading intensity on sludge clarification and thickening characteristics. *Water Res.* 13: 1213–1221.
72. Jorand, F., Zartarian, F., Thomas, F., Block, J.C., Bottero, J.Y., Villemin, G., Urbain, V., and Manem, J. 1995. Chemical and structural (2D) linkage between bacteria within activated sludge flocs. *Water Res.* 29(7): 1639–1647.
73. Leppard, G.G. 1986. The fibrillar matrix component of lacustrine biofilms. *Water Res.* 20: 697–702.
74. Leppard, G.G. 1993. Organic Flocs in surface waters: Their native state and aggregation behavior in relation to contaminant dispersion in *Particulate Matter and Aquatic Contaminants*, S.S. Rao (ed.). Lewis Publishers, Boca Raton, fl, pp. 169–195.
75. Zartarian, F., Mustin, C., Bottero, J.Y., Villemin, G., Thomas, F., Aillères, L., Champerois, M., Grulois, P., and Manem, J. 1994. Spatial arrangement of components of activated sludge flocs. *Water Sci. Technol.* 30: 243–250.
76. Leppard, G.G., Droppo, I.G., West, M.M., and Liss, S.N. 2003. Compartmentalization of metals within the diverse colloidal matrices comprising activated sludge microbial flocs. *J. Environ. Qual.* 32: 2100–2108.
77. Decho, A.W. and Kawaguchi, T. 1999. Confocal imaging of in situ natural microbial communities and their extracellular polymeric secretions using Nanoplast resin. *Biotechniques*, 27(6): 1246–1252.
78. Caldwell, D.E., Korber, D.R., and Lawrence, J.R. 1992. Imaging of bacterial cells by fluorescence exclusion using scanning confocal laser microscopy. *J. Microbiol. Meth.* 15: 249–261.
79. Holloway, C.F. and Cowen, J.P. 1997. Development of scanning confocal laser microscopic technique to examine the structure and composition of marine snow. *Limnol. Oceanogr.* 42: 1340–1352.
80. Schuster, K.C., Reese, I., Urlaub, E., Gapes, J.R., and Lendl, B. 2000a. Multidimensional information on the chemical composition of single bacterial cells by Confocal Raman Microspectroscopy. *Anal. Chem.* 72(22): 5529–5534.
81. Schuster, K.C., Urlaub, E., and Gapes, J.R. 2000b. Single-cell analysis of bacteria by Raman Microscopy: Spectral information of the chemical composition of cells and on the heterogeneity in a culture. *J. Microbiol. Meth.* 42: 29–38.
82. Burks, G.A., Velegol, S.B., Paramanova, E., Lindenmuth, B.E., Feick, J.D., and Logan, B.E. 2003. Macroscopic and nanoscale measurements of the adhesion of bacteria with varying outer layer surface composition. *Langmuir* 19(6): 2366–2371.
83. Velegol, S.B., Pardi, S., Li, X., Velegol, D., and Logan, B.E. 2003. AFM imaging artifacts due to bacterial cell height and AFM tip geometry. *Langmuir* 19: 851–857.
84. Lawrence, J.R., Swerhorne, G.D.W., Leppard, G.G., Araki, T., Zhang, X., West, M.M., and Hitchcock, A.P. 2003. Scanning transmission X-ray, laser scanning, and transmission electron microscopy mapping of the exopolymeric matrix of microbial biofilms. *Appl. Environ. Microbiol.* 69: 5543–5554.
85. Decho, A.W. 1990. Microbial exopolymer secretions in ocean environments: Their roles in food webs and marine processes. *Oceanogr. Mar. Biol. Annu. Rev*. 28: 73–153.
86. Wilen, B.-M., Jin, B., and Lant, P. 2003. The influence of key chemical constituents in activated sludge on surface and flocculating properties. *Water Res.* 37: 2127–2139.
87. Gehr, R. and Henry, J.G. 1983. Removal of extracellular materials: Techniques and pitfalls. *Water Res.* 17(12): 1743–1748.
88. Spaeth, R. and Wuertz, S. 2000. Extraction and quantification of extracellular polymeric substances from wastewater in *Biofilms: Investigative Methods and Applications*. H-C. Flemming, U. Szewzyk, and T. Griebe (eds.). Technomic Publishing Company Inc., Lancaster, Pennsylvania, pp. 51–68.

89. Brown, M.J. and Lester, J.N. 1980. Comparison of bacterial extracellular polymer extraction methods. *Appl. Environ. Microbiol.* 40: 179–185.
90. Liu, Y. and Fang, H.P. 2003. Influences of extracellular polymeric substances (EPS) on flocculation, settling and dewatering of activated sludge. *CRC Crit. Rev. Environ. Sci. Technol.* 33(3): 237–273.
91. Rudd, T., Sterritt, R.M., and Lester, J.N. 1983. Extraction of extracellular polymers from activated sludge. *Biotechnol. Lett.* 5(5): 327–332.
92. Frølund, B., Palmgren, R., Keiding, K., and Nielsen, P.H. 1996. Extraction of extracellular polymers from activated sludge using a cation exchange resin. *Water Res.* 30(8): 1749–1758.
93. Lowry, O.H., Rosebrough, N.J., Farr, A.L., and Randall, R.J. 1951. Protein Measurement with the Folin phenol reagent. *J. Biol. Chem.* 193: 265–275.
94. Gaudy, A.F. 1962. Colorimetric determination of protein and carbohydrate. *Industrial Water and Wastes*. Jan–Feb: 17–22.
95. Filisetti-Cozzi, T.M. and Carpita, N.C. 1991. Measurement of uronic acids without interference from neutral sugars. *Anal. Biochem.* 197: 159–162.
96. Del Gallo, M., Negi, M., and Neyra, C.A. 1989. Calcofluor- and lectin-binding exocellular polysaccharides of *Azospirillum brasilense* and *Azospirillum lipoferum*. *J. Bacteriol.* 171: 3504–3510.
97. Stewart, P.S., Murga, R., Srinivasan, R., and de Beer, D. 1995. Biofilm structural heterogeneity visualized by three microscopic methods. *Water Res.* 29: 2006–2009.
98. Allison, D.G. and Sutherland, I.W. 1984. A staining technique for attached bacteria and its correlation to extracellular carbohydrates production. *J. Microbiol. Meth.* 2: 93–99.
99. Michael, T. and Smith, C.M. 1995. Lectins probe molecular films in biofouling: characterization of early films on non-living and living surfaces. *Mar. Ecol. Prog. Ser.* 119(1–3): 229–236.
100. Lawrence, J.R., Neu, T.R., and Swerhone, G.D.W. 1998. Application of multiple parameter imaging for the quantification of algal, bacterial and exopolymer components of microbial biofilms. *J. Microbl. Meth.* 32: 253–261.
101. Wolfaardt, G.M., Lawrence, J.R., Robarts, R.D., and Caldwell, D.E. 1998. In situ characterization of biofilm exopolymers involved in the accumulation of chlorinated organics. *Microbial Ecol.* 35: 213–223.
102. Johnsen, A.R., Hausner, M., Schnell, A., and Wuertz, S. 2000. Evaluation of fluorescently labeled lectins for noninvasive localization of extracellular polymeric substances in *Sphingomonas* biofilms. *Appl. Environ. Microbiol.* 66(8): 3487–3491.
103. Sharon, N. and Lis, H. 1989. *Lectins*. Chapman and Hall, New York, pp. 1–127.
104. Neu, T.R. and Marshall, K.C. 1991. Microbial 'footprints' — A new approach to adhesive polymers. *Biofouling* 3: 101–112.
105. Morgan, J.W., Forster, C.F., and Evison, L. 1900. A comparative study of the nature of biopolymers extracted from anaerobic and activated sludges. *Water Res.* 24: 743–50.
106. Liao, B., Allen, D.G., Droppo, I.G., Leppard, G.G., and Liss, S.N. 2001. Surface properties of activated sludge and their role in bioflocculation and settling. *Water Res.* 35: 339–350.
107. Mikkelsen, L.H. 2003. Applications and limitations of the colloid titration method for measuring activated sludge surface charges. *Water Res.* 37: 2458–2466.
108. Rosenberg, M., Gutnick, D., and Rosenberg, E. 1980. Adherence of bacteria to hydrocarbons: A simple method for measuring cell surface hydrophobicity. *FEMS Microbiol. Lett.* 9: 29–33.

109. Rosenberg, M. and Doyle, R.J. 1990. Microbial cell surface hydrophobicity: history, measurement and significance in *Microbial Cell Surface Hydrophobicity*, R.J. Doyle and M. Rosenberg (ed.). Chapter 1, American Society for Microbiology, Washington, D.C., pp. 1–29.
110. Duncan-Hewitt, W.C., Policova, Z., Cheng, P., Vargha-Butler, E.I., and Neumann, A.W. 1989. Semiautomatic measurement of contact angles on cell layers by a modified axisymmetric drop shape analysis. *Colloids Surf.* 42: 391–403.
111. Neumann, A.W., Li, D., Spelt, G., and Cheng, P. 1996. *Applied Surface Thermodynamics*. Marcel Dekker, Inc. New York.
112. Lindahl, M., Fairs, A., Wadstrom, T., and Hjerten, S. 1981. A new test based on "salting out" to measure relative surface hydrophobicity of bacterial cells. *Biochem. Biophys. Acta.* 677: 471–476.
113. Rozgoni, F., Szitha, K.R., Ljungh, A., Baloda, S.B., Hjerten, F., and Wadstrom, T. 1985. Improvement of the salt aggregation test to study bacterial cell-surface hydrophobicity. *FEMS Microbiol. Lett.* 30: 131–138.
114. Urbain, V., Block, J.C., and Manem, J. 1993. Bioflocculation in activated sludge: An analytic approach. *Water Res.* 27(5): 829–838.
115. Wagner, M., Amann, R., Lemmer, H., and Schleifer, K. 1993. Probing activated sludge with oligonucleotides specific for proteobacteria: Inadequacy of culture-dependent methods for describing microbial community structures. *Appl. Environ. Microbiol.* 59: 1520–1525.
116. Wagner, M., Amann, R., Kampfer, P., Assmus, B., Hartmann, A., Hutzler, P., Springer, N., and Schleifer, K. 1994a. Identification and in situ detection of Gram-negative filamentous bacteria in activated sludge. *Syst. Appl. Microbiol.* 17: 405–417.
117. Wagner, M., Erhart, R., Manz, W., Amann, R., Lemmer, H., Wedi, D., and Schleifer, K. 1994b. Development of an rRNA-targeted oligonucleotide probe specific for the genus Acinetobacter and its application for in situ monitoring in activated sludge. *Appl. Environ. Microbiol.* 60: 792–800.
118. Mobarry, B.K., Wagner, M., Urbain, V., Rittman, B., and Stahl, D.A. 1996. Phylogenetic probes for analyzing the abundance and spatial organization of nitrifying bacteria. *Appl. Environ. Microbiol.* 62: 2156–2162.
119. Wagner, M., Rath, G., Koops, H.-P., Flood, J., and Amann, R. 1996. In situ analysis of nitrifying bacteria in sewage treatment plants. *Water Sci. Technol.* 34(1–2): 237–244.
120. Wagner, M., Rath, G., Amann, R., Koops, H., and Schleifer, K. 1995. In situ identification of ammonia-oxidizing bacteria. *Syst. Appl. Microbiol.* 18: 251–264.
121. Wagner, M., Noguera, D.R., Juretschko, S., Rath, G., Koops, H., and Schleifer, K. 1997. Combining fluorescent *in situ* hybridization (FISH) with cultivation and mathematical modelling to study population structure and function of ammonia-oxidizing bacteria in activated sludge in *Proceedings 2nd International Conference on Microorganisms in Activated Sludge and Biofilm Processes*, Berkeley, California, pp. 273–281.
122. Grossart, H.-P. and Simon, M. 1998. Bacterial colonization and microbial decomposition of limnetic organic aggregates (lake snow). *Aquat. Microb. Ecol.* 15: 127–140.
123. Simon, M., Grossart, H.-P., Schweitzer, B., and Ploug, H. 2002. Microbial ecology of organic aggregates in aquatic ecosystems. *Aquat. Microb. Ecol.* 28: 175–211.

124. Victorio, L., Gilbride, K.A., Allen, D.G., and Liss, S.N. 1996. Phenotypic fingerprinting of microbial communities in wastewater treatment systems. *Water Res.* 30: 1077–1086.
125. Brock, T.D. and Brock, M.L. 1966. Autoradiography as a tool in microbial ecology. *Nature* 209: 734–736.
126. Brock, T.D. 1967. Bacterial growth rates in the sea: direct analysis by thymidine autoradiography. *Science* 155: 81–83.
127. Juniper, S.K. 1981. Stimulation of bacterial activity by a deposit feeder in two New Zealand intertidal inlets. *Bull. Mar. Sci.* 3: 691–701.
128. Carman, K.R. 1990. Radioactive labeling of a natural assemblage of marine sedimentary bacteria and microalgae for trophic studies: An autoradiographic study. *Microbial Ecol.* 19: 279–290.
129. Gray, N.D., Howarth, R., Pickup, R.W., Gwyn Jones, J., and Head, I.M. 1999. Substrate uptake by uncultured bacteria from the genus *Achromatium* determined by microautoradiography. *Appl. Environ. Microbiol.* 65: 5100–5106.
130. Lee, N., Nielsen, P., Andreasen, K., Juretschko, S., Nielsen, J., Schleifer, K., and Wagner, M. 1999. Combination of fluorescent in situ hybridization and microautoradiography — a new tool for structure–function analyses in microbial ecology. *Appl. Environ. Microbiol.* 65: 1289–1297.
131. Nielsen, P.H., Andreasen, K., Lee, N., and Wagner, M. 1999. Use of microautoradiography and fluorescent *in situ* hybridization for characterization of microbial activity in activated sludge. *Water Sci. Technol.* 39: 1–9.
132. Nielsen, P.H., Andreasen, K., Lee, N., Wagner, M., Blackall, L.L., Lemmer, H., and Seviour, R.J. 1998. Variability of Type 021N in activated sludge as determined by in situ substrate uptake pattern and in situ hybridization with fluorescent rRNA targeted probes. *Water Sci. Technol.* 37: 423–430.
133. Andreasen, K. and Nielsen, P.H. 2000. Growth of *Microthrix parvicella* in nutrient removal activated sludge plants: studies of *in situ* physiology. *Water Res.* 34: 1559–1569.
134. Ouverney, C.C. and Fuhrman, J.A. 1999. Combined microautoradiography-16S rRNA probe technique for determination of radioisotope uptake by specific microbial cell types *in situ*. *Appl. Environ. Microbiol.* 65: 1746–1752.
135. Thomsen, T.R., Kjellerup, B.V., Nielsen, J.L., Hugenholtz, P., and Nielsen, P.H. 2002. *In situ* studies of the phylogeny and physiology of filamentous bacteria with attached growth. *Environ. Microbiol.* 4(7): 383–391.
136. Zarda, B., Hahn, D., Chatzinotas, A., Schonhuber, W., Neef, A., Amann, R., and Zeyer, J. 1997. Analysis of bacterial community structure in bulk soil by *in situ* hybridization. *Arch. Microbiol.* 168: 185–192.
137. Davenport, R.J., Curtis, T.P., Goodfellow, M., Stainsby, F.M., and Bingley, M. 2000. Quantitative use of fluorescent *in situ* hybridization to examine relationships between mycolic acid-containing Actinomycetes and foaming in activated sludge plants. *Appl. Environ. Microbiol.* 66: 1158–1166.

I

Freshwater Environments

2 Overview of Flocculation Processes in Freshwater Ecosystems

Gary G. Leppard and Ian G. Droppo

CONTENTS

2.1 INTRODUCTION

Globally, freshwater represents only 2.5% of the world's water resources.[1] Water, particularly freshwater, is the most essential and significant component for sustaining human life and many other aspects of global survival. Globally, the integrity of freshwater is jeopardized by contaminant and particulate inputs from soil erosion, atmospheric deposition, and anthropogenic point and nonpoint sources of pollution. With clean drinking water one of the most significant issues impacting mankind,[1] a better understanding of its particulate component, the component carrying the majority of contaminants, is critical for freshwater sustainable development.

Flocculation is a universal process occurring within aquatic ecosystems that incorporate both inorganic and organic cohesive particles. Certainly the freshwater systems, consisting primarily of rivers and lakes (although other systems such as urban sewer systems and stormwater detention ponds also have been studied[2]), are dominated by cohesive sediments from a variety of sources and with a variety of compositions.

1-56670-615-7/05/$0.00+$1.50

While some river loads such as that for the Mississippi will be dominated by sand transport, flocculation of the cohesive fraction will play an equally important role in moderating contaminant transport.[3] Within the majority of cohesive sediment transport rivers, flocculated particles are consistently shown to represent greater than 80% of the total volume of sediment in transport.[4,5] This fact has been dismissed within many engineering and scientific applications of the past. In fact, coastal and estuarine models and researchers often treated the river inputs to the marine system as unflocculated, and only when mixed with saltwater was flocculation believed to be significant (due to electrochemical effects). Over the last few decades though, there has been enlightenment as to the importance of flocculation in the freshwater system. For example, freshwater flocs are shown to be an integral component of interstitial pores within gravel bed rivers, with concomitant effects on salmonid egg survival.[6,7] Urban engineering projects such as storm, sanitary and combined sewer systems, stormwater detention ponds, inline detention basins, artificial marsh lands, and other products of best management practices are taking into account the influence that flocculation has on the controls of sediment and contaminant transport.[2] Models of urban environments, however, lag behind those of the natural water systems, owing largely to the purely engineering approach to system design. Flocculated particles have also been given greater consideration as to their impact on the transport of contaminants.[8–14] A tangible impact of flocculation is its effect on reservoir infilling by significantly increasing the deposition rate of sediments. Flocculation's impact on reservoir infilling, fisheries, habitat destruction, and contaminant transport have resulted in significant financial burdens for remediation and restoration projects. All of the above examples are related to the important relationship of floc structure to floc behavior. Specifically, floc form or structure will impact floc physical (transport), chemical (uptake/transformation), and biological (biocommunity dynamics) behavior within the floc itself or within a given system as a whole.[9,14–22]

This chapter provides an overview of freshwater flocculation, and the nature of the resultant flocs, with subsequent chapters addressing studies which have investigated many of the above issues as they relate to flocculation. While our focus is on freshwater, other studies/methods from the engineering and marine fields are discussed in this chapter when they are applicable to freshwater.

2.2 DEFINITION OF FRESHWATER FLOCS

Flocculation is an aggregation process (or processes) leading to the formation of larger particles from smaller particles suspended within a natural or engineered water.[23] The process usually involves some form of physical or chemical destabilization, and a step in which particles collide.[23,24] For aquatic scientists, flocculation is sometimes equated with "aggregation due to polymers," whereas "aggregation due to electrolytes" is often called coagulation.[25] For our purposes, both processes can be treated as similar in mechanism.[23,26] From the action of either aggregation process, or from both operating together, the resultant sedimenting particle is a floc.[17]

The aggregating particles in the bulk water will be heterogeneous and composed of dissolved, colloidal, and particulate materials of varying size and composition[27]

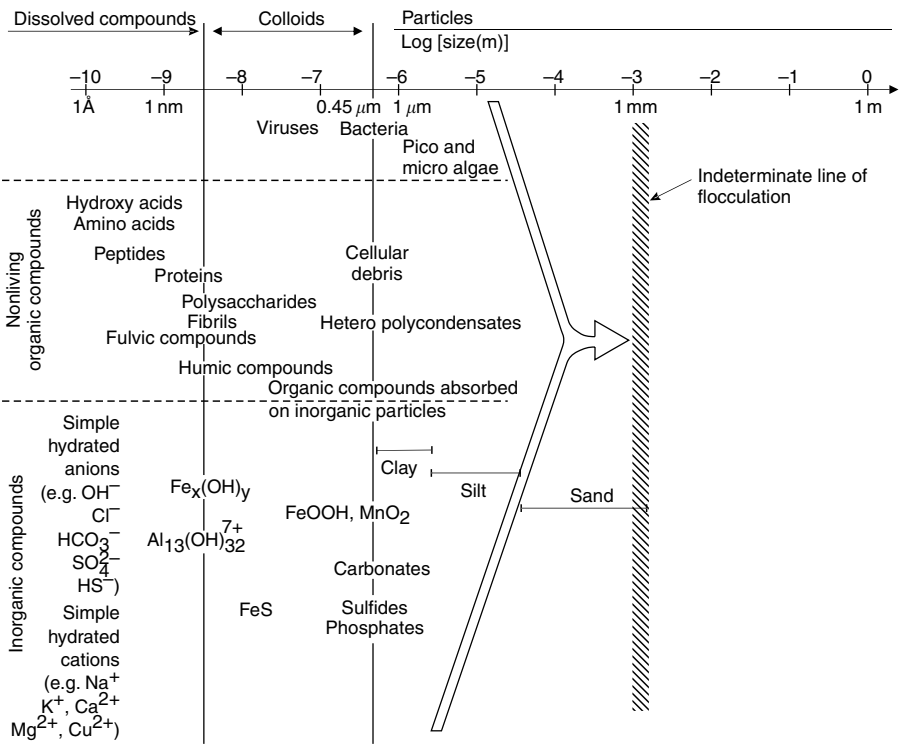

FIGURE 2.1 Schematic classification of what environmental science generally considers as dissolved, colloidal, and particulate materials as defined by size and organic and inorganic components. All of the components to the left of the flocculation wedge can be incorporated into flocculated or aggregated particles with a subsequent increase in effective size. No upper size range for floc size can be determined as it is dependent on a number of physical, chemical, and biological factors, although marine snow has been observed in the order of centimeters. (Reproduced with permission from Droppo (2000).)

(Figure 2.1). A proportion of these particles will be of an organic (living and nonliving) and inorganic nature. All of the components to the left of the flocculation wedge in Figure 2.1 can be incorporated into flocculated or aggregated particles with a subsequent increase in effective size. While the dissolved ionic component of Figure 2.1 may not be considered true particles, they can still influence flocculation through precipitation on and complexation with other components of the floc. Note, however, that there is no static upper size range for floc size as it is dependent on a number of physical, chemical, and biological factors.[3]

A freshwater floc is defined here as a suspended particulate (in the micrometer to multi-millimeter range) which is (a) derived by freshwater aggregation processes and (b) typically rich in subcomponents whose least dimensions can span the entire colloidal size range and above. Subcomponents (Figure 2.2) include bacteria and other small organisms, extracellular polymeric substances (EPS), aggregated humic

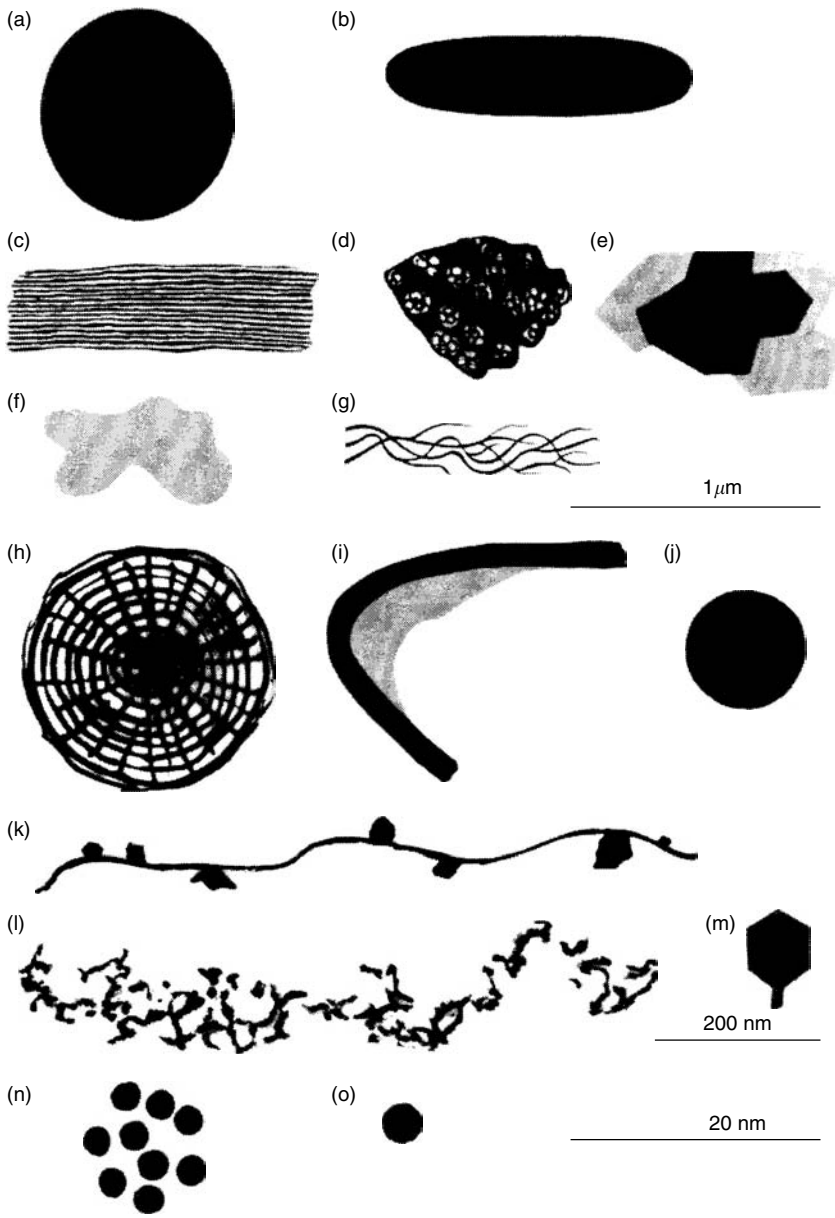

FIGURE 2.2 The shape and dimensions of some common aquatic colloids: (a) submicrometer eukaryote cell, an alga; (b) prokaryote cell, a Gram-negative bacterium; (c) microfibrillar cell wall fragment from higher plant or alga; (d) frustule fragment from the mineral cell wall of a diatom alga; (e) a clay mineral; (f) amorphous organic debris; (g) mucilaginous aggregate of fibrils; (h) discarded scale from the surface of an alga; (i) refractory wall fragment from Gram-negative bacterium; (j) amorphous iron oxyhydroxyphosphate; (k) individual fibril with associated small colloids; (l) fractal aggregate of humic substance; (m) marine virus; (n) fulvic acid aggregate; and (o) extracellular enzyme. (Reproduced with permission from Leppard and Buffle (1998).)

substances, clay minerals, colloidal iron and manganese oxyhydroxides, biogenic silicates, bacterial envelope fragments, algal cell wall fragments, algal scales, viruses, identifiable cell lysis products, and both mineral and organic nanoscale coatings.[28,29] The EPS is frequently packaged by microbiota into nanoscale fibrils,[15,30] which cross-connect the various floc subcomponents, and which can be oriented in three dimensions by bacterial secretion processes to establish intra-floc pores, and also densely packed microzones which may represent a structural basis for diffusional gradients.[3,16,17,21]

A paradoxical description of a floc, which focuses on the structural and behavioral characteristics, was provided by Droppo et al.[17] It was paradoxical relative to a much earlier concept of the floc as a "black box." From recent multidisciplinary work, a floc can now be defined as "an individual microecosystem, composed of a matrix of water, inorganic and organic colloidal particles with autonomous and interactive physical, chemical, and biological functions or behaviors operating within the floc matrix."[17] The rationale for this definition and the relationships among architecture, biology, chemistry, behavior, and environmental activities are outlined in Droppo[3] and elaborated in the following sections.

2.3 TYPES OF FRESHWATER FLOCS

Flocs in freshwater ecosystems are fundamentally no different from those in saltwater (Section II) or engineered (Section III) ecosystems, although saltwater flocs are sometimes exceptionally large.[22,31] At first this similarity may seem nonsensical, given the extreme differences in overlying conditions and industrial manipulations. However, if one examines flocs from these environments they are all composed of inorganic particles, organic (living and nonliving) particles (Figure 2.2), and water. The difference lies in the relative proportions and specific composition of individual entities comprising these general base components. In addition, it is evident that the factors influencing flocculation will remain the same regardless of environment, only the relative importance of each will vary as defined by site specific conditions. It is these relative compositional and mechanistic differences which will give the floc population its site specific distinctive characteristics. As such, while extreme examples within this generalized view of flocs have been defined in the literature (biota-rich flocs,[10,16,17] mineral-rich flocs,[32] and aggregated humic substances[33–35]) their common link is that they all have an inorganic and organic (living and nonliving) component and water as constituents, although in some instances a single component may be dominant.

Within freshwater systems, flocs can be classified into four categories based on their location of origin: (a) formed within the water column, (b) eroded from the bed, (c) derived from the terrestrial environment and washed into the system by overland or subsurface flow (and usually referred to as "aggregates"), and (d) decaying organic matter (e.g., from plants). This chapter focuses primarily on the first classification of flocs. While these categories of flocs are known because of our understanding of soils, microbiology, hydraulics, and flocculation theory, they, at this point in time, cannot be differentiated within a single sample.[36] The lack of differentiation reflects a lack of existing methods to discriminate these forms, as the majority of sediment analysis instruments are indirect and nondiscriminative (e.g., laser particle sizers).

Flocs formed in the water column via various physical, chemical, and biological means, as discussed in this chapter, will generally appear as open matrix, low density, high water content particles which may be more fragile than those derived from the other three categories.[36] Flocs derived from bed sediment erosion are generally more compact but with a larger organic fraction due to biofilm growth providing for a low density. The compaction is a result of self weighted consolidation processes and biostabilization.[37] The significant biological component provides the floc with strength due to the sticky nature of the material. These particles will often have denser areas within them that may represent water stable soil "aggregates" that have settled quickly to the bed. Such particles can be referred to as hybrid particles (i.e., a particle composed of both floc and aggregate components). Flocs derived from soil surfaces are typically not truly flocs but rather aggregates formed through soil processes. Nonetheless, these particles are similar in structure, containing similar constituent particles, and once within the water, are quickly colonized by aquatic bacteria. These particles are compact and dense with settling velocities one to two orders of magnitude higher than flocs formed directly in a water body.[36]

Freshwater flocs derived from the microbial decomposition of suspended plant, algal, and zooplankton debris are receiving renewed attention as a result of an accelerating interest in aquatic microbial ecology.[22,38] The focus of many recent studies has been on bacterial colonization, bacterial/algal interactions, decomposition phenomena, the cycling of nutrients and elements of biogeochemical interest, and the flux of energy in aquatic ecosystems. Some of this research reveals the fact that a small chunk of decomposing debris takes on the aspect of a microbiota-rich floc, as the debris per se becomes increasingly consumed during its conversion to microbial biomass and associated EPS. In fact, Grossart and Simon[38] point out similarities between such biota-rich flocs and activated sludge flocs in sewage treatment plants. The association of microbiota and suspended debris during the decomposition process is sometimes called a macroscopic organic "aggregate," not to be confused with the soil "aggregate" (described earlier in the chapter) or the submicrometer-scale "aggregate" of nanoscale colloids to be described in the following sections.

In the authors' examination of thousands of floc images from multiple freshwater environments (rivers, lakes, storm waters, and combined sewer systems)[5,13,16,17,39,40] and also of those in the literature,[6,11,41–43] very rarely are flocs seen in excess of 500 μm, with the majority of flocs below 100 μm. As with all environments, the size of freshwater flocs will be dictated by local shear conditions and developmental factors described in Figure 2.3 to Figure 2.7 below. On average, Droppo[44] demonstrated that the general size of flocs relative to environment is as follows: combined sewers $>$ lakes $>$ rivers. This relative difference is related to organic concentrations being highest in the sewer systems and shear being the strongest in river systems.

Density relationships for flocs in freshwater are no different than those in engineered or marine systems. In all cases, as floc size increases the density decreases, approaching that of water. This relationship is related to larger flocs becoming more porous (approaching 100%) due to an increase in contact points and therefore retaining more bound water. As described below, pores in freshwater flocs are generally small,

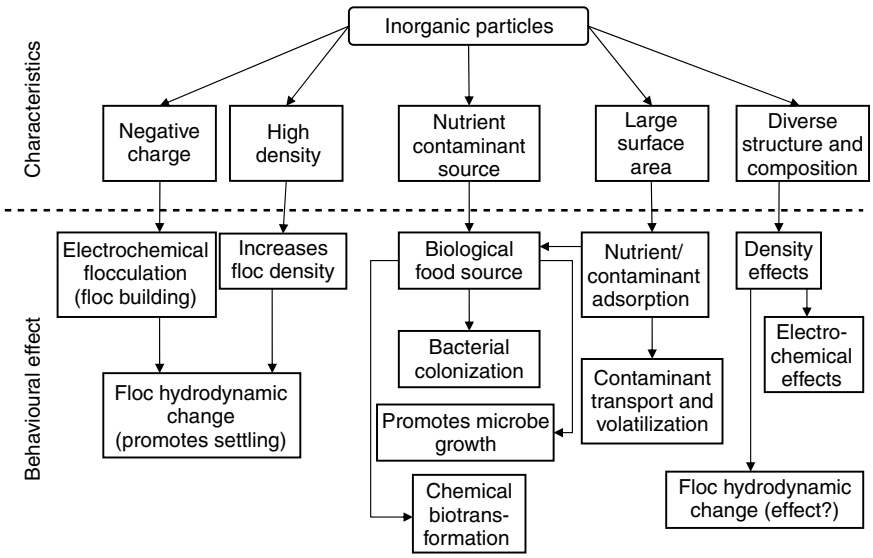

FIGURE 2.3 The characteristics of inorganic particles that will influence the internal and external behavior of flocs. (Adapted from Droppo (2001) and reproduced with permission.)

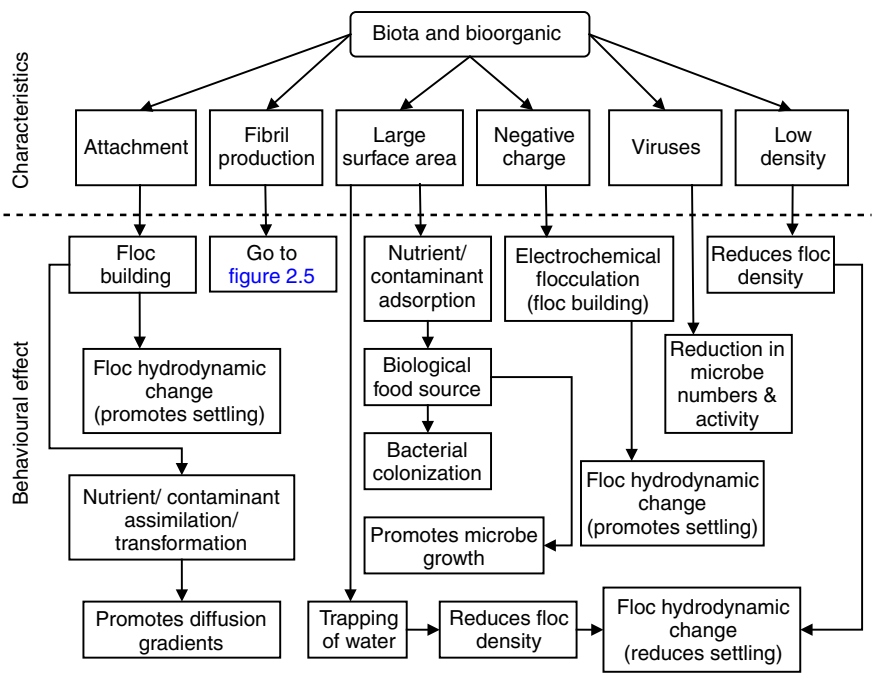

FIGURE 2.4 The characteristics of the microbial community/organic particles that will influence the internal and external behavior of flocs. (Adapted from Droppo (2001) and reproduced with permission.)

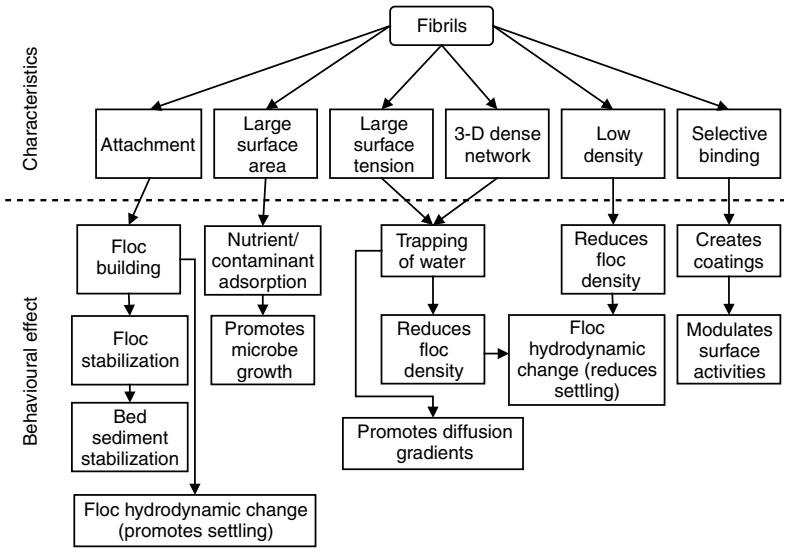

FIGURE 2.5 The characteristics of microbial extracellular polymeric fibrils and their influence on the internal and external behavior of flocs. (Adapted from Droppo (2001) and reproduced with permission.)

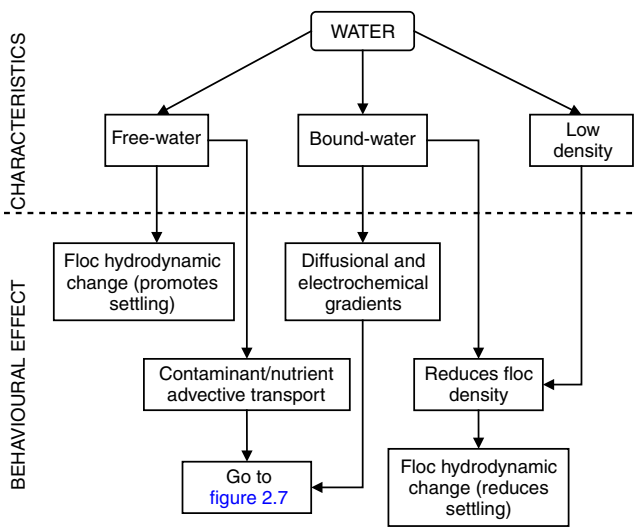

FIGURE 2.6 The characteristics of water within a floc and its influence on the internal and external behavior of flocs. (Adapted from Droppo (2001) and reproduced with permission.)

particularly due to the prominent functional existence of EPS fibrils, and thus they "trap" water rather than allowing convective flow through flocs. This has concomitant effects on diffusion gradients within the floc. A comparison of densities from multiple environments can be found in Droppo[44] and Leppard and Droppo.[40] While data on

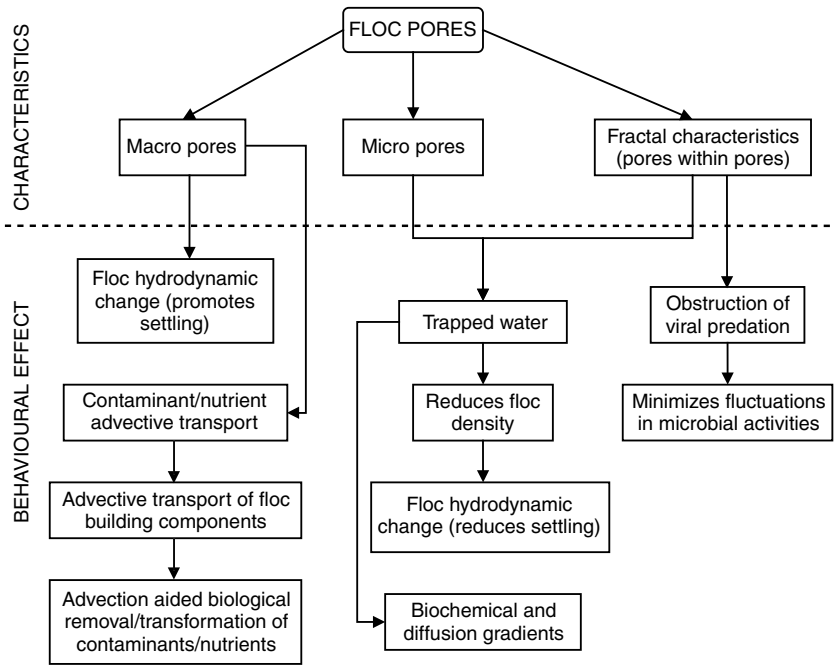

FIGURE 2.7 The characteristics of floc pores and their influence on the internal and external behavior of flocs. (Adapted from Droppo (2001) and reproduced with permission.)

freshwater floc density is limited, the authors have demonstrated that generally the typical range is from 1.01 to 1.3 mg cm^{-3}.

Generally within the literature, researchers have illustrated flocs to comprise three gross scale morphological and compositional forms; they show flocs which are highly enriched in either microbiota or mineral colloids or humic substances. While these characterizations were based on the dominant primary particle within the floc, such characterization is misleading as the freshwater floc is highly heterogeneous in structure and composition (although extreme exceptions do occur such as mineral flocs collected at the snout of glaciers — Woodward et al.[32]). From our experience, freshwater floc types tend to differ in terms of the relative amounts of common colloidal subcomponents; different floc types grade into each other. While the relative importance of each of these components will vary greatly with differing flocs, the processes operating within the floc are the same. Commonly found compounds, materials and life forms within flocs are revealed in Figure 2.1, while specific colloids found within flocs as abundant subcomponents are shown in Figure 2.2. The associations between various colloids typically appear almost random, with little repetitiveness of specific arrangements. Nevertheless, there is order and this order is related to microbial function and to microbial modifications to improve habitat, a fact being increasingly well demonstrated in related researches with biofilms[45–48] and with experimental bacterial populations.[49] As is the case for biofilms, among the spectrum of floc types there may be environmentally significant "machines" for adjusting water quality and modulating biogeochemical processes.

2.4 GROWTH AND STABILITY OF FRESHWATER FLOCS

This section deals only with those flocs undergoing flocculation within the water column as these are the "true" flocs. Growth of a floc may occur (a) through continued aggregation in the bulk water (i.e., through collision processes), (b) through invasion by biota, and (c) by the intra-floc generation of particles by microbes.

Increasingly, the roles of microorganisms and their secretions are coming under intensive scrutiny, in efforts to understand floc growth and potential manipulation of growth and behavior.[3,14–16,18,20,21,50] Mechanisms of floc formation, the interfacial forces involved, and the effects of physiological factors have been reviewed recently by Liss,[21] who emphasizes the importance of surface properties in floc interactions. Important interfacial forces considered by Liss[21] are: van der Waals; electrostatic double-layer; hydrophobic/hydrophilic; and steric.

There is increasing interest in the role(s) played by transparent exopolymer particles (TEP) in freshwater ecosystems; in essence, they "glue" small flocs together to yield large flocs. TEP, initially described by Alldredge et al.[51] in a marine ecosystem, are loosely defined as (abundant) suspended particles formed from the polysaccharides secreted by bacteria and phytoplankton; individual particles are a sticky mixed material which promotes aggregation, and are difficult to detect in water with simple lenses. Grossart et al.,[18] working at a site in Lake Constance (Germany) suggest that TEP may be of major importance for the formation of flocs in lakes, as they are known to be in marine waters where TEP has EPS fibrils as a major component.[52] Relative abundances of freshwater and marine flocs in different ecosystems, in relation to TEP as an aquatic adhesive, are shown in Simon et al.[22]

The aggregation of nanoscale particles in rivers (Rhine River, western Europe) and lakes (Lake Bret, Switzerland) has been investigated for almost two decades,[29] with the nanoscale formally referring to particle diameters of 1 to 100 nm.[53] Regarding nanoscale aggregation in bulk water, a generalized description of aquatic colloidal interactions has been published by Buffle et al.[54] for major classes of colloids. They concluded that aggregation is dominated by three classes of colloids: these are (a) compact inorganic colloids, (b) large rigid biopolymers, and (c) fulvic compounds, with fulvic compounds acting to stabilize the inorganic colloids and rigid biopolymers acting to destabilize them. Buffle et al.[54] state that the concentration of stable colloids in a given aquatic ecosystem will depend on the relative proportions of the three general classes of colloids. Factors controlling the stability of colloids in natural waters, with a focus on nanoscale particles, are assessed in Filella and Buffle.[55]

In aggregation studies, the term "stability" is not used in the thermodynamic sense; a stable aggregate is one which is slow in changing its state of dispersion during an observation period. The common modes of destabilization and their characteristics have been known and documented for decades.[26,56] Current studies of floc stability and integrity focus on the effects of various natural organic substances,[57] on interparticle interactions,[20] on the composition of the extracellular polymeric substances,[21,58] on microbial associations,[58] and on freshwater physical processes.[5,6,41,50] Recent research on engineered systems, applicable to freshwater

flocs, indicates that floc/floc interactions may be dominated by the specific nature of the EPS present at the floc/water interface, as opposed to the overall composition (core plus peripheral layer) of the EPS in a floc.[20]

While particles are diverse, the colloidal particles are believed to dominate the aggregation process. A colloid is defined operationally as any particle with a least dimension in the range of 1.0 to 0.001 μm,[26] a range which includes macromolecules.[29] The significance of this size range of ultradivided matter is that the individual suspended particles can be adhesive in natural waters. Such colloidal suspensions differ fundamentally from true solutions; colloidal particles are unstable because of large interfacial energies, and the particle–particle interactions are stronger than kT.

There is a growing and valuable school of thought[59] which seeks to redefine an aquatic colloid, for environmental science purposes, as any particle that provides a molecular milieu into and onto which chemicals can escape from aqueous solution, and whose movement is not significantly affected by gravitational settling. In this context, it has long been known that aquatic colloids can carry significant burdens of contaminants and nutrients; in this burdened condition, they can aggregate to form subsequent settling particles which are capable of burying the associated contaminants and nutrients.[60] Thus, a capture of contaminants by suspended colloids, prior to and during the incorporation of those colloids into sedimenting flocs, can be a linked process leading to water column decontamination. Honeyman and Santschi[61] take this concept one step further by providing evidence that colloid-associated elements are likely to have a behavior markedly different from the dissolved version and versions associated with suspended "true" particles. Their studies of "colloidal pumping" suggest that sorption of chemicals onto colloids may be coupled directly to the role of flocculation in regulating the fate of trace metals in aquatic ecosystems.

2.5 RELEVANT INFORMATION FROM MICROFLOCS

In addition to TEP and to conventional flocs, there exist discrete freshwater microflocs consisting of aggregated nanoparticles, which are likely to contribute to the growth of conventional flocs. Recently, Kerner et al.[62] described the self-organization of dissolved organic matter (DOM) into micelle-like microparticles (0.4 to 0.8 μm) in river water (Elbe River, Germany). This abiotic transfer of dissolved organic carbon to microparticles has great ecological significance because it occurs without carbon loss, while depending only on temperature and the aggregation capacity of the DOM molecules involved. For the characterization of DOM molecules, the analytical chemical technology continues to evolve well.[63]

In earlier work on heterogeneous microparticles in river water samples (Rhine River, near Basle, Switzerland), Filella et al.[64] demonstrated the capture of nanoscale mineral particles at the surfaces of suspended meshworks of long organic fibrils whose diameters were in the lowest part of the nanoscale range. This discovery led to a focus on colloidal organic fibrils[30] as bridging structures and as accumulators of nanoscale mineral coatings; these flocculation events provided an impetus for the development of analytical electron microscopy (AEM) for addressing the need

to characterize the nanoscale components of microflocs initially,[65–67] and then of large flocs.[14] The research on microfloc nanocomponents and their biogeochemical roles were done in the following natural ecosystems: Lake Lugano, Switzerland;[66] Paul Lake, MI, USA;[66,67] and the peatlands of the Bied River, Switzerland.[65,66] The research thrust on fibril/mineral colloid aggregation accompanied an earlier, ongoing, microbiology-based thrust which focused on biomineralization initiated at the nanoscale on biological surfaces.[68] Such nanoscale studies have great relevance to the transformations of metals within flocs[10] and within consolidated sediments.[69]

2.6 THE ARCHITECTURE OF FRESHWATER FLOCS

Floc architecture is a major determinant of floc activities and behavior; it can evolve in complexity under the influence of biological activity, leading to the development of specific features which enhance microbial habitat while conferring environmentally relevant activities and behavior to a floc.[3] The capacity to analyze floc architecture by microscopical means is evolving quickly,[14,16,17,39,58,70] with the microscopical observations being increasingly well integrated into an interdisciplinary context.[14,20,21,40] Sample sites for the analysis of floc architecture have included five in Ontario, Canada (Hamilton Harbour, Port Stanley Harbour, Nith River, Sixteen-Mile Creek, and Fourteen-Mile Creek) and the Elbe River in Germany. Current emphasis is placed on relationships between floc architecture and the (a) activities of microbes and (b) surface-active nanoscale subcomponents, the (c) composition and (d) three-dimensional (3D) distribution of the various EPS and the (e) behavior of flocs with regard to the transport of environmentally significant materials. With regard to the 3D distribution of the various families of EPS molecules, there is great interest in EPS contributions to the following: pore structures; barriers which establish chemical gradients; barriers which obstruct viral predators; and transposable layers which can adjust the stickiness at the floc/water interface.

2.6.1 Architecture in Relation to Floc Activities, Properties, and Behavior

In order to understand better the relevance of floc architecture in terms of the floc physical, chemical, and biological behavior, Droppo[3] developed a conceptual model of floc form and behavior. The model breaks the floc down into five subcomponents: (a) inorganic particles, (b) biota and bioorganic particles, (c) fibrils, (d) water, and (e) pores. Each of these components is then further subdivided into specific physical characteristics. The associated physical (e.g., transport/settling), chemical (e.g., chemical assimilation/transformation), and biological (e.g., microbial community development) behaviors are then broken out in relation to each of these characteristics (Figure 2.3 to Figure 2.7). While in reality one cannot segregate specific components of a floc and their behaviors (they all work together to influence floc development, structure, and behavior), this modeling approach allows for insight into the significance of the micro- and macro-architecture on outward floc behavior.

In the model[3] the inorganic component (Figure 2.3) may represent mineral particles (silt and clay) or structural chemical precipitates which exhibit characteristic electrochemical double layers and are influenced by van der Waals forces.[71] Conceptually, inorganic particles will most significantly influence the physical transport of a flocculated particle due to their density effects (they increase floc density and relative settling velocity) and potential for electrochemical flocculation. In addition, however, they also will influence the floc's chemical behavior by affecting the adsorption and transformation of contaminants and nutrients,[72,73] and their biological behavior in terms of their ability to act as sites for bacterial colonization and subsequent chemical and biological activity.[3,4,16]

The biological component (Figure 2.4) is the most dynamic component of a floc as it can influence not only floc development and therefore transport through mediation of electrochemical flocculation, floc density, bacterial attachment, and EPS production (Figure 2.5), but will also have an impact on the chemical, physicochemical, and biological processes operating within the floc through diffusional gradients and biotransformation of nutrients and contaminants.[3,16,74–76]

There is increasing evidence that the most important component influencing floc behavior is the EPS fibril produced by bacteria (and by some microalgae). Figure 2.5 illustrates the important characteristics of this material and its influence on behavior. Examination of the three-dimensional matrix of EPS within freshwater flocs reveals that it truly represents a framework for the floc. Fibrils are completely integrated within the floc, forming physical and chemical links to adjacent constituent particles. This network strengthens flocs and binds flocs together, giving them a pseudo-plastic rheology.[3,15–17,30,77] In addition, the EPS network influences the floc transport behavior through modifying floc density primarily by promoting the retention of water within the floc. This retention is related to the significant surface area of the fibrils, promoting micropores with significant surface tension. The large surface area of the fibrils and retention of pore water also affect the floc's chemical behavior by influencing the uptake of nutrients and contaminants and promoting diffusional and electrochemical gradients for parameters such as contaminants, pH, and redox potential.[3,14,16,40,78]

Both free flowing and bound water will impact a floc's structure and behavior (Figure 2.6). The free movement of water within a floc can enhance the removal of contaminants and nutrients from water by bacterial actions and general adsorption because of the advective delivery of compounds.[79] Movement of water through a floc can also increase its settling velocity due to a reduction in drag around the floc.[80] Bound water on the other hand will promote molecular diffusion and electrochemical gradients of contaminants[16,78] and will reduce settling velocity due to its impact on reducing floc density. The greater the water content the closer the overall floc's density will be to that of water. Droppo et al.[17] showed that most riverine flocs over 300 μm had densities close to that of water. As such, water retained within a floc matrix will have significant hydrodynamic influences on floc behavior.

As is evident from the above discussion, floc pores as defined by the interparticle and interfibril voids play a significant role in influencing floc structure and behavior (Figure 2.7). Pores, which appear to be devoid of physical structures when imaged by optical microscope techniques, are sometimes observed to be composed of complex

matrices of nanoscale fibrillar EPS when imaged by the much higher resolution of transmission electron microscopy.[16] Pores are responsible for much of the floc physical, chemical, and biological behavior as they control water content and movement within the floc proper. As a result and as discussed above, pores will influence floc density, transport and chemical and biological activities, and diffusional and electrochemical gradients.[79–81] Figure 2.7 provides the resultant behavioral effects of pores.

The pore structure of flocs could very well have a profound effect on predation of the microbiota by viruses, with consequent effects on the population density and speciation of microbiota. Viruses in the nanoscale size range have a high abundance in aquatic environments;[82,83] their abundance is sufficient to make them major predators in many microbial niches. Since the rate of lytic infection depends on the rate of virus adsorption to its host,[84] the pore structure of a floc may serve to prevent predation by keeping an effective separation distance between virus and microbe. Using transmission electron microscopy, applied to ultrathin sections of flocs, the authors are currently accumulating evidence that viruses may be unable to penetrate into regions of a floc where the packing of fibrils yields a pore structure in the lower part of the nanoscale range.

2.6.2 Relevant Findings for Floc Architecture from the Biofilm Literature

In terms of architecture, biota-rich flocs often resemble biofilms which had been stripped from their substratum and turned back on themselves.[16] This is true even when one considers the complex model of biofilm architecture introduced by de Beer et al.[45] to relate specific aspects of structure to oxygen distribution and mass transport. Diffusion in a biofilm is hindered relative to diffusion in the nearby bulk solution[85] while oxygen distribution can be strongly correlated to structure, being facilitated by voids as it is delivered from the bulk water to microbial cell clusters.[45] Interest in relating specific entities of biofilm structure to molecular composition, activities, and physiological phenomena[86] has been strong and some resultant case histories are worthy of note for floc specialists.

Because biofilms are attached to a solid substratum, many investigations of biofilm structure/function relationships are technically less complicated than the same work would be for flocs, whose overall morphology becomes distorted when they fall out of suspension onto a rigid surface. This situation has been addressed by the floc stabilization technique of Droppo et al.,[39] thus making available an improved capacity to extend to flocs some investigations formerly confined to biofilms.

Consider the following case study of a biofilm and the utility of relating it directly to the transport and transformation activities of flocs. Microbial exopolymers (EPS) were demonstrated to provide a mechanism for the bioaccumulation of the herbicide, diclofop methyl.[87] This study used confocal laser scanning microscopy (CLSM) to directly visualize accumulation of the herbicide and its breakdown products within a biofilm community. Correlated mass spectroscopic analysis confirmed the accumulation of the herbicide and its breakdown products within the biofilm. The diclofop-degrading biofilm developed distinctive spatial relationships among diverse members of its microbial community, implying that unique consortial relationships facilitated diclofop degradation by cooperative interactions.[88]

Subsequent physiological experiments demonstrated that the EPS could act as a storage site for the herbicide, prior to its degradation.[89] These results led to analyses of the three-dimensional distributions of biofilm exopolymers involved in the accumulation of chlorinated organics, using fluorescent probes in conjunction with CLSM.[90] Using fluorescent lectins,[91] a nearly 1:1 correspondence could be demonstrated between the distribution of regions that accumulated diclofop and regions which bound a lectin which is specific for an EPS polymer containing α-L-fucose.[90]

This highly evolved case study shows for biofilms what is almost certainly to be evidenced soon for flocs. The matrix material (EPS) binds a chemical of environmental interest, leading to bioaccumulation followed by metabolically directed degradation of the chemical. The microbial consortia develop distinct spatial relationships to promote cooperative interactions among diverse members of the microbial community, in relation to what they sense as either food or toxicant. The biological activity restructures the overall architecture to improve adaptation to stimuli coming from the bulk water. Some of the restructuring consists of the secretion of specific EPS molecules which facilitate the interactions between microbes and an incoming chemical. Given the similarities between biofilm and floc architecture (and the ability of their constituent microbes to adjust that architecture to gain ecological advantage), improved technology should soon permit the kinds of biofilm research done by Wolfaardt et al.[87–90] to be done also on flocs.

2.7 APPLICABLE NEW TECHNOLOGIES

Scanning transmission x-ray microscopy (STXM) is a promising new technology for the analysis of flocs and biofilms, as shown by recent progress in mapping the three-dimensional disposition of diverse exopolymeric matrix materials in a biofilm[92] developed from water of the South Saskatchewan River (Canada). STXM represents a new frontier in the use of synchrotron radiation to characterize heterogeneous aggregated materials, yielding nanoscale structural resolution accompanied by data on the atomic environment of selected elements within a preselected colloid. It exploits the fact that soft x-rays interact with almost all elements to allow mapping of chemical species based on bonding structure. With STXM analysis, there is a potential to follow the evolution of biofilm and floc architecture over time, while relating the chemical transformations of specific toxic metals to the specific colloids involved in the transformations. Such research has already begun on freshwater flocs using x-ray absorption spectroscopy (XAS), a precursor of STXM, in combination with electron microscope-based, energy-dispersive spectroscopy. Gaillard et al.[93] showed for Lake DePue (a lake contaminated by zinc in Illinois, United States) that, close to the contaminant source, zinc is bound to relatively labile phosphate and carbonate ligands associated spatially with aggregated microbiota. Far from the source, however, the zinc is predominantly coordinated with sulfides.

Atomic force microscopy (AFM) is a promising new tool for measuring the interaction forces between one colloid and another, and also between a colloid and a surface.[94] AFM is applicable to the analysis of colloids found in flocs,[95,96] as is the related technique of biological force microscopy, or BFM.[97] Camesano and Logan[95] used AFM to probe the effects of pH, ionic strength, and the presence of bacterial

surface polymers on interaction forces between individual bacteria and silicon nitride surfaces, finding that the bacterial surface polymers dominated interactions between bacteria and AFM silicon nitride tips. Continuation of this work could provide insight into specific roles for individual kinds of EPS molecules. Currently, Muirhead and Lead[98] are using AFM to measure the size and nanostructure of natural aquatic colloids in river waters, including humic substances and fibrillar EPS of probable microbial origin.

Environmental genomics is a genetics-based, interdisciplinary field of research that seeks to understand external factors affecting organisms when they are exposed to environmental stresses, such as contaminants and pathogens. Host responses to these stresses include changes in gene expression and genetic products, changes that culminate with alterations in host phenotype. Applications to floc research are imminent, including the development of labeled probes which will identify which microbe is which in a floc or biofilm. In fact, at the level of light microscopy, this can now be done quite well for the direct identification of individual microbes in mixed communities using FISH, or fluorescence *in situ* hybridization, with rRNA-targeted nucleic acid probes.[99]

2.8 CONCLUSIONS

This chapter has defined flocculation, described its environmental importance, and elaborated in detail on the nature of the resultant flocs. Considerable attention has been focused on the structural characteristics of freshwater flocs, from the colloidal components up to gross scale aspects of an entire floc. The composition and interaction of constituent components have been addressed with a conceptual model used to demonstrate how floc architecture influences floc behavior, physically (e.g., transport), chemically (e.g., contaminant uptake and transformation), and biologically (e.g., microbial community structure and biochemical activities). The growth and evolution of flocs and their stability is shown to be a combination of electrochemical and biological influences, with EPS often dominating in this regard. Consideration is given to the roles of suspended nanoscale and colloidal particles in aggregation processes which yield surface active materials for subsequent microbial colonization and floc formation. Flocs are shown to possess many of the same characteristics and functions as biofilms, with relevant biofilm research reported. Finally, the evolution of new technologies applicable to an improved understanding of flocculation processes is described. We anticipate that technology-driven investigations will reveal further relationships between the three-dimensional disposition of individual entities within a floc and specific important activities attributable to specific associations of floc components.

REFERENCES

1. UNEP, Global Environmental Outlook 3. State of the Environment and Policy Retrospective 1972–2002. Nairobi, Kenya: UNEP, 2002.
2. Droppo, I.G., Irvine, K.N., and Jaskot, C., Flocculation of cohesive sediments in the urban continuum: Implications for stormwater management, *Environ. Tech.*, 23, 27, 2002.

3. Droppo, I.G., Rethinking what constitutes suspended sediment, *Hydrol. Process.*, 15, 1551, 2001.
4. Droppo, I.G. and Ongley, E.D., Flocculation of suspended sediment in rivers of southeastern Canada, *Water Res.*, 28, 1799, 1994.
5. Petticrew, E.L. and Droppo, I.G., The morphology and settling characteristics of fine-grained sediment from a selection of Canadian rivers. In: *Contributions to IAP-V by Canadian Experts, IHP-V — Technical Documents in Hydrology*, No. 33, UNESCO, Paris, 2000, pp. 111–126.
6. Krein, A., Petticrew, E., and Udelhoven, T., The use of fine sediment fractal dimensions and colour to determine sediment sources in a small watershed, *Catena*, 53, 165, 2003.
7. Petticrew, E.L and Arocena., J.M., Organic matter composition of gravel-stored sediments from salmon bearing streams. *Hydrobiologia*, 494, 17, 2003.
8. Ongley, E.D., Krishnappan, B.G., Droppo, I.G., Rao, S.S., and Maguire, R.J., Cohesive sediment transport: Emerging issues for toxic chemical management, *Hydrobiologia*, 235/236, 177, 1992.
9. Leppard, G.G., Flannigan, D.T., Mavrocordatos, D., Marvin, C.H., Bryant, D.W., and McCarry, B.E., Binding of polycyclic aromatic hydrocarbons by size classes of particulate in Hamilton Harbor water, *Environ. Sci. Technol.*, 32, 3633, 1998.
10. Webb, S.M., Leppard, G.G., and Gaillard, J.-F., Zinc speciation in a contaminated aquatic environment: Characterization of environmental particles by analytical electron microscopy, *Environ. Sci. Technol.*, 34, 1926, 2000.
11. Walling, D.E. and Woodward, J.C., Effective particle size characteristics of fluvial suspended sediment transported by lowland British rivers. In: *The Role of Erosion and Sediment Transport in Nutrient and Contaminant Transfer*, M. Stone, Ed., IAHS Publication No. 263, 2000, pp. 129–139.
12. Krishnappan, B.G., In situ size distribution of suspended particles in the Fraser River, *J. Hydraul. Eng. — ASCE*, 126, 561, 2000.
13. Droppo, I.G., Walling, D.E., and Ongley, E.D., The influence of floc size, density and porosity on sediment and contaminant transport. In: *Role of Erosion and Sediment Transport in Nutrient and Contaminant Transfer*, M. Stone, Ed., IAHS Publ. No. 263 2000, pp. 141–147.
14. Leppard, G.G., Droppo, I.G., West, M.M., and Liss, S.N., Compartmentalization of metals within the diverse colloidal matrices comprising activated sludge microbial flocs, *J. Environ. Qual.*, 32, 2100, 2003.
15. Leppard, G.G., Organic flocs in surface waters — their native state and aggregation behavior in relation to contaminant dispersion. In: *Particulate Matter and Aquatic Contaminants*, S.S. Rao, Ed., Lewis Pubs., Chelsea, MI, 1993, chap. 7.
16. Liss, S.N., Droppo, I.G., Flannigan, D.T., and Leppard, G.G., Floc architecture in wastewater and natural riverine systems, *Environ. Sci. Technol.*, 30, 680, 1996.
17. Droppo, I.G., Leppard, G.G., Flannigan, D.T., and Liss, S.N., The freshwater floc: A functional relationship of water and organic and inorganic floc constituents affecting suspended sediment properties, *Water Air Soil Pollut.*, 99, 43, 1997.
18. Grossart, H.-P., Simon, M., and Logan, B.E., Formation of macroscopic organic aggregates (lake snow) in a large lake: The significance of transparent exopolymer particles, phytoplankton and zooplankton, *Limnol. Oceanogr.*, 42, 1651, 1997.
19. Finlayson, J.C., Liao, B., Droppo, I.G., Leppard, G.G., and Liss, S.N., The relationship between the structure of activated sludge flocs and the sorption of hydrophobic pollutants, *Water Sci. Tech.*, 37(4–5), 353, 1998.

20. Liao, B.Q., Allen, D.G., Leppard, G.G., Droppo, I.G., and Liss, S.N., Interparticle interactions affecting the stability of sludge flocs, *J. Colloid Interface Sci.*, 249, 372, 2002.
21. Liss, S.N., Microbial flocs suspended biofilms. In: *The Encyclopaedia of Environmental Microbiology*, Vol. 4, G. Bitton, Ed., Wiley-Interscience, New York, 2002, pp. 2000–2012.
22. Simon, M., Grossart, H.-P., Schweitzer, B., and Ploug, H., Microbial ecology of organic aggregates in aquatic ecosystems, *Aquat. Microb. Ecol.*, 28, 175, 2002.
23. Gregory, J., Fundamentals of flocculation, *CRC Crit. Rev. Environ. Control*, 19, 185, 1989.
24. O'Melia, C.R., Particle-particle interactions. In: *Aquatic Surface Chemistry*, W. Stumm, Ed., John Wiley & Sons, New York, 1987. chap. 14.
25. Stumm, W. and Morgan, J.J., *Aquatic Chemistry — An Introduction Emphasizing Chemical Equilibria in Natural Waters*, 2nd ed., Wiley-Interscience, New York, 1981.
26. Vold, R.D. and Vold, M.J., *Colloid and Interface Chemistry*, Addison-Wesley, London, 1983.
27. Droppo, I.G., Filtration in particle size analysis. In: *Encyclopedia of Analytical Chemistry*, R.A. Meyers, Ed., John Wiley & Sons, Ltd., Chichester, 2000, pp. 5397–5413.
28. Leppard, G.G., Evaluation of electron microscope techniques for the description of aquatic colloids. In: *Environmental Particles, Vol. 1*, J. Buffle and H.P. van Leeuwen, Eds., Lewis Pubs., Chelsea, MI, 1992, chap. 6.
29. Leppard, G.G. and Buffle, J., Aquatic colloids and macromolecules: Effects on analysis. In: *The Encyclopedia of Environmental Analysis and Remediation, Vol. 2*, R.A. Meyers, Ed., John Wiley & Sons, New York, 1998, pp. 349–377.
30. Leppard, G.G., Colloidal organic fibrils of acid polysaccharides in surface waters: Electron-optical characteristics, activities and chemical estimates of abundance, *Colloids Surf. A.*, 120, 1, 1997.
31. Heissenberger, A., Leppard, G.G., and Herndl, G.J., Ultrastructure of marine snow: II. Microbiological considerations, *Mar. Ecol. Prog. Ser.*, 135, 299, 1996.
32. Woodward, J.C., Porter, P.R., Lowe, A.T., Walling, D.E., and Evans, A.J., Composite suspended sediment particles and flocculation in glacial meltwaters: Preliminary evidence from Alpine and Himalayan basins, *Hydrol. Proc.*, 16, 1735, 2002.
33. Myneni, S.C.B., Brown, J.T., Martinez, G.A., and Meyer-Ilse, W., Imaging of humic substance macromolecular structures in water and soils, *Science*, 286, 1335, 1999.
34. Senesi, N., Aggregation patterns and macromolecular morphology of humic substances: A fractal approach, *Soil Sci.*, 164, 841, 1999.
35. Mondi, C., Leifer, K., Mavrocordatos, D., and Perret, D., Analytical electron microscopy as a tool for accessing colloid formation processes in natural waters, *J. Microsc.*, 207, 180, 2002.
36. Droppo, I.G., Nackaerts, K., Walling, D.E., and Williams, N., Can Flocs and Water Stable Soil Aggregates be Differentiated Within Fluvial Systems? Catena, in press.
37. Droppo, I.G. and Amos, C.L., The structure, stability and transformation of contaminated lacustrine surface fine-grain laminae, *J. Sed. Res.*, 71, 718, 2001.
38. Grossart, H.-P. and Simon, M., Bacterial colonization and microbial decomposition of limnetic organic aggregates (lake snow), *Aquat. Microb. Ecol.*, 15, 127, 1998.
39. Droppo, I.G., Flannigan, D.T., Leppard, G.G., Jaskot, C., and Liss, S.N., Floc stabilization for multiple microscopic techniques, *Appl. Environ. Microbiol.*, 62, 3508, 1996.

40. Leppard, G.G. and Droppo, I.G., The need and means to characterize sediment structure and behavior prior to the selection and implementation of remediation plans, *Hydrobiologia.*, 494, 313, 2003.
41. Phillips, J.M. and Walling, D.E., The particle size characteristics of fine-grained channel deposits in the River Exe Basin, Devon, UK, *Hydrol. Proc.*, 13, 1, 1999.
42. de Boer, D.H., Stone, M., and Lévesque, L.M.J., Fractal dimensions of individual particles and particle populations of suspended solids in streams, *Hydrol. Proc.*, 14, 653, 2000.
43. Stone, M. and Krishnappan, B.G., Floc morphology and size distributions of cohesive sediment in steady state flow, *Water Res.*, 37, 2739, 2003.
44. Droppo, I.G., A new definition of suspended sediment: Implications for the measurement and prediction of sediment transport. In: *Erosion and Sediment Transport Measurement in Rivers: Technological and Methodological Advances*, J. Bogen, T. Fergus, and D. Walling, Eds., IAHS Pub. no. 283, 2003, pp. 3–12.
45. de Beer, D., Stoodley, P., Roe, F., and Lewandowski, Z., Effects of biofilm structures on oxygen distribution and mass transport, *Biotechnol. Bioeng.*, 43, 1131, 1994.
46. Tolker-Nielsen, T. and Molin, S., Spatial organization of microbial biofilm communities, *Microb. Ecol.*, 40, 75, 2000.
47. Lawrence, J.R., Neu, T.R., and Marshall, K.C., Colonization — adhesion, bioaggregates and biofilms. In *Manual of Environmental Microbiology*, 2nd ed., C.J. Hurst, G.R. Knudsen, R.L. Crawford, M. McInerney, and L.D. Stetzenbach, Eds., American Society for Microbiology, Washington, D.C., 2002, 466.
48. Battin, T.J., Kaplan, L.A., Newbold, J.D., Cheng, X., and Hansen, C., Effects of current velocity on the nascent architecture of stream microbial biofilms, *Appl. Environ. Microbiol.*, 69, 5443, 2003.
49. Rainey, P.B. and Rainey, K., Evolution of cooperation and conflict in experimental bacterial populations, *Nature,* 425, 72, 2003.
50. Lartiges, B.S., Deneux-Mustin, S., Villemin, G., Mustin, C., Barres, O., Chamerois, M., Gerard, B., and Babut, M., Composition, structure and size distribution of suspended particulates from the Rhine River, *Water Res.*, 35, 808, 2001.
51. Alldredge, A.L., Passow, U., and Logan, B.E., The abundance and significance of a class of large transparent organic particles in the ocean, *Deep-Sea Res.*, 40, 1131, 1993.
52. Passow, U., Alldredge, A.L., and Logan, B.E., The role of particulate carbohydrate exudates in the flocculation of diatom blooms, *Deep-Sea Res. Part I*, 41, 335, 1994.
53. Hochella, M.F., Jr., There's plenty of room at the bottom: Nanoscience in geochemistry, *Geochim. Cosmochim. Acta*, 66, 735, 2002.
54. Buffle, J., Wilkinson, K.J., Stoll, S., Filella, M., and Zhang, J., A generalized description of aquatic colloidal interactions: The three-colloidal component approach, *Environ. Sci. Technol.*, 32, 2887, 1998.
55. Filella, M. and Buffle, J., Factors controlling the stability of submicron colloids in natural waters, *Colloids Surf. A.*, 73, 255, 1993.
56. Stumm, W. and O'Melia, C.R., Stoichiometry of coagulation, *J. AWWA*, 60, 514, 1968.
57. Walker, H.W. and Bob, M.M., Stability of particle flocs upon addition of natural organic matter under quiescent conditions, *Water Res.*, 35, 875, 2001.
58. Bockelmann, U., Manz, W., Neu, T.R., and Szewzyk, U., Investigation of lotic microbial aggregates by a combined technique of fluorescent in situ hybridization and lectin-binding-analysis, *J. Microbiol. Methods*, 49, 75, 2002.
59. Gustaffson, O. and Gschwend, P.M., Aquatic colloids: Concepts, definitions, and current challenges, *Limnol. Oceanogr.*, 42, 519, 1997.

60. O'Melia, C.R., The influence of coagulation and sedimentation on the fate of particles, associated pollutants, and nutrients in lakes. In: *Chemical Processes in Lakes*, W. Stumm, Ed., Wiley-Interscience, New York, 1985, pp. 207–224.
61. Honeyman, B.D. and Santschi, P.H., Coupling adsorption and particle aggregation: Laboratory studies of "colloidal pumping" using ^{59}Fe-labeled hematite, *Environ. Sci. Technol.*, 25, 1739, 1991.
62. Kerner, M., Hohenberg, H., Ertl., S., Reckermann, M., and Spitzy, A., Self-organization of dissolved organic matter to micelle-like microparticles in river water, *Nature*, 422, 150, 2003.
63. Leenheer, J.A. and Croué, J.-P., Characterizing aquatic dissolved organic matter, *Environ. Sci. Technol.*, 37, 18A, 2003.
64. Filella, M., Buffle, J., and Leppard, G.G., Characterization of submicrometre colloids in freshwaters: Evidence for their bridging by organic structures, *Water Sci. Technol.*, 27(11), 91, 1993.
65. Mavrocordatos, D., Mondi-Couture, C., Atteia, O., Leppard, G.G., and Perret, D., Formation of a distinct class of Fe-Ca(-Corg)-rich particles in a complex peat-karst system, *J. Hydrol.*, 237, 234, 2000.
66. Perret, D., Gaillard, J.-F., Dominik, J., and Atteia, O., The diversity of natural hydrous iron oxides, *Environ. Sci. Technol.*, 34, 3540, 2000.
67. Taillefert, M., Lienemann, C.-P., Gaillard, J.-F., and Perret, D., Speciation, reactivity, and cycling of Fe and Pb in a meromictic lake, *Geochim. Cosmochim. Acta*, 64, 169, 2000.
68. Fortin, D. and Beveridge, T.J., Mechanistic routes to biomineral surface development. In: *Biomineralization — From Biology to Biotechnology and Medical Application*, E. Baeuerlein, Ed., Wiley-VCH, New York, 2000, chap. 2.
69. Jackson, T.A. and Leppard, G.G., Energy dispersive X-ray microanalysis and its applications in biogeochemical research. In: *Soil Mineral-Organic Matter-Microorganism Interactions and Ecosystem Health*, A. Violante, P.M. Huang, J.-M. Bollag, and L. Gianfreda, Eds., Elsevier, Amsterdam, 2002, pp. 219–260.
70. Neu, T.R., In situ cell and glycoconjugate distribution in river snow studied by confocal laser scanning microscopy, *Aquat. Microb. Ecol.*, 21, 85, 2000.
71. de Boer, J.J., *The Dynamical Character of Adsorption*, 2nd ed., Clarendon Press, Oxford, 240, 1968.
72. Allan, R.J., *The Role of Particulate Matter in the Fate of Contaminants in Aquatic Ecosystems*. Inland Waters Directorate, National Water Research Institute, Burlington, Ontario, Canada, Scientific Series No. 142, 1986.
73. Horowitz, A.J., *A Primer in Sediment-Trace Element Chemistry*, 2nd Ed., Lewis, Chelsea, MI, 1991, p. 136.
74. Decho, A.W., Microbial exopolymer secretions in ocean environments: Their role(s) in food webs and marine processes, *Oceanogr. Mar. Biol. Annu. Rev.*, 28, 73, 1990.
75. Leppard, G.G., Transmission electron microscopy applied to water fractionation studies — A new look at DOC, *Water Pollut. Res. J. Can.*, 20(2), 100, 1985.
76. Leppard, G.G., The characterization of algal and microbial mucilages and their aggregates in aquatic ecosystems, *Sci. Total Environ.*, 165, 103, 1995.
77. Defarge, C., Trichet, J., Jaunet, A.-M., Robert, M., Tribble, J., and Sansone, F.J., Texture of microbial sediments revealed by cryo-scanning electron microscopy, *J. Sed. Res.*, 66, 935, 1996.
78. Costerton, J.W., Cheng, K.-L., Geesey, G.G., Ladd, T., Nickel, J.C., Dasgupta, M., and Marrie, T.J., Bacterial biofilms in nature and disease, *Annu. Rev. Microbiol.*, 41, 435, 1987.

79. Logan, B.E. and Hunt, J.R., Advantages to microbes of growth in permeable aggregates in marine systems, *Limnol. Oceanogr.*, 32, 1034, 1987.
80. Li, D.H. and Ganczarczyk, J., Flow through activated sludge flocs. *Water Res.*, 22, 789, 1988.
81. Logan, B.E. and Hunt, J.R., Bioflocculation as a microbial response to substrate limitations, *Biotechnol. Bioeng.*, 31, 91, 1988.
82. Bergh, O., Borsheim, K.Y., Bratbak, G., and Heldal, M., High abundance of viruses found in aquatic environments, *Nature (London)*, 340, 476, 1989.
83. Borsheim, K.Y., Bratbak, G., and Heldal, M., Enumeration and biomass estimation of planktonic bacteria and viruses by transmission electron microscopy, *Appl. Environ. Microbiol.*, 56, 352, 1990.
84. Bratbak, G., Thingstad, F., and Heldal, M., Viruses and the microbial loop, *Microb. Ecol.*, 28, 209, 1994.
85. Lawrence, J.R., Wolfaardt, G.M., and Korber, D.R., Determination of diffusion coefficients in biofilms by confocal laser microscopy, *Appl. Environ. Microbiol.*, 60, 1166, 1994.
86. Laspidou, C.S. and Rittmann, B.E., A unified theory for extracellular polymeric substances, soluble microbial products, and active and inert biomass, *Water Res.*, 36, 2711, 2002.
87. Wolfaardt, G.M., Lawrence, J.R., Headley, J.V., Robarts, R.D., and Caldwell, D.E., Microbial exopolymers provide a mechanism for bioaccumulation of contaminants, *Microb. Ecol.*, 27, 279, 1994.
88. Wolfaardt, G.M., Lawrence, J.R., Robarts, R.D., Caldwell, S.J., and Caldwell, D.E., Multicellular organization in a degradative biofilm community, *Appl. Environ. Microbiol.*, 60, 434, 1994.
89. Wolfaardt, G.M., Lawrence, J.R., Robarts, R.D., and Caldwell, D.E., Bioaccumulation of the herbicide diclofop in extracellular polymers and its utilization by a biofilm community during starvation, *Appl. Environ. Microbiol.*, 61, 152, 1995.
90. Wolfaardt, G.M., Lawrence, J.R., Robarts, R.D., and Caldwell, D.E., In situ characterization of biofilm exopolymers involved in the accumulation of chlorinated organics, *Microb. Ecol.*, 35, 213, 1998.
91. Nilsson, C.L., Lectins: Proteins that interpret the sugar code, *Anal. Chem.*, 75, 348A, 2003.
92. Lawrence, J.R., Swerhone, G.D.W., Leppard, G.G., Araki, T., Zhang, X., West, M.M., and Hitchcock, A.P., Scanning transmission x-ray, laser scanning, and transmission electron microscopy mapping of the exopolymeric matrix of microbial biofilms, *Appl. Environ. Microbiol.*, 69, 5543, 2003.
93. Gaillard, J.-F., Webb, S.M., and Leppard, G.G., The chemical speciation of Zn in the sediments of a lake impacted by a Zn smelter, *Proc. Int. Conf. Heavy Metals in the Environment: Silver Anniversary*, Ann Arbor, MI, 2000, Contribution No. 1142: CD-ROM format.
94. Claesson, P.M., Ederth, T., Bergeron, V., and Rutland, M.W., Techniques for measuring surface forces, *Adv. Colloid Inter. Sci.*, 67, 119, 1996.
95. Camesano, T.A. and Logan, B.E., Probing bacterial electrosteric interactions using atomic force microscopy, *Environ. Sci. Technol.*, 34, 3354, 2000.
96. Mosley, L.M., Hunter, K.A., and Ducker, W.A., Forces between colloid particles in natural waters, *Environ. Sci. Technol.*, 37, 3303, 2003.
97. Lower, S.K., Tadanier, C.J., and Hochella, Jr., M.F., Measuring interfacial and adhesion forces between bacteria and mineral surfaces with biological force microscopy, *Geochim. Cosmochim. Acta*, 64, 3133, 2000.

98. Muirhead, D. and Lead, J.R., Measurement of the size and structure of natural aquatic colloids in an urbanised watershed by atomic force microscopy, *Hydrobiologia*, 494, 65, 2003.
99. Wagner, M., Horn, M., and Daims, H., Fluorescence *in situ* hybridisation for the identification and characterization of prokaryotes, *Curr. Opin. Microbiol.*, 6, 302, 2003.

3 Intra-Storm and Seasonal Variations in the Effective Particle Size Characteristics and Effective Particle Density of Fluvial Suspended Sediment in the Exe Basin, Devon, United Kingdom

John M. Phillips and Desmond E. Walling

CONTENTS

1-56670-615-7/05/$0.00+$1.50

3.1 INTRODUCTION

Fine-grained ($<62.5\ \mu$m) sediment-associated transport dominates the land–ocean flux of many natural[1] and anthropogenically derived nutrients and contaminants to the fluvial system.[2] Globally, transport during storm events dominates the suspended sediment flux of most rivers.[3–5] In addition to its role in the sediment-associated transport of nutrients, contaminants, and other geochemical materials, suspended sediment frequently represents a significant form of nonpoint source pollution in its own right, with both environmental, for example, ref. [6,7] and economic costs.[8]

The hydrodynamic properties of suspended sediment particles are determined primarily by their size (diameter), density, and shape. Of these parameters, particle size represents the principal physical factor controlling both the hydrodynamic properties and chemical activity of fluvial suspended sediment particles. Particle size is a key variable in many numerical models of the transport and geochemical dynamics of fine sediment. A sound understanding of the *in situ* particle size characteristics of fluvial suspended sediment is, therefore, clearly essential to many areas of research, and particularly our ability to predict and manage the environmental impacts of fine-grained sediment transport.

It is increasingly being demonstrated that fluvial suspended sediment is typically composed of composite particles, comprising aggregates or flocs, as well as discrete particles, and that composite particles may comprise a significant proportion of the total sediment load, as well as being important determinants of the particle size characteristics of fluvial suspended sediment.[9–14] In this chapter the following terminology is adopted; "composite particle" is a generic term used to describe a particle formed of smaller primary particles. "Degree of aggregation" (DOA) is the term used to describe the percentage reduction in volume median particle size of the *in situ*, or effective particle size distribution (EPSD) following laboratory treatment and measurement of the chemically dispersed mineral fraction, or absolute particle size distribution (APSD). These terms do not imply particular causal processes, as might be inferred from the use of "floc" or "flocculation" which are strongly associated in the literature with a specific set of physicochemical processes confined to the water column.[15–17]

Although the primary impact of aggregation upon the hydrodynamic properties of suspended sediment is one of coarsening the particle size distribution, an important secondary effect is the associated impact on the relationship between particle size and particle density. A growing number of studies have established that, in fluvial and other freshwater systems, composite particles may consist of a mixture of mineral grains and low density organic matter, as well as pores containing water or gas and thus regions of neutral buoyancy.[16,18] Although the potentially unique structure of individual composite particles within a suspended sediment sample is likely to confound any simple relationship between particle size and settling velocity, an inverse relationship between composite particle size and density has been reported by numerous studies of particle density in the freshwater environment.[11,19–21] The reduction in effective particle density (EPD) associated with an increased DOA has, however, been shown in the above studies to be typically of secondary importance compared

to the increase in particle size, with the net impact of aggregation being an increase in sedimentation rates.

Characterization of the at-a-station *in situ* particle size regime is dependent upon a sound understanding of the temporal dynamics of the EPSD and associated DOA, at both the storm event and seasonal temporal scales. Furthermore, an appreciation of the temporal dynamics of these parameters of the suspended sediment load of river systems is essential for both spatial analysis of effective particle size data, and the calibration of reach specific sediment transport models. Although seasonal variations in the EPSD and DOA have been described by a number of studies from contrasting physiographic regions,[9,22] there is a relative paucity of data concerned with the quantification and explanation of the degree of variation in the EPSD over shorter temporal scales, in particular at the storm event scale. Evidence of significant intra-storm variation in the EPSD of fluvial suspended sediment is provided by several recent studies,[12,23,24] however, this phenomenon, and its relative importance compared to seasonal variations in the EPSD, is still poorly documented, and not yet fully understood.

A representative measure of the EPSD is dependent upon the use of a measurement technique that is conservative, that is, one that does not modify the EPSD by breaking up existing composite particles,[25] or encouraging the formation of additional, or larger, composite particles.[26] Furthermore, in view of the "operationally defined" nature of particle size data,[27] the same measurement technique should, where possible, be used for derivation of both the EPSD and APSD in any comparative analysis. Although these uncertainties can be minimized by making measurements *in situ,* few devices currently exist that are capable of making nondisruptive *in situ* measurements of the EPSD of fluvial suspended sediment, especially during storm events when ambient channel conditions may be characterized by significant turbulence and high flow velocities (e.g., $>2\ \mathrm{m\ s^{-1}}$), as well as elevated suspended sediment concentrations (e.g., $>1000\ \mathrm{mg\ l^{-1}}$).

This chapter details the effective particle size characteristics and degree of aggregation of suspended sediment in eight rivers in the Exe Basin, Devon, United Kingdom Over a 13-month period, high-frequency nondisruptive *in situ* measurements of the EPSD were obtained during flood events using a laser backscatter probe,[12,28] which was also used for measurement of the APSD of the suspended sediment. Temporal and spatial variations in the EPSD and degree of aggregation are examined, together with an assessment of effective particle density in the study area. The origin of the composite particles within the EPSD is also considered, with particular reference to the relative importance of "inherited" composite particles from in-channel and catchment slope sediment sources.

3.2 THE STUDY SITES

The location of the eight study sites within the Exe Basin, Devon, United Kingdom, is shown in Figure 3.1. Each site was associated with an existing discharge gauging station operated by the Environment Agency for England and Wales, or the Geography Department, University of Exeter, and was equipped with continuous turbidity

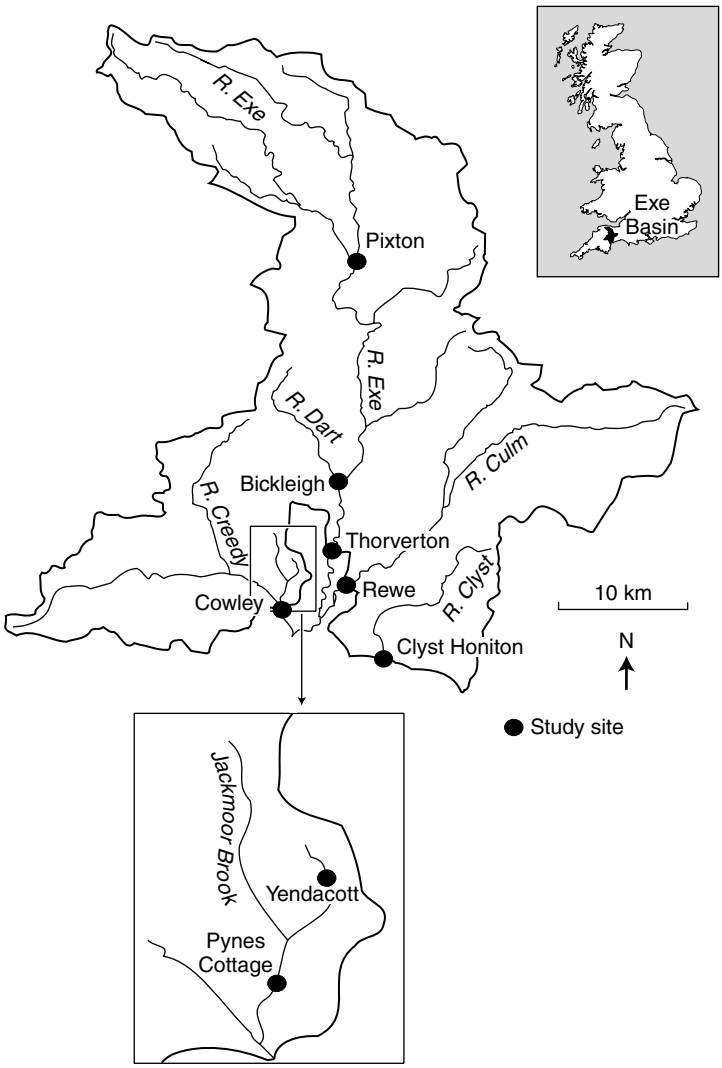

FIGURE 3.1 Study sites within the River Exe drainage basin, Devon, United Kingdom.

and suspended sediment monitoring equipment maintained by the Geography Department, University of Exeter. A number of previous studies have demonstrated that the contrasting physiographic characteristics of the study site drainage basins combine to produce a range of suspended sediment regimes.[29,30]

Typical annual sediment yields for the study area have been estimated as being greatest for the River Dart basin (58 t km^2 yr^{-1}), and at a minimum for the River Culm (20 t km^2 yr^{-1}) and Upper Exe (19 t km^2 yr^{-1}) basins. The mean annual sediment yields of the remaining study basins range from 26 t km^2 yr^{-1} (River Clyst)

to 39 t km^2 yr^{-1} (River Creedy).[3] The maximum suspended sediment concentration sampled at each of the study sites during the study period follows a similar trend. Sampled suspended sediment concentrations were at a maximum in the River Dart at Bickleigh (2024 mg l^{-1}) while the lowest recorded values of this parameter were associated with the Upper Exe (241.7 mg l^{-1}) at Pixton and the River Culm at Rewe (406 mg l^{-1}). Intermediate values of maximum sampled suspended sediment concentration were obtained for the River Clyst at Clyst Honiton (667 mg l^{-1}), River Creedy at Cowley (887 mg l^{-1}), and River Exe at Thorverton (805 mg l^{-1}), while relatively high values of 1040 mg l^{-1} and 1275 mg l^{-1} were recorded for the Jackmoor Brook at Pynes Cottage and Yendacott, respectively. The APSD of suspended sediment has also been previously shown to differ between the study sites.[29,30] While the precise values of the absolute particle size statistics reported depend on the measurement technique employed, the study period mean values of the median absolute particle size (Ad_{50}) measured in this study are consistent with those of the previous studies in the Exe Basin. In particular, suspended sediment collected from the Upper Exe at Pixton had a characteristically coarser Ad_{50} (7.7 μm) than all the other study sites. In addition, suspended sediment samples collected from those basins underlain primarily by Permian strata (the Clyst, Yendacott, Jackmoor Brook, and Culm catchments) were characterized by a considerably finer median particle size (4.2 μm, 4.3 μm, 4.6 μm, and 5.0 μm, respectively) than those collected from the River Exe at Thorverton (6.5 μm), and River Dart at Bickleigh (6.1 μm), which are underlain primarily by Devonian and Carboniferous rocks, respectively.

3.3 METHODOLOGY

Particle size measurements were made using a Par-Tec 200 laser backscatter probe. At each study site, rapid and nondisruptive *in situ* measurements of the EPSD of suspended sediment were made by immersing the probe at ca. 1 to 2 hourly intervals in the thalweg zone of the channel during flood events. The Par-Tec 200 was typically immersed for ca. 3 min on each periodic deployment, during which time seven replicate measurements of the EPSD of ambient suspended sediment were made. A total of 204 deployments of the Par-Tec equipment were made during 37 storm events at the eight study sites. The operating principles, and full details of the field application of this device are given in Phillips and Walling.[12,28] During the *in situ* measurement process, two representative grab samples of suspended sediment were collected adjacent to the submerged Par-Tec 200 probe. Suspended sediment concentration at the time of *in situ* measurement of the EPSD was determined by filtration of the contents of one of the samples through a tared 0.45 μm filter. Suspended sediment was recovered from the second sample by centrifugation and its APSD measured using the Par-Tec 200 after removal of the organic fraction by treatment with hydrogen peroxide, and chemical dispersion in 0.4% sodium hexametaphosphate solution.

Particle density was investigated using a combination of the physical measure of median effective particle size derived from the Par-Tec 200 laser backscatter probe, and the hydraulically derived estimate of median settling velocity obtained from

sedimentation analysis using a Valeport (SK110) Bottom Withdrawal Tube (BWT). The BWT was used to take *in situ* samples of suspended sediment adjacent to the Par-Tec 200, with sedimentation taking place immediately afterwards by placing the BWT in a vertical stand on the river bank. The median EPD was derived by simple rearrangement of the settling velocity equation of Gibbs et al.[31]

3.4 RESULTS AND DISCUSSION

3.4.1 The Degree of Aggregation of Suspended Sediment in the Study Area

The influence of aggregation on the mean storm-period contribution of specific size fractions to the EPSD is summarized in Table 3.1, which presents the mean storm-period percentage of total effective volume for specific particle size fractions, together with the associated EPSD/APSD ratio for the storm event exhibiting the greatest event mean value of DOA. From these data, it is evident that at all sites the aggregated nature of the suspended sediment has caused a relative enrichment (ratio values of >1) of the $>16\ \mu$m (coarse silt–sand) fraction of the EPSD, while the $<2\ \mu$m to $16\ \mu$m (clay–medium silt) fraction evidences relative depletion at all sites except that of the River Clyst. Furthermore, maximum enrichment and depletion at all sites are associated with the $>62.5\ \mu$m (very fine sand) and $<2\ \mu$m to $4\ \mu$m (clays–very fine silt) fractions, respectively.

Median particle size is a key descriptive statistic for the characterization of particle size data, and in this study the DOA, as defined above, has been adopted as the main index of aggregation of suspended sediment at the study sites.

The importance of aggregation as a phenomenon within all of the 204 intra-storm effective particle size measurements made at the Exe Basin study sites is illustrated in Figure 3.2. A strong relationship is evident in Figure 3.2(a) between Ed_{50} and the DOA for all 204 intra-storm measurements made in the study area. The relationship between Ed_{50} and DOA is reasonably well described by an exponential trend with an r^2 of 0.86. Figure 3.2(b) presents the relationship between Ed_{50} and the associated Ad_{50}. From the scatter, and the limited range in the value of Ad_{50} ($3.0\ \mu$m to $9.6\ \mu$m) evident in Figure 3.2(b), it is clear that the APSD exerts little control upon Ed_{50}, the magnitude of which is strongly related to the relative incidence of composite particles. This phenomenon is examined for the River Exe at Thorverton in Figures 3.2(c) and (d), this being the study site with the most complete data set. A strongly exponential relationship between Ed_{50} and DOA, similar to that established for the study areas as a whole (r^2 of 0.87), is evident for the Exe data set in Figure 3.2(c). The limited range of the value of Ad_{50}($4.9\ \mu$m to $8.1\ \mu$m), combined with the significant degree of scatter in the relationship between Ed_{50} and Ad_{50} evident in Figure 3.2(d) further demonstrates that the principal determinant of Ed_{50} in the Exe Basin is the DOA, rather than temporal variations in the APSD of the sediment.

The above data emphasize that the *in situ* hydrodynamic properties of fluvial suspended sediment in the Exe Basin can only be meaningfully characterized by reference to the EPSD. Furthermore, the data presented in Figure 3.2 and Table 3.1, clearly indicate that the EPSD and associated DOA both vary at the inter-storm and

TABLE 3.1
Storm Period Mean Percentage of Total Volume for Particular Size Fractions, and Associated EPSD/APSD Ratio for the Storm Event Having the Greatest Mean DOA

Particle size Class	R. Clyst 03/04/94 ($n = 9$)[a]	R. Creedy 17/05/93 ($n = 10$)	Jackmoor Brook 29/11/93 ($n = 5$)	The Yendacott 15/07/93 ($n = 4$)	R. Dart 30/03/94 ($n = 6$)	R. Culm 25/05/94 ($n = 4$)	Upper Exe 31/03/94 ($n = 6$)	Exe 25/05/94 ($n = 5$)
<2 μm	11.2[b]/0.47[c]	2.2/0.16	5.3/0.31	3.8/0.21	4.0/0.23	1.6/0.09	4.8/0.43	3.9/0.23
Ratio range	0.59–0.36	0.27–0.08	0.58–0.09	0.30–0.12	0.32–0.17	0.17–0.04	0.67–0.48	0.33–0.16
2–4 μm	14.0/0.61	5.3/0.25	6.9/0.3	6.1/0.25	8.5/0.41	3.5/0.17	10.6/0.57	7.0/0.33
Ratio range	0.66–0.53	0.41–0.15	0.46–0.13	0.35–0.16	0.51–0.32	0.26–0.09	0.69–0.58	0.42–0.25
4–8 μm	18.8/0.79	12.0/0.46	11.0/0.46	11.0/0.44	16.0/0.66	7.8/0.31	20.4/0.76	12.1/0.49
Ratio range	0.87–0.73	0.66–0.32	0.70–0.25	0.56–0.33	0.81–0.55	0.47–0.18	0.84–0.75	0.57–0.37
8–16 μm	**17.4/1.06**[d]	17.0/0.82	13.0/0.69	14.4/0.81	18.0/0.92	12.2/0.63	22.7/0.94	13.9/0.69
Ratio range	1.22–0.92	1.03–0.64	0.81–0.44	1.07–0.57	1.09–0.80	0.85–0.43	1.02–0.91	0.80–0.56
16–32 μm	**18.6/1.81**	**25.6/1.76**	**18.2/1.33**	**21.1/1.77**	**22.7/1.63**	**20.0/1.39**	**23.6/1.36**	**17.4/1.29**
Ratio range	1.93–1.56	1.87–1.64	1.54–1.04	2.00–1.44	2.01–1.51	1.80–1.12	1.39–1.19	1.38–1.09
32–62.5 μm	**15.5/6.56**	**30.1/8.09**	**28.1/6.07**	**29.1/9.07**	**23.4/6.68**	**34.9/8.72**	**14.8/3.46**	**21.3/6.41**
Ratio range	8.91–5.05	10.22–6.49	7.68–4.23	9.96–7.74	7.57–5.57	9.47–8.13	2.99–2.38	7.86–5.10
>62.5 μm	**4.4/75.83**	**7.8/167.61**	**17.6/104.59**	**14.6/113.67**	**7.4/63.81**	**20.1/141.5**	**3.0/14.21**	**24.3/327.16**
Ratio range	178.32–45.63	253.07–82.39	123.56–91.02	169.26–59.83	117.87–27.36	171.86–94.97	16.94–5.28	549.74–137.99

[a] Number of intra-storm measurements.
[b] Storm period mean % of total effective particle volume.
[c] Ratio of % of total volume: effective/absolute particle size distribution.
[d] Bold type indicates relative enrichment within the EPSD (i.e., a ratio >1).

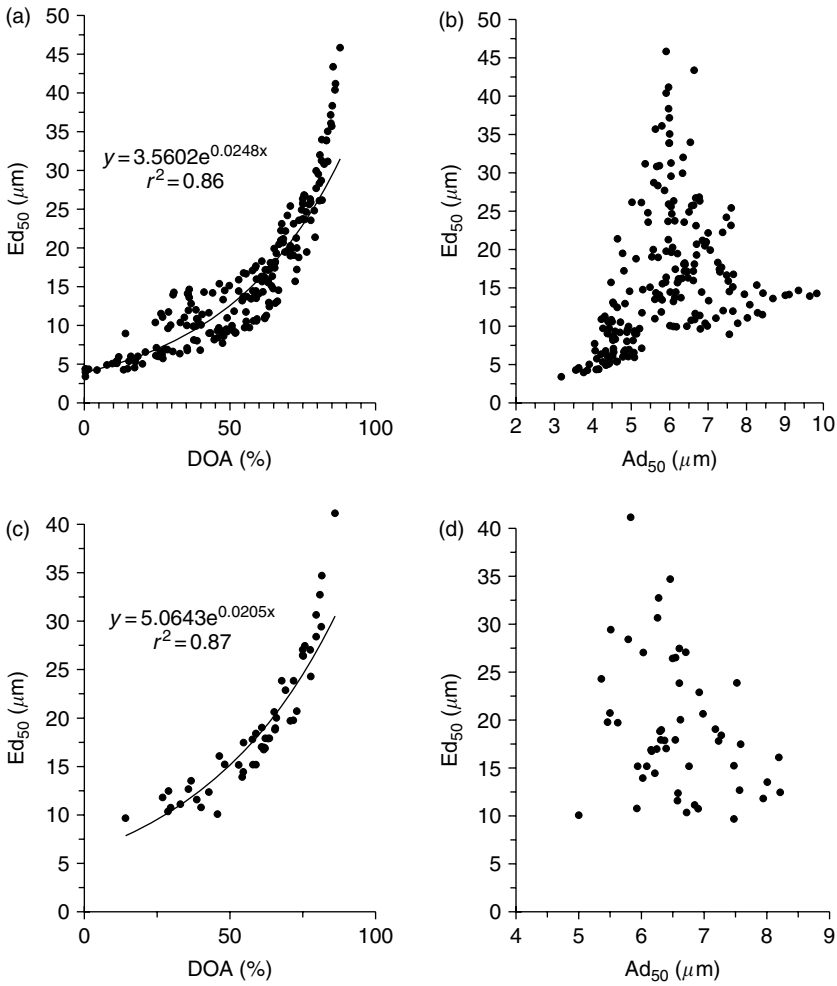

FIGURE 3.2 (a) The relationship between Ed_{50} and the DOA and (b) the relationship between Ed_{50} and Ad_{50} for all 204 intra-storm measurements (b), (c) the relationship between Ed_{50} and the DOA, and (d) the relationship between Ed_{50} and Ad_{50} based on the measurements made on the River Exe at Thorverton.

intra-storm temporal scales, respectively. These aspects of EPSD behavior at the study sites are considered in detail below.

3.4.2 Short-Term Variability in the EPSD

Short-term (<1 min) variations in the effective particle size characteristics of suspended sediment were assessed by analysis of the replicate measurements of the EPSD made during each periodic deployment of the Par-Tec equipment. During each periodic deployment of ca. 3 min, replicate measurements were made at intervals of

25.6 sec. For each set of replicate measurements, the temporal variability of the EPSD was defined by the standard error (S.E.) of three key descriptive statistics, namely, the mean value of the volume mean and median particle size, as well as the degree of sorting as defined by Buller and McManus[32] which describes the spread of the particle size data.

Mean variation in any of the three parameters did not exceed ± 0.3 μm at any site, and in the majority of cases the maximum variation on any occasion, in any parameter, did not exceed ± 2.0 μm. Maximum variation in the three parameters was shown by the S.E. of the median particle size at ± 2.2 μm at the R. Culm and Exe study sites on the May 25, 1994, and this value principally reflects the significantly coarser EPSD of suspended sediment on this date, relative to that measured during all other storm events at the eight study sites. In view of the limited variation evident in the replicate EPSD data, and taking account of the considerably greater degree of intra- and inter-storm event variation in EPSD discussed below, the EPSD of suspended sediment at the study sites can be considered to be stable over periods of ca. 3 min. Accordingly, in the following analyses the EPSD of suspended sediment transported during each periodic ca. 3 min deployment of the Par-Tec equipment has been characterised by averaging the associated replicate measurements.

3.4.3 Intra-Storm Variability in the EPSD and Associated DOA

The most detailed intra-storm measurements of the EPSD were made at Jackmoor Brook on the April 8, 1994, and the River Exe at Thorverton on February 23, 1994. On these occasions the Par-Tec equipment was deployed for extended periods through the storm event, during which time *in situ* measurements were made every 25.6 sec and averaged over intervals of ca. 3 min. Figure 3.3(a) and (b) present the semi-continuous median effective particle size data for these two sites, together with the median APSD of periodic samples taken during the events. Figure 3.3(c) and (d) present the associated hydrograph and suspended sediment concentration data for the Jackmoor Brook and River Exe storm events, respectively.

The EPSD data for the Jackmoor Brook event encompasses both the rising and falling limb of the hydrograph and a range in suspended sediment concentration of ca. 800 mg l^{-1}, with a maximum value of 1040 mg l^{-1}. The data for the River Exe event are confined to the peak and falling limb of the hydrograph and suspended sediment concentrations are generally less than at the Jackmoor Brook, with a range of ca. 220 mg l^{-1} and a maximum value of 358 mg l^{-1}. At both sites, the Ed_{50} data exhibit a gradual reduction in magnitude through the storm event, the pattern of which approximates an exponential trend. At both sites it is apparent from the Ad_{50} data that the Ed_{50} reflects aggregation throughout the sampling period, and, given the limited range in the Ad_{50} data, that the magnitude of this phenomenon follows a similar trend to that of the Ed_{50}, with the DOA being greatest during the earlier parts of the hydrograph, and in particular, declining rapidly through the falling limb.

Table 3.2 summarizes the intra-storm range in Ed_{50} and associated DOA for all storm events at the eight study sites. From these data it is clear that in every case Ed_{50} exhibits measurable variation at the intra-storm temporal scale. The magnitude of this

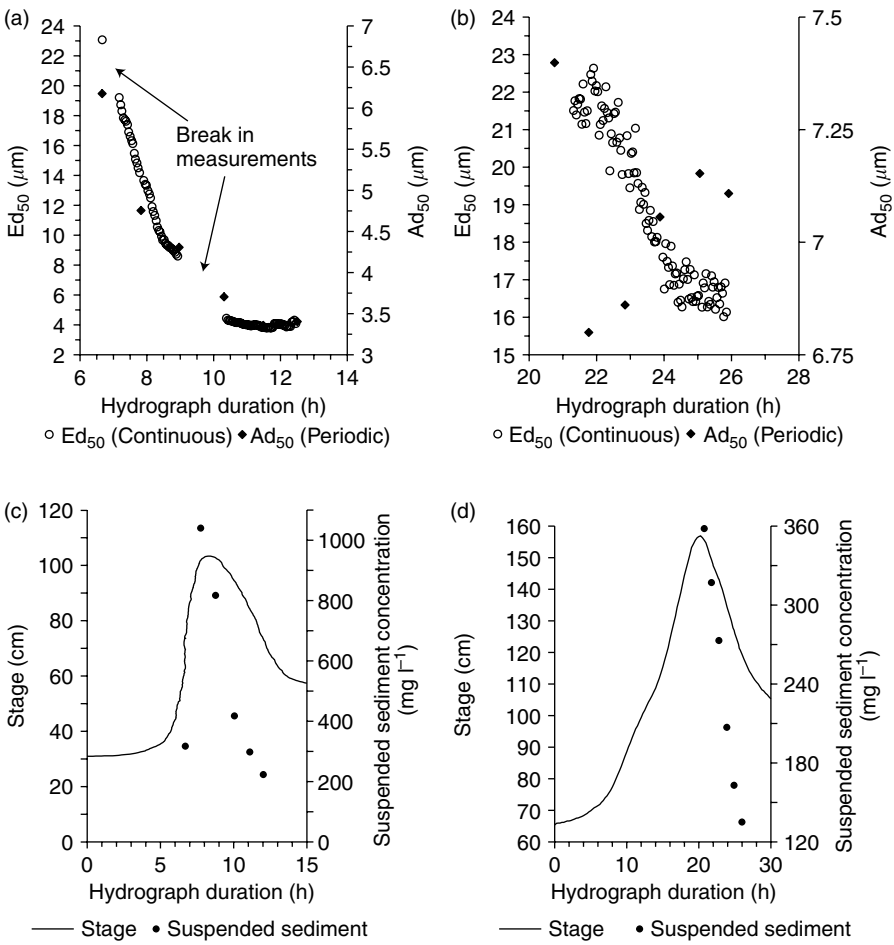

FIGURE 3.3 High frequency *in situ* intra-storm measurement of Ed_{50}: (a) Pynes Cottage on the Jackmoor Brook on 08/04/94, (b) Thorverton on the River Exe on 23/02/94, (c) hydrograph and sampled suspended sediment concentration at Pynes Cottage on 08/04/94, and (d) hydrograph and sampled suspended sediment concentration at Thorverton on 23/02/94.

variation ranges from less than 1 μm in the case of the Upper Exe to more than 20 μm in the Exe and Jackmoor Brook, with a study area mean value of 8.8 μm. In common with the trends in Ed_{50} evident in Figure 3.3(a) and (b), the Ed_{50} "Change" data in Table 3.2 (defined as the difference (μm) between the last and the first intra-storm measurement) also show a characteristic reduction in Ed_{50} at the end of each sampling period, with 32 of the 37 storm events showing a reduction in Ed_{50} relative to that at the start of the storm event. The magnitude of this variation ranges from less than 1 μm (Upper Exe) to 28.3 μm (Jackmoor Brook), with a study area average value of 7.4 μm. It is useful to note that in only one case where an increase in Ed_{50} was recorded was the value greater than 1 μm. This case is associated with the Upper Exe

TABLE 3.2
Intra-Storm Variation in Ed_{50} and the DOA for all Sampled Storm Events

River/Storm Event	*n*	Mean (μm)	2 S.E. (μm)	Max. (μm)	Min. (μm)	Change[a] (μm)	Mean DOA	2 S.E.	Max. DOA	Min. DOA	Change Ratio[b]
Clyst											
13/10/93	3	5.1	0.8	5.8	4.6	−1.1	15.4	11.0	26.3	9.3	0.4
05/01/94	6	4.5	0.7	5.9	3.8	−2.1	9.8	10.6	32.4	0.0	0.0
03/04/94	9	10.0	0.7	12.5	8.6	−2.3	56.5	3.0	65.2	50.3	0.9
Creedy											
17/05/93	10	23.8	2.9	30.9	15.3	−15.5	74.5	3.4	81.1	62.8	0.8
J. Brook											
01/10/93	7	13.9	6.0	30.5	8.0	−21.9	61.6	9.9	81.9	45.6	0.6
29/11/93	5	27.3	10.4	43.0	14.7	−28.3	77.1	7.7	85.0	63.9	0.8
09/01/94	5	5.4	1.6	7.7	3.6	−4.2	19.2	20.6	44.2	0.0	0.0
23/02/94	5	6.3	0.9	7.9	5.5	−2.4	23.9	11.5	44.4	11.4	0.3
08/04/94	6	9.7	6.3	23.1	3.9	−19.2	39.0	22.0	73.3	13.1	0.2
Yendacott											
16/06/93	5	14.6	5.9	25.8	10.5	−14.9	67.7	7.8	81.3	61.6	0.8
15/07/93	4	26.5	7.8	35.3	19.1	−16.2	80.7	4.0	84.6	76.0	0.9
09/01/94	6	5.4	1.6	7.3	3.0	−3.4	24.1	23.3	47.1	0.0	0.0
Dart											
03/04/93	7	13.2	4.8	26.4	8.6	−17.8	54.7	9.1	75.1	42.4	0.6
11/06/93	11	16.5	1.8	20.8	13.0	+0.2	63.0	2.4	67.9	56.9	1.0
11/10/93	5	21.5	2.8	25.0	17.0	−8.0	66.3	4.3	70.4	58.3	0.8
23/01/94	6	14.5	3.1	20.6	10.5	−10.0	57.4	5.9	67.3	48.6	0.7
25/02/94	4	11.1	0.4	11.6	10.6	+0.1	34.5	6.2	40.1	25.9	0.6
30/03/94	6	18.1	3.2	23.2	12.5	−6.5	68.7	3.6	75.2	63.0	0.9
Culm											
13/09/93	4	34.1	2.8	36.7	30.4	−6.3	83.3	1.1	84.3	82.0	1.0
15/12/93	6	7.3	1.2	9.1	5.7	−3.1	35.7	8.9	48.6	24.2	0.5
05/01/94	5	5.6	0.9	6.7	4.7	−1.8	17.0	7.7	28.2	10.7	0.4
03/02/94	5	6.5	1.5	8.8	5.0	−3.2	28.6	12.1	46.8	14.9	0.5
25/05/94	6	35.0	6.5	45.4	24.4	−21.0	83.3	2.8	87.4	78.5	0.9
Upper Exe											
19/12/93	5	13.8	0.2	14.2	13.5	+0.1	33.3	2.5	35.6	30.1	1.0
20/12/93	3	13.6	0.4	13.9	13.2	−0.7	40.0	4.7	43.7	35.6	0.9
03/02/94	3	9.7	0.3	10.0	9.5	+0.4	32.3	8.5	38.1	24.0	0.6
31/03/94	6	13.2	2.3	16.2	9.5	+5.2	46.7	6.0	55.1	37.0	1.3
Exe											
26/05/93	5	24.8	5.4	31.6	18.6	−7.3	75.7	4.1	80.5	70.4	0.9
16/06/93	7	19.3	5.3	33.6	13.3	−9.4	65.2	6.7	81.1	54.2	0.8
13/09/93	4	16.0	0.5	16.8	15.6	−1.2	61.2	0.5	61.7	60.5	1.0

TABLE 3.2
Continued

River/Storm Event	*n*	Mean (μm)	2 S.E. (μm)	Max. (μm)	Min. (μm)	Change[a] (μm)	Mean DOA	2 S.E.	Max. DOA	Min. DOA	Change Ratio[b]
06/10/93	7	22.2	3.4	26.3	15.7	−9.6	70.2	4.4	75.4	61.7	0.8
19/12/93	4	12.1	2.9	16.3	10.0	−5.0	35.5	12.8	54.3	26.5	0.5
20/12/93	5	9.8	0.9	11.2	8.5	−2.7	30.4	9.9	42.3	13.8	0.3
05/01/94	4	13.2	1.6	14.9	11.5	−2.6	41.4	6.4	47.8	35.4	0.7
03/02/94	5	11.9	2.2	14.0	8.9	−3.9	49.8	6.4	57.5	39.7	0.8
23/02/94	6	19.3	2.0	22.7	16.7	−6.1	62.9	3.9	68.7	57.3	0.9
25/05/94	5	27.7	6.9	40.0	19.6	−20.4	79.2	4.3	85.7	72.5	0.8
Mean	5.5	15.2	2.9	20.3	11.5	−7.4	50.4	7.6	61.2	41.0	0.7

n = Number of samples within the storm event.
[a] Ed_{50} of last minus the first intra-storm measurement.
[b] Ratio of the DOA associated with last/first intra-storm measurement.

which also recorded two of the remaining three cases of a net increase in Ed_{50}, and is indicative of a particle size regime in this upland catchment that is anomalous within the study area.

Table 3.3 presents the Spearmans Rank correlation coefficients for the relationship between Ed_{50} and sample time within the storm event. Sample time is defined as time (h) from the initial rise of the hydrograph. The majority of the correlation coefficients are negative, and, despite the small sample size of a number of the data sets, all study sites except the Upper Exe have at least one statistically significant negative correlation. The results of this analysis indicate that the net change in Ed_{50} is typically the product of a systematic change through the hydrograph, as was identified by the more detailed measurements presented in Figure 3.3. This conclusion is also supported by the finding that of the 29 storm events for which *in situ* measurements were made on both the rising and falling limbs of the hydrograph, rising limb samples accounted for the maximum value of Ed_{50} on 25 occasions, while falling limb measurements also accounted for the minimum value of Ed_{50} on 25 occasions.

The aggregation data presented in Table 3.2 display a similar pattern of intra-storm variability to that of the effective particle size data. There is a wide intra-storm range in the value of DOA, with values varying by between 1.2% (Exe 13/09/93) to 60.2% (Jackmoor Brook 08/04/94), with a study area mean value of 20.2%. On three occasions the value of DOA fell to zero, in every case a phenomenon associated with the final sample of a mid-winter storm event. This finding may reflect antecedent conditions in the sediment source areas, where biological processes leading to aggregation can be expected to be at a minimum as a result of low winter temperatures.

Perhaps most significantly, the DOA "Change" data are also indicative of a reduction in aggregation at the end of the measurement period, relative to the initial value. The only case of a net increase in the DOA is also associated with a net increase

TABLE 3.3
Spearmans Rank Correlation Coefficients for the Relationship Between Ed_{50} and Sample Time (Hours from Start of Hydrograph Rise) at the Intra-Storm Temporal Scale

Storm[a] Event	R. Clyst	R. Creedy	Jackmoor Brook	The Yendacott	R. Dart	R. Culm	Upper Exe	R. Exe
1	−0.50	**−0.87**	**−0.93**	−0.60	**−1.00**	−0.80	0.50	−0.60
2	**−0.94**[b]		**−1.00**	**−1.00**	−0.40	**−0.94**	−1.0	**−0.86**
3	−0.23		−0.91	−0.70	−0.90	−0.90	1.00	−0.80
4			**−1.00**		**−1.00**	−0.90	0.77	**−0.82**
5			**−0.94**		0.60	**−1.00**		−0.20
6					−0.49			−0.90
7								−0.80
8								−0.60
9								**−1.00**
10								**−1.00**

[a] Storm event in chronological order of storm events listed in Table 3.2.
[b] Bold type indicates statistically significant at the 0.05 level (two-tailed test).

TABLE 3.4
Spearmans Rank Correlation Coefficients for the Relationship Between the DOA and Sample Time (Hours from Start of Hydrograph Rise) at the Intra-Storm Temporal Scale

Storm[a] Event	R. Clyst	R. Creedy	Jackmoor Brook	The Yendacott	R. Dart	R. Culm	Upper Exe	R. Exe
1	−0.50	−0.80	−0.86	−0.60	−0.96	−0.40	−0.10	−0.60
2	−0.83		**−1.00**	**−1.00**	−0.41	**−0.94**	−0.50	**−0.86**
3	0.05		−0.90	−0.70	−0.09	−0.90	−1.00	−0.80
4			**−1.00**		**−1.00**	−0.70	0.77	**−0.90**
5			−0.94		−0.80	**−1.00**		−0.80
6					−0.60			−0.90
7								**−1.00**
8								−0.60
9								**−0.94**
10								**−1.00**

[a] Storm event in chronological order of storm events listed in Table 3.2.
[b] Bold type indicates statistically significant at the 0.05 level (two-tailed test).

in Ed_{50} over the measurement period (Upper Exe 31/03/94). The close relationship between the intra-storm dynamics of Ed_{50} and the DOA is supported by the data contained in Table 3.4 in which the Spearmans Rank correlation coefficients for the relationship between the DOA and sample time within the storm event are

TABLE 3.5
Results of Mann–Whitney U-Test Analysis Showing the Percentage of Statistically Significant Differences (0.05 Confidence Level) Determined Between the Mean, Median, and Degree of Sorting of each Group of Replicate Measurements Within Each Storm Event Data Set

Parameter	Clyst $n = 54$	Creedy $n = 45$	Jackmoor Brook $n = 65$	Yendacott $n = 26$	Dart $n = 122$	Culm $n = 64$	Upper Exe $n = 31$	Exe $n = 115$
Mean	87	89	75	88	84	80	71	82
Median	80	91	88	85	80	75	71	84
Sorting	85	89	82	88	80	70	71	83

presented. In common with the Ed_{50} data in Table 3.3, the generally negative correlation coefficients are indicative of a systematic intra-storm trend, rather than a random variation through the hydrograph.

Mann–Whitney U-test analysis of the statistical significance of the intra-storm variability in the EPSD is summarized in Table 3.5. Using this test it is possible to identify if the EPSD of replicate measurements from two sample sets have been taken from a common statistical population. Accordingly, for each storm event, comparisons were made between the values of the mean and median EPS, as well as the degree of sorting for all possible pairs of the replicate sample sets comprising the periodic intra-storm deployments of the Par-Tec equipment. The data presented in Table 3.5 demonstrate that, for all the study sites, the EPSD measured during each periodic intra-storm deployment was in the majority of cases statistically significantly different in all three tested parameters from the EPSD measured during the remaining periodic deployments in the storm event.

3.4.4 Inter-Storm and Seasonal Variability in the EPSD and Associated DOA

From the data presented in Table 3.2 it is evident that there is significant inter-storm variability of both the EPSD and DOA of fluvial suspended sediment in the study area. At every study site, each storm event is characterized by a unique mean storm-period value of Ed_{50}, and intra-storm range in Ed_{50} and DOA, with an inter-storm range in the mean storm-period Ed_{50} of between 4.1 μm (Upper Exe) and 29.4 μm (Culm). Similarly, with only one exception (R. Culm 13/09/93 and 25/05/94), the mean storm-period value of the DOA is unique to each event, with an inter-storm range of between 14.4% (Upper Exe) and 66.3% (Culm).

Mann–Whitney U-test analysis of the statistical significance of the inter-storm variability in the EPSD is summarized in Table 3.6. For each study site, all possible comparisons were made between the intra-storm periodic data sets for the mean

TABLE 3.6
Results of Mann–Whitney U-Test Analysis Showing the Percentage of Statistically Significant Differences (0.05 Confidence Level) Determined Between the Mean, Median, and Degree of Sorting of the Inter-Storm Data

Parameter	Clyst $n = 3$	Jackmoor Brook $n = 10$	Yendacott $n = 3$	Dart $n = 15$	Culm $n = 10$	Upper Exe $n = 6$	Exe $n = 45$
Mean	67	60	67	47	70	50	62
Median	100	60	67	40	60	17	62
Sorting	67	70	67	60	80	50	53

and median effective particle size, as well as the degree of sorting. This analysis indicates that in the majority of cases inter-storm variation in the EPSD is a statistically significant phenomenon. The generally lower degree of significance in Table 3.6, relative to that in Table 3.5 can be explained by reference to the greater degree of variability within the intra-storm periodic data sets (Table 3.6), compared to the magnitude of variation within the replicate sets comprising the periodic measurements through an individual storm event (Table 3.5).

Seasonal variation in the factors controlling sediment mobilization and transport (e.g., rainfall intensity, variable source area, and land use), as well as the biological and physicochemical processes that may control aggregation (e.g., microorganism activity, water chemistry, water and soil temperature, suspended sediment concentration, and velocity and turbulence within the water column) can be expected to be important determinants of the inter-storm variations in EPSD and DOA summarized in Table 3.2. In this context, the measurements made on consecutive days in the Upper Exe and Exe study sites on the December 19 and December 20, 1993 provide an opportunity for investigating the magnitude of nonseasonally influenced inter-storm variation in the EPSD and DOA of suspended sediment in the study area. From Table 3.2 it can be seen that at both sites the median EPSD of the second event is characterized by a general reduction in Ed_{50}, both on average, and in range. This trend is also exhibited by the DOA data for the Exe, although in the case of the Upper Exe the second event is characterized by an increase in aggregation. The general fining in the EPSD was also associated with a similar trend in the APSD, such that the silt/clay ratios of the EPSD for the two events were 24.7 and 21.4 for the Upper Exe, and 17.0 and 10.0 for the Exe, while the associated values for the APSD were 16.6 and 12.3 for the Upper Exe, and 10.7 and 8.4 for the Exe, respectively.

The inter-storm range in Ed_{50} at both sites, and also in the DOA in the case of the Exe is, however, relatively small and not statistically significant when assessed by Mann–Whitney U-test analysis (0.05 level). This phenomenon is illustrated more fully in Figure 3.4 which presents the event mean EPSDs for both sites (the mean

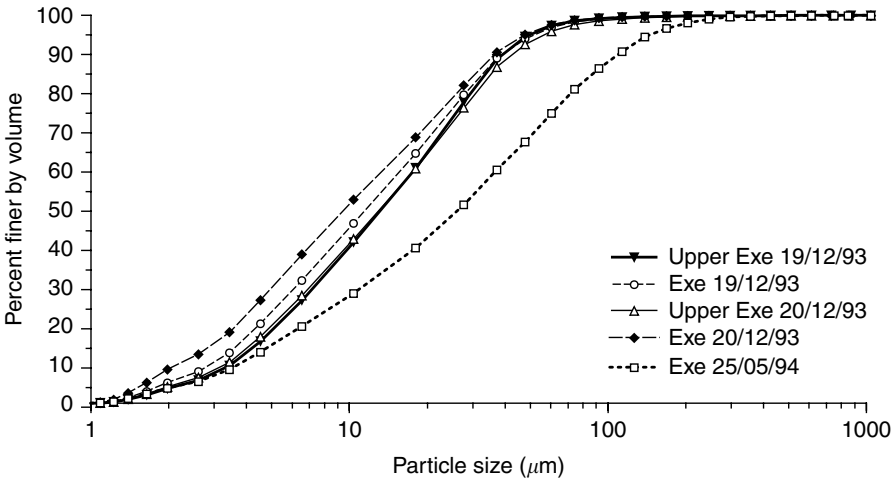

FIGURE 3.4 Inter-storm variation in the EPSD on the Upper Exe at Pixton, and the Exe at Thorverton.

of the full EPSD for each periodic measurement), together with the mean EPSD for a summer event on the River Exe (no summer sample available for the Upper Exe). The greater difference between the summer and winter events on the River Exe, relative to the two consecutive winter events, clearly necessitates a consideration of the relative importance of inter-storm variations in the EPSD and DOA over seasonal time scales.

Figure 3.5 presents the storm-period mean values of Ed_{50} and the DOA for all study sites plotted against the Julian day (day 1 being January 1) of the storm event. A clear seasonal trend is evident in both data sets, with the Ed_{50} and DOA being at a minimum during the mid-winter period of December and January (days 335–331), increasing through the spring to a summer–autumn (May to October; days 121–304) maxima before a general reduction in both parameters is evident toward winter.

The statistical significance of the observed seasonality in the EPSD and DOA of the study sites was assessed by Mann–Whitney U-test analysis of the summer/autumn and winter/spring values of mean and median effective particle size, as well as the degree of sorting, and the DOA. Analysis was restricted to those sites considered to have a sufficient seasonal range in samples (all except the River Clyst, Upper Exe, and River Creedy, with data from the Jackmoor Brook and Yendacott being amalgamated to be representative of the Jackmoor Brook as a whole). This analysis established that for both the EPSD and DOA there was a significant difference (0.05 level) in all three variables between the summer/autumn and winter/spring grouped data sets. The lack of a statistically significant seasonal difference in the three parameters for the seasonally grouped APSD data emphasizes the importance of seasonal variability in aggregation in influencing the patterns described above.

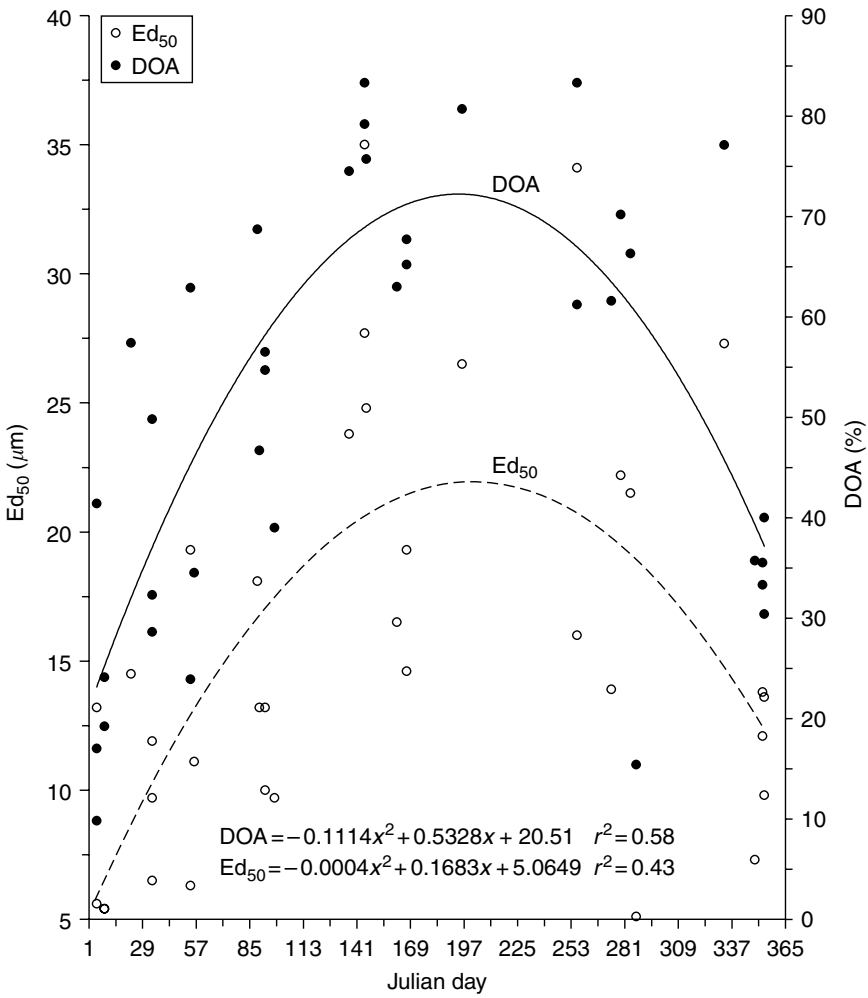

FIGURE 3.5 Seasonality in the magnitude of the storm-period mean values of Ed_{50} and the DOA at all sites.

The scatter in the relationships depicted in Figure 3.5 reflects in part spatial variation in the EPSD dynamics of the different rivers in the study area. Figure 3.6(a) and (b) present data for the study site at Thorverton on the River Exe only, this being the study site with the most complete seasonal data set and from which seasonality in the EPSD and DOA can best be considered without the additional influence of spatial variations in the data. In both Figure 3.6(a) and (b) the strength of the seasonal trend in the storm event mean value of both Ed_{50} and DOA, as described by the value of r^2 for the polynomial relationship, is higher than that determined for the study area as a whole in Figure 3.5. Similarly strong seasonal trends are evident for the maximum and minimum storm event values of Ed_{50} and DOA that are also shown in

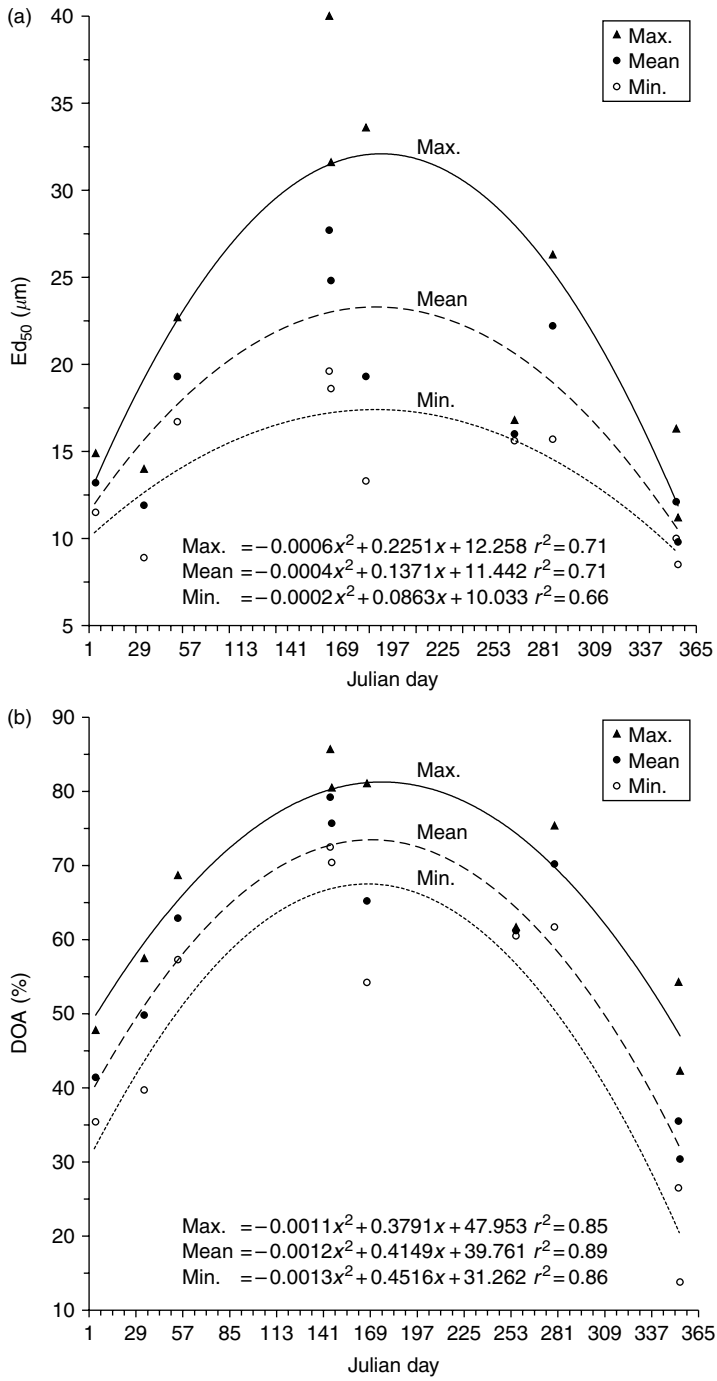

FIGURE 3.6 (a) Seasonality in the magnitude of the storm-period mean, minimum and maximum value of Ed_{50} for the River Exe at Thorverton and (b) seasonality in the magnitude of the storm-period mean, minimum and maximum value of the DOA for the River Exe at Thorverton.

Figure 3.6(a) and (b). These data, together with those of Figure 3.5, demonstrate that seasonal variations in the EPSD and DOA are significant phenomena, and add a further temporal dimension to any attempt to characterize the hydrodynamic properties of fluvial suspended sediment in the study area.

3.4.5 Effective Particle Density

Temporal variations in the DOA have been demonstrated to be the major determinant of the EPSD of fluvial suspended sediment in the study area. The significance of aggregation upon the second key hydrodynamic property of fluvial suspended sediment in the study area, namely, particle density is considered below.

Figure 3.7 presents the results of the five quantitative assessments of EPD undertaken using the Par-Tec 200 laser backscatter probe and the Valeport (SK110) BWT. These data indicate that the median EPD of all samples is considerably less than the ca. 2.65 g cm^3 that could be expected from a dispersed sample of mineral sediment with the same size distribution. Furthermore, an inverse size/density relationship is apparent, which is in accordance with that previously reported for fluvial suspended sediment.[11,18,21]

When considering the significance of the EPD data presented in Figure 3.7 to the intra-storm and seasonal variations in effective particle size described above, it should be noted that the relationship between effective particle size and density presented in Figure 3.7 is generalized both spatially and temporally. With this caveat in mind, it is reasonable to conclude that EPD will vary significantly throughout the study area, both at the intra-storm and seasonal temporal scales. For example, application of the power function contained in Figure 3.7 to the Ed_{50} data in Table 3.2 results in an intra-storm range in EPD of between 0.01 g cm^3 (Upper Exe, 19/12/93, 20/12/93, and 03/02/94 and Exe 13/09/93) and 0.35 g cm^3 (Jackmoor Brook 08/04/94), with a study area average intra-storm range of 0.10 g cm^3. Seasonal variation in EPD is illustrated in Figure 3.8 which presents the estimated mean storm-period EPD using the power

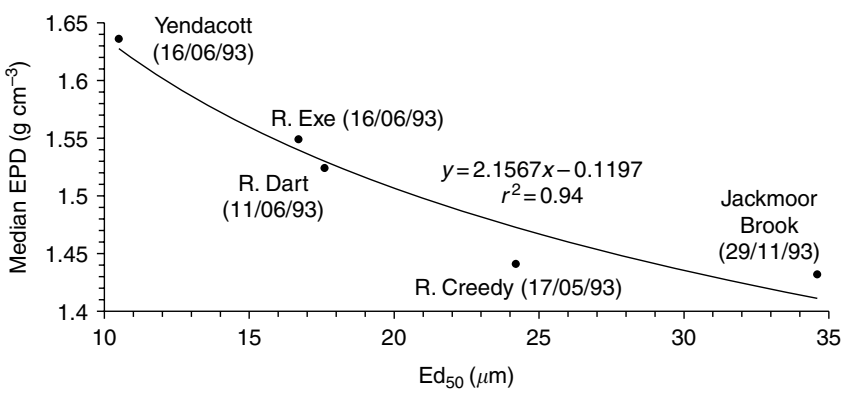

FIGURE 3.7 The inverse relationship between median effective particle size and median particle density determined for the study area.

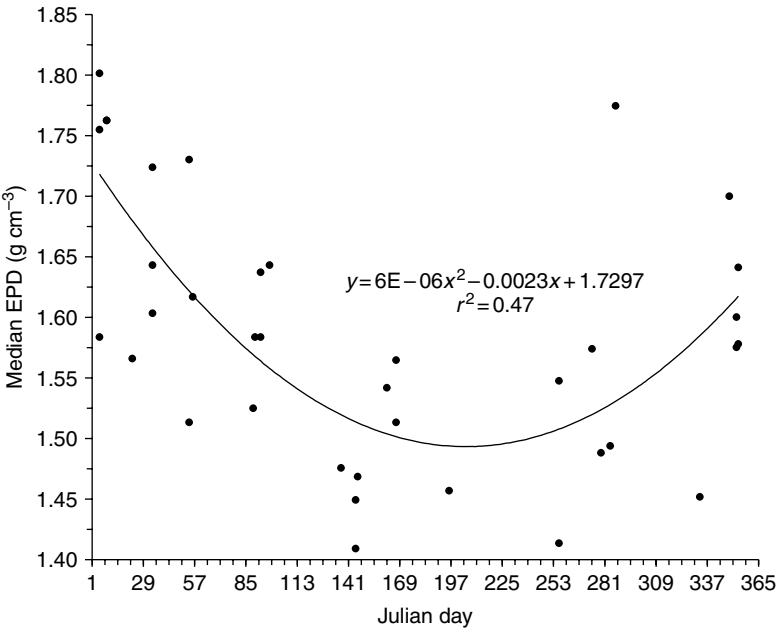

FIGURE 3.8 Estimated seasonal variation in effective particle density for the combined study site data set.

function contained in Figure 3.7. As would be expected, the trend approximates the inverse of the seasonal trend in EPS, with EPD being a minimum during the summer–autumn period.

3.5 SOURCES OF AGGREGATED SEDIMENT IN THE EXE BASIN

Detailed consideration of the origin of the composite particles comprising the EPSD in the study area is beyond the scope of this chapter. However, data obtained from Jackmoor Brook during the storm event of April 8, 1994 do provide an important insight into this issue. Measurements were made of the EPSD and DOA of four suspended sediment samples comprising runoff from slopes draining to the channel. The samples were collected from four cultivated fields immediately prior to the commencement of the detailed *in situ* measurements in the stream at this site, using 500 ml wide-mouthed bottles. EPSD measurements were made on-site using the Par-Tec 200, with the chemically dispersed APSD of each sample being determined subsequently in the laboratory. The EPSD of all four runoff samples evidenced aggregation, with a mean Ed_{50} of 13.5 μm and DOA of 64.9%. The APSDs of the runoff and stream samples were virtually identical, with mean values of Ad_{50} of 4.2 μm and 4.3 μm, respectively. These results suggest that external slope processes

are potentially important determinants of the EPSD and DOA of fluvial suspended sediment in the study area.

Phillips and Walling[33] have described the aggregated nature of fine-grained bed sediment at the River Dart, Jackmoor Brook, River Exe, and River Culm study sites within the Exe Basin, with the EPSD of fine-grained bed sediments being consistently coarser than that of suspended sediment at these sites. Furthermore, when resuspended, the EPSD of the bed sediments was shown to become finer in response to the break up of composite particles. This phenomenon is likely to be of greatest importance to the EPSD of ambient suspended sediment during the rising limb of the hydrograph when the bed sediment is resuspended, as critical bed shear-stresses are first exceeded. In this context, the observed intra-storm trend of a fining of the EPSD through the hydrograph (Figure 3.3(a) and (b) and Table 3.2) may be hypothesized to result, in part, from the resuspension and subsequent break up of highly aggregated fine-grained bed sediments.

Phillips and Walling[33] also identified a seasonal trend in the EPSD and associated DOA of resuspended fine-grained bed sediments that essentially mirrored that of the suspended sediment described in this study. Given their considerably coarser EPSD, it is reasonable to conclude that resuspended fine-grained bed sediments may be an important variable in determining the observed seasonal variation in the EPSD and DOA of fluvial suspended sediment in the study area.

3.6 CONCLUSION

The effective particle size distributions of fluvial suspended sediment collected at eight study sites in the Exe Basin have been shown to be characterized by a significant degree of aggregation. Intra-storm variation in the effective particle size distribution was measured in all 37 of the sampled storm events and the magnitude of this variation was closely related to the degree of aggregation of the suspended sediment. The pattern of intra-storm variation was characterized by a relatively systematic reduction of both the median effective particle size, and degree of aggregation through the hydrograph. Inter-storm variation in the effective particle size distribution was not significant over periods of days, however seasonal variations in the effective particle size distribution and degree of aggregation dominate the effective particle size regime of the study area, with both parameters being at a maximum during the summer/autumn period.

The effective particle density of suspended sediment was reduced relative to that which could be expected from a single mineral grain, and evidenced an inverse relationship between effective particle size and effective particle density. Temporal variations in effective particle density have been considered and it is possible to infer that particle density typically increases through an individual runoff event, while seasonally EPD may also vary, being at a minimum during the summer/autumn period.

If more widely applicable, the dynamic nature of the effective particle size regimes identified in this study has important implications for the characterization of fluvial suspended sediment particle size regimes. In particular, and of particular significance for the modeling of suspended sediment transport, measurement strategies must be appropriate and detailed enough to encompass significant intra-storm and seasonal

variation in the effective particle size distribution and degree of aggregation of fluvial suspended sediment. Finally, further research is needed to elucidate more fully the origin of the composite particles comprising the effective particle size distribution of storm-period suspended sediment. In particular, it is important to establish the extent to which aggregation reflects dynamic flocculation within the water column during the storm event or "inherited" aggregation from preexisting flocs/aggregates derived from in-channel and catchment slope sediment sources.

ACKNOWLEDGMENTS

The support of the U.K. Natural Environment Research Council in providing a Research Grant (D.E.W.) and a Research Studentship (J.M.P.) for work on the effective particle size characteristics of fluvial sediment is gratefully acknowledged. Thanks are also extended to the Environment Agency for their cooperation in the provision of precipitation data for the Exe Basin, and stage data for the River Exe at Pixton and Thorverton, and the River Creedy at Cowley.

REFERENCES

1. Meybeck, M., *Les fleuves et le Cycle Geochimique des Elements*, These de Doctorat d'Etat, Universite Pierre et Marie Curie, Paris, 1984.
2. Walling, D.E., Webb, B.W., and Russell, M.A., Sediment-associated nutrient transport in U.K. rivers, in *Freshwater Contamination*, Proceedings of Rabat Symposium S4, April–May 1997, IAHS Publ. No. 243, 1997.
3. Walling, D.E. and Webb, B.W., Suspended load in gravel-bed rivers: UK experience, in *Sediment Transport in ravel Bed Rivers*, C.R. Thorne, J.C. Bathurst, and R.D., Hey, Eds., Wiley, Chichester, 1987, 691.
4. Wolman M.G. and Miller, J.P., Magnitude and frequency of forces in geomorphic processes, *J. Geol.*, 68, 54–74, 1960.
5. Megnounif, A., Terfous, A., and Bouanani, A., Production and transport of suspended sediment transport in the Upper-Tafna river basin (North West Algeria). *Revue des Sciences de l'Eau* 16 (3), 369–380, 2003.
6. Acornley, R.M. and Sear, D.A., Sediment transport and siltation of brown trout (*Salmo trutta* L.) spawning gravels in chalk streams, *Hydrol. Process.*, 13, 447, 1999.
7. Richards, C. and Bacon, K.L., Influence of fine sediment on macroinvertebrate colonization of surface and hyporehic stream substrates, *Great Basin Naturalist*, 54, 106, 1996.
8. Clark, E.H., Haverkamp, J.A., and Chapman, W. *Eroding Soils: the Off-farm Impacts*, The Conservation Foundation, Washington, DC, 1985.
9. Droppo, I.G. and Ongley, E.D., Aggregation of suspended sediment in rivers of Southeastern Canada, *Water Res.,* 28, 1799, 1994.
10. Droppo, I.G., Jeffries, D., Jaskot, C., and Backus, S., The prevalence of freshwater flocculation in cold regions: A case study from the Mackenzie River Delta, northwest territories, Canada, *Arctic*, 51 (2), 155, 1998.
11. Petticrew, E.L. and Droppo, I.G., The morphology and settling characteristics of fine-grained sediment from selection of Canadian rivers, *in Contributions to the*

International Hydrological Programme V by Canadian Experts, IHP-V Technical Documents in Hydrology, No 33, pp 111, UNESCO, Paris, 2000.
12. Phillips, J.M. and Walling, D.E., Measurement *in situ* of the effective particle-size characteristics of fluvial suspended sediment by means of a field-portable Laser backscatter probe: Some preliminary results, *Mar. Freshwater Res*., 46, 349, 1995a.
13. Walling, D.E. and Woodward, J.C., Effective particle size characteristics of fluvial suspended sediment transported by lowland British rivers, in *The Role of Erosion and Sediment Transport in Nutrient and Contaminant Transfer*, Proceedings of Waterloo Symposium, July 2000, IAHS Publ. No. 263, 2000, 129.
14. Woodward, J.C., Porter, P.R., Lowe, A.T., Walling, D.E., and Evans, A J., Composite suspended sediment particles and flocculation in glacial meltwaters: Preliminary evidence from Alpine and Himalayan basins, *Hydrol. Process.*, 16 (9), 1735, 2002.
15. Droppo, I.G., Rethinking what constitutes suspended sediment, *Hydrol. Process.*, 15 (9), 1551, 2001.
16. Droppo, I.G., Leppard, G.G., Flannigan, D.T., and Liss, S.N., The freshwater floc: A functional relationship of water and organic and inorganic floc constituents affecting suspended sediment properties, *Water Air Soil Pollut*., 99, 43, 1997.
17. Lick, W. and Huang, H., Flocculation and the physical properties of flocs, in *Nearshore and estuarine cohesive sediment transport*, A.J. Mehta, Ed., Coastal and Estuarine Studies, 42, Amer. Geophys. Union, Washington, DC, 1993, 21.
18. Droppo, I.G., Walling, D.E., and Ongley, E.D., The influence of floc size, density and porosity on sediment and contaminant transport, *in The Role of Erosion and Sediment Transport in Nutrient and Contaminant Transfer.* IAHS Publ. No. 263, Reading, IAHS Press, 2000, 141.
19. Kranck, K., Experiments on the significance of aggregation in the settling of fine-grained sediment in still water, *Can. J. Earth Sci.*, 17, 1517, 1980.
20. Lau, Y.L. and Krishnappan, B.G., *Measurements of Size Distributions of Settling Flocs*, NWRI Contribution No. 97–223, National Water Research Institute, Burlington, Ontario, Canada, 1997.
21. Tipping, E., Woof, C., and Clarke, K., Deposition and resuspension of fine particles in a riverine "dead zone", *Hydrol. Process*., 7, 263, 1993.
22. Skvortsov, A.F., River suspensions and soils, *Sov. Soil Sci*., 4, 409, 1959.
23. Droppo, I. G. and Ongley, E.D., Flocculation of suspended solids in Southern Ontario rivers, in *Sediment and the Environment*, R.J. Hadley and E.D. Ongley, Eds., IAHS Publ. No. 184, 1989, 95.
24. Sinawi, G. and Walling, D.E., The characteristics of composite suspended sediment particles transported during storm events in the River Exe, Devon, U.K., *Geomorphologie*, 2, 29, 1996.
25. Gibbs, R.J., Floc breakage by pumps, *J. Sediment Petrol.*, 51, 670, 1981.
26. Phillips, J.M. and Walling, D.E., An assessment of the effects of sample collection, storage and resuspension on the representativeness of measurements of the effective particle size distribution of fluvial suspended sediment, *Water Res.*, 29 (11), 2498, 1995b.
27. Horowitz, A.J., *A Primer in Sediment-Trace Element Chemistry*, (2nd edition), Lewis, Chelsea, MI, U.S., 1991, 136.
28. Phillips, J.M. and Walling, D.E., Calibration of a Par-Tec 200 laser back-scatter probe for in situ sizing of fluvial suspended sediment, *Hydrol. Process*., 12, 221, 1998.
29. Walling, D.E. and Kane, P.W., Suspended sediment properties and their geomorphological significance, in *Catchment experiments in Fluvial Geomorphology*, T.P Burt and D.E. Walling, Eds., Geobooks, Norwich, 1984, 311.

30. Walling, D.E. and Moorehead, P.W., The particle size characteristics of fluvial suspended sediment: an overview, *Hydrobiology*, 176/177, 125, 1989.
31. Gibbs, R.J., Matthews, M.D., and Link, D.A., The relationship between sphere size and settling velocity, *J. Sediment. Petrol.*, 41 (1), 7, 1971.
32. Buller, A.T. and McManus, J., Simple metric sedimentary statistics used to recognise different environments, *Sedimentology*., 18, 1, 1972.
33. Phillips, J.M. and Walling, D.E., The particle size characteristics of fine-grained channel deposits in the River Exe Basin, Devon, U.K. *Hydrol. Process.*, 13, 1, 1999.

4 The Composite Nature of Suspended and Gravel Stored Fine Sediment in Streams: A Case Study of O'Ne-eil Creek, British Columbia, Canada

Ellen L. Petticrew

CONTENTS

4.1 INTRODUCTION

In the past decade there has been a concerted research emphasis on the structure, settling, and storage of suspended sediments in freshwater riverine environments.[1–5] This body of work has recognized the significance of flocculation and aggregation (terms which are used interchangeably in the literature) in riverine sediment transport processes, and the concomitant implications for the storage of both sediments and

1-56670-615-7/05/$0.00+$1.50

sediment-associated contaminants. While the mechanisms and factors regulating flocculation, defined as the combination of two or more particles of mineral or organic material to create larger composite particles, have been research interests in the marine literature for decades they were only reported as being significant in natural freshwater systems in the 1990s.[6–8] While the process of flocculation increases both the effective size of the particle and modifies its density it has been shown that the propensity for particle settling is influenced more by the particles altered size rather than its density or porosity.[5]

While the literature details the conditions or mechanisms which promote the flocculation and aggregation of sediments in rivers (increased sediment concentrations, increased collision encounters, decreased shear velocities, high ionic strength, increased bacterial activity, and increased temperatures) there has also been some effort in the literature to subdivide composite particles into two separate populations comprising flocs and aggregates. Different processes and different composite structures have been suggested as a means to differentiate flocs and aggregates. Petticrew and Droppo[9] differentiated flocs and aggregates by visual evaluation, with flocs being characterized as irregularly shaped and porous while aggregates appeared opaque and compact. It was postulated by them, and reiterated by Woodward et al.[10] that the sources of the two structures were different with the fragile, loosely bound flocs being formed in the water column while aggregates are delivered to the stream from the catchment as robust, compact particles. Petticrew and Droppo[9] also considered the fact that the floc structures stored in or on the gravels could be dewatered and potentially become more compact due to biological processes or physical reworking. Droppo et al.[11] have proposed a floc cycle for riverine composite particles that suggested a downsizing and consolidation of particles with increased exposure to bed shearing environments, indicating a change in structure over time spent in the river system. While it may be important to determine the source of the composite types it is also of interest to determine the relative abundance of aggregates and flocs in the stream channel and to determine if they behave differently in the context of settling and storage.

The objective of this chapter is to evaluate the morphology, settling behaviour, and characteristics of composite sediments that are transported and stored in a relatively undisturbed productive headwater stream. A case study of a highly productive salmon bearing stream is presented here with both the hydrologically important and biologically important periods of the open water season being investigated over several years. The focus of this chapter is the relationship of these changing environmental conditions with the sediment particle populations in both the water column and gravel storage. The changes in composite particle morphology and their resultant dynamic characteristics (settling rate and densities) were evaluated temporally over a range of open water conditions (May through October) while both the physical environment (suspended sediment load, stream velocities, and shear stresses) and the biological inputs to the stream changed.

Earlier work on O'Ne-eil Creek, reporting on the structure and composition of suspended and gravel stored sediment, indicated that in these biologically active headwater streams the fines (sediments $< 63\mu$m) were well flocculated.[3,12] The aggregates or flocs exhibited maximum sizes 7 (suspended) to 14 (gravel stored) times greater

than the maximum size of the constituent inorganic material comprising the composite structures.[3] Petticrew and Droppo[9] visually identified different composite structures and observed that these loosely bound flocs and compact aggregates exhibited different settling behaviors and size ranges. As these data were collected during the 1996 die-off of 10,722 sockeye salmon (*Oncorhynchus nerka*) that had returned to the stream to spawn, follow-up work was undertaken to evaluate the importance of the biological and physical influence of the fish upon the morphometric and dynamic properties of the sediment.

The hydrologically important period in terms of sediment transport in streams of this region is the spring melt which occurs in late May. High flows on the rising limb of this flood event scour and break down the armoured layer in this creek[13] mobilizing the supply of channel surface and gravel stored fine sediment. Terrestrial contributions from the floodplain and from the headwater slopes are also observed during this event. Cyclonic summer storms can also generate high intensity rainstorms which act to move sediment into and within the channel. The high flow spring melt events exhibit increased concentrations of suspended fine sediment, increased local shear stresses, and contributions of organic matter which are predominantly terrestrially derived. It was of interest to determine the resultant size, structure, and settling behavior of the composite particle population generated by these interacting set of factors.

Alternately the influence of the dominant biological influence in the stream was of concern, as this stream can have annual sockeye returns of up to 50,000, although on average it receives approximately 10,000 per year.[13] The physical effect of the digging of redds, or egg nests dug to about 25 cm into the gravels, is to both modify the surface morphology of the gravel bed and to resuspend the gravel stored fines,[14] possibly many times in one spawning season. Following this major physical disturbance of both the gravels and the water column, the fish die in the stream and decay in the late summer low flows. The flux of organic matter to the stream is immense and abrupt[15,16] as these salmon spawn in only the lower 2 km of the channel and die in a period of about 10 days, resulting in a high unit area loading of fish breakdown products. Petticrew and Arocena[17] observed a chemical signature of salmon flesh in the gravel stored sediments, indicating that either the breakdown products or bacteria with the salmon signature are associated with the fine grained gravel stored aggregates. Given the potential role of organic matter and microbial activity in the generation of composite particles this highly productive stream was seen as a good venue to evaluate the effect of both the supply of organic matter and the physical disturbance of spawning on the structure of flocs and aggregates being transported and stored in streams.

4.2 METHODS

4.2.1 Study Area

The O'Ne-eil Creek catchment is approximately 75 km^2 and is located in an experimental forest in the central interior of northern British Columbia. It is a tributary to the Middle River which drains into the Stuart Lake system which is well known for its highly productive sockeye salmon runs. Fish escapements to streams in this region,

including O'Ne-eil, have been monitored using counting fences for nearly 50 years. The O'Ne-eil catchment drains part of the Hogem Range of the Omenica Mountains, and has its mouth at 700 metres above sea level (masl) and its drainage divide at approximately 1980 masl.[18] The channel is approximately 20 km in length with a steep upper reach which drains well-developed cirques, a steeper middle reach that passes through a rock-walled canyon, and a gentle, low gradient depositional reach in the lower 2 km.[19] In the lower reaches of the stream, the channel bed is comprised of clean gravel with very low concentrations of fine sediments, well suited for salmon redds. This lower reach is underlain by fine grained glaciolacustrine sediments and the only anthropogenic disturbance to date consists of a road (constructed in 1980) which cuts through this material. This road bridges the stream and allows access approximately 1500 m upstream of the river mouth. There has been no harvesting in the catchment, so the system represents a nearly pristine environment.

4.2.2 Field Methods

Data collected over five seasons of sampling are presented here comprising various periods of 1995, 1996, 1997, 2000, and 2001. Within each year various hydrological or biological events were sampled including spring melt floods, active salmon spawning, post-spawning die-off, and low flows when no visual evidence of adult fish were evident, which in this chapter is called post-fish, were represented. Table 4.1 identifies the events, the conditions, and the variables that were collected each year. The conditions of sampling are characterized as either "ambient" or "resuspended" with ambient conditions representing the undisturbed, natural suspended sediment concentration conditions. In order to characterize the gravel stored fine sediment, a resuspension technique that was an attempt to rework the surface gravels using approximately the same energy expended by spawning salmon, was used. Several minutes after the collection of the ambient sample, a second sample of suspended sediment was taken, following the disturbance, or mixing, of the top layer (0.04 to 0.06 m) of gravels by a field assistant, positioned 3 to 5 m upstream of the collection site. This distance provided sufficient travel time for the resettling of heavier sand particles thereby allowing the collected material to comprise the aggregated fine sediment stored within the surface gravel matrix. In this chapter, that material is termed "resuspended gravel stored fines."

Stream velocities and depths at the time of sampling were determined using a Swoffer current meter and are presented in Table 4.1.

4.2.3 Suspended Sediment Measurements

Stream water with suspended sediment was collected approximately 10 cm below the surface of the water in several large mouthed 1 l Nalgene bottles for the determination of

(i) suspended particulate matter (SPM) concentration
(ii) the disaggregated or absolute particle size distribution (APSD)
(iii) the aggregated or effective particle size distribution (EPSD)
(iv) morphometric characteristics of the aggregated suspended sediment population
(v) the fractal dimensions of the filtered particle population

TABLE 4.1
O'Ne-eil Creek Sampling Schedule, Conditions and Variables for Five Sample Years

Year	Date	Event type	Conditions sampled	Cumulative fish return	SPM (mg l^{-1})	Water depth (m) and velocity (m s^{-1})	SPM filter fractals	Settling chamber sizing	Settling chamber visual characterization
1995	Aug. 2	Active spawn	Ambient	26,456	11.70	0.20/0.26	N[a]	Y[b]	N
1996	Aug. 26	Die-off	Ambient	10,772	0.93	0.22/0.23	Y	N	N
			Resupended gravel stored fines	10,772	7.22	0.22/0.23	Y	Y	Y
1997	May 28	Spring melt rising limb	Ambient	0	8.38	0.70/1.04	Y	Y	N
	May 30	Spring melt rising limb	Ambient	0	6.79	0.77/1.59	Y	Y	N
	Jun. 1	Spring melt rising limb	Ambient	0	8.70	1.40/1.28	Y	Y	N
2000	Aug. 10	Active spawn	Ambient	10,601	2.47	0.22/0.31	N	Y	Y
			Resupended gravel stored fines	10,601	15.73	0.22/0.31	N	Y	Y
2000	Aug. 12	Active spawn	Ambient	10,709	3.76	0.21/0.28	Y	N	N
			Resupended gravel stored fines	10,709	7.12	0.21/0.28	Y	N	N
2000	Sep. 21	Post-fish	Ambient	10,890	0.69	0.26/0.35	Y	N	N
			Resupended gravel stored fines	10,890	15.48	0.26/0.35	Y	N	N
2000	Oct. 5	Post-fish	Ambient	10,890	1.00	0.20/0.29	Y	Y	Y
			Resupended gravel stored fines	10,890	20.89	0.20/0.29	Y	Y	Y
2001	Jul. 17	Pre-fish arrival	Gravel stored fines	0			Y	Y	N
2001	Jul. 28	Early spawn	Gravel stored fines	8,211			Y	Y	N
2001	Aug. 3	Mid-spawn	Gravel stored fines	10,931			Y	Y	N
2001	Aug. 12	Die-off	Gravel stored fines	13,757			Y	Y	N
2001	Aug. 16	Die-off	Gravel stored fines	13,892			Y	Y	N
2001	Sep. 22	Post-fish	Gravel stored fines	13,893			Y	Y	N

[a] N = no samples analyzed.
[b] Y = yes, samples analyzed.

The water samples were returned to the laboratory and processed in a variety of ways. SPM was determined gravimetrically by filtering a known volume of water (commonly 1000 to 4000 ml, depending on concentration) onto preweighed and preashed 47 mm diameter glass fiber filters. A second, smaller volume (100 to 1000 ml) was filtered through preweighed 0.8 μm Millipore cellulose-acetate filters. These were used for determining the disaggregated inorganic grain size distribution also known as the ASPD. The weighed, dried filters were ashed in a low-temperature asher (<60°C) and wet digested with an excess of 35% H_2O_2 before analysis on a Coulter counter.[20] A Coulter Multisizer IIE was used to determine the ASPD. Results are expressed as a volume/volume concentration in ppm and are plotted as smoothed histograms of log concentration versus log diameter.[20] The Multisizer was set to a lower detection limit of 0.63 μm and an upper detection limit of 1200 μm.

The EPSD was determined by filtering smaller volumes of water (10 to 100 ml, depending on the sediment concentration) through 0.45 μm Millipore filters at low levels of suction (<80 kPa). Care in handing the collected water and in the filtering process ensured minimal disturbance to the aggregate structures. EPSD was measured optically, using a method similar to that of de Boer[21] and reported in Biickert.[22] These filters were air dried, cut and mounted onto microscope slides to obtain particle morphometrics using the BioQuant OS/2 image analysis system which was connected to a microscope. The filtered particles were counted and characterized for perimeter, area, long axis, equivalent spherical diameter (ESD) and circularity. The population of particles counted per filter was in excess of 1000 and in most cases triplicate filters were analyzed to allow a determination of the variability. To obtain the ESPD, the population's equivalent spherical diameters were grouped into size classes which correspond to the same intervals as the Coulter counter and plotted as volume/volume concentration in parts per million against ESD. The lower limit of the image analysis technique when linked to the microscope is an areal size of 5.4 μm^2 and presumably the upper limit would be defined by the area of the filter visible at the given magnification setting which would be in the order of 100,000 μm^2. However as the volume of water filtered is often small, because this minimizes overlap of particles on the filter, and because the probability of capturing the larger, rarer flocs is lower due to reduced sample volume, this method tends to artificially restrict the upper limit of the size spectra. For almost all filters analyzed for this study, the maximum aggregate diameter observed was of the order of 400 μm while larger aggregated particles (>700 μm) were observed in the bigger sample volume of the same origin in the settling chamber.

The morphometric parameters collected from the image analysis of the filtered population of aggregates were used to determine the fractal dimension (D) of the populations. D is a measure of the perimeter–area relationship for a set of objects. Collections of natural objects tend to have a perimeter–area (P, A) relationship of $A \propto P^{2/D}$.[23] Euclidean objects such as squares or circles have a D value of 1. Values of $D>1$ indicate that as area increases, perimeter increases at a greater rate.[21,24] This means that these larger particles have more edge complexity and are less Euclidean or evenly shaped. Fractal D values were determined from perimeter and

area relationships for populations of filtered aggregates as well as particle populations sized and characterized in the settling chamber.

4.2.4 Settling Chamber Measurements

The collection of a larger volume of suspended sediment to determine the fall velocities and densities of suspended sediment structures employed a rectangular plexiglass settling box ($1.5 \times 0.14 \times 0.06$ m) with two removable end caps that was built to hold approximately 13 l of water. A scale was mounted on the outside back wall of the settling chamber using white adhesive paper which aided in photographing and sizing particles. The settling chamber was aligned into the stream flow such that water and suspended sediment passed through it. When a sample was required the ends were capped and the box carried in a horizontal position to the side of the creek, where it was placed vertically onto a stable platform 20 to 30 cm in front of a 35 mm single lens reflex (SLR) camera mounted on a tripod. After a period of several minutes, during which fluid turbulence decayed, a series of timed photographs were taken. Pairs of sequential images were then projected onto a large surface and examined to identify individual flocs. The particle size, shape, and position in the two images were determined using image analysis packages (Mocha and Bioquant) allowing an estimate of the fall velocity.

In the spring of 1997, the same settling chamber was used to collect suspended sediment samples from the snowmelt flood events in O'Ne-eil Creek. Due to the fast overbank flows at this time the box was lowered and returned to the bridge platform using a winch system. The box was filled and capped by persons standing in the stream. The photographic system employed in the field at this time was a video capture system. A black and white digital camera (a charged-coupled device — CCD), with a resolution of 512×512 pixels, was connected to a personal computer running Empix Imaging's Northern Exposure software. This field setup allowed an automated image grabbing system, which recorded the current time (accurate to 10^{-2} s) on each image. A run of 45 images could be grabbed in just over a 90 sec. The resultant images had individual pixel resolution of $55\,\mu\text{m} \pm 10\,\mu\text{m}$. The images were then analyzed via a custom-developed[22] settling rate measurement program.

Due to colder weather, and shorter day lengths that contributed to poor conditions for outdoor photography, the samples from October 5, 2000 were collected in the field but returned to the laboratory for analysis. In this case up to 12 l of ambient and resuspended sediment-laden water was collected and introduced into the settling chamber for analysis using the SLR camera.

Measurements of particle size and settling velocity for both the SLR and video imaging method allowed for the derivation of particle Reynolds numbers as well as particle density using the equations presented in Namer and Ganczarczyk.[25] The lower resolution of particle diameters using these techniques was approximately $150\,\mu$m while the upper limit would be defined by the field of view of the cameras, which given the distance from the settling chamber allows a photographic image of a particle with a long axis in excess of $10{,}000\,\mu$m.

4.2.5 Infiltration Gravel Bags

On July 13, 2001, twelve infiltration gravel bags were installed in two riffles near the bridge site of O'Ne-eil Creek. A hole approximately 25 cm in depth was dug and the gravels removed were cleaned through a 2 mm sieve. The bags are a modification of the design presented by Lisle and Eads[26] and consist of watertight bags, with a maximum volume of 10,000 cm^3 clamped onto a 20 cm diameter iron ring. The bag is folded down on itself at the bottom of the hole, while straps attached to the ring are placed along the sides of the hole and left at the gravel–water interface. The cleaned gravel is then returned to the hole, being placed on top of the folded bag and left for a known period of time to accumulate fine sediments in the intergravel spaces. The bag traps were retrieved over a 71-day period following installation. The retrieval dates (cf. Table 4.1) represent (i) the period before the fish return to the river to spawn (July 17), (ii) the early spawn (July 28), (iii) mid-spawn (August 3), (iv) two dates during the major fish die-off (August 12 and August 16), and (v) a sample when there was no visual evidence of live or dead carcasses in the stream, termed post-fish (September 22).

Upon retrieval a lid is placed over the surface gravels between the emergent straps that are pulled up, moving the iron ring and the bag up through the gravels ensuring a minimal loss of fine sediment. The gravels and water collected in the bags were passed through a 2 mm sieve such that the finer sediment was collected in a calibrated bucket. This material was mixed to resuspend all grain sizes, settled for 10 sec to allow the settling of large sands from the top water layer from which a 250 ml subsample was taken for use in the settling chamber. These gravel stored fine sediments were introduced into the settling chamber which was filled with filtered (0.45 μm) O'Ne-eil Creek water. The CCD digital video method of image collection was used for these samples. Around 100–250 individual particles were tracked for each set of bags, providing size and settling characteristics while larger populations ($n = 1000$ to 2500) of particles photographed in the settling chamber were used to determine morphometric characteristics of the total population of gravel stored aggregated fine sediment.

4.2.6 Visual Characterization of Aggregate Particles

The images of particles captured in the settling chamber when the SLR camera is used were very clear and distinct such that more detailed structure of individual particles could be evaluated. It was obvious upon viewing the particles for the first time in the year 1995 that some were opaque, appearing to exhibit no open pores while others were a loose and open matrix of material attached together. In some cases the aggregates were a combination of both of these forms. In 1996, we decided to label each particle that we had tracked and for which we had estimated a settling velocity, in order to determine if differences in settling behavior existed between these visual subpopulations. The compact, opaque subset was termed compact particles while the open, loose matrices were called flocs. The combination particles and those which we were unable to define were classed in a group as mixed particles. A fourth subset was added in the year 2000 as visual evaluation of the compact subpopulation indicated

that some dense, dark particles had visual indicators that they were organics or parts of organisms. For further clarity these were separated and labeled compact-organic particles.

4.3 RESULTS

The settling chamber was used for the first time in August 1995, sampling ambient water during the active spawn of a very large return of salmon (26,456) to O'Ne-eil Creek. On this first use, 23 individual particles were identified and tracked for 46 settling velocity determinations, but the data set was not characterized visually for particle type (Table 4.2). The visual identification of floc and compact particles was first undertaken and reported[9] for the 1996 settling population. When the two subpopulations (i.e., floc and compact particles) are plotted as diameter against density (Figure 4.1) it is clear that while both floc and compact particle diameters range between 300 to 1300 μm, the larger particles tend to be flocs and they exhibit lower densities. In this data set flocs with the equivalent diameter as compact particles are always of lower density. An exponential decrease of density with increasing size is apparent for the compact particle population as it exhibits a wider range of densities. Figure 4.2 shows the same general pattern for the August and October 2000 settling data. The total population of settled particles exhibits the exponential decrease in density with diameter more clearly than in the 1996 data in Figure 4.1. Note that a third set of particles, visually identified as compact-organic, is also shown here. They tend to fall into the central part of the size–density spectrum.

Table 4.2 provides a summary of particle numbers and types identified in the ambient and resuspended settling chamber runs of 1996 and 2000. Visual identification of particle types was not undertaken in 1995 or 1997. In each case

TABLE 4.2
Settling Chamber Image Analysis Characterization

Date	Event	Sample type	Number of individual particles	Percent floc	Percent compact	Percent mixed
Aug. 2, 1995	Active spawn	Ambient	23[a]	N/A	N/A	N/A
Aug. 26+27, 1996	Die-off	Resuspended	43[b]	35	23	42
May 28+30, 1997	Spring melt rising limb	Ambient	280	N/A	N/A	N/A
Aug. 10, 2000	Active spawn	Ambient	117	7	75	18
Aug. 10, 2000	Active spawn	Resuspended	113	13	77	10
Oct. 5, 2000	Post-fish	Ambient	37	14	51	35
Oct. 5, 2000	Post-fish	Resuspended	315	12	71	17

[a] 46 settling counts performed.
[b] 70 settling counts performed.

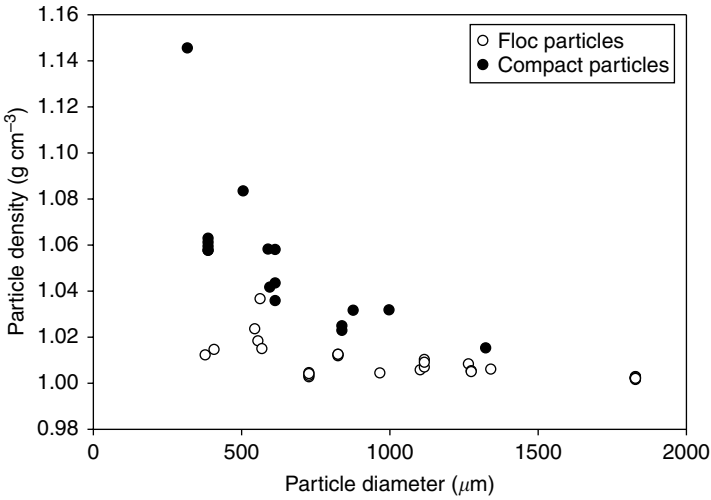

FIGURE 4.1 Size–density relationship for visually determined floc and compact particles from resuspended gravel stored sediment during the salmon die-off of 1996.

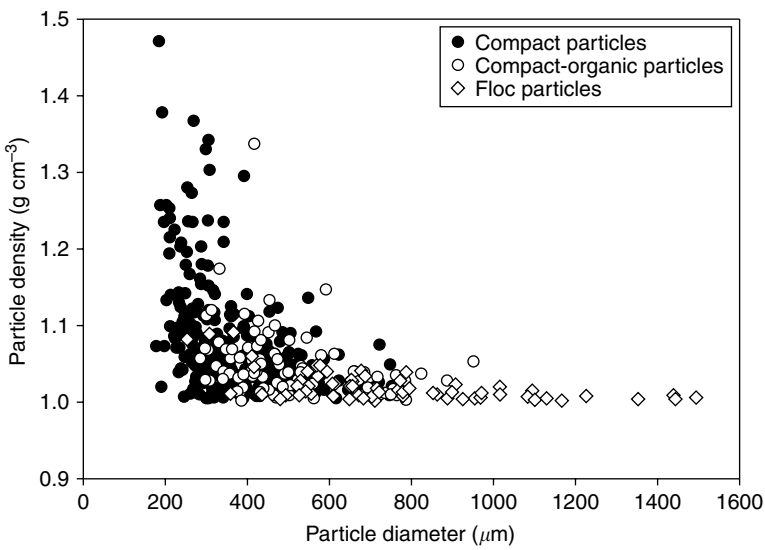

FIGURE 4.2 Size–density relationship for visually identified floc, compact and compact-organic particles from both ambient and resuspended sediment in mid- and post-spawn of 2000. Note the separation of flocs and compact particles into the arms of the distribution.

when the particle subpopulations were differentiated the proportion of flocs never comprise as much as half of the population, although the maximum value occurs in the die-off period of 1996 when 35% were identified as flocs. Of note in Table 4.2 is the proportion of compact particles observed in the resuspended sediment in the

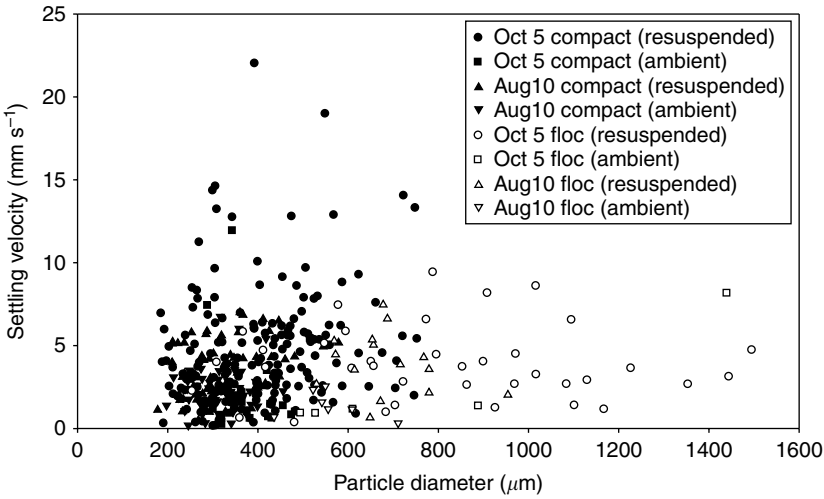

FIGURE 4.3 Settling velocities of aggregated particles observed in the ambient suspended and resuspended, gravel stored sediment in mid-spawn (August 10) and post-fish (October 5) 2000.

active spawn and post-fish samples of 2000, calculated as 77% and 71%, respectively. These values are similar to the 75% of compact particles observed in the ambient suspended sediment during the active spawn of 2000. The ambient waters of the October post-spawn period have only 51% compact particles in the suspended sediment.

When the data from August and October 2000 settling runs are plotted together the different sizes and behaviors of the two populations are apparent (Figure 4.3). The compact particles are generally smaller, all being $<760\,\mu$m and tend to exhibit the fastest settling rates with 6% actually exceeding the settling rate of 100 μm quartz sand (8.7 mm s^{-1}). The open matrix floc particles exhibit the largest sizes as indicated by the fact that all particles in excess of 760 μm are identified as flocs that generally settle at slower rates. Note that there are few large flocs in the ambient suspended sediments of both August and October, but upon resuspension of the gravel stored sediment the floc structures increase in number.

Table 4.3 summarizes the data from all available settling chamber runs and provides statistics for the particle populations' size (diameter), shape (sphericity), and density by particle type where possible. The data for the relative abundance of floc and compact particles indicates that in all but the die-off period compact particles dominate both the suspended (ambient) and gravel stored (resuspended) samples. The proportion of floc particles tracked for settling varied between 7% and 35% of the total population. The percentage of flocs exceeded the compact particles only during the fish die-off in August 1996. Once again it is clear that the compact particle sizes are significantly smaller than floc sizes, as shown by viewing both the population means and maximum diameters. The largest sizes occur in the resuspended gravel stored sediments during the fish die-off of 1996. The compact particle population mean during die-off is significantly larger ($p = 0.05$) than compact particles observed at

TABLE 4.3
Size and Density Characterisation of Settling Chamber Particle Populations

Date	Event	Sample type	Particle type	Percent of total population	Mean diameter and SE[a] (μm)	Maximum diameter (μm)	Smaller diameter % <500 (μm)	Larger diameter % >500 μm	Greater density % >1.10 g cm^{-3}	Lower density % <1.10 g cm^{-3}	Shape as sphericity and SE
Aug. 2, 1995	Active spawn	Ambient	Total population	100	514 (58.2)	1162	52	48	42	58	N/A
Aug. 27, 1996	Die-off	Resuspended	Compact	23	704 (96.6)	1323	35	65	6	94	N/A
			Floc	35	897 (107.8)	1828	6	94	0	100	N/A
May 28+30, 1997	Spring melt rising limb	Ambient	Total population	100	276 (6.5)	712	96	4	32	68	N/A
Aug. 10, 2000	Active spawn	Ambient	Compact	75	342 (8.4)	685	96	4	10	90	0.62 (0.011)
			Floc	7	564 (31.8)	711	15	85	0	100	0.47 (0.025)
Aug. 10, 2000	Active spawn	Resuspended	Compact	77	365 (13.2)	723	86	14	30	70	0.63 (0.014)
			Floc	13	685 (27.3)	954	0	100	0	100	0.56 (0.025)
Oct. 5, 2000	Post-fish	Ambient	Compact	51	384 (15.5)	515	95	5	11	89	0.67 (0.020)
			Floc	14	791 (176)	1439	20	80	0	100	0.54 (0.058)
Oct. 5, 2000	Post-fish	Resuspended	Compact	71	400 (9.5)	752	79	21	22	78	0.67 (0.007)
			Floc	12	816 (52.4)	1494	19	81	0	100	0.56 (0.020)

[a] SE = standard error shown in brackets.

any other time. The spring melt rising limb population was not visually differentiated into compact and floc particles but exhibits the lowest population particle diameter mean and its maximum particle size is similar to that of resuspended gravel stored compact particles of the active spawn of August 2000 and the post-spawn of October 2000. Note that the ambient active spawn particles (August 2000) exhibit the smallest floc and compact sizes even though water velocities are similar to those observed in September and October sampling periods (Table 4.1). In fact its maximum floc size is slightly smaller than the maximum aggregate measured in the 1997 spring melt when flows were four times as fast.

To differentiate size and density, each subpopulation was separated into size categories based on a criterion diameter of 500 μm while low density and high density particles were separated at 1.10 g cm^{-3}. These values were selected as they characterize the boundaries of the bulk of overlapping data points in Figure 4.2. In Table 4.3 the floc subpopulations are classified as large (>80% of the particles always exceed 500 μm) and low density (100% < 1.1 g cm^{-3}). Compact particle subpopulations tend to be comprised predominantly (>79%) of smaller (<500 μm) particles. The exception is the 1996 die-off when larger compact particles comprised 65% of the population with the other 35% being <500 μm. The compact particles also predominate in the high density classification with 11 to 30% of their population exhibiting densities >1.1 g cm^{-3}, excluding the 1996 post-spawn die-off when only 6% were of higher density. Compact-organic particles were not included in this evaluation of compact particles but comprised a separate subpopulation not presented in Table 4.3.

In the data sets that were also characterized for sphericity (all 2000 settling runs) all floc populations are significantly less circular than the compact particles (Table 4.3). While the floc shapes are not significantly different ($p = 0.05$) over time or by source (suspended or gravel stored) the compact particles do exhibit differences over time. The compact particles become significantly more rounded in the post-fish ambient and resuspended samples.

Fractal (D) values and their 95% confidence limits for the population of particles measured for settling velocities in 2000 are shown in Figure 4.4. A fractal value for the total population is shown for each sample date as well as the fractal value for the floc, compact and compact-organic particle subpopulations. The fractal values for the total populations indicate that there is no significant difference by source (ambient versus resuspended sediment) but there is by time, in that the suspended (ambient) sediment has significantly smaller fractal values in October than in August for the total population. Fractals for gravel stored (resuspended) sediment do not vary significantly between these dates. An evaluation of the subpopulations indicates that the floc and compact-organic particles exhibit a large amount of variation, while the compact particles have smaller confidence limits, indicating less variability in shape.

A similar fractal analysis of particles collected on filters is shown in Figure 4.5 for the years 1996 through to 2000. The sampling dates are not graphed chronologically by year, but rather grouped by date within the season so that the periods of spring melt, active spawn, fish die-off, and post-spawn can be viewed consecutively. The fractal values are lowest for the ambient suspended sediment of the spring melt period

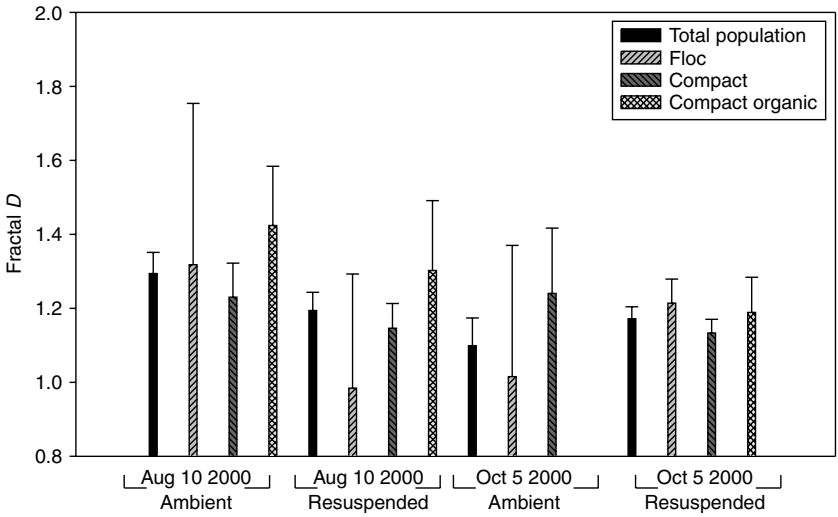

FIGURE 4.4 Fractal values for total particle populations and the visually identified subpopulations for ambient and resuspended sediment in the mid-spawn (August 10) and post-fish (October 5) periods of 2000. Error bars represent the 95% confidence intervals.

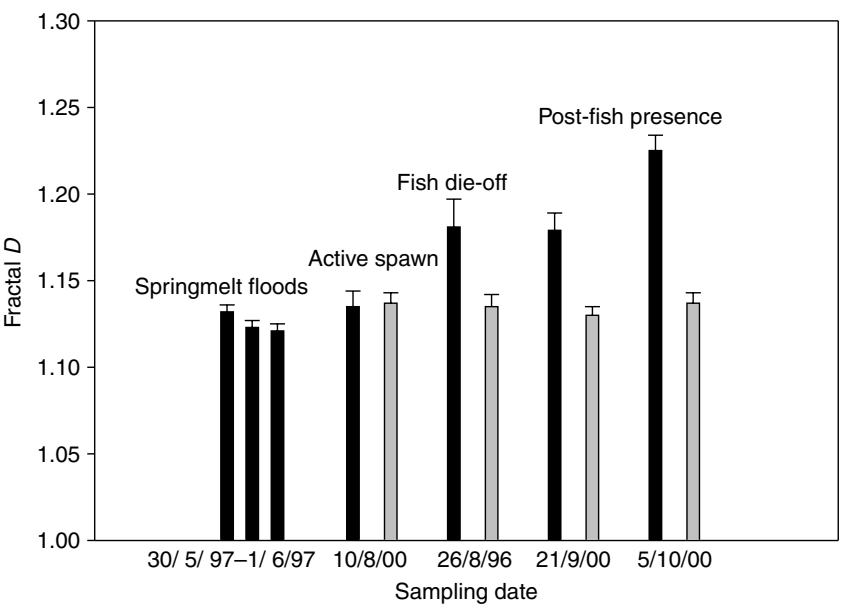

FIGURE 4.5 Fractal values for aggregates sampled and analyzed on filters over three years, comprising four different bio-physical open water conditions. Dark bars represent ambient suspended sediment conditions while lighter colored bars are resuspended, gravel stored fine sediments. Error bars represent the 95% confidence intervals.

indicating that the particles are more rounded. In contrast to the results of the settling particle fractal analysis (Figure 4.4) the *D* values for filtered suspended sediment increase later in the season, becoming significantly less rounded during fish die-off and in post-fish periods (Figure 4.5). In the active spawn sampled in August 2000, the suspended and gravel stored fractals are not significantly different from each other. These low *D* values represent more rounded particles and are similar statistically to the suspended sediment of the spring melt flood and the gravel stored samples throughout the full sampling season.

In 2001, gravel stored fine sediments collected from infiltration bags were introduced into the settling chamber and analyzed for size, shape (fractal), and settling characteristics (density). Table 4.4 shows these data along with the cumulative number of spawning fish returned to O'Ne-eil Creek by that date. Particle diameters were largest pre-fish and post-fish with the smallest mean values occurring at mid-spawn. Particle densities increased chronologically until die-off when they significantly decreased. Density increases were significant again in the post-fish sediments. The temporal pattern is that pre-spawn gravel stored aggregates are large and low density, mid-spawn aggregates are small and high density while at seasons end (post-fish) the gravel stored aggregates are again large but high density. While the fractal values for all of the infiltration bag sediments are low, the smallest *D* values, representing the roundest particles, were noted at mid-spawn and post-fish which is also when densities were highest. Figure 4.6 shows the changing pattern of fractal values over time along with a temporal plot of the cumulative spawner numbers in 2001. This indicates the number of individual fish having passed the counting fence by that date. On August 3, when 10,931 have returned to the stream to rework the gravels for redd construction the particles are more rounded than at all times except for the period when no visual evidence of fish carcasses are apparent in the stream (post-fish).

TABLE 4.4
Characteristics of Gravel Stored Fine Sediment Collected in Infiltration Bags in 2001

Event type	Date in 2001	Cumulative fish returns	Particle diameter (μm)		Particle density (g cm^{-3})		Fractal *D*	95% CL D
Pre-fish arrival	Jul. 17	0	332 (109)	b	1.047 (0.033)	a	1.060	0.009
Early spawn	Jul. 28	8211	261 (112)	a	1.092 (0.068)	b	1.073	0.004
Mid-spawn	Aug. 3	10931	244 (89)	a	1.116 (0.079)	c	1.052	0.007
Die-off	Aug. 12	13757	**262 (95)**[a]	a	**1.032 (0.048)**[a]	a	1.063	0.004
Die-off	Aug. 16	13892					1.061	0.004
Post-fish	Sep. 21	13893	316 (157)	b	1.121 (0.033)	c	1.051	0.004

Note: Means (and standard deviations) of particle diameter and particle density are shown. In each column, means followed by similar letters are not significantly different ($p < 0.05$).
[a] Values in bold represent composite value for Aug. 12 and Aug. 16.

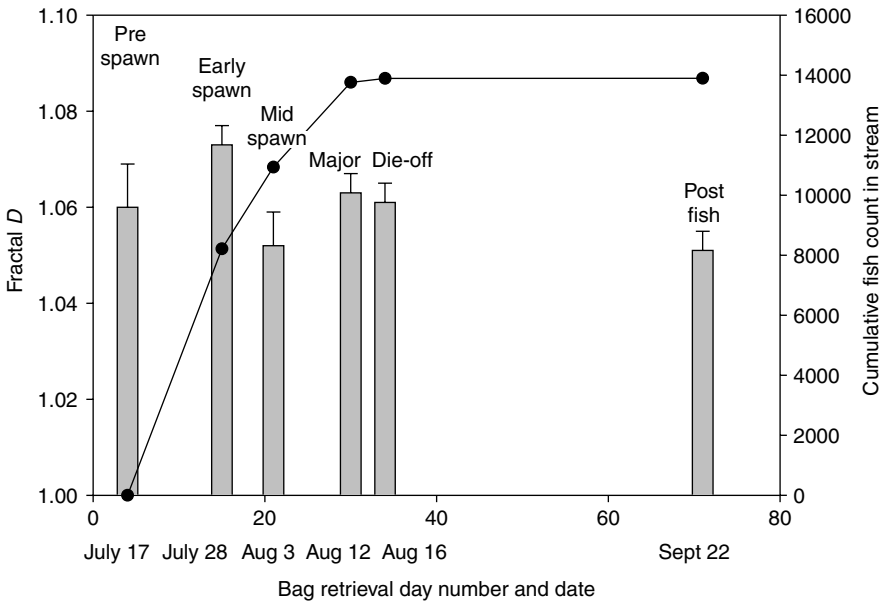

FIGURE 4.6 Fractal values for fine sediment collected in infiltration gravel bags in the summer of 2001 are shown as bars with the 95% confidence limits depicted. These sediment populations ($n > 1000$) were characterized for size and shape from charge-coupled device (CCD) images in the settling chamber. The 2001 cumulative fish count for O'Ne-eil Creek is shown by sample date (dots).

4.4 DISCUSSION

The particle populations sampled in O'Ne-eil Creek have been shown to be highly aggregated with floc factors (EPSD/APSD) exceeding ten.[3] All of the particles evaluated in this paper for size, morphology, and settling characteristics can be shown to be aggregates as the maximum particle sizes of the disaggregated inorganic sediment (APSD) of these samples do not exceed 130 μm, while each of the particles evaluated visually (EPS) was larger than 150 μm. The only particles which should be considered separately in this context are the compact-organics as they in fact may not be composite particles, but could be parts of organisms or aggregates of organism parts. The organics are removed from the sediment sample before characterizing the ASPD and so their constituent size is not determined.

Visual differentiation of aggregate particles in freshwater allowed an investigation of the size, shape, and behavior of particle subpopulations identified as flocs and compact particles. The loosely packed, open matrix floc particles are observed to be larger, less dense, less rounded, and slower settling than the opaque, compact particles. They were noted to be less abundant than compact particles in all periods sampled except for the fish die-off. While the smaller, rounder, denser compact particles are carried in ambient low flow conditions (0.23 to 0.35 m s^{-1}) their proportions are smaller in the post-fish quiescent flows (79%) than in low flows with active spawning

occurring (93%). In the resuspended gravel stored sediment of active spawn and post-fish they comprise 85% and 83%, respectively (Table 4.3). It is unfortunate that the spring melt population could not be visually differentiated as the energy environment of that period was high and both the proportion of floc and compact particles would be of interest as well as their respective sizes and shapes.

In any case, the characteristics of the total population can still be useful as it is clear that the particle size of the populations change over the open water season with the smallest mean sizes observed during spring melt when local flows are deepest and fastest and the concentration of suspended sediment is higher (mean of 7.96 mg l^{-1}) for this system. The shear stress measured in spring melt flows of this scale in O'Ne-eil Creek has been reported as being approximately 70 N m^{-1} [27] which would act to break apart weakly bound aggregate structures resulting in smaller mean and maximum population sizes as observed. Interestingly, aggregate particles are small during the active spawn of 1995 and 2000, while the largest sizes were observed during the die-off of fish in 1996. This variability in size occurs despite the fact that measured water velocities, which reflect local shear stresses of approximately 6 N m^{-1} at this site in O'Ne-eil Creek[27] were not very different during these sample periods (Table 4.1). This implies that the activity of spawning fish resuspending sediment could be having a similar shearing effect. Evidence to support this can be seen in the concentrations of suspended sediment during ambient flow conditions. In 2000, the background concentrations were between 2.47 and 3.76 mg l^{-1} after approximately 10,700 fish had entered the stream to spawn, while in 1995 the ambient concentration was 11.70 mg l^{-1} with 26,985 spawners in the stream. Undisturbed ambient suspended sediment concentrations are measured in O'Ne-eil Creek as <1 mg l^{-1}. The physical activity of these fish in digging their redds results in the reworking of the gravel bed, resuspension of the gravel stored fine sediments, and the downstream transport and deposition of these fines. The energy imparted in moving the gravels to release fine sediment, along with the action of being transported in the turbulent water column before settling again, would act to break apart weakly held structures, generating smaller and stronger and potentially more compact aggregates. In the ambient flow of active spawn in August 2000 only 7% of the total population of aggregate particles is loose floc structures. Alternately the largest aggregate sizes as well as the largest abundance of floc structures (35%) are observed in the salmon die-off period which exhibits low flow velocities with resuspended sediment concentrations of 7.22 mg l^{-1}. While these same low shear conditions and higher resuspended particle concentrations are sampled in post-fish periods (September and October 2000) the particle aggregates do not reach the same large sizes as during die-off. Clearly some other environmental factor aside from shear velocities and suspended sediment concentrations is controlling the size of these aggregate structures. The changing size and density of the infiltration gravel bag particle populations also supports the influence of the physical role of spawning salmon on the aggregate size. Smallest mean population sizes at mid-spawn, which are also associated with high densities, suggest that the smaller compact particles that predominate have been collected in the infiltration bags during spawn. The larger less dense aggregates collected in the bags earlier in the season have presumably been modified by the fish spawning activity. While the particles stored in the gravel bed during salmon die-off

are not statistically larger than at mid-spawn they are significantly less dense, which corresponds to the higher proportion of low density flocs observed in the water column (Tables 4.3 and 4.4). This could reflect the fact that the larger floc particles are less stable, breaking up when they enter the gravel matrix, or potentially being broken into smaller particles by the physical action of sieving through 2 mm mesh when the gravels are separated from the fines in the field.

The change in the particle composition and structure noted during fish die-off is associated with a temporal change in the organic composition of the aggregates. Petticrew and Arocena[17] reported on these same gravel stored samples and stated that over the open water season the biofilms that cover gravel stored aggregates changed from weak, web-like structures at mid-spawn to a less porous, film-like covering in post-spawn. The stronger more extensive biofilm was associated with large aggregates while the weaker web structure existed when the aggregates were being exposed to repetitive reworking of the gravel bed (e.g., resuspension) during mid-spawn.

The sediment moving in the spring melt has the lowest mean particle size as well as the lowest fractal values, as determined from filtered samples (Figure 4.5). The sediment moving in the melt is small, dense, and rounded. In an evaluation of the filter fractals there is a significant decrease in D over the three day high flow sampling period in 1997. The suspended sediment becomes more rounded with time, indicating either a change of source[21] or a modification of the particle shape with changing energy conditions. In Figure 4.5 there does not appear to be any significant differences between sediments resuspended from the gravel artificially over the season and the ambient suspended sediment from the active spawn of 2000. This would indicate that the sediments are from the same source, which we know to be the case, and experiencing similar energy conditions. This then would support the assumption that the energy imparted to the surface gravels to resuspend the stored fine sediments is similar to the work perpetrated by the fish. To corroborate this effect of physical resuspension note the timing of significant differences observed in the fractal dimensions and structure of the infiltration gravel bag sediments over the 2001 season (Figure 4.6, Table 4.4). Particles are growing more amorphous from pre-spawn through early spawn but then decrease in D values becoming rounder at the same time as becoming smaller and denser at mid-spawn when the majority of the physical reworking of the bed has been completed. As this reworking abates and die-off occurs, delivering carcass breakdown products to the stream the particle roundness decreases, density decreases, and particle size starts to increase again.

The ambient suspended sediments analyzed from the filtered populations show a significant increase in D following active spawn (Figure 4.5). This indicates that these particles are more amorphous than those of active spawn but also less rounded than the gravel stored sediment resuspended on the same dates. Intuitively this would make sense as there is less energy in the low flow water velocities which could break up the larger more amorphous particles.

In the post-spawn period the artificially resuspended (gravel stored) sediment has similar fractal values as the material comprising the ambient suspended sediment during the active spawn (August 2000) (Figure 4.5). This indicates that the material resuspended by spawning fish which remains in the water column is similar in shape to the gravel stored sediment later in the season. This is corroborated by looking at the

fractal results of the infiltration gravel bags (Table 4.4, Figure 4.6). The mid-spawn and post-fish fractals indicate they are the roundest populations of particles over the season, but as well they are the densest populations. Petticrew and Arocena[17] presented scanning electron microscope evidence indicating that these mid-spawn aggregates were held together with a weak-looking web of biofilm while pre- and post-spawn periods exhibited a more extensive coating of biofilm. The strength of these biofilms may relate to the physical action these particles are exposed to (low flows, active spawning) and could also play a role in regulating their size.

4.4.1 Fractal Concerns

Note that the fractal results for the filtered populations (Figure 4.5) are not the same as is found in the fractal analysis of the settling chamber populations shown in Figure 4.4. In this latter data set there are no significant differences within the subpopulations by either source (ambient versus resuspended) or date but there is a statistically smaller D value for the total population of the ambient post-fish (October 2000) suspended sediment as compared to the ambient active spawn samples. This indication that the ambient suspended sediment is becoming more rounded with time is opposite to the results of the filtered samples. A comparison of fractal values for samples from the same date and source material indicates that the filtered particle populations are always lower than the settling chamber populations. This would be a result of both the larger number of particles that are counted by filters as well as the lack of inclusion of the larger particles ($>400\,\mu$m) which have the higher proportion of amorphous, less rounded flocs. Inclusion of these bigger particles, which also exhibit larger variability, increases the fractal value of the settling chamber populations as seen in Figure 4.4. Another inconsistency is that the fractal values of the gravel stored sediment (Figure 4.6) are consistently much lower than that of the resuspended sediment shown in Figure 4.4, which is meant to represent the gravel stored sediment. This could be a function of the artificially disturbed samples being mixed with low concentrations of ambient sediment or the fact that the structure of the aggregates changes with depth in the gravels. The infiltration gravel bags collect material stored to a depth of approximately 25 cm while the artificial resuspension mobilizes only the top 5 or 6 cm. In Figure 4.3 it is clear that the majority of large floc particles are associated with the artificially resuspended gravel stored samples from August and October 2000, as opposed to being abundant in the ambient suspended sediment. Aside from periods of high flow, or just following scouring events, a layer of fine grained loosely aggregated sediment is often observed to be coating the surface of the channel.[28] These fine grained aggregates are more floc like than compact and are easily resuspended and moved downstream with increases in entrainment flows. These aggregates would be collected in both the artificially resuspended and the infiltration bag sediment sampling but would represent a larger portion of the population in the artificially resuspended sample as it disturbs a larger surface area and smaller depth of gravels. These surface fines would be less abundant in the gravel infiltration bag samples as they are deeper (25 cm) and have a specific surface area sampled (314 cm^2). This bias of surface sampling would then result in higher fractal D values

for the former (i.e., more amorphous) and lower D values, or more rounded particles in the gravel bags as observed in this comparison.

As the fractal values presented here reflect the measurement of potentially different populations (e.g., sediment populations with different upper and lower size limits as well as populations from different depths of gravel storage) care should be taken to compare results of fractal analyses between methods. Changing the upper and lower limits of the population analyzed in a fractal analysis has been found to have a significant effect on the results. For the settling chamber samples the lower limit was defined by the resolution of the image analysis technique (diameter approx. 150 μm) and the upper limit was not restricted. The regressions were always strong ($r^2 > 0.90$) and significant, but the subpopulation sizes were not always very large ($n = 5$ to 182). A test was done on the largest settling chamber data set (total population, Oct 2000 resuspended, $n = 315$), where the sample was altered to include only the aggregate population <600, <500, <400, and <300 μm in order to determine the effect of the size limits on the fractal D values. While the D's are not significantly different as the upper size limit is reduced and the sample size becomes smaller, the 95% confidence limits increase resulting in reduced ability to distinguish statistical differences. This observation is important if one plans to use fractals for identifying source sediments or for implying processes affecting sediment structure. The results of the filter population fractals presented in Figure 4.5 were analyzed using the same method as de Boer and Stone[29] who identified source differences in suspended sediment during a spring melt period. The lower limits and presumably the upper limits (as they are defined by the sampling technique) are similar to de Boer's which are detailed in his 1997 paper.[21] Using this method between 1,500 and 15,000 particles can easily be counted ensuring a representative population size. In viewing this lower end of the aggregate population (7 to 400 μm) we see significant differences over a 3-day period in spring melt and a difference in the ambient suspended sediment over the season. As the data for Figure 4.4 are comprised of subpopulations of quite variable, and in some cases small sizes, these data would be considered problematic. A better method of evaluating the fractal dimensions of these samples would be to measure a large number of particles from the general population photographed in the settling chamber as opposed to using just particles that have been tracked for settling velocities. This approach was used to determine fractal values for the infiltration bag fine sediments from 2001. An excess of 1,000 particles were sized to determine the D values of the gravel stored sediment over the season. The fractal D values indicate that on all dates the particles are very rounded with the only significant differences being that the mid-spawn is rounder than the sample before it from early spawn and that the final post-fish sample is roughly the same roundness as mid-spawn with a significantly smaller D than in the period of fish die-off preceding it.

4.5 CONCLUSIONS

Visual differentiation of aggregated sediment particles both moving in the stream and stored in the gravel bed indicates the presence of variable subpopulations of particle types. The settling behavior of the particles is modified by their size, density, and

shape which appear to be modified by the hydrological, physical, and biological conditions within the stream. Both the energy of turbulent streamflow and the energy imparted by fish reworking the gravel bed are associated with a predominance of small, denser compact particles. In periods when internal stream energy is lower and when there is abundant organic matter delivery to the stream the composite structures are largest and are comprised predominantly of loosely bound flocs.

While structural and behavioral differences are associated with the different events occurring in the system, a more complete investigation of the open water season, incorporating storm events and summer base flows would be valuable. As well an evaluation of the types of organic matter comprising the composite structures throughout the season could potentially elucidate the processes which regulate the structure and morphology of these particles.

ACKNOWLEDGMENTS

I would like to acknowledge the field assistance of Simon Biickert, Chris Spicer, Leslie Chamberlist, Jenia Yanick, Dirk deBoer, Jen McConnachie, Beka McConnachie, and Matt Riley. Various types of sample analysis and laboratory assistance were also provided by Lito Arocena, Tim Milligan, Tauqeer Waqar, Leslie Chamberlist, and Jen McConnachie. I would also like to thank Ian Droppo for many beneficial discussions about flocs. Funding for this work was provided by National Science and Engineering Research Council and Fisheries Renewal British Columbia.

REFERENCES

1. Kranck, K., et al., In situ particle size distributions resulting from flocculation of suspended sediment, in *Nearshore and Estuarine Cohesive Sediment Transport*. A. J. Metha, Ed., A.G.U. Washington, D.C., 1993, 60.
2. Droppo, I.G. and Ongley, E.D., Flocculation of suspended sediment in rivers of southeastern Canada, *Water Res.*, 28, 1799, 1994.
3. Petticrew, E.L., Sediment aggregation and transport in northern interior British Columbian streams, in *Erosion and Sediment Yield: Global and Regional Perspectives*, Walling, D.E. and Webb, B.W., Eds., Publ. 236, IAHS Press, Wallingford, 1996, 313.
4. Phillips, J.M. and Walling, D.E., The particle size characteristics of fine-grained channel deposits in the River Exe Basin, Devon, UK, *Hydrol. Process.*, 13, 1, 1999.
5. Droppo, I.G., Rethinking what constitutes suspended sediment, *Hydrol. Process.*, 15, 1551, 2001.
6. Burban, P. et al., Settling speeds of flocs in freshwater and seawater, *J. Geophys. Res.*, 95, 213, 1990.
7. Ongley, E.D. et al., Cohesive sediment transport: Emerging issues for toxic chemical management, *Hydrobiologia*, 235/236, 177, 1992.
8. Woodward, J.C. and Walling, D.E., A field sampling method for obtaining representative samples of composite fluvial suspended sediment particles for SEM analysis, *J. Sediment. Petrol.*, 62, 742, 1992.
9. Petticrew, E.L. and Droppo, I.G., The morphology and settling characteristics of fine-grained sediment from a selection of Canadian rivers, in *Contributions to the*

International Hydrological Programme V by Canadian Experts. IHP-V Technical Documents in Hydrology. No 33, UNESCO, Paris, 2000, 111.
10. Woodward, J.C. et al., Composite suspended sediment particles and flocculation in glacial meltwaters: Preliminary evidence from alpine and Himalayan basins, *Hydrol. Process.*, 16, 1735, 2002.
11. Droppo, I.G., Walling, D.E., and Ongley, E.D., Suspended sediment structure: Implications for sediment and contaminant transport modeling, in *Modelling Soil Erosion, Sediment Transport and Closely Related Hydrological Processes*, Summer W., Klaghofer E., and Zhang, W., Eds., IAHS Publ. 249, Wallingford, 1998, 437.
12. Petticrew, E.L., The influence of aggregation on storage of fine grained sediments in salmon bearing streams, in *Forest-fish Conference: Land Management Practices Affecting Aquatic Ecosystems*, Brewin, M.K. and Monita, D.M.A., Eds., Canadian Forest Service Information Report NOR-X-356, Edmonton, 1998, 241.
13. Poirier, R., The effects of floods and sockeye salmon on stream bed morphology, M.Sc. thesis, University of Northern British Columbia, Prince George, 2003.
14. Kondolf, G.M., Sale, M.J., and Wolman, M.G., Modification of fluvial gravel size by spawning salmonids, *Water Resour. Res.*, 29, 2265, 1993.
15. Ritchie, J.E., Perkins, M.A., and Goldman, C.R., Effects of kokannee salmon (*Oncorhynchus nerka*) decomposition on the ecology of a subalpine stream, *J. Fish. Res. Board Can.*, 32, 817, 1975.
16. Wold, A.K.F. and Hershey, A.E., Effects of salmon carcass decomposition on biofilm growth and wood decomposition, *Can. J. Fish. Aquat. Sci.*, 56, 767, 1999.
17. Petticrew, E.L. and Arocena, J.M., Organic matter composition of gravel-stored sediments from salmon bearing streams, *Hydrobiologia*, 494, 17, 2003.
18. Macdonald, J.S., Scrivner, J.C., and Smith, G., *The Stuart-Takla Fisheries/Forestry Interaction Project*, Can. Tech. Rep. Fish. Aquat. Sci. Publ. No. 1899, 1992.
19. Ryder, J.M., *Stuart-Takla Watersheds: Terrain and Sediment Sources*, Work Pap. 03/1995. British Columbia Ministry of Forests, Victoria, 1995.
20. Milligan, T.G. and Kranck, K., Electroresistance particle size analysers, in *Principles, Methods and Applications of Particle Size Analysis*, Syvitski, J.P.M., Ed., Cambridge University Press, 1991, 109.
21. de Boer, D.H., An evaluation of fractal dimensions to quantify changes in the morphology of fluvial suspended sediment particles during baseflow conditions, *Hydrol. Process.*, 11, 415, 1997.
22. Biickert, S., The effect of pulp mill effluent on fine-grained sediment morphology and storage in the Fraser River at Prince George, British Columbia, M.Sc. thesis, University of Northern British Columbia, Prince George, 1999.
23. Mandelbrot, B.B., Passoja, D.E., and Paullay, A.J., Fractal character of fracture surfaces of metals, *Nature*, 308, 721, 1984.
24. Krein, A., Petticrew, E.L., and Udelhoven, T., The use of fine sediment fractal dimensions and colour to determine sediment sources in a small watershed, *Catena*, 53, 165, 2003.
25. Namer, J. and Ganczarczyk, J.J., Settling properties of digested sludge particle aggregates, *Water Res.*, 27, 1285, 1993.
26. Lisle, T.E. and Eads, R.E., *Methods to Measure Sedimentation of Spawning Gravels*. USDA Forest Service, Research Note PSW 411, 1991.
27. McConnachie, J.L., Seasonal variability of fine-grained sediment morphology in a salmon-bearing stream, M.Sc. thesis, University of Northern British Columbia, Prince George, 2003.

28. Droppo, I.G. and Stone, M., In-channel surficial fine-grained laminae (Part 1): Physical characteristics and formational processes, *Hydrol. Process.*, 8, 101, 1994.
29. de Boer, D.H. and Stone, M., Spatial and temporal variability in fractal dimensions of suspended solids in two southern Ontario rivers, in *Modelling Soil Erosion, Sediment Transport and Closely Related Hydrological Processes*, Summer, W., Klaghofer, E., and Zhang W., Eds., IAHS Publ. 249, Wallingford, 1998, 445.

5 Effects of Floc Size and Shape in Particle Aggregation

Joseph F. Atkinson, Rajat K. Chakraborti, and John E. VanBenschoten

CONTENTS

5.1 INTRODUCTION

Particle aggregation is a complex process affected by various physical, chemical, and hydrodynamic conditions. It is of interest for understanding, modeling, and design in natural and engineered water and wastewater treatment systems. In natural aquatic

1-56670-615-7/05/$0.00+$1.50

systems such as lakes, rivers, and estuaries, particle aggregation is important because it controls the fate of both the particles themselves, as well as potentially hazardous substances adsorbed to the particles.[1–5] In water and wastewater treatment, flocculation is used to produce larger aggregates that can more effectively be removed from the treatment stream by sedimentation and filtration.[6–8] The growth of aggregates depends on the relative size of the colliding particles or clusters of particles, their number density, surface charge and roughness, local shear forces, and the suspending electrolyte. Specific factors that affect aggregation include coagulant dose, mixing intensity, particle concentration, temperature, solution pH, and organisms in the suspension.[3,7,9] These factors contribute not only to changes in particle size and shape, but also affect flow around and possibly through the aggregate, with corresponding effects on transport and settling rates.

Historically, efforts to understand individual processes of aggregation have been based on relatively simple systems, assuming impervious spherical particles, with various mechanisms of particle interaction explained using Euclidean geometry. More recently, it has been recognized that aggregates are porous and irregularly shaped, and that these characteristics suggest different behavior than for impervious spheres. Fractal concepts have been adapted from general theoretical considerations originally discussed by Mandelbrot[10] and later by Meakin.[11–14] For specific applications in environmental engineering, much of the fundamental fractal theory for particle aggregation has been developed by Logan and his coworkers.[15–18] Fractal theories have been used mainly as a quantifying tool for describing the structure of the aggregate, but several studies have also looked at the application of fractal characteristics as a means of analyzing the kinetics of aggregation.[11,18]

In addition to the assumption of impervious spherical particles, earlier studies also assumed that volume is conserved when two particles join (known as the coalesced sphere assumption). However, these assumptions are exact only for liquid droplets. When two aggregates collide, the resulting (larger) aggregate often has higher permeability than the parent aggregates, and the volume of the new aggregate is generally larger than the sum of the two original volumes. The overall goal of this study is to conceptualize and develop an aggregation model using fractal concepts, based on measurements from coagulation–flocculation experiments under a variety of environmental/process conditions, and to determine the potential impact of aggregate geometry on particle dynamics in natural and process oriented environments. The study is motivated by the idea that improvements in particle and aggregation modeling may be achieved by incorporating more realistic aggregate geometry; and fractal concepts are used to characterize the impacts of aggregate shape in relation to traditional models that have assumed spherical aggregates. In particular, incorporating realistic aggregate geometry is expected to provide improvements in our ability to describe such features as aggregate growth rates under different hydrodynamic and chemical conditions. Relationships between aggregate size and geometry, as characterized by fractal dimension, are sought, which can provide additional information for understanding and modeling particle behavior. To avoid potential problems associated with sample collection and handling, a nonintrusive image-based technique is used for the measurements.

This technique uses digital image analysis to obtain information for aggregates in suspension that can be used in model development. It is expected that results of this study will lead to a better understanding of particle behavior in aqueous suspensions, and will advance our capability to model aggregate interaction and transport.

5.2 BACKGROUND

5.2.1 Fractal Aggregate Properties

The assumptions of aggregates as impervious, spherical objects have facilitated the development of particle interaction models and provided an obvious simplification of their geometric properties, defined by a single variable, the diameter, d. Perimeter, P, is then proportional to d, projected area, A, is proportional to d^2, and volume, V, is proportional to d^3. Under the coalesced sphere assumption, volume conservation can be easily computed in terms of changes in diameter, since when two particles collide and stick, the resulting volume is just the sum of the two original volumes and the diameter is found by assuming the resulting volume is again spherical. Other features of aggregation, including particle interaction terms and hydrodynamic interactions, also have been explored on the basis of spherical particles. In this approach aggregate density, ρ, is essentially constant and equal to the density of the primary particles from which the aggregate was formed, since ρ is defined as the total mass of the aggregate divided by its volume. In addition, porosity, ϕ is zero in this case.

In reality, aggregates are highly irregular, with complex geometry and relatively high porosity. Shape cannot be defined in terms of spherical, Euclidean geometry, and fractal geometry must be used instead. The primary geometric parameters of interest are the one-, two-, and three-dimensional fractal dimensions, which may be defined, respectively, by[16,18]

$$P \propto l^{D_1}; \quad A \propto l^{D_2}; \quad V \propto l^{D_3} \tag{5.1}$$

where l is a characteristic length for an aggregate, and D_1, D_2, and D_3 are the one-, two-, and three-dimensional fractal dimensions, respectively. In general, l has been defined differently in different studies, but the most common definition, which will be used here, is to take l as the longest side of an aggregate. Note also that l takes the place of d in the Euclidean definitions of P, A, and V. Here, D_1, D_2, and D_3 do not in general take integer values, as in Euclidean geometry. These fractal dimensions are obtained from the slope of a log–log plot between the respective aggregate property and l. In essence, fractal geometry expresses the mass distribution in the body of an aggregate, which is often nonhomogeneous and difficult to assess. Aggregates with lower fractal dimension exhibit a more porous and branched structure and, as shown below, have higher aggregation rates.

By taking into account the shape of primary particles and their packing characteristics in an aggregate, Logan[15–18] derived various aggregate properties in terms of the fractal dimensions defined in Equation (5.1). The number of primary particles in

an aggregate was shown to be

$$N = \psi^{D_3/3} \left(\frac{l}{l_0} \right)^{D_3} \tag{5.2}$$

where N is the number of primary particles, ψ is a constant defined by $\psi = \zeta\xi/\xi_0$, ζ is the packing factor, ξ_0 and ξ are shape factors for the primary particles and the aggregate, respectively, and l_0 is the characteristic length for the primary particles. The density of the primary particles is ρ_0 and the volume of one primary particle is $V_0 = \xi_0 l_0^3$. The total solid mass in an aggregate, m_s, is then $(N\rho_0 V_0)$, or

$$m_s = \rho_0 \psi^{D_3/3} \xi_0 l_0^{3-D_3} l^{D_3} \tag{5.3}$$

Using similar parameters, the aggregate solid density, ρ_s, is calculated as the ratio of mass and encased volume of the fractal aggregate, defined as the combined volume of particles and pores within the aggregate, $V_e = \xi l^3$. The aggregate solid density is then

$$\rho_s = \frac{m_s}{V_e} = \rho_0 \psi^{D_3/3} \left(\frac{\xi_0}{\xi} \right) \left(\frac{l}{l_0} \right)^{D_3-3} \tag{5.4}$$

Solid volume, V_s, is the volume associated with the primary particles, which is just $V_s = N(\xi_0 l_0^3)$. In addition, the porosity of the aggregate is $\phi = 1 - V_s/V_e$, or

$$\phi = 1 - \psi^{D_3/3} \left(\frac{\xi_0}{\xi} \right) \left(\frac{l}{l_0} \right)^{D_3-3} \tag{5.5}$$

Finally, the total, or effective density of the aggregate is the total mass (solid plus fluid) divided by the encased volume, which can be shown to be

$$\rho = \rho_0 - \phi(\rho_0 - \rho_w) \tag{5.6}$$

where ρ_w is the water density. The net gravitational force for settling depends on the difference between ρ and ρ_w, which can be written as

$$\rho - \rho_w = (1 - \phi)(\rho_0 - \rho_w) \tag{5.7}$$

This last result demonstrates the intuitive idea that aggregate porosity should be important in controlling settling rate.

In the present experiments it was found that ϕ is related to size (discussed in the later part of this section), and indirectly to D_2 and D_3. Drag on an aggregate moving through the water column depends on the flow of water around and possibly through the aggregate, which in turn depends on overall shape, porosity, and distribution of primary particles within the aggregate structure. For example, flow through an aggregate with a uniform distribution of primary particles would be different from flow

through an aggregate in which primary particles are more clustered, with relatively large and interconnected pore spaces, and these differences would lead to differences in overall drag (however, it should be noted that most researchers (e.g., ref. [17,18]) believe there is little or no flow through an aggregate). Even without flow through an aggregate, the distribution of primary particles would affect the manner in which an aggregate would move through the fluid.

Aggregate settling rate can be evaluated from a standard force balance between gravity, buoyancy, and drag,

$$(\rho - \rho_w)V_e = \tfrac{1}{2}C_D\rho_w A w_s^2 \tag{5.8}$$

where C_D is a drag coefficient, w_s is the settling velocity, and A is the projected area in the direction of movement (i.e., vertical). Since V_e is proportional to l^3, A is proportional to l^{D_2}, and ρ depends on l^{D_3-3}, Equation (5.8) shows that w_s^2 is proportional to $(l^{D_3-D_2})/C_D$. Note that if Euclidean values are used for D_2 and D_3 ($D_2 = 2$ and $D_3 = 3$), then w_s^2 is proportional to l/C_D. If it is further assumed that laminar conditions apply, and the relationship for C_D for drag on a sphere is used, $C_D \propto Re^{-1}$, where $Re = w_s l/\nu$ is a particle Reynolds number and ν is kinematic viscosity of the fluid in which the settling occurs, then

$$w_s \propto l^{(D_3-D_2+1)} \tag{5.9}$$

which shows that for a given l, larger D_3 (more compact aggregate) facilitates faster settling, while larger D_2 appears to inhibit settling. This is a somewhat contradictory result, since both D_2 and D_3 increase with greater compaction, and this contradiction may be a factor in explaining differing results reported for settling in the literature. However, in the case of the most compact (impermeable) aggregates (with $D_2 = 2$ and $D_3 = 3$), the relationship represented in Equation (5.9) converges to a typical Stokes' settling expression (for spheres) where the settling rate is a function of diameter squared. As shown below, results from the present study support an exponent in the settling relationship that is <2, suggesting that a fractal description of settling is needed.

5.2.2 Model Development

Models of suspended sediment transport are important for evaluating efficiency of removal in treatment plant operations and also in predicting the distribution of suspended load and associated (sorbed) contaminant fluxes in water quality models. These models require some description of aggregation processes and must simulate changes in particle size distribution. Aggregation models may generally be classified as either microscale or macroscale. An example of a microscale model is the classic diffusion-limited aggregation (DLA) model,[19,20] or one of its various derivatives such as reaction-limited aggregation (RLA). Such models have an advantage in that they consider particle interactions directly, and allow examination of individual aggregates. However, they are generally not very convenient for incorporation into more general sediment transport and water quality models.

Macroscale models address general properties of the suspension, and not individual aggregates. The most well-known macroscale modeling framework was originally described by Smoluchowski,[21] and it considers mass conservation for aggregates in different size classes. A basic form of the equation may be written in discrete form as

$$\frac{dn_k}{dt} = \frac{1}{2}\alpha \sum_{i+j=k} \beta(i,j) n_i n_j - n_k \alpha \sum_{i=1}^{\infty} \beta(i,k) n_i \tag{5.10}$$

where n_k represents the number of aggregates in size class k, t is time, α is collision efficiency, $\beta(i,j)$ is the rate at which particles of volumes V_i and V_j collide (collision frequency function), and i, j, and k represent different aggregate size classes. The first summation accounts for the formation of aggregates in the k class, from collisions of particles in the i and j classes. The second summation reflects the loss of k-sized aggregates as they combine with all other aggregate sizes to form larger aggregates. Additional terms such as breakup, settling, and internal source or decay may be added on the right-hand side of Equation (5.10), or terms may be dropped, depending on the processes of importance for a given application. For simplicity, these terms are neglected in the present discussion.

In the discrete form suggested by Equation (5.10), size distribution is determined simply by the number of particles, n_k, in each of the k size classes considered for a given problem. Separate equations are written for each size class and the interaction terms determine how the size distribution changes over time. Various forms of this equation may be incorporated into more general advection diffusion type models written to evaluate the distribution of sediment and associated (sorbed) contaminant in water quality models (e.g., ref. [22]).

Major assumptions of the Smoluchowski approach (Equation (5.10)) are that only two particles take part in any single collision, particles follow rectilinear paths (i.e., the particles move in a straight line up to the collision point), and particle volume is conserved during the agglomeration process (again, the coalesced sphere assumption). The rectilinear assumption tends to over predict aggregation rates, while the coalesced sphere assumption under predicts them.[3] In reality, as the coagulation of solid particles proceeds, fluid is incorporated into pores in the aggregates that are formed, resulting in a larger collision diameter than the coalesced sphere diameter.[23] However, this process is not explicitly included in the traditional model.

The collision frequency function, $\beta(i,j)$, reflects the physical factors that affect coagulation, such as temperature, viscosity, shear stress, and aggregate size and shape. The three major mechanisms that contribute to collisions are Brownian motion or perikinetic flocculation, fluid shear or orthokinetic flocculation, and differential settling. The total collision frequency is the sum of contributions from these three transport mechanisms,

$$\beta_{\text{total}} = \beta_{\text{Br}} + \beta_{\text{Sh}} + \beta_{\text{DS}} \tag{5.11}$$

where β_{Br}, β_{Sh}, and β_{DS} are the contributions due to Brownian motion, fluid shear, and differential sedimentation, respectively. If the colliding particles are submicron in size, Brownian motion is appreciable. However, with larger particles, Brownian motion becomes less important.[24] In traditional methods, β is calculated from constant parameters describing aggregation kinetics, assuming spherical particles. In other words, there is no dependence on the actual shape and size of the aggregates in calculating β. Formulas have been developed to calculate β based on fractal geometry for each of the three above-mentioned transport mechanisms (Table 5.1). These expressions are based on solid volume of the aggregate, V_s, defined previously. The degree to which the values determined from Table 5.1 differ from those determined using the traditional approach assuming spherical aggregates depends on how far the respective fractal dimensions are from their Euclidean counterparts. The functions in Table 5.1 reduce to corresponding traditional estimates when Euclidean values are used, but in general they produce larger values for β.[18] The present results (Figure 5.12) also confirm this relationship.

In the experiments described below, collision frequencies and, as a secondary effect, collision efficiencies, are examined as they depend on geometric characteristics of the interacting particles. Density also is shown to be dependent on particle size, which in general is a function of time.

5.2.2.1 Conceptual Fractal Model of Aggregation

Although useful for general modeling purposes, the Smoluchowski model does not provide a basis for developing insight into the details of the physical processes that take

TABLE 5.1
Collision Frequency Functions for Fractal Aggregates (from ref. [15, 18])

Mechanism	Collision Frequency Function
Brownian motion	$\beta_{Br} = \frac{2k_B T}{3\mu_w}\left(v_i^{-1/D_3} + v_j^{-1/D_3}\right)\left(v_i^{1/D_3} + v_j^{1/D_3}\right)$
Fluid shear	$\beta_{sh} = \frac{G}{6\xi_0 b_D^{3/D_3}} v_0^{1-(3/D_3)}\left(v_i^{1/D_3} + v_j^{1/D_3}\right)^3$
	$\beta_{DS} = \frac{\pi}{4}\left(\frac{2g(\rho_0 - \rho_w)}{a\rho_w \xi_2 \nu^{b_D}}\right)\xi_0^{-1/3} b_D^{-(2+(b_D-D_2)/(2-b_D))}$
Differential sedimentation	$*v_0^{(1/3)-(1/D_3)(2+(b_D-D_2)/(2-b_D))}\left\lvert v_i^{(1/D_3)((D_3+b_D-D_2)/(2-b_D))}\right.$
	$\left. -v_j^{(1/D_3)((D_3+b_D-D_2)/(2-b_D))}\right\rvert \left(v_i^{1/D_3} + v_j^{1/D_3}\right)^2$

Note: The parameters in these functions are: β = collision frequency function ($cm^3\,sec^{-1}$); k_B = Boltzmann's constant (1.38×10^{-16} g cm^2 sec^{-2} K^{-1}); T = absolute temperature (293 K); G = velocity gradient (sec^{-1}); μ_w = dynamic viscosity of water (0.01002 g cm^{-1} sec^1); ρ_w = density of water (0.99821 g cm^{-3}); ρ_0 = density of primary particle; g = gravitational constant (981 cm sec^{-2}); ξ_2 = aggregate area shape factor; a and b_D = fractal functions depending on Reynolds number ($a = 24$ and $b_D = 1$ for $Re < 0.10$); ν = kinematic viscosity (0.01004 cm^2 sec^{-1}), and v_i, v_j = solid volume of i and j size class particles, and v_0 = primary particle volume.

place during aggregation. Microscale models are more helpful in this regard, and also helpful for present purposes is a more general conceptual description of aggregation, in terms of geometric properties (fractal dimensions) of the interacting aggregates. Several studies have already shown, for example, the effect of fractal dimension on collision frequencies,[15,16,18] and similar results were found in the present study, as described later in this section.

The present conceptual model is based on general ideas presented in the literature describing aggregation processes, and is applied to a specific experiment in which an initially monodisperse suspension of primary particles, either spherical or at least with known fractal dimension, is mixed with or without coagulant addition. The model focuses on the initial stages of aggregation, before particles grow large enough that further growth may be limited by breakup. It is assumed that mixing speed and chemical conditions are constant during any given experiment.

Referring to Figure 5.1, the initial state of the suspension is characterized by initial values for average size and fractal dimension of the primary particles. Here, fractal dimension refers to either D_2 or D_3, and size refers to the longest dimension for an aggregate. As particles collide and stick, average size increases and fractal dimension decreases, according to processes discussed earlier in this section. For example, following a successful collision (i.e., one that results in the two particles sticking), the resulting volume is larger than the sum of the volumes of the two colliding particles, as additional pore space is incorporated in the aggregate.

As the process continues, both growth and breakup occur, but growth is faster. Eventually, a state, represented by point A in Figure 5.1, is reached in which there is a temporary balance between growth and breakup. During this period there may be some restructuring of the aggregates, as particles and clusters penetrate into the pore spaces of larger aggregates, not necessarily increasing size appreciably, but increasing

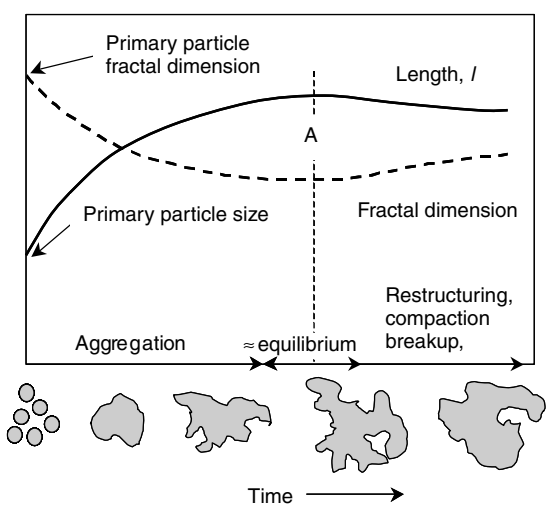

FIGURE 5.1 Conceptual model of temporal changes in fractal dimensions and average size (characteristic length) during initial stages of an aggregation process.

density, with a corresponding reduction in fractal dimension. With additional time, aggregates become more compact and average size may even decrease slightly, as particles and clusters that are only loosely joined break off and rejoin other aggregates in a more stable manner. The overall effect is a slight reduction in average size and a slight increase in fractal dimension. These changes also are illustrated with the floc sketches at the bottom of Figure 5.1.

The length of time in the initial phase (before point A) will vary, depending on chemical and mixing conditions, as well as the initial state of the suspension. In the experiments reported below, this phase lasts approximately 40 to 60 min. In a typical treatment process, the length of time allowed for mixing is on the order of several tens of minutes, so the later processes of restructuring and compaction are probably not significant. In natural systems particular conditions may last longer, and there is a greater chance particles will be in a near-equilibrium state.

5.3 EXPERIMENTAL SETUP

5.3.1 Image Analysis

Three sets of experiments were conducted in this study (Table 5.2), each one using an image-based analysis of aggregates. A nonintrusive imaging technique was used to capture images of aggregates and to analyze changes in aggregate properties with time. Using this technique, aggregates could be maintained in suspension and images were captured without sample extraction or any other interruption of the experiment. In one set of tests (Experiment Set 1, Section 5.3.2.1), the images were taken of the mixing jar containing suspensions immediately at the end of the flocculation step, assuming the particle shape and size did not change during the settling period. In another set of

TABLE 5.2
Summary of Experiments

Experiments	Coagulant	Measurements	Shear rate (sec^{-1})
Experiment Set 1 (lake water and montmorillonite)	Alum	Initial conditions, charge neutralization, sweep floc	n/a-tested supernatant after mixing (during settling)
Experiment Set 2 (latex particles) (Expts. 1–8)	Alum	10, 20, 30 min	20, 80
Experiment Set 3 (latex particles, Buffalo River) (Expts. 9–11)	Polymer	2–150 min	10, 40, 100

experiments (Experiment Set 2, Section 5.3.2.2), images were taken from the sample while slow mixing was still in progress, that is, particles were photographed *in situ*.

A schematic of the general experimental setup is shown in Figure 5.2. Images of the suspended particles were illuminated by a strobe light, which provided a coherent backlighting source. Depending on conditions for a particular experiment, the strobe pulse rate and intensity were adjusted to produce one pulse during the time the camera shutter was open. The projected images were captured by a computer-controlled CCD camera (Kodak MegaPlus digital camera, model 1.4) placed on the opposite side of the mixing jar from the strobe. Generally the shutter exposure time was between about 80 and 147 ms. The camera captured digital images on a sensor matrix consisting of 1320 (horizontal) × 1035 (vertical) pixels. Each pixel was recorded using 8 bit resolution, that is, with 256 gray levels. For the present tests, a resolution of 540 pixels per mm was achieved. This was determined by imaging a known length on a stage micrometer and counting the number of pixels corresponding to that length. The camera was mounted on a traversing device so that it could be moved in each of the three coordinate directions, and images were stored on the hard drive of a PC. Camera settings were varied to obtain the best quality (greatest contrast between aggregates and background) for each set of experimental conditions (see Chakraborti[25] for further details), but pixel resolution was held constant throughout the tests. Pixel resolution was always sufficient to adequately describe the smallest particles in these experiments.[26] Experiments were conducted in a darkened room to eliminate light contamination.

Once saved, images were processed using a public domain image analysis software program (NIH *Image*). Processing steps included contrast enhancement and thresholding, resulting in a binary image consisting of solids (black) and background (white). *Image* was then applied to calculate basic geometric properties for each aggregate in the image, which included perimeter and area. In addition, an ellipse was fitted to each aggregate, by matching moment of inertia and area of the original aggregate. This step resulted in the definition of major and minor ellipse axes, and the major axis was taken as the characteristic (longest) length, l, of the aggregate. In order to estimate volumes to calculate D_3 (Equation (5.1)), the two-dimensional fitted ellipse was rotated about the long axis. As shown by Chakraborti et al.,[27]

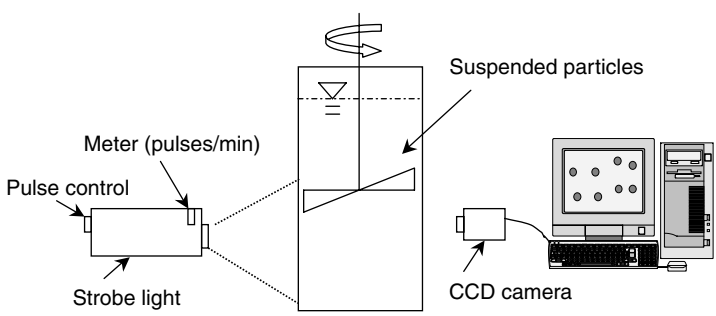

FIGURE 5.2 Experimental setup consisting of strobe light, CCD camera attached to a computer, and the suspended sample in a mixing jar.

this procedure produces estimates of volume that are preferable to using a spherical encased volume assumption, although there is still obviously greater uncertainly in the volume estimates than in the calculations based on area. Since direct measurements of volume using an image-based method are not available, the ellipse approximation provides a reasonable approach. After application of *Image*, all data were transferred to a spreadsheet for further processing, including calculations of size distributions, fractal dimensions, and other parameters as described in the following paragraphs.

Before conducting the aggregation experiments, preliminary tests were conducted to ensure that the imaging procedures were providing accurate data. Monodisperse suspensions of several different latex particle sizes with known concentration were photographed to determine the accuracy of size analysis and also to evaluate the degree to which concentration could be reproduced. Initial experiments were conducted by Cheng et al.,[28] who showed that both 10 μm and 6 μm monodisperse latex solutions were correctly analyzed. Chakraborti[25] conducted additional tests and, in addition, used the known concentration to evaluate the sampling volume, defined by the field of focus of the camera. The sampling volume was found to be approximately 20 mm square and 3 mm deep. In addition, he conducted a number of sensitivity analyses to further refine the imaging procedures and evaluate the accuracy and reproducibility of the imaging results.

5.3.2 Materials and General Procedures

Three sets of experiments were designed to provide data for analysis of particles resulting from coagulation and flocculation under different process conditions (Table 5.2). In these experiments, alum and polymer were used as coagulants. In Experiment Set 1, particle size distributions and morphology of aggregates obtained from lake water samples and laboratory suspensions of montmorillonite clay were measured. Results of these experiments were reported previously,[27] and they demonstrated that fractal dimension could be used to characterize different stages of aggregation, ranging from initial untreated suspensions, to conditions of sweep floc with relatively large alum dose. Experiments were conducted to test the hypothesis that charge neutralization and sweep floc mechanisms produce fundamentally different particle characteristics, including differences in fractal dimension. In Experiment Set 2, images of aggregates were obtained while the suspension was still being stirred during flocculation. Results demonstrated that images could be obtained *in situ* and also provided direct observation of temporal changes in floc characteristics during mixing. Again, alum was used as a coagulant. The goal of these experiments was to test the hypothesis that changes in fractal dimension are correlated with the physicochemical conditions of a particular experiment. These experiments were reported by Chakraborti et al.[26] The third set of experiments was designed to provide a description of the aggregation process over longer periods of time for both inorganic and natural suspensions. Polymer was used as coagulant, to avoid additional mass that may be introduced by alum particles and to focus on fundamental aggregate growth due to primary particles only. The previous flocculation experiments were restricted to durations of only 30 min. For treatment plant operation this length of time may be relevant, but the aggregates were probably still undergoing changes in their shape and size. In particular, disaggregation

and restructuring were relatively unimportant during this earlier period, and become more important only for longer times. Results from the second and third sets of experiments provided the basis for model conceptualization and model development described above. Because Experiment Sets 1 and 2 have been previously reported, they are only briefly summarized here.

5.3.2.1 Experiment Set 1

Water samples were collected from a shallow lake located on the campus of the University at Buffalo, Buffalo, New York. The lake has an average depth of 3 m, with maximum depth of 8 m and a total area of 243,000 m^2. Experiments also were conducted for clay suspensions prepared by adding montmorillonite clay powder (K-10) to deionized water to produce a sample with a solids concentration of 100 mg/l. Montmorillonite is an aluminum hydrosilicate where the ratio between SiO_2 and Al_2O_3 is approximately 4 to 1. It has a bulk density of 370 g/l, surface area of 240 m^2/g and pH 3.2 observed at 10% suspension (Fluka Chemicals, Buchs, Switzerland). For coagulant, a stock solution of alum was prepared by dissolving $Al_2(SO_4)_3 \cdot 18\ H_2O$ (Fisher Scientific, Pittsburgh, PA) in deionized water to a concentration of 0.1 M (0.2 M as aluminum). Standard jar tests were conducted with these samples to determine an appropriate dose of alum to generate a "sweep floc" condition. Changes of both surface charge (measured as zeta potential) and residual turbidity with alum dose also were measured. After addition of alum, the suspension was mixed rapidly (@$\sim$100 rpm) for 1 min and then slow-mixed for 20 min with a mean velocity gradient, $G = 20\ \text{sec}^{-1}$. The mixing was then stopped and images of the resulting aggregated particles in suspension were taken. All experiments were conducted at room temperature ($\sim$20°C to 23°C), and the analyzed images were obtained with an alum dose of 20 mg/l, and with pH maintained at 6.5 by manual addition of acid or base as required.

5.3.2.2 Experiment Set 2

Monosized polystyrene latex microspheres with a density of 1.05 g/ml (Duke Scientific Corporation, Palo Alto, CA, United States) were used as the primary particles for these experiments. The nominal particle diameter was 9.975 μm, with a standard deviation of $\pm$0.061 μm. Particles were taken from a 15 ml sample of aqueous suspension with 0.2% solids content (manufacturer's specification). The number concentration of particles in the concentrated suspension was 3.66×10^6 particles/ml ($\pm$10%). Aliquots of 0.06 ml or 0.1 ml of the suspension were added to the mixing jar along with 1 l of deionized water, resulting in initial number concentrations of 220 and 366 particles/ml, respectively. The higher and lower concentrations yielded total suspended solids of 0.12 and 0.20 mg/l. The images were analyzed to track changes in aggregate morphology for a given test, as well as differences between tests resulting from varying coagulant (alum) dose, particle concentration and mixing speed, or shear rate.

A freshly prepared stock solution of alum was prepared for each test as in Experiment Set 1. For each test, after addition of coagulant and an initial rapid

mixing period (with $G = 100\ \text{sec}^{-1}$) for 1 min, the mixing speed was reduced to either $G = 20\ \text{sec}^{-1}$ or $G = 80\ \text{sec}^{-1}$ and continued until the end of the experiment. All tests were conducted at room temperature (20°C to ~23°C) and a constant pH of 6.5 was maintained by adding acid or base as required. Measurements were taken at 10, 20, and 30 min after the initial rapid mixing period. Experiments were performed to evaluate temporal changes in the fractal dimensions of aggregates formed during flocculation of the microspheres. Particle size distributions, collision frequency, and aggregate geometrical information at different mixing times were obtained under variable conditions.

5.3.2.3 Experiment Set 3

Typically, two types of suspension were used in the third set of experiments: abiotic (latex) and natural (collected from a local river), containing both inorganic and organic constituents. These experiments were conducted using the same equipment and general procedures as in Experiment Sets 1 and 2. Polystyrene latex particles (Duke Scientific Corporation, Palo Alto, CA) of 6 μm diameter (6.038 μm $\pm$ 0.045 μm; density 1.05 g/ml) with a particle concentration of 4000 /ml were used as the primary particles for the abiotic suspensions. Suspensions were prepared by adding a predetermined quantity of particles in deionized water and stirring vigorously to insure homogeneity. These solutions contained 4.52×10^{-5}% solids by volume, or 0.5 mg/l. A constant pH = 6.5 was maintained by adding acid or base as required.

The natural suspension was obtained from the Buffalo River (Buffalo, New York). This sample was collected at about 0.5 m below the water surface at a point where the channel is about 50 m wide and total water depth is about 7 m (in the mid-section). The wind velocity recorded on the sampling day was 27 kmph (17 mph), and water temperature was 10.55°C (51°F). The organic content was measured by oven drying a filtered 500 ml sample for 24 h at 105°C, followed by 24 h of oven drying at 550°C. The measured total solids content (TSS) was 14.6 mg/l (measured using a 0.22 μm filter), which is fairly typical for rivers, and the volatile organic solids (VSS) was 0.4 mg/l, resulting in a 2.74% organic content.

Since the surface charge of suspended particles is negative, cationic polymer was used for coagulant. Polymer was chosen since it does not form gel or add particles in suspension like alum floc, and it allows quick aggregation. Alken solutions (Alken-Murray Corporation, New York) supplied the polymer Ethanediamine (C193K) for these experiments. This polymer has a molar mass less than one million (~700,000) and contains the quaternary amine (ammonium) group that produces the positive charge. According to the manufacturer, it is completely soluble and has an effective pH range of 0 to 13, with good floc formation at solution pH between 4 and 6. Fresh polymer (0.5% stock solution, per manufacturer's specifications) was prepared for each experiment, and the solution was shaken vigorously before each use.

The selected mixing speeds for the experiments were 15 rpm, 46 rpm, and 100 rpm, resulting in average velocity gradients, $G = 10\ \text{sec}^{-1}$, $40\ \text{sec}^{-1}$, and $100\ \text{sec}^{-1}$, respectively. These values were chosen to span the range of mixing environments found in engineered and natural aquatic systems, although some natural environments may have even lower mixing intensities. For each experiment, samples

were rapid mixed for 1 min to provide thorough mixing of the particles with the coagulant. The stirring rate was then adjusted to the desired level and images of the flocs were taken at different times throughout the experiment.

Preliminary tests were performed to determine the quantity of coagulant needed to produce particle aggregation at the desired rate. Measurements of zeta potential and resulting residual turbidity (measured at 30 min after stopping the mixing) are shown in Figure 5.3 for different polymer doses added to Buffalo River suspensions. Basic stages of aggregation may be seen with increasing coagulant dose. Initially (Stage I), particle surface charge is reduced as the particles become destabilized. The principle aggregation mechanism in this stage is the reduction of electrostatic repulsion between particles as a result of surface charge reduction. Charge neutralization (Stage II) is reached when sufficient coagulant is added so that the originally negatively charged particles are just neutralized, and aggregates are formed when contacts occur. Further addition of coagulant leads to charge reversal and restabilization (Stage III) where aggregation is not chemically favored. When alum is used as coagulant, $Al(OH)_3(s)$ is produced, which coats particles with a gelatinous and "sticky" sheath. At higher doses and for appropriate pH range, "sweep floc" may occur, which causes aggregates to settle more quickly and reduce turbidity. This stage is not present for the polymer, which does not produce "sweep floc."

As the surface charge of the suspended particles changes with increasing coagulant dose, the resulting residual turbidity decreases, reaching a minimum for a dose near the dose corresponding to neutral surface charge (Figure 5.3). The initial turbidity for the Buffalo River suspension was 28 NTU, and the coagulant dose causing charge neutralization was 520 μg/l. For doses higher than the neutral surface charge dose,

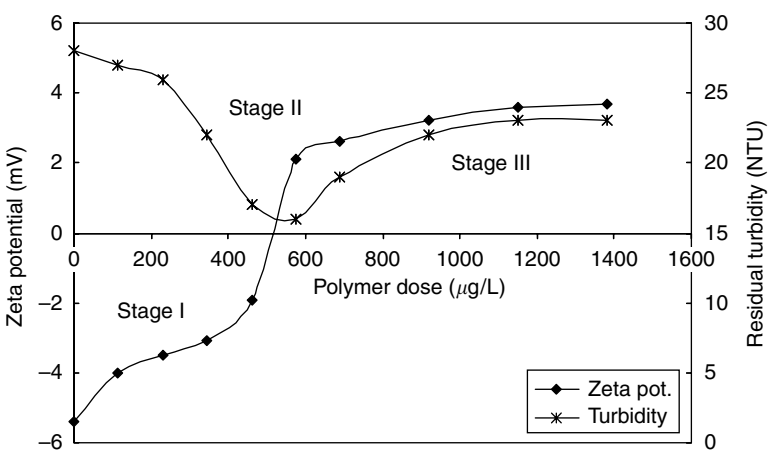

FIGURE 5.3 Zeta potential and residual turbidity measurements as a function of coagulant dose for Buffalo River suspension; different stages of aggregation are indicated with increasing dose.

turbidity increases slightly. Once the dose of coagulants was selected for a particular experimental condition (the charge neutralization dose), the next step was to photograph and analyze images of particles from the mixing jar, as described above.

5.4 RESULTS AND DISCUSSION

5.4.1 Observations and Analysis of Data

5.4.1.1 Coagulation–Flocculation

A time series of floc images formed by Buffalo River particles at different mixing times is shown in Figure 5.4 (these images were obtained as a prelude to the tests in Experiment Set 3). After only 2 min, the initially monodispersed particles are seen to form flocs of various shapes and sizes, and larger flocs formed with additional time. The larger aggregates at later times appear to be more porous and spread out than the smaller aggregates observed at earlier times, and are associated with lower fractal dimensions. The images show that the aggregate structure is an agglomerate of particles/clusters, with a highly irregular surface. Qualitatively at least, this observation supports the characterization of natural aggregates in terms of fractal geometry. The series of images in Figure 5.4 also is consistent with the aggregation

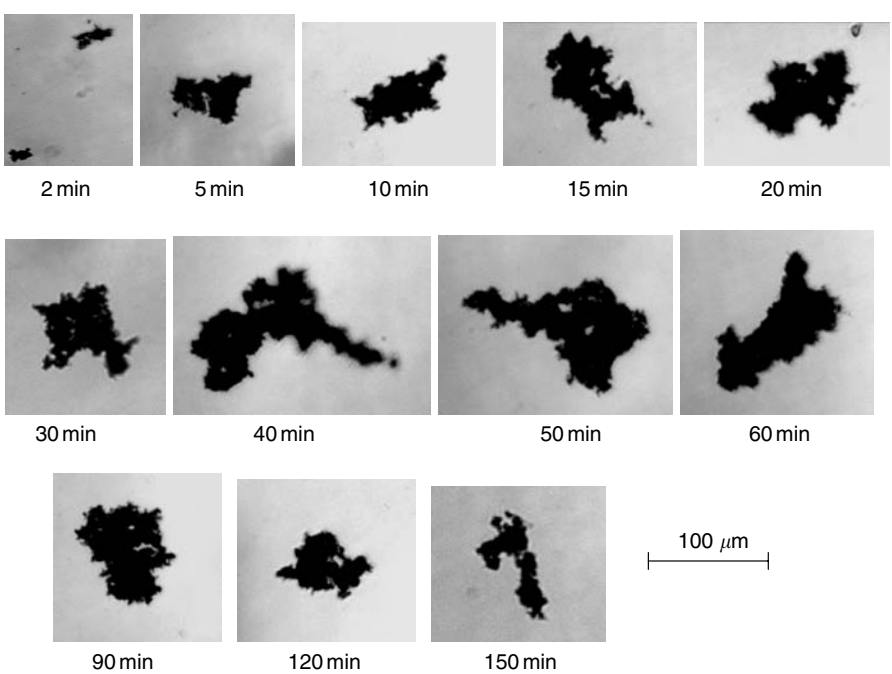

FIGURE 5.4 Images of aggregates from Buffalo River suspensions at different times of aggregation.

stages described in Figure 5.1. During the initial period of coagulation, aggregates quickly grow and become more convoluted and porous. Later, after about 50 or 60 min, aggregates appear to be more regular, with a smoother surface. This condition corresponds with the later stages described in Figure 5.1, where more loosely bound clusters have been broken off and the aggregates become denser as inner pore spaces become occupied. The period between about 40 and 60 min shows only minor changes, which should correspond with the state indicated around point A in Figure 5.1. For times greater than about 90 min, the aggregate size seems to decrease slightly, again consistent with the later stages described in Figure 5.1.

5.4.1.2 Particle Size and Shape

Geometric information from the image analysis was used to characterize particles. Temporal changes in aggregate size distribution for experiments with latex particles mixed with $G = 20\ \text{sec}^{-1}$ and $G = 10\ \text{sec}^{-1}$ are shown in Figure 5.5, where frequency of occurrence (number) in each size class is plotted against the aggregate characteristic length (major ellipse axis) using a logarithmic scale. Test results using alum (Experiment Set 2) and polymer (Experiment Set 3) are shown. In both cases the gradual movement of the peak of the distribution toward larger size is clearly seen, indicating that aggregate growth was the primary mechanism during this period (also shown in Figure 5.4). In this period (0 to 30 min) conditions are such that the model of Equation (5.10) is applicable, that is, breakup is negligible. Compared with the results using polymer, alum treatment seems to result in more peaked size distributions, with less spread about the mode. The peak size for the polymer treated experiment showed a more significant increase with time and the peak had smaller magnitudes than with the alum treated test. The higher peak associated with the alum

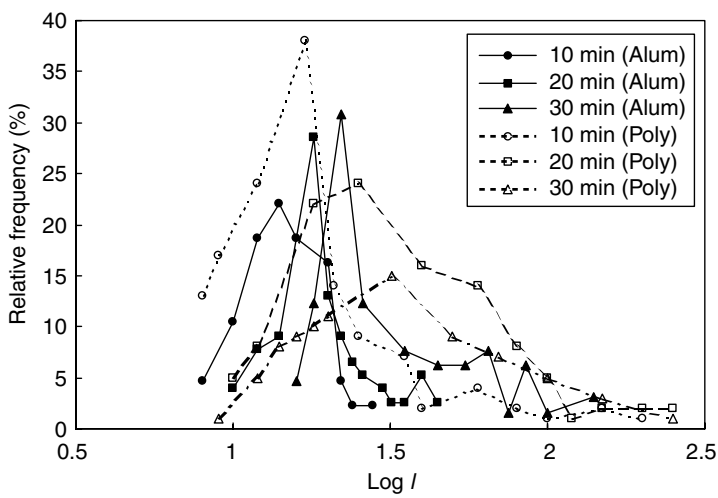

FIGURE 5.5 Temporal plot of particle size distribution for latex suspensions mixed at $G = 20\ \text{sec}^{-1}$ using alum, and mixed at $G = 10\ \text{sec}^{-1}$ using polymer (Poly).

treated tests may be related to additional solids added by the alum, and to different particle concentrations used in the two sets of experiments. It is difficult to compare the two suspensions directly since different coagulants were used and the zeta potentials for the two suspensions at charge neutralization were different, as were the mixing speeds. Keeping these differences in mind, the polymer treated coagulation produced larger (and possibly stronger) particles more quickly than coagulation by alum at the charge neutralization stage.

Temporal changes in the peak of the particle size distribution for Buffalo River suspensions mixed with polymer at $G = 10\ \text{sec}^{-1}$ are illustrated in Figure 5.6. The peak size gradually increases (until about 50 to 60 min) and then it decreases. The decrease at later times is thought to be due to the breakup effect, which has been described in several previous studies. For example, Williams et al.[29] reported a breakup of particle size after reaching a peak for silica particles mixed at various speeds. Their study suggested that smaller G would induce a larger peak and a relatively smaller decrease of peak size over time, compared to a higher mixing rate. A similar observation was reported by Selomulya et al.,[30] who found that the average aggregate size (for latex particles) decreased with time after reaching a peak, using a range of shear rates (40 to 80 sec^{-1}).

Further evidence of this type of behavior is seen in Figure 5.7 and Figure 5.8, where temporal changes in median aggregate size and D_2 are plotted for both latex (LT) and Buffalo River (BR) suspensions treated with polymer under three different mixing rates. Although not shown here, similar results were found with D_3 as with D_2. In general, slower mixing produced larger aggregates (Figure 5.7) and lower D_2 (Figure 5.8) for both these experiments, and changes in the Buffalo River suspensions were relatively more pronounced. This may be due to higher solids concentration for the Buffalo River suspension, or to the presence of organic material, which was not a factor in the latex tests. In addition, there was greater heterogeneity in aggregate size and shape for Buffalo River suspensions. In both cases there is a gradual increase in size and decrease in D_2, followed by the attainment of approximately steady-state

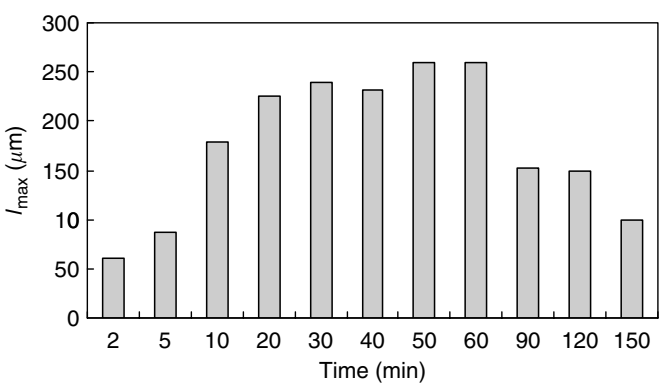

FIGURE 5.6 Temporal change in the peak of the particle size distribution for Buffalo River suspensions mixed at $G = 10\ \text{sec}^{-1}$.

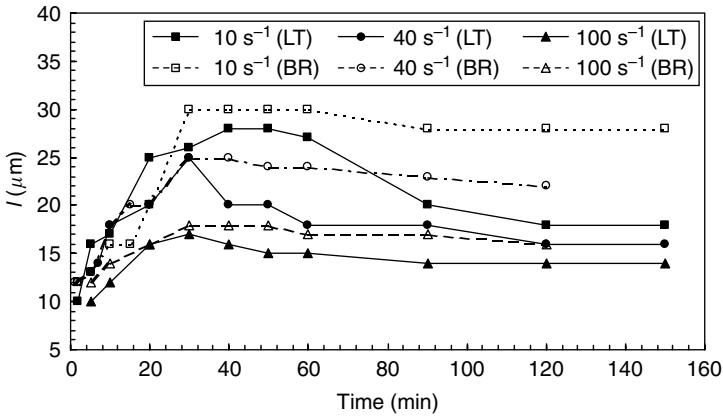

FIGURE 5.7 Temporal changes in the particle size (median) for latex (LT) and Buffalo River (BR) suspensions with various shear rates.

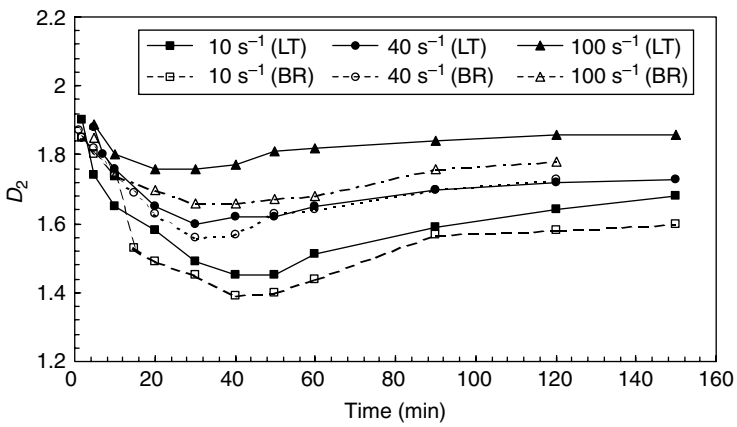

FIGURE 5.8 Temporal plot of D_2 for experiments with latex (LT) and Buffalo River (BR) suspensions with 10 sec^{-1}, 40 sec^{-1} and 100 sec^{-1} mixing speeds.

values. The final steady-state size was found to be higher than the initial size, but lower than the peak size, and final D_2 was lower than the initial value, but higher than the minimum, consistent with the above conceptual model description (Figure 5.1).

The effect of mixing speed, suggested in the results of Figure 5.7, is further demonstrated in Figure 5.9, where aggregate area is plotted as a function of size for two experiments from Experiment Set 2, using a relatively high and a relatively low mixing speed. The slopes for the lines (estimated as D_2 — see Equation (5.1)) corresponding to $G = 20$ sec^{-1} and $G = 80$ sec^{-1} were 1.62 ($\pm$0.02) and 1.75 ($\pm$0.03), respectively, where the $\pm$ values are the standard errors for the regression lines. The results verify that aggregate size correlates with mixing speed (and fractal dimension), with smaller size corresponding to larger G and larger D_2. For comparison, lines with $D_2 = 1$ and

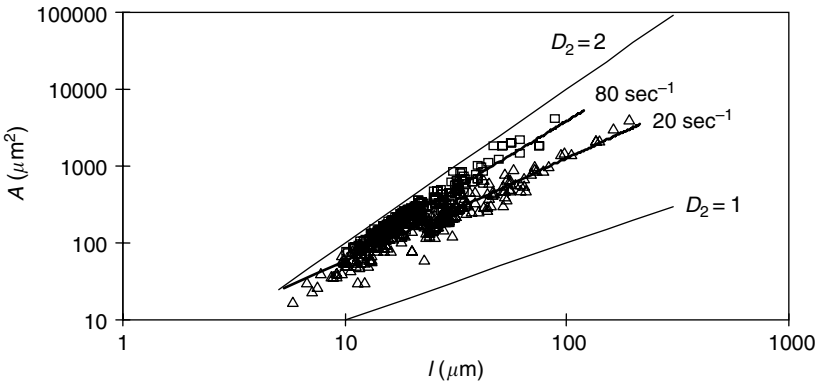

FIGURE 5.9 Effect of shear rate ($G = 20\ \text{sec}^{-1}$ and $80\ \text{sec}^{-1}$) on aggregate size, as represented by area, and comparison with Euclidean relationship ($D_2 = 2$).

$D_2 = 2$ also are drawn in Figure 5.9. With all data points falling between these two lines, it is clear that the aggregate size depends on a fractal relation.

5.4.1.3 Density and Porosity

Solid density and porosity for aggregates produced in Experiment Set 1 at sweep floc condition were calculated using Equations (5.4) and (5.5) and plotted as functions of aggregate size, taken as the major axis of the ellipse fitted to each aggregate (Figure 5.10). Various parameters needed in these definitions (e.g., shape factors) were evaluated using the imaging technique.[18,31] Primary particle density was assumed to be 2.65 g/cm^3, corresponding to clay or silt particles. For larger aggregates, large portions of the aggregate contained pores, with porosity varying between 0.92 and 0.99. Floc density varied from 1.01 to 1.10 g/cm^3, considerably less than the primary particle density. Curves were fit to the data for porosity and density, along with corresponding data from Amos and Droppo.[32] As shown in Figure 5.10, the smoothness of the fit for these curves indicates that aggregate properties scale with size. A similar relationship between floc size, density, and porosity has been observed in several previous studies.[5,33,34] As previously noted, these properties are important for settling and general transport calculations.

5.4.1.4 Collision Frequency Function

Collision frequency (β) was calculated using relations summarized in Table 5.1. To illustrate the general results, β values for a latex suspension mixed with $G = 20\ \text{sec}^{-1}$ and treated with alum are shown in Figure 5.11. Results for other tests and other particle size combinations showed similar trends and are not shown here (see Chakraborti [25] for further details). To calculate collision frequency functions, two particle sizes (i and j) are required. In these calculations, the primary particle size was taken as 10 μm, and different sizes for the second colliding particle were assumed, varying between 10 μm and 1 mm. Results also are shown when variable fractal

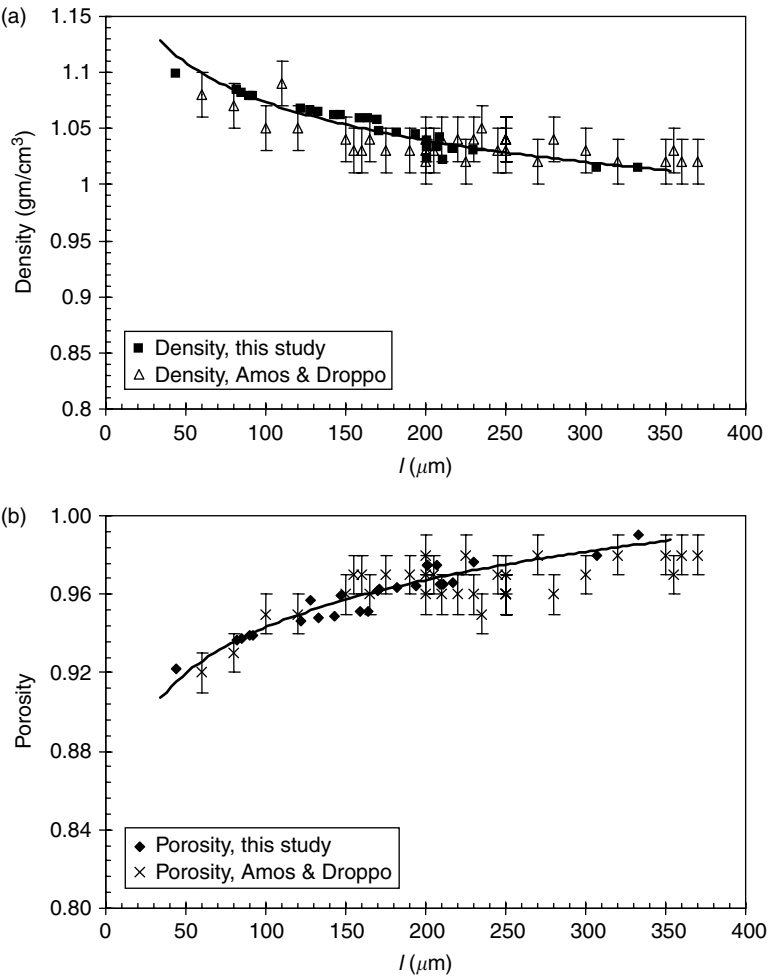

FIGURE 5.10 Aggregate properties as a function of size for lake water suspensions and measurements by Amos and Droppo[32] for (a) density and (b) porosity. Bars represent the observed range of data.

dimensions are used. In this case, the fractal dimensions obtained from Experiment Set 2, corresponding to the three different measurement times, were incorporated in the calculations ($D_2 = 1.84, 1.75$, and 1.65, and $D_3 = 2.77, 2.62$, and 2.47, for $t = 10$ min, 20 min, and 30 min, respectively). As expected, the effects of shear rate and differential sedimentation were much greater than the effects of Brownian motion. Furthermore, except for the largest particles, the impact of shear rate was greater than differential sedimentation.

Noting that the fractal dimensions decreased with time, it is seen that β generally increased with time during these experiments. The increase is particularly evident for colliding particles larger than about 100 μm, where nearly an order of magnitude

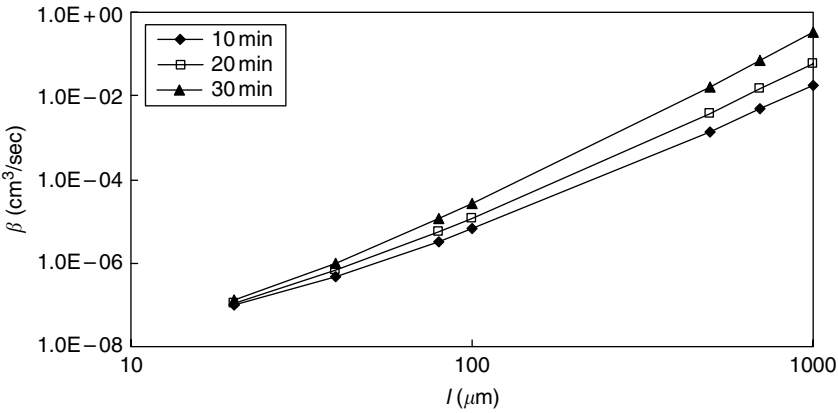

FIGURE 5.11 Total collision frequency (β) as a function of particle size (l) at different times of aggregation for latex suspensions mixed at $G = 20\ \text{sec}^{-1}$.

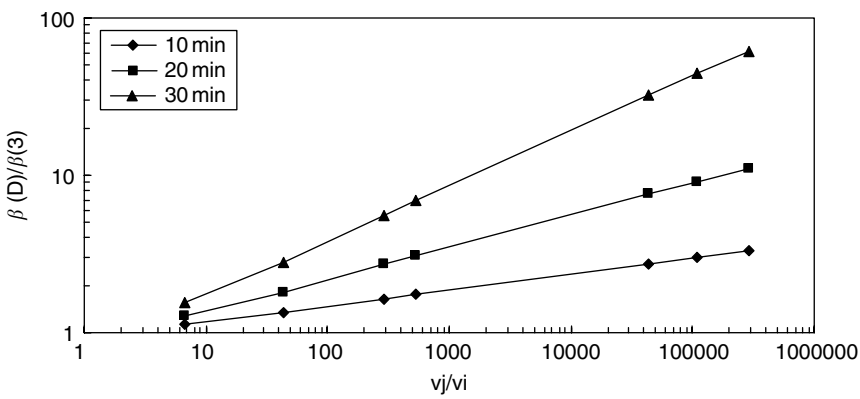

FIGURE 5.12 Comparison of total collision frequency function calculated according to fractal ($\beta(D)$) and Euclidean ($\beta(3)$) formulas at different times of aggregation.

increase is seen in the values of β for the fractal dimension corresponding to 30 min, relative to the values for 10 min. This is due to the effect of larger collision radii for aggregates that sweep out a larger volume and provide greater opportunity for collisions with other particles.

It also should be noted that the β values shown in Figure 5.11 are significantly greater than the values that would be calculated based on Euclidean dimensions. For example, setting $D_2 = 2$ and $D_3 = 3$ in the formulas in Table 5.1 gives β values consistent with traditional models that assume spherical particles. A comparison of β calculated using the Euclidean values ($\beta(3)$) and β from the fractal formulas ($\beta(D)$) is shown in Figure 5.12, where it can be seen that order of magnitude and greater increases are obtained using the fractal calculations. Chakraborti[25] provides a more detailed comparison of different calculation results for a range of particle sizes.

5.4.1.5 Settling Velocity

Using results from Experiment Set 1, the exponent in Equation (5.9) was found to be 1.96 for initial conditions, 1.73 at the charge neutralization dose, and 1.47 for sweep floc, for the lake water samples. Corresponding values for the montmorillonite suspensions were 1.82, 1.70, and 1.62, respectively. Although the exponent in these results becomes smaller for higher alum dose, l also increases with each successive coagulation stage, suggesting more rapid collision rates.[35] Thus, larger aggregate size appears to offset the effect of lower fractal dimension and helps to explain the common observation from water treatment practice that sweep coagulation results in better (lower turbidity water) settling than charge neutralization.

However, in order to fully evaluate settling, the aggregate density also must be taken into account. With increasing size (l), results from Figure 5.10(a) show that density decreases, which should reduce w_s (Equation (5.9)). Calculations based on the present samples show that w_s increases with increasing l, but at a slower rate than would be expected using a traditional (Stokes-based) model (Figure 5.13). Data in this figure were obtained by taking images of samples from the Buffalo River, which were allowed to passively settle in the mixing jar. The images were double exposed so that each aggregate was pictured twice. The difference in locations of each of the aggregate pairs was then divided by the known time interval between the two images to obtain settling rate. These rates were then plotted as a function of aggregate size. The best fit line drawn through the data has $w_s \propto l^{1.30}$, an exponent value clearly less than 2 and, in fact, even less than the exponent suggested in Equation (5.9) (discussed earlier). Thus, an additional factor must be affecting the settling, which may be due to changes in density or changes in the drag coefficient, as previously suggested. The net effect of these various factors is unknown in general, and further data are needed to determine the correct relationship for settling.

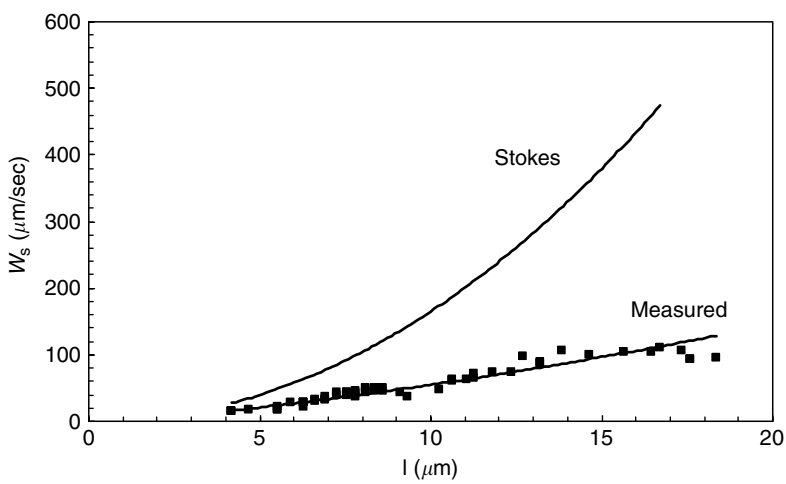

FIGURE 5.13 Settling velocity of Buffalo River solids.

5.5 CONCLUSIONS AND RECOMMENDATIONS

The focus of this study is on developing relationships between aggregate size and shape, and transport and growth behavior. Experiments were conducted to demonstrate the dependence of aggregate properties on fractal dimensions, consistent with the supposition that improvements could be made in describing aggregate characteristics and behavior in aqueous solutions using a fractal-based analysis, rather than relying on the common approach of assuming the aggregates are impervious spheres. An image-based analysis was used to develop basic geometrical properties of aggregates in suspension, from which properties such as fractal dimension could be derived. Basic properties such as density and porosity were shown to be functions of size, which also was correlated with fractal dimension. Along with relatively high porosity, these results show that the solid sphere assumption has obvious drawbacks, although it clearly has facilitated progress in aggregation theory.

To develop a full model of particle transport and behavior in an aqueous system, an extended version of Equation (5.10) would serve as a reasonable starting point, with additional terms added according to the needs of a particular application. Those terms might include breakup, settling, and internal reactions, or sources and sinks of material. The present experiments were designed to shed light on the particle aggregation and settling mechanisms, and although progress has been made, the results here are far from complete. For example, there is still uncertainty in the volume calculations, and methods are needed for nonintrusive measurement of aggregate volume. Much work remains to be done to complete a full model description, particularly with respect to settling.

From a modeling point of view, an approach needs to be developed that can incorporate changes in fractal dimensions directly into the aggregation modeling framework (Equation 5.10). Once fractal dimensions are known, they can be used to calculate collision frequency functions (Table 5.1) which are needed in the aggregation calculations. Experimental results were shown to be consistent with the conceptual model, and indicated that the basic Smoluchowski approach (Equation 5.10) could still be used, but that collision frequencies should be updated as functions of time, as fractal dimensions change. For the present tests fractal dimensions were supplied to the model using a simple empirical fit to the observed data, but ideally these values would be developed in a separate submodel. At this stage, the only approach available to accomplish this is with a DLA or RLA-type model, which would account for each individual aggregate (or at least some representative number of aggregates) and keep track of changes in fractal dimensions. While theoretically appealing, this approach is at best cumbersome for general modeling purposes, and is computationally unrealistic, even with today's computer capabilities. Nonetheless, as a research tool, this type of model may be useful and is worth a more detailed look.

Values for β are considerably different when fractal dimensions are taken into account, and an unexpected result of incorporating better resolved β in the calculations has been the realization of the need for further evaluation of α, in particular as a time-varying parameter that depends not only on the chemistry of the solution and the surface of the aggregate, but also on aggregate structure. In other words, noting that α is generally used as a fitting parameter, and that aggregation is controlled

by the product of α and β, then changes in β suggest that corresponding changes in α will be required. In addition, since β changes with time, it may be expected that α should change with time. This makes intuitive sense, as the likelihood of two colliding aggregates sticking together should be greater when they have a rougher surface, compared with a smooth sphere. So far, very little research has been directed at a finer description of collision efficiency, and this is an important area for further improvement of aggregation models.

The conceptual model developed here has been useful in explaining the different stages of aggregation for the present experiments and, more importantly, the relationship between fractal dimensions and different aggregation processes. Although designed with the specific conditions of the present experiments in mind, the model provides a framework within which one may conceptualize the correspondence between fractal dimensions and physical changes occurring among the aggregates. The model is easily extended to consider situations where an initially monodisperse suspension is not required, as the basic ideas are also applicable when a change in mixing or chemistry is induced in a system where at least the initial size distribution is known.

A property of particular interest is the settling rate, and results shown in Figure 5.13 indicate that Stokes' law is inadequate for estimating settling for fractal aggregates. Particular problems with the application of Stokes' law include determination of appropriate aggregate size and density, as well as the assumption of laminar flow around the aggregate, and the associated formulation of the drag coefficient. This last point also applies for the fractal-based expression (Equation (5.9)), since the correct formulation for drag coefficient has not been demonstrated, only assumed. The results shown in Figure 5.13 suggest the dependence of w_s on l is different than in Equation (5.9), and this difference may be due to an inadequate description of the drag coefficient. The drag coefficient assumed in Equation (5.9) comes from the expression for a sphere in laminar flow, but it would be more consistent to assume C_D as a function of fractal dimensions, which characterize general aggregate shape and would introduce the impact of different shapes on settling characteristics. Along with collision frequency and efficiency, this is another specific area where fractal dimensions can improve our ability to model particle aggregation and behavior in suspensions.

NOMENCLATURE

A	Projected area
C_D	Drag coefficient
D_1	One dimensional fractal dimension
D_2	Two dimensional fractal dimension
D_3	Three dimensional fractal dimension
g	Gravitational constant
G	Shear rate
k_B	Boltzmann constant
l	Object characteristic length

m	Mass
m_s	Solid mass (in an aggregate)
n_i	Number of particles, i-th size
N	Number of primary particles
P	Perimeter
Re	Particle Reynolds number
t	Time
T	Absolute temperature
V	Volume
w_s	Settling velocity
α	Collision efficiency
β	Total collision frequency function
β_{Br}	Collision frequency function due to Brownian motion
β_{Sh}	Collision frequency function due to shear rate
β_{DS}	Collision frequency function due to differential sedimentation
ρ	Density
ϕ	Porosity
ψ	Fractal constant
ξ	Shape factor
μ	Dynamic viscosity
ν	Kinematic viscosity
ζ	Packing factor

REFERENCES

1. O'Connor, D.J., Models of sorptive toxic substances in freshwater systems. III Streams and Rivers, *J. Environ. Eng.*, 114 (3), 552–574, 1988.
2. Droppo, I.G. and Ongley, E.D., The state of suspended sediment in the freshwater fluvial environment: A method of analysis, *Water Res.*, 26 (1), 65–72, 1992.
3. O'Melia, C.R., and Tiller, C.L., Physicochemical aggregation and deposition in aquatic environments, in *Environmental Particles* (Vol 2), J. Buffle and H.P. van Leewen, Eds., Lewis Publishers, Boca Raton, FL, 1993, chap. 8.
4. Chapra, S.C., *Surface Water Quality Modeling*, McGraw Hill, New York, 1997.
5. Droppo, I.G., et al., The freshwater floc: A functional relationship of water and organic and inorganic floc constituents affecting suspended sediment properties, *Water Air Soil Pollut.*, 99, 43–54, 1997.
6. Lawler, D.F., Removing particles in water and wastewater, *Environ. Sci. Technol.*, 20 (9): 856–861, 1986.
7. Elimelech, M., Gregory, J., Jia, X., and Williams, R.A., Particle deposition and aggregation — Measurement, modeling and simulation, Butterworth-Heinemann Ltd., London, U.K., 1995.
8. O'Melia, C.R., Coagulation, in *Water Treatment Plant Design for the Practicing Engineer*, R.L. Sanks, Ed., Ann Arbor Science, MI, 1979, chap. 4.
9. Gregory, J., Fundamentals of flocculation, *Crit. Rev. Env. Con.*, 19 (3), 185–230, 1989.
10. Mandelbrot, B.B., *The Fractal Geometry of Nature*, W.H. Freeman, San Francisco, CA, 1983.
11. Meakin, P., Fractal aggregates, *Adv. Coll. Int. Sci.*, 28, 249–331, 1988.

12. Meakin, P., Simulations of aggregation processes, in *The Fractal Approach to Heterogeneous Chemistry*, D. Avnir, Ed., John Wiley and Sons, NY, 131–158, 1989.
13. Meakin, P., Fractal aggregates in geophysics, *Rev. Geophysics*, 29, 317–354, 1991.
14. Meakin, P., A historical introduction to computer models for fractal aggregates, *J. Sol-Gel Sci. Tech.*, 15, 97–117, 1999.
15. Jiang, Q. and Logan, B.E., Fractal dimensions of aggregates determined from steady state size distributions, *Environ. Sci. Technol.*, 25 (12), 2031–2038, 1991.
16. Jiang, Q. and Logan, B.E., Fractal dimensions of aggregates from shear devices, *J. Amer. Water Works Assoc.*, 88 (2), 100–113, 1996.
17. Johnson, C.P., Li, X., and Logan, B.E., Settling velocities of fractal aggregates, *Environ. Sci. Technol.*, 30, 1911–1918, 1996.
18. Logan, B.E., *Environmental Transport Processes*, John Wiley and Sons Inc, 1999.
19. Witten, T.A. and Sander, L.M., Diffusion-limited aggregation: A kinetic critical phenomenon, *Phy. Rev. Lett.*, 47 (19), 1400–1403, 1981.
20. Witten, T.A. and Sander, L.M., Diffusion-limited aggregation, *Phys. Rev.*, B 27, (9), 5686–5697, 1983.
21. Smoluchowski, M., Versuch einer Mathematischen Theorie der Koagulation-Kinetik Kolloider Losungen, *Z. Physik. Chem.*, 92, 129, 1917.
22. Xavier, C. and Schladow, G., Vertical Distribution of Particles in Stratified Lake, *J. Environ. Eng.*, 119 (3), 443–462, 1993.
23. Wiesner, M.R., Kinetics of aggregate formation in rapid mix, *Water Res.*, 26(3), 379–387, 1992.
24. Kusters, K.A., Wijers, J.G., and Thoenes, D., Aggregation kinetics of small particles in agitated vessels, *Chem. Eng. Sci.*, 52, 107–121, 1997.
25. Chakraborti, R.K., *Application of Fractal Concepts for Analysis and Modeling of Particle Aggregation*, Ph.D. Dissertation, Dept. of Civil Struct. Environ. Eng., University at Buffalo, Buffalo, New York, 2004.
26. Chakraborti, R.K. et al., Changes in fractal dimensions during aggregation, *Water Res.*, 37 (4), 873–883, 2003.
27. Chakraborti, R.K., Atkinson, J.F., and Van Benschoten, J.E., Characterization of alum floc by image processing, *Environ. Sci. Tech.*, 34 (18), 3969–3976, 2000.
28. Cheng, C.-Y. et al., An image-based system for particle counting and sizing, *J. Environ. Eng.*, 126 (3), 258–266, 2000.
29. Williams, R.A., Peng, S.J., and Naylor, A., In-situ measurement of particle aggregation and breakage kinetics in concentrated suspension, *Powder Tech.*, 73, 75–83, 1992.
30. Selomulya, C. et al., Evidence of shear rate dependence on restructuring and break up of latex aggregates, *J. Colloid Int. Sci.*, 236, 67–77, 2001.
31. Vicsek, T., *Ractal Growth Phenomena*, World Scientific, New Jersey, 1992.
32. Amos, C.L. and Droppo, I.G., *The Stability of Remediated Lake Bed Sediment*, Hamilton Harbour, Lake Ontario, Canada, Geological Survey of Canada, open file report No. 2276, 1996.
33. Tambo, N. and Watanabe, Y., Physical characteristic of flocs I. The floc density function and aluminum floc, *Water Res.*, 13, 409–419, 1979.
34. Klimpel, R.C., Dirican, C., and Hogg, R., Measurement of agglomerate density in flocculated fine particle suspensions, *Particulate Sci. Tech.*, 4, 45–59, 1986.
35. Serra, T. and Logan, B.E., Collision frequencies of fractal bacterial aggregates with small particles in a sheared fluid, *Environ. Sci. Tech.*, 33, 2247–2251, 1999.

6 Mapping Biopolymer Distributions in Microbial Communities

John R. Lawrence, Adam P. Hitchcock, Gary G. Leppard, and Thomas R. Neu

CONTENTS

1-56670-615-7/05/$0.00+$1.50

6.1 INTRODUCTION

Microbial communities or aggregates also known as biofilm systems may be divided into stationary ones and mobile ones. Stationary ones are the classical microbial films usually on solid surfaces. Mobile ones have been named with a variety of terms such as assemblages, aggregates, flocs, snow, or mobile biofilms.[1] The techniques described in the following chapter apply to both biofilms and flocs. Aquatic aggregates (river, lake, marine, technical) may be very different in terms of size, composition, density, and stability.[2] Lotic aggregates are structurally very stable as they are exposed to a constant shear force resulting in relatively small aggregates ($\approx$ 5 to 300 μm), whereas lake or marine snow may be very fragile and much larger (millimeters to meters). Both environmental aggregates are colonized to a certain degree by prokaryotic and eukaryotic microorganisms (bacteria, algae, fungi, protozoa). The bacterial composition of environmental aggregates was studied *in situ*, for example, by Weiss et al.[3] In comparison to natural aggregates, technical aggregates are heavily colonized mainly by bacteria, for example, in activated sludge.[4] The microbial population structure of activated sludge was first analyzed *in situ* by Wagner et al.[5] Another example for man-made aggregates are mobile biofilms growing on carrier material, for example, in fluidized bed reactors. Due to high shear force, these immobilized aggregates are extremely dense and stable.[6] A major understudied component of all these microbial systems is their exopolymeric matrix.

Exopolymeric substances have correctly been referred to as the mystical substance of biofilms and aggregates[7] and a challenge to properly characterize.[8] The extracellular polymeric substances (EPS) are defined as organic polymers of biological origin which in biofilm systems are responsible for the interaction with interfaces.[7] Although EPS are understood as extracellular polymers mainly composed of microbial polysaccharides, by definition other extracellular polymeric substances may also be present, for example, proteins, nucleic acids and polymeric lipophilic compounds.[8–11] In biofilm systems we can expect two types of structural polymeric carbohydrate structures. First, those associated with cell surfaces and second, those located extracellularly throughout the extracellular biofilm matrix. The importance of EPS in flocs and biofilm systems is fundamentally twofold: (i) they represent a major structural component of flocs and (ii) they are responsible for sorption processes.[12,13]

Particularly in complex environmental systems, the EPS are difficult if not impossible to chemically characterize on the traditional basis of isolating single polymer species. Chemical approaches are limited to pure culture, chemically defined systems. Despite this problem, chemical quantification of EPS constituents in biofilm systems have been reported.[14] These confirm the complex nature of the material and the extensive range of polymers present. Increasingly attempts have been made to examine natural biofilm and floc polysaccharides *in situ*.[1,8,15–18]

The critical need for *in situ* analyses and visualization of EPS is due to its complex chemical nature and the importance of its molecular structure in its behavior. Indeed, the challenge remains to characterize its chemical composition in the context of its biological form. To do this we have proposed a variety of *in situ* methods based on the application of chemical probes and 1P (1-photon) and 2P (2-photon) laser microscopy. In addition, synchrotron radiation using the interaction of x-rays with

the molecular structure of intact hydrated biofilms has proven an effective approach. In this overview we assess *in situ* analyses of EPS using light of various wavelengths ultraviolet, visible, infrared, and x-ray in combination with targeted probes to assess the structure of biofilms and flocs.

6.2 METHODOLOGY

6.2.1 Handling Flocs for Microscopic Examination

Due to their size, location and relative fragility, river, lake, or marine flocs are difficult to examine under *in situ* conditions. Lotic aggregates are often sampled in bottles with, for example, one or two liter volume. Similarly, lake or marine flocs maybe sampled directly into special containers by scuba divers.[19] However, within 30 min, these sampling procedures will result in settling and co-aggregation of smaller flocs into larger loosely associated aggregates of several 100 μm diameter thus analyses of these specimens are extremely time sensitive. Leppard[20] reported the occurrence of artifactual aggregation where small aggregates combine to yield a few large aggregates. In addition, it was noted that rough handling (high flow, centrifugation) storage longer than 24 h, and most concentration steps will all result in coagulation of the flocs.

In order to maintain structural integrity of the sample some care must also be exercised in the preparation for microscopic examination. In general, biofilm and floc samples are exposed to physical stress in the real-world environment, therefore in most instances they are resilient enough to be manipulated and mounted for staining and observation. However, laboratory treatments such as drying, freezing, washing, dehydration etc. will all perturb the native structure of the floc. Leppard,[20,21] Leppard et al.,[22] and Droppo et al.[23] provide useful instruction on the handling of flocs for microscopic examination and preservation of their native state and properties. Staining may be carried out by careful addition of the stain and its withdrawal using tissues or small sponges, with subsequent replacement and washing with sterile medium (variously 3× to 5×) or environmental water (river, lake, pond, etc.). In some instances removal of excess stain must be carried out by centrifugation of the floc and resuspension in stain/probe free water. Only careful evaluation can determine at what point these treatments will alter the floc under investigation and this should be assessed for each type of floc examined. Conventional wet mounts and other slide preparations may also be usefully performed to examine flocs.[24] Floc or aggregate samples may be fixed to the bottom using flowable silicon adhesives or allowed to settle to the bottom of a small petri dish (diameter 5 cm). In these cases an upright microscope may be used to examine the preparation. In the case of flocs an inverted microscope in combination with a settling chamber having a cover slip bottom such as those provided by NalgeNunc International, Denmark, may be a preferred method of preparation for 1-photon laser scanning microscopy (1P-LSM), 2-photon laser scanning microscopy (2P-LSM), or fluorescence microscopy.[1] Although if an inverted microscope is used, access to the sample is limited and the working distance of the objective lens may further limit examination of the material. It is also possible that lotic aggregates be collected directly in the LabTek coverslip chambers (NalgeNunc International). By this sampling procedure the settling and co-aggregation of small flocs is kept to

a minimum. Subsequently, the aggregates can be microscopically examined using LSM for reflection signals and autofluorescence (general, algal, cyanobacterial). In addition, flocs may be stained inside the chamber using nucleic acid specific stains to record bacterial distribution and fluorescently labeled lectins to record glycoconjugate distribution.

In the case of synchrotron based imaging such as scanning transmission x-ray microscopy (STXM) the sample must be prepared on an x-ray transparent holder. STXM measurements must be performed with the sample in a wet cell constructed with a silicon nitride window (Silson Inc, Northampton, U.K.) by placing the sample onto one half of the silicon nitride cell and sealing it with the other half. Figure 6.1 shows a typical completed wet cell with enclosed biofilm material. The wet cell is then placed directly in the beamline for imaging.[25,26]

6.2.2 Epifluorescence Microscopy

Conventional widefield epifluorescence microscopy provides simple effective means to examine the results of most staining of the exopolymers of microbial cells, flocs, and biofilms provided a suitable range of optical filters are available. Optical sectioning may be achieved using epifluorescence, a stepper motor, and a digital video imaging device. The major limitation of the image series collected is poor axial resolution, however, this may be improved by computing intensive restoration procedures or deconvolution (see Section 6.2.3).

6.2.3 CLSM and 2P-LSM

Confocal laser scanning microscopy (CLSM or 1P-LSM) has become an indispensable technique for the study of interfacial microbial communities.[27] This is particularly due to the increasing number of fluorescent stains and reporter

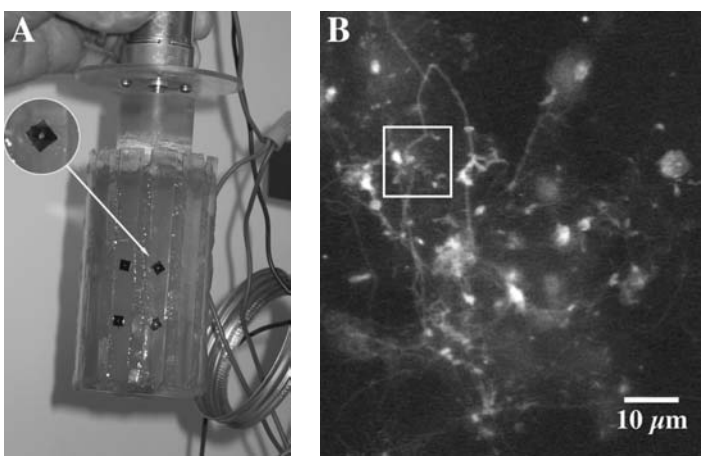

FIGURE 6.1 (A) Image shows a silicone nitride window attached to a rotating annular biofilm reactor, and detail in inset shows window and central x-ray transparent region for STXM imaging; (B) CLSM image of x-ray transparent region showing biofilm development on the window.

systems suitable for application in the study of flocs and biofilms. Specific techniques include those for detection and quantification of cellular and polymeric compounds in biofilms.[9,16,27] In addition, Neu et al.[28] demonstrated that 2P-LSM could be effectively applied to the study of highly hydrated microbial systems such as flocs and that a range of fluorescent reporters for both cell and exopolymer identity could be applied in combination with this imaging approach. Figure 6.2 provides a comparison of the excitation for 1P versus 2P for the common fluor fluorescein illustrating the different response of the fluor in the two forms of LSM. Extensive details of these microscopy techniques and their use in combination with biofilms and flocs are provided in Lawrence et al.[27] Neu,[1] Lawrence and Neu,[29] and Lawrence et al.[30]

6.2.3.1 CLSM Limitations

A limitation of 1-photon excitation is laser penetration of samples (excitation) and detection of emission signal in thick samples. This problem is very much dependent upon the density and light scattering properties of the sample. Consequently thick samples have to be embedded and physically cut into slices using embedding resins or cryosectioning.

6.2.3.2 2P-LSM Limitations

The major problems are the overall stability of the laser system, maintenance of signal intensity, and excessive noise in the image. In addition, images may be degraded by reaction of the light source with the substratum or mounting materials causing, for example, streaks in the image due to adsorption of infrared light (e.g., plastics). Although laser penetration is better (twofold) in 2P-LSM over CLSM, light scattering in thick biological samples remains a problem.

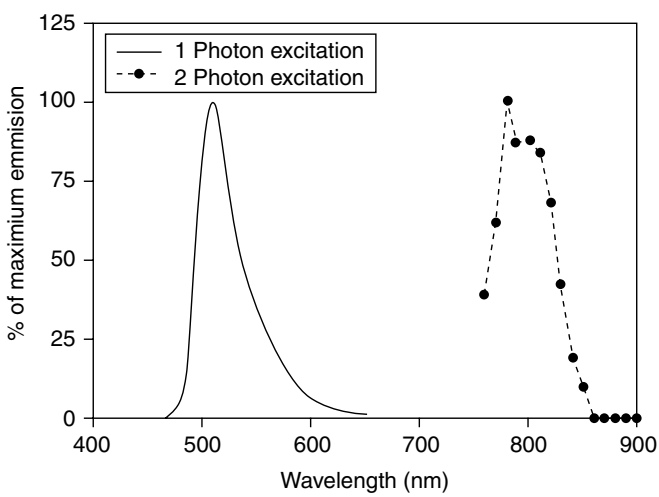

FIGURE 6.2 Comparison of the 1P and 2P emission for fluorescein when excited at wavelengths between 400 and 900 nm.

6.2.4 Synchrotron Radiation (Soft x-ray Imaging)

Scanning transmission x-ray microscopy (STXM) is a powerful tool that may be applied to fully hydrated biological materials. This is due to the capacity of soft x-rays to penetrate water and have minimal radiation damage relative to electron techniques. In addition, soft x-rays interact with nearly all elements and also allow mapping of chemical species based on bonding structure.[31] Soft x-ray microscopy also provides suitable spatial resolution and chemical information at a microscale relevant to bacteria. Most importantly, the method uses the intrinsic x-ray absorption properties of the sample eliminating the need for the addition of reflective, absorptive, or fluorescent probes and markers which may introduce artifacts or complicate interpretation. Figure 6.3 shows the representative absorption spectra for protein, nucleic acid, saccharide, lipid, and calcium carbonate. The potential of soft x-rays for imaging early stage *Pseudomonas putida* biofilms using a full field transmission x-ray microscope with synchrotron radiation was demonstrated by Gilbert et al.[32] They measured at single photon energy and did not explore the analytical capability of x-ray microscopy. Lawrence et al.[25] demonstrated the application of analytical soft x-ray microscopy to map protein, nucleic acids, lipids, and polysaccharides in biofilm systems. Hard

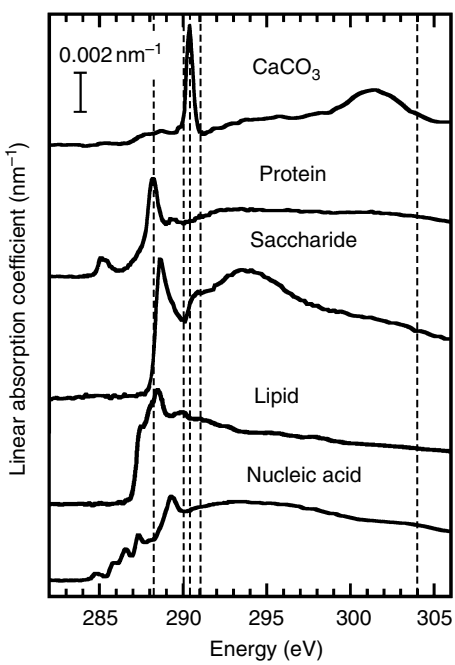

FIGURE 6.3 C 1s NEXAFS spectra of protein (albumin), polysaccharides (sodium alginate), lipid(1-Palmitoyl-2-Hydroxy-sn-Glycero-3-Phosphocholine), and nucleic acid (calf thymus DNA). All spectra except that of DNA were recorded with the ALS 7.0.1 STXM. The spectrum of DNA was recorded on ALS 5.3.2 STXM. (Copyright American Society for Microbiology, Lawrence, J.R. et al. *Appl. Environ Microbiol*: 69: 5543–5554, 2003.)

x-ray analyses also have potential for application to biofilm–floc materials having been used for bacterial cell–metal interaction studies.[33]

6.2.4.1 STXM Limitations

Limitations to STXM include: suitability of the model compounds relative to biofilm/floc material, data acquisition without undue radiation damage, requirement for very thin samples (<200 nm equivalent thickness of dry organic components, less than 5 micron of water when wet), use of fragile silicon nitride windows, sample preparation, that is, encapsulation in a wet cell, and absorption saturation distortion of analysis in thick regions of a specimen.

6.3 TARGETS AND PROBES

The *in situ* analyses of hydrated biofilms may be carried out using a variety of probes targeted generally at polysaccharides, proteins, lipids, or nucleic acids. In addition, other probes such as dextrans, ficols, and polystyrene beads may be used to assess general properties such as charge, hydrophobicity, permeability, or the determination of diffusion coefficients. Probes are most frequently conjugated to fluors although colloidal reflective conjugates (gold, silver) may be used.[27] Recently, quantum dots (QDs) have shown great promise as multiwavelength fluorescent labels. Colloidal QDs are semiconductor nanocrystals whose photoluminescence emission wavelength is proportional to the size of the crystal. Kloepfer et al.[34] reported that cell surface molecules, such as glycoproteins, made excellent targets for QDs conjugated to wheat germ agglutinin. This new class of fluorescent labels may open opportunities for *in situ* detection of matrix chemistry. As indicated above, the option exists for probe independent examination of major biopolymers and other constituents in hydrated biofilm and floc material providing a basis for detailed examination of these structures and ground truthing of the fluorescent and reflection based probe dependent approaches.

6.3.1 Polysaccharides

6.3.1.1 General Probes

A range of stains with specificity for beta-D-glucan polysaccharides are used as general stains, these include calcofluor white and congo red. Ruthenium red has also been used as a light microscopy stain for detection of EPS. Probes for glycoaminoglycan such as Alcian blue may also be used as a general stain for "polysaccharides." Wetzel et al.[35] demonstrated its use for determination of total EPS in microbial biofilms, in this case it was used indirectly and not for microscopy. Due to the complexity of the EPS the likelihood of finding a true total polysaccharide probe appears to be very limited.

6.3.1.2 Lectins

Lectin-like proteins have a long history of application in the biological sciences.[36] Currently, lectins are regarded as proteins with a lectin–carbohydrate and a lectin–protein binding site and are characterized on the basis of their interactions with specific monosaccharides. Lectins are produced by many organisms including plants, vertebrates, protists, slime molds, and bacteria where they function as cell/surface-recognition molecules.[37] Recognition of the specific site is controlled by stereochemistry, however, the carbohydrates also interact with lectins via hydrogen bonds, metal coordination, van der Waals, and hydrophobic interactions.[38] (See also review articles and comprehensive books on lectins.[39–42])

The difficulty of isolating a single polymer type from a complex biofilm matrix may be comparable to the situation at the cellular level.[43] Neu et al.[16] noted that if one considers the potential of carbohydrates to encode information in terms of saccharides it is even larger than that of amino acids and nucleotides. The latter two compounds can only build 1 dimer whereas one type of monosaccharide can form 11 different disaccharides. Further, 4 monosaccharides, a common number in the repeating unit of polysaccharides, may form 35,560 different disaccharides.[37] If each of the estimated number of bacterial species (4,800,000) secretes one protein and one polysaccharide this would be 9,600,000 EPS compounds; a very conservative estimate.[44] As a consequence, there is a need to establish an *in situ* technique for the assessment of glycoconjugate distribution in floc systems. At present the most promising approach to achieve this is the application of fluorescent-lectin-binding-analysis (FLBA) in combination with CLSM. Labeled lectins have been successfully used in many microbial pure culture studies to probe for cell surface structures.[45–48] Fluor conjugated lectins have also been used fairly extensively in complex environments including, marine habitats[49] and freshwater systems.[1,15,16,18,30,50,51]

As noted by Neu and Lawrence[9] lectins may represent a useful probe for *in situ* techniques to three-dimensionally examine the distribution of glycoconjugates in fully hydrated microbial systems. The many lectins available, offer a huge and diverse group of carbohydrate specific binding molecules waiting to be employed for an *in situ* approach.[52] The above listed studies all suggest that lectins may be applied successfully to extract information regarding the nature of the EPS. Fluor-conjugated lectins effectively reveal the form, distribution, and arrangement of EPS in three dimensions. Figure 6.4 illustrates this phenomenon showing the distribution of EPS using *Solanum tuberosum, Cicer arietinum*, and *Tetragonolobus purpureas* lectins and confocal laser microscopy to examine a microcolony in a river biofilm, note the multiple layers of EPS identified by each lectin and their spatial distribution. Figure 6.5 illustrates the distribution of binding sites for lectins within a river floc from the Elbe River. As also shown in Figure 6.5, FLBA has been combined with fluorescent *in situ* hybridization (FISH; see review by Amann et al.)[53] to allow localization and identification of bacteria associated with the binding of specific lectins.[17] This visualization is extremely useful as a starting point for additional questions regarding the EPS. However, the major goals of quantification and chemical identification remain more elusive. Neu et al.[16] evaluated lectin binding in complex habitats in detail. They showed that it was possible, through digital

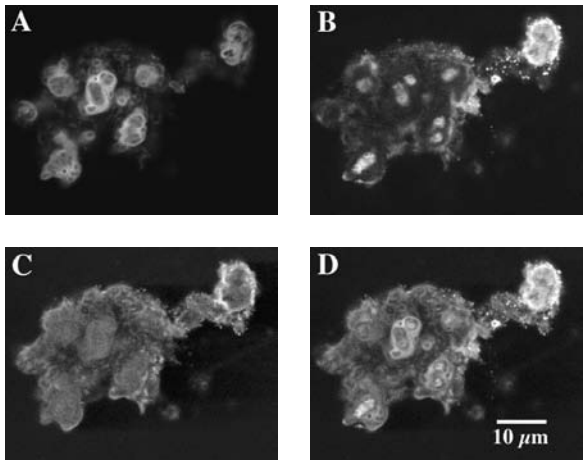

FIGURE 6.4 CLSM micrographs of a bacterial microcolony stained with lectins (A) *Cicer arietinum*-Alexa-568; (B) *Solanum tuberosum*-FITC; (C) *Tetragonolobus purpureas*-CY5; and (D) the overlay image of all three channels showing the layers and differential lectin binding.

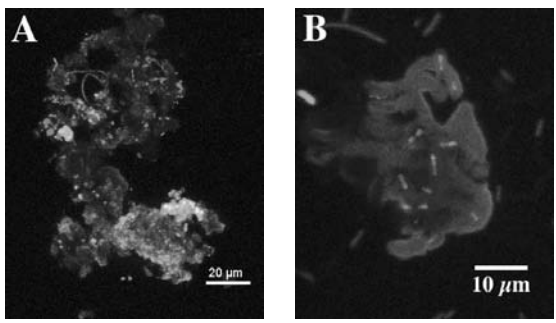

FIGURE 6.5 (**Color Figure 6.5 appears following page 236.**) Images of the combined FLBA–FISH approach showing (A) staining of an Elbe River floc where the gene probe EUB-CY3 and lectin *Canavalia ensiformis*–FITC were applied; and (B) the binding of the lectin *Cicer arietinum*–Alexa-568 and the lectin *Arachis hypogaea*–CY5 with localization of beta-proteobacterial cells using the probe Bet42a.

image analyses of confocal image stacks, to quantitatively evaluate the binding of different lectins spatially and with time. Neu et al.[18] were able to detect clear statistically significant effects of nutrient treatments and time on the EPS composition of river biofilms using CLSM and FLBA. Figure 6.6 shows a typical data set with variation in lectin binding in response to the addition of nutrients during biofilm development. There were however, effects of the fluor, the matrix, and the lectin on the apparent specificity of lectin binding and limitations on the interpretation of the nature of binding site of the lectin. Recent comparative STXM–CLSM studies of biofilms demonstrated significant agreement between the probe target dependent

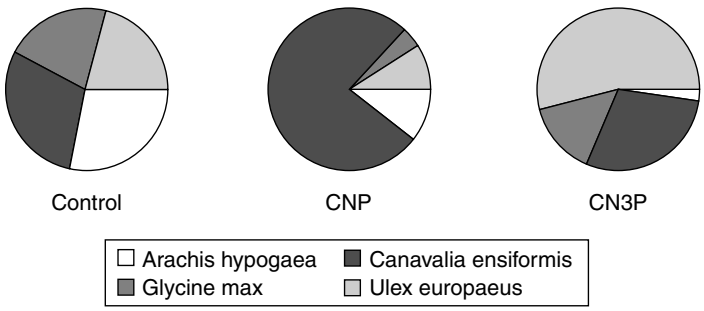

FIGURE 6.6 Sample data set illustrating the effect of nutrient additions on the EPS composition as determined by a panel of fluor-conjugated lectins. Note the increase in *Canavalia ensiformis* lectin binding in the carbon, nitrogen, phosphorus treatment versus the increase in *Ulex europeaus* lectin binding when 3x phosphorus is added to the river water during biofilm development.

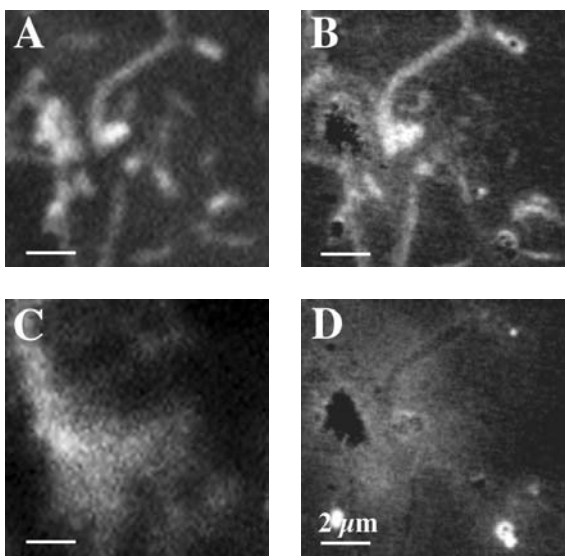

FIGURE 6.7 (A) CLSM image of mixed species river biofilm stained with nucleic acid sensitive stain Syto9; (B) STXM image of the same location showing the location of nucleic acids as detected by fitting models based on spectra in Figure 6.3; (C) localization of fucose containing polysaccharide using the fucose sensitive lectin *Tetragonolobus purpureas*; and (D) the same area imaged using STXM and fitting of general polysaccharide.

identification of polysaccharide by CLSM and the probe independent detection based on soft x-ray spectroscopy. Lectin binding could be shown to identify subsets of the total polysaccharide regions detected using STXM (Figure 6.7). Significant questions remain however regarding the precise chemical interpretation of the binding of a specific lectin.

6.3.1.3 Antibodies

Antibodies have been suggested as potential probes for sugars and carbohydrates, however there are limitations to their application in complex microbial communities. For example, (i) the production of antibodies against carbohydrates is in general difficult relative to proteins, (ii) it requires the isolation of pure polysaccharide material from the complex polysaccharide matrix of a complex microbial biofilm community, and (iii) if the antibody could be produced its specificity would allow only the detection of a very limited fraction of the carbohydrates present in a complex biofilm community. Thus the application of antibodies presents significant technical and interpretative barriers for *in situ* characterization procedures.

6.3.2 Proteins–Lipids

Proteins are major constituents of the exopolymeric matrix of floc and biofilm systems. Particularly in activated sludge flocs, protein can be the most important contributor representing 50% or more of the extractable EPS.[14,54] Both extractive analysis and *in situ* detection of protein is complicated by the presence of lipoproteins and glycoproteins, molecules that have a chemistry representative of more than one class of biomolecule.

Neu and Marshall[55] applied a "protein specific" probe Hoechst 2495 to detect bacterial footprints on surfaces. In this case these remnant structures were readily detected with this dye, consistent with the presence of a high level of protein in the EPS. The SYPRO series of protein stains, although developed for protein in gels and solutions have been proposed for application *in situ*. Lawrence et al.[25] applied SYPRO orange alone and in combination with other macromolecular stains. These SYPRO stains bound extensively in the biofilm system, both in a cell associated and matrix distributed pattern. They found strong colocalization of protein, lipid, and polysaccharide. Parallel studies using STXM verified that colocalization was a valid interpretation and representative of conditions in the biofilm matrix. Again this may reflect the lipoprotein, glycoprotein distribution in the matrix polymer.

The hydrophobic lipid stain Nile Red has also been used extensively to detect lipids in algal and bacterial cells and associated materials. Wolfaardt et al.[56] reported using Nile Red to detect hydrophobic cell surfaces within a degradative biofilm community, while Lamont et al.[57] indicated that lipid deposits associated with *Frankia* could be localized.

6.3.3 Nucleic Acids

Nucleic acids are also abundant in biofilms both as cell associated DNA–RNA and within the extracellular matrix of the biofilm or floc. Although noncellular binding of nucleic acid stains has often been classified as nonspecific staining, it has become apparent that DNA may be a structural component of biofilms. Indeed extractive studies have often indicated that a considerable fraction of the biofilm EPS is DNA. Some reports reviewed in Nielsen and Jahn[14] indicate that nucleic acids may comprise 5 to 15% of the extracellular materials in pure culture biofilms and activated sludge.

Recently, Whitchurch et al.[58] indicated using pure cultures that this extracellular DNA may be structural in nature and required for biofilm development. Similarly, Lawrence et al.[25] detected extracellular nucleic acids in biofilm materials using STXM. Correlation of fluorescent nucleic acid staining with the results of soft x-ray analyses indicated that both detected regions of non-cellular nucleic acids within a biofilm.

6.3.4 Charge/Hydrophobicity

The essential approach to *in situ* determination of surface charge involves the application of probes with known characteristics with assessment of their binding patterns in the floc matrix. The use of fluorescent beads with sulfated or carboxylated surface chemistry has been used for determination of hydrophobicity and hydrophilicity of bacterial cells and may be used for flocs. Zita and Hermannson[59] describe the essential method using beads obtained from Molecular Probes Inc. (Molecular Probes, Eugene, OR). Fluorescent beads have also been used to analyze under *in situ* conditions the surface properties of filamentous bacteria in activated sludge flocs.[60] As noted above the binding of the hydrophobic dye Nile Red a lipophilic compound may also be interpreted as recognition of hydrophobic regions. Similarly, dextrans may be obtained with anionic, polyanionic, neutral, or positive charges, these may also be reacted with microbial EPS to assess charge and charge distribution. This approach has been applied by Wolfaardt et al.[56] Figure 6.8 are three-dimensional (3D) stereo pairs of the binding of 100 nm carboxylate and 20 nm sulfate modified beads at the same location in a river biofilm. The image shows differential binding based on hydrophobicity and penetration of the biofilm material based on hydrated radius of the probe.

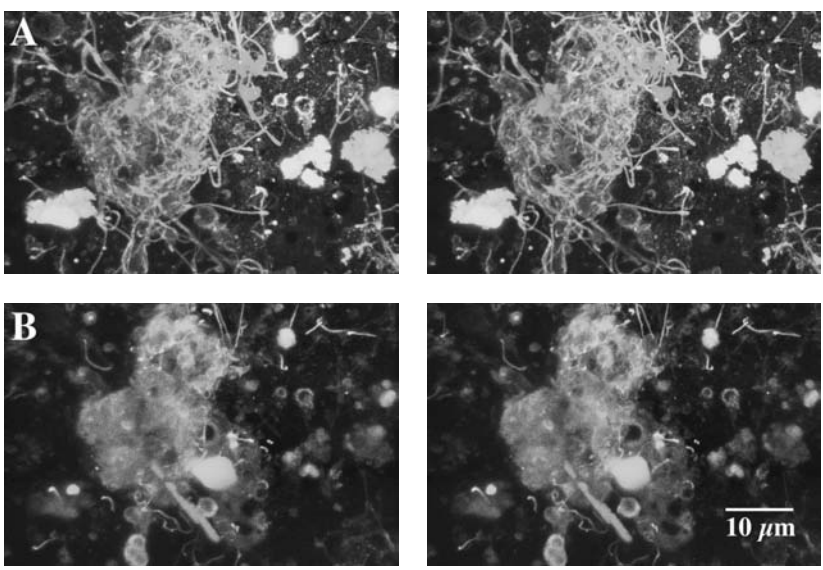

FIGURE 6.8 CLSM stereo pairs A and B showing the differential sorption of the 100 nm carboxylate modified beads and 20 nm sulfate modified beads in river biofilm.

6.3.5 Permeability

There are a number of fluor conjugated probes that may be used to assess permeability and diffusion coefficients of bacterial cells and polymer, these include ficols, size fractionated dextrans, and a range of fluorescent beads (10 nm to 15 μm diameter) (see, e.g., Molecular Probes, Eugene, OR). Lawrence et al.[61] used 1P-LSM to monitor the migration of fluor conjugated dextrans to determine effective diffusion coefficients for biofilm systems. Microinjection and 1P-LSM has been developed by De Beer et al.[62] to determine diffusion coefficients in biofilm materials. The standard FRAP (fluorescence recovery after photobleaching) approach may also be applied to bacteria, aggregates, and biofilms. Figure 6.9 (see also Section 6.3.4) illustrates the penetration of biofilm microcolonies by 100 and 20 nm diameter fluorescent beads.

6.4 EXAMINATION OF EPS BOUND AND ASSOCIATED MOLECULES

Due to its chemical heterogeneity the EPS of biofilms is an important site for the sorption of carbon, metals, contaminants, and enzymes.[12] A number of studies indicate that the EPS of biofilms functions to maintain long-term reserves of metabolizable carbon.[63,64] Wolfaardt et al.[65] demonstrated that autofluorescence could be used to localize the herbicide diclofop methyl in biofilm polymers and to follow its sorption and subsequent metabolism. Antibodies may be used to map the locations of specific enzymes, specific compounds such as pesticides, and a variety of other biologically relevant molecules. Specific enzyme activity associated with EPS may be localized using antibodies or fluorescent reporters of enzyme activity.[66] Figure 6.10 shows the results of incubation of biofilm material with ELF 97 (Molecular Probes, Eugene, OR), illustrating the binding of the lectin *Phaseolus vulgaris*–TRITC and the combination of the exopolymer image with ELF positive locations in the biofilm. This shows the presence of both cellular and EPS localized phosphatase activity. Lawrence et al.[67] localized the herbicide atrazine within river biofilms using antibody staining. As indicated in the publication of Wuertz et al.[68] ion or metal sensitive probes such as

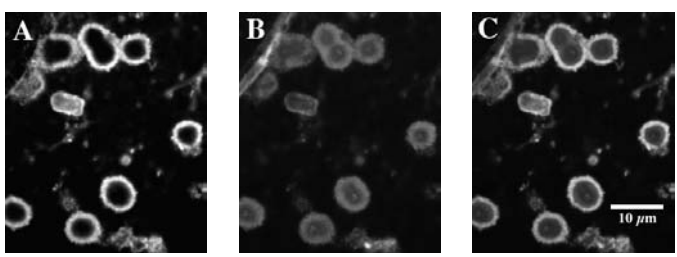

FIGURE 6.9 CLSM images showing the differential penetration of microcolonies with (A) binding and retention of 100 nm sulfate modified beads on the outside; (B) penetration of the 20 nm aldehyde–sulfate modified beads to the inside of the colony; and (C) the overlay of the two channels showing localization of the two probes.

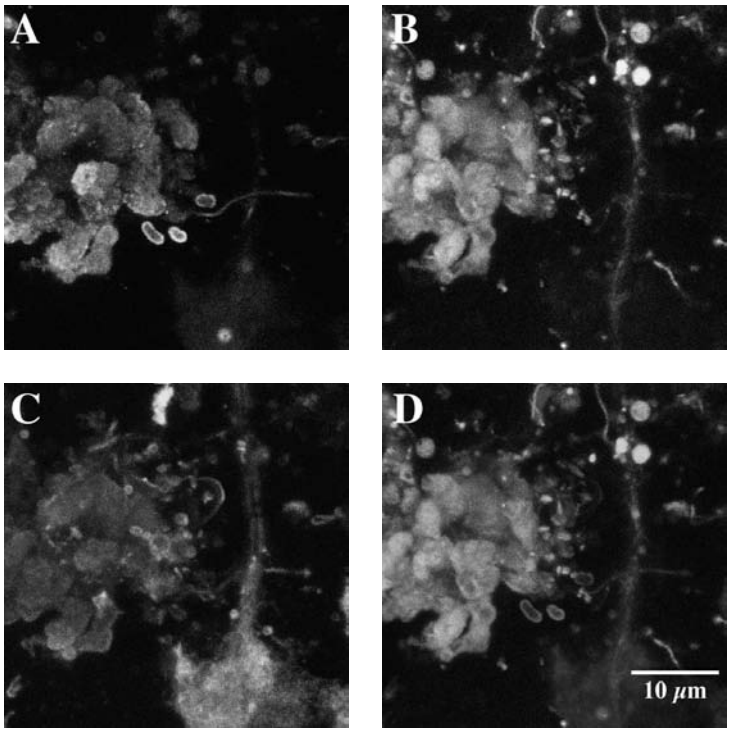

FIGURE 6.10 CLSM micrographs illustrating (A) the binding of *Phaseolus vulgaris*–TRITC lectin; the development of ELF97 (Molecular Probes, Eugene, OR) phosphatase activity reporting fluorescence (B); and (C) *Arachis hypogaea*-CY5 lectin binding pattern; and (D) the combination of the three signals shows the presence of both cellular and EPS localized phosphatase activity.

Newport Green may be used to detect the presence of metals in biofilms and within the EPS matrix.

6.5 DIGITAL IMAGE ANALYSES

Digital images may be collected by a wide range of options, digital camera or digital video on wide field epifluorescence microscope, 1P-LSM, and 2P-LSM. Collection and analyses of synchrotron images is a specialized area not covered in detail in this chapter.[25,26] Once an image series or image stack is generated there are many options to analyse these images and depending on the specific requirements many commercial or freeware systems can be chosen. Key points to consider include: gray level resolution, programming language, capacity for modification, design of macros or plug-ins, and memory requirements, capacity to perform operations on serial image stacks produced in confocal microscopy, or to perform object-based image analysis. Software may be from the microscope company directly or special software companies. All the major companies constantly extend the features on

their microscope software. However, in general no software is suitable for every data set and can perform every type of analysis. Consequently, the data has to be treated with different software. The most sophisticated general packages are Imaris (Bitplane), Amira (TGS), and Volocity (Improvision). All of these packages have the usual options plus rendering capacity. Others available include Quantimet System, Leica (Heidelburg, Germany), MicroVoxel (Indec Systems, Sunnyvale, California), VoxelView (Vital Images, Fairfield, Iowa), or VoxBlast (VayTek, Inc., Fairfield, Iowa), a complete listing of commercial image analyses software may be found most easily by an internet search. Alternately freeware may meet the requirements, the following are widely used systems, Comstat, a program for windows platforms (see http://www.im.dtu.dk/comstat/), NIH Image for Apple platforms (http://rsb.info.nih.gov/nih-image/), or the Windows-based version (ScionImagePC at www.scioncorp.com), and the new Java version ImageJ from NIH or ImageTool (http://ddsdx.uthscsa.edu/dig/itdesc.htlm). There is also Linux based software produced by the French INRA, Nantes, called QUANT3D. An example of how macros developed in NIH Image were used to achieve quantitative measurements in FLBA is provided in Section 6.5.1.

6.5.1 Quantitative *In Situ* Lectin Analyses

Neu et al.[16] provided a detailed analysis of lectin binding in complex systems and proposed a standardized method for digital imaging, image analyses, and calculation of lectin binding. Image analysis was used to define the area of the biofilm binding a specific lectin. In addition, the average gray value of the defined area was determined. These two parameters were used to quantify the area binding a specific lectin according to Equation (6.1).

$$\%\text{ICBA} = \frac{\text{TA} \times \text{AGV} \times 100}{255 \times 393216} \tag{6.1}$$

% ICBA is the Intensity Corrected Binding Area, TA is the Thresholded Area of lectin binding, AGV is the Average Gray Value within thresholded area, 255 the gray value of saturated pixels, and 393216 is the number of pixels in a full image (768×512).

They noted the importance of incubation time, lectin concentration, the nature of the fluor labeling, presence of carbohydrate inhibition, order of addition, and lectin interactions. An incubation time of 20 min was found to be sufficient; tests indicated that fluorescein isothiocyanate (FITC) conjugated lectins had more specific binding characteristics than tetramethyl rhodamine isothiocyanate (TRITC) or cyanine dye (CY5) labeled lectins. They concluded that the selection of a panel of lectins for investigating the EPS matrix required a full evaluation of their behavior in the microbial system to be studied. Neu et al.[16] used macros developed in NIH Image and the above equation to analyze 1P-LSM image stacks and determine the quantitative abundance of specific lectin binding sites in river biofilms. Neu et al.[18] has applied this approach to examine the impact of nutrients on the glycoconjugate make up of the EPS of river biofilms an approach that may be easily applied to flocs.

6.6 DECONVOLUTION

Deconvolution may be required to remove out-of-focus information from the images in the stack. Essentially, deconvolution is an algorithm for calculation that places extended signals in the *z* direction to their correct *xy–xz* location in the image stack. A variety of programs are available that allow the user to carryout this mathematical process including, AutoDeblur (AutoQuant), HazeBuster/Microtome (Vaytek), Huygens (SVI), Amira DECONV (TGS), TILLvisION deconvolution (TILL Photonics), 3-d deconvolution (Zeiss). The 3D rendering may be carried out using ray tracing or surface contour based programs such as Huygens (SVI). An example of application of deconvolution to images of bacteria and biofilm associated with sponges is presented with color illustration in Manz et al.[69]

6.7 3D RENDERING

The use of visualization techniques such as confocal, 2P-LSM, or synchrotron based imaging necessitates the presentation of the data in the most meaningful form. In general, this has meant the use of a range of color and three-dimensional presentation

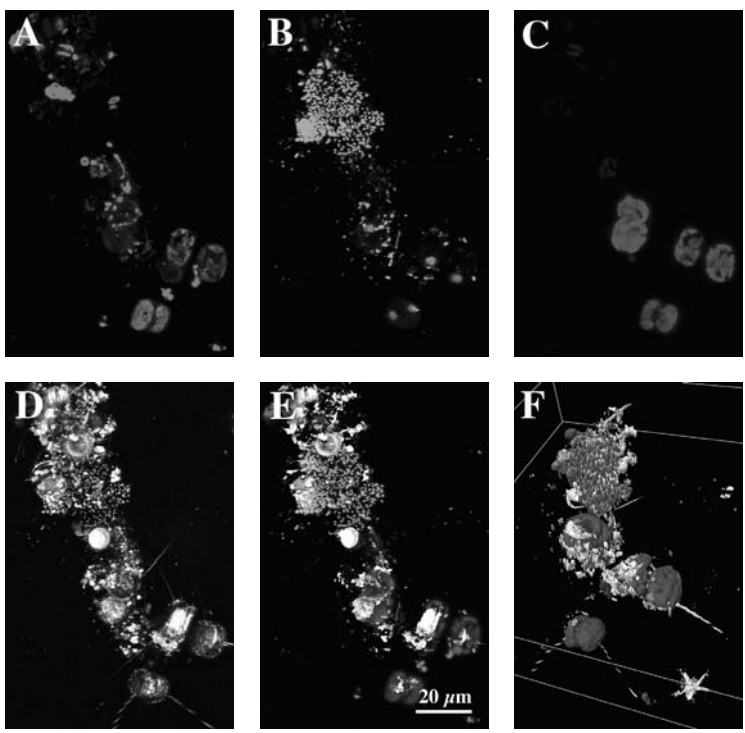

FIGURE 6.11 (**Color Figure 6.11 appears following page 236.**) 3D rendering of Elbe river floc showing the individual channels (A) staining with the lectin *Triticum vulgaris*–TRITC; (B) nucleic acid staining with SYTO9; (C) an autofluorescence signal for algae; (D) reflectance of particulate colloidal materials; (E) merged 3D image; and (F) oblique view of the 3D rendering of the four image stack.

formats including: simulated fluorescence, stereo pairs, red–green anaglyph projections, and two or three color stereo pairs. These approaches allowing the presentation of multichannel information sets providing a synthesis of large data sets for the readers examination. Additional approaches involve the application of 3D rendering of these data sets. Figure 6.11 provides an example of a series of images of an Elbe river floc showing: four images, the reflection image of particulate matter in the floc, autofluorescence showing the presence of autotrophic algae and cyanobacteria, staining with the nucleic acid stain Syto 9 showing all bacteria, and staining with a lectin *Triticum vulgaris*–TRITC revealing the exopolymer matrix of the floc as single channel maximum intensity projection (MIP) and then combined as MIP and a rendering image all of the same floc. Finally, images are often adjusted in terms of color balance for publication using programs such as Photoshop (Adobe Systems Inc., San Jose, California)

6.8 CONCLUSIONS

What is needed to further fine tune the *in situ* analysis of exopolymeric substances of microbial communities? Primarily, we require a more detailed characterization of the probes and a greater understanding of the nature of their affinities for targets such as protein, lipid, nucleic acids, and carbohydrates. Further studies of their behavior in complex microbial communities must also be carried out in order to establish the "ground truth" for imaging based studies. This has been carried out in part through the correlative application of STXM and 1P-LSM imaging[25] which indicated considerable agreement between the probe free and the probe dependent mapping of major biopolymers in biofilm systems. However, new probes specific for major biopolymers will have to continue to be developed and evaluated in complex systems. These highly specific probes will be critical for the assessment of floc properties as well as for structural examination of these microbial communities.

ACKNOWLEDGMENTS

The authors gratefully acknowledge the excellent technical assistance of Ute Kuhlicke (Germany) and George D.W. Swerhone (Canada). The studies reported here were supported by the Canada–Germany Agreement on Scientific Research (1995–2003), Health Canada through the Toxic Substances Research Initiative of Health Canada, the National Water Research Institute, Environment Canada, the National Research Council of Canada, the Natural Sciences and Engineering Research Council of Canada, and the UFZ Centre for Environmental Research.

REFERENCES

1. Neu, T.R. In situ cell and glycoconjugate distribution of river snow as studied by confocal laser scanning microscopy. *Aquatic Microb Ecol* 21: 85–95, 2000.
2. Eisma, D. *Suspended Matter in the Aquatic Environment*. Springer-Verlag, New York, 1993.

3. Weiss, P., Schweitzer, B., Amann, R., and Simon, M. Identification in situ and dynamics of bacteria on limnetic organic aggregates (lake snow) Appl Environ Microbiol 62: 1998–2005, 1996.
4. Kämpfer, P., Erhart, R., Beimfohr, C., Böhringer, J., Wagner, M., and Amann, R. Characterisation of bacterial communities from activated sludge: Culture-dependent numerical identification versus in situ identification using group- and genus-specific rRNA-targeted oligonucleotide probes. *Microb Ecol* 32: 101–121, 1996.
5. Wagner, M., Amann, R., Lemmer, H., and Schleifer, K.H. Probing activated sludge with oligonucleotides specific for proteobacteria: Inadequacy of culture-dependent methods for describing microbial community structure Appl Environ Microbiol 59: 1520–1525, 1993.
6. Boessmann, M., Staudt, C., Neu, T.R., Horn, H., and Hempel, D.C. Investigation and modelling of growth, structure and oxygen penetration in particle supported biofilms. *CET Chem Eng Technol* 26: 219–222, 2003.
7. Cooksey, K.E. Extracellular polymers in biofilms. In *Biofilms — Science and Technology. NATO ASI Series — Vol 223*, pp 137–147. Edited by L.F. Melo, T.R. Bott, M. Fletcher, and B. Capdeville. Kluwer Academic Publishers, Dordrecht, The Netherlands, 1992.
8. Neu, T.R. The challenge to analyse extracellular polymers in biofilms. In *Microbial Mats, Structure, Development and Environmental significance. NATO ASI Series — Vol G 35*, pp 221–227. Edited by L.J. Stal and P. Caumette. Springer-Verlag Berlin, Germany, 1994.
9. Neu, T.R. and Lawrence, J.R. In situ characterization of extracellular polymeric substances (EPS) in biofilm systems. Chapter 2. In *Microbial Extracellular Substances*, pp 21–48, Edited by, J. Wingender, T.R. Neu, and H.-C. Flemming, Springer-Verlag, Berlin, Germany, 1999.
10. Wingender, J., Neu, T.R., and Flemming, H.-C. *Microbial Extracellular Polymeric Substances*, p. 258, Springer-Verlag, Berlin, Germany, 1999.
11. Sutherland, I.W. The biofilm matrix — an immobilized but dynamic microbial environment. *Trends Microbiol* 9: 222–227, 2001.
12. Flemming, H.-C., Schmitt, J., and Marshall, K.C. Sorption properties in biofilms. In *Sediment and Toxic Substances*. pp 115–157, Edited by W. Calmano and U. Förstner Springer-Verlag, Berlin, Germany, 1996.
13. Neu, T.R. and Marshall, K.C. Bacterial polymers: Physicochemical aspects of their interaction at interfaces. *J Biomat Appl* 5, 107–133, 1990.
14. Nielsen, P.H. and Jahn, A. Extraction of EPS. In *Microbial Extracellular Polymeric Substances. Characterization, Structure and Function*, pp 49–72. Edited by J. Wingender, T.R. Neu, and H.-C. Flemming. Springer-Verlag, Berlin, Germany, 1999.
15. Neu, T.R. and Lawrence, J.R. Development and structure of microbial stream biofilms as studied by confocal laser scanning microscopy. *FEMS Microb Ecol* 24: 11–25, 1997.
16. Neu, T.R., Swerhone, G.D.W., and Lawrence, J.R. Assessment of lectin-binding-analysis for in situ detection of glycoconjugates in biofilm systems. *Microbiology* 147: 299–313, 2001.
17. Böckelmann, U., Manz, W., Neu, T.R., and Szewzyk, U. A new combined technique of fluorescent in situ hybridization and lectin-binding-analysis (FISH-LBA) for the investigation of lotic microbial aggregates. *J Microbiol Meth* 49: 75–87, 2002.
18. Neu, T.R., Swerhone, G.D.W., Bockelmann, U., and J.R. Lawrence. Effect of carbon, nitrogen and phosphorus on the nature and development of lectin-specific glycoconjugates in lotic biofilms. *Aquatic Microb Ecol*, accepted, 2004.

19. Simon, M., Alldredge, A.L., and Azam, F. Bacterial carbon dynamics on marine snow. *Mar. Ecol. Prog. Ser*. 65: 205–211, 1990.
20. Leppard, G.G. Organic flocs in surface waters: Their native state and aggregation behavior in relation to contaminant dispersion. In *Particulate Matter and Aquatic Contaminants*, pp 169–195. Edited S.S. Rao, Lewis Publ., Chelsea MI, 1993.
21. Leppard, G.G. Evaluation of electron microscope techniques for the description of aquatic colloids. In, *Environmental Particles, Vol. 1., IUPAC Environmental Chemistry Series*, pp 231–289. Edited by J. Buffle and H.P. van Leeuwen, Lewis Publ., Chelsea, MI, 1992.
22. Leppard, G.G., Burnison, B.K., and Buffle, J. Transmission electron microscopy of the natural organic matter of surface waters. *Anal Chim Acta* 232: 107–121, 1990.
23. Droppo, I.G., Flannigan, D.T., Leppard, G.G., Jaskot, C., and Liss, S.N. Floc stabilization for multiple microscopic techniques. *Appl Environ Microbiol* 62: 3508–3515, 1996.
24. Murray, R.G.E., Doetsch, R.N., and Robinow, C.F. Determinative and cytological light microscopy. Chpt. 2. In *Methods for General and Molecular Bacteriology*. pp 21–40, Edited by P. Gerhardt, R.G.E. Murray, W.A. Wood, and N.R. Krieg, American Society for Microbiology Press, Washington, D.C., 1994.
25. Lawrence, J.R., Swerhone, G. D.W., Leppard, G.G., Araki, T., Zhang, X., West, M.M., and Hitchcock, A.P. Scanning transmission x-ray, laser scanning, and transmission electron microscopy mapping of the exopolymeric matrix of microbial biofilms. *Appl Environ Microbiol* 69: 5543–5554, 2003.
26. Hitchcock, A.P., Morin, C., Tyliszczak, T., Koprinarov, I.N, Ikeura-Sekiguchi, H., McCrory, C.T., Childs, R.F., Lawrence, J.R., and Leppard, G.G. Soft X-ray microscopy of soft matter–hard information from two softs. *Surface Rev Lett* 9: 193–202, 2002.
27. Lawrence, J.R., Korber, D.R., Wolfaardt, G.M., Caldwell, D.E., and Neu, T.R. Analytical imaging and microscopy techniques. 2nd Ed. In *Manual of Environmental Microbiology*, pp 39–61. Edited by C.J. Hurst, Ronald L. Crawford, G.R. Knudsen, M. McInerney, and L.D. Stetzenbach, American Society for Microbiology Press, Washington, D.C., 2002.
28. Neu, T.R., Kuhlicke, U., and Lawrence, J.R. Assessment of fluorochromes for 2-Photon Laser Scanning Microscopy (2-PLSM) of biofilms. *Appl Environ Microbiol* 68: 901–909, 2002.
29. Lawrence, J.R. and Neu, T.R. Confocal laser scanning microscopy for analysis of microbial biofilms. Chpt 9. In *Biofilms, Meth Enzymol* Vol 310 pp 131–144. Edited by R.J. Doyle, Academic Press, Orlando, FL, 1999.
30. Lawrence, J.R., Wolfaardt, G.M., and Neu, T.R. The study of biofilms using confocal laser scanning microscopy. Chpt 16. In *Digital Analysis of Microbes, Imaging, Morphometry, Fluorometry and Motility Techniques and Applications*. pp 431–465, Edited by M.H.F Wilkinson and F. Schut, Modern Microbiological Methods Series, John Wiley and Sons Ltd, Sussex, UK. 1998.
31. Ade, H. and Urquhart, S.G., NEXAFS Spectroscopy and Microscopy of Natural and Synthetic Polymers. In *Chemical Applications of Synchrotron Radiation*. Edited by T.K. Sham, World Scientific Publishing, Hackensack, NJ, 285–355, 2002.
32. Gilbert, E.S., Khlebnikov, A., Meyer-Ilse, W., and Keasling, J.D. Use of soft X-ray microscopy for the analysis of early-stage biofilm formation. *Water Sci Technol* 39: 269–272, 1999.

33. Kelly, S.D., Boyanov, M.I., Bunker, B.A., Fein, J.B., Fowle, D.A., Yee, N., and Kemner, K.M. XAFS determination of the bacterial cell wall functional groups responsible for complexation of Cd and U as a function of pH. *J Synchrotron Radiat* 8: 946–948, 2001.
34. Kloepfer, J. A., Mielke, R. E., Wong, M. S., Nealson, K. H., Stucky, G., and Nadeau, J. L. Quantum dots as strain- and metabolism-specific microbiological labels. *Appl Environ Microbiol* 69: 4205–4213, 2003.
35. Wetzel. R.G., Ward, A.K., and Stock, M. Effect of natural dissolved organic matter on mucilaginous matrices of biofilm communities. *Arch Hydrobiol* 139: 289–299, 1997.
36. Sharon, N. and Lis, H. A century of lectin research (1888–1988). *Trends Biochem Sci* 12: 488–491, 1987.
37. Sharon, N. and Lis, H. Lectins as cell recognition molecules. *Science* 246, 227–234, 1989.
38. Elgavish, S. and Shaanan, B. Lectin-carbohydrate interactions: Different folds, common recognition principles. *Trends Biochem Sci* 22: 462–467, 1997.
39. Bog-Hansen, T.C. *Lectins — Biology, Biochemistry, Clinical Biochemistry*. Volume 1, 2, and 3. de Gruyter, Berlin 1981.
40. Doyle, R.J. and Slifkin, M. *Lectin-Microorganism Interactions*. Marcel Dekker, New York, 1994.
41. Weis, W.I. and Drickamer, K. Structural basis of lectin-carbohydrate recognition. *Annu Rev Biochem* 65: 441–473, 1996.
42. Brooks, S.A., Leathem, A.J.C., and Schuhmacher, U. *Lectin Histochemistry.* Bios Scientific Publishers, Oxford, U.K., 1997.
43. Amann, R. Who is out there? Microbial aspects of biodiversity. *Syst Appl Microbiol* 23:1–8, 2000.
44. Staudt, C., Horn, H., Hempel, D.C., and Neu, T.R. Screening of lectins for staining lectin-specific glycoconjugates in the EPS of biofilms. In P. Lens, A.P. Moran, T. Mahony, P. Stoodley, and V. O'Flaherty *Biofilms in Medicine, Industry and Environmental Biotechnology*. pp 308–327, Edited by IWA Publishing, UK, 2003.
45. Jones, A.H., Lee, C.-C., Moncla, B.J., Robinovitch, M.R., and Birdsell, D.C. Surface localization of sialic acid on *Actinomyces viscosus. J Gen Microbiol* 132, 3381–3391, 1986.
46. Morioka, H., Tachibana, M., and Suganuma, A. Ultrastructural localization of carbohydrates on thin sections of *Staphylococcus aureus* with silver methenamine and wheat germ agglutinin-gold complex. *J Bacteriol* 169: 1358–1362, 1987.
47. Merker, R.I. and Smit, J. Characterization of the adhesive holdfast of marine and freshwater Caulobacters. *Appl Environ Microbiol* 54: 2078–2085, 1988.
48. Hood, M.A. and Schmidt, J.M. The examination of *Seliberia stellata* exopolymers using lectin assays. *Microb Ecol* 31: 281–290, 1996.
49. Michael, T. and Smith, C.M. Lectins probe molecular films in biofouling: Characterization of early films on non-living and living surfaces. *Mar Ecol Prog Ser* 119: 229–236, 1995.
50. Liss, S.N., Droppo, I.G., Flannigan, D.T., and Leppard, G.G. Floc architecture in wastewater and natural riverine systems. *Environ Sci Technol* 30: 680–686, 1996.
51. Mohamed, M.N., Lawrence, J.R., and Robarts, R.D. Phosphorus limitation of heterotrophic biofilms from the Fraser River, British Columbia, and the effect of pulp mill effluent. *Microb Ecol 36*: 121–130, 1998.
52. Cummings, R.D. Use of lectins in analysis of glycoconjugates. *Meth Enzymol* 230: 66–86, 1994.

53. Amann, R., Ludwig, I.W., and Schleifer, K.H. Phylogenetic identification and *in situ* detection of individual microbial cells without cultivation. *Microbiol Rev* 59: 143–169, 1995.
54. Frolund, B., Griebe, T., and Nielsen, P.H. Extraction of extracellular polymers from activated sludge using a cation exchange resin. *Water Res*. 30: 1749–1758, 1996.
55. Neu, T.R. and Marshall, K.C. Microbial "footprints" — A new approach to adhesive polymers. *Biofouling* 3: 101–112, 1991.
56. Wolfaardt, G.M., Lawrence, J.R., Robarts, R.D., and Caldwell, D.E. In situ characterization of biofilm exopolymers involved in the accumulation of chlorinated organics. *Microb Ecol* 35: 213–223, 1998.
57. Lamont, H.C., Silvester, W.B., and Torrey, J.G. Nile red fluorescence demonstrates lipid in the envelope of vesicles form N2-fixing cultures of Frankia. *Can J Microbiol* 34: 656–660, 1987.
58. Whitchurch, C.B., Tolker-Nielsen, T., Ragas, P.C., and Mattick, J.S. Extracellular DNA required for bacterial biofilm formation. *Science* 295: 1487, 2002.
59. Zita, A. and Hermansson, M. Determination of bacterial cell surface hydrophobicity of single cells in culture and in wastewater in situ. *FEMS Microbiol Ecol* 152: 299, 1997.
60. Nielsen, J.L., Mikkelsen, L.H., and Nielsen, P.H. *In situ* detection of cell surface hydrophobicity of probe-defined bacteria in activated sludge. *Water Sci Tech* 43(6): 97–103, 2000.
61. Lawrence, J.R., Wolfaardt, G.M., and Korber, D.R. Monitoring diffusion in biofilm matrices using scanning confocal laser microscopy. *Appl Environ Microbiol* 60: 1166–1173, 1994.
62. De Beer, D., Stoodley, P., and Lewandowski, Z. Measurement of local diffusion coefficients in biofilms by microinjection and confocal microscopy. *Biotechnol Bioeng* 53: 151–158, 1997.
63. Freeman, C. and Lock, M.A. The biofilm polysaccharide matrix: A buffer against changing organic substrate supply. *Limnol Oceanog* 40: 273–278, 1995.
64. Freeman, C., Chapman, P.J., Gilman, K., Lock, M.A., Reynolds, B., and Wheater, H.S. Ion exchange mechanisms and the entrapment of nutrients by river biofilms. *Hydrobiologia* 297: 61–65, 1995.
65. Wolfaardt, G.M., Lawrence, J.R, Robarts, R.D., and Caldwell, D.E. Bioaccumulation of the herbicide diclofop in extracellular polymers and its utilization by a biofilm community during starvation. *Appl Environ Microbiol* 61: 152–158, 1995.
66. Van Ommen Kloeke, F., and Geesey, G.G. Localization and identification of populations of phosphatase-active bacterial cells associated with activated sludge flocs. *Microb Ecol* 38: 201–214, 1999.
67. Lawrence, J.R., Kopf, G., Headley, J.V., and Neu, T.R. Sorption and metabolism of selected herbicides in river biofilm communities. *Can J Microbiol*. 47: 634–641, 2001.
68. Wuertz, S., Mueller, E., Spaeth, R., Pfleiderer, P., and Flemming, H.-C. Detection of heavy metals in bacterial biofilms and microbial flocs with the fluorescent complexing agent Newport Green. *J Ind Microbiol Biotechnol* 24: 116–123, 2000.
69. Manz, W., Arp, G., Schmann-Kindel, G., Szewzky, U., and Reitner, J. Widefield deconvolution epifluorescence microscopy combined with fluorescence in situ hybridization reveals the spatial arrangement of bacteria in sponge tissue. *J Microbiol Meth* 40: 125, 2000.

7 Contrasting Roles of Natural Organic Matter on Colloidal Stabilization and Flocculation in Freshwaters

Kevin J. Wilkinson and Alain Reinhardt

CONTENTS

7.1 INTRODUCTION

A large proportion of trace compounds (typically 40% to 90%) are adsorbed to aquatic colloids via covalent, electrostatic, or hydrophobic interactions.[1,2] Based

1-56670-615-7/05/$0.00+$1.50

upon size and density considerations, colloids will generally remain suspended in the water column and be transported over long distances. On the other hand, coagulation or flocculation can facilitate the elimination of colloids from the water column by producing aggregates that are large enough to sediment.[3,4] In complex systems such as natural waters, colloidal aggregation is ubiquitous due to the large number of colloid types and reactive sites. Indeed, size fractionation analysis has often demonstrated that each colloid type may be found in all size fractions.[5] This suggests that it is at least as important to understand interactions among the colloids as it is to determine the binding energies of trace compounds to each colloid type.[6] While considerable research has focused on determinations of binding constants of trace compounds with colloids (e.g., ref. [1,2,7,8]), relatively few data are available on the precise structural properties of the colloids[9] and their interactions in natural systems.

In this context, the exact role of natural organic matter (NOM) in freshwaters is yet to be resolved. Although it is often shown that NOM can stabilize inorganic colloids in natural waters,[10,11] the opposite phenomenon, that is, destabilization, has also been shown to occur with specific groups of NOM, in particular, the polysaccharides.[12–14] Therefore, in order to understand colloidal aggregation in freshwaters, it is necessary to take into account the specific behavior of each of the major groups of NOM by considering relevant physicochemical parameters such as molar mass, size, electric charge density, and conformational information such as the persistence length, radius of gyration, or fractal dimensions.[15,16]

This information is more difficult to obtain than the corresponding parameters that are necessary to model the behavior of inorganic colloids (mainly hydrodynamic radius and electric charge density[17]). It is therefore not surprising that no generalized predictive model of colloidal interactions exists that includes the different types of organic macromolecules that comprise the majority of NOM. The main objective of this chapter will be to improve our understanding of the role(s) of NOM on colloidal aggregation in freshwaters in order to facilitate the development of such a model.

7.2 CHARACTERIZATION OF THE MAJOR AQUATIC COLLOIDS

In this chapter, colloids are defined as any organic or inorganic entity large enough to have supramolecular structure and properties (e.g., possibility of conformational changes for organic colloids or an electrical surface field for inorganic colloids), but small enough not to sediment quickly (hours to days) in the absence of aggregation. This definition implies that the colloidal size range will typically be between 1 nm and 1 μm. In freshwaters, colloids include significant organic and inorganic components, with the proportions of each component depending upon the nature of the water body and surrounding watershed, the vertical and horizontal position in the water body, the climate, etc. Typical size distributions and some important physicochemical characteristics of the principal freshwater colloids are given in Figure 7.1 and Table 7.1.

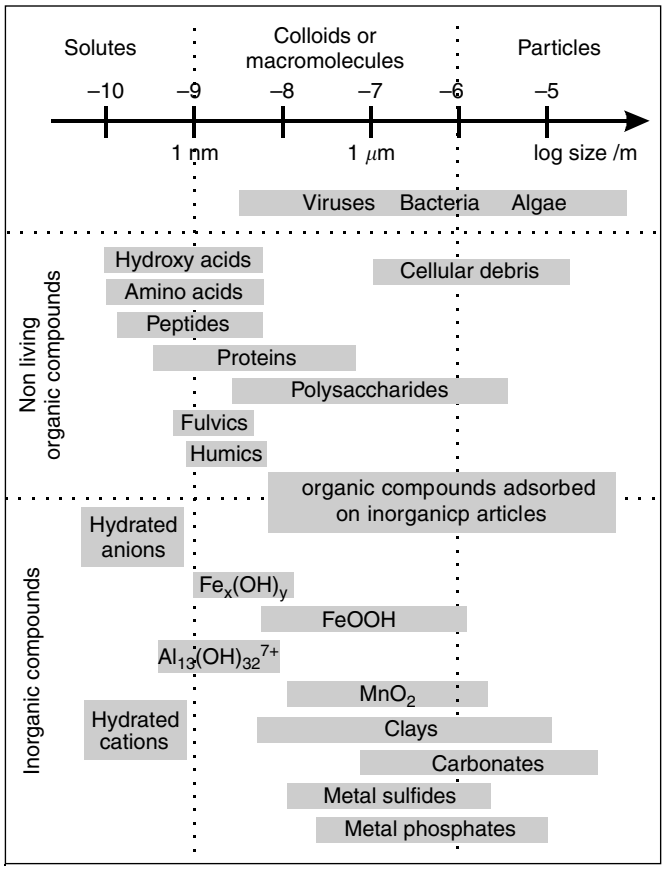

FIGURE 7.1 Schematic representation, by size, of some of the important organic and inorganic components of freshwaters. (Modified from Buffle, J. and H.P. van Leeuwen, *Environmental Particles*. 1992, Chelsea, Michigan: Lewis Publishers, Inc. with permission from Lewis Publishers.)

7.2.1 Inorganic Colloids

The major *inorganic colloids* found in oxic freshwaters include alumino-silicates (clays), silica, and iron oxyhydroxyde particles.[2,20,21] Other inorganic colloids can also be found, but they are usually minor components (e.g., aluminum or manganese oxides) or are only present in anoxic waters (e.g., elemental sulfur or FeS). Calcium carbonate is found in significant quantities in freshwaters, especially during periods of high primary productivity, but it is mostly particulate (i.e., $>1\ \mu$m). Inorganic particles are generally electrically charged due to the isomorphic substitution of ions in the bulk solid phase, or to the reactions of surface functional groups with dissolved ions in the aqueous phase.[22] Apart from the iron oxyhydroxides which are neutral or positively charged in the circumneutral pH range, the major inorganic colloids are generally negatively charged in water due to their low zero point of charge (Table 7.1; see ref. [6,21]).

TABLE 7.1
Important Physicochemical Characteristics of Some Representative Freshwater Colloids

Nature of colloid and macromolecule	Molar mass or specific surface area	Site or charge density	Comments
		Non living organic compounds	
Small, organic molecules including amino acids, hydroxy acids, peptides, monosaccharides	Molar mass <1 kDa	Variable	Extremely labile compounds, residence time often hours
Humic substances (including fulvic and humic acids and the so-called marine humic acids)	Molar mass 0.5–5 kDa, spherical	Electrical charge of -2 to -11 meq g^{-1}, mainly carboxylic acid dissociation	Residence time of centuries
Proteins	Molar mass 3–100 kDa, flexible		Residence time of hours to days
Reserve polysaccharides	Molar mass 10–1000 kDa, flexible	Typical electrical charge of -0.3–0.8 meq g^{-1}, minimum 0, maximum 6 meq g^{-1}	Some modification of diameter as a function of pH, ionic strength and the presence of cations; Residence times of hours to days
Structural polysaccharides	Molar mass 10–1000 kDa, fibrillar structures, often double or triple helical structure	Typical electrical charge of -0.3–0.8 meq g^{-1}, minimum 0, maximum 6 meq g^{-1}	Structure often highly dependent upon pH, ionic strength and the presence of cations; Residence time of months to centuries
Peptidoglycans	Molar mass 10–1000 kDa, rigid structures		Residence time of months

Inorganic compounds			
Amorphous-SiO_2	40–260 $m^2\ g^{-1}$	4.5–12 nm^{-2}	$pH_{zpc} = 3.0–3.5$
Amorphous-FeOOH	160–700 $m^2\ g^{-1}$	0.1–0.9 mol/mol of Fe	$pH_{zpc} = 7.9–8.1$
Amorphous-Al_2O_3		2–12 nm^{-2} (crystalline)	$pH_{zpc} \approx 9.4$
Amorphous-MnO_2	260 $m^2\ g^{-1}$	6–20 nm^{-2} (crystalline)	$pH_{zpc} \approx 2.3$
Kaolinite	10–20 $m^2\ g^{-1}$	0.6–3.6 nm^{-2}	pH at isoelectric point = 3.3–4.6
Smectite	750–800 $m^2\ g^{-1}$	0.5–1.0 nm^{-2}	$pH_{zpc} \leq 2.5$
Allophanes	500–700 $m^2\ g^{-1}$	0.4–1.2 nm^{-2}	
Illite	90–130 $m^2\ g^{-1}$	0.9–2.7 nm^{-2}	

Note: Values are representative (rather than exhaustive). Where possible, values are given for the amorphous phases of the inorganic colloids. For the inorganic colloids, the site densities refer to the maximum negative charge density for $pH \gg pH_{zpc}$.

Source: (Modified from Buffle, J., et al., *Environmental Science and Technology*, 1998. **32**(19): p. 2887–99 (and references therein) with permission from the American Chemical Society. Based in part on Buffle, J., *Complexation Reactions in Aquatic Systems: An Analytical Approach*. 1988, Chichester: Ellis Horwood; Thurman, *Organic Geochemistry of Natural Waters*. 1985, Dordrecht: Kluwer Academic Publishers Group; and Davis, J.A. and D.B. Kent, *Reviews in Mineralogy*, 1990, Mineralogical Society of America: Washington, D.C. p. 177–260.

It is therefore reasonable to represent the submicron inorganic colloids as compact, often negatively charged particles that cover the whole colloidal size range.

7.2.2 Allochthonous Macromolecules: Humic Substances

Humic substances (HS) generally represent the largest NOM fraction in freshwaters (typically 40 to 80%; ref. [9,19]. Because they are primarily of pedogenic origin, they may also be present in the coastal waters of oceans but are generally absent from the pelagic zones. HS are chemically heterogeneous polymers with small molar masses (typically ~1000 Da; see ref. [23]), high charge densities at neutral or alkaline pH's (Figure 7.2A), and typical average lifetimes of several hundred years. Due to the significant degree of branching of HS, their high charge density (above pH 5; see ref. [24]) and degree of hydration (40% strongly bond water[9]), they are less flexible than linear biopolymers such as proteins. In dilute solutions (<10 mg l^{-1}) at circumneutral pH and low ionic strength ($\leq 10^{-2}$ M), HS generally behave as small rigid globules, with diameters of 1 to 3 nm (Figure 7.2A and 7.2B; ref. [24–27]). HS aggregate formation is favored at high concentrations of electrolyte, protons (i.e., low pH), HS, or divalent cations.[23,28,29] Although HS are sometimes represented as linear polyelectrolytes, the linear representation of the HS does not fit with either the experimental measurements discussed earlier in the chapter or the more modern models that consider HS as highly branched molecules.[30] Nonetheless, because HS are both chemically heterogeneous and polydisperse, both within a given HS sample and with respect to samples isolated from different sources, there is no single useful structural model of a "typical" HS. Rather, most of the interesting properties of the HS result from their inherent

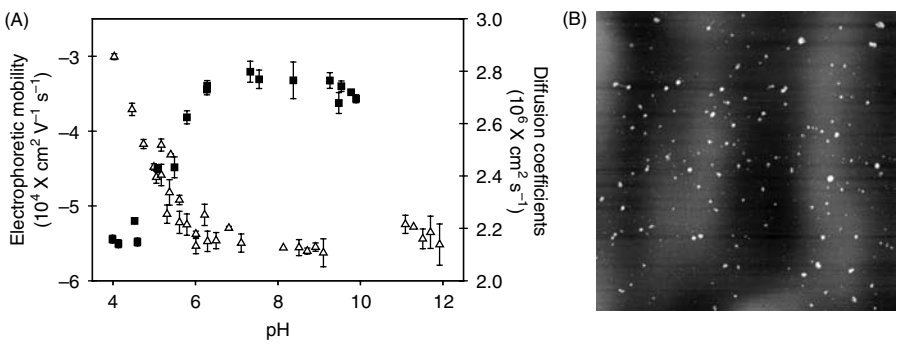

FIGURE 7.2 (A) Electrophoretic mobilities (EPM) and diffusion coefficients (D) of the International Humic Substances Society (IHSS) standard Suwannee River aquatic fulvic acid (SRFA) versus pH (△ EPM; ■ D). Adapted from Hosse, M. and K.J. Wilkinson, *Environmental Science and Technology*, 2001. **35**(21): p. 4301–6; Lead, J.R., et al. *Environmental Science and Technology*, 2000. **34**(7): p. 1365–9 with permission from the American Chemical Society. (B) AFM image of the IHSS SRFA (10 mg l^{-1}, 50 mM NaCl, pH 5.5) adsorbed to mica. Scan size is 600 nm x 600 nm. The image shows mainly isolated points (as opposed to aggregates) with adsorbed heights that averaged 0.8 ± 0.3 nm[31]. (Adapted from Balnois, E., et al. *Environmental Science and Technology*, 1999. **33**(21): p. 3911–17 with permission from the American Chemical Society.)

polydispersity and heterogeneity, implying that knowledge of property distributions will be more useful than mean values. For the above reasons, much still remains to be learned about the structure of HS, in particular, at low (i.e., environmentally relevant) concentrations.

7.2.3 Autochthonous Macromolecules: Proteins, Lipids, and Polysaccharides

In freshwaters, a large number of organic compounds, including polysaccharides, aminosugars, peptidoglycans, proteins, polyphenolic compounds, lignins, tannins, DNA, and polyhydroxybutyrates,[28] are produced in the water column by the exudation or degradation of phytoplankton, aquatic bacteria, and aquatic macrophytes. Part of the autochthonous organic matter, especially structural components of plankton that are resistant to degradation, are subject to recombination and thus are similar to the HS except that they are generally more aliphatic and less hydrophilic, with slightly smaller charge densities and molar masses (~800 Da).[9] Other classes of organic macromolecules, such as the *reserve polysaccharides*, are degraded within hours to days of their release into the water column.[32] Aquatic *proteins* generally have a molar mass that is in the tens of thousands and a significant proportion of hydrophobic moieties, favoring the formation of globules with typical diameters of <3 to 4 nm.[9] Nonetheless, the concentration of free protein in the water column is generally low due to its rapid degradation (hours to days) upon microbe death.[33,34] Such observations are consistent with data showing that the amino acid contents of sediment traps decline rapidly with depth[35] and that protease activity is high in surface water aggregates.[36]

Structural, fibrillar polysaccharides and peptidoglycans are also released from plankton as exudates or cell wall components.[32,37–39] They can constitute a significant proportion of freshwater NOM, varying seasonally between ca. 5% and 30% in the surface waters of lakes (Figure 7.3; ref. [13,39]) and often accounting for an even larger proportion of the NOM in the surface waters of marine systems.[40–42] In marine systems, fibrillar polysaccharides have been shown to be refractory enough to be found in the deep ocean where they may have lifetimes of hundreds of years[4] while peptidoglycans appear to be degraded much faster (turnover time of weeks to months[34]). Freshwater polysaccharides are generally quite rigid due to a large quantity of strongly bound hydration water (up to 80%) and the association of the molecules into double or triple helices that can be stabilized by hydrogen or calcium bridges.[43] TEM and AFM images of freshwater and marine biopolymers (e.g., Figure 7.3; ref. [40,44]) show that their total length may be larger than 1 μm, whereas their thickness is often only a few nanometers. Furthermore, because they are often charged molecules (i.e., charge densities of the polysaccharides are typically in the range of 0 to -0.8 meq g^{-1}, ref. [9]) their conformations can change as a function of the pH and ionic strength (Figure 7.3A,B). Indeed, in natural waters, the charge density of the natural organic polyelectrolytes is often lower than their maximum value due to partial protonation, complexation by metals, and electrolyte screening. In addition to the association of molecules into dimers and trimers, aggregation of those structures is thought to lead to the

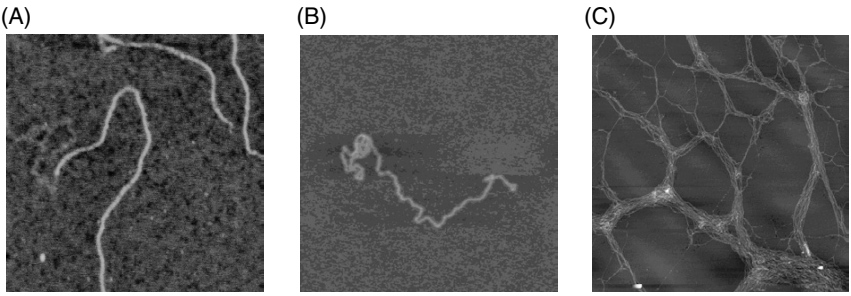

FIGURE 7.3 (A) AFM image of the bacterial (*Rhizobium meliloti*) polysaccharide, succinoglycan (10 mg l^{-1}) in water. Scan size 500 nm × 500 nm. (B) AFM image of succinoglycan (10 mg l^{-1}) in 0.01 M KCl. Scan size 705 nm × 705 nm. (C) AFM image of succinoglycan (10 mg l^{-1}) in 0.5 M KCl. Scan size 2.3 μm × 2.3 μm. (All three images were adapted from Balnois, E., et al. *Macromolecules*, 2000. **33**(20): p. 7440–7 with permission from the American Chemical Society.)

formation of rigid, poorly defined structures including gels, flocs, and biofilms[45] (Figure 7.3C).

7.3 PRINCIPAL MECHANISMS OF COLLOIDAL STABILIZATION AND DESTABILIZATION

Colloids of a given type (e.g., clays, fulvic acids, iron hydroxides) may aggregate together (homoaggregation) or with colloids of other types (heteroaggregation). General quantitative physicochemical theory exists only for the (irreversible) homocoagulation of compact particles, based on the Smoluchowski equations and Derjaguin, Landau, Verwey and Overbeek (DLVO) theory.[1,47,48] According to DLVO theory, the interaction energy between two compact, spherical colloids results essentially from (i) their surface charge, which defines the electrical field around each particle, and (ii) the attractive van der Waals forces between them. The electrical and van der Waals forces define an energy barrier which, if overcome by the kinetic energy of the particles moving in water, will lead to aggregation and an unstable suspension. For submicron colloids, this kinetic energy results mainly from Brownian motion and little from hydrodynamic or gravitational forces[49,50] whereas for larger particles or aggregates, hydrodynamic processes such as differential sedimentation and fluid shear can provide the necessary energy (e.g., ref. [51,52]). The barrier to aggregation is decreased with increasing ionic strength or protonation of the colloidal surface. In fact, the critical coagulation concentration (CCC) of the suspension is defined as the ionic strength for which the energy barrier has been eliminated, resulting in a rapid, diffusion limited aggregation. Finally, for large particles (>micrometers), a secondary minimum, resulting in the formation of aggregates with relatively small cohesion energies, exists in solutions of moderate ionic strength (10^{-2} to 10^{-3} M).

Non-DLVO forces such as steric interactions, hydration pressure, hydrogen bonding, and hydrophobic effects, although rarely considered in quantitative attempts to

model colloidal interactions, are more recently being recognized as important forces contributing to the coagulation of environmental colloids.[53] For example, in environmental (aqueous) systems, it is now clear that non-DLVO hydration effects are possible due to the reorganization of surface bound water upon approach of the colloidal particles. Furthermore, hydrophobic surfaces have a greater tendency to aggregate than predicted by DLVO theory alone due to the migration of water from the solid–water interface to the bulk solution and the subsequent formation of hydrogen bonds. Indeed, under conditions for which the energy barrier for aggregation lies at subnanometer distances, there appear to be significant discrepancies between theory and experimentally measured coagulation rates (e.g., ref. [54–57]).

Little work has directly examined the role of biopolymers on the flocculation process. Based on the literature examining synthetic polymers, one would expect the biopolymers to influence the above processes either by being adsorbed to the colloidal surface[58] or by being expulsed from the area between the particles (depletion layer).[59,60] Indeed, the adsorption of small quantities of polymer is known to facilitate colloidal aggregation due to bridging flocculation or charge neutralization while the adsorption of larger quantities is thought to restabilize the colloidal suspensions due to charge inversion or steric restabilization. The presence of large quantities of non-adsorbing biopolymer can result in an excess pressure that pushes the colloids together, resulting in a destabilization of the colloidal suspension (i.e., depletion flocculation). The adsorption of natural biopolymers to dispersed mineral particles can be facilitated by Coulombic interactions, surface complexation, hydrogen bonding, hydrophobic interactions, and even surface catalyzed polymerization reactions.[61,62] In spite of an important literature on the physicochemical properties of the polymers and their interactions with compact colloids (e.g., ref. [15,16]), there is no general theory for aggregation involving biopolymers. One of the principal difficulties when evaluating the role of biopolymers on the aggregation process is that the conformation of the adsorbed biopolymer will greatly influence whether the colloidal system is stabilized or destabilized. Several parameters, including the affinity of the biopolymer for the particle surface, its chemical structure and molar mass, and the physicochemical conditions existing at the particle–water interface will greatly influence the conformation of the macromolecule on the particle surface[16] (Figure 7.4).

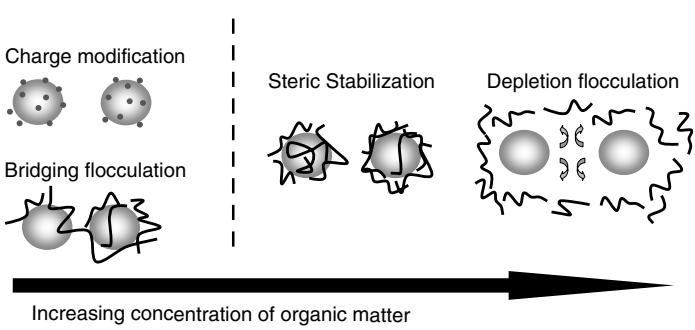

FIGURE 7.4 Schematic representation of some of the potential roles of organic matter on colloidal flocculation and stabilization processes in natural freshwaters.

7.3.1 Charge Modification

A quantitative understanding of the role of biopolymer (polyelectrolyte) adsorption on colloidal stabilization and destabilization processes requires knowledge on: (i) the variation of the thickness of the adsorbed layer as a function of pH and ionic strength; (ii) the repulsive forces between noncovered particles; (iii) the competition between polymer segments and ions for surface sites; and (iv) the potential energy barrier between the adsorbed polymer and the solution. Destabilization by charge neutralization generally occurs at low concentrations of biopolymer for which the repulsive Coulombic forces between the particles, reflected by low electrophoretic mobilities or zeta potentials, approach zero.[61,63] For a strong interaction between the biopolymer and the colloidal surface, adsorption and a subsequent charge inversion (and restabilization) is possible. Over time, the strongly adsorbing polymer will have a tendency to be flattened on the surface of the particle, greatly reducing the opportunity for interaction with other particles. In this case, the charge density of the polymer is more important than its molar mass.

Gregory demonstrated that in certain cases, the aggregation rate depended upon the molar mass of the polymer and the ionic strength of the solution.[64] This mechanism is generally observed when particles having a low charge density are neutralized by polyelectrolytes with high charge densities. In such a case, a local charge heterogeneity can occur that results in the arrangement of the polyelectrolytes in patches on the particle surface.[61] The most important consequence of the charge heterogeneity is that oppositely charged regions of different particles can react, even in the presence of an overall negligible particle charge. In that case, at low ionic strength, the maximal aggregation rates will be greater than those observed in the presence of a simple electrolyte. At high ionic strength, the additional attraction is reduced and the aggregation rate will approach that observed for a simple charge neutralization.

7.3.2 Bridging Flocculation

Bridging flocculation occurs when the loops and tails of a polymer adsorbed to one particle become attached to one or more other particles. The process is optimized for polymers which have several points of attachment on the colloidal surface and are large enough to have free segments (loops and tails) outside the zone of electrostatic repulsion and available to bind to other surfaces. The surface coverage of the adsorbed polymer appears to be a fundamental parameter controlling the probability of bridging[65] with the half surface coverage postulated as the optimum condition for flocculation to occur.[66] While flocculation can occur for polymers that are at equilibrium with the colloidal surface,[67] nonequilibrium flocculation, occurring before the polymers are able to completely collapse on the colloidal surface, is thought to predominate.[68] In that case, the dynamics of bridging flocculation are related to both the thermodynamics and kinetics of polymer adsorption, including: transport of the polymer to the colloidal surface, attachment of the polymers to the surface, and relaxation (reconformation) of the attached polymers. Furthermore, the time that the polymer remains in its nonequilibrium conformation will be an important parameter controlling flocculation efficiency. The time scale will be influenced by the

particle : polymer ratio, the size of the particle, the surface area of the particle, the adsorption energy of the polymer segments, and the collision frequency among the particles.[69,70] The polymer rigidity,[71] charge and spacing of charged groups, the polymer dosage, the particle surface charge,[72] and the particle mixing regime[52] are also important parameters controlling the flocculation efficiency.[69] For neutral polymers, the optimal polymer dose will also depend upon the molar mass of the polymer and the ionic strength. In that case, larger polymers will flocculate particles more efficiently while a higher ionic strength will decrease the electrostatic repulsion among particles so that fewer polymer molecules are required to attain the same effect. In the presence of charged polymers, both polymer and colloid charge are influenced by the ionic strength. An increased ionic strength will generally decrease the rigidity of polyelectrolyte chains resulting in more limited possibilities for flocculation. On the other hand, as discussed earlier, the interparticle repulsive forces are screened at high ionic strength, allowing for an easier approach of the particles. For this reason, optimal bridging of particles by polyelectrolytes will generally occur at intermediate charge densities or salt concentrations.[73]

It is relatively difficult to distinguish between the bridging and charge neutralization mechanisms. In the presence of neutral polymers, there is little doubt that bridging flocculation is responsible for particle aggregation. On the other hand, polyelectrolytes can both reduce electrostatic repulsion and act as bridging molecules. A charge neutralization mechanism is generally identified for cases in which the optimal polymer dosage (maximum aggregation rate) (i) coincides with a zero zeta potential; (ii) decreases with increasing polymer charge density; and (iii) increases proportionally with particle concentration.[74,75] In the presence of polyelectrolytes, the simple charge neutralization mechanism is not sufficient to explain the flocculation of colloidal particles for (i) failures of the above observations; (ii) effects due to the molar mass of the polymer (width of the flocculation zone; shifts in the optimal dosage), or (iii) an observation of a higher aggregation rate than would be observed in the presence of a simple electrolyte.[64,74] Discrepancies have been attributed to both an uneven distribution of charge on the particles (electrostatic patch model[64]) or to the likely possibility that both flocculation and charge neutralization mechanisms are likely to occur simultaneously.[74]

7.3.3 Depletion Flocculation

Depletion flocculation occurs for cases in which the polymer has a stronger affinity for the water than it does for the particle surface (or a polymer covered particle surface). In that case, the polymer remains predominantly as a nonadsorbing coil in the solution phase. When the particles in solution approach each other to a distance that is less than the effective polymer diameter (i.e., twice the gyration radius), then the polymer will be excluded from the space between the particles, reducing its concentration with respect to the bulk solution. The imbalance of osmotic pressure generates an attractive force among the particles, causing flocculation. The driving force for the existence of the depletion zone is due to conformational entropic restrictions of the polymer coils that are not compensated by an adsorption energy.[59] In the presence of a sufficient quantity of nonadsorbing polymer, the interparticle interaction energy curve shows a

secondary minimum at a distance corresponding to twice the radius of gyration of the polymer. Recent direct measurements of the interparticle interaction forces by atomic force microscopy have confirmed that the depth of the secondary minima increased with increasing free polymer concentration.[76,77] The most important parameter governing depletion flocculation in aqueous solutions is the size of the polymer with respect to the particle.[78] Although an increase in molar mass has opposing effects on the depletion energy,[79] overall, an increase of the particle concentration or an increase of the molar mass of the polymer will favor depletion flocculation.[77,79–81]

7.3.4 Steric Stabilization

The adsorption of large concentrations of a neutral polymer or polyelectrolyte can lead to steric stabilization. In this case, the particle surface is saturated with polymer such that the polymer loops and trains form a relatively thick layer (several nanometers) of adsorbed polymer. Stabilization depends upon several factors including the thickness of the adsorbed polymer layer, the size of the particles, and the effective Hamaker constant of the covered particles. Indeed, the spatial extension of the adsorbed layer must be thick enough to prevent the particles from approaching to distances at which London–van der Waals attractive forces become significant. Although, the adsorbed polymers may overlap and become compressed, such overlap is generally unfavorable, due to a strong repulsion that increases very sharply with increasing penetration.[82] Because van der Waals attractive forces increase with particle size, larger particles require thicker polymer layers to ensure a similar particle stability. Note that for concentrations of polymers that are greater than those required for steric stabilization, the excess polymer will remain unadsorbed in the bulk solution, potentially leading to depletion flocculation.

7.4 PRIMARY COLLOIDAL INTERACTIONS IN FRESHWATERS

In most oxic waters, Pareto law size distributions[50] and microscopic imaging (e.g., ref. [14,83]) obtained in the nanometer to micrometer size range suggest that colloids are often found associated in aggregate structures[84] rather than existing solely as isolated entities. Based upon the physicochemical nature of natural organic matter (Section 7.2) and the known mechanisms leading to stabilization or flocculation (Section 7.3), Section 7.4 summarizes our current understanding of the aggregation properties of the major aquatic colloids.

7.4.1 Homocoagulation

Colloids may aggregate among themselves (homoaggregation) or among other colloid types (heteroaggregation). In homoaggregation, the electric field is always repulsive, whereas it may be attractive or repulsive in heteroaggregation, depending on the nature of particles. An apparent contradiction in environmental colloidal sciences is that models invoking homoaggregation have been reasonably successful in predicting

colloidal and aggregate size distributions in natural waters,[5,50] despite the obvious large chemical heterogeneity of colloids in freshwaters. Such an observation is probably due in part to the fact that, in natural waters, most inorganic colloids are covered by an adsorbed layer of HS[11,62,85] that can modify their surface charge, resulting in an "effective" single class of compounds with similar surface properties. Homoaggregation of HS covered inorganic colloids is usually a slow process due to a low collision efficiency resulting from a significant repulsive charge of the surface bound HS. This results in compact aggregates that do not exceed 1 micron even after a week[50] and are unlikely to be responsible for major sedimentation fluxes.

Little is known about the aggregation of HS.[86] More traditional opinion proposes that observations of large HS entities can be attributed to that fact that the HS are polymers that can assume a random coil conformation in solution.[87] Another view suggests that large HS entities are, in fact, associations of relatively small molecules held together by weak interaction forces including hydrophobic forces and hydrogen bonds.[88] Although the conceptual model for HS aggregation is still under discussion, it is clear that HS can form large macromolecular structures or aggregates in aqueous media at low pH[26] (Figure 7.5), in the presence of multivalent ions,[89] or in the solid state, such as in soils. Indeed, homoaggregates of HS have been observed by light scattering,[90,91] turbidmetry,[92] fluorescence spectroscopy,[93] atomic force microscopy,[26] and fluorescence correlation spectroscopy,[27] even in the pH range 5 to 8 for which COOH groups of the HS are predominantly dissociated.[24] Under these conditions, HS can be considered as charged globules and DLVO theory would appear to be at least partly applicable,[94] although for such small, chemically heterogeneous colloids, hydration effects, hydrogen bonding, non polar interactions, polyvalent cation interactions,[95] and reversible aggregation must also be considered. Indeed, in an attempt to explain the observed slow *disaggregation* kinetics of a peat humic acid (Figure 7.5C), Avena and Wilkinson[96] postulated that at least two different disaggregation mechanisms were involved simultaneously. Although the disaggregation rate increased significantly above the pH corresponding to the deprotonation of the carboxylic groups, another mechanism, likely involving the breaking of hydrogen bonds holding the HS aggregate together, was also identified. Note finally, that in contrast to what is generally assumed in the DLVO models, aggregation, though slow, was reversible.

In order to understand the formation of biological flocs and biofilms, it is extremely important to determine the mechanisms for the homoaggregation of other biopolymers than the HS, including polysaccharides, peptidoglycans, and proteins. In recent years, there has been a substantial increase of interest in the biomedical literature with respect to protein aggregation and its implications (reviews see ref. [97,98]). As mentioned above, protein aggregation in freshwaters is not thought to be important due to the high lability of the proteins in the water column. In biofilms, polysaccharides appear to play a predominant though not singular role.[99] Most investigations of the physicochemical behavior of polysaccharides in solution have concentrated on their conformational helix–coil transitions and their interactions with metal ions. These contributions have demonstrated that transitions between a helical and random coil conformation are dependent upon temperature, pH, ionic strength, and calcium content.[46,100] Less attention has been paid to the self association of the

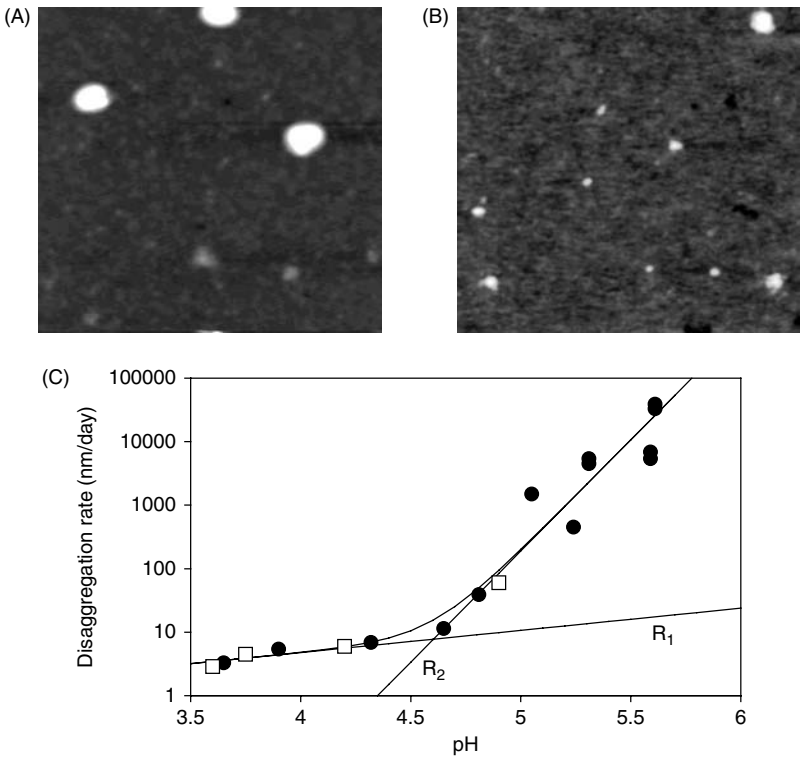

FIGURE 7.5 Tapping mode atomic force microscopy (TM-AFM) images and disaggregation rates (rate of decrease of an equivalent spherical aggregate) of the U.K. Geological Survey peat humic acid (PHA). (A) TM-AFM of a 10 mg l^{-1} PHA solution adsorbed on mica at pH 3.2, 5 mM NaCl. Scan size is 2 μm × 2 μm. (B) TM-AFM of a 10 mg l^{-1} solution adsorbed on mica at pH 6.8, 5 mM NaCl. (C) Disaggregation rates of the PHA as a function of pH. (C) shows that the aggregates observed in (A) were not at equilibrium (at this concentration, equilibrium corresponds to complete disaggregation, a process that will take months). (The figures were taken from [A, B] Balnois, E., et al. *Environmental Science and Technology*, 1999. **33**(21): p. 3911–17; [C] Avena, M.J. and K.J. Wilkinson, *Environmental Science and Technology*, 2002. **36**(23): p. 5100–05 with permission from the American Chemical Society.)

polysaccharides, including their gelation properties. Furthermore, most work in the field of gelation has examined polysaccharides used in encapsulation and physico-chemical techniques such as electrophoresis rather than freshwater polysaccharides. In addition to the intermacromolecular coordination bonds of metal ions, hydrogen bonds and hydrophobic interactions are of great importance in the homocoagulation process.

7.4.2 Heterocoagulation: Role of HS

As discussed in Section 7.4.1, HS diameters are typically 1 to 3 nm. Therefore, the interaction of the HS with colloids larger than 10 to 20 nm corresponds to their

adsorption[101,102] and results primarily in a modification of the surface properties of the colloid (surface potential and dielectric constant). Indeed, inorganic colloids in contact with HS tend to have a similar negative surface charge,[11,62,85,103] irrespective of their intrinsic chemical nature. In the normal ranges of pH (5 to 8), ionic strength (1 to 50 mM) and HS concentrations (0.5 to 10 mg l^{-1}) that are found in freshwaters, HS adsorption should stabilize colloidal suspensions,[11,12,104,105] due to a significant electrostatic repulsion among the HS covered colloids. The net effect will depend on surface coverage of the mineral surface by the HS and the corresponding degree of charge neutralization. For model compounds, it has been shown that the adsorption of negatively charged polyelectrolytes on positively charged colloids may also result in destabilization but only for a limited range of surface coverages, that is, those very close to charge neutralization.[75,106] Laboratory studies of both metal oxides and clays,[11,12,105,107] suggest that strong adsorption of the HS occurs and that very low concentrations ($\leq$1 mg l^{-1}) are sufficient to stabilize colloidal particles for colloid concentrations that are typical of natural waters ($<$10 mg l^{-1}) (Figure 7.6). Where coagulation does occur, a low collision efficiency is expected to lead to compact aggregate structures, especially for low ionic strength waters.

Although steric repulsion of inorganic colloids by adsorbed HS might be thought to increase the stabilization effect compared to electrostatic repulsion alone, it is unlikely to be significant, given that the thickness of adsorbed HS molecules is small (few nanometers on mica; ref. [26,108], Figure 7.7). Indeed, these results[26] show that it is unlikely that multiple layers of HS form on mica by adsorption from dilute solution ($<$10 mg l^{-1}) at circumneutral pH. Note that it might be possible to arrive at a different conclusion for colloid suspensions in marine systems where due to ionic strength effects (compression of the Debye layer), the Debye layer can be of a similar order of magnitude as the adsorbed HS layer.

7.4.3 Heterocoagulation: Role of Rigid Polysaccharides and Peptidoglycans

In freshwaters, fibrillar material likely corresponding to rigid polysaccharides or peptidoglycans can be observed in the water column, especially in zones dominated by photosynthetic plankton (especially phytoplankton and cyanobacteria) (Figure 7.8). These long chain, semi-rigid biopolymers contrast with the organic material remaining in solution at depth which is primarily "processed" organic material. Furthermore, during periods of high productivity, inorganic colloids are depleted in surface waters at depths corresponding to the maximum production of polysaccharides.[13] In laboratory experiments, flocculation has been shown to increase with increasing concentrations of added polysaccharide while showing the opposite tendency in the presence of humic substances. Finally, microscopic images of freshwater aggregates (e.g., ref. [84,109]) often show small inorganic colloids embedded into networks of fibrillar material.

For the heterocoagulation of compact colloids and fibrils, chemical reactivity is expected to depend on the electric charge, van der Waals forces, hydrogen and coordination bonds, as well as hydrophobic interactions of the two entities, as would

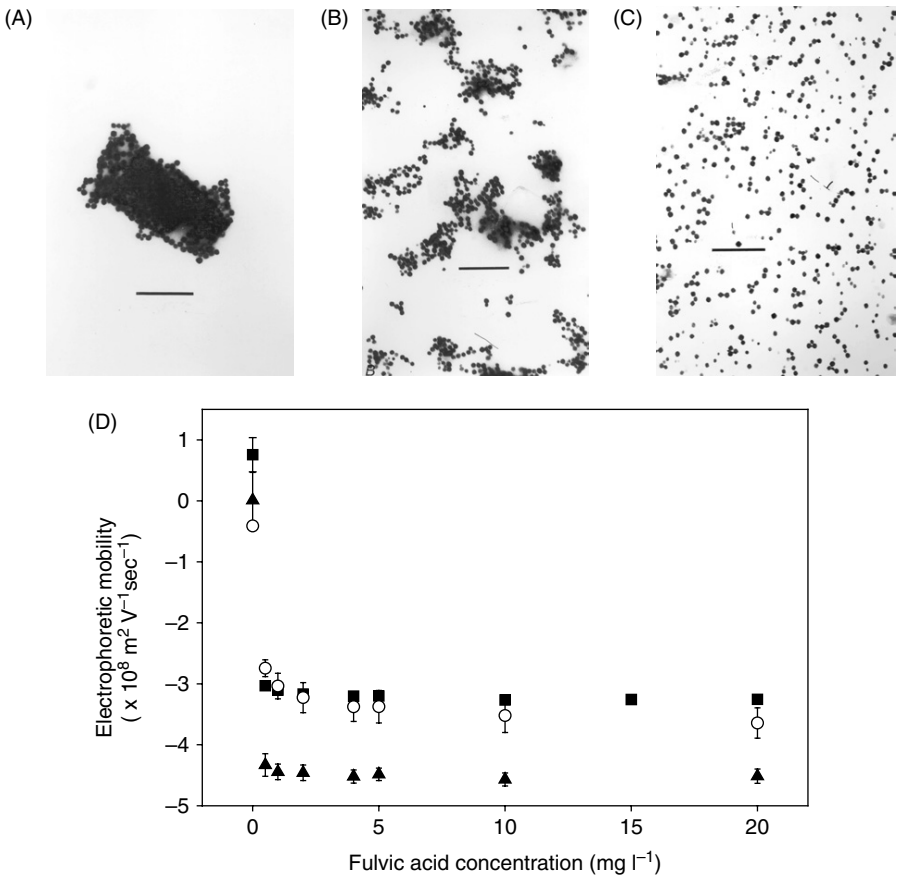

FIGURE 7.6 Transmission electron microscopy of hematite (Fe_2O_3) colloids in the presence of (A) 0, (B) 0.7, and (C) 4.9 mg l^{-1} of added Suwannee River standard natural organic matter (pH 7). Bars in the figure correspond to 500 nm. (D) Electrophoretic mobilities of hematite colloids (10 mg l^{-1}) as a function of an increasing concentration of the standard Suwannee River fulvic acid at pH 6.5 and three different ionic strengths: (NaCl: 5 mM, ■; 50 mM, ▲; 250 mM, ◯.) (Taken from Wilkinson, K.J., J.C. Negre, and J. Buffle. *Journal of Contaminant Hydrology*, 1997. **26**(1–4): p. 229–43 with permission from Elsevier.)

be the case for homocoagulation. On the other hand, since most fibrillar biopolymers have a zero or slightly negative charge density, electrostatic repulsion and thus the energy barrier preventing aggregation will be small. Furthermore, due to the formation and interactions of helices comprising the rigid biopolymers, their thickness and thus the van der Waals forces of the fibril segments may be significantly larger than for a corresponding segment of a single chain. Because freshwater fibrils may be much longer than the diameter of the colloids (Table 7.1), they can serve as rigid (or semi-rigid) long distance bridges between the colloids. Furthermore, attached, compact colloids may serve as the binding center for polymers, leading to the formation of loose aggregate networks that extend to very large dimensions.

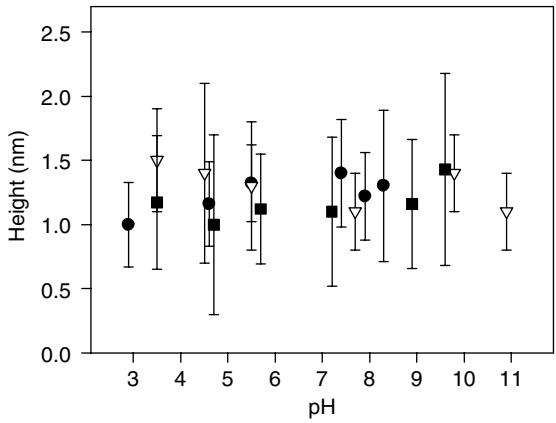

FIGURE 7.7 Variation of the height of adsorbed standard Suwannee River humic acid on mica between pH 3 and pH 11 for ionic strengths of 5 mM NaCl (■), 50 mM NaCl (Δ) or 5 mM $CaCl_2$ (●). (Figure is taken from Balnois, E., et al. *Environmental Science and Technology*, 1999. **33**(21): p. 3911–17 with permission from the American Chemical Society.)

Indeed, several recent studies of model systems have demonstrated that small concentrations of polymer can facilitate the bridging flocculation process (e.g., polystyrene latex and methylcellulose or polyvinylpyrrolidone,[112] silica and polyacrylamide,[113] alumina and modified polyacrylamide[114,115]). In these colloidal systems, flocculation is often first observed at lower concentrations followed by stabilization at significantly higher ones. For example, Solberg and Wagberg[113] observed bridging flocculation of silica nanoparticles for an addition of 0.4 mg l^{-1} polyacrylamide and dispersion due to electrosterical stabilization for concentrations exceeding 1.2 mg g^{-1} of the polymer. Nonetheless, only a few studies have examined the bridging flocculation process in the presence of microbial polysaccharides and environmental colloids. For example, Labille et al.[116] recently showed that the anionic bacterial polysaccharide succinoglycan induced the destabilization of a polydisperse suspension of montmorillonite, presumably by bridging flocculation. Using dynamic light scattering, Ferretti et al.[117] demonstrated bridging flocculation of hematite colloids by the neutral triple helical schizophyllan (Figure 7.9). In that case, environmentally realistic (low) polysaccharide concentrations, that is, <1 mg C l^{-1} were observed to induce bridging flocculation. At higher and lower polysaccharide concentrations, the hematite suspensions were stabilized.

7.4.4 Heterocoagulation: Contributions of Other Types of Organic Matter

To our knowledge, there is very little specific information on the interactions of the *proteins or reserve polysaccharides* with inorganic surfaces in natural waters. Some recalcitrant proteins have the potential to play a role similar to that of HS in fresh waters, since they are small (hydrodynamic diameters of 1 to 5 nm) polymers with

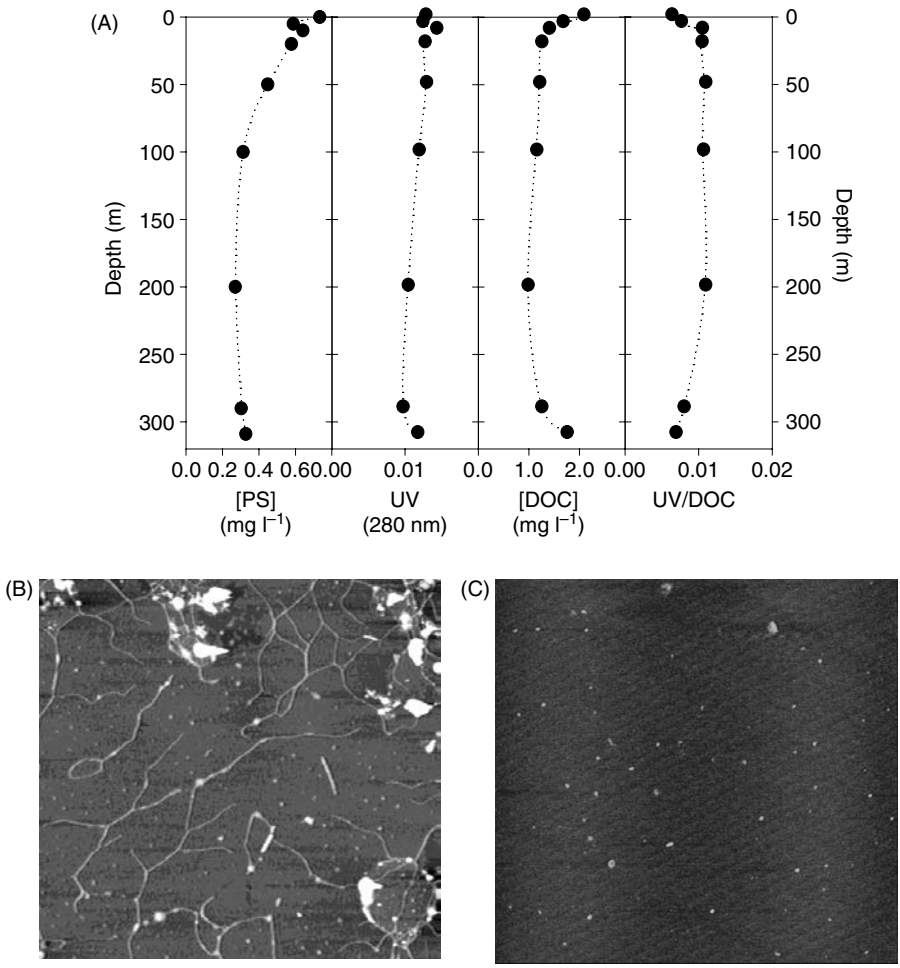

FIGURE 7.8 (A) Organic matter profiles obtained in a oligotrophic lake (Lake Geneva, Switzerland). In this figure, the increase in dissolved organic carbon (DOC) in the surface waters can be attributed to an added presence of fibrillar polysaccharides (PS) rather than HS (represented by the vertical curve of ultraviolet (UV) absorbance). Polysaccharides were determined by the spectrometric technique detailed in ref. [110,111]. (B) AFM image showing some important organic macromolecules isolated from a Lake Geneva surface water sample at 15 m (B) and 309 m. (C) Scan size was 5 μm × 5 μm at 15 m and 3 μm × 3 μm at 309 m. (B is taken from Wilkinson, K.J., et al. *Colloids and Surfaces, A: Physicochemical and Engineering Aspects*, 1999. **155**(2–3): p. 287–310 with permission from Elsevier.)

hydrophobic moieties that will favor their adsorption on surfaces as thin films. Indeed, for model systems, a stabilizing role of certain flexible polysaccharides has also been demonstrated. For example, the adsorption of the flexible (globular) polysaccharide, dextran (40, 150, and 500 kDa) stabilized monodisperse suspensions of sulfate- and amidine-modified polystyrene colloids, similar to what was observed for a HS.[118]

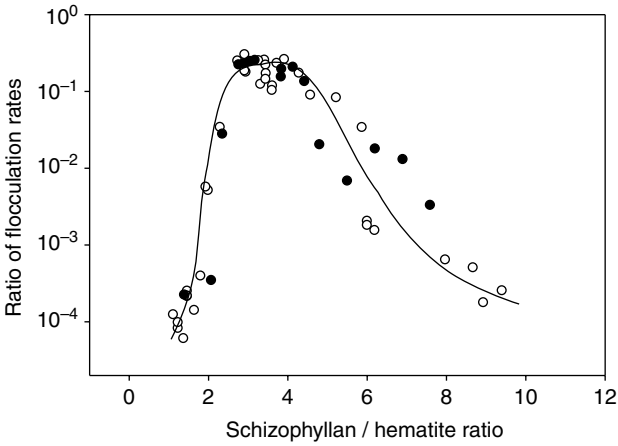

FIGURE 7.9 Ratio of flocculation rates of a 10 mg l^{-1} colloidal hematite suspension as a function of the ratio between the total number of schizophyllan entities and the total number of hematite particles (◯) pH 4.5, ionic strength = 1 mM and (●) pH 3, ionic strength = 1 mM. The flocculation rate ratio is equal to the flocculation rate under consideration divided by the maximum rate of flocculation obtained using 0.1 M NaCl. (Figure is taken from Ferretti, R., et al. *Journal of Colloid and Interface Science*, 2003. **266**: p. 328–38 with permission from Elsevier.)

Although all of the biopolymers stabilized the colloidal suspensions, the HS and the large molar masses of dextran were the most effective in reducing the rate of aggregation of the colloidal particles. On the other hand, none of the biopolymers fragmented already formed aggregates (in contrast to the results observed in Figure 7.6 and ref. [119,120]). In another study, the adsorption of even extremely large molecules of a flexible polymer, polyacrylic acid (molar masses of 1 to 2 × 10^6 Da), did not result in surface thicknesses exceeding 13 nm[121] discounting the role of a potential steric stabilization. In this case, the polyacrylic acid was clearly demonstrated to induce coagulation by charge neutralization, irrespective of its molar mass.[75] Indeed, coil-like polymers will tend to collapse at the colloid surface due to a strong electrostatic attraction, especially for interactions between oppositely charged colloids and biopolymers. Furthermore, most flexible biopolymers in aquatic systems have molar masses which are too small to produce significant layer thicknesses. Nonetheless, the role of large extended biopolymers such as alginic acid have been largely unstudied (with the possible exception of their role in biofilms, e.g., ref. [122]).

Finally, when evaluating the role of proteins, polypeptides, reserve polysaccharides, etc., it is important to compare the time scales for the decomposition of the macromolecules with that of their adsorption and coagulation. As discussed in the previous section, most measurements of proteins and reserve polysaccharides in natural freshwaters indicate that they constitute a minor component with a rapid turnover.[19] As observed for the HS, it is likely that the adsorption of certain recalcitrant, flexible biomacromolecules onto comparatively large inorganic surfaces will result primarily in a modification of the particle surface charge.

7.5 SUMMARY AND FUTURE PERSPECTIVES

In natural freshwaters, the association of all classes of "natural organic matter" into a single, homogeneous reacting entity with a single set of properties is clearly an oversimplification. The physicochemical nature of the organic macromolecules, including their chemical nature, inherent chemical heterogeneity and polydispersity, will greatly influence their role in the flocculation process. The aggregation of inorganic freshwater colloids in the presence of natural organic matter can nonetheless be simplified as the result of at least two major but opposing effects: their stabilization by humic substances and their destabilization by large, rigid biopolymers. In the presence of polysaccharides, large, loose flocs are generally formed (Figure 7.10(A)) in marked contrast with the effect of the humic substances. In that case, the significant repulsive charge of the colloids leads either to colloidal stabilization or to the formation of small, compact aggregates (Figure 7.10(B)) due to a low collision efficiency between the particles. Under such a scenario, colloidal aggregates exceeding 1 μm are likely to form slowly[50] and are thus unlikely to be responsible for major sedimentation fluxes. Nonetheless, the simple explanation based upon each of the flocculation mechanisms in isolation is rarely encountered in natural freshwaters. Typically, the bridging role of the organic biopolymers becomes less and less significant and the application of DLVO/Smoluchowski theory becomes more and more valid for larger primary particles (>100 nm). Rigid biopolymers appear to dominate aggregate structures[84] when the size of the primary particles making up the aggregates are small (<100 nm), even though, under optimal conditions, aggregates formed by flocculation will be much larger that those obtained by the coagulation of compact colloids. For the larger colloidal aggregates, stability and aggregate structure will also depend on the shear

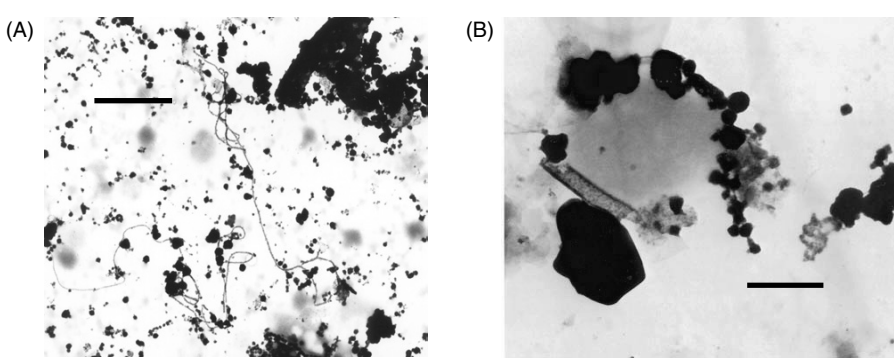

FIGURE 7.10 (A) Inorganic colloids associated with fibrillar organic macromolecules. Scale bar corresponds to 1 μm. (B) Compact heteroaggregate from Lake Bret, Switzerland. The picture shows a spherical silica particle (gray at center) aggregated with smaller iron hydroxide particles (black spheroids), a clay particle and some biological debris. Scale bar corresponds to 250 nm. For experimental detail on transmission electron microscopy (TEM) preparation, see ref. [123,124]; for further discussion, see ref. [6]. (B was taken from Buffle, J., et al. *Environmental Science and Technology*, 1998. **32**(19): p. 2887–99 with permission from the American Chemical Society.)

forces in solution, the tensile strength of the bridging biopolymers, and the weight of the particles, all factors that may influence fragmentation and collapse. In any case, environmental systems generally contain mixed heteroaggregates that are likely the result of both a charge modification by the small molecules and bridging flocculation by the large biopolymers, the net result being a network of rigid biopolymers that are interconnected by isolated or aggregated compact colloids.

Unfortunately, only limited data are available that examine the effects of organic biopolymer mixtures (especially HS and polysaccharides) on the flocculation and stabilization processes (e.g., ref. [125–127]). For example, in one recent study on a model system, low concentrations of polyvinyl alcohol (PVA) were shown to induce the flocculation of amidine polystyrene latex particles via polymer bridging;[126] an effect that was prevented in the presence of a low concentration of HS (2.5 $mg\,l^{-1}$).[126] On the other hand, colloidal montmorillonite suspensions (3 $mg\,l^{-1}$) were shown to aggregate in the presence of 2 and 4 $mg\,C\,l^{-1}$ of algal exopolymers isolated from a small eutrophic lake, even in the (stabilizing) presence of 0.1 $mg\,C\,l^{-1}$ of a soil fulvic acid. Future research into the three-colloidal component system (compact inorganic colloids; large rigid biopolymers; humic substances) is thus clearly merited.[6]

Much more detailed information is especially needed on the interactions of the natural rigid biopolymers with freshwater colloids and the modifying role of the HS. Since both natural colloids and biopolymers are physically and chemically heterogeneous, neighboring zones of a same particle surface may have different charges or charge densities. Aggregation might then occur due to interactions of surface patches[61,64] which do not represent the average characteristics of the surface. Conclusions drawn from studies using model monodisperse, chemically homogeneous polymers and colloids must therefore be applied with great caution to predictions of the role of natural organic matter in "real" environmental systems.

In addition to developing a better understanding of heterocoagulation in freshwaters, future research should also examine the nature of the chemical interactions and kinetics of biopolymer associations (HS, polysaccharides, proteins). Indeed, the formation mechanisms of biofilms and humic aggregates and the kinetics of the two processes have been largely ignored in the literature. It is hoped that future research might provide a detailed and quantitative insight into the principle mechanisms regulating the role of each of the main classes of organic macromolecules and their mixtures.

Although it is obvious that measurements of total organic carbon are poor indicators of the role(s) of natural organic matter in a given aquatic system, separate determinations of HS, polysaccharides, peptidoglycans, proteins, etc. are analytically very difficult to perform (e.g., ref. [28,128,129]). Physicochemical separation techniques such as chromatography, filtration, field flow fractionation, etc. have been proposed but are largely inadequate for a complete separation of the principal structures. Studies using enriched fractions of the important components are useful, albeit oversimplified surrogates of natural freshwaters. It is likely that increased resolution of the spectroscopic techniques, including nuclear magnetic resonance spectrometry[130,131] may one day be able to provide a quantitative distinction of the important components of freshwaters, especially at environmentally relevant (i.e., low) concentrations.

ACKNOWLEDGMENTS

We gratefully acknowledge the scientific contributions of M. Avena, E. Balnois, J. Buffle, M. Filella, M. Hosse, J.R. Lead, K. Starchev, S. Stoll, and J. Zhang. Some sampling performed by the CIPEL (Commission internationale pour la protection des eaux du Léman) and funding from INTERREG II (Project 740075/GE0045) is gratefully acknowledged. Funding from the Swiss National Funds (Project 2000-061648) is also greatly appreciated.

REFERENCES

1. Stumm, W., *Chemistry of the Solid-Water Interface*. 1992, New York: John Wiley and Sons.
2. Stumm, W., *Aquatic Chemistry. Chemical Equilibria and Rates in Natural Waters*. 1996, New York: Wiley.
3. Martin, J.-M., M.-H. Dai, and G. Cauwet, Significance of colloids in the biogeochemical cycling of organic carbon and trace metals in the Venice Lagoon (Italy). *Limnology and Oceanography*, 1995. 40: p. 119–31.
4. Guo, L. and P.H. Santschi, Composition and cycling of colloids in marine environments. *Reviews of Geophysics*, 1997. 35: p. 17–40.
5. Newman, M.E., et al., Submicron particles in the Rhine River — II. Comparison of field observations and model predictions. *Water Research*, 1994. 28: p. 107–18.
6. Buffle, J., et al., A generalized description of aquatic colloidal interactions: The three-colloidal component approach. *Environmental Science and Technology*, 1998. 32(19): p. 2887–99.
7. Kinniburgh, D.G., et al., Metal ion binding by humic acid: Application of the NICA-donnan model. *Environmental Science and Technology*, 1996. 30(5): p. 1687–98.
8. Benedetti, M.F., W.H. van Riemsdijk, and L.K. Koopal, Humic substances considered as a heterogeneous Donnan gel phase. *Environmental Science Technology*, 1996. 30: p. 1805–1813.
9. Buffle, J., *Complexation Reactions in Aquatic Systems: An Analytical Approach*. 1988, Chichester: Ellis Horwood.
10. Jekel, M.R., The stabilization of dispersed mineral particles by adsorption of humic substances. *Water Research*, 1986. 20: p. 1543–54.
11. Tipping, E. and D.C. Higgins, The effect of adsorbed humic substances on the colloid stability of haematite particles. *Colloids and Surfaces, A: Physicochemical and Engineering Aspects*, 1982. 5: p. 85–92.
12. Wilkinson, K.J., J.C. Negre, and J. Buffle, Coagulation of colloidal material in surface waters: The role of natural organic matter. *Journal of Contaminant Hydrology*, 1997. 26(1–4): p. 229–43.
13. Wilkinson, K.J., A. Joz-Roland, and J. Buffle, Different roles of pedogenic fulvic acids and aquagenic biopolymers on colloid aggregation and stability in freshwaters. *Limnology and Oceanography*, 1997. 42(8): p. 1714–24.
14. Filella, M., J. Buffle, and G.G. Leppard, Characterization of submicron colloids in freshwaters: Evidence for their bridging by organic structures. *Water Science Technology*, 1993. 27: p. 91–102.
15. Tanford, C., *Physical Chemistry of Macromolecules*, 1961. New York: Wiley.
16. Fleer, G.J., et al., *Polymers at Interfaces*, 1993. London: Chapman and Hall.

17. Lyklema, J., *Fundamentals of Interface and Colloid Science*, Vol. II. 1995, London: Academic Press.
18. Buffle, J. and H.P. van Leeuwen, Foreword, in *Environmental Particles*, J. Buffle and H.P. van Leeuwen, Editors, Vol. 1. 1992, Chelsea, Michigan: Lewis Publishers, Inc. p. 554.
19. Thurman, *Organic Geochemistry of Natural Waters*. 1985, Dordrecht: Kluwer Academic Publishers Group.
20. Davis, J.A. and D.B. Kent, Mineral-water interface geochemistry, in *Reviews in Mineralogy*, M.F. Hochella and A.F. White, Editors. 1990, Mineralogical Society of America: Washington, DC. p. 177–260.
21. Lerman, A., *Geochemical Processes*. 1979, New York: Wiley Interscience.
22. Sposito, G., Characterization of particle surface charge, in *Environmental Particles*, J. Buffle and H.P. von Leeuwen, Editors. 1993, Boca Raton: Lewis Publishers. p. 291–314.
23. Leenheer, J.A., et al., Molecular resolution and fragmentation of fulvic acid by electrospray ionization/multistage tandem mass spectrometry. *Analytical Chemistry*, 2001. 73(7): p. 1461–71.
24. Hosse, M. and K.J. Wilkinson, Determination of electrophoretic mobilities and hydrodynamic radii of three humic substances as a function of pH and ionic strength. *Environmental Science and Technology*, 2001. 35(21): p. 4301–06.
25. Goldberg, M.C. and E.R. Weiner, Fluorescence measurements of the volume, shape and fluorophore composition of fulvic acid from the Suwannee River, in *Humic Substances in the Suwannee River, Georgia: Interactions, Properties, and Proposed Structures*, R.C. Averett, et al., Editors. 1994, USGS Water Supply paper 2373: Denver. p. 99–113.
26. Balnois, E., et al., Atomic force microscopy of humic substances: Effects of pH and ionic strength. *Environmental Science and Technology*, 1999. 33(21): p. 3911–17.
27. Lead, J.R., et al., Determination of diffusion coefficients of humic substances by fluorescence correlation spectroscopy: Role of solution conditions. *Environmental Science and Technology*, 2000. 34(7): p. 1365–69.
28. Leenheer, J.A. and J.-P. Croue, Characterizing aquatic dissolved organic matter. *Environmental Science and Technology*, 2003. 37(1): p. 18A–26A.
29. Conte, P. and A. Piccolo, Conformational arrangement of dissolved humic substances. Influence of solution composition on association of humic molecules. *Environmental Science and Technology*, 1999. 33(10): p. 1682–90.
30. Schulten, H.-R., P. Leinweber, and M. Schnitzer, in *Structure and Surface Reactions of Soil Particles*, M. Huang, N. Senesi, and J. Buffle, Editors. 1998, Wiley: New York. p. 281–324.
31. Lead, J.R., et al., Diffusion coefficients and polydispersities of the suwannee river fulvic acid: Comparison of fluorescence correlation spectroscopy, pulsed-field gradient nuclear magnetic resonance, and flow field-flow fractionation. *Environmental Science and Technology*, 2000. 34(16): p. 3508–13.
32. Wetzel, R.G., *Limnology*. Vol. 1st edition. 1975, Philadelphia: Saunders.
33. Smith, D.C., et al., Intense hydrolytic enzyme activity on marine aggregates and implications for rapid dissolution. *Nature*, 1992. 359 p. 139–141.
34. Nagata, T., B. Meon, and D.L. Kirchman, Microbial degradation of peptidoglycan in seawater. *Limnology and Oceangraphy*, 2003. 48: p. 745–54.
35. Wakeham, S.G., et al., Biogeochemistry of particulate organic matter in the oceans: Results from sediment trap experiments. *Deep-Sea Research Part A. Oceanographic Research Papers*, 1984. 31: p. 509–28.

36. Amy, P.S., et al., Microbial activity and ultrastructure of mineral-based marine snow from Howe Sound, British-Columbia. *Canadian Journal of Fisheries and Aquatic Sciences*, 1987. 44: p. 1135–42.
37. Jensen, T.E. and W.A. Corpe, Elemental analysis of non-living particles in picoplankton fractions from oligotrophic lake water. *Water Research*, 1994. 28: p. 901–7.
38. Strycek, T., et al., Extracellular fibril production by freshwater algae and cyanobacteria. *Microbial Ecology*, 1992. 23: p. 53–74.
39. Leenheer, J.A., et al., in *Natural Organic Matter and Disinfection By-Products*, S.E. Barrett, S.W. Krasner, and G.L. Amy, Editors. 2000, American Chemical Society: Washington, DC. p. 68–83.
40. Santschi, P.H., et al., Fibrillar polysaccharides in marine macromolecular organic matter as imaged by atomic force microscopy and transmission electron microscopy. *Limnology and Oceanography*, 1998. 43(5): p. 896–908.
41. Aluwihare, L.I., D.J. Repeta, and R.F. Chen, A major biopolymeric component to dissolved organic carbon in surface sea water. *Nature*, 1997. 387: p. 166–9.
42. McCarthy, M.D., J.I. Hedges, and R. Benner, Major bacterial contribution to marine dissolved organic nitrogen. *Science*, 1998. 281: p. 231–4.
43. Morris, E.R., D.A. Rees, and G. Robinson, Mechanism and dynamics of conformational ordering in xanthan polysaccharide. *Journal of Molecular Biology*, 1980. 138: p. 349–62.
44. Wilkinson, K.J., et al., Characteristic features of the major components of freshwater colloidal organic matter revealed by transmission electron and atomic force microscopy. *Colloids and Surfaces, A: Physicochemical and Engineering Aspects*, 1999. 155(2–3): p. 287–310.
45. Muzzarelli, R.A.A., *Natural Chelating Polymers*. 1973, Oxford: Pergamon Press.
46. Balnois, E., et al., Conformations of succinoglycan as observed by atomic force microscopy. *Macromolecules*, 2000. 33(20): p. 7440–7.
47. O'Melia, C.R., The Influence of coagulation and sedimentation on the fate of particles, associated pollutants and nutrients in lakes, in *Chemical Processes in Lakes*, W. Stumm, Editor. 1985, John Wiley and Sons: New York.
48. O'Melia, C.R., in *Aquatic Chemical Kinetics*, W. Stumm, Editor. 1990, Wiley: New York. p. 447–74.
49. O'Melia, C.R., Aquasols: The behavior of small particles in aquatic systems. *Environmental Science Technology*, 1980. 14: p. 1052–60.
50. Filella, M. and J. Buffle, Factors controlling the stability of submicron colloids in natural waters. *Colloids and Surfaces, A: Physicochemical and Engineering Aspects*, 1993. 73: p. 255–73.
51. Hunt, J.R., Particle dynamics in seawater: Implications for predicting the fate of discharged particles. *Environmental Science and Technology*, 1982. 16: p. 303–9.
52. Adachi, Y., T. Matsumoto, and M.A. Cohen Stuart, Effects of hydrodynamic mixing intensity coupled with ionic strength on the initial stage dynamics of bridging flocculation of polystyrene latex particles with polyelectrolyte. *Colloids and Surfaces, A: Physicochemical and Engineering Aspects*, 2002. 207(1–3): p. 253–61.
53. Grasso, D., A review of non-DLVO interactions in environmental colloidal systems. *Reviews in Environmental Science and Biotechnology*, 2002. 1: p. 17–38.
54. Lips, A. and E. Willis, Low angle light scattering technique for the study of coagulation. *Transaction of the Faraday Society*, 1973. 69: p. 1226–36.
55. Kihira, H., N. Ryde, and E. Matijevic, Kinetics of heterocoagulation. 1. A comparison of theory and experiment. *Colloids and Surfaces*, 1992. 64(3–4): p. 317–24.

56. Kihira, H. and E. Matijevic, Kinetics of heterocoagulation. 3. Analysis of effects causing the discrepancy between the theory and experiment. *Langmuir*, 1992. 8(12): p. 2855–62.
57. Behrens, S.H., et al., Charging and aggregation properties of carboxyl latex particles. Experiments versus DLVO theory. *Langmuir*, 2000. 16(6): p. 2566–75.
58. Dickinson, E. and L. Eriksson, Particle flocculation by adsorbing polymers. *Advances in Colloid and Interface Science*, 1991. 34: p. 1–29.
59. Jenkins, P. and M. Snowden, Depletion flocculation in colloidal dispersions. *Advances in Colloid and Interface Science*, 1996. 68: p. 57–96.
60. Tuinier, R., J. Rieger, and C.G. de Kruif, Depletion-induced phase separation in colloid polymer mixtures. *Advances in Colloid and Interface Science*, 2003. 103: p. 1–31.
61. Gregory, J., Polymer adsorption and flocculation. *Special Publication — Royal Society of Chemistry*, 1996. 186(Industrial Water Soluble Polymers): p. 62–75.
62. Tombacz, E., et al., Particle aggregation in complex aquatic systems. *Colloids and Surfaces, A: Physicochemical and Engineering Aspects*, 1999. 151(1–2): p. 233–44.
63. Gregory, J., Flocculation by polymers and polyelectrolytes, in *Solid/Liquid Dispersions*, T.T. F., Editor. 1987, Academic Press: London. p. 163.
64. Gregory, J., Rates of flocculation of latex particles by cationic polymers. *Journal of Colloid Interface Science*, 1973. 42: p. 448–56.
65. La Mer, V.K., Filtration of colloidal dispersions flocculated by anionic and cationic polyelectrolytes. *Discussions of the Faraday Society*, 1966. 42: p. 248–254.
66. Healy, T.W. and V.K. La Mer, Energetics of flocculation + redispersion by polymers. *Journal of Colloid Science*, 1964. 19(4): p. 323–332.
67. Pelssers, E.G.,M., M.A. Cohen Stuart, and G.J. Fleer, Kinetic aspects of polymer bridging: Equilibrium flocculation and nonequilibrium flocculation. *Colloids and Surfaces*, 1989. 38: p. 15–25.
68. Gregory, J., Polymer adsorption and flocculation in sheared suspensions. *Colloids and Surfaces*, 1988. 31: p. 231–53.
69. Biggs, S., et al., Aggregate structures formed via a bridging flocculation mechanism. *Chemical Engineering Journal*, 2000. 80: p. 13–22.
70. Stoll, S. and J. Buffle, Computer simulation of bridging flocculation processes: the role of colloid to polymer concentration ratio on aggregation kinetics. *Journal of Colloid Interface Science*, 1996. 180: p. 548–63.
71. Walker, H.W. and S.B. Grant, Factors influencing the flocculation of colloidal particles by a model anionic polyelectrolyte. *Colloids and Surfaces, A: Physicochemical and Engineering Aspects*, 1996. 119(2/3): p. 229–39.
72. Walker, H.W. and S.B. Grant, Influence of surface charge and particle size on the stabilization of colloidal particles by model polyelectrolytes. *Colloids and Surfaces, A: Physicochemical and Engineering Aspects*, 1998. 135(1–3): p. 123–133.
73. Matsumoto, T. and Y. Adachi, Effect of ionic strength on the initial dynamics of flocculation of polystyrene latex with polyelectrolyte. *Journal of Colloid and Interface Science*, 1998. 204(2): p. 328–35.
74. Vincent, B., Effect of adsorbed polymers on dispersion stability. *Advances in Colloid and Interface Science*, 1974. 4(2–3): p. 193–277.
75. Ferretti, R., J. Zhang, and J. Buffle, Kinetics of hematite aggregation by polyacrylic acid: effect of polymer molecular weights. *Colloids and Surfaces, A: Physicochemical and Engineering Aspects*, 1997. 121: p. 203–215.
76. Milling, A.J. and B. Vincent, Depletion forces between silica surfaces in solutions of poly(acrylic acid). *Journal of the Chemical Society, Faraday Transactions*, 1997. 93(17): p. 3179–83.

77. Biggs, S., et al., Molecular weight dependence of the depletion interaction between silica surfaces in solutions of sodium poly(styrenesulfonate). *Langmuir*, 2000. 16(24): p. 9242–48.
78. Otsubo, Y., Flocculation of colloids by soluble polymers and its effect on rhelogy. *Heterogeneous Chemistry Reviews*, 1996. 3: p. 327–49.
79. Burns, J.L., et al., The effect of molecular weight of nonadsorbing polymer on the structure of depletion-induced flocs. *Journal of Colloid and Interface Science*, 2002. 247(1): p. 24–32.
80. Sperry, P.R., H.B. Hopfenberg, and N.L. Thomas, Flocculation of latex by water-soluble polymer: Experimental confirmation of a non-bridging, non-adsorptive, volume-restriction mechanism. *Journal of Colloid and Interface Science*, 1981. 82: p. 62–76.
81. Burns, J.L., et al., Relationship between interaction forces and the structural compactness of depletion flocculated colloids. *Colloids and Surfaces, A: Physicochemical and Engineering Aspects*, 1999. 162(1–3): p. 265–77.
82. Tadros, T., Interaction forces between particles containing grafted or adsorbed polymer layers. *Advances in Colloid and Interface Science*, 2003. 104: p. 191–226.
83. Perret, D., et al., Submicron particles in the Rhine river — I. Physico-chemical characterization, in *Water Research* 1993. p. 91–106.
84. Buffle, J. and G.G. Leppard, Characterization of aquatic colloids and macromolecules. 1. Structure and behavior of colloidal material. *Environmental Science and Technology*, 1995. 29: p. 2169–75.
85. Davis, J.A. and R. Gloor, Adsorption of dissolved organics in lake water by aluminum oxide. Effect of molecular weight. *Environmental Science and Technology*, 1981. 15: p. 1223–29.
86. Clapp, C.E. and M.H.B. Hayes, Sizes and shapes of humic substances. *Soil Science*, 1999. 164: p. 777–89.
87. Swift, R., Macromolecular properties of soil humic substances: Fact, fiction, and opinion. *Soil science*, 1999. 164: p. 790–802.
88. Piccolo, A., The supramolecular structure of humic substances. *Soil Science*, 2001. 166(11): p. 810–32.
89. Plaschke, M., et al., Combined AFM and STXM *in situ* study of the influence of Eu(III) on the agglomeration of humic acid. *Colloids and Surfaces, A: Physicochemical and Engineering Aspects*, 2002. 197: p. 245–56.
90. Pinheiro, J.P., et al., Dynamic properties of humic matter by dynamic light scattering and voltammetry. *Analytica Chimica Acta*, 1996. 329(1–2): p. 15–24.
91. Tombacz, E., J.A. Rice, and S.Z. Ren, Fractal structure of polydisperse humic acid particles in solution studied by scattering methods. *Models in Chemistry*, 1997. 134: p. 877–88.
92. Senesi, N., et al., Fractal humic acids in aqueous suspensions at various concentrations, ionic strengths, and pH values. *Colloids and Surfaces A: Physicochemical and Engineering Aspects*, 1997. 127(1–3): p. 57–68.
93. Engebretson, R.R., T. Amos, and R. von Wandruszka, Quantitative approach to humic acid associations. *Environmental Science and Technology*, 1996. 30: p. 990–97.
94. Tombacz, E. and E. Meleg, A theoretical explanation of the aggregation of humic substances as a function of pH and electrolyte concentration. *Organic Geochemistry*, 1990. 15: p. 375–81.
95. Kam, S.-K. and J. Gregory, The interaction of humic substances with cationic polyelectrolytes. *Water Research*, 2001. 35(15): p. 3557–66.

96. Avena, M.J. and K.J. Wilkinson, Disaggregation kinetics of a peat humic acid: Mechanism and pH effects. *Environmental Science and Technology*, 2002. 36(23): p. 5100–05.
97. Harper, J.D. and P.T. Lansbury, Jr., Models of amyloid seeding in Alzheimer's disease and scrapie: mechanistic truths and physiological consequences of the time-dependent solubility of amyloid proteins. *Annual Review of Biochemistry*, 1997. 66: p. 385–407.
98. Dobson, C.M., Protein misfolding, evolution and disease. *Trends in Biochemical Sciences*, 1999. 24(9): p. 329–32.
99. Neu, T.R. and J.R. Lawrence, *In situ* characterization of extracellular polymeric substances (EPS) in biofilm systems, in *Microbial Extracellular Polymeric Substances*, J. Wingender, T.R. Neu, and H.-C. Flemming, Editors. 1999, Springer-Verlag: Berlin. p. 22–47.
100. Crescenzi, V., M. Dentini, and T. Coviella, Conformation-dependent solution properties of microbial polysaccharides. *Frontiers in Carbohydrate Research*, 1992. 2: p. 100–114.
101. Sposito, G., *The Surface Chemistry of Soils*. 1984, New York: Oxford University Press.
102. Gu, B., et al., Adsorption and desorption of natural organic matter on iron oxide: Mechanisms and models. *Environmental Science Technology*, 1994. 28: p. 38–46.
103. Beckett, R. and N.P. Le, The role of organic matter and ionic composition in determining the surface charge of suspended particles in natural waters. *Colloids and Surfaces*, 1990. 44: p. 35–49.
104. Amal, R., J.A. Raper, and T.D. Waite, Effect of fulvic acid adsorption on the aggregation kinetics and structure of hematite particles. *Journal of Colloid and Interface Science*, 1992. 151(1): p. 244–57.
105. Gibbs, R.J., Effect of natural organic coatings on the coagulation of particles. *Environmental Science and Technology*, 1983. 17(4): p. 237–40.
106. Liang, L. and J.J. Morgan, Chemical aspects of iron oxide coagulation in water: Laboratory studies and implications for natural systems. *Aquatic Science*, 1990. 52: p. 32–55.
107. Tipping, E., The adsorption of aquatic humic substances by iron oxides. *Geochimica et Cosmochimica Acta*, 1981. 45(2): p. 191–9.
108. Plaschke, M., et al., *In situ* AFM study of sorbed humic acid colloids at different pH. *Colloids and Surfaces*, A: Physicochemical and Engineering Aspects, 1999. 160: p. 269–79.
109. Pizarro, J., et al., Coagulation/sedimentation of submicron particles in a eutrophic lake. *Water Research*, 1995. 29: p. 617–32.
110. Burney, C.M. and J.M. Sieburth, Dissolved carbohydrates in seawater. II. A spectrophotometric procedure for total carbohydrate analysis and polysaccharide determination, in *Marine Chemistry*, 1977. p. 15–28.
111. Johnson, K.M., C.M. Burney, and J.M. Sieburth, Doubling the production and precision of the MBTH spectrophotometric assay for dissolved carbohydrates in seawater. *Marine Chemistry*, 1981. 10: p. 467–73.
112. Csempesz, F., Enhanced flocculation of colloidal dispersions by polymer mixtures. *Chemical Engineering Journal*, 2000. 80: p. 43–49.
113. Solberg, D. and L. Wagberg, Adsorption and flocculation behavior of cationic polyacrylamide and colloidal silica. *Colloids and Surfaces, A: Physicochemical and Engineering Aspects*, 2003. 219(1–3): p. 161–72.
114. Glover, S.M., et al., Bridging flocculation studied by light scattering and settling. *Chemical Engineering Journal*, 2000. 80: p. 3–12.

115. Ovenden, C. and H. Xiao, Flocculation behaviour and mechanisms of cationic inorganic microparticle/polymer systems. *Colloids and Surfaces, A: Physicochemical and Engineering Aspects*, 2002. 197: p. 225–34.
116. Labille, J., et al., Destabilisation of montmorillonite suspensions by Ca^{2+} and succinoglycan. *Clay Minerals*, 2003. 38: p. 173–85.
117. Ferretti, R., et al., Flocculation of hematite particles by a comparatively large rigid polysaccharide: schizophyllan. *Journal of Colloid Interface Science*, 2003. 266: p. 328–38.
118. Walker, H.W. and M. Mustafa, B., Stability of particle flocs upon addition of natural organic matter under quiescent conditions. *Water Research*, 2001. 35: p. 875–82.
119. Ouali, L. and E. Pefferkorn, Fragmentation of colloidal aggregates induced by polymer adsorption. *Journal of Colloid and Interface Science*, 1994. 168(2): p. 315–22.
120. Pefferkorn, E. and L. Ouali, Polymer induced fragmentation of colloids: Mechanism and kinetics. *Progress in Colloid and Polymer Science*, 1994. 97 *(Trends in Colloid and Interface Science VIII)*: p. 65–70.
121. Zhang, J. and J. Buffle, Kinetics of hematite aggregation by polyacrylic acid: importance of charge neutralization. *Journal of Colloid and Interface Science*, 1995. 174(2): p. 500–9.
122. Sutherland, I.W., Biofilm exopolysaccharides, in *Microbial Extracellular Polymeric Substances. Characterization, Structure and Function*, J. Wingender, T.R. Neu, and H.-C. Flemming, Editors. 1999, Springer-Verlag: Berlin. p. 73–92.
123. Perret, D., et al., Electron microscopy of aquatic colloids: Non-perturbing preparation of specimens in the field, in *Water Research*, 1991. p. 1333–43.
124. Wilkinson, K.J., S. Stoll, and J. Buffle, Characterization of NOM-colloid aggregates in surface waters: coupling transmission electron microscopy staining techniques and mathematical modeling. Fresenius' *Journal of Analytical Chemistry*, 1995. 351(1): p. 54–61.
125. Lurie, M. and M. Rebhun, Effect of properties of polyelectrolytes on their interaction with particulates and soluble organics. *Water Science and Technology*, 1997. 36(4, Role of particle Characteristics in separation processes): p. 93–101.
126. Bob, M.M. and H.W. Walker, Effect of natural organic coatings on the polymer-induced coagulation of colloidal particles. *Colloids and Surfaces, A: Physicochemical and Engineering Aspects*, 2001. 177: p. 215–22.
127. Kim, E.K. and H.W. Walker, Effect of cationic polymer additives on the adsorption of humic acid onto iron oxide particles. *Colloids and Surfaces, A: Physicochemical and Engineering Aspects*, 2001. 194(1–3): p. 123–31.
128. Zumstein, J. and J. Buffle, Circulation of pedogenic and aquagenic organic matter in an eutrophic lake. *Water Research*, 1989. 23: p. 229–39.
129. Krasner, S.W., et al., Three approaches for characterizing NOM. *Journal - American Water Works Association*, 1996. 88(6): p. 66–79.
130. Hatcher, P.G., et al., Modern analytical studies of humic substances. *Soil Science*, 2001. 166(11): p. 770–94.
131. Simpson, A.J., et al., Improvements in the two-dimensional nuclear magnetic resonance spectroscopy of humic substances. *Journal of Environmental Quality*, 2002. 31(2): p. 388–92.

8 An Example of Modeling Flocculation in a Freshwater Aquatic System

Bommanna G. Krishnappan and Jiri Marsalek

CONTENTS

8.1 INTRODUCTION

Flocculation in natural freshwater systems has been suggested and inferred by many researchers,[1–4] and was explicitly investigated by Droppo and Ongley.[5] These studies and others[6–9] have concluded that in addition to the electrochemical processes, the bacterial processes also play a role in the formation of freshwater flocs. It is believed (Ongley et al.[10]) that the biological processes contribute for flocculation in two different ways: bacterial bonding and bacterial "glue." Marshall[6] had shown that the

1-56670-615-7/05/$0.00+$1.50

bacteria have a high affinity for fine grained sediment particles and thereby promotes flocculation by increasing the surface area and bonding two or more mineral particles together. Biddanda[11] and Muschenheim et al.[8] had shown that secretion of extracellular polymeric exudates by certain bacteria provide the necessary bonding material (glue) to hold particles together.

Modeling of the flocculation process in freshwater system has been attempted by several investigators.[12–15] The approach used by these investigators is based on the premise that the freshwater flocculation is a two step process in which the particles are first brought into contact by collision mechanisms such as Brownian motion, laminar and turbulent fluid shear, inertia, and differential settling, and subsequently, a certain amount of such collisions result in the formation of flocs because of the electrochemical and bacterial bonding and bacterial "glue." While our knowledge on the collision mechanisms and the collision frequencies is reasonably well established, the same cannot be said for the actual mechanism of flocculation (i.e., how collided particles bind and form flocs). The approach used in the existing models is to introduce a collision efficiency parameter that is a measure of the probability of successful collisions, and to determine the value of this parameter as part of the calibration process of the model. A flocculation modeling approach proposed by Krishnappan and Marsalek[15] for a stormwater detention pond is reviewed here to highlight the current state of knowledge in the area of modeling of freshwater flocculation.

8.2 THE STORMWATER DETENTION SYSTEM

The freshwater system that was considered by Krishnappan and Marsalek[15] is a stormwater detention pond in Kingston, Ontario, Canada. The layout of the pond is shown in Figure 8.1. The pond consists of two cells; a wet pond and a dry pond. The surface area of each pond is about one half of a hectare. The permanent depth of water in the wet pond is about 1.2 m. The pond was constructed in 1982 to minimize the impact of runoff from a newly built shopping plaza on the Little Cataraqui Creek.

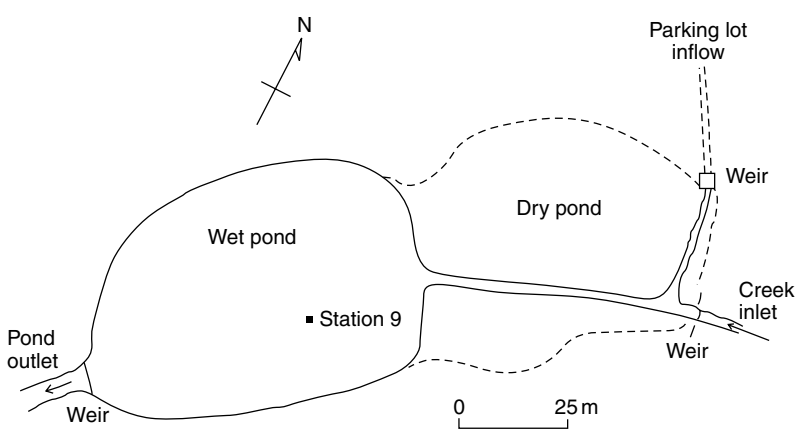

FIGURE 8.1 Schematic layout of the Kingston Stormwater Detention pond.

This creek drains an urban catchment with a drainage area of about 4.5 km^2. Since the construction of the pond, continued development in the catchment basin has increased the stream flow and hence reduced the effectiveness of the pond. Ongoing sedimentation in the pond has further exasperated the problem. To assess the effectiveness of the pond to trap sediment, a fine sediment transport study was initiated. As part of this study, deposited sediment from the pond and the pond water were collected and tested in a rotating circular flume to ascertain the sediment behavior under different boundary shear stress conditions (Krishnappan and Marsalek[16]). These experiments had indicated that the pond sediment underwent flocculation when subjected to a flow field, and consequently the settling behavior of the sediment differed significantly from that of the constituent primary particles.

Existing methods for analyzing suspended solids settling in stormwater ponds do not consider flocculation of the sediment, and treat the particles as discrete and noninteracting particles. Such an approach is not satisfactory, and hence there is a definite need for a model that would take into account the flocculation process of the stormwater sediment. To meet this need, Krishnappan and Marsalek[15] formulated a flocculation and settling model for the Kingston pond sediment. The formulation of the model was based on their experimental study in the rotating flume for the sediment from the Kingston stormwater pond.

8.3 EXPERIMENTAL STUDY

Deposited sediment from the pond was collected at a number of sampling stations within the wet pond using an Ekman dredge and combined to form a composite sample. The sample and a large volume (500 l) of pond water were brought to the Hydraulics Laboratory of the National Water Research Institute in Burlington, Ontario, Canada and were tested in the Rotating Circular Flume. Use of the pond water as the suspending medium preserved the chemical and biological characteristics of the sediment–water mixture in the laboratory experiments.

8.3.1 Rotating Circular Flume

A sectional view of the rotating circular flume is shown in Figure 8.2. The flume is supported by a rotating platform, which is 7.0 m in diameter. The flume is 5.0 m in diameter at the centre-line, 30 cm wide, and 30 cm deep. The annular top cover fits inside the flume with close tolerance. The gap between the edges of the top cover and the flume walls is about a millimeter. The height of the cover inside the channel can be adjusted by raising or lowering the top cover. The flume and the cover are rotated in opposite directions. The maximum rotational speed of both components is three revolutions per minute. The flume is equipped with a Laser Doppler Anemometer to measure the flow field and a Malvern Particle size analyzer to measure the size distribution of sediment flocs in suspension. The Malvern Particle size analyzer was placed directly underneath the flume, and the sampling cell of the instrument was connected to a short sampling tube that was inserted through the bottom plate of the flume into the flow. The sample was drawn through the sampling cell continuously

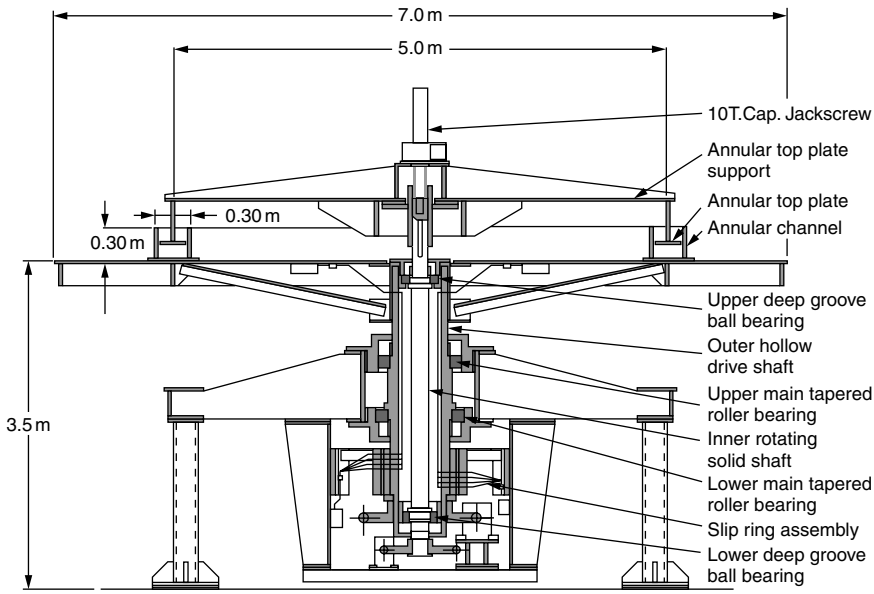

FIGURE 8.2 A sectional view of the rotating circular flume used in the experimental study.

and the instrument was operated in its flow-through mode. The size distribution of the sediment flocs were monitored at regular intervals of time. The complete details of the flume and the instruments can be found in Krishnappan.[17]

8.3.2 Deposition Tests

Deposition tests were carried out by placing the pond water and a known amount of sediment in the flume and operating the flume at the maximum speed to mix the sediment thoroughly. The amount of sediment added was enough to produce a fully mixed concentration of about 200 mg/l. The flume and the top cover were operated at the maximum speed for about 20 min, and then the speed was lowered to the desired shear stress level. The flume was then operated at this level for about 5 h. During this time, both suspended sediment concentration and the size distribution of sediment in suspension were monitored at regular intervals of time.

Figure 8.3 shows the variation of suspended sediment concentration as a function of time for five different bed shear stress conditions. From this figure, we can see that after the initial 20-min mixing period, the concentration decreases gradually and tends to reach a steady state value for all the shear stresses tested. The steady state concentration is a function of the bed shear stress. From such data, it is possible to calculate the amount of sediment that would deposit under a particular bed shear stress under a steady flow condition.

The size distribution data measured during the deposition experiments are summarized in Figure 8.4. In this figure, the median sizes of the distributions are plotted as a function of time for three of the five deposition tests. For the lowest bed shear stress

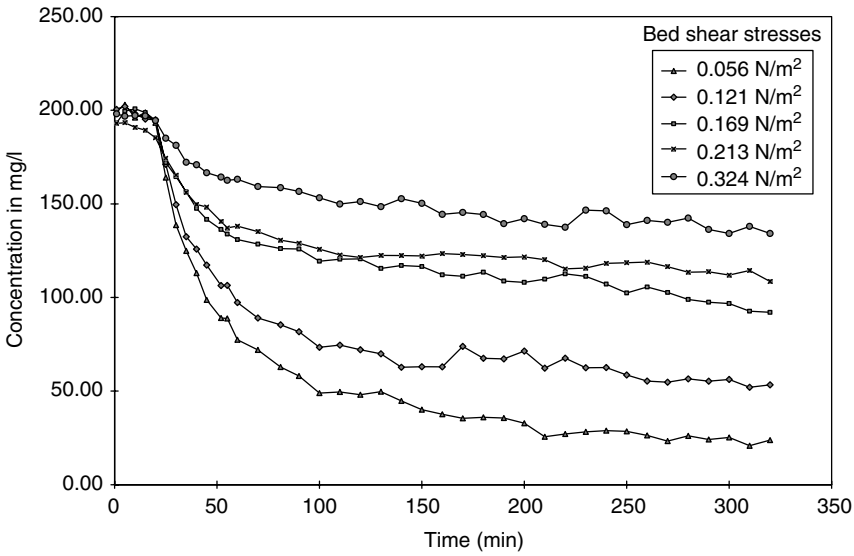

FIGURE 8.3 Concentration vs. time curves for different shear stresses during deposition.

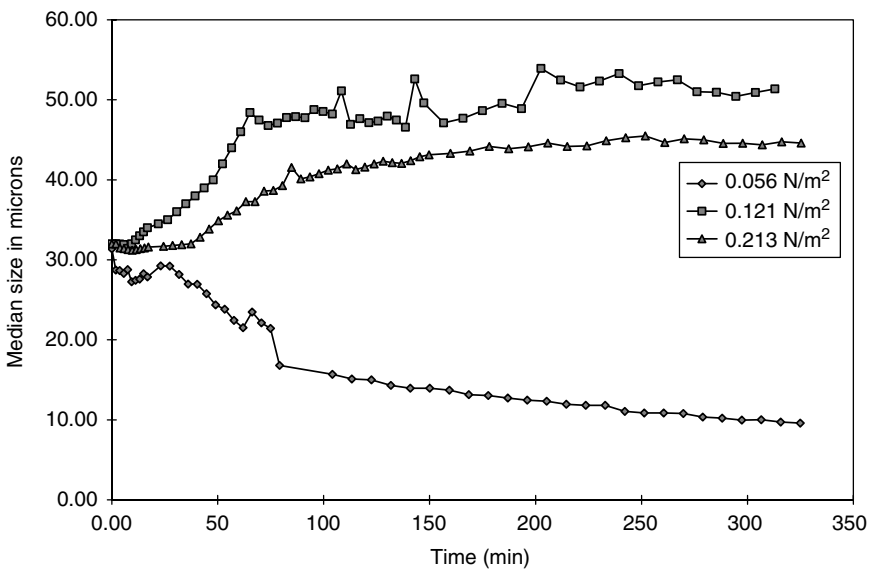

FIGURE 8.4 Median-size variations as a function of time for different bed shear stresses.

test ($0.056\,\mathrm{N/m^2}$) the median size of the sediment decreases gradually suggesting that larger particles are settling out leaving the finer fractions in suspension, in a manner analogous to the settling of discrete particles. When the bed shear stress is low such as in this case, the particles were undergoing settling without particle interaction and flocculation. On the other hand, when the bed shear stress was increased

to 0.121 N/m^2, there was a clear evidence of flocculation as can be inferred from the median size variation shown in Figure 8.4 for this shear stress. From this curve, we can see that the distributions were becoming progressively coarser starting from a median size of 30 μm to a final steady state size of about 55 μm. As the bed shear stress was further increased, the floc sizes decreased as shown by the curve corresponding to the bed shear stress of 0.213 N/m^2. At this shear stress, the increased turbulence has limited the floc growth and hence the maximum size of the floc formed was only about 45 μm.

The size distribution data shown in Figure 8.4 have demonstrated that the sediment from the stormwater detention pond undergoes flocculation when subjected to the flow field in the rotating circular flume. For formulating the flocculation model, Krishnappan and Marsalek[15] selected three tests among the five deposition tests and the concentration and the size distribution data collected from these three tests were used to calibrate and verify the model.

8.4 MATHEMATICAL MODEL

The mathematical model considers the motion of sediment particles in the rotating circular flume in two stages: a transport or a settling stage and a flocculation stage. The settling stage is modeled using an unsteady advection–diffusion equation. For flow conditions that exist in the rotating flume, the equation can be simplified to a one dimensional form as follows:

$$\frac{\partial C_k}{\partial t} + w_k \frac{\partial C_k}{\partial z} = \frac{\partial}{\partial z}\left(D \frac{\partial C_k}{\partial z}\right) \tag{8.1}$$

where C_k is the volumetric concentration of sediment of the kth size fraction and w_k is the fall velocity of the same fraction. D is the turbulent diffusion coefficient in the vertical direction; t is time and z is the vertical distance from the water surface. This equation was solved using a finite difference scheme proposed by Stone and Brian,[18] which minimizes the numerical dispersion. The boundary conditions specified for solving the equation are, (a) no net flux at the water surface and (b) the net upward flux at the sediment water interface is calculated as the difference between the erosion flux and the deposition flux. A uniform concentration of sediment over the water column was used as the initial condition for the model.

The flocculation stage was modeled using a coagulation equation shown in the following equation:

$$\frac{\partial N(i,t)}{\partial t} = -\beta N(i,t) \sum_{j=1}^{\infty} K(i,j) N(j,t) + \frac{1}{2} \beta \sum_{j=1}^{\infty} K(i-j,j) N(i-j,t) N(j,t) \tag{8.2}$$

This equation expresses the number–concentration balance of particles undergoing flocculation as a result of collisions among particles. The terms $N(i,t)$ and $N(j,t)$ are number concentrations of particles in size classes i and j, respectively at time t; $K(i,j)$ is the collision frequency function, which is a measure of the probability that

a particle of size i collides with a particle of size j in unit time, and β is the collision efficiency, which defines the probability that a pair of collided particles coalesce and form a new particle. The collision efficiency parameter β accounts for the coagulation properties of the sediment–water mixture. This includes the bacterial bond and the bacterial "glue" referred to earlier.

The first term on the right-hand side of Equation (8.2) gives the reduction in the number of particles of size class i by the flocculation of particles in class i and all other size class particles. The second term gives the generation of new particles in size class i by the flocculation of particles in smaller size classes. In this process, it is assumed that the mass of the sediment particles is conserved.

Equation (8.2) was solved after simplifying it into a discrete form by considering the particle size space in discrete size ranges. Each range was considered as a bin containing particles of certain size range. The size ranges in various bins were selected in such a way that the mean volume of particles in bin i is twice that of the preceding bin. When the particles of bin i flocculate with particles of bin j ($j < i$), the newly formed particles will fit into bins i and $i + 1$. The proportion of particles going to bins i and $i + 1$ is calculated by considering the mass of the particles before and after flocculation.

The collision frequency function, $K(i,j)$ assumes different functional forms depending on the type of the collision mechanism considered. The collision mechanisms that were considered in the model were: (a) Brownian motion (K_b); (b) turbulent fluid shear (K_{sh}); (c) inertia of particles in turbulent flows (K_I); and (d) differential settling of particles (K_{ds}). An effective collision frequency function K_{ef} was calculated in terms of the individual collision functions as follows:

$$K_{ef} = K_b + \sqrt{(K_{sh}^2 + K_I^2 + K_{ds}^2)} \tag{8.3}$$

The geometric addition in Equation (8.3) above is necessary because of the geometric addition of velocity vectors involved in the last three collision frequency functions (Huebsh).[19]

The collision frequency functions for the different collision mechanisms considered assume the following functional forms (Valioulis and List[20]):

$$K_b(r_i, r_j) = \frac{2}{3}\frac{kT}{\mu}\frac{(r_i + r_j)^2}{r_i r_j} \tag{8.4}$$

$$K_{sh}(r_i, r_j) = \frac{4}{3}\left(\frac{\varepsilon}{\nu}\right)^{0.5}(r_i + r_j)^3 \tag{8.5}$$

$$K_I(r_i, r_j) = 1.21\frac{\rho_f}{\rho}\left(\frac{\varepsilon^3}{\nu^5}\right)^{0.25}(r_i + r_j)^2 abs(r_i^2 - r_j^2) \tag{8.6}$$

$$K_{\mathrm{ds}}(r_i, r_j) = \frac{2}{9}\frac{\pi g}{\nu}\left(\frac{\rho_f - \rho}{\rho}\right)(r_i + r_j)^2 abs(r_i^2 - r_j^2) \tag{8.7}$$

In the above equations, k is the Boltzmann constant, T is the absolute temperature in Kelvin, μ is the absolute viscosity of the fluid, ν is the kinematic viscosity of the fluid, ε is the turbulent energy dissipation rate per unit mass, ρ and ρ_{f} are densities of fluid and sediment flocs, respectively, and g is the acceleration due to gravity.

8.5 APPLICATION OF THE MODEL TO THE LABORATORY DATA

The result from the deposition experiment with the highest bed shear stress of 0.324 Pa (Test No 1) was chosen for calibrating the model. The other two tests with bed shear stresses of 0.213 Pa (Test No 2) and 0.121 Pa (Test No 3) were used as verification tests. The input parameters for the settling stage of the model include, settling velocity of the sediment flocs, the turbulent diffusion coefficient, and deposition and erosion fluxes of the sediment at the sediment water interface. For the flocculation stage, additional input parameters needed are: (a) the collision efficiency parameter; (b) the collision frequency functions; and (c) a model for the growth-limiting effect of turbulence. A discussion of the various input parameters and their assigned values are given in the following section.

8.5.1 Input Parameters

8.5.1.1 Settling Velocity of the Flocs, w_k

Settling velocity of the flocs is calculated in the model using the Stokes' Law and a size dependent density relationship developed by Lau and Krishnappan.[21] Accordingly, the expression for the settling velocity becomes:

$$w_k = (1.65/18)\exp(-ad_k^b)gd_k^2/\nu \tag{8.8}$$

where w_k is the settling velocity of the kth fraction and d_k is the size of the sediment floc. The parameters a and b are empirical coefficients that need to be determined as part of the calibration process.

8.5.1.2 Turbulent Diffusion Coefficient, D

The turbulent diffusion coefficient, D was assumed to be equal to the momentum diffusivity, which was obtained by simulating the flow characteristics of the rotating flume using the PHOENICS model.[22] The PHOENICS model is a three-dimensional turbulent flow model and it employs the $k - \varepsilon$ turbulence model to close the system of equations. A depth averaged value of D was calculated from the three-dimensional prediction of the turbulent eddy viscosity.

8.5.1.3 Deposition Flux, F_d

Deposition flux at the sediment water interface was calculated using the Krone's equation as follows:

$$F_d = pw_k C_k \tag{8.9}$$

In this equation, p is the probability that a sediment floc reaching the bed stays at the bed. This probability is related to the bed shear stress and the critical shear stress for deposition, which is defined as the shear stress above which none of the sediment in suspension would deposit. The equation for p takes the following form:

$$p = \left(1 - \frac{\tau}{\tau_{crd}}\right) \tag{8.10}$$

where τ is the bed shear stress and τ_{crd} is the critical shear stress for deposition. The bed shear stress corresponding to the high speed operation of the flume was taken as the critical shear stress for deposition for the current application of the model. It is possible to measure the critical shear stress for deposition precisely by successively lowering the shear stress until the deposition of the sediment begins.

8.5.1.4 Erosion Flux, F_e

The erosion flux F_e is taken as zero. This is in accordance with the recent finding of Winterwerp,[23] who argued that the equation of Krone can be interpreted as a combined erosion–deposition formula for erosion-limited conditions. Considering the erosion flux, while using the Krone's equation for deposition is equivalent to considering the erosion flux twice.

8.5.1.5 Collision Efficiency Parameter, β

As indicated earlier, the collision efficiency parameter accounts for the different coagulation mechanisms that are present in the freshwater flocculation process. Here, the parameter is treated as a calibration factor and was determined as part of the calibration process. If this parameter is determined through calibration as it has been done here, then the model can also be used for saltwater flocculation.

8.5.1.6 Collision Frequency Functions K_b, K_{sh}, K_l, K_{ds}

The collision frequency functions given by Equations (8.4) to (8.7) were determined for flows in the rotating flume using the dissipation rate of kinetic energy of turbulence ε given by the PHOENICS' model simulations.

8.5.1.7 Model for the Growth-Limiting Effect of Turbulence

The growth-limiting effect of turbulence was modeled using the scheme proposed by Tambo and Watanabe.[24] According to their scheme, a collision–agglomeration

function was used as a multiplier for the collision-frequency function to produce an effective collision frequency that produced an optimum floc size distribution for the given turbulence level. The collision–agglomeration function recommended by Tambo and Watanabe[24] is as follows:

$$\alpha_R = \alpha_0 \left(1 - \frac{R}{S+1}\right)^n \tag{8.11}$$

where R is the number of primary particles contained in a floc under consideration and S is the number of primary particles contained in the maximum floc for the given turbulence level. The parameters α_0 and n assumed values of $\frac{1}{3}$ and 6, respectively, as recommended by Tambo and Watanabe.[24] This approach is an indirect way in which the breakup of particles during collision is handled.

8.6 COMPARISION OF MODEL PREDICTIONS WITH THE MEASURED DATA

Comparison of model predictions of suspended sediment concentration with the measured data is shown in Figure 8.5. The test with the highest shear stress was used as the calibration test and the calibration coefficients a, b, and β were determined by matching the predicted concentration vs. time curve and the size distribution profiles with the measured data. The calibration was carried out using a trial and error approach. The starting values for the coefficients a and b were obtained from Lau and Krishnappan,[21] and a range of values were tried for β. The predicted size distributions were then compared with the measured distributions and a value of β that gave a

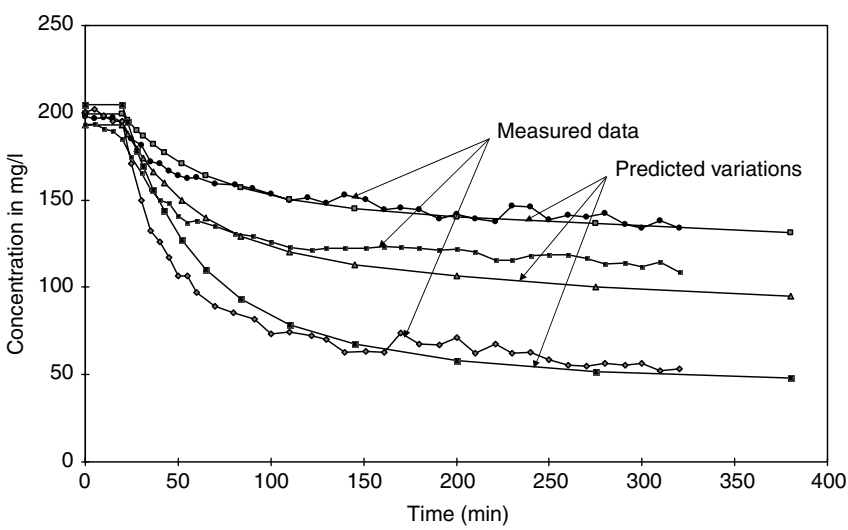

FIGURE 8.5 Comparison between model predictions and measured concentration vs. time curves.

reasonable match was chosen. Then, using this β value, the coefficients a and b were adjusted until the predicted concentration vs. time curve matched reasonably well with the measured curve. The procedure was repeated, and within a few iterations, all three coefficients were estimated. The calibrated values of these parameters were found to be $a = 0.02$, $b = 1.45$, and $\beta = 0.075$. The predicted concentration vs. time curves for the other two tests were produced using these calibrated values. From the comparison in Figure 8.5, we can see that the predicted concentration variation agrees reasonably well with the measured data for all the three tests.

Comparison of the predicted size distribution data with the measurement is shown in Figure 8.6 to Figure 8.9 for Test No 1 and in Figure 8.10 to Figure 8.13 for Test No 2 for various elapsed times. These figures show that the agreement between the model predictions and the measurement is reasonable for the size distribution data as well. The comparison carried out for Test No 3 is not shown here as it was similar to the other two tests.

Reasonable agreement between the model predictions of concentration vs. time curves and the size distribution of the flocs in suspension at various elapsed times imply that the model is capable of predicting the settling and flocculation process of the Kingston pond sediment in the rotating circular flume. For predicting the sediment behavior in the actual pond, the flocculation and the settling components of the model can be used in conjunction with a hydrodynamic model that is capable of predicting the flow conditions in the pond. Plans are underway to initiate such a study in a number of stormwater detention ponds in Ontario, Canada.

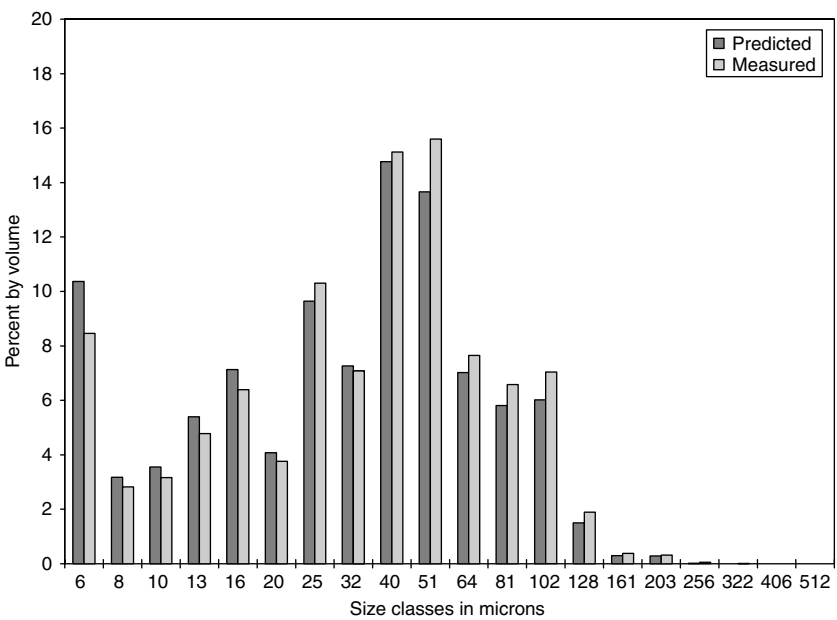

FIGURE 8.6 Comparison of size distributions for Test No 1 at elapsed time of 30 min.

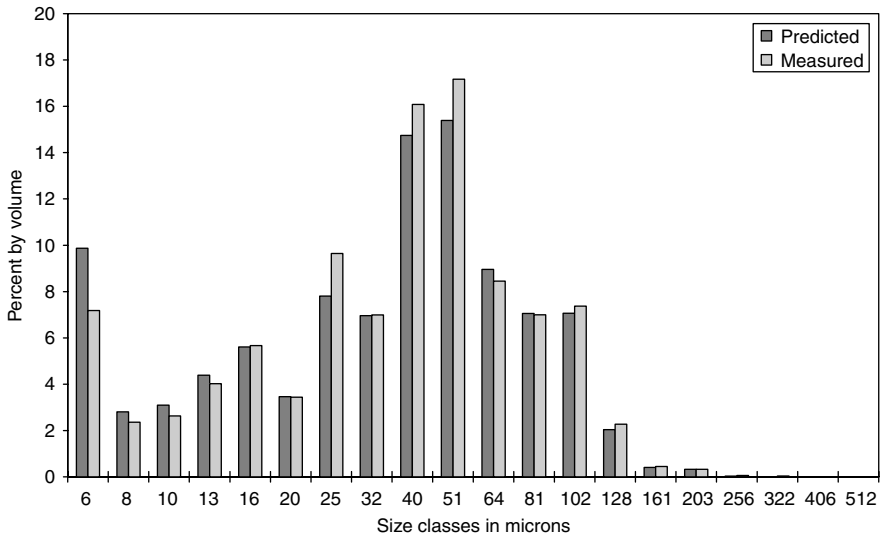

FIGURE 8.7 Comparison of size distributions for Test No 1 at an elapsed time of 48 min.

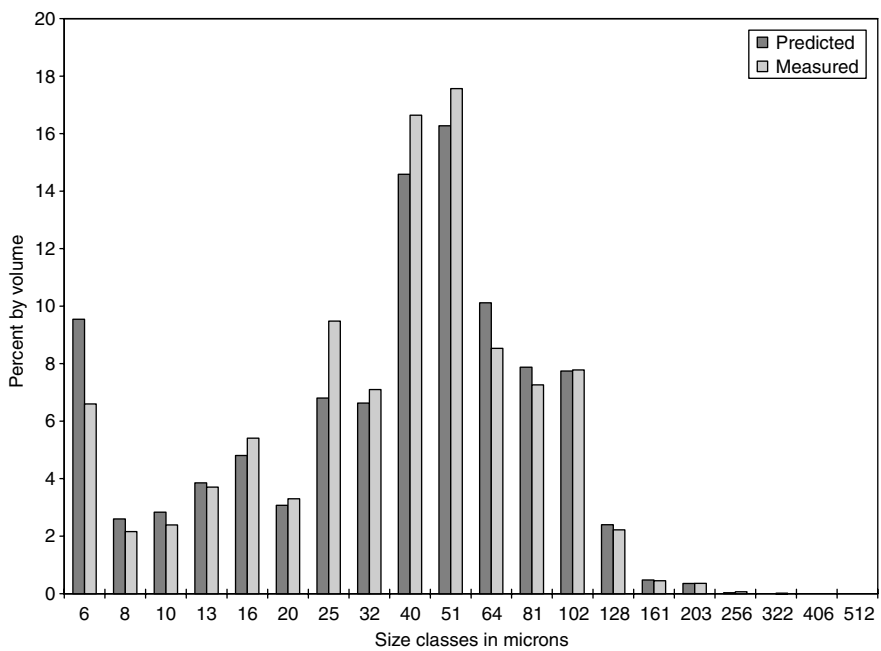

FIGURE 8.8 Comparison of size distributions for Test No 1 at an elapsed time of 60 min.

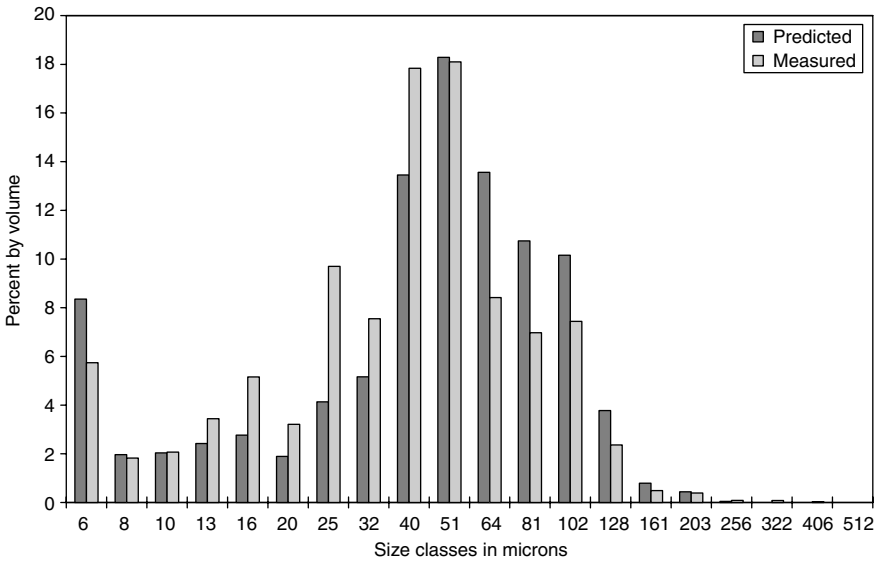

FIGURE 8.9 Comparison of size distributions for Test No 1 at an elapsed time of 110 min.

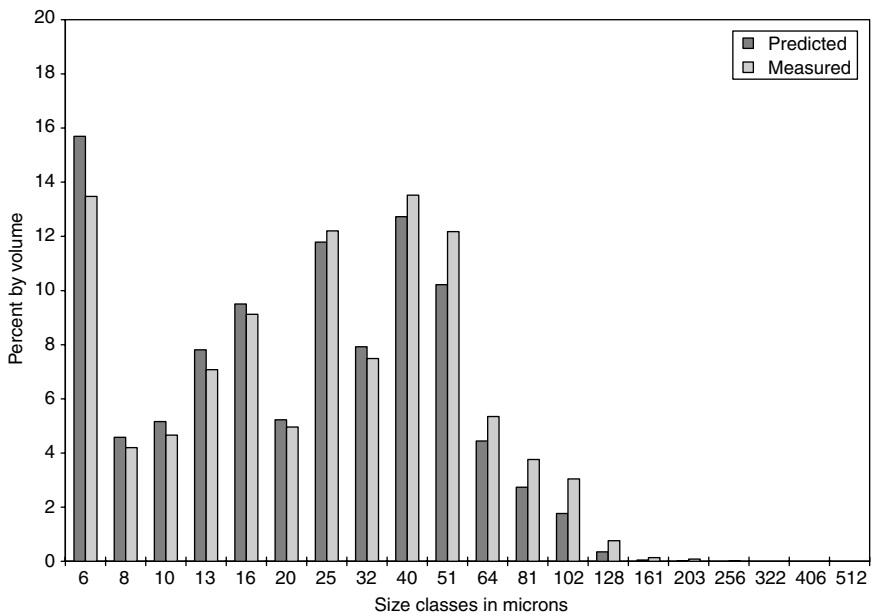

FIGURE 8.10 Comparison of size distributions for Test No 2 at an elapsed time of 30 min.

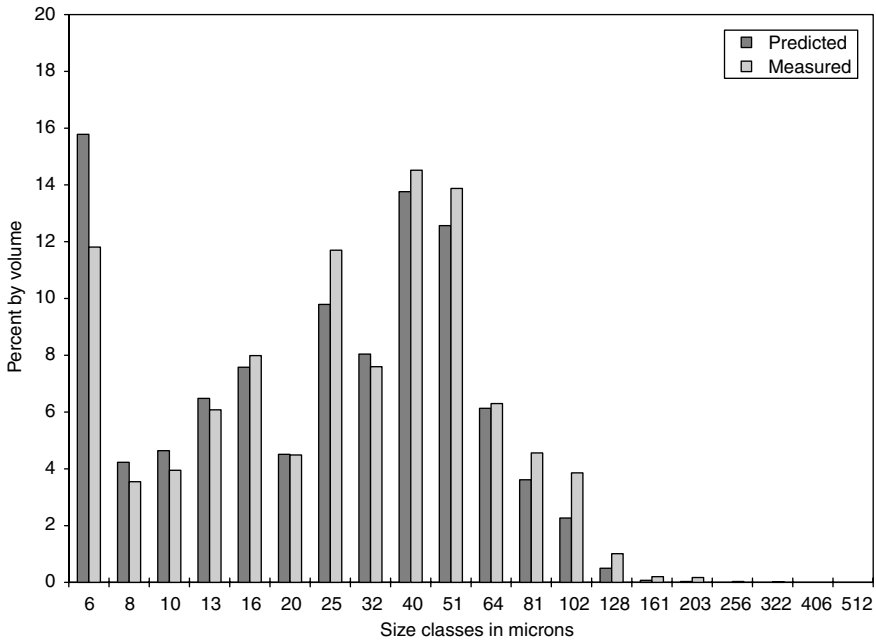

FIGURE 8.11 Comparison of size distributions for Test No 2 at an elapsed time of 55 min.

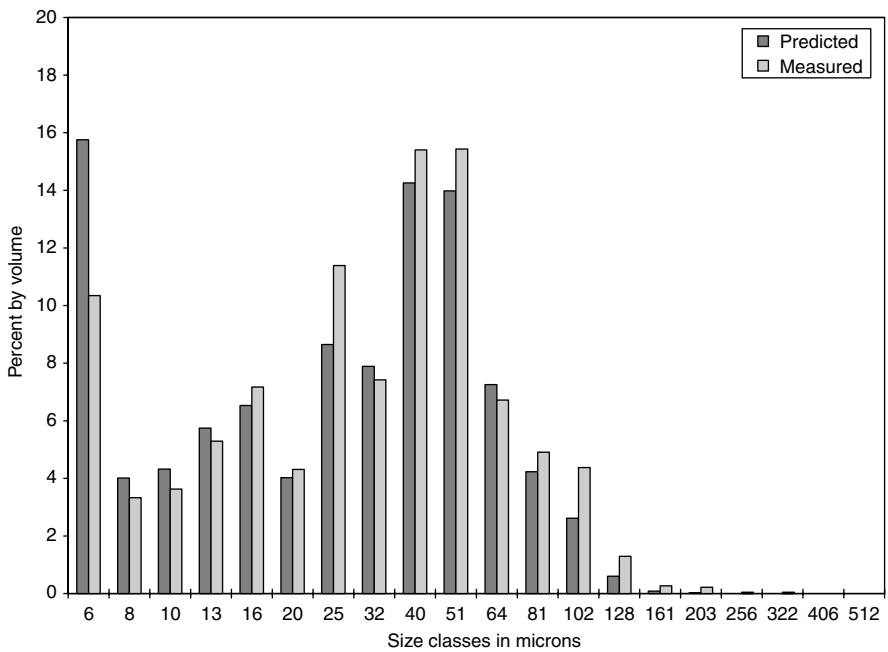

FIGURE 8.12 Comparison of size distributions for Test No 2 at an elapsed time of 72 min.

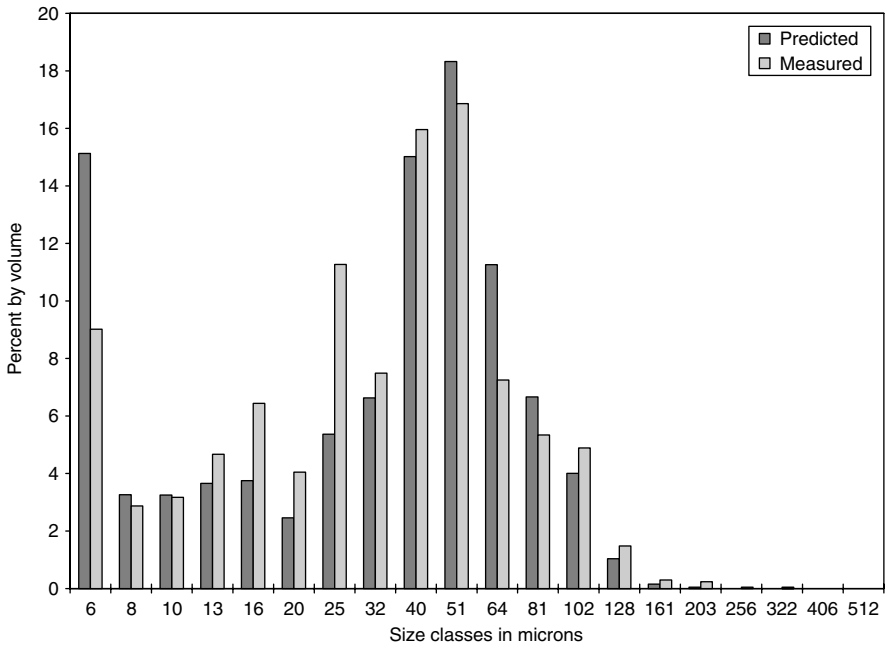

FIGURE 8.13 Comparison of size distributions for Test No 2 at an elapsed time of 106 min.

Even though the development of the model was based on the behavior of specific stormwater detention pond sediment, it has the potential for application for sediment from other freshwater systems as well. For example, the present model was applied to predict the behavior of sediment from the Hay River near the town of Hay River in Northwest Territories in the rotating flume. The details of this study can be found in Krishnappan and Milburn.[25] The study showed that the model performed equally well for the Hay River sediment, and yielded a different set of calibration parameters. The model, therefore, can become a useful tool for testing sediments from different environments to gain a better understanding of the flocculation mechanisms and the role of bulk properties of the system that are responsible for the flocculation of sediment in freshwater systems.

8.7 SUMMARY AND CONCLUSIONS

A model to predict the settling and flocculation of sediment from a stormwater detention pond was proposed. The model was applied to the rotating flume experiments in which the deposition characteristics of the pond sediment were measured. The deposition experiments carried out in the rotating flume showed that the pond sediment underwent flocculation when subjected to the flow field in the flume. The shear stress producing flocculation has to exceed certain critical level. The experiments also demonstrated the growth-limiting character of turbulence at high bed shear stresses. The formulated model was calibrated and tested using the data from the rotating

flume experiments. The model predictions of concentration and size distribution as a function of time, agreed reasonably well with the measured data. The model has the potential to be used as a management and research tool for assessing the flocculation and transport of fine sediments in freshwater systems.

ACKNOWLEDGMENTS

The authors wish to acknowledge the contribution of Mr. Robert Stephens of the National Water Research Institute in carrying out the rotating flume experiments for the sediment. The authors also wish to thank Dr. Ian Droppo of the National Water Research Institute, Environment Canada, and Mr. T.G. Milligan of the Department of Fisheries and Oceans, for their constructive suggestions for the improvement of the manuscript during its review. The critical review of the manuscript by the anonymous reviewer is also very much appreciated.

NOMENCLATURE

a Empirical coefficient
b Empirical coefficient
C Volumetric concentration of sediment [*Dimensionless*]
D Turbulent diffusion coefficient [m^2/s]
F Sediment flux [m^3/m^2s]
g Acceleration due to gravity [m/s^2]
i Sediment size class notation
j Sediment size class notation
K Collision frequency function
N Number concentration [number/m^3]
p Probability [*Dimensionless*]
R Number of primary particles in a floc [number]
S Number of primary particles in the biggest floc [number]
r Radius of sediment particles [m]
T Temperature [degree Kelvin]
t Time axis [s]
w Settling velocity [m/s]
z Vertical distance axis [m]
α_R Collision–agglomeration function of Tambo and Watanabe[21]
α_0 Parameter
α_0 Collision efficiency parameter
ε Turbulent energy dissipation rate
μ Absolute viscosity of the fluid
ν Kinematic viscosity of the fluid
ρ Density
τ Shear stress

Subscripts

b Pertains to Brownian motion
ds Pertains to differential settling
ef Pertains to an effective value
I Pertains to inertia
k Pertains to size class of sediment

REFERENCES

1. Ongley, E.D., Bynoe, M.C., and Percival, J.B. Physical and geochemical characteristics of suspended solids, Wilton Creek, Ontario. *Can. J. Earth Sci*. 18: 1365–1379, 1981.
2. Partheniades, E. The present state of knowledge and the need for future research on cohesive sediment dynamics, in *Proc. 3rd Int. Symp. on River Sedimentation*, School of Engineering, The University of Mississippi, USA: 3–25, 1986.
3. Umlauf, G. and Bierl, R. Distribution of organic micropollutants in different size fractions of sediment and suspended solid particles of the River Rotmain, *Z. Wasser-Abwasser-Forsch.* 20: 203–209, 1987.
4. Tsai, C.H., Iacobellies, S., and Lick, W. Flocculation of fine grained lake sediments due to uniform shear stress, *J. Great Lakes Res.* 13: 135–146, 1987.
5. Droppo, I.G. and Ongley, E.D. Flocculation of suspended solids in southern Ontario rivers, *Water Res.* 28: 1799–1809, 1994.
6. Marshall, K.C. Sorptive interaction between soil particles and microorganisms, in *Soil Biochemistry,* McLaren, A.D. and Skujins, J., Eds., Marcel and Dekker, Inc., New York, 1971.
7. Paerl, H.W. Detritus in Lake Takoe: structural modification by attached microflora, *Science* 180: 496–498, 1973.
8. Muschenheim, D.K., Kepkay, P.E., and Kranck, K. Microbial growth in turbulent suspension and its relation to marine aggregate formation, *Neth. J. Sea Res.* 23: 283–292, 1989.
9. Zabawa, C.F. Microstructure of agglomerated suspended sediments in Northern Chesapeake Bay Estuary, *Science* 202: 49–51, 1978.
10. Ongley, E.D. et al. Cohesive sediment transport: emerging issues for toxic chemical management, *Hydrobiologia* 235/236: 177–187, 1992.
11. Biddanda, B.A. Structure and function of marine microbial aggregates, *Oceanol. Acta* 9: 209–211, 1986.
12. Lick, W. and Lick, J. Aggregation and disaggregation of fine grained lake sediments, *J. Great Lakes Res.* 14(4): 514–523, 1988.
13. Krishnappan, B.G. Modelling of settling and flocculation of fine sediments in still water, *Can. J. Civil Eng.* 17(5): 763–770, 1990.
14. Krishnappan, B.G. Modelling of cohesive sediment transport, in *Intl. Symp. on the Transport of Suspended Sediment and its Mathematical Modeling*, Florence (Italy), September 2–5, 1991.
15. Krishnappan, B.G. and Marsalek, J. Modelling of flocculation and transport of cohesive sediment from an on-stream stormwater detention pond, *Water Res.* 36: 3849–3859, 2002.

16. Krishnappan, B.G. and Marsalek, J. Transport characteristics of fine sediments from an on-stream stormwater management pond, *Urban Water* 4: 3–11, 2002.
17. Krishnappan, B.G. Rotating circular flume, *J. Hyd. Eng.* ASCE, 119(6): 758–767, 1993.
18. Stone, H.L. and Brian, P.L.T. Numerical solution of convective transport problems, *J. Hyd. Div.* ASCE, 98(9): 1963.
19. Huebsh, I.O. *Relative Motion and Coagulation of Particles in a Turbulent Gas.* USNRDL-TR-67-49. U.S. Naval Radiological Defence Laboratory, San Francisco, California, 94 pages, 1967.
20. Valioulis, I.A. and List, E.J. Numerical simulation of a sedimentation basin. 1. Model Development, *Environ. Sci. Technol.* 18(4): 242–247, 1984.
21. Lau, Y.L. and Krishnappan, B.G. *Measurement of Size Distribution of Settling Flocs*, Report 97–223, National Water Research Institute, Environment Canada, Burlington, Ontario, Canada, 1997.
22. Rosten, H.I. and Spalding, D.B. *The PHOENICS Reference Manual, TR/200*, CHAM Ltd., Wimbledon, London, 1984.
23. Winterwerp, J.C. On the deposition of cohesive sediment, presented at *INTERCOH 2003*, Virginia Institute of Marine Science, October 1–4, 2003.
24. Tambo, N. and Watanabe, Y. Physical aspects of flocculation process-I. Fundamental Treatise, *Water Res.* 13: 429–439, 1979.
25. Krishnappan, B.G. and Milburn, D. Flocculation of fine sediment from Hay River in Northwest Territories, Canada, presented at *INTERCOH 2003*, Virginia Institute of Marine Science, October 1–4, 2003.

II

Saltwater Environments

9 Transport of Materials and Chemicals by Nanoscale Colloids and Micro- to Macro-Scale Flocs in Marine, Freshwater, and Engineered Systems

Peter H. Santschi, Adrian B. Burd, Jean-Francois Gaillard, and Anne A. Lazarides

CONTENTS

9.1 INTRODUCTION

Particles are the vehicles of vertical transport of material in aquatic systems. Large, heterogeneous aggregates can sink through the water column at rates of 10 to 100 m per day carrying with them carbon, nutrients, and trace metals.[1] In the open ocean, sinking particles carry carbon (e.g., in the form of phytoplankton, detritus, and mucilage) from the surface waters to the sediments, thereby playing an important role in the global

1-56670-615-7/05/$0.00+$1.50

carbon cycle.[2] These particles also carry nutrients, which help support food webs in the mid-depths and benthos.[3] In estuarine and coastal systems, terrigenous particles settle out of the water column removing clays and a large and variable amount of trace elements. In rivers, large quantities of suspended material are transported in the form of nanoparticles.[4] Nanoscale particles of Fe and Mn are also formed at oxic/anoxic transitions in aquatic systems.[5–7] Aggregation and subsequent settling of particulate material is a crucial step in many industrial processes such as those used in water treatment plants.[8] This removal process, whose efficiency depends on the presence of some principal components, that is, fibrillar microbial exudates, humic-type material, and mineral matter,[9,10] as well as environmental conditions, that is, pH and ionic strength, is depicted in Figure 9.1.

Particulate material in aquatic systems covers a range of sizes greater than a million-fold, from nanoscale colloidal particles to millimeter-sized flocs.[1,9,11–14] Particle size distributions in marine environments tend to follow a power-law distribution.[15–19] Large particles ($>100\ \mu$m) are relatively rare and represent the dominant agent of sedimentation. For example, for aggregates with equivalent spherical diameters >1.5 mm, numbers of 4 to 40 aggregates/l, peaking at the euphotic zone and in mid-depth and near-bottom nepheloid layers, have been reported for the Middle Atlantic Bight.[20] Aggregate peak concentration regions coincided with strong ^{234}Th deficiencies in the water column, demonstrating their high efficiency for scavenging particles and particle-reactive elements.[20] Sediment trap data and *in situ* camera observations[21–23] indicate that marine particles settle as large, heterogeneous aggregates, such as marine snow (Figure 9.2). The sinking rate of an aggregate is a function of its size, composition, and structure. Dense, compact particles (e.g., fecal pellets) sink faster than larger, porous marine snow particles. Differences in the timing between peaks in surface particle concentrations and peaks detected by sediment traps throughout the water column indicate that these aggregates can have settling velocities of 50 to 100 m per day or more.[24–26]

Colloidal particles (operationally defined in environmental aquatic chemistry as microparticles and macromolecules with sizes between about 1 μm and 1 nm)

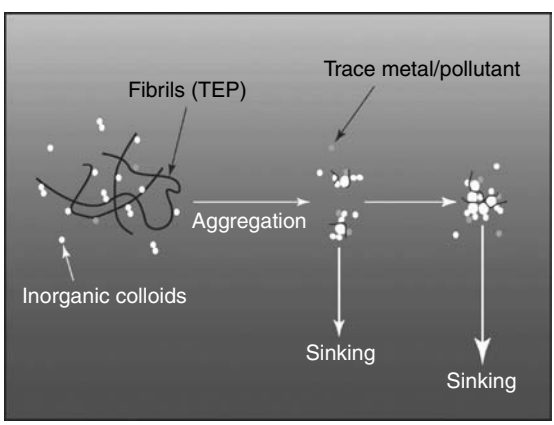

FIGURE 9.1 Diagram representing the major routes of the formation of large-scale aggregates from the aggregation of fibrils and colloidal particles.

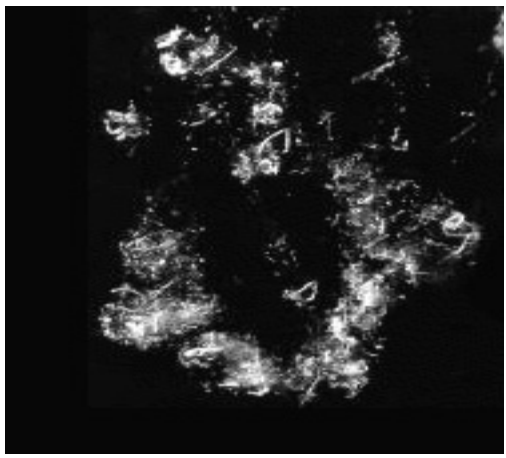

FIGURE 9.2 Marine snow. Clear organic matrix that enmeshes fecal pellets and smaller biomolecules.[11]

dominate the particle number density and surface area. Ultrafiltration measurements[27] revealed typical concentrations of colloidal organic carbon (COC) in oceanic surface waters with sizes between about 1 nm (1 kDa) and $<0.2\ \mu$m, of about 30 to 40 μM-C (about 1 mg, organic matter/l), COC >3 kDa about 11 μM, and COC $>$ 10 kDa about 3 μM. If marine colloids are present as spherical particles, the average molecular weight of COC $>$ 1 kDa in marine environments would be about 2 to 3 kDa. This should give an average particle number density in surface ocean water of 10^{14} to 10^{15} nanoparticles per milliliter. However, Wells and Goldberg[28,29] reported number densities of at most 10^9 per milliliter of spherical nanoparticles they called "Koike" particles, a concentration that is similar to that in ground water where colloid concentrations are in the range of a few micrograms per liter.[30] This large discrepancy between expected and measured colloids concentration in marine environments indicates that (1) the majority of the colloidal fraction was undetected by Wells and Goldberg,[12,28,29] which is likely, since the colloids were not stained for transmission electron microscopy (TEM); (2) the assumption of spherical shape for calculating the average molecular weight is incorrect; this is likely, since many biomolecules are not spherical but fibrillar; (3) colloids are present as aggregates.

Colloids are indeed present as aggregates, since recent observations of colloidal particles using TEM[31] and atomic force microscopy (AFM)[14,32] have revealed that an important fraction of colloidal organic matter (COM) in aquatic systems is present as nanoscale fibrils that also contain smaller molecules assembled like pearls on a necklace (Figure 9.3). These fibrils are acid-polysaccharide rich, have diameters of 1 to 3 nm and can be missed by standard fractionation techniques.[14,31] Fibrils have estimated molecular weights between 10^5 and 10^6 kDa and yet, because of their shape, they are able to pass through a 10 kDa filter.[14] Wells and Goldberg[12] did not use state-of-the-art preparatory and staining techniques for electron microscopy imaging and, therefore, were not able to document existing colloids in a representative manner. Santschi et al.,[14] Leppard et al.,[33] and Wilkinson et al.[32] used state-of-the-art electron

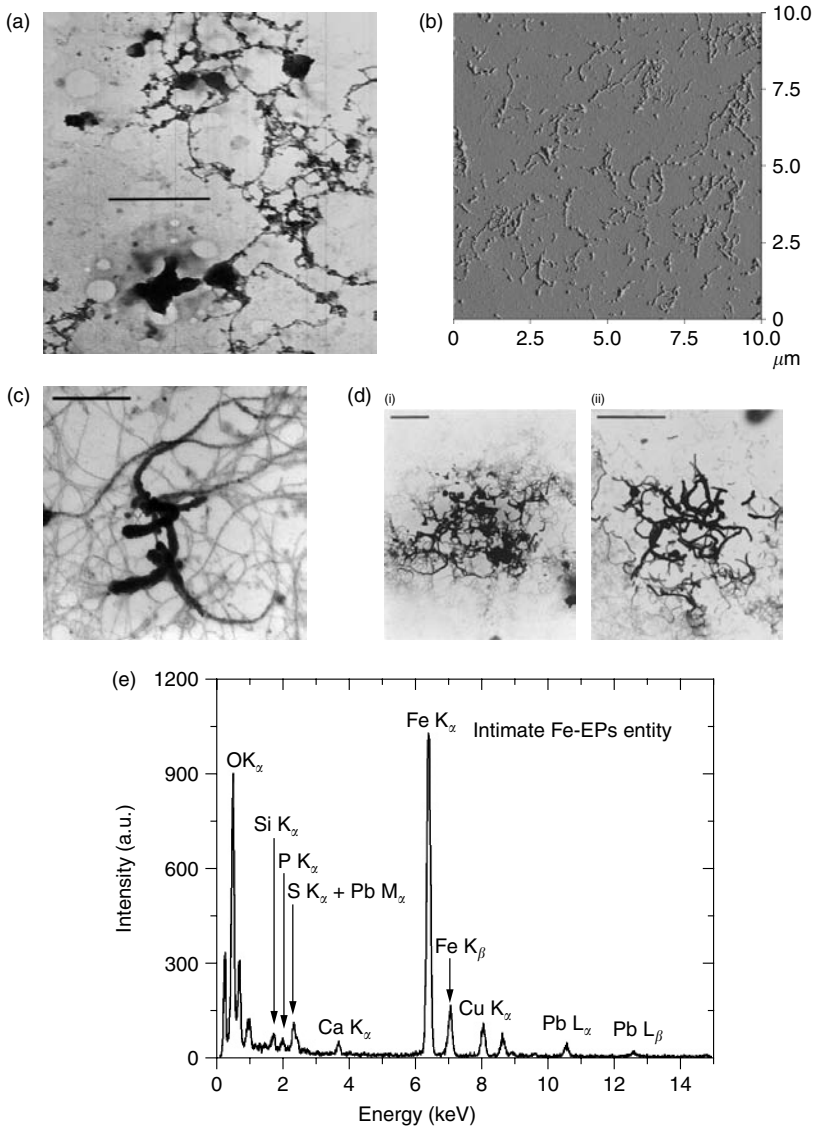

FIGURE 9.3 Transmission Electron Microscopy (TEM) and Atomic Force Microscopy (AFM) micrographs of nanoscale fibrils in aquatic systems. (a) TEM whole mount specimen showing the interconnections between fibrils and nanoscale particles from the Middle Atlantic Bight (courtesy of K. Wilkinson; scale bar = 500 nm). (b) AFM image of fibrils and small nano-colloids from the Middle Atlantic Bight, with an architecture like pearls on a necklace.[14] (c) A specimen collected by centrifugation from a freshwater lake, Paul Lake (MI), imaged by TEM, showing fibrils rendered electron dense by the attachment of nanoscale globules of natural iron oxide (scale bar: 500 nm)[6]; (d) natural hydrous iron oxide aggregates found between 6.5 and 7.5 m in the water column of Paul Lake, where particulate Fe shows a maximum, and below which $[Fe^{2+}]$ is increasing in concentration (scale bar = 1 μm).[6] The TEM micrographs in (d) display intimate mixtures of organic fibrils naturally stained by natural iron oxides. The EPS spectrum shown in (e) of these mixtures shown in (d) displays some Fe–Pb elemental association. The Cu peak originates from the TEM grid.

and atomic force microscopy techniques to document the various forms, shapes, and architectures of marine and freshwater colloids from different environments. For the first time, polysaccharide-rich fibrils of recent (determined by radiocarbon analysis; ref. [14]) origin were documented to make up a significant fraction of all colloidal sized nanoparticles (Figure 9.3). It is also important to realize that these fibrillar extracellular polymeric substances (EPS) molecules are much more abundant in the $\leq 0.5\ \mu$m "dissolved" than in the $\geq 0.5\ \mu$m particulate fraction. This is due to the approximately two orders of magnitude higher concentration of DOC than POC in the ocean, and the relative abundances of total and acid polysaccharides (APSs) that are similar in the two size fractions of organic carbon.[34] Being able to accurately detect these nanoparticles is important because, although they are too small to settle out of the water column at appreciable rates, they do aggregate and are capable of forming the matrix for the formation of larger aggregates that can settle faster.[35,36] However, so far no quantitative estimate exists of their number concentration in marine systems.

Transparent exopolymer particles (TEP, Figure 9.2 and Figure 9.3) form an important component of aggregates in natural waters.[37–41] These particles are natural exudates from marine algae and bacteria.[42] They consist of surface active polysaccharides rich in acidic functional groups[43,44] and are formed from the aggregation of nanoscale fibrils.[45,46] Recent results, however, indicate that only a small fraction of the total carbohydrate content of marine suspended and sinking matter consists of surface-active acid polysaccharide compounds, with total uronic acids making up about 7% (0.2% to 2% of POC), and total acid polysaccharides about 11% of the total carbohydrate, or about 1% of the POC content.[34,47,48] Thus, it appears that, much like small amounts of glue needed to hold man-made materials together, surface-active substances that provide the stickiness of the TEP do not have to be in high abundance to be effective.

TEPs have a high stickiness and their presence has been shown to stimulate aggregation amongst phytoplankton cells.[43] As a matter of fact, times of highest particulate organic carbon export from the ocean coincide with times of large phytoplankton blooms, diatoms in particular,[49] which are strong TEP producers as well as providers of "mineral ballast," enhancing density and settling velocity of sinking particle aggregates. This relationship was documented by a close relationship between diatom pigments (fucoxanthin) and ^{234}Th-derived POC flux from the surface ocean,[49,50] producing a higher efficiency of the "biological pump" (i.e., ratio of POC flux to primary production). In addition to phytoplankton species, bacteria also produce abundant acidic polysaccharide-rich compounds,[31,42,51] especially when attached to particles as a "micro-biofilm." Indeed, significant relationships between APS concentrations and heterotrophic bacterial production (BP), and ^{234}Th/POC ratios and BP were recently demonstrated by Santschi et al.,[47] which strongly suggest microbial involvement through production of Th(IV)-binding APS compounds, while their enzymatic activities can produce smaller but more stable filter-passing Th(IV)-binding fragments.

Macromolecular COM, a result of exopolymer formation by algae and bacteria, makes up 30% to 40% of conventionally defined dissolved organic matter.[27,52–54] The aggregation of fibrils and other biopolymers, with an architecture like pearls on a necklace (Figure 9.3), into rapidly sinking marine snow provides an important

pathway for the removal of DOM and associated metals and radionuclides[55,56] from surface waters (Figure 9.1).

This important transport system is not, however, well understood. A promising research direction is suggested by potential gaps in conventional aggregation models. These models predict lower coagulation rates than those observed in nature. It has been suggested by Hill[57] that one could reconcile the model results with observations if there existed a background distribution of particles, and by Alldredge and others that this background distribution can be accounted for by TEP (Figure 9.2 and Figure 9.3). Therefore, it would be important to characterize the hitherto neglected nanoscale components of heterogeneous aquatic aggregates and integrate these components into aggregation models, so that the models will be able to account for observed coagulation rates.

It is of great interest to aquatic scientists to better understand the processes by which components of these aggregates scavenge metals and pollutants and thereby endow the assembled aggregates with their pollutant-clearing properties. Suspended particles can scavenge trace metals, providing an efficient mechanism for removing chemicals from solution.[5,6,58–61] Colloidal particles dominate the particulate surface area distribution, making them excellent at scavenging chemicals from the bulk water. In particular, metal oxides have been observed to coat fibrils (Figure 9.3c,d). So, to understand the removal of trace metals from solution requires understanding the properties and dynamics of both the dissolved species and the properties of the particles that scavenge them.

Extracellular polymeric substances (EPS) in specific marine or freshwater environments are known to initiate or modify precipitation of MnO_2 and FeOOH,[62] SiO_2,[63] $CaCO_3$,[64] and uptake of different trace metals.[56] Thus, the organic template can be important for mineral formation in the ocean. These exopolymers are part of the marine DOC pool and have a modern radiocarbon age,[14] as compared to the bulk of the DOC. Microbially produced APS-rich compounds do not only have chelating properties for trace metals,[31] but also emulsifying properties through a protein trace component, with the hydrophilic polysaccharide chains providing protective layers that confer effective steric stabilization over time.[65]

In activated sludge flocs, EPS have been shown to be important for establishing the floc pore structure,[8] whereby their relative composition can govern floc surface properties and bioflocculation.[66,67] For example, the ratios of protein to total carbohydrates, hydrophobicity and surface charge are a function of EPS composition at the floc/water interface, and thus are important parameters for predicting the extent of bioflocculation.[66–68] Bacterial hydrophobicity appears to be a good overall parameter for predicting the adhesion potential of their EPS to soil particles.[69]

9.2 THE STRUCTURE AND PROPERTIES OF FIBRILS

Aggregates in natural waters are composed of a disparate mixture of material: clay particles, fulvics, fecal material, phytoplankton, extracellular polysaccharides, etc.[1] The essential ingredient of floc structure is a matrix composed mainly from structural polysaccharides and peptidoglycans derived from cell exudates.[31,70,71] These molecules form nanoscale fibrillar structures, which can be identified in a variety of

aquatic environments.[8,14,31,33,72] These polysaccharide-rich fibrils form 30% of the organic material in freshwaters[9,70] and up to 60% in marine systems.[14,73] Fibrils are distinct from terrestrially derived humic substances which account for the largest fraction (40% to 80%) of organic material in freshwater systems[70] and which typically behave as small nanoscale spherical particles.[74–76]

Early work on fibrils[31] using transmission electron microscopy (TEM) showed that, in the presence of phytoplankton and bacteria, a large fraction of autochthonous organic material is composed of fibrillar particles rich in acid polysaccharides. These fibrillar particles have been shown to stimulate aggregation (see ref. [31] for a review) and to scavenge colloidal particles.[10] These fibrils have been found linked with iron particles (Figure 9.3c,d) in both freshwater systems and batch reactors, leading to the suggestion that fibrils can act as nucleation centers during oxidation reactions.[6]

Properties of an aggregate, such as its settling speed, are dependent on its architecture. Aggregates typically possess a fractal structure.[77–79] For example, Alldredge and Gotschalk,[80] demonstrated that marine snow aggregates settle with a velocity, v, proportional to $d^{0.26}$ rather than the Stokes relationship of d^2, where d is the diameter (Figure 9.4).

The relationship between mass (M) and size (L) of an aggregate is $M = aL^D$, where a is a constant and D is the fractal dimension of the aggregate. Aggregates which preserve volume upon collision have $D = 3$; aggregates with $D < 3$ are more porous and have a density which decreases as aggregate size increases.[80] Fractal dimensions have been measured for aggregates in aquatic systems; in marine systems, D ranges between 1.3 and 2.3.[19,81–84] In lacustrine systems, fractal dimensions range between 1.19 and 1.69,[81,85,86] and in engineered systems from 1.4 to about 2.0 (see ref. [87], and references therein). In general, for loose flocs, fractal dimensions are in the 1.7 to 1.8 range, and for more compact aggregates, they are of the order of 2.3 to 2.5.[88,89] After addition of small amounts (1 wt%) of cationic polymers, fractal dimensions of aggregates in dewatered sludges from a waste water treatment plant decreased from 2.2 to 1.75, amounting to a 2.5-fold decrease in density and a large increase in permeability.[90]

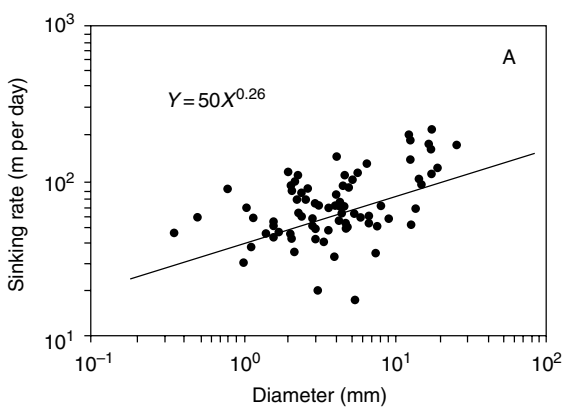

FIGURE 9.4 Relationship between settling velocity (v) and diameter for marine snow aggregates.[80]

Both fractal dimension and aggregate composition affect sinking rate. Aggregates with lower fractal dimensions are more porous and settle at slower rates than those with higher values. Engel and Schartau[91] have shown that aggregates with a greater proportion of TEP have lower sinking velocities and a less pronounced size-versus velocity relationship indicating that the amount of TEP affects the architecture of the aggregate, possibly decreasing its fractal dimension. It would therefore be important to investigate the role of TEP in determining aggregate architecture, through structural and modeling studies.

9.3 MECHANISMS AND MODELS OF COLLOIDAL AGGREGATION AND SCAVENGING

Scavenging of pollutants and trace metals depends upon the size spectrum of the particulate material. Large particles (e.g., greater than 50 μm), although relatively scarce, dominate the vertical flux because of their mass and large sinking velocity. On the other hand, colloidal particles dominate the particle number concentration and adsorption kinetics. Particle aggregation and disaggregation provide physical mechanisms linking these two particle sizes — this is demonstrated in the Brownian Pumping model[92–96] where trace metals are absorbed onto colloidal particles, which subsequently aggregate thereby incorporating the trace metals into larger particles. Scavenging and transport of materials, therefore, depend upon both the kinetics of aggregation and adsorption, resulting in a particle concentration dependence of kinetic constants of metal transfer to particles with broken exponents.[92,94,95]

Two types of mechanism contribute to the formation of aggregates: particle collision and adhesion. The classical theory of particle collisions is well developed, at least for particles of a simple shape.[35,57,97,98] The physical processes that bring particles together (Brownian motion, shear, differential sedimentation) are well described and hydrodynamic forces that can alter collision efficiencies can be taken into account.[57,97] Simple models assume that a single physical collision process operates in a given particle size range, but observations and more sophisticated models suggest that this is not the case.[99–101] However, on the whole, size distributions calculated from aggregation models agree favorably with observed particle size distributions.[102]

The probability that two particles will adhere once they have collided is less well understood. Traditionally, the DLVO (Derjaguin, Landau, Verwey, and Overbeek) theory has been used where the electrostatic and van der Waals forces between the two particles (and their environment) are evaluated to determine if the overall force is attractive or repulsive.[103] A coupling of statistical-based particle aggregation models with DLVO theory gives a good representation of the formation of aggregates comprised of inorganic particles.[103,104] However, it has recently become apparent that such a model cannot fully describe colloidal interactions between abiotic and biotic colloids in aquatic systems.[105] This is particularly important since biologically produced transparent exopolymer particles (TEP) are thought to form the matrix around which larger aggregates form.[43,45,71] Indeed, steric forces may determine exopolymer interactions in seawater.[106] In addition, hydrophobic interactions and Brownian movement forces may also be important in particle adhesion involving bacterial exopolymers.[107]

New experiments and models are needed to improve our understanding of exopolymer interactions, and hence our ability to predict the stickiness of aquatic particles under various environmental conditions.

In many aggregation models, particularly those used to model aggregation between a broad range of heterogeneous particles, adhesion is usually described using a single, constant stickiness coefficient, α. When $\alpha = 1$, all collisions result in attachment. This produces aggregates that have open, highly porous structures because small particles will have a low probability of diffusing to the central regions of a larger aggregate before colliding with, and adhering to, some part of it. Small values of the stickiness coefficient result in more compact, less porous aggregates. Because of these structural differences, the value of the stickiness coefficient should affect the sinking velocity of the particle since this depends on the particle's excess density, and hence porosity. Indeed, Engel[108] has shown that increased TEP concentrations enhance the stickiness coefficient during a diatom bloom. In addition, Engel and Schartau[91] have shown that particles with higher specific TEP content have lower settling velocities and a less pronounced variation of settling velocity with particle size. This indicates that the presence of biologically produced polymers can affect the fundamental structure and physical properties of large-scale macroparticles, specifically their porosity or fractal dimension and settling velocity.

Stickiness (α) is a function of many factors including pH, ionic strength, etc. Using a combination of models and observational data, Mari and Burd[41] estimated the stickiness between TEP particles as being 0.6, and that between TEP and non-TEP particles as being lower at 0.3. Using radio-labeled colloidal organic matter, which was passed through silica columns, Quigley et al.[55] determined a slightly higher stickiness factor of 0.88 for the polysaccharide enriched fraction (containing mostly fibrils) vs. 0.7 for the bulk fraction. These estimates indicate that TEP concentration is important for determining the structure of aquatic particles; however, they are rarely included explicitly in models.

Simulations of particle aggregation in aquatic systems have usually been restricted to considering aggregates composed of homogeneous primary particles, usually spheres. In these simulations, all aggregates are assumed to have the same fractal dimension regardless of their size. Aggregation dynamics proceeds by the standard Smoluchowsi model.[97] These models have successfully incorporated particle sizes ranging from 1 nm to 1 μm and have been used to examine the scavenging of thorium from surface oceanic waters.[96] These models indicate the importance of particle size in determining the adsorption rate of trace metals.

In reality, environmental aggregates are highly heterogeneous.[1,11] The structure and physical properties of aggregates formed from monomers of different sizes differ from those formed from monomers of a single size.[109] More sophisticated models that can include different particle types (e.g., phytoplankton and fecal pellets) have been developed[110,111] and indicate the importance of particle aggregation for understanding the vertical flux of material from the ocean surface.

A different modeling approach has used combinations of small spherical particles and polymer chains — bridging flocculation,[112–114] shown in Figure 9.5. The structure of polymer chains varies with environmental conditions such as pH, and both aggregation kinetics and aggregate structure depend upon the concentration and conformation

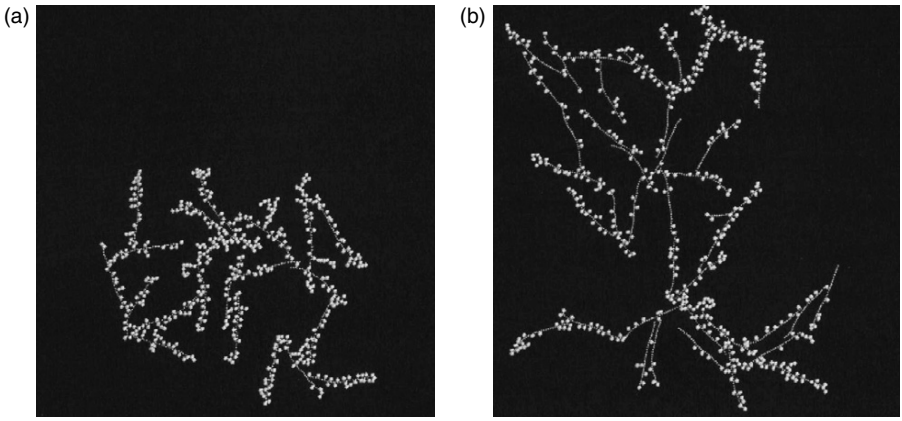

FIGURE 9.5 The effect of the relative concentration of chains and particles on aggregate structure: (a) 20 chains, (c) 40 chains. Aggregates have a structure similar to that arising from cluster–cluster aggregation when the relative concentration of chains is low. For high chain concentration, the aggregate has a network structure. (Taken from ref. [113].)

of these chains. Constant, prescribed stickiness coefficients were used, though different values were chosen for chain–chain interactions, particle–particle interactions, and chain–particle interactions. The resulting simulations indicate that polymer chain fractal dimension and the relative concentration of particles and chains are important in determining the rate of aggregate formation. Interestingly, this work also indicates that bridging flocculation can be described using simple scaling laws.

Looking into the future, full molecular dynamics simulations of large polysaccharides in aqueous environments may soon be feasible. This is a computationally difficult problem because polysaccharides contain a large number of flexible and polar hydroxyl (neutral sugars) and carboxyl or sulfate (acidic sugars) groups. These can form hydrogen bonds not only between molecules but also between groups in the same molecule. Improved models of the force fields for carbohydrates[115,116] bring closer the possibility of molecular dynamics models of acid polysaccharides.

9.4 UNRESOLVED QUESTIONS

9.4.1 How Does the Presence of Metals Affect the Properties of Fibrils?

Metal oxide precipitates have been found coating fibrillar material in aquatic systems[5–7] and Ca ions are known to form "egg-box" structures with alginic acids.[42] Whether metal ions are preferentially scavenged from the water column by fibrils, and how metal binding influences fibril conformation and interaction both with inorganic colloids and other fibrils is generally not known. It is likely that metal–fibril and fibril–inorganic–colloids interactions will render the electrical and chemical properties of the fibrils similar to those of the metal oxides. However, the association of metal ions with fibrils is expected to alter their aggregation characteristics and stickiness

factors. In addition, the presence of inorganic colloids would, in general, accelerate floc formation.

Currently, there are no experimental values for stickiness between natural inorganic colloids and organic chains, and no quantitative information about interactions between metals and natural biopolymers. Reported values for stickiness factors of inorganic colloids in freshwater are as low as 10^{-3} to 10^{-2}.[117] Fibrils will have different stickiness properties depending on their chemical composition and nanoscale structure. Stickiness will also almost certainly vary according to the concentration of metals such as Fe and Mn oxide colloidal particles as these will bind to the fibrils and affect the surface charge distribution. Metals are likely to bind at specific sites on the fibrils and can consequently alter the fibril conformation.

9.4.2 How Does the Presence or Absence of Fibrils Affect Particle Formation and Particle Aggregation Rates?

Colloid formation and particle aggregation rates are determined by the rates at which components are brought together (e.g., by Brownian diffusion, turbulent shear) and the probability that they will adhere once they have collided. In almost all models of aggregation in aquatic environments, interparticle adhesion is represented by a single parameter, the stickiness coefficient. It is likely that interparticle interactions depend significantly on the physical and chemical properties of fibrils and thus are crucial for predicting rates of particle aggregation. One example is the presence of covalently bound proteins in acid polysaccharidic hydrocolloids,[65] or their general hydrophobicity,[69] which determine the degree of stickiness. Furthermore, the presence of metal nucleation sites on fibrils likely alters the dynamics of inorganic colloid formation and, hence, the structure and function of the inorganic colloid fraction.

9.4.3 What Role Do Nanoscale Fibrils Play in Determining the Structure of Larger Scale Aggregates?

Typically, models of particle aggregation in aquatic systems use only a single monomer, which is regarded as being a spherical particle. Recent simulations by Stoll and Buffle[112,113] have incorporated a mixture of polymer chains and spherical monomer particles. Different proportions of polymer chains and spherical monomers result in different fractal dimensions for the resulting aggregates. These simulations used constant stickiness factors for different interactions, whereas, in reality, the stickiness will change with the environment. A combination of computer simulations and Small Angle X-ray Spectroscopy (SAXS) experiments would be needed to examine how fibril properties influence the properties (such as the fractal nature of the assemblage) of aggregates.

Theoretical models of fibrils need to be improved. While the heterogeneous composition of fibrils and their high molecular weight poses challenges for detailed molecular modeling, techniques for simulating sections of polysaccharide models are available[118]; models of solvated proteins have also been constructed.[119] Fibrils and their dynamics can be represented using relatively simple models, such as the "pearls-on-a-necklace" (Figure 9.3 and Figure 9.4) construction[112,113] or using the optimized Rouse–Zimm theory.[120] Simulations need to be performed using both

rigid and flexible chains and charge distributions estimated through a combination of experimental data and modeling — for example, using the Macro Model modeling system.[121] Similar approaches have been used elsewhere.[120,122,123] These models will make use of persistence-length measurements from AFM,[75,76] the coordination environment of metals attached to the fibrils from the x-ray Absorption Near Edge Structure (XANES) measurements, as well as charge and structural characteristics from scattering experiments.

Fibril properties (e.g., hydrodynamic radii, adhesion forces) change with the pH and ionic strength of the bulk medium.[124] In these simulations, the bulk medium can be represented as a dielectric medium entering the model through its dielectric permittivity.[125] Changes in salinity, pH, and ionic strength could be modeled by changes to the dielectric medium used in the simulation, and predictions of aggregation and scavenging will be made for freshwater, estuarine, and coastal environments.

What will be needed is to assess potential changes at the molecular scale of metal oxide nanoparticles entrapped by the fibrils and also to probe the coordinative environment of the metals that are interacting with the fibrils. It is likely that binding of either Fe or Mn nanoparticles by fibrils affect their chemical identity. Nanoparticles of MnO_x when precipitated using various trace metals show different features in spectra of XANES measurements (Figure 9.6). These differences in the XANES features show that the Mn local environment is responsive to the type of metal sorbed. In the case of the metals attaching to the fibrils, the average coordination environment of the metal will hold the answer to this question. To follow the "aggregation" process

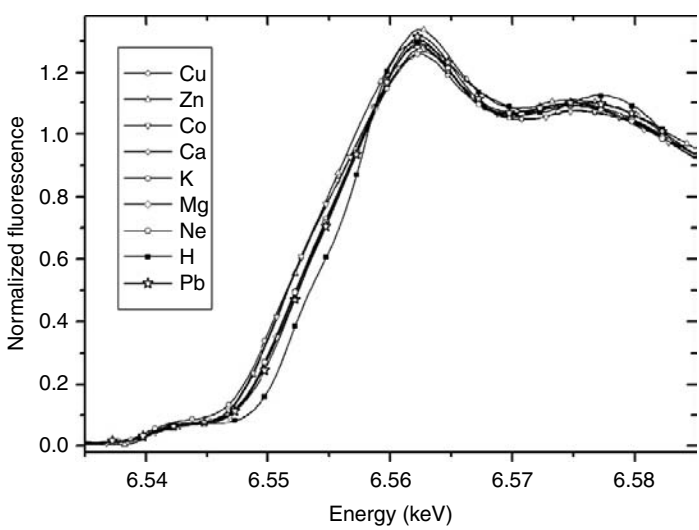

FIGURE 9.6 Mn K-edge XANES spectroscopy of colloidal MnO_2 particles prepared according to the method of Perez-Benito et al.[126] that were precipitated/aggregated by addition of either protons or various metals. The sorption of the different metals leads to shifts in the characteristic energy of the white line and changes in the pre-edge features illustrating that the coordination of Mn in the nanoparticles is affected.[127]

at a molecular scale, time resolved analyses to determine how various metals develop chemical bonds with the fibrils, as well as the formation of metal clusters on the fibrils as a function of time need to be studied.

A better understanding of fibril–metal interactions by theoretical methods is thus necessary. The adsorption of metals onto the fibril affects the charge density and hence the physico-chemical properties of the fibril. In particular, the aggregation (e.g., stickiness) and chemical (e.g., scavenging) properties will change depending on the form of interaction between the fibril and the metal ion. Different forms of interaction can occur: interactions may involve the sharing of electrons (inner-sphere bonds) or electrostatic interactions (outer-sphere bonds). Models need to utilize a combination of standard particle simulation techniques[128] and molecular dynamics techniques.[129–131] In particular, simulations to examine how fibril interactions change with changing environmental conditions (e.g., changing pH) and metal content would need to be carried out.

Finally, a better understanding of the role of natural organic matter, both humics and fibrils, is required, as they support the self-cleansing capacity of fresh, estuarine, and marine waters, and regulate the export of production of organic matter in open water systems. Knowledge of the detailed mechanisms of trace metal removal, pollutant transport, and formation of sedimentary deposits in aquatic environments hinges on an improved knowledge of the nano-science of natural organic matter.

ACKNOWLEDGMENTS

We are indebted to Drs Kevin Wilkinson and Jacques Buffle for numerous stimulating discussions. This work was funded, in parts, by grants from NSF (#9906823 and #0210865), and the Texas Institute of Oceanography. XAS experiments were performed at the Advanced Photon Source, Sector 5, on the DND-CAT bending magnet beam-line that is supported by the E.I. DuPont de Nemours & Co., the Dow Chemical Company, the NSF through Grant DMR-9304725, and the State of Illinois through the Department of Commerce and the Board of Higher Education Grant IBHE HECA NWU 96. DOE-BES under Contract No. W-31-102-Eng-38 supported use of the APS.

REFERENCES

1. Fowler, S.W. and Knauer, G.A., Role of large particles in the transport of elements and organic compounds through the oceanic water column, *Prog. Oceanogr.*, 16, 147, 1986.
2. Hanson, R.B., Ducklow, H.W., and Field, J.G., *The Changing Ocean Carbon Cycle: A Midterm Synthesis of the Joint Global Ocean Flux Study*, Cambridge University Press, 2000.
3. Angel, M.V., Does mesopelagic biology affect the vertical flux?, in *Productivity of the Oceans: Present and Past*, Berger, W.H., Smetacek, V.S., and Wefer, G., Eds., John Wiley, New York, 1989.
4. Perret, D. et al., Electron microscopy of aquatic colloids: non-perturbing preparation of specimens in the field, *Water Res.*, 25, 1333, 1991.

5. Lienemann, C.-P. et al., Association of cobalt and manganese in aquatic systems: chemical and microscopic evidence, *Geochim. Cosmochim. Acta*, 61, 1437, 1997.
6. Taillefert, M. et al., Speciation, reactivity, and cycling of Fe and Pb in a meromictic lake, *Geochim. Cosmochim. Acta*, 64, 169, 2000.
7. Perret, D. et al., The diversity of natural hydrous iron oxides, *Environ. Sci. Technol.*, 34, 3540, 2000.
8. Liss, S.N. et al., Floc architecture in wastewater and natural riverine systems, *Environ. Sci. Technol.*, 30, 680, 1996.
9. Wilkinson, K.J., Joz-Roland, A., and Buffle, J., Different roles of pedogenic fulvic acids and aquagenic biopolymers on colloidal aggregation and stability in freshwaters, *Limnol. Oceanogr.*, 42, 1714, 1997.
10. Buffle, J. et al., A generalized description of aquatic colloidal interactions: the three-colloidal component approach, *Environ. Sci. Technol.*, 32, 2887, 199.
11. Alldredge, A.L. and Gotschalk, C., Direct observations of the mass flocculation of diatom blooms: characteristics, settling velocities and formation of diatom aggregates, *Deep Sea Res.*, 36, 159, 1989.
12. Wells, M.L. and Goldberg, E.D., Colloid aggregation in seawater, *Mar. Chem.*, 41, 353, 1992.
13. Heissenberger, A., Leppard, G.G., and Herndl, G.J., Ultrastructure of marine snow: II. Microbiological considerations, *Mar. Ecol. Prog. Ser.*, 135; 299, 1996.
14. Santschi, P.H. et al., Fibrillar polysaccharides in marine macromolecular organic matter as images by atomic for microscopy and transmission electron microscopy, *Limnol. Oceanogr.*, 43, 896, 1998.
15. Sheldon, R.W., Prakash, A., and Sutcliffe, W.H., The size distribution of particles in the ocean. *Limnol. Oceanogr.*, 17, 327, 1972.
16. Hunt, J.R., Prediction of oceanic particle size distributions from coagulation and sedimentation mechanisms, in *Particles in Water*, Kavanaugh, M.C. and Leckie, J.O., Eds., American Chemical Society, pp. 234–257, 1980.
17. Eisma, D., Flocculation and de-flocculation of suspended matter in estuaries, *Neth. J. Sea Res.*, 20, 183, 1986.
18. Sternberg, R.W. et al., Suspended sediment transport under estuarine tidal channel conditions, *Sediment. Geol.*, 57, 257, 1988.
19. Jackson, G.A. et al., Particle size spectra between 1 μm and 1 cm at Monterey Bay determined using multiple instruments, *Deep Sea Res.*, 44, 1739, 1997.
20. Santschi, P.H. et al., Boundary exchange and scavenging of radionuclides in continental margin waters of the Middle Atlantic Bight. Implications for organic carbon fluxes, *Continental Shelf Res.*, 19, 609, 1999.
21. Asper, V.L., Measuring the flux and sinking speed of marine snow aggregates, *Deep Sea Res.*, 34, 1, 1987.
22. Silver, M.W. and Gowing, M.W., The "particle" flux: origins and biological components, *Prog. Oceanogr.*, 26, 75, 1991.
23. Lampitt, R.S., Hillier, W.R., and Challenor, P.G., Seasonal and diel variations in the open ocean concentration of marine snow aggregates, *Nature*, 362, 737, 1993.
24. Deuser, W.G. et al., Seasonal changes in the species composition, numbers, mass, size, and isotopic composition of planktonic foraminifera settling into the deep Sargasso Sea, *Paleogeogr. Paleoclimat. Paleoecol.*, 33, 103, 1981.
25. Asper, V.L. et al., Rapid coupling of sinking particle fluxes between surface and deep ocean waters, *Nature*, 357, 670, 1992.
26. Conte, M.H., Ralph, N., and Ross, E.H., Seasonal and interannual variability in deep ocean particle fluxes at the Oceanic Flux Program (OFP)/Bermuda Atlantic Time Series

(BATS) site in the western Sargasso Sea near Bermuda, *Deep Sea Res. II*, 48, 1471, 2001.
27. Guo, L., Santschi, P.H., and Warnken, K.W., Dynamics of dissolved organic carbon (DOC) in oceanic environments, *Limnol. Oceanogr.*, 40, 1392, 1995.
28. Wells, M.L. and Goldberg, E.D., Occurrence of small colloids in seawater, *Nature*, 353, 342, 1991.
29. Wells, M.L. and Goldberg, E.D., The distribution of colloids in the North Atlantic and Southern Oceans, *Limnol. Oceanogr.*, 39, 286, 1994.
30. Degueldre, C. et al., Colloid properties in granitic groundwater systems. I: Sampling and characterization, *Appl. Geochem.*, 11, 677, 1996.
31. Leppard, G.G., Colloidal organic fibrils of acid polysaccharides in surface waters: electron-optical characteristics, activities and chemical estimates of abundance, *Colloids Surf. A*, 120, 1, 1997.
32. Wilkinson, K.J. et al., Characteristic features of the major component of freshwater colloidal organic matter revealed by transmission electron and atomic force microscopy, *Colloids Surf. A. Physiochem. Eng. Aspects*, 155, 287, 1999.
33. Leppard, G.G. et al., A classification scheme for marine organic colloids in the Adriatic Sea: colloid speciation by transmission electron microscopy, *Can. J. Fish. Aquat. Sci.*, 54, 2334, 1997.
34. Hung, C.-C. et al., Distributions of carbohydrate species in the Gulf of Mexico, *Mar. Chem.*, 81, 119, 2003a.
35. McCave, I.N., Size spectra and aggregation of suspended particles in the deep ocean, *Deep Sea Res.*, 31, 329, 1984.
36. Jackson, G.A. and Burd, A.B., Aggregation in the marine environment: a critical review. *Environ. Sci. Technol.*, 32, 2805, 1998.
37. Alldredge, A.L., Passow, U., and Logan, B.E., The abundance and significance of a class of large, transparent organic particles in the ocean, *Deep Sea Res.*, 40, 1131, 1993.
38. Passow, U., Alldredge, A.L., and Logan, B.E., The role of particulate carbohydrate exudates in the flocculation of diatom blooms, *Deep Sea Res.*, 41, 335, 1994.
39. Mopper, K.J. et al., The role of surface-active carbohydrates in the flocculation of a diatom bloom in a mesocosm, *Deep Sea Res. II*, 42, 47, 1995.
40. Grossart, H.-P., Simon, M., and Logan, B., Formation of macroscopic organic aggregates (lake snow) in a large lake: the significance of transparent exopolymer particles (TEP), phytoplankton and zooplankton, *Limnol. Oceanogr.*, 42, 1651, 1997.
41. Mari, X. and Burd, A.B., Seasonal size spectra of transparent exopolymeric particles (TEP) in a coastal sea and comparison with those predicted using coagulation theory, *Mar. Ecol. Prog. Ser.*, 163, 63, 1998.
42. Leppard, G.G., The characterization of algal and microbial mucilages and their aggregates in aquatic systems, *Sci. Total. Environ.*, 165, 103, 1995.
43. Passow, U. and Alldredge, A.L., Aggregation of a diatom bloom in a mesocosm: the role of transparent exopolymer particles (TEP), *Deep Sea Res. II*, 42, 99, 1995.
44. Zhou, J., Mopper, K., and Passow, U., The role of surface-active carbohydrates in the formation of transparent exopolymer particles (TEP) by bubble adsorption of seawater, *Limnol. Oceanogr.*, 43, 1860, 1998.
45. Passow, U., Formation of transparent exopolymer particles, TEP, from dissolved precursor material. *Mar. Ecol. Prog. Ser.*, 192, 1, 2000.
46. Passow, U., Production of transparent exopolymer particles (TEP) by phyto- and bacterioplankton, *Mar. Ecol. Prog. Ser.*, 236, 1, 2002.

47. Santschi, P.H. et al., Control of acid polysaccharide production, and ^{234}Th and POC export fluxes by marine organisms, *Geophysical Res. Lett.*, 30(2), doi: 10.1029/2002GL016046, 2003.
48. Hung, C.-C. et al., Production and fluxes of carbohydrate species in the Gulf of Mexico, *Global Biogeochem. Cycles*, 17(2), 1055, doi:10.1029/2002GB001988, 2003b.
49. Buesseler, K.O., The de-coupling of production and particle export in the surface ocean, *Global Biogeochem. Cycles*, 12, 297, 1998.
50. Baskaran, M. et al., ^{234}Th:^{238}U disequilibria in the Gulf of Mexico: importance of organic matter and particle concentration, *Continental Shelf Res.*,16, 353, 1996.
51. Leppard, G.G., Massalski, A., and Lean, D.R.S., Electron-opaque microscopic fibrils in lakes: their demonstration, their biological derivation and their potential significance in the redistribution of cations, *Protoplasma*, 92, 289, 1977.
52. Benner, R.J.D. et al., Bulk chemical characteristics of dissolved organic carbon, *Science*, 255, 1561, 1992.
53. Guo, L., Coleman, C.H., Jr., and Santschi, P.H., The distribution of colloidal and dissolved organic carbon in the Gulf of Mexico, *Mar. Chem.*, 45, 105, 1994.
54. Santschi, P.H. et al., Isotopic evidence for the contemporary origin of high molecular-weight organic matter in oceanic environments, *Geochim. Cosmochim. Acta*, 59, 625, 1995.
55. Quigley, M.S. et al., Sorption irreversibility and coagulation behavior of ^{234}Th with surface-active marine organic matter, *Mar. Chem.*, 76, 27, 2001.
56. Quigley, M.S. et al., Importance of polysaccharides for ^{234}Th complexation to marine organic matter, *Limnol. Oceanogr.*, 47, 367, 2002.
57. Hill, P.S., Reconciling aggregation theory with observed vertical fluxes following phytoplankton blooms, *J. Geophys. Res.*, 97, 2295, 1992.
58. Balistrieri, L.S. and Murray, J.W., The surface chemistry of sediments from the Panama Basin: the influence of Mn oxides on metal adsorption, *Geochim. Cosmochim. Acta*, 50, 2235, 1986.
59. Buffle, J., *Complexation Reactions in Aquatic Systems*, Ellis Horwood, Chichester, West Sussex, England 1988.
60. Stumm, W., *Chemistry of the Solid–Water Interface: Processes at the Mineral–Water and Particle–Water Interface in Natural Systems*, Wiley, New York, 1992.
61. Santschi, P.H., Lenhart, J., and Honeyman, B.D., Heterogeneous processes affecting trace contaminant distribution in estuaries: the role of natural organic matter, *Mar. Chem.*, 58, 99, 1997.
62. Cowen, J.P. and Bruland, K.W., Metal deposits associated with bacteria-implications for Fe and Mn marine biogeochemistry, *Deep Sea Res.*, 32, 253, 1985.
63. Kinrade, S.D. and Knight, C.T.G., Silicon-29 NMR evidence of a transient hexavalent silicon complex in the diatom Navicula pelliculosa, *J. Chem. Soc. Dalton Trans.*, 3, 307, 2002.
64. Leveille, R.J., Fyfe, W.S., and Longstaffe, F.J., Geomicrobiology of carbonate-silicate microbioalites from Hawaiian basaltic sea caves, *Chem. Geol.*, 169, 339, 2000.
65. Dickinson, E., Hydrocolloids at interfaces and the influence on the properties of dispersed systems, *Food Hydrocolloids*, 17, 25, 2003.
66. Liao, B.Q. et al., Surface properties of sludge and their role in bioflocculation and settleability. *Water Res.*, 35, 339, 2001.
67. Liao, G.Q., et al., Interparticle interactions affecting the stability of sludge flocs. *J. Colloid Interface Sci.*, 249, 372, 2002.

68. Leppard, G.G., Droppo, I.G., West, M.M., and Liss, S.N., Compartmentalization of metals within the diverse colloidal matrices comprising activated sludge microbial flocs. *J. Environ. Quality*, 32, 2100.
69. Stenstörm, T.A., Bacterial hydrophobicity, an overall parameter for the measurement of adhesion potential to soil particles, *Appl. Environ. Microbiol.*, 55, 142, 1989.
70. Thurman, E.M., *Organic Geochemistry of Natural Waters*, Martinus Nijhoff/ Dr. W. Junk Publishers, Dordrecht, 1985.
71. Decho, A.W., Microbial exopolymer secretions in ocean environments: their role(s) in food webs and marine processes, *Oceanogr. Mar. Biol. Ann. Rev.*, 28, 73, 1990.
72. Buffle, J. and Leppard, G.G., Characterization of aquatic colloids and macromolecules. I. Structure and behavior of colloidal material, *Environ. Sci. Technol.*, 29, 2169, 1995.
73. Aluwihare, L.I., Repeta, D.J., and Chen, R.F., A major biopolymeric component to dissolved organic carbon in surface sea water, *Nature*, 387, 166, 1997.
74. Pinheiro, J.P. et al., The pH effect in the diffusion coefficient of humic matter: influence in speciation studies using voltammetric techniques. *Colloids Surf. A-Physiochem. Eng. Aspects*, 137, 165, 1998.
75. Balnois, E. et al., Conformations of succinoglycans as observed by atomic force microscopy. *Macromolecules*, 33, 7440, 2000.
76. Balnois, E. and Wilkinson, J.K., Sample preparation techniques for the observation of environmental biopolymers by atomic force microscopy, *Colloids Surf. A: Physicochem. Eng. Aspects*, 207, 229, 2002.
77. Meakin, P., *Fractals, Scaling and Growth Far from Equilibrium*, Cambridge University Press, 1998.
78. Vicsek, T., *Fractal Growth Phenomena*, 2nd edition, World Scientific, Singapore, 1992.
79. Gouyet, J.-F., *Physics and Fractal Structures*, Springer, 1996.
80. Alldredge, A.L. and Gotschalk, C., In-situ settling behavior of marine snow, *Limnol. Oceanogr.*, 33, 339, 1988.
81. Logan, B.E. and Wilkinson, D.B., Fractal geometry of marine snow and other biological aggregates, *Limnol. Oceanogr.*, 39, 130, 1990.
82. Klips, J.R., Logan, B.E., and Alldredge, A.L., Fractal dimensions of marine snow determined from image analysis of in situ photographs, *Deep Sea Res.*, 41, 1159, 1994.
83. Li, X. and Logan, B.E., Size distributions and fractal properties of particles during a simulated phytoplankton bloom in a mesocosm, *Deep Sea Res. II*, 42; 125, 1995.
84. Jackson, G.A. et al., Combining particle size spectra from a mesocosm experiment measured using photographic and aperture impedance (Coulter and Elzone) techniques, *Deep Sea Res.* II, 42, 139, 1995.
85. Hawley, N., Settling velocity distribution of natural aggregates, *J. Geophys. Res.*, 87, 9489, 1982.
86. De Boer, D.H., Stone, M., and Levesque, L.M.J., Fractal dimensions of individual flocs and floc populations in streams, *Hydrolog. Proc.*, 14, 653, 2000.
87. Li, D.-H. and Ganczarczyk, J.J., Fractal geometry of particle aggregated in water and wastewater treatment processes, *Environ. Sci. Technol.*, 23, 1385, 1989.
88. Amal, R., Raper, J.A., and Waite, T.D., Fractal structure of hematite aggregates, *J. Colloid Interface Sci.*, 140, 158, 1990.
89. Johnson, C.P., Li, X., and Logan, B., Settling velocities of fractal aggregates, *Environ. Sci. Technol.*, 30, 1911, 1996.

90. Guan, J., Waite, T.D., and Amal, R. Rapid structure characterization of bacterial aggregates, *Environ. Sci. Technol.*, 32, 3735, 1996.
91. Engel, A. and Schartau, M., Influence of transparent exopolymer particles (TEP) on sinking velocity of Nitzchia closterium aggregates, *Mar. Ecol. Prog. Ser.*, 182, 69, 1999.
92. Honeyman, B.D. and Santschi, P.H., A Brownian-pumping model for oceanic trace metal scavenging: evidence from Th isotopes, *J. Mar. Res.*, 47, 951, 1989.
93. Honeyman, B.D. and Santschi, P.H., Coupling of trace metal adsorption and particle aggregation: kinetic and equilibrium studies using ^{59}Fe-labeled hematite, *Environ. Sci. Technol.*, 25, 1739, 1991.
94. Stordal, M.C., Santschi, P.H., and Gill, G.A., Colloidal pumping: evidence for the coagulation process using natural colloids tagged with ^{203}Hg, *Environ. Sci. Technol.*, 30, 3335, 1996.
95. Wen, L.S., Santschi, P.H., and Tang, D., Interactions between radioactively labeled colloids and natural particles: evidence for colloidal pumping, *Geochim. Cosmochim. Acta*, 61, 2867, 1997.
96. Burd, A.B., Moran, S.B., and Jackson, G.A., A coupled adsorption-aggregation model of the POC/Th ratio of marine particles, *Deep Sea Res.*, 47, 103, 2000.
97. Pruppacher, H.R. and Klett, J.D., *Microphysics of Clouds and Precipitation*, Riedel, 1980.
98. Burd, A.B. and Jackson, G.A., The evolution of particle size spectra I: pulsed input, *J. Geophys. Res.*, 102, 10545, 1997.
99. Li, X. and Logan, B.E., Collision frequencies of fractal aggregates with small particles by differential sedimentation, *Environ. Sci. Technol.*, 31, 1229, 1997.
100. Li, X. and Logan, B.E., Collision frequencies between fractal aggregates and small particles in a turbulently sheared fluid, *Environ. Sci. Technol.*, 31, 1237, 1997a.
101. Burd, A.B. and Jackson, G.A., Modeling steady state particle size spectra, *Environ. Sci. Technol.*, 36, 323, 2002.
102. Jackson, G.A., Comparing observed changes in particle size spectra with those predicted using coagulation theory, *Deep Sea Res. II*, 42, 159, 1995.
103. van Oss, C.J., *Interfacial Forces in Aqueous Media*, Marcel Dekker, New York, 1994.
104. Israelachvili, J., *Intermolecular and Surface Forces*, 2nd edition, Academic Press, New York, 1992.
105. Grasso, D. et al., A review of non-DLVO interactions in environmental colloidal systems, *Rev. Env. Sci. Biotechnol.*, 1, 17, 2002.
106. Rijnaarts, H.H.M. et al., DLVO and steric contributions to bacterial deposition in media of different ionic strengths, *Colloids Surf. B: Biointerfaces*, 14, 179, 1999.
107. Azeredo, J., Visser, J., and Oliveira, R., Exopolymers in bacterial adhesion: interpretation in terms of DLVO and XDLVO theories, *Colloids Surf. B: Biointerfaces*, 14, 141, 1999.
108. Engel, A., The role of transparent exopolymer particles (TEP) in the increase in apparent particle stickiness during the decline of a diatom bloom, *J. Plankton Res.*, 22, 485, 2000.
109. Bushell, G. and Amal, R., Fractal aggregates of polydisperse particles, *J. Colloid Interface Sci.*, 205, 459, 1998.
110. Jackson, G.A., Using fractal scaling and two-dimensional particle size spectra to calculate coagulation rates for heterogeneous systems, *J. Colloid Interface Sci.*, 202, 20, 1998.
111. Jackson, G.A., Effect of coagulation on a model planktonic food web, *Deep Sea Res. I*, 48, 95, 2001.

112. Stoll, S. and Buffle, J., Computer simulation of bridging flocculation processes: the role of colloid to polymer concentration ratio on aggregation kinetics, *J. Colloid Interface Sci.*, 180, 548, 1996.
113. Stoll, S. and Buffle, J., Computer simulation of flocculation processes: the roles of chain conformation and chain/colloid concentration ratio in the aggregate structures, *J. Colloid Interface Sci.*, 205, 290, 1998.
114. Stoll, S., Computer simulations of aggregate formation and colloid/polymer mixtures, *SAMS*, 42, 219, 2002.
115. Kony, D.W. et al., An improved OPLS-AA force field for carbohydrates, *J. Comput. Chem.*, 23, 1416, 2002.
116. Eklund, R. and Widmalm, G., Molecular dynamics simulations of an oligosaccharide using a force field modified for carbohydrates, *Carbohydr. Res.*, 338, 393, 2003.
117. O'Melia, C.R., Particle–particle interactions, in *Aquatic Surface Chemistry. Chemical Processes at the Particle–Water Interface*, Stumm, W., Ed., John Wiley & Sons, New York, p. 385, 1987.
118. Cros, S. et al., Solution conformations of pectin polysaccharides: determination of chain characteristics by small angle neutron scattering, viscometry, and molecular modeling, *Biopolymers*, 39, 339, 1996.
119. Eichinger, M., Heller, H., and Grumbuller, H., EGO — an efficient molecular dynamics program and its application to protein dynamics simulations, in *Workshop on Molecular Dynamics on Parallel Computers*, Esser, R., Grassberger, P., Grotendorst, J., and Lewerenz, M., Eds., World Scientific, Singapore, 2000.
120. Perico, A., Local dynamics in biological macromolecules, *Biopolymers*, 28, 1527, 1989.
121. Schrodinger Inc., *MacroModel Interactive Modeling System*, Version 7.0: A Primer, 1999.
122. Wallin, T. and Linse, P., Monte Carlo simulations of polyelectrolytes at charged hard spheres with different numbers of polyelectrolyte chains, *J. Chem. Phys.*, 109, 5089, 1998.
123. Liu, H.-Y. et al., Equilibrium spatial distribution of aqueous pullulan: small-angle X-ray scattering and realistic computer modeling, *Macromolecules*, 32, 8611, 1999.
124. Frank, B.P. and Belfort, G., Intermolecular forces between extracellular polysaccharides measured using the atomic force microscope, *Langmuir*, 13, 6234, 1997.
125. Wallin, T. and Linse, P., Monte Carlo simulations of polyelectrolytes at charged micelles: 2. Effects of linear charge density, *J. Phys. Chem.*, 100, 17873, 1996.
126. Perez-Benito, J.F., Brillas, E., and Pouplana, R., Identification of a soluble form of colloidal manganese (IV), *Inorg. Chem.*, 28, 390, 1989.
127. Gaillard, J.-F., Webb, S.M., and Quintana, J.P.G., Quick x-ray absorption spectroscopy for determining metal speciation in environmental samples, *J. Synchrotron Radiat.*, 8, 928, 2001.
128. Hockney, R.W. and Eastwood, J.W., *Computer Simulation Using Particles*, IOP Publishing, Bristol, UK, 1988.
129. Haile, J.M., *Molecular Dynamics Simulation: Elementary Methods*, Wiley, New York, 1992.
130. Deuflhard, P. et al., Eds., *Computational Molecular Dynamics: Challenges, Methods, Ideas*, Springer, New York, 1999.
131. Esser, R., et al., Eds., *Workshop on Molecular Dynamics on Parallel Computers*, World Scientific, Singapore, 2000.

10 Variability of Suspended Particle Concentrations, Sizes, and Settling Velocities in the Chesapeake Bay Turbidity Maximum

Lawrence P. Sanford, Patrick J. Dickhudt, Laura Rubiano-Gomez, Marissa Yates, Steven E. Suttles, Carl T. Friedrichs, David D. Fugate, and Heidi Romine

CONTENTS

10.1 INTRODUCTION

Estuarine Turbidity Maxima (ETMs) are zones of elevated suspended sediment concentration and reduced light availability typically found near the limit of salt intrusion in the upper reaches of estuaries. ETMs often are characterized by sharp gradients in physical, biological, geological, and chemical properties, as freshwater rivers with their suspended sediments, plankton, and nutrients transform into brackish, tidal estuaries. Trapping of riverine sediment and detritus in ETMs is thought to contribute to the maintenance of unique and important zooplankton and fish populations[1–5] and to promote rapid rates of sedimentation[6] and reduced phytoplankton productivity.[7]

1-56670-615-7/05/$0.00+$1.50

Flocculation has long been recognized as an important contributing factor to ETM particle trapping[8–11] through associated increases in settling velocity. However, flocculation in early ETM studies was largely interpreted as a one-time transition between small riverine particles and large estuarine flocs bound together by electrochemical attractive forces,[12] a view now recognized as incomplete.

The ETM of the Chesapeake Bay, USA was first studied in the late 1960s and 1970s. The most extensive work was carried out by Schubel and coworkers,[13–16] followed by the work of Zabawa[8] and Gibbs[17] on the behavior of suspended particles and agglomerates. The results of these studies indicated several consistent characteristics of particles in the Chesapeake ETM. Particle populations were divided into two groups: large flocs (or aggregates or agglomerates, depending on individual preference) between 20 and 250 μm in size settling at rates between 0.1 and 1 mm sec^{-1}, and smaller background particles consisting of primary particles or very small flocs. This distinction was operational with the large flocs making up the pool of tidally resuspended and deposited bottom sediments and the background particles remaining essentially unchanged over the tidal cycle. Zooplankton fecal pellets were identified as an important component of the large agglomerate population. Note that these studies necessarily relied on a limited number of point samples obtained with sampling techniques that may have disrupted weaker flocs.

Subsequent work carried out by some of the present authors in upper Chesapeake Bay confirmed the apparent two-component nature of the particle population,[6,18–21] though settling velocities measured with bottom withdrawal settling tubes were higher than the 1 mm sec^{-1} upper limit observed previously. Recently, settling speeds of the large flocs were observed to vary seasonally, with maxima at the end of the summer and minima in winter. Models of tidal resuspension and deposition assuming that the two particle populations were independent and that the settling speed of the large flocs was constant over tidal cycles compared quite reasonably to observations. However, these studies were focused on sediment transport patterns and parameterizations and did not attempt to distinguish details of the size and settling velocity distributions of the particles.

The research reported here was carried out during a large, interdisciplinary investigation of the coupled physical and biological dynamics of the Chesapeake Bay ETM ("BITMAX," Bio-physical Interactions in the Turbidity MAXimum). This research was carried out during seasonal cruises to the upper Bay in 2001 and 2002, employing a new suite of instrumentation that for the first time allowed a detailed, simultaneous examination of the changing sizes and settling speeds of particles in this region, in relation to physical structure and dynamics. We concentrate here on data collected during 2002, primarily because our methods were better developed in the second year of the study.

Though obviously of interest for local, Chesapeake Bay research, this study also explores environmental conditions that have not received a great deal of attention in the marine and estuarine flocculation literature. Eutrophic estuarine transition zones with moderate physical energy, moderate turbidity, and moderate biological activity are, in a sense, midway between the oceanic, oligotrophic environments studied by Alldredge, Jackson, and coworkers,[22–27] the coastal and continental shelf environments studied by Hill, Milligan, and colleagues,[28–30] and the highly energetic,

turbid estuaries studied by Dyer, van Leussen, and colleagues.[31–34] Interested readers are referred to work in similar estuarine environments to this study by Kranck and Milligan[35] and Fugate and Friedrichs,[36] among others.

10.2 SITE DESCRIPTION

The ETM zone of Chesapeake Bay is almost always found between latitudes 39° 10′ N and 39° 28′ N, a range of approximately 40 km (Figure 10.1). This region of the Bay has a mean volume of approximately 2.63 km^3 and a mean depth of approximately 4.1 m,[37] not counting the small tributaries. It is incised by a narrow shipping channel maintained by dredging at a depth of approximately 12 m, which connects the Chesapeake and Delaware Canal with the Port of Baltimore and serves as the primary pathway for up-Bay salt intrusion. The average astronomical tidal range increases northward from 0.36 to 0.5 m, with typical maximum tidal current speeds of 0.5 m sec^{-1} in the channel and 0.3 m sec^{-1} over the broad shoals.[38] Wind-forced water level fluctuations can be much larger than the astronomical tide (up to 1 m in range), with associated current fluctuations of up to 0.2 m sec^{-1}.[6,39,40] Net nontidal gravitational circulation varies strongly in response to fluctuations in river flow, changing from a riverine, barotropic downstream flow above the limit of salt to

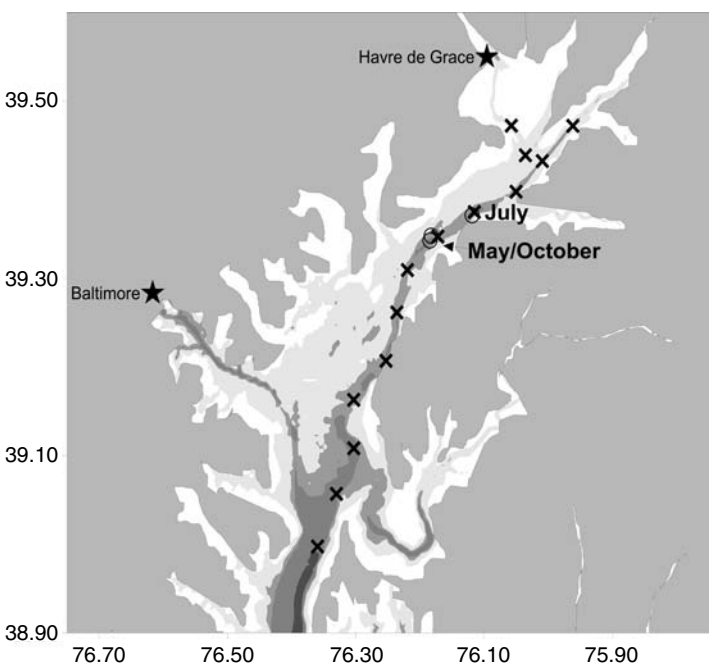

FIGURE 10.1 Map of Upper Chesapeake Bay with station locations. Gray shading indicates depth intervals of 3, 7, 10, and 20 m. Xs indicate axial stations repeated during each axial hydrographic survey. Os indicate locations of 12-h anchor stations.

a well-developed estuarine circulation below the limit of salt. Almost all of the fresh water flow enters from the Susquehanna River. At the average Susquehanna River flow of 1100 $m^3\ sec^{-1}$, the freshwater replacement time of the ETM region of the Bay is approximately 1 month.

More than 80% of the sediment entering the upper Bay comes down the Susquehanna, with almost all of the rest resulting from shoreline erosion.[41,42] The bottom sediments gradually fine southward from the broad, sandy delta known as Susquehanna Flats, through short transition zones of silty sands and sandy silts, through the clayey silts that dominate the ETM region, to the silty clays that dominate the broad lower reach of the upper Bay. The deep channels of the upper Bay sediment rapidly[6,43] and require constant dredging to maintain navigable depths. Suspended sediments comprise silts, clays, and aggregates thereof, with a low organic matter fraction.[13,16,41] Total suspended sediment (TSS) concentrations in the entire upper Bay are elevated relative to the rest of the estuary, with typical background concentrations of very slowly settling particles between 5 and 25 $mg\ l^{-1}$.[6,13,19,44] The ETM itself typically has TSS concentrations 20 to 100 $mg\ l^{-1}$ higher than background, with the largest concentrations resulting from tidal resuspension in near-bottom waters.[6,13]

Freshwater flow and sediment load data from the Susquehanna River were obtained from the United States Geological Survey (USGS). The sediment load data were calculated from flow using a calibrated USGS estimation procedure.[45] Monthly averaged data for 2002 are presented in Figure 10.2 for comparison to the 23-year mean monthly averages between 1979 and 2002. It is apparent from this figure that 2002 was a low to average flow year for the Susquehanna, except for May and June. Sediment loads were even lower relative to the long-term mean, except for May.

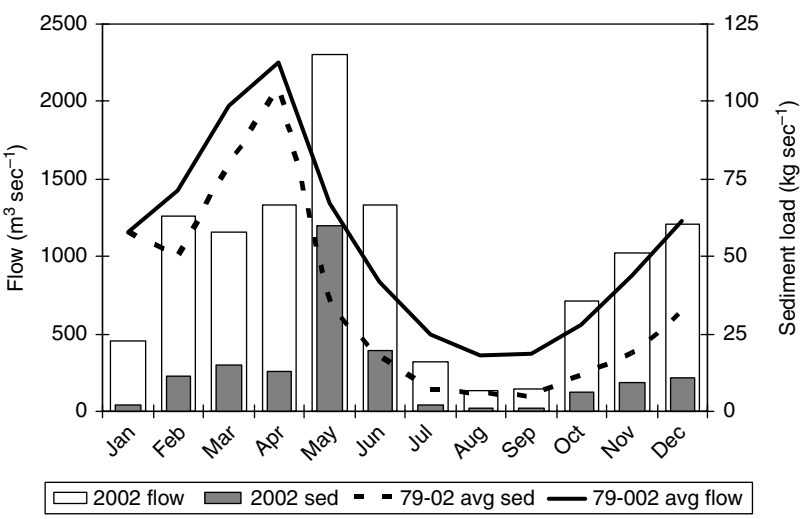

FIGURE 10.2 Freshwater discharge and sediment load from the Susquehanna River at Conowingo Dam. Bars depict monthly averages for calendar year 2002 and lines represent long term monthly averages from 1979 to 2002. Data from USGS internet sites.

The year 2001 was also quite dry with low sediment delivery. This is in marked contrast to the 1996 data presented by Sanford et al.,[6] which were collected during one of the wettest years of the 1990s.

10.3 METHODS

A total of six seasonal, interdisciplinary cruises, each of 9 days duration, were carried out in the ETM region of the upper Chesapeake Bay during May, July, and October of 2001 and 2002. Daylong axial surveys were carried out before, between, and after the seasonal cruises at approximately 6-week intervals. In this chapter, we concentrate on the seasonal cruises carried out during 2002, since these cruises yielded the most complete and reliable data sets on particle characteristics. During each of the seasonal cruises, an initial rapid axial survey was run from the R/V Cape Henlopen to locate the ETM, after which reference moorings were deployed and fisheries surveys were carried out. A full axial survey with suspended sample collections and coordinated lateral sampling followed. Lateral sampling was carried out using the R/V Coot, a small, shallow draft vessel outfitted with a similar set of instrumentation to that used on the Henlopen. The remainder of each cruise was taken up by additional full axial/lateral sampling, 6-h repeated surveys in the vicinity of the ETM, 12-h tidal cycle surveys concentrating on interactions between turbulence and particle characteristics, bottom sediment sampling and erodibility testing, and zooplankton/fish sampling.

Three full axial surveys were conducted during the May 2002 cruise, and four axial surveys during both the July and October 2002 cruises. Each survey consisted of 12 to 14 stations up the shipping channel, spaced approximately 6 km apart (Figure 10.1). They began near the Chesapeake Bay Bridge before maximum tidal current and ended near Turkey Point shortly after maximum tidal current. Both flood and ebb tides were surveyed. Profiles were taken at each station with a SBE 9/11 CTD equipped with a Downing and Associates OBS-3a backscatterance sensor and a Sea Tech 5 cm pathlength transmissometer. A Sequoia Scientific LISST-100C (Laser *in situ* Scattering and Transmissometry) and well pump were mounted at the same elevation and in close proximity to the OBS, transmissometer, and CTD sampling pump. The sample volumes of the LISST-100C and transmissometer were oriented horizontally and centered over a large open space in the CTD frame to ensure sampling of an undisturbed water column during profiling. Only data collected on the downcast were analyzed. Pump samples collected with the well pump were used for TSS calibrations for the OBS, transmissometer, and LISST-100C. Data were interpolated onto a uniform grid at 0.5 m vertical resolution and 3 km horizontal resolution using the kriging algorithm in Surfer (Golden Software), and contoured using the same software.

The LISST-100C measured optical transmission and multi-angle forward scattering of a 670 nm laser. The LISST sampled at a rate of 5 Hz. Five samples were averaged and recorded to an internal datalogger at a rate of 1 Hz. An optically transparent path reduction module was added to the LISST, reducing the optical path length from 5 to 2.5 cm and effectively doubling the maximum concentration in which the instrument could operate from $\approx$80 to $\approx$160 mgl^{-1}. Optical percent transmission data were converted to total suspended solids (TSS, mgl^{-1}) using

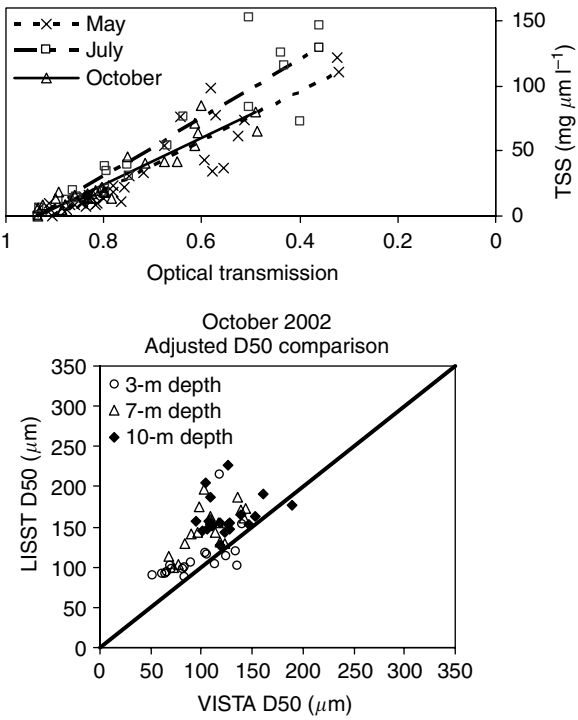

FIGURE 10.3 (a) Linear regressions correlating TSS from pump samples to optical transmission measured with LISST-100C. (b) comparisons between D50 as measured by the LISST-100C and D50 as measured by the VISTA. The LISST data are adjusted to remove particles that are too small to resolve with the VISTA and to remove large, rare particles that are extremely improbable to have been observed with the VISTA.

a linear calibration derived from pump samples (Figure 10.3). Laser scattering data were inverted to produce particle size distributions as described by Agrawal and Pottsmith.[46] The inversion process was applied with a modified version of a Matlab routine provided by Sequoia Scientific. Data quality was ensured by eliminating data with an optical transmission of less than 15% as advised by Sequoia Scientific. The inversion produced a size distribution reported as volume concentration ($\mu l l^{-1}$) in 32 logarithmically spaced size classes including particles from 2.5 to 500 μm in diameter. Size classes for the LISST are fixed by the physical configuration of the scattering sensors. The cumulative volume concentration from all size classes was reported as total volume concentration ($\mu l l^{-1}$) and was used to calculate median particle diameter by volume (D50). Data from the 20 smallest classes were combined to calculate volume concentration <66.5 μm. The remaining 12 large size classes were combined to calculate volume concentration >66.5 μm. Bulk density (ρ_b) was estimated as follows: The density of water (ρ_{water}) was calculated using temperature and salinity data from the CTD. Mineral solids density (ρ_{solid}) was assumed to be 2.65 g cm^{-3}. Solids fraction (ϕ_s) was calculated as TSS/Total Volume Concentration/ρ_{solid}, and $\rho_b = (\rho_{solid} * \phi_s) + \rho_{water} * (1 - \phi_s)$.

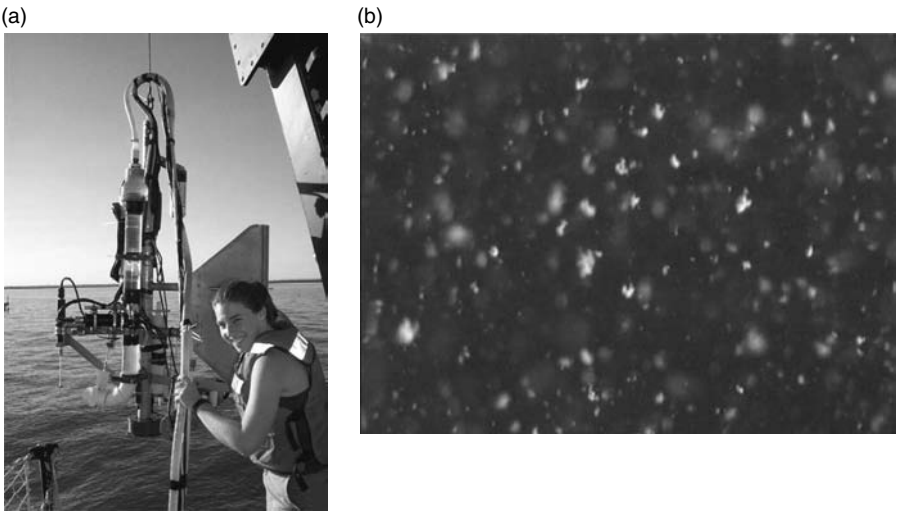

FIGURE 10.4 (a) Photograph of M. Yates recovering the profiling rig during a tidal cycle anchor station. The VISTA settling tube is clearly visible, with the ADV to its left and the CTD immediately to its right in the image. (b) Captured image from VISTA from 10:10 AM (EDT) on October 10, 2002 in ETM region. Sample depth is approximately 9.5 m. Field of view is 11.5 mm wide by 8.5 mm high.

Tidal cycle anchor stations were conducted as two vessel efforts over 12 daylight hours on one day of each seasonal cruise. A water column profiling rig with a transmissometer, a LISST-100C, a CTD, an Acoustic Doppler Velocimeter (ADV), and a video settling tube was lowered repeatedly to 3, 7, and 10 m depths at 0.5 h per cycle from the Cape Henlopen (Figure 10.4). A modified Valeport settling tube (based on the Owen tube design[47]) was used to estimate settling velocities of relatively undisturbed particles collected just above the bottom at several times during the tidal cycle. A LISST-100C and a Precision Measurement Engineering Self-Contained Autonomous MicroProfiler (SCAMP) temperature microstructure profiler were deployed repeatedly from the Coot, with LISST-100C casts between each set of SCAMP profiles. Only the Coot LISST and SCAMP CTD data are presented here; analysis of the thermal dissipation rate data has been problematic. The different data types were analyzed individually and combined into depth–time contour plots using Surfer.

During the tidal cycle anchor stations, disaggregated size distributions of suspended sediment were evaluated by high volume pumping and filtering. Samples were collected at 1 m above the bottom, over both flood and ebb tides, using a submersible pump. The output of the pump was connected to three separate onboard filtration housings in parallel to enhance the speed of filtration, and immediately filtered through Millipore Durapore 0.65 μm membrane filters. Filters were wrapped in aluminum foil and stored on ice until returned to the laboratory. Sediment was removed from the filters via sonication. Fractional pipette grain size analysis[48] was performed on the combined material from all filters collected during each flood or ebb sampling period.

The Valeport settling tube, approximately 5 cm in diameter by 1 m long, was modified by constructing a flow-through water jacket around it. It was deployed horizontally in the water column at the desired depth and oriented into the flow by a vane. A messenger was sent to close the ends of the tube, which was then raised back to the surface, still in the horizontal. On deck, the tube was wrapped with reflective bubble wrap insulation and placed vertically into its stand, after which a hose running from a pump lowered to the sampling depth was connected to the water jacket. The combination of reflective insulation and flowing water jacket effectively eliminated internal circulations in the tube, one source of uncertainty in previous settling tube studies.[49] Samples were withdrawn from the bottom for TSS analysis at specified, geometrically increasing time intervals starting 2 min and ending 80 min after inversion. The sequence of bottom-withdrawal TSS values was analyzed using a spreadsheet implementation of the procedure of Owen,[47] similar to that described by Jones and Jago.[50] This procedure yielded the distribution of settling particle mass in specific settling velocity intervals. Settling speed data from ETM surveys in 1996 and 2001 were collected and analyzed using the same methods.

Questions have been raised about data from both bottom withdrawal settling tubes and LISSTs in the literature,[32,49,51–53] especially when used to characterize fine, flocculated sediment particles. For these reasons, and also because we hoped to be able to directly relate particle size and settling velocity, we developed a Video *In situ* Settling Tube Apparatus (VISTA) for use on the profiling rig (Figure 10.4). The VISTA used an on-deck pump to pull water through a tube attached to the profiling rig. The opening of the tube was directed into the flow by a fin. The pump pulled water into the mouth of the tube, through a 90° turn and up a vertical section of clear tubing at a flow rate approximating isokinetic sampling. The pump was run for 1 to 2 min at each depth to flush the settling tube, then valves at the top and bottom of the vertical section were triggered to trap a water sample and create a settling chamber. A PULNiX CCD underwater video camera was used to record images of the settling particles. The camera was mounted on the side of the settling tube with its faceplate about 5 mm from the side of the tube. The in-focus field of view in the center of the sampling tube was 8.3 mm high by 11.2 mm wide. Lighting was provided by a collimated underwater video light, shown in a sheet through the side of the tube that overlapped the focal plane of the camera. The camera output an analog signal that was recorded on Hi-8 tapes. An example of the image is shown in Figure 10.4.

For particle sizing, images were digitized and captured using the frame grabber software DVStill at a resolution of approximately 640 × 480 pixels. Selected frames were saved as bitmap files and analyzed using the Image Toolbox in MATLAB. The image processing technique converted the image to a 256 shade grayscale, sharpened it to enhance the edges of the particles, removed the background by use of a threshold filter, and then linearly enhanced the contrast to cover the range of the grayscale. Levels of sharpening and thresholding were adjusted depending on lighting conditions. The particles were identified using a Prewitt edge detector, and the final size and shape were determined using dilation and erosion functions. Equivalent particle diameters were calculated by taking the average of the minor and major axis lengths, and particle volumes were calculated using the equivalent diameters. Particles under the size of three pixels (approximately 30 μm) were not considered. Approximately

ten frames from each video clip were processed. All analyzed particle diameters and volumes were used to calculate the overall size distribution and D50 for comparison with simultaneously collected LISST-100C data, while individual particle diameters were used for comparisons to estimated floc settling speed.

Particle settling speeds were estimated using an *ExpertVision (EV) Motion Analysis* system. The EV Video Processor captured analog video data directly from the Hi-8 tapes, then created digitized outlines to facilitate particle tracking. The subsampled field of view was represented as a grid 256 pixels wide by 240 pixels tall. A distance scaling of 0.035 mm/pixel was used. The EV Motion Analysis software was used to calculate the vertical motion of particles. Due to the 90° turn at the tube's intake and rapid closure of the valves, some turbulence was created in the settling chamber. Small fluctuations due to ship motion were also present. Thus, it was necessary to estimate a background velocity by calculating the speeds of small particles that moved with the flow. Floc settling speeds were calculated by subtracting interpolated background vertical velocity from the vertical velocity of each large particle.

Relationships between particle size and particle settling speed were assessed by comparison with the floc fractal relationship defined by Hill[54] as

$$\frac{w_{sf}}{w_{sr}} = \left(\frac{d_f}{d_r}\right)^{D3-1} \tag{10.1}$$

where w_{sf}, d_f and w_{sr}, d_r are the settling speed and diameter of a floc and the smallest particle in the floc (the reference particle), respectively, and D3 is the fractal dimension. The settling speed of the reference particle is given by Stoke's equation:

$$w_{sr} = \frac{1}{18}\frac{g}{\nu}(s_r - 1){d_r}^2 \tag{10.2}$$

where g is the acceleration due to gravity, ν is the kinematic viscosity of the water, and s_r is the specific gravity of the reference particle. Defining $\beta = g(s_r - 1)/(18\nu)$, assuming $s_r = 2.65\ \mathrm{g\,cm^{-3}}$ and $\nu = 0.012\ \mathrm{cm^2\,sec^{-1}}$ and substituting (10.2) into (10.1), we obtain

$$w_{sf} = \beta {d_r}^{3-D3} {d_f}^{D3-1} \tag{10.3}$$

which was fit to the data in a least squares sense to obtain estimates of D3 and d_r.

Estimates of turbulent shear were made using data collected with a 10 MHz Sontek Acoustic Doppler Velocimeter (ADV) deployed on the profiling rig during the tidal cycle anchor station studies. The ADV on the profiling rig measured velocity in three dimensions in a single sampling volume (0.25 $\mathrm{cm^3}$), burst sampling 4096 samples at 10 Hz every 10 min. This allowed time for the profiling rig to be repositioned at the next depth between bursts. The ADV was mounted such that the sampling volume was at the same elevation as the LISST sampling volume and the intake for the VISTA. Vertical velocity spectra were used to estimate turbulent dissipation rate (ε) by the inertial subrange technique,[55,56] removing the (minimal) effects of ship motion with the technique developed by Gross et al.[57] for estimating dissipation in the presence of

wave motions. Small scale shear, γ, was calculated as $\gamma = (\varepsilon/\nu)^{1/2}[\text{sec}^{-1}]$, where ν is the kinematic viscosity.

Time series current velocity profiles were collected for the duration of each seasonal cruise using a 1,200 kHz Broadband Acoustic Doppler Current Profiler (ADCP) mounted in the hull of a surface buoy in a downward looking configuration. The ADCP buoy was deployed at 39° 22.098′ N, 76° 07.523′ W in approximately 11 m of water. The ADCP collected data at 5-min intervals, sampling 0.5-m bins through the water column starting at 1.56 m below the surface and extending to approximately 1 m above the seabed. For each sample, 120 water column pings were averaged, which gives an estimated standard deviation of the measured velocity of about 0.5 cm sec^{-1}. ADCP data was post-processed using MATLAB software, where all bad data points (including all data below 0.75 m above the seabed) were removed. North and east velocities were translated into along and cross-channel components, using a projected angle for the along channel direction of 230° T (ebb positive).

A microcosm erosion testing system was used to test the erodibility of bottom sediments collected using the Cape Henlopen Ocean Instruments multicorer. The erosion system consisted of two 10 cm Gust Microcosms,[58] which use a spinning disk with central suction to generate a controllable, nearly uniform shear stress. A Campbell Datalogger controlled the system and stored data. During erosion experiments, a sequence of increasing levels of shear stress was applied to undisturbed cores. The effluent from each Microcosm was passed through a turbidimeter and time series of turbidity were measured. The effluent was collected, filtered, and weighed to determine the actual mass eroded during each step, which was used to calibrate the turbidimeter. Erosion rate was subsequently calculated as the product of pumping rate and suspended sediment concentration, and the data were analyzed according to the formulation of Sanford and Maa.[59]

10.4 RESULTS

Disaggregated particle sizes of suspended sediment in upper Chesapeake Bay were very fine, consisting of either clays or fine silts (Table 10.1). The four pumped samples listed in Table 10.1 were all collected from just above the bottom at anchor during two of the seasonal cruises in 2002. No data are available from the October cruise because insufficient material was collected to run a standard gravimetric analysis. Slightly more coarse material ($d_{75} = 16\ \mu$m) appears to have been resuspended under strong tidal forcing, but over the weakest flood tide sampled, only clay particles smaller than 1 μm were in suspension. There were few apparent seasonal differences in disaggregated suspended particle size, with greater differences between sequential flood and ebb tides than between May and July.

In contrast to these very fine disaggregated particle size distributions, much of the material in suspension was packaged in large flocs. These particles were often visible to the naked eye in the settling tubes and erosion microcosm, and were even more apparent in the magnified video images from the VISTA (Figure 10.4). The flocs visible in Figure 10.4b, collected approximately 1.5 m above bottom during

TABLE 10.1
Disaggregated Particle Size Distributions from High-Volume Filtering 1 m Above Bottom During May and July 2002 Tidal Cycle Anchor Stations

Sample	Sampling Duration (h)	Total Mass (g)	d_{25} (μm)	d_{50} (μm)	d_{75} (μm)
May Flood (25 cm sec^{-1})	2.5	7.05	<1	<1	<1
May Ebb (45 cm sec^{-1})	6	35.78	<1	3	9
July Flood (75 cm sec^{-1})	2.5	28.32	<2	3	16
July Ebb (40 cm sec^{-1})	9	13.37	<2	<2	2

maximum flood resuspension on October 10, 2002, range in size from the limit of resolution of the video system (approximately 30 μm) to approximately 400 μm. Large flocs also dominated the LISST data (see below).

Encouragingly, the floc size estimates from the VISTA and LISST were reasonably similar. Figure 10.3b shows a comparison between the D50 estimates from the LISST and VISTA deployed on the profiling rig during the October 10, 2002 anchor station. The LISST size distributions have been adjusted by excluding particles below the resolution of the VISTA and too rare (large) to have at least a 1% probability of being observed by the VISTA, before calculation of D50. LISST D50 estimates are generally between 80% and 200% of the VISTA D50 estimates. The LISST and VISTA D50 estimates are significantly correlated ($r^2 = 0.37$) and the mean of the LISST estimates is significantly larger than the mean of the VISTA estimates (paired t-test, $p < 0.05$). Although it is possible that the LISST slightly overestimated D50, a more likely explanation is that the VISTA sampling procedure disrupted the largest, weakest flocs, and therefore resulted in a slight underestimation of D50 relative to the LISST. In either case, Figure 10.3b does not establish the absolute accuracy of either technique but lends considerable confidence to the use of both as reasonable estimators of *in situ* particle size.

Calibration of the transmissometer on the LISST to TSS sampled *in situ* was quite reasonable (Figure 10.3a), with r^2 values for the three linear fits shown ranging between 0.82 and 0.85. The scatter in the data are due to the facts that the suspended sediment samples were taken over a 70 km reach of the upper Chesapeake Bay over all depths and over a 1-week period, and that there is a certain amount of unavoidable error associated with collection and analysis of suspended sediment samples themselves. Differences in, or departures from, a linear relationship between optical transmission and TSS are most often attributed to changes in particle size,[60] with coarser particle sizes (and higher settling velocities) corresponding to a higher calibration slope (lower sensitivity). This was shown previously for the upper Chesapeake Bay by Sanford et al.,[6] who pointed out corresponding seasonal and interannual variabilities in transmissometer calibrations. In 2002, these calibration differences were less apparent. In particular, the calibrations for the May and October 2002

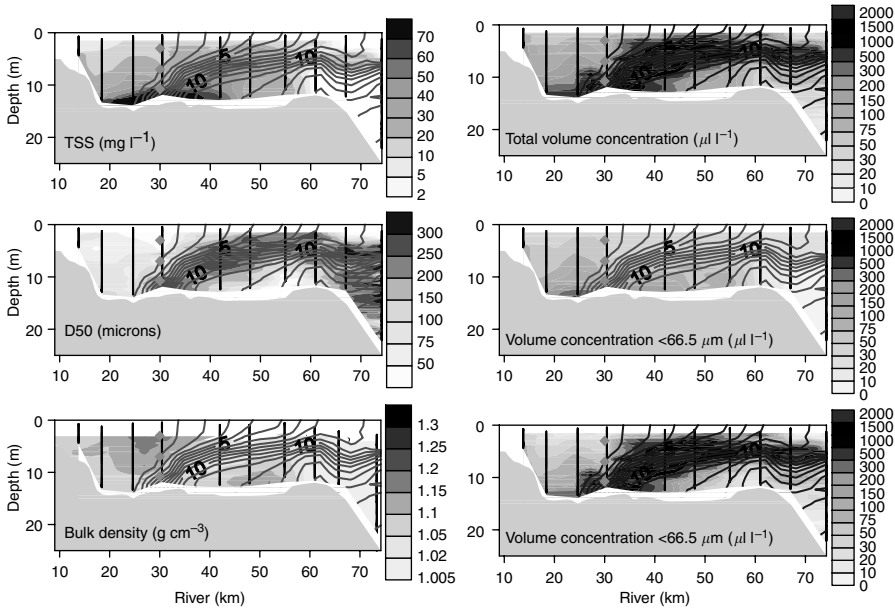

FIGURE 10.5 (**Color Figure 10.5 appears following page 236.**) Contour plots from LISST-100C data collected during an axial hydrographic survey on May 11, 2002 beginning at 9:45 and ending at 15:30 EDT. The survey was performed coincident with an ebb tide with currents of 60 cm sec^{-1} at the surface and 45 cm sec^{-1} near bottom. Diamonds indicate the location of 12 h anchor station occupied on May 10, 2002.

cruises were essentially identical, with the July calibration exhibiting a slightly higher slope.

Axial distributions of particle characteristics measured with the LISST on May 11, 2002 during a moderate ebb tide are shown in Figure 10.5. The salinity contours overlaid on each of the panels of Figure 10.5 provide a common reference frame, and illustrate several features of the particle distributions. May 2002 was wetter and delivered more sediment to the upper Bay than normal (Figure 10.2), in contrast to most of the rest of 2002, though this particular survey occurred before the largest pulse of fresh water inflow. As a result, the limit of salt intrusion was located at approximately km 25 and the water column was highly salt (hence density) stratified. A pronounced turbidity maximum was located near the limit of salt, with near-bottom TSS levels approximately 50 mg l^{-1} higher than background. Slightly elevated TSS levels were also apparent in the pycnocline stretching downstream from the limit of salt. Interestingly, this latter feature was not apparent in the data from the Sea Tech 5 cm pathlength transmissometer also located on the CTD frame (not used here). One of the most striking features of the LISST particle data was the high particle volume concentrations also concentrated in the pycnocline stretching downstream from the limit of salt. The only way that high volume concentrations can coincide with relatively lower TSS is if the particles are large, relatively watery flocs. This is confirmed in the D50 and ρ_b distributions, where it is apparent that a large population

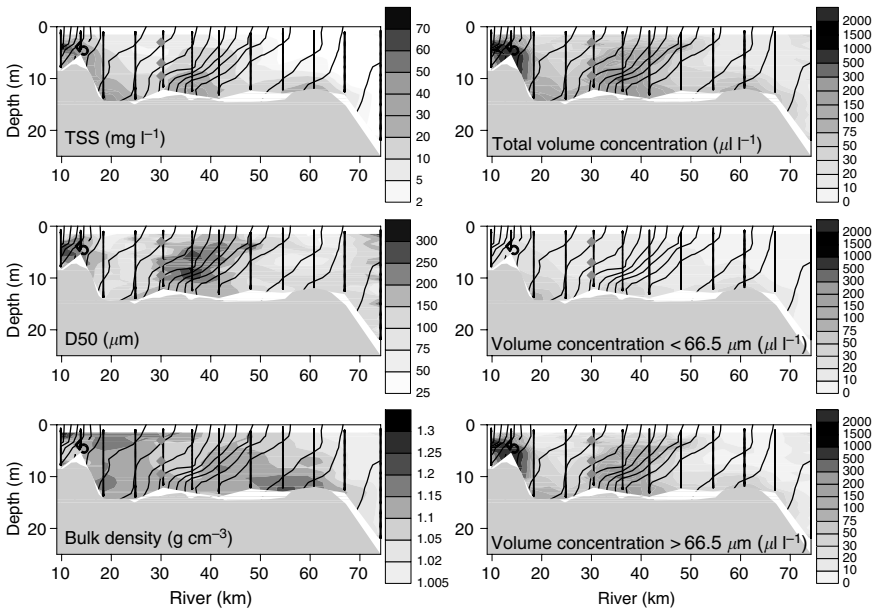

FIGURE 10.6 (**Color Figure 10.6 appears following page 236.**) Contour plots from LISST-100C data collected during an axial hydrographic survey on October 11, 2002 beginning at 8:30 and ending at 15:10 EDT. The survey was performed coincident with a flood tide of 30 cm sec^{-1}. Diamonds indicate the location of 12-h anchor station occupied on October 10, 2002.

of >200 μm, low bulk density particles made up this pycnocline feature. The turbidity maximum itself consisted of high concentrations of both large and small particles, though the median particle size at the center of the feature was >200 μm.

Axial distributions of particle characteristics measured with the LISST on October 11, 2002 during a weak flood tide are shown in Figure 10.6. October 2002 was an average month for flow, though sediment delivery was lower than average (Figure 10.2). However, this survey occurred just as the pulse of flow that made October an average month was beginning, after a long, very dry summer. Some possible indications of this pulse are the crowding of the isohalines and elevated TSS at approximately km 12. No completely fresh water was observed during this survey, and stratification was much weaker than during the May surveys. A weak turbidity maximum coincided with a near-bottom convergence in the axial salinity near km 35, with near-bottom TSS levels approximately 30 $mg\,l^{-1}$ higher than background. TSS concentrations were in general very low in upper Chesapeake Bay. A patch of relatively high particle volume concentration was concentrated in the pycnocline just downstream of this turbidity maximum, again coincident with large, low bulk density particles. Average particle bulk densities were generally higher than during the May survey (Figure 10.5), but remained far below the densities of solid, unflocculated particles.

Time-depth distributions of various physical data from an anchor station the day before the axial survey of Figure 10.6 are presented in Figure 10.7. The anchor

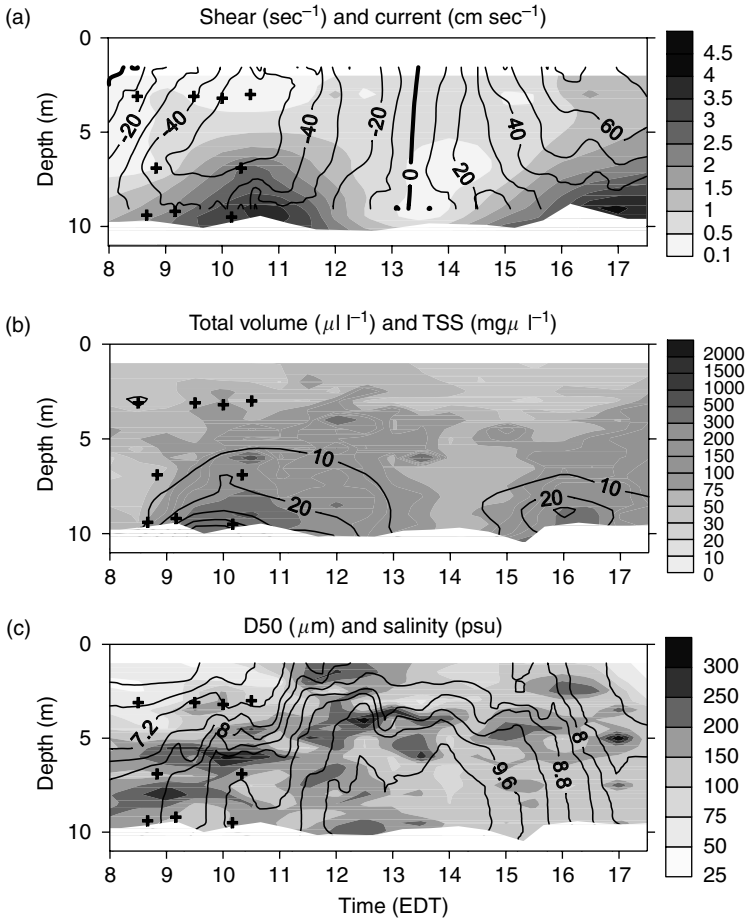

FIGURE 10.7 Contour plots of LISST-100C data collected at 12 h anchor station on October 10, 2002. The black plus symbols represent time and depth of video clips used to calculate particle size and settling velocity. In (a), the ADCP velocity is contoured and turbulent shear is shaded. In (b), TSS is contoured and Total Volume Concentration is shaded. In (c), salinity is contoured and D50 is shaded.

station was carried out in approximately 11 m of water just to the west of the shipping channel at approximately km 30 (Figure 10.1 and Figure 10.6). The observational period spanned moderately strong flood and ebb tides. The contours are based on a mix of underlying data resolution, ranging from 3 depth intervals at 0.5 to 1 h resolution for the turbulent shear and TSS data through 0.25 m by 0.5 h resolution for the volume concentration, D50, and salinity data to 0.25 m by 5 min resolution for the ADCP velocity contours. Many of the observed changes in the mid- and upper water column appear to be dominated by advection, as indicated most strongly by salinity. Comparing Figure 10.7 to Figure 10.6, it is apparent that the anchor station was located just upstream of a strong axial salinity convergence. This convergence was advected through the anchor station site during the flood tide and advected back out during the

ebb tide of the anchor station. The patch of large, high volume concentration particles in the pycnocline noted in Figure 10.6 advected with the salinity structure, with little apparent dynamical relationship to physical energy. More interesting was the change in near-bottom concentrations and particle sizes, especially during the flood tide. Both TSS and volume concentration maxima corresponded to maximal tidal velocities and turbulent shears, indicating local resuspension. Higher D50 values during the resuspension period indicate that much of the resuspended material consisted of large, robust flocs, in spite of the high turbulent shears (up to 3.5 sec^{-1}). However, maximum near-bottom D50 values occurred as the flood tide was decelerating and turbulent shear was decreasing, likely indicating the importance of local flocculation (or decreasing disaggregation).

Estimates of the space- and time-varying distributions of settling velocity derived from the LISST data of Figure 10.6 and Figure 10.7 are presented in Figure 10.8. These estimates were calculated using D50 and ρ_b estimated from the LISST and Stokes law (Equation 10.2). As such, they use an unusual mix of mass and volume weighted bulk parameters, such that their absolute validity is not clear. However, they are useful as an indication of potential variability in w_s, and also for comparison to other estimates of settling velocity below. Three results are apparent from these

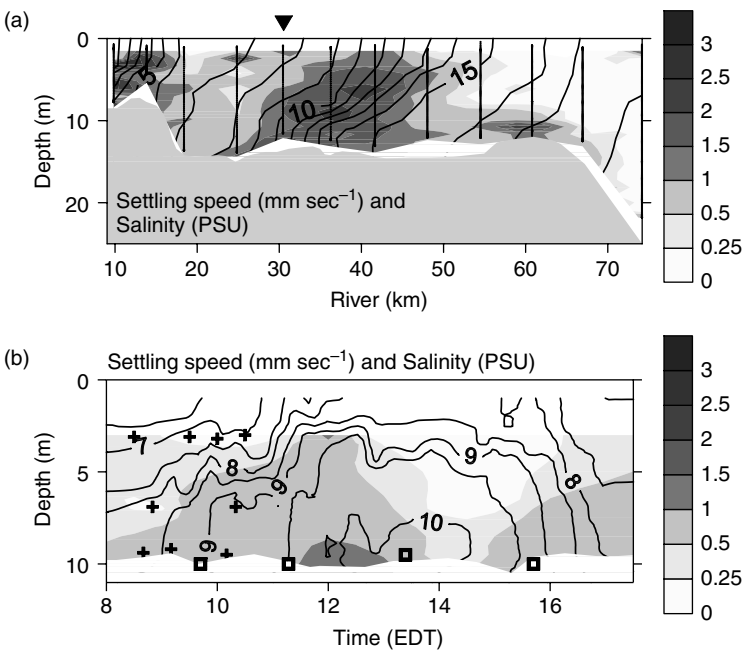

FIGURE 10.8 Contour plots of settling velocity (mm sec^{-1}) estimated from the LISST data presented in Figure 10.6 and Figure 10.7, using estimated D50 and bulk density and assuming Stokes settling. (a) Axial distribution of settling velocity on October 11, 2003 with salinity contours overlaid for reference. The inverted triangle shows the location of the anchor station on October 10, 2003. (b) Time series distribution of settling velocity during anchor station on October 10, 2003, with salinity contours overlaid for reference.

calculations. First, settling speeds in the vicinity of the turbidity maximum varied by an order of magnitude, in these plots between approximately 0.25 to 2.5 mm sec^{-1}, and the upper Bay appeared to be a very efficient trap for particles that settle in this range. Second, settling velocity was most clearly correlated with distributions of D50, though not perfectly because of its dependence on bulk density. Third, the highest settling speeds tended to occur at mid-depth or near-bottom and as the tide was decelerating toward slack.

Figure 10.9 summarizes the relationships between settling velocity and floc diameter derived from the VISTA, using data collected at the times and depths indicated by the + symbols in Figure 10.7 and Figure 10.8b. The regression equations noted in each panel are of the form of Equation (10.3), and are indicated by the heavy solid lines on each plot. Table 10.2 summarizes the VISTA data presented in this figure, and presents the fractal parameters derived from the regressions. Both mean settling velocity and floc size tended to increase with depth, significantly so for settling velocity (from 0.66 to 2.26 mm sec^{-1}) and marginally so for floc size (from 170 to 294 μm). Average bulk density derived from each pair of settling velocities and sizes remained nearly constant with depth at 1.05 to 1.06, similar to the LISST estimates in Figure 10.6. The fractal dimensions of the surface, middle, and bottom distributions were not significantly different, averaging 2.02. However, the reference particle size of the bottom regression (16 μm) was much greater than those of the middle (3.2 μm) and top (3.9 μm) regressions. Clearly, though there is significant scatter, a fractal description of the relationship between particle size and settling

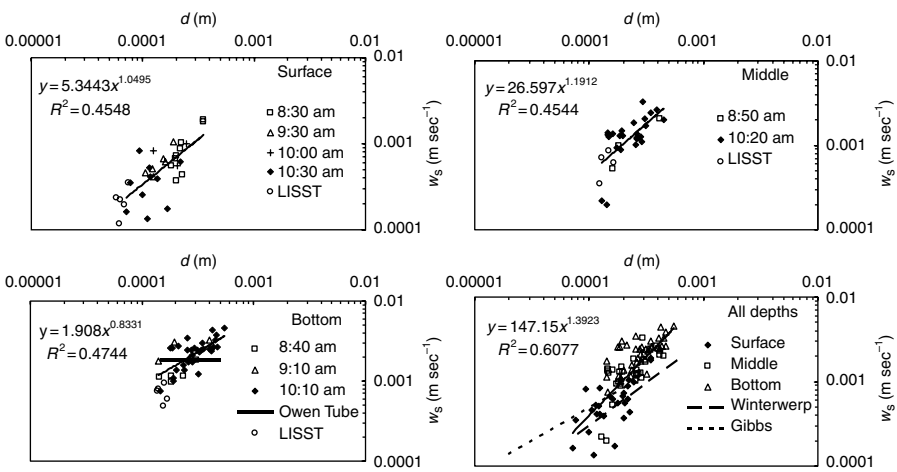

FIGURE 10.9 Plots of floc diameter vs settling speed as determined from image analysis of VISTA samples collected during the first 2 h of the tidal cycle anchor station on October 10, 2002: From (a) approximately 3 m depth, (b) approximately 7 m depth, (c) approximately 9.5 m depth, and (d) all depths together. Open squares represent simultaneous LISST estimates, Owen tube line represents Valeport settling tube sample, Winterwerp indicates fractal relationship for Ems estuary (see text), and Gibbs represents data collected in upper Chesapeake Bay in the early 1980s.[17]

TABLE 10.2
Depth-Stratified Summary of Particle Characteristics Determined from Analysis of VISTA Data Presented in Figure 10.9

Depth (m)	ws_ave (mm sec^{-1})	ws_std (mm sec^{-1})	d_ave (μm)	d_std (μm)	ρ_{bulk} (g cm^{-3})	D3	d_r (μm)
3	0.66[a]	±0.42	170[b]	±71	1.05	2.05	3.85
7	1.41[a]	±0.67	243	±86	1.05	2.19	3.15
9.5	2.26[a]	±0.91	294	±105	1.06	1.83	16.07
All	1.54	±0.99	243	±104	1.06	2.39	0.79

[a] Settling speeds at each depth are significantly different from settling speeds at the other depths ($p < 0.05$).
[b] Diameter at surface is significantly different from diameters at middle and bottom, which are not significantly different from each other ($p < 0.05$).

velocity explains much of their co-variability. It is notable that combining the data from all three depths resulted in an artificially high estimate of the fractal dimension and an artificially low estimate of the reference particle size, reinforcing the idea that these (especially the bottom) represented distinct particle pools.

Other data are included in Figure 10.9 for comparison. The LISST estimates are from the same locations and times as the VISTA data, calculated in the same way as the data presented in Figure 10.8b. While they are consistent with the fractal relationships, the LISST estimates were at the low end of the scale for both particle size and settling velocity. This is most likely due to the fact that the VISTA estimates were for large, visible settling flocs, while the LISST estimates incorporated the entire spectrum of particles and thus are strongly affected by the fine, slow settling fraction. The Valeport tube estimate of w_{s50} indicated in Figure 10.9c (1.9 mm sec^{-1}) is from a sample mid-way between the second and third VISTA bottom samples, as indicated in Figure 10.8. It is quite encouraging that it is in the center of the cluster of VISTA estimates. The second and third Valeport tube estimates were very similar, but the last sample of the anchor station contained significantly more material settling at very high speeds (>7 mm sec^{-1}). The long-dash line in the "all depths" panel corresponds to the reference particle size and fractal dimension quoted for the Ems estuary flocs by Winterwerp[61]; it is reproduced here because of its striking similarity to our surface layer data. Finally, the short-dash line in the "all depths" panel corresponds to the Chesapeake ETM data collected by Gibbs.[17] Clearly, though the basic trends are similar to our data (with a slightly lower fractal dimension), the ranges of settling speeds and particle sizes are considerably lower in Gibbs' data. This is likely because the sampling techniques available at the time disrupted the largest, fastest settling flocs.

A summary of all of the Valeport tube data we collected in upper Chesapeake Bay during 1996, 2001, and 2002 is presented in Figure 10.10. Some arguments against the use of static bottom withdrawal settling tubes[51] have focused on the possibility of biases induced by flocculation in the tube itself due to differential settling, which would result in the previously reported strong correlation between settling velocity

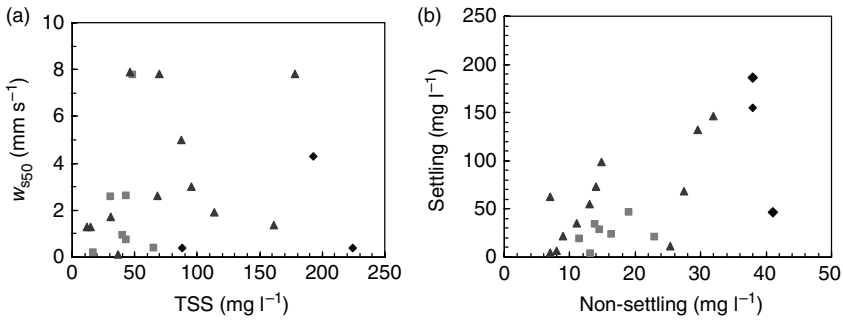

FIGURE 10.10 Valeport settling tube results from 1996 (♦), 2001 (■), and 2002 (▲). In (a) the median settling speed of the settling particles is plotted vs TSS, and in (b) concentration of nonsettling and settling fractions are compared.

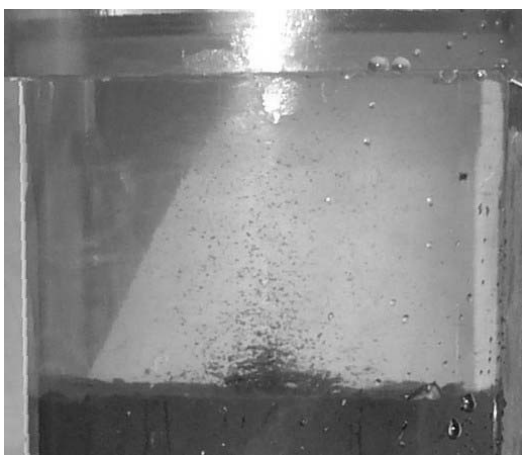

FIGURE 10.11 Large flocs remained intact during erosion of this core collected in the Upper Chesapeake Bay in May 2001. This photo was taken during an intermediate shear stress step of an erosion experiment, at an applied stress of approximately 0.15 Pa. The core tube is 10 cm in diameter.

and TSS.[62] However, there is no apparent relationship between settling velocity and particle concentration in Figure 10.10a; very high settling speeds occurred at relatively low concentrations, and relatively low speeds occurred at high concentrations. There is, however, a reasonable correlation between settling concentration (defined as all material collected before the last bottom withdrawal sample) and nonsettling concentration. In particular, the maximum settling concentration seems to be approximately five times the nonsettling concentration. This is consistent with either flocculation of the nonsettling population to form the settling population, or resuspension of large flocs and their consequent disaggregation into the nonsettling population, or both.

Figure 10.11 is a photograph taken during an erosion experiment on a core collected in upper Chesapeake Bay in May 2001, at an intermediate applied shear stress. This

photograph confirms that direct resuspension of large flocs occurs from the surface of the sediment bed. The diameter of the core tube is 10 cm, such that the visible flocs collecting near the center of the core and resuspending upward are at least several hundred micrometers in size. Visual observations of this and many similar erosion experiments have indicated that these flocs move initially as bedload, followed by resuspension at slightly higher stresses.

10.5 DISCUSSION

The data presented here represent only a preliminary look at the data set generated during our study of the dynamics of the Chesapeake Bay ETM, but they suggest a scenario in which dynamically variable flocculation and disaggregation are integral aspects of particle dynamics, particle trapping, and ecosystem function in this region. Based on this data and on additional analysis of the larger data set, we have formulated a conceptual model of ETM particle dynamics, presented in Figure 10.12. This model serves both to organize the data presented here and as a hypothesis to be tested through future data collection and analysis.

According to this model, an assemblage of inorganic and organic particles enters the estuary as smaller flocs and primary particles with the inflowing freshwater, approaches the ETM, and is swept up and over the leading edge of the salt front. Salinity increases due to mixing, enhancing particle stickiness and aggregation due to electrochemical flocculation, phytoplankton cell lysis, sloppy feeding by zooplankton, and bacterial production. In surface waters, floc size is limited by sinking losses and turbulent disaggregation. Large flocs that sink into the low energy pycnocline

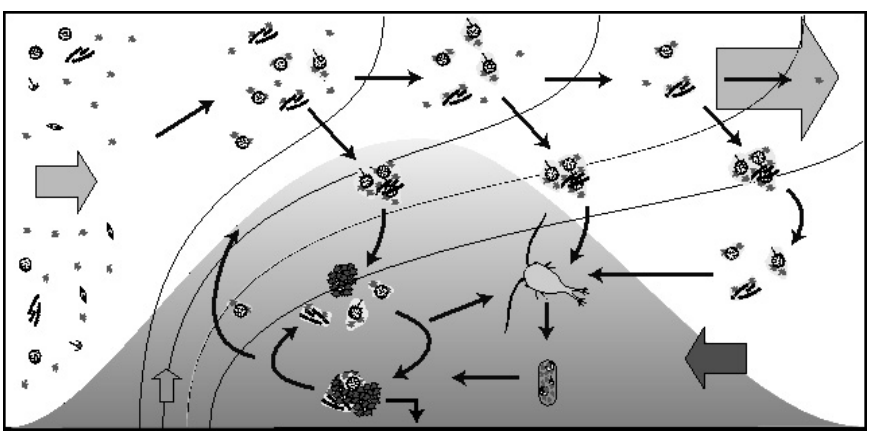

FIGURE 10.12 Conceptual model of particle dynamics in the Chesapeake Bay ETM. See text for discussion. Wide arrows indicate residual current velocities, averaged over tidal cycles. Narrow arrows indicate direction of particle transport. Key: relatively unflocculated inorganic (▪) and organic particles (); ETM (gray dome-shaped area); salt front (black contour lines); particle stickiness (shading); flocculated particles (); robust resuspended aggregates (); zooplankton (); fecal pellets ().

are preserved by the lack of turbulent shear and accumulate due to reduced settling speeds as they encounter denser water; they may also continue to grow through flocculation due to differential settling. Flocs that sink below the pycnocline are partially disaggregated and transported toward the ETM convergence by the estuarine circulation. Within the ETM convergence, more robust resuspended flocs/aggregates interact with fresher particles, carrying some of them to the bottom. Zooplankton also feed on organic material and bacteria in the flocs and produce relatively robust fecal pellets with high settling speeds. An unknown number of relatively fine particles is recycled from the ETM zone into surface or pycnocline waters. Although some finer particles wash through the ETM under high flow or unfavorable flocculation conditions, most flocculated particles are trapped. In the Chesapeake ETM, these trapped particles are eventually buried due to high sedimentation rates, though they may be removed later by dredging. The schematic in Figure 10.12 is presented in the context of an ETM at the limit of salt intrusion (Figure 10.5), but it is also applicable with small modification to an ETM at a local axial convergence (Figure 10.6). The modification is primarily that changes in particle stickiness might not play as strong a role, but changes in turbulence, particle size, and particle concentration associated with the frontal zone should be just as important as at the limit of salt.

There are several differences between this model and the traditional idea that flocculation occurs once through an increase in electrochemical attraction when freshwater particles first encounter salt. One-time flocculation cannot explain the existence of the observed large flocs in the pycnocline, with finer particles both above and below, nor can it explain the concentration of both large and small particles near bottom in the center of the ETM. These phenomena imply active exchange between large and small floc populations, at least at certain times and places. The precise mechanisms that control flocculation and disaggregation in the Chesapeake Bay ETM cannot be distinguished at this time, but it is quite likely that they vary in time and space. It is also quite likely that an equilibrium flocculation state is seldom reached in this dynamic environment, especially near the bottom within the ETM. This is because the time scales of flocculation and disaggregation are most likely equivalent to or longer than the time scales of tidal variability in near-bottom turbulence, particle concentration, and large aggregate resuspension/deposition.[30,61] Finally, traditional thinking does not adequately allow for the influences of biogenic stickiness and fecal pellet production, which are likely to be significant factors in ETM particle dynamics. For example, Sanford et al.[6] reported a seasonal variability in settling velocity that was repeated, albeit without exactly the same timing, in the settling tube data collected in 2001 and 2002. This is in spite of the lack of seasonal variability in primary particle size (Table 10.1).

Fractal scaling of the relationship between floc size and settling velocity (Equation 10.1) has been applied to particles from many different aquatic environments in recent years,[26,34,54,63,64] but this was the first attempt that the authors have made to apply it to Chesapeake Bay particles. The novelty of the analysis for us was because of technology limitation; development of the VISTA eliminated that barrier, and we hope to pursue improvements to the video technique and accompanying analyses in the future. While the fractal representations presented here only accounted for

approximately half of the observed variability, fractal scaling nevertheless presents itself as a powerful tool for summarizing the characteristics of estuarine particles in two parameters, facilitating intercomparison and modeling. For example, the agreement between the Ems fractal relationship quoted by Winterwerp[61] and the fractal relationship of our surface water samples shown in Figure 10.9 suggests a similarity that is currently leading us to apply Winterwerp's flocculation model and parameterizations to the Chesapeake Bay ETM. Another candidate model is that of Jackson,[27,65] who also bases his formulation explicitly on fractal scaling. Thus, it behooves estuarine particle researchers to identify the fractal scales that describe their systems, along with sources of variability in those scales. Dyer and Manning,[34] for example, have characterized the influences of different mechanisms of floc formation and destruction on fractal properties of the resulting particle populations. This approach may help to diagnose sources and mechanisms of flocculation in other environments through comparison of fractal scales.

In this chapter, we have shown that both the fractal scales and the dynamic variability of near bottom, resuspended particles in the Chesapeake ETM separate them from particles further up in the water column. In particular, it appears that direct resuspension of relatively robust large flocs is the rule rather than the exception, but that a combination of simple settling of these same flocs along with interactions with other particles controls deposition. This same phenomena of direct resuspension of large flocs has also been observed on the continental margin by Thomsen and Gust[66] and in lower Chesapeake Bay by Fugate and Friedrichs,[36] both observations from low to moderate energy environments with active benthos. It is in direct opposition to the expectation that high levels of shear stress should erode primary particles only, and/or that high turbulent shears in the bottom boundary layer should immediately destroy large flocs. In fact, Fugate and Friedrichs found that resuspended floc sizes in the bottom boundary layer of a more energetic and turbid, but less biologically active estuary were governed by the expected inverse relationship between local turbulent shear and floc size. Thus, the presence of directly resuspended large flocs/aggregates may indicate the dominance of biogenic particle packaging. Alternately, it may represent a threshold of turbulent energy below which resuspended flocs survive and above which disaggregation occurs[30]; this threshold is likely specific to the strength of the flocs in question. The distinction may not be important, since biological domination of the sediment–water interface may be inversely correlated with the level of physical energy and sediment mixing.[67]

Ultimately, of course, fine sediment transport is much more influenced by settling velocity than it is by particle size, such that knowing particle size alone is of limited utility. New techniques such as the LISST and *in situ* macro-photography have made it much easier to determine distributions of particle size, but measurement of settling velocity and its variability is still difficult. Readily available techniques such as the Valeport settling tube have been legitimately questioned, while specialized, more accurate video settling techniques are limited in availability and require painstaking analysis. That is why defining relationships between settling speed and particle size and understanding how these relationships respond to environmental variability are so important. It is also why intercomparison and standardization of particle size and settling speed measurement techniques[32,33] are critical.

We have presented and compared two methods for estimating particle size, and three methods for estimating settling speed, with generally encouraging results. The VISTA video technique is as close to a standard as we could achieve, though it needs refinement. In particular, we need to increase resolution and further reduce the potential for floc breakup during sampling and the presence of background motion inside the closed tube. The reasonable agreement between the Valeport settling tube and VISTA settling speed estimates is quite encouraging, given the history of problems with other bottom withdrawal settling tube measurements noted above. This may be due to several factors specific to our implementation of the technique, including almost always sampling the pool of tidally resuspended flocs (i.e., break-up resistant) very near the bottom, sampling low enough TSS concentrations that interactions between particles were negligible, and carefully insulating the tube from external temperature fluctuations. This echos the findings of Dyer et al.,[32] who concluded that adopting well-controlled protocols for settling tubes improved the consistency of results. An attractive feature of bottom-withdrawal settling tubes in general is that they also allow investigation of the biogeochemical characteristics of particles segregated by settling speed. Finally, we have explored a simple technique using calibrated LISST transmissometer and volume concentration data to estimate the variability of settling speed. The results are encouraging, though slightly slower than other measurements. They should be regarded as tentative but deserving of further study.

ACKNOWLEDGMENTS

We are grateful to the captains and crews of the RV Cape Henlopen and the RV Coot for their invaluable assistance in the field, and to the workshop organizers for inviting this chapter. This research was supported by Award No. OCE-0002543 from the U.S. National Science Foundation Division of Ocean Sciences and the Maryland Sea Grant NSF Research Experiences for Undergraduates program. UMCES Contribution No. 3597.

REFERENCES

1. North, E.W. and Houde, E.D., Retention of white perch and striped bass larvae: Biological–physical interactions in Chesapeake Bay estuarine turbidity maximum, *Estuaries* 24(5), 756–769, 2001.
2. Dauvin, J.C. and Dodson, J.J., Relationship between feeding incidence and vertical and longitudinal distribution of rainbow smelt larvae (Osmerus mordax) in a turbid well-mixed estuary, *Marine ecology progress series. Oldendorf* (*Mar. Ecol.* (*Prog. Ser.*)) 60(1–2), 1–12, 1990.
3. Kimmerer, W.J., Physical, biological, and management responses to variable freshwater flow into the San Francisco estuary, *Estuaries* 25(6B), 1275–1290, 2002.
4. Roman, M.R., Holliday, D.V., and Sanford, L.P., Temporal and spatial patterns of zooplankton in the Chesapeake Bay turbidity maximum, *Marine Ecology Progress Series* 213, 215–227, 2001.

5. Kimmerer, W.J., Burau, J.R., and Bennett, W.A., Tidally oriented vertical migration and position maintenance of zooplankton in a temperate estuary, *Limnology and Oceanography* 43(7), 1697–1709, 1998.
6. Sanford, L.P., Suttles, S.E., and Halka, J.P., Reconsidering the physics of the Chesapeake Bay estuarine turbidity maximum, *Estuaries* 24(5), 655–669, 2001.
7. Goosen, N.K., Kromkamp, J., Peene, J., Rijswijk, P.v., and Breugel, P.v., Bacterial and phytoplankton production in the maximum turbidity zone of three European estuaries: the Elbe, Westerschelde and Gironde, *Journal of Marine Systems* 22(2–3), 151–171, 1999.
8. Zabawa, C.F., Microstructure of agglomerated suspended sediments in northern Chesapeake Bay Estuary, *Science* 202(4363), 49–51, 1978.
9. Kranck, K., Dynamics and distribution of suspended particulate matter in the St. Lawrence Estuary, *Naturaliste Canadien* 106(1), 163–173, 1979.
10. Krone, R.B., Aggregation of suspended particles in estuaries, in *Estuarine Transport Processes*, Kjerfve, B.J., Ed., University of South Carolina Press, Columbia, SC, pp 177–190, 1978.
11. Krone, R.B., Sedimentation in the San Francisco Bay system, in *San Francisco Bay: The Urbanized Estuary Pacific Division*, AAAS, San Francisco, pp 85–96, 1979.
12. Einstein, H.A. and Krone, R.B., Experiments to determine modes of cohesive sediment transport in salt water, *Journal of Geophysical Research* 67(4), 1451–1461, 1962.
13. Schubel, J.R., Turbidity maximum of the Northern Chesapeake Bay, *Science* 161, 1013–1015, 1968.
14. Schubel, J.R. and Biggs, R.B., Distribution of Seston in Upper Chesapeake Bay, *Chesapeake Science* 10(1), 18–23, 1969.
15. Schubel, J.R., Tidal variation of the size distribution of suspended sediment at a station in the Chesapeake Bay turbidity maximum, *Netherlands Journal of Sea Research* 5(2), 252–266, 1971.
16. Schubel, J.R. and Kana, T.W., Agglomeration of fine-grained suspended sediment in Northern Chesapeake Bay, *Powder Technology* 6, 9–16, 1972.
17. Gibbs, R.J., Estuarine flocs: their size, settling velocity and density, *Journal of Geophysical Research-Oceans* 90(NC2), 3249–3251, 1985.
18. Sanford, L.P., Panageotou, W., and Halka, J.P., Tidal resuspension of sediments in northern Chesapeake Bay, *Marine Geology* 97(1–2), 87–103, 1991.
19. Sanford, L.P. and Halka, J.P., Assessing the paradigm of mutually exclusive erosion and deposition of mud, with examples from upper Chesapeake Bay, *Marine Geology* 114(1–2), 37–57, 1993.
20. Sanford, L.P., Wave-forced resuspension of Upper Chesapeake Bay Muds, *Estuaries* 17(1B), 148–165, 1994.
21. Sanford, L.P. and Chang, M.-L., The bottom boundary condition for suspended sediment deposition, *Journal of Coastal Research* Special Issue 25, 3–17, 1997.
22. Alldredge, A.L., In situ collection and laboratory analysis of marine snow and large pecal pellets, in *Marine Particles: Analysis and Characterization*, Hurd, D.C. and Spencer, D.W., Eds, American Geophysical Union, Washington, D.C, pp 43–46, 1991.
23. MacIntyre, S., Alldredge, A.L., and Gotshalk, C.C., Accumulation of marine snow at density discontinuities in the water column, *Limnology and Oceanography* 40(3), 449–468, 1995.
24. Kiorboe, T., Hansen, J.L.S., Alldredge, A.L., Jackson, G.A., Passow, U., Dam, H.G., Drapeau, D.T., Waite, A., and Garcia, C.M., Sedimentation of phytoplankton during a

diatom bloom: rates and mechanisms, *Journal of Marine Research* 54(6), 1123–1148, 1996.
25. Jackson, G.A., Maffione, R., Costello, D.K., Alldredge, A.L., Logan, B.E., and Dam, H.G., Particle size spectra between 1 μm and 1 cm at Monterey Bay determined using multiple instruments (vol. 44, p. 1739, 1997), *Deep-Sea Research Part I-Oceanographic Research Papers* 45(9), 1575–1575, 1998.
26. Jackson, G.A. and Burd, A.B., Aggregation in the marine environment, *Environmental Science and Technology* 32(19), 2805–2814, 1998.
27. Jackson, G.A., Effect of coagulation on a model planktonic food web, *Deep-Sea Research Part I-Oceanographic Research Papers* 48(1), 95–123, 2001.
28. Hill, P.S., Sherwood, C.R., Sternberg, R.W., and Nowell, A.R. M., In-situ measurements of particle settling velocity on the Northern California Continental-Shelf, *Continental Shelf Research* 14(10–11), 1123–1137, 1994.
29. Hill, P.S., Milligan, T.G., and Geyer, W.R., Controls on effective settling velocity of suspended sediment in the Eel River flood plume, *Continental Shelf Research* 20(16), 2095–2111, 2000.
30. Hill, P.S., Voulgaris, G., and Trowbridge, J.H., Controls on floc size in a continental shelf bottom boundary layer, *Journal of Geophysical Research-Oceans* 106(C5), 9543–9549, 2001.
31. Fennessy, M.J., Dyer, K.R., and Huntley, D.A., Size and settling velocity distributions of flocs in the Tamar Estuary during a tidal cycle, *Netherlands Journal of Aquatic Ecology* 28(3–4), 275–282, 1994.
32. Dyer, K.R., Cornelisse, J., Dearnaley, M.P., Fennessy, M.J., Jones, S.E., Kappenberg, J., McCave, I.N., Pejrup, M., Puls, W., vanLeussen, W., and Wolfstein, K., A comparison of in situ techniques for estuarine floc settling velocity measurements, *Journal of Sea Research* 36(1–2), 15–29, 1996.
33. Eisma, D., Dyer, K.R., and van Leussen, W., The in situ determination of the settling velocities of suspended fine-grained sediment — a review, in *Cohesive Sediments*, Burt, N., Parker, R., and Watts, J., Eds, John Wiley & Sons, New York, pp 17–44, 1997.
34. Dyer, K.R. and Manning, A.J., Observation of the size, settling velocity and effective density of flocs, and their fractal dimensions, *Journal of Sea Research* 41(1–2), 87–95, 1999.
35. Kranck, K. and Milligan, T.G., Characteristics of suspended particles at an 11-hour anchor station in San Francisco Bay, California, *Journal of Geophysical Research* 97(C7), 11373–11382, 1992.
36. Fugate, D.C. and Friedrichs, C.T., Controls on suspended aggregate size in partially mixed estuaries, *Estuarine Coastal and Shelf Science* 58(2), 389–404, 2003.
37. Cronin, W.B., *Volumetric, Areal, and Tidal Statistics of the Chesapeake Bay Estuary and Its Tributaries*, The Chesapeake Bay Institute of the Johns Hopkins University, Baltimore, MD, 1971.
38. Browne, D.R. and Fisher, C.W., *Tide and Tidal Currents in the Chesapeake Bay* NOAA, Rockville, MD, 1988.
39. Elliott, A.J., Wang, D.P., and Pritchard, D.W., The circulation near the head of Chesapeake Bay, 36(4), 643–655, 1978.
40. North, E.W., Chao, S.-Y., Sanford, L.P., and Hood, R.R., The Influence of Wind and River Pulses on an Estuarine Turbidity Maximum: Numerical Studies and Field Observations, *Estuaries* 27(1), 132–146, 2004.
41. Biggs, R.B., Sources and distribution of suspended sediment in Northern Chesapeake Bay, *Marine Geology* 9(3), 187–201, 1970.

42. Cronin, T.M., Sanford, L.P., Langland, M.L., Willard, D., and Saenger, C., Chapter 6: Estuarine sediment transport, deposition, and sedimentation, in *A Summary Report of Sediment Processes in Chesapeake Bay and Watershed, Water Resources Investigations Report 03-4123*, Cronin, T.M., Langland, M.L., and Phillips, S., Eds, U.S. Geological Survey, New Cumberland, Pennsylvania, pp 129–160, 2003.
43. Officer, C.B., Lynch, D.R., Setlock, G.H., and Helz, G.R., Recent sedimentation rates in Chesapeake Bay, in *The Estuary as a Filter*, Kennedy, V.S. Ed., Academic Press, pp 131–157, 1984.
44. Schubel, J.R., Sedimentation in the upper reaches of the Chesapeake Bay, in *Estuaries and Estuarine Sedimentation* American Geological Institute, Washington, DC, pp VII1–29, 1971.
45. Yochum, S.E., Report No. Water Resources Investigations Report 00–4156, 2000.
46. Agrawal, Y.C. and Pottsmith, H.C., Instruments for particle size and settling velocity observations in sediment transport, *Marine Geology* 168(1–4), 89–114, 2000.
47. Owen, M.W., *Determination of the Settling Velocities of Cohesive Muds*, Hydraulics Research, Wallingford, 1976.
48. Komar, P.D. and Cui, B., The analysis of grain-size measurements by sieving and settling tube techniques, *Journal of Sedimentary Petrology* 54, 603–614, 1984.
49. Dearnaley, M.P., Direct measurement of settling velocities in the Owen Tube: a comparison with gravimetric analysis, in *Cohesive Sediments*, Parker, W.R., Parker, R., and Watts, J. Eds, John Wiley & Sons, New York, pp 75–85, 1997.
50. Jones, S.E. and Jago, C.F., Determination of settling velocity in the Elbe estuary using QUISSET tubes, *Journal of Sea Research* 36(1–2), 63–67, 1996.
51. Hill, P.S. and Milligan, T.G., Suspicions about settling columns, in *Coastal Ocean Processes Symposium: A Tribute to William D. Grant*, Woods Hole Oceanographic Institute, Woods Hole, MA, WHOI-99-04, pp 107–110, 1998.
52. Gartner, J.W., Cheng, R.T., Wang, P.F., and Richter, K., Laboratory and field evaluations of the LISST-100 instrument for suspended particle size determinations, *Marine Geology* 175(1–4), 199–219, 2001.
53. Traykovski, P., Latter, R.J., and Irish, J.D., A laboratory evaluation of the laser in situ scattering and transmissometry instrument using natural sediments, *Marine Geology* 159(1–4), 355–367, 1999.
54. Hill, P.S. and McCave, I.N., Suspended Particle Transport In Benthic Boundary Layers, in *The Bentic Boundary Layer*, Boudreau, B.P.J., Bo Barker Oxford University Press, New York, pp. 78–103.
55. Terray, E.A., Donelan, M.A., Agrawal, Y.C., Drennan, W.M., Kahma, K.K., Williams, I.I.I., AJ, Hwang, P.A., and Kitaigorodskii, S.A., Estimates of kinetic energy dissipation under breaking waves, *Journal of Physical Oceanography* 26(5), 792–807, 1996.
56. Sanford, L.P., Turbulent mixing in experimental ecosystems, *Marine Ecology Progress Series* 161, 265–293, 1997.
57. Gross, T.F., Williams, A.J., and Terray, E.A., Bottom boundary layer spectral dissipation estimates in the presence of wave motions, *Continental Shelf Research* 14 (10/11), 1239–1256, 1994.
58. Gust, G. and Mueller, V., Interfacial hydrodynamics and entrainment functions of currently used erosion devices, in *Cohesive Sediments*, Burt, N., Parker, W.R., and Watts, J. Eds, John Wiley & Sons, New York, pp 149–174, 1997.
59. Sanford, L.P. and Maa, J.P.-Y., A unified erosion formulation for fine sediments, *Marine Geology* 179(1–2), 9–23, 2001.

60. Gardner, W.D., Biscaye, P.E., Zaneveld, R.V., and Richardson, M.J., Calibration and comparison of the LDGO nephelometer and the OSU transmissometer on the Nova Scotian Rise, *Marine Geology* 66(1–4), 323–344, 1985.
61. Winterwerp, J.C., On the flocculation and settling velocity of estuarine mud, *Continental Shelf Research* 22(9), 1339–1360, 2002.
62. Burt, T.N., Field settling velocities of estuary muds, in *Estuarine Cohesive Sediment Dynamics*, Mehta, A.J. Ed., Springer-Verlag, Berlin, Heidelberg, New York, Tokyo, pp 126–150, 1986.
63. Manning, A.J. and Dyer, K.R., A laboratory examination of floc characteristics with regard to turbulent shearing, *Marine Geology* 160(1–2), 147–170, 1999.
64. Winterwerp, J.C., A simple model for turbulence induced flocculation of cohesive sediment, *Journal of Hydraulic Research* 36(3), 309–326, 1998.
65. Jackson, G.A., Using fractal scaling and two-dimensional particle size spectra to calculate coagulation rates for heterogeneous systems, *Journal of Colloid and Interface Science* 202(1), 20–29, 1998.
66. Thomsen, L. and Gust, G., Sediment erosion thresholds and characteristics of resuspended aggregates on the Western European continental margin, *Deep-Sea Research Part I-Oceanographic Research Papers* 47(10), 1881–1897, 2000.
67. Dellapenna, T.M., Kuehl, S.A., and Schaffner, L.C., Sea-bed mixing and particle residence times in biologically and physically dominated estuarine systems: a comparison of lower Chesapeake Bay and the York River subestuary, *Estuarine Coastal and Shelf Science* 46(6), 777–795, 1998.

11 Organic Rich Aggregates in the Ocean: Formation, Transport Behavior, and Biochemical Composition

Laurenz Thomsen

CONTENTS

11.1 INTRODUCTION

The biogeochemical significance of organic rich aggregates (marine snow) in the vertical flux of organic matter into the oceans' interior and sea floor is widely acknowledged.[1,2] The aggregates, which form during phytoplankton blooms and, to a lesser extent, by the resuspension of benthic biofilms, are a primary source of marine snow.[3] A considerable part of the aquatic primary production is removed from the surface through processes of particle aggregation and sedimentation.[4–6] These aggregates are the most important components of the organic matter flux to the deep sea[7] and appear to be hotspots of heterotrophic activity in the water column, being an important carbon source for free-living bacteria throughout their descent.[8] After sedimentation and during an extended period of resuspension loops, almost all of the remaining carbon is then remineralized. Nevertheless, a part of this organic matter is too refractory to be recycled, thus becoming buried in ocean sediments, sequestering carbon and so influencing atmospheric carbon dioxide concentrations.[9,10] This chapter will concentrate on the fate of organic aggregates in the size range of tens to

1-56670-615-7/05/$0.00+$1.50

thousands of micrometers, their production and descent through the water column as well as their residence and further modification within the benthic boundary layer. The term "benthic boundary layer" (BBL) is used for the water layers above the sediments although in sedimentological/physical-oceanography terminology "bottom boundary layer" would be the right phrase to use. Most examples will be given from continental margin studies. Continental margins can be defined as the region between the upper limit of the tidal range and the base of the continental slope. The burial of aggregate-associated organic matter in continental margin sediments is directly linked to the global cycles of carbon over geologic time.[11] Although continental margins account only for ≈15% of total ocean area and 25% of total ocean primary production, today more than 90% of all organic carbon burial occurs in sediments built up by particle deposition on continental shelves, slopes, and in deltas.[12] In this whole chapter, useful new references are predominantly cited which lead the interested reader to important previous work on the topic.

11.2 FORMATION OF ORGANIC RICH AGGREGATES

In their review of the microbial ecology of organic aggregates, Simon et al. gave an overview of the present knowledge of macroscopic organic aggregates (>500 μm).[5] These macroaggregates are heavily colonized by bacteria and other heterotrophic microbes and greatly enriched in organic and inorganic nutrients as compared to the surrounding water. The authors point out that during the last 15 years, many studies have been carried out to examine the various aspects of the formation of aggregates, their microbial colonization and decomposition, nutrient recycling, and their significance for the sinking flux. The significance of aggregate-associated microbial processes as key processes and also for the overall decomposition and flux of organic matter varies greatly among limnetic and oceanic systems, and is affected by the total amount of suspended particulate matter. A conclusion from these studies is that the significance of bacteria for the formation and decomposition of aggregates appears to be much greater than previously estimated. For a better understanding of the functioning of aquatic ecosystems it is of great importance to include aggregate-associated processes in ecosystem modeling approaches. Knoll et al. studied the early formation and bacterial colonization of diatom microaggregates (<150 μm) during the phytoplankton spring bloom and showed that these are colonized by bacterial populations that differ from those in the surrounding water.[13] They conclude that the bacterial community on aggregates develops largely from seeds on their precursor microaggregates.

Theoretical analyses of particle coagulation processes predict that aggregate formation depends on the probability of particle collision and on the efficiency with which two particles that collide stick together afterwards (stickiness).[14,15] The former is a function of particle concentration, size, and the mechanism by which particles are brought into contact, for example, Brownian motion, shear or the differential settlement of particles. The latter depends mainly on the physicochemical properties of the particle surface and may vary with the particle type. Particle collision does not necessarily result in aggregation, as the stickiness or sticking efficiency is often only 10% or less but can increase up to 60% depending on the particle type involved.[4]

Depending on its intensity, shear can either increase particle collision or increase particle destruction. This is particularly the case at the base of the surface mixed layer, where internal waves, wind driven shear and tidal shear are pronounced; and within the benthic boundary layer where turbulence is increased again.

In surface waters, changes in particle coagulation efficiency have been attributed to the abundance of single species or as part of the life cycle strategy of cells.[16,17] The occurrence of aggregates does not, for example, always coincide with the peak of phytoplankton abundance. Rather, it is often postponed toward the decline of the bloom.[18] This has been hypothesized to be due to an increase in particle stickiness.[19] A decade ago, a special class of particles was found to be readily abundant during phytoplankton blooms in water and in aggregates as well. These gels, called transparent exopolymer particles (TEP),[20] are thought to play a central role in coagulation processes. Laboratory experiments have demonstrated that diatoms produce more gels under nutrient limitation, although little is known about how limitation by different nutrients affects the quantity and composition of the gels and subsequent stickiness. Because of the great abundance in shelf seas and in the open ocean and because of the stickiness of TEP, the probability of particle collisions is enhanced.[21] Logan et al. proposed two hypotheses[22] to account for the precipitous formation of large, rapidly settling aggregates at the termination of phytoplankton blooms in nature: aggregation due primarily to cell–cell collisions, and aggregation resulting from the presence of TEP. By comparing TEP and phytoplankton half-lives in these systems, it is concluded that the formation of rapidly sinking aggregates following blooms of mucous-producing diatoms is primarily controlled by concentrations of TEP, not phytoplankton.[22]

Engel conducted measurements of diatom species composition, TEP, bulk particle abundance, as well as chemical and biological variables in order to reveal the determinants of coagulation efficiency.[19] The investigation showed that an increase in TEP concentration relative to conventional particles at the decline of the bloom significantly enhanced apparent coagulation efficiencies. High proportions of TEP led to apparent values of stickiness of 1, which indicates that collision rates can be substantially underestimated when the stickiness parameter alpha is calculated on the basis of conventional particle counting only, for example, with the Coulter Counter.

11.3 THE DESCENT THROUGH THE WATER COLUMN

The physical and biological properties of the aggregates determine their transport behavior in the water column. The excess density over that of the surrounding water controls the speed with which aggregates descend to the sea floor. For particles with Reynolds numbers <1, Stokes' law can be applied to determine the settling velocity:

$$W_S = \frac{d^2(\Delta\rho)g}{18\nu}$$

where d is the particle diameter, $\Delta\rho$ is the excess density of the particle over seawater, g is the gravitational constant and ν is the kinematic viscosity of the fluid. The kinematic viscosity is strongly temperature dependent and has an enormous influence on the behavior of particles of low Reynolds numbers. ν nearly doubles from warm surface waters (0.01 cm^2 sec^{-1} at 20°C) to cold bottom waters (0.018 cm^2 sec^{-1} at 1°C). As Stokes law was originally applied to rigid, impermeable spherical particles of known density, it is difficult to apply to nonspherical aggregated particles which virtually represent most particulate material in the ocean. However, Stokes can then be used to back-calculate the particle density of the aggregates as discussed by.[14] During the last two decades empirical particle-size/settling-velocity relationships have been developed for different oceanic regimes (Figure 11.1). The data reveal that organic rich aggregates from surface waters at continental margins show much lower settling velocities than those of similar size but enriched in ballast. This lithogenic ballast is added to the organic aggregates during resuspension events.

The surface mixed layer at the top of the ocean varies in thickness from tens to hundreds of meters and aggregate concentrations inside this layer are related to the processes of production, destruction, and sinking. Peak concentrations are often located at the base of the surface mixed layer, which can extend up to a few hundred meters during winter. This layer is subject to rapid changes in heat, turbulence, nutrients, and depth of mixing. The peak concentrations at the base of the surface mixed

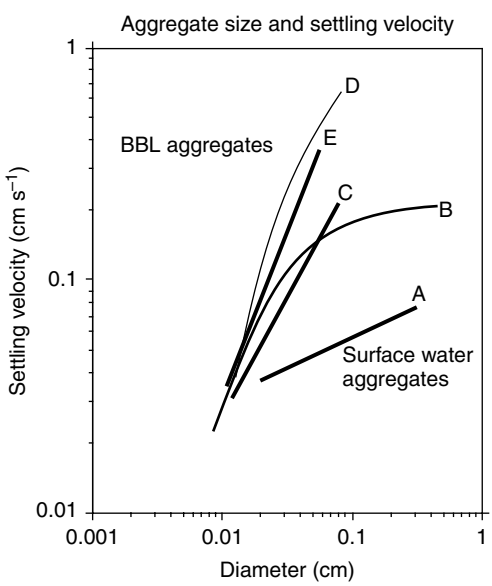

FIGURE 11.1 Particle settling velocities/particle diameter relationships of aggregates from ocean surface waters (A), intermediate and bottom nepheloid layers (B), and from the benthic boundary layer (C, D, E) determined by Alldredge and Gottschalk[4] for A, McCave[14] for B, Thomsen et al.[23] for C (Celtic margin), Thomsen et al.[24] for D (Iberian margin), and Sternberg et al.[25] for E (North East Pacific margin).

layer mainly coincide with the occurrence of pycnoclines, where rapid changes in seawater-density (and thus excess-density of aggregates) can reduce or even stop the vertical flux of the aggregates. The physical forcing in the mixed layer creates changes in the biological processes, which depend on them. Here, organic rich aggregates are formed which are derived from gelatinous housing of zooplankton species, mucous feeding webs used by others, faecal material, and from phytoplankton cells and their component particles.[26] The proportion of free water within the aggregates, its porosity, determines how fast the internal environment changes in response to varying external conditions; the porosity also influences the rate at which small particles accumulate on the aggregates. After their slow descend through the pycnocline, differential settling is mainly responsible for additional aggregate formation as well as the migrating zooplankton, which consume the aggregates to depth of up to 1000 m.

11.4 TRANSPORT WITHIN THE BENTHIC BOUNDARY LAYER: THE RESUSPENSION LOOP

Once on the sea floor, the aggregates are more easily remobilized into the benthic boundary layer than the bulk sediments beneath,[23] and are resuspended back into the water column, being again subjected to aggregation and disaggregation processes.[27] Long-term studies at different continental margins revealed that the bottom sediments consist of a thin surface layer of organic rich aggregates (mean diameter 100 to 2500 μm). These resuspend under critical shear velocities [u_{*c}] of 0.4 to 1.2 cm sec^{-1} (mean u_{*c} of 0.8 ± 0.1 cm sec^{-1}) and have median diameters of 140 to 450 μm and settling velocities of 0.05 to 0.35 cm sec^{-1} (Figure 11.1). The aggregates consist of up to 75% of organic matter, which is mostly refractory with a carbon/nitrogen ratio exceeding 10, and the lithogenic material is embedded in the amorphous matrix of the organic matter. The BBL aggregates contain remnants of faecal pellets, meiofauna organisms, and shell debris of foraminifera. Approximately 35 to 65% of the bacteria of the BBL are particle attached and live within the organic matrix of the aggregates and approximately 1% of the organic fraction is labile bacterial organic carbon.[23,24] The BBL aggregates in >100 μm size range are resuspended under similar flow conditions as particles of similar size but higher density (sand). However, they are transported over much greater distances due to their lower density and porous structure, which reduces their settling velocity (Figure 11.2, compare Figure 11.1). These aggregates can subsequently be transported in tide-related resuspension–deposition loops over long distances. Table 11.1 summarizes typical particle characteristics from continental margin BBLs. A cohesion effect for the aggregates is visible at about 30 μm (Figure 11.2). Thus, organomineral aggregates with average sizes <30 μm behave in the same way as clay (<2 μm), and particles coarser than 30 μm should display size sorting behaviour. The last result is different from the calculations of McCave et al., who propose 10 μm as threshold between noncohesive and cohesive sediment behavior.[31] This difference seems due to particle stabilization from microbial exudates.[32] The erosion threshold data were mainly obtained in summer, when biological activity in surface sediments at the study site is high.[33] Evidence for the importance of biological adhesion on critical stress for incipient transport has been

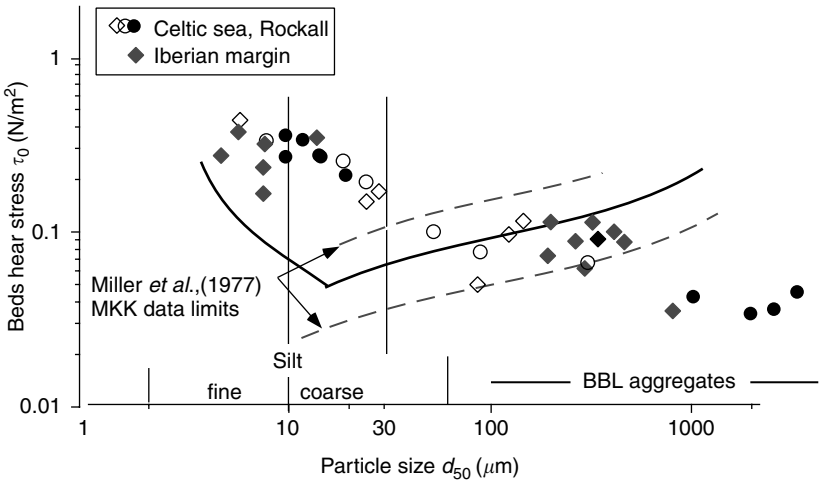

FIGURE 11.2 Critical bed shear stress for erosion of continental margin sediments showing the onset of a cohesion effect at about 30 μm. The black curve represents the modified Shields curve after Unsöld.[28] The dashed lines refer to the limits of available high quality data evaluated by Miller et al.[29] and Self et al.[30]

TABLE 11.1
Typical Flow and Particle Characteristics from Continental Margin BBLs

u	(cm sec^{-1})	2–50
u_{*c}	(cm sec^{-1})	0.1–2
τ_c	(N m^{-2})	0.01–0.4
Total particulate matter	(g m^{-3})	0.1–8
Particulate organic carbon	(mg m^{-3})	10–150
Chlorophyll equivalents	(mg m^{-3})	0.01–0.3
BBL aggregate number	(n m^{-3})	(10–1500) $\times$ 10^3
BBL aggregate diameter	d_{50}	140–2400

Note: u = mean velocity, u_{*c} = critical shear velocity, τ_c = critical bed shear stress, d_{50} = median aggregate diameter (μm).

demonstrated by various authors (e.g., ref. [32]) who showed that microbial exudates could increase the critical bed stress by a factor up to 5.

During times of enhanced flow conditions, aggregates are formed and compacted by shear, which accounts for the fact that they do not disaggregate when they enter the viscous sublayer at mid- and lower slope sediments. The formation of these BBL aggregates and the minerals incorporated into the particles might be responsible for the organic matter preservation on continental slopes. Statistical analyses of

TABLE 11.2
Model Particle Parameters

d (μm)	$\Delta\rho$ (g cm^{-3})	W_s (cm sec^{-1}) $r^2 = 0.8; n = 191$ $r^2 = 0.8; n = 31$	u_{*c} (cm s^{-1}) $r^2 = 0.7;$ $n = 15$*	τ_0 (N m^{-2})	$\approx u_{100}$	u_{*li} $r^2 = 0.9;$ $n = 6$	τ_0 (N m^{-2})	$\approx u_{100}$
50	0.139	0.013	0.98	0.10	16	0.7	0.050	11
100	0.137	0.050	0.90	0.084	14	0.9	0.083	15
185	0.091	0.114	0.89	0.082	14	0.8	0.066	14
200	0.086	0.125	0.89	0.081	14	0.8	0.066	14
400	0.047	0.275	0.86	0.076	13	0.6	0.038	10
500	0.038	0.350	0.84	0.073	12	0.5	0.026	8
1000	5.90×10^{-3}	0.215	0.76	0.060	11			
2000	2.07×10^{-3}	0.303	0.61	0.038	10	0.5	0.026	8
4000	8.17×10^{-4}	0.477	0.50	0.026	8			

Note: d = aggregate diameter, $_*\rho$ = excess density with fluid density taken as 1.028g cm^{-3} 5°C, salinity = 36, w_s = settling velocity, u_{*c} = critical shear velocity, τ_0 = bed shear stress, u_{100} = flow velocity at 100 cm a.b. calculated after Middleton and Southard (1984) with z_0 taken as 0.1 cm, u_{*li} = critical deposition velocity, $n = 15^* = d_{50}$ data from 15 stations with 50 to 200 single datapoints.

the available BBL flow and particle and biogeochemical data of the Iberian margin (15 stations with u_{*c} data, 3 stations with u_{*li} data, 191 experimental w_s measurements, 31 *in situ* w_s measurements, ≈1200 aggregates analyzed), were used to determine the basic parameters for a simple particle transport model (Table 11.2). For a particle size spectrum from 50 to 4000 μm in diameter, estimated excess densities, critical shear velocities, and critical deposition velocities decreased with increasing particle size, while the settling velocity increased over the same particle size spectrum.[24]

11.5 DEGRADATION AND DECOMPOSITION OF THE AGGREGATES

11.5.1 BACTERIA

The breakdown of the generally strongly degraded organic matter deposited on deep-sea sediments is mainly accomplished by bacteria. The rates of degradation depend largely on the proportion of biologically labile material which decreases with advancing decay.[7] Despite the possible protection mechanisms, like bacterial community pressure inhibition and sorption to mineral surfaces,[11] if the net vertical and downslope transport is too slow, it is likely that mainly refractory organic matter will reach the deep ocean floor. Once the aggregates enter the benthic boundary layer, their fate is to a large extent controlled by the benthic flora and fauna which play a major role in determining their geochemical behavior. The reworking of the aggregates may further inhibit the degradation of organic matter, since the sorption of organic matter to the larger amount of lithogenic material in these aggregates may provide some degree

of protection against microbial activity.[11] However, the resuspension of the particles can also enhance their remineralization. Ritzrau showed that microbial activities and concentrations of various parameters (particulate organic carbon, Chlorophyll a, utilization of ^{14}C-amino acids) displayed distinct distribution patterns in the BBL and were up to a factor of 7.5 higher than in the adjacent water column and concluded that turbulence increases the microbial activity in the benthic boundary layer.[35] For BBL aggregates, Lind et al. presented a comparison between phytoplankton and bacterioplankton production[36] with each modified by high concentrations of suspended clays. High clay turbidity caused light-limitation of water column phytoplankton production. However, the clay combined with DOC to form aggregates which supported bacterioplankton production. Leipe et al. collected particles from the water column, the bottom nepheloid layer, and the "fluffy layer" in the Baltic Sea and revealed that suspended particulate matter (SPM) in the bottom nepheloid layer and the "fluffy layer" overlying sediments was enriched in organic carbon and clay minerals, whereas the nonaggregated SPM was dominated by quartz and biogenic opal.[37] It appeared that separation effects operate during aggregation of mineral particles and organic matter in repeated cycles of resuspension and settling. No clear seasonal variations in the composition of the SPM were found, in spite of high spatial and temporal variability of biological and physical variables. Their results suggest that preferential incorporation, possibly aided by microbiological colonization, of silicates into the organic flocs is a process that occurs under a wide range of conditions.

11.5.2 Fauna

In their classic study on the effects of benthos on sediment transport, Jumars and Nowell summarize that no consistent functional grouping of organisms as stabilizers vs. destabilizers, respectively decreasing or enhancing erodibility, is possible.[38] Benthic organisms can affect erodibility in particular — and sediment transport in general — via alternation of (1) fluid momentum impinging on the bed, (2) particle exposure to the flow, (3) adhesion between particles, and (4) particle momentum. The net effects of a species or individual on erosion and deposition thresholds or on transport rates are not generally predictable from extant data. Furthermore, they depend upon the context of flow conditions, bed configuration, and community composition into which the organism is set. Suspension-feeding fauna actively remove the aggregates from the water column and deposit it as faeces either within or on top of the sediment, a process called biodeposition.[39] Feeding pits, faecal pellet mounds, and tube-structures of the benthos locally can change the current regime and cause resuspension and passive biodeposition of particles.[38,40] Bioturbation due to moving animals or due to bulk feeding by deposit feeders substantially modifies the physical and geochemical properties of the aggregates.[41,42] Muschenheim and Milligan studied BBL characteristics in the Bay of Fundy and summarized that seston concentration and composition were found to vary greatly throughout the course of a tidal cycle, with periodic dilution of the organic content due to resuspended sand.[43] Examination of the particle size distributions suggests that flocculation plays a major role in packaging the material ingested by these benthic communities.

Heip et al. summarize that at continental margins the overall metabolism in shelf and upper slope sediments is dominated by the macrofauna, which are responsible for 50% of the organic aggregate mineralization.[44] At the lower slope and abyssal depth microbiota dominate in terms of total biomass (>90%) and organic matter respiration (about 80%). Because large animals have a lower share in total metabolism, mixing of the aggregates within the sediments is reduced by a factor of 5, whereas mixing of bulk sediment is one to two orders of magnitude lower than on the shelf. The lability of the organic aggregates in the sediments at the upper slope and shelf is significantly higher than in sediments in the deeper parts. The residence time of mineralizable carbon which is mainly transported in form of organic rich aggregates is about 120 d on the shelf and more than 3000 d at the lower slope. These conclusions for the lower slope and deep sea are supported by studies of Smith et al.[45] They carried out an important experiment on the biological reaction of incoming seasonal pulses of particulate matter in the open Pacific (4100 m depth, 220 km west of the central California coast) and hypothesized that the incoming aggregates would create localized regions of intense biological activity on the sea floor. However oxygen consumption of organic aggregates was similar to that of the background sediment and had no measurable influence on the chemical composition of the underlying sediment on time scales from 23 to 223 d or on sediment oxygen consumption after 222 d. The aggregates produced a minimal impact on sediment mineralization rates. The results are supporting the ideas of a fast benthic pelagic coupling, where the labile organic aggregates are rapidly consumed and elevated values of benthic activities are reduced to background values after a period of 2–3 weeks. There are, however, some areas in the oceans where the transport of aggregates can be enhanced: the submarine canyons.

Submarine canyons are areas where potentially the residence time can be short and net transport fast enough to supply the lower slope with labile material.[24] Recent studies point to the existence of a fast and continuous downward sediment transport along the axis of the canyon, independently of the current regime operating on the shelf. Aggregates being transported down a canyon would be subjected to aggregation and disaggregation cycles in the benthic boundary layer, but also to a continuous variation of the pressure to which they are subjected. So, it is possible that the organic matter, present in aggregates transported down a canyon, might be partially preserved due to both mineral particle sorption and increasing hydrostatic pressure.

11.6 CONCLUSIONS

In conclusion there is now an increasing amount of information on the formation and transport behavior of organic rich aggregates but lack of knowledge on the compositional changes over long time periods. The organic rich aggregates within the resuspension loop can still show a greenish color after several weeks or months but seem highly refractory and are thus exposed to low bacterial decomposition. Further studies are needed to investigate this effect of possible carbon protection within the BBL and the implication for long-term carbon storage in the ocean.

REFERENCES

1. Asper, V.L., Deuser, W.G., and Knauer, G.A., Rapid coupling of sinking particle fluxes between surface and deep ocean waters. *Nature* 357, 6380, 670–672, 1992.
2. Jackson, G.A. and Burd, A.B., Aggregation in the marine environment. *Environmental Science and Technology* 32, 19, 2805–2814, 1998.
3. Thornton, D.C.O. Diatom aggregation in the sea: Mechanisms and ecological implications. *Journal of Phycology* 37, 2, 149–161, 2002.
4. Alldredge, A.L. and Silver, M.W., Characteristics, dynamics and significance of marine snow. *Progress in Oceanography* 20, 1, 41–82, 1988.
5. Simon, et al. (Authors are Grossart, Schweitzer, Ploug), Microbial ecology of organic aggregates in aquatic ecosystems. *Aquatic-Microbial-Ecology* 28, 2, 175–211, 2002.
6. Hill, P.S. and Nowell, A.R.M., Comparison of two models of aggregation in continental-shelf bottom boundary layers. *Journal of Geophysical Research* 100, C11, 22,749–722, 76, 1995.
7. Turley, C., Bacteria in the cold deep-sea benthic boundary layer and sediment-water interface of the NE Atlantic. *FEMS Microbiology Ecology* 33, 2, 89–99, 2000.
8. Kiørboe, -T., Ploug, -H., and Thygesen, -U.H. (2001). Fluid motion and solute distribution around sinking aggregates. 1. Small-scale fluxes and heterogeneity of nutrients in the pelagic environment. *Marine-Ecology-Progress-Series* 211, 1–13, 2001.
9. Siegenthaler, U. and Sarmiento, J.L., Atmospheric carbon dioxide and the ocean. *Nature* 365, 644, 119–125, 1993.
10. Hedges, J.I. and Lee, C., and Peterson, M.L., The biochemical and elemental compositions of marine plankton: A NMR perspective. *Marine Chemistry* 78, 1, 47–63, 2002.
11. Hedges, J.I. and Keil, R.G., Organic geochemical perspectives on estuarine processes: Sorption reactions and consequences. *Marine Chemistry* 65, 1–2, 55–65, 1999.
12. Hartnett et al. (Authors are Keil, Hedges, Devol), Influence of oxygen exposure time on organic carbon preservation in continental margin sediments. *Nature* 391, 6667, 572–574, 1998.
13. Knoll,-S., Zwisler,-W., and Simon, -M., Bacterial colonization of early stages of limnetic diatom microaggregates. *Aquatic-Microbial-Ecology* 25, 2, 141–150, 2001.
14. McCave, I.N., Size spectra and aggregation of suspended particles in the deep ocean. *Deep-Sea Research* 31, 4, 329–335, 1984.
15. Jackson, G.A., A model of the formation of marine algal flocs by physical coagulation processes. *Deep-Sea Research* 37, 8, 1197–1211, 1990.
16. Kiørboe, T. and Hansen, J.L.S. Phytoplankton aggregate formation: Observations of patterns and mechanisms of cell sticking and the significance of exopolymeric material. *Journal of Plankton Research* 15, 9, 993–1018, 1993.
17. Crocker, K.M. and Passow U., Differential aggregation of diatoms. *Marine Ecology Progress Series* 117, 1–3, 249–257, 1995.
18. Riebesell, U., Particle aggregation during a diatom bloom. I. Physical aspects. *Marine Ecology Progress Series* 69, 3, 273–28, 1991.
19. Engel, A., The role of transparent exopolymer particles (TEP) in the increase in apparent particle stickiness (alpha) during the decline of a diatom bloom. *Journal-of-Plankton* 22, 3, 485–497, 2000.
20. Alldredge, A.L., Passow, U. and Logan B.E., The abundance and significance of a class of large, transparent organic particles in the ocean. *Deep-Sea Research*, Part I 6, 1131–1140, 1993.

21. Passow, U., Transparent exopolymer particles (TEP) in aquatic environments. *Progress in Oceanography* 55, 3–4, 287–333, 2000.
22. Logan, et al. (Authors are Passow, Alldredge, Grossart, and Simon), Rapid formation and sedimentation of large aggregates is predictable from coagulation rates (half-lives) of transparent exopolymer particles (TEP). *Deep-Sea Research* II 42, 1, 230–214, 1995.
23. Thomsen, L. and G. Gust, Sediment stability and characteristics of resuspended aggregates of the western European continental margin. *Deep Sea Research* I 47, 1881–1897, 2000.
24. Thomsen, L., Weering, T.V., and Gust, G., Benthic boundary layer characteristics at the Iberian continental margin. *Progress in Oceanography* 54, 315–329, 2002.
25. Sternberg, R. and Nowell, A.R.M., Continental shelf sedimentology: Scales of investigation define future research opportunities. *Journal of Sea Research* 41/1–2, 55–73, 1999.
26. Lampitt, R.S., In *Oceanography, An Illustrated Guide*, Eds Summerhayes, C.P. and Thorpe, S.A., Manson Publishing 96–112, Snow falls in the Open Ocean, 1996.
27. Ransom, B., Bennett, R.H., and Baerwald, R., Comparison of pelagic and nepheloid layer marine snow: Implications for carbon cycling. *Marine Geology* 150, 1–4, 39–5, 1998.
28. Unsöld, G., Der Transportbeginn rolligen Materials in gleichförmigen turbulenten Strömungen, Ph.D, Dissertation, Kiel-University, 145 pp., 1982.
29. Miller, M.C., McCave, I.N., and Komer, P.D., Threshold of sediment motion under unidirectional currents. *Sedimentology*, 24, 507–527, 1977.
30. Self, R.F.L., Nowell, A.R.M., and Jumars, P.A., Factors controlling critical shears for deposition and erosion of individual grains. *Marine Geology*, 86, 181–199, 1989.
31. McCave, I.N., Manighetti, B., and Robinson, S., Sortable silt and fine sediment size/composition slicing: Parameters for palaeocurrent speed and palaeoceanography. *Palaeoceanography* 10/3, 593–610, 1995.
32. Dade B. et al. (Authors are Davis, Nichols, Nowell, Thistle, Trexler, White) Effects of bacterial exopolymer adhesion on the entrainment of sand. *Geomicrobiology Journal* 8, 1–16, 1990.
33. Duineveld et al. (Authors are Lavaleye, Berghuis, de Wilde, Weele, Kok Batten, de Leeuw), Patterns of benthic fauna and benthic respiration on the Celtic continental margin in relation to the distribution of phytodetritus. *Int Revue Hydrobiology* 82/3, 395–424, 1997.
34. Middleton, G.V. and Southard, J.B. Mechanics of sediment movement. *S.E.P.M. Short course Number 3, 2nd Edition*, Tulsa, 787 pp., 1984.
35. Ritzrau, W., Microbial activity in the benthic boundary layer: Small-scale distribution and its relationship to the hydrodynamic regime. *Journal of Sea Research* 36, 3–4, 171–180, 1996.
36. Lind,-O.T., Chrzanowski,-T.H. and Davalos-Lind,-L., Clay turbidity and the relative production of bacterioplankton and phytoplankton. *Hydrobiologia* 353, 1–3, 1–18, 1997.
37. Leipe et al. (Authors are Loeffler, Emeis, Jaehmlich, Bahlo, and Ziervogel), Vertical patterns of suspended matter characteristics along a coastal-basin transect in the western baltic Sea. *Estuarine,-Coastal-and-Shelf* 51, 6, 789–804, 2000.
38. Jumars,-P.A. and Nowell,-A.R.M. Effects of benthos on sediment transport. Difficulties with functional grouping. *Continental Shelf Research* 3, 2, 115–130, 1984.

39. Graf, G. and Rosenberg, R., Bioresuspension and Biodeposition — A Review. *Journal of Marine System*, 11, 269–278, 1997.
40. Miller, D.C., Bock, M.J., and Turner, E.J., Deposit and suspension feeding in oscillary flows and sediment fluxes. *Journal of Marine Research*, 50, 489–520, 1992.
41. Bodreau, B.P., A mathematical model for coupled sediment-suspended particle exchange. *Journal of Marine System* 11, 297–302, 1996.
42. Soetaert et al. (Authors are Herman, Middelburg, Heip, de Stigter, van Weering, Epping, and Helder) Modelling Pb_{210}-derived mixing activity in ocean sediments: Diffusive versus non-local mixing. *Journal of Marine Research* 54, 23–41, 1996.
43. Muschenheim,-D.K. and Milligan,-T.G., Benthic boundary layer processes and seston modification in the Bay of Fundy (Canada). *Milieu* 48, 4, 285–294, 1998.
44. Heip, et al. (Authors are de Wilde, Duineveld, Flach, Graf, Lavalaye, Pfannkuche, Soetaert, Soldwedel, Thomsen, and Vanaverbeke), The carbon and particle requirements of benthic communities a long Goban Spur transect, a synthesis. *Deep Sea Research* II/48, 3223–3243, 2001.
45. Smith, et al. (Authors are Baldwin, Glatts, Kaufmann, Fisher), Detrital aggregates on the sea floor: Chemical composition and aerobic decomposition rates at a time-series station in the abyssal NE Pacific. *Deep-Sea-Research*-II 45, 4–5, 843–880, 1998.

12 Equilibrium and Nonequilibrium Floc Sizes

Johan C. Winterwerp

CONTENTS

12.1 INTRODUCTION

Cohesive sediment is a mixture of clay, silt, sand, organic material, water, and, sometimes, gas. The clay, silt, and organic particles can form flocs, sometimes also incorporating some larger sand particles. These flocs contain large amounts of water (70% to 95% by volume) and are much larger than the individual floc-building particles. As a result, the settling velocity of flocs is much higher than that of the individual clay, silt, and organic particles. Moreover, the flocculation process affects the density of fluid mud or slurries formed by these cohesive sediment flocs.

One of the first researchers who studied flocculation processes in the natural environment was Krone.[1,2] He suggested that flocs are built up in a hierarchical way: large third-order flocs would be formed by a number of smaller second-order flocs, which themselves would consist of a number of even smaller first-order flocs, etc.

In sanitary engineering, Argaman and Kaufman[3] and Parker et al.[4] studied the flocculation process in wastewater. They found that floc sizes first increase with increasing turbulence shear, and then decrease in size. This would imply a variation in floc size over the tidal cycle in natural systems. Indeed, Van Leussen[5] measured floc sizes 2.8 m below the water surface in the Ems estuary, The Netherlands, and found large variations in settling velocity, as shown in Figure 12.1. Further to these ideas, Dyer[6] proposed the conceptual diagram of Figure 12.2, indicating floc size increase with increasing suspended sediment concentration and an increasing–decreasing trend in floc size with increasing turbulence intensity.

1-56670-615-7/05/$0.00+$1.50

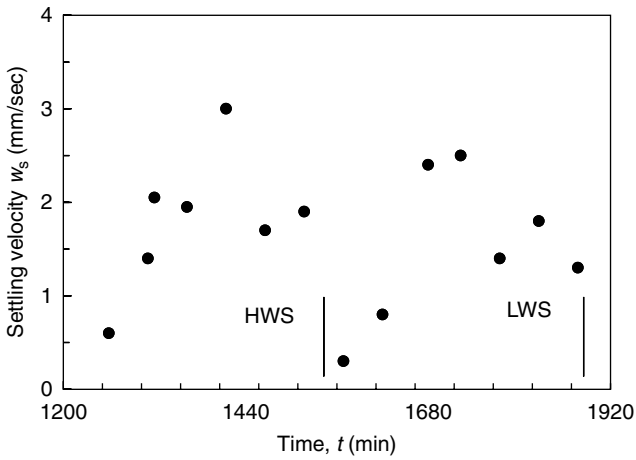

FIGURE 12.1 Variation in settling velocity in the Ems estuary, The Netherlands, measured 2.8 m below the water surface. (After Van Leussen, PhD thesis, University of Utrecht, The Netherlands, 1994.)

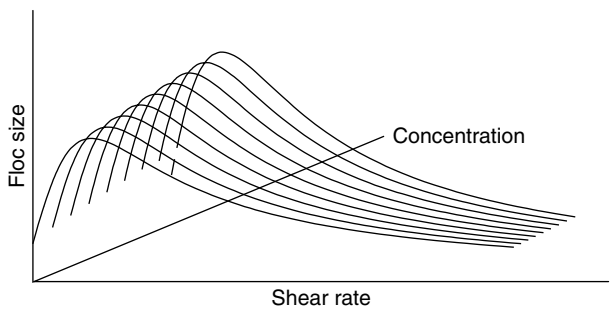

FIGURE 12.2 Conceptual flocculation diagram of Dyer.[6]

Based on this diagram, Van Leussen[5] further suggested that large flocs, formed in the upper part of the water column are broken down near the bed, as sketched in Figure 12.3. This diagram would also explain the sedimentation formula found by Krone,[1] which predicts that cohesive sediment particles can only settle if the bed shear stress is smaller than a threshold value. This threshold value would be determined by the strength of the flocs.

In this chapter, we analyze the data and concepts in Figures 12.1 through 12.3 further. To a large extent it is based on the work presented in Winterwerp.[8,9] However, here we focus on the role of the flocculation time, that is, the time necessary for flocs to achieve their equilibrium size at given hydro-sedimentological conditions, and the consequences on the time evolution of floc size. Our main presumption herein is that flocculation takes time, as shown in Figure 12.4. This figure presents the time evolution of flocs, as measured by Hogg et al.[10] on a suspension of kaolinite clay, peptized with a polymeric flocculant. The clay concentration was about 80 g/l, and

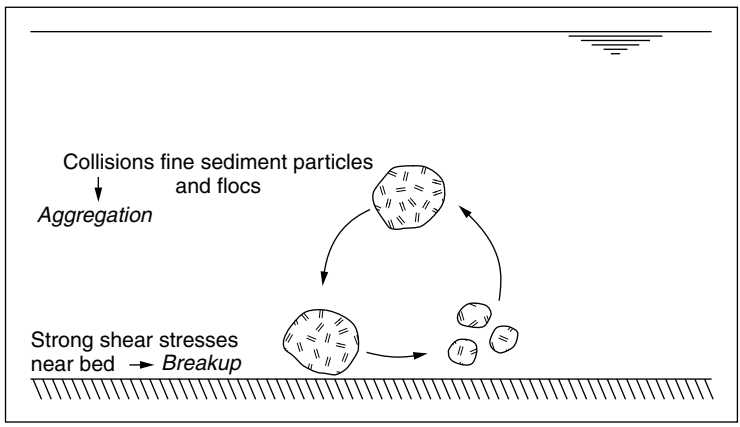

FIGURE 12.3 Schematic picture of flocculation processes in the water column. (After Van Leussen, *Physical Processes in Estuaries*, ed. J. Dronkess and W. Van Leussen, Springer-Verlag, Heidlelberg, 1988.)

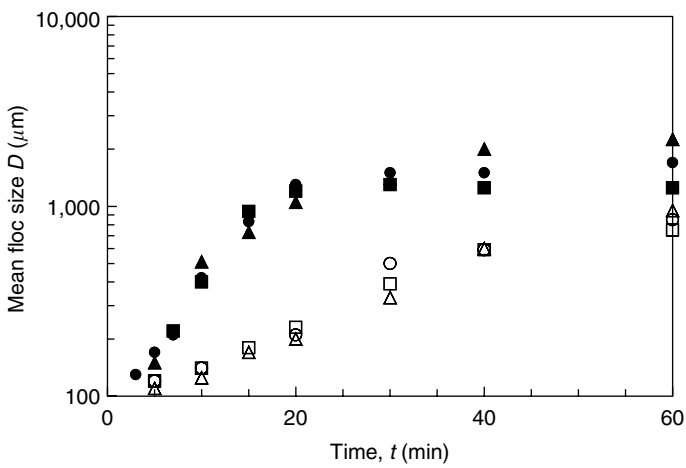

FIGURE 12.4 Floc growth measured by Hogg et al.[10] — the various symbols refer to various test conditions.

flocculation conditions were made extremely favorable through the addition of the flocculant. Yet, the flocculation time was still about 1 h. Also McAnally and Mehta[11] found flocculation times of many hours, depending on the turbulence intensity and sediment concentration.

The evolution of flocs in the natural environment is governed by a large number of physical, and often also chemical and biological processes. At present it is impossible to quantify all these processes, as many basic questions have not yet been answered. An analysis of these processes is, therefore, only possible when making severe simplifications. Here we schematize the floc size distribution with one mean floc size

only. We first treat a number of processes in isolation to establish their relevance and scaling rules, upon which these processes are integrated to understand the effect of nonlinear interactions as occurring in the real world. It is emphasized that this chapter yields qualitative conclusions only, as model schematizations are crude and the data scarce.

In Section 12.2, we present a simple relation between floc size and settling velocity and a Lagrangian model for flocculation of cohesive sediment under turbulent conditions; here we also present our formal definition of the flocculation time. Note that from studies by McCave,[12] Wacholder and Sather,[13] and Stolzenbach and Elimelech,[14] it can be concluded that Brownian motion and differential settling play a small role in the high-dynamic coastal and estuarine environments. In Section 12.3, we elaborate on the vertical floc size distribution, discussing the role of residence times on maximal floc size. In Section 12.4, we integrate the various physical processes and study the evolution of floc size over the tidal cycle, elaborating on the processes behind rapid settling and sediment-induced stratification. Whereas Sections 12.3 and 12.4 deal with low concentrated suspensions, Section 12.5 treats the effects of flocculation on the sediment concentration in fluid mud layers. In Section 12.6, we present some conclusions, and contemplate on the role of flocculation time on floc size and settling velocity, and how to measure these.

12.2 A LAGRANGIAN FLOCCULATION MODEL

This section summarizes the flocculation model developed by Winterwerp.[8,9] We assume that the bulk properties of the suspended sediment, relevant for the present study, can be captured with one floc size only (denoted by D_f in this chapter), which may vary with time and over space, however. We treat flocs of cohesive sediment as self-similar fractal entities, as proposed by Kranenburg[15] and in line with Krone's[1] hierarchical floc structure. The fractal dimension n_f is obtained from the description of a growing object with linear size La, consisting of L seeds of linear size a, and volume $V(La)$ (e.g. Vicsek[16]). Assuming that the linear size of the primary objects has unit dimension, $V(La) \propto N(La)$, where N is the number of primary objects (seeds), the fractal dimension n_f is defined as

$$n_f = \lim_{L \uparrow \infty} \frac{\ln(N(L))}{\ln(L)} \tag{12.1}$$

From this approach, it follows that the differential (or excess) density $\Delta\rho_f$ of mud flocs is given by (Kranenburg[15]):

$$\Delta\rho_f = \rho_f - \rho_w = (\rho_s - \rho_w)\left[\frac{D_p}{D_f}\right]^{3-n_f} \tag{12.2}$$

where ρ_f, ρ_w, and ρ_s are the densities of the mud flocs, the (interstitial) water, and the sediment (primary particles), and D_f is a characteristic (mean) diameter of the flocs, and D_p is the diameter of the primary particles. From (12.2), it follows that

the relation between mass (c) and volumetric concentration (ϕ_f) reads:

$$\phi_f = \left(\frac{\rho_s - \rho_w}{\rho_f - \rho_w}\right)\frac{c}{\rho_s} = \frac{c}{\rho_s}\left[\frac{D_f}{D_p}\right]^{3-n_f} \tag{12.3}$$

At the gelling point, defined as the condition that flocs form a space-filling network, the volumetric concentration of the flocs ϕ_f becomes unity by definition. Hence, the gelling concentration c_{gel} can be obtained from (12.3):

$$c_{gel} = \rho_s\left[\frac{D_p}{D_f}\right]^{3-n_f} \tag{12.4}$$

Such gelling conditions are found in fluid mud layers (e.g. Section 12.5); the gelling concentration is also known as the structural density in soil mechanics, as a measurable strength builds up in the network.

Measurements of the fractal dimension of flocs of cohesive sediment in the water column reveal values from about $n_f \approx 1.4$ for very fragile flocs, like some marine snow to $n_f \approx 2.2$ for strong estuarine flocs. Typical values within estuaries and coastal waters range from $n_f \approx 1.7$ to 2.2, with an average value of $n_f \approx 2.0$ (e.g. Kranenburg[15]).

This fractal approach implies that the relation between settling velocity w_s of a single mud floc in still water, and floc size D_f, which is based on a balance between gravitational and drag forces, does not follow Stokes' law, but (e.g. Winterwerp[8])

$$w_s = \frac{\alpha}{18\beta}\frac{(\rho_s - \rho_w)g}{\mu}D_p^{3-n_f}\frac{D_f^{n_f-1}}{1 + 0.15Re_p^{0.687}} \quad \left[\approx \frac{\alpha' g \mathrm{D} D_p}{\nu}D, \text{ for } n_f = 2\right] \tag{12.5}$$

in which $\mu(\nu)$ is the dynamic (kinematic) viscosity of the fluid, and $Re_p = w_s D_f/\nu$ is the particle Reynolds number. For spherical ($\alpha = \beta = 1$), Euclidean ($n_f = 3$) particles in the Stokes' regime, for which $Re_p \ll 1$, the well-known Stokes' formula for a stationary settling particle is retrieved:

$$w_s = \frac{(\rho_s - \rho_w)gD_f^2}{18\mu} \tag{12.6}$$

Figure 12.5 presents the settling velocity as established with Equation (12.5) with $\alpha = \beta = 1$, $D_p = 4\ \mu$m (which is a typical value found by Van Leussen[5] for Ems mud), $\rho_s = 2650$ kg/m^3, $\rho_w = 1020$ kg/m^3, and $\mu = 10^{-3}$ Pasec, for three values of n_f, that is, $n_f = 1.7$, 2, and 2.3, together with observations. These observations comprise of data on settling velocity and floc size measured in the Delft Hydraulics settling column, in the Ems estuary and in the North Sea (Van Leussen[5]; VIS in Figure 12.5 means size and settling velocity measurements with a Video *In Situ* camera system), in Chesapeake Bay (Gibbs[17]), and in the Tamar estuary (Fennessy et al.[18]). It is observed that Equation (12.5) matches the data adequately. This is also the case for data presented by Hawley,[19] who summarizes the work of Japanese researchers

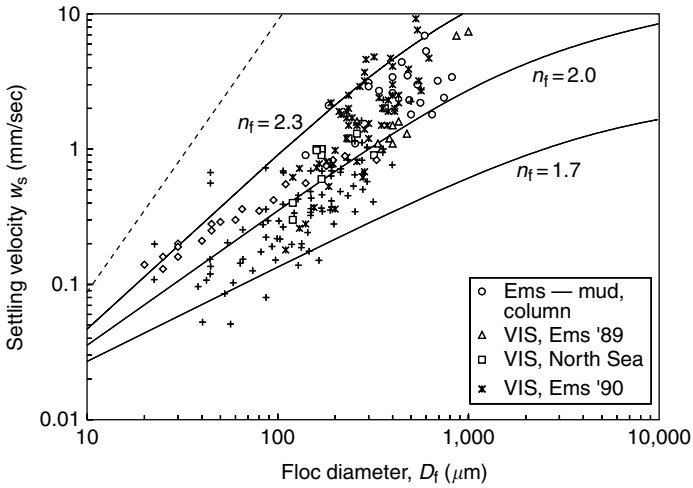

FIGURE 12.5 Relation between settling velocity and floc size (Equation (12.5)) for self-similar flocs.

in the ocean (not shown here). The overall trend of the data points seems slightly steeper than the fit with $n_f = 2$, because no data are available in the lower right corner of the graph, that is, small w_s and large D_f. However, when the individual data sets are studied, the slopes agree better with $n_f = 2$.

Figure 12.5 shows that for particles with a diameter up to a few 100 μm, the data can be properly represented with the fit $w_s \propto D_f$, that is, with an average fractal dimension, $n_f = 2$. At floc diameters beyond $D_f = 1$ mm, Equation (12.5) predicts a rapid deviation from a simple power law behavior because of the increasing role of the particle Reynolds number. We can expect that the validity of (12.5) becomes limited at floc sizes beyond a few millimetres.

Winterwerp[9] has developed a Eulerian flocculation model, which is identical to a Lagrangian model (Winterwerp[8]) in case of no advection and constant sediment concentration. This flocculation model is used in Sections 12.2 and 12.3 of this chapter to analyze the effects of the flocculation time, and reads:

$$\frac{dD_f}{dt} = k_A c G D_f^2 - k_B G^{3/2}(D_f - D_p)D_f^2 \tag{12.7}$$

where c is the suspended sediment concentration by mass, G is a measure for the shear rate at the smallest turbulence length scale ($G \equiv \sqrt{\varepsilon/\nu}$), k_A (m^2/kg) is a dimensional aggregation parameter and k_B(sec$^{1/2}$/m^2) is a floc break-up parameter. Here we have assumed that the fractal dimension n_f attains its mean value of $n_f = 2$.

For small values of D_f, the first term on the right-hand side of (12.7), that is, the aggregation term dominates, whereas for large D_f, the second term, that is, the break-up term dominates. From this flocculation equation, an equilibrium floc size $D_{f,e}$ is obtained for $dD_f/dt = 0$. A mathematically trivial but physically unsound and unstable solution is $D_{f,e} = 0$. In this case, small particles always grow. The other

equilibrium solution for the Lagrangian model reads:

$$D_{f,e} = D_p + \frac{k_A c}{k_B \sqrt{G}} \tag{12.8}$$

which is a stable equilibrium, as for $D_f < D_{f,e}$, the flocs grow and for $D_f > D_{f,e}$, the flocs break up. For the chosen fractal dimension, $n_f = 2$, the differential equation (12.7) can be easily solved analytically, if the sediment concentration by mass c is constant. First, a time scale parameter T' is defined:

$$T' = \left(k_B G^{3/2} D_{f,e}^2\right)^{-1} \tag{12.9}$$

The solution of Equation (12.7) then has the implicit form:

$$t = T' \left[\ln\left(\frac{D_{f,e} - D_0 D_f}{D_{f,e} - D_f D_0}\right) + \frac{D_{f,e}}{D_0} - \frac{D_{f,e}}{D_f} \right] \tag{12.10}$$

in which D_0 is the floc size at $t = 0$. This solution describes the aggregation/floc-break-up process for flocs initially either smaller or larger than the flocs at equilibrium size.

From (12.10), a time constant for flocculation T_f can be defined in the case that the initial floc size D_0 is much smaller or much larger than the equilibrium value, yielding the maximum time scales of the aggregation and floc break-up processes:

$$\begin{aligned} &\text{for } D_{f,e} \gg D_0\text{: } T_f \approx T' D_{f,e}/D_0 \approx \frac{1}{k_A c G D_0} \\ &\text{for } D_{f,e} \ll D_0\text{: } T_f \approx 2T' \approx \frac{2k_B}{k_A^2 c^2 \sqrt{G}} \\ &\text{hence } T_f \propto \left(\frac{U^3}{h}\right)^{-n} c^{-m} \quad \text{with } \frac{1}{4} \le n \le \frac{1}{2},\ 1 \le m \le 2 \end{aligned} \tag{12.11}$$

The flocculation model contains a flocculation parameter k_A and a floc break-up parameter k_B, which have to be determined empirically. This has been done at present for one set of data only, that is, on the basis of flocculation experiments carried out in the settling column of Delft Hydraulics (see Van Leussen[5]). This column is a 4.25 m high perspex cylinder with an inner diameter of 0.29 m. Within the column, a grid can be oscillated at various frequencies and amplitudes to generate a homogeneous turbulence field. For details on the calibration, the reader is referred to Winterwerp.[8,9,20] From this analysis, we found $k_A = 14.6\ \text{m}^2/\text{kg}$ and $k_B = 14.10^3\ \text{sec}^{1/2}/\text{m}^2$ (NB: $n_f = 2$). It is stressed that these parameters have been obtained for cohesive sediment from the Ems estuary in The Netherlands, and that no other data are available at present. One would expect, though, that these parameters are not universally applicable. However, as no other data are available, these values will be used anyway in this chapter.

12.3 FLOC SIZE DISTRIBUTION OVER THE WATER DEPTH

From the analysis of the Lagrangian flocculation model in Section 12.2, we obtained the time scales for flocculation (e.g. Equation (12.11)). The flocculation time can vary between a few minutes to many days, and even more, depending on the hydrodynamic conditions and the suspended sediment concentration. As a result, flocs of cohesive sediment, observed in marine environments, are often not in equilibrium with the local hydrodynamic conditions.

Let us first compute the time evolution of floc size, as predicted with the Lagrangian flocculation model (12.7). The results are shown in Figure 12.6, together with some data obtained in a settling column (for details, see Winterwerp[8]). We observe that for two sets of experimental data, equilibrium conditions are obtained within a few hundred seconds. For one experiment though, the flocculation time exceeds 1 h. From a qualitative point of view, Figure 12.6 shows the same trend as Figure 12.4. However, we cannot analyze the results in Figure 12.4 further, as no details of the experimental conditions are given.

These observations have important implications for the flocculation behavior in marine conditions. Flocs settle continuously due to gravity and are remixed/resuspended by turbulence. Hence, they experience varying hydrodynamic conditions (shear rates) during their journey through the water column. This implies that the ratio between flocculation time and residence time in a specific turbulent environment becomes an important parameter.

This can be further analyzed for schematic conditions by considering a situation where the turbulence field is homogeneous over the water depth, as can be realized in a settling column, for example. The mean residence time T_r for all particles in the

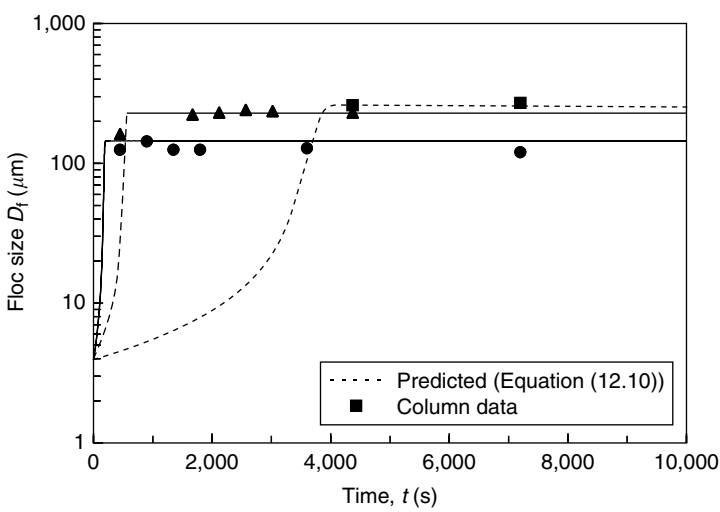

FIGURE 12.6 Floc growth as a function of time (Equation 12.10, after Winterwerp, *Continental Shelf Res.*, 22, 1339–1360, 2002) — particle size at $t = 0$ measures 4 μm.

water column with initial height Z_0 above the bottom of the water column can be obtained from

$$\int_0^{T_r} w_s \, dt = \alpha'' \int_0^{T_r} D_f \, dt = Z_0 \tag{12.12}$$

in which w_s is the settling velocity and $\alpha'' = \alpha' D_p g \Delta / \nu (\approx 3 \text{ sec}^{-1}$ for $D_p = 4 \ \mu\text{m})$. The residence time T_r can be solved directly from this equation through integration of the simplified flocculation model (12.7) to yield

$$T_r = \frac{Z_0}{\alpha'' D_{f,e}} + \frac{D_f - D_0}{k_A c G D_f D_0} = \frac{Z_0}{w_{s,e}} + T' \left[\frac{D_{f,e}}{D_0} - \frac{D_{f,e}}{D_f} \right] \tag{12.13}$$

in which $w_{s,e}$ is the equilibrium settling velocity for equilibrium floc size (e.g. Equation (12.5) and (12.8)). The maximum settling velocity, as a function of a limited residence time, follows from (12.12) and (12.13) ($t = T_r$):

$$w_{s,max} = \frac{w_{s,0}}{((D_{f,e} - D_0)/D_{f,e}) e^{-Z_0/(w_{s,e} T')} + D_0/D_{f,e}} \tag{12.14}$$

The maximum settling velocity predicted with Equation (12.14) is plotted in Figure 12.7 for the k_A and k_B values given before, a suspended sediment concentration of 1 g/l, and $Z_0 = 1$, 2, and 4 m, respectively. It is shown that for small values of G, the flocs cannot attain equilibrium conditions, given by Equation (12.8) because of the limited residence time. If the concentration would decrease by a factor 10,

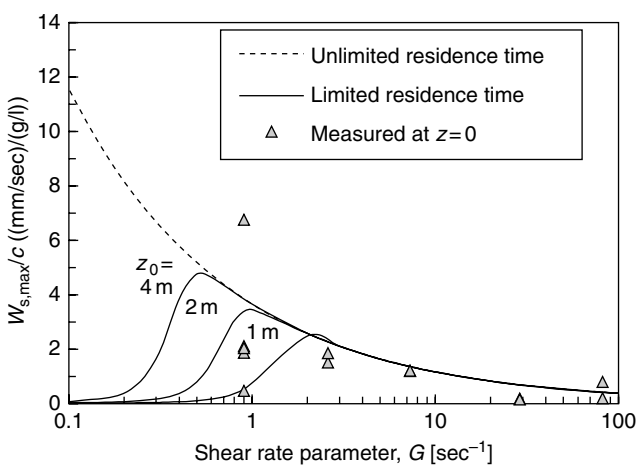

FIGURE 12.7 Effects of limited residence time on the relation between floc size and shear rate (Equation 12.14, after Winterwerp, *Continental Shelf Res.*, 22, 1339–1360, 2002) compared with data by Van Leussen (PhD thesis, University of Utrecht, The Netherlands, 1994) measured in settling column.

the shear rate at which equilibrium would be possible, would increase by the same factor. We have also plotted some data presented by Van Leussen,[5] which appear to be properly modeled by Equation (12.14). As the experiments by Van Leussen were carried out at various sediment concentrations, the settling velocity in Figure 12.7 is divided by c to allow mutual comparison.

Note that Figure 12.7 is qualitatively similar to the diagram by Dyer in Figure 12.2. We conclude that the left part of this graph is affected by a limited residence time, or similarly by too long flocculation times.

We can substantiate these observations further, and investigate when the classical diagram by Van Leussen[7] of flocculation processes in the water column, sketched in Figure 12.3 is correct. It shows larger flocs higher in the water column, where turbulent shear is relatively small, and smaller flocs near the bed, where turbulent shear is high.

This diagram can of course only hold when the flocculation time is small when compared to the mixing and settling time of sediment. As the settling velocity of mud flocs is generally of the order of a few 0.1 to 1 mm/sec, or smaller, the vertical mixing time h^2/ε_z (where h is the water depth and ε_z is the vertical eddy diffusivity) is generally much smaller than the settling time h/w_s. Moreover, the time scale for floc break-up is almost always smaller than the time scale for aggregation, as follows from Equation (12.11). Hence, to compare flocculation time with residence time, we may compare aggregation time with settling time only. The relevant aggregation time is the time necessary to form larger flocs with size D_u higher in the water column through aggregation of smaller flocs with size D_l originating from the lower part of the water column. The latter are more or less in equilibrium with the hydrodynamic conditions near the bed as G (and often c) is large. Also, for the present analysis, we assume that the vertical gradient in suspended sediment concentration is small.

The flocculation time T_f for $D_u > D_l$ is obtained from Equation (12.11):

$$T_f \approx \frac{1}{k_A c G_u D_l} \tag{12.15}$$

where G_u is assumed to be represented by the mean value of the shear rate in the upper 25% of the water column. We assume further that D_l is the floc size in equilibrium with the shear rate G_l in the lower 25% of the water column. G_u and G_l are found from averaging G, using Nezu and Nakagawa's approximation [21] of the dissipation rate $\varepsilon = u_*^3(1-\zeta)/\kappa h\zeta$, where $\zeta = z/h$ and u_* is the shear velocity:

$$G_u = \frac{1}{0.25}\int_{0.75}^{1} G\,\mathrm{d}\zeta = 0.36\sqrt{\frac{u_*^3}{\kappa\nu h}} \tag{12.16a}$$

and

$$G_l = \frac{1}{0.25}\int_{0}^{0.25} G\,\mathrm{d}\zeta = 3.82\sqrt{\frac{u_*^3}{\kappa\nu h}} \tag{12.16b}$$

and the equlibrium floc size in the lower part of the water column D_l follows from (12.8):

$$D_l = \frac{k_A c}{k_B \sqrt{G_l}} \tag{12.17}$$

The settling time of large flocs in the upper part of the water column T_s is found from Equation (12.5):

$$T_s = \frac{h}{w_s} \approx \frac{h}{\alpha'' D_u} \tag{12.18}$$

where D_u is the floc size in equilibrium with G_u and α'' is defined before. If the relative flocculation time $T_f/T_s < 1$, we expect that considerable aggregation can take place so that flocs higher in the water column are much larger than those near the bed. Substitution from Equation (12.15) through (12.18) yields T_f/T_s:

$$\frac{T_f}{T_s} = \frac{\alpha''}{k_A c h} \frac{1}{G_u} \sqrt{\frac{G_l}{G_u}} \approx 0.0012 \sqrt{\frac{1}{h c^2 u_*^3}} \tag{12.19}$$

where we use the various parameter values obtained for Ems mud. The relative flocculation time T_f/T_s is depicted in Figure 12.8 for a variety of suspended sediment concentrations, showing under which conditions considerable vertical gradients in

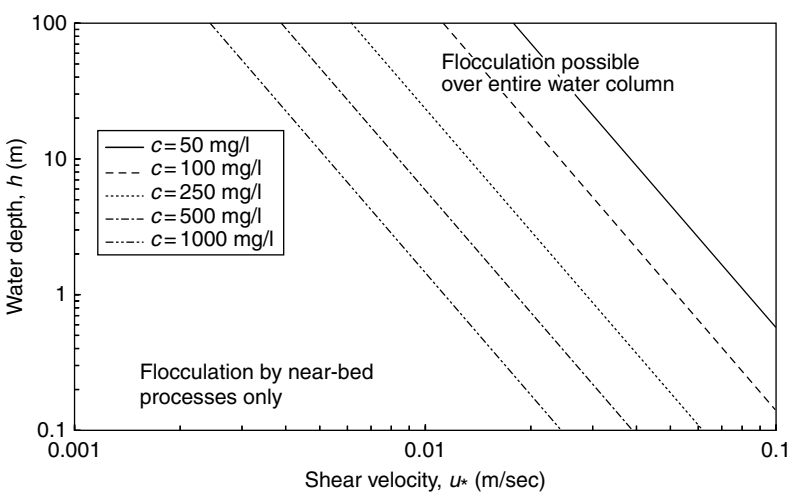

FIGURE 12.8 Relative flocculation time of mud flocs in water column (Equation (12.19)). At large h and u_*, residence time is large, c.q. flocculation time is small and we expect $D_u \gg D_l$. At small h and u_*, residence time is small, c.q. flocculation time is large and we expect $D_u \approx D_l \approx D_{l,e}$.

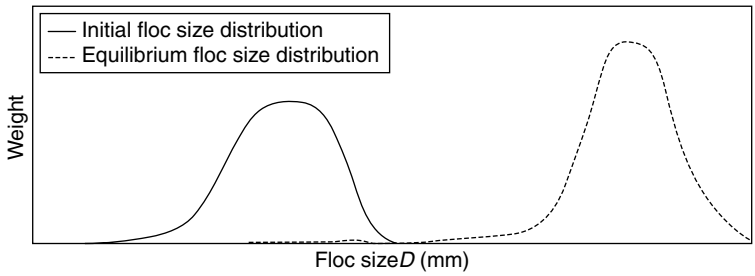

FIGURE 12.9 Particle size distribution for initial and equilibrium conditions. (After Kranck and Milligan, *J. Geoph. Res.*, 97(C7), 11373–11382, 1992.)

floc size (i.e., $D_u \gg D_l$) are expected to occur. This graph suggests that for estuarine conditions, with shear velocities of a few centimeters per second, vertical gradients in floc size only occur for suspended sediment concentrations beyond a few 100 mg/l. Around slack water, suspended sediment concentrations should even be much larger to generate significant vertical gradients in floc size (e.g. Winterwerp[9]). It is noted that these results are obtained for the parameter settings obtained from laboratory experiments with Ems mud, and therefore cannot be considered to be universally valid. However, this analysis clearly indicates that flocculation processes higher in the water column, as depicted in Figure 12.3, can only occur if the residence time of the flocs in the water column is large enough.

If the flocculation time is much larger than the residence time (i.e. lower left corner of Figure 12.8) vertical gradients in floc size are small: $D_u \approx D_l$. As D_l is expected to be in equilibrium with the local near-bed hydro-sedimentological conditions (i.e. local G and c), the mean floc size throughout the water column can be estimated from these conditions only.

This analysis was dedicated to one floc size only. However, a limitation in residence times will also have implications for wide floc size distributions, as observed in nature. Figure 12.9 presents the initial floc size distribution, that is, prior to flocculation, and the floc size distribution for equilibrium conditions, as measured by Kranck (Kranck and Milligan[22]). It shows a shift toward larger flocs in the equilibrium situation, as expected. However, if equilibrium conditions are not met, more or less any floc size distribution in between the two curves of Figure 12.9 may occur. Of course, this observation also holds for the median floc size. It is clear that this has major implications on the interpretation of floc size data obtained in the marine environment.

12.4 FLOC SIZE DISTRIBUTION OVER THE TIDAL CYCLE

Let us next examine how flocculation affects the sediment dynamics in a turbidity maximum. For this purpose, we analyze the field measurements carried out in the Ems estuary at the border of The Netherlands and Germany (Van Leussen[5]) with the use of a IDV-model. Contrary to Sections 12.2 and 12.3, we now include all physical processes in our analysis, such as settling and turbulent mixing, the effects of sediment–fluid interaction and flocculation. For details on this model, the reader is referred to Winterwerp.[9]

These measurements were carried out in June 1990 along five stretches of the river. At each stretch, two anchor stations at a mutual distance of approximately 1 km were deployed to measure the flow velocity with an Ott meter, the salinity from conductivity and temperature measurements, and the suspended sediment concentration with a Partech turbidity meter, or by taking water samples at high suspended sediment concentrations. During 13 h these parameters were measured every $\frac{1}{2}$ h at 0.3, 0.5, 1, 2 m, etc. above the bed, till 1.5 m below the water level. Along these stretches, measurements were also taken from a moving vessel, determining the relative flow velocity, salinity, and suspended sediment concentration with identical instruments, and the floc size and settling velocity with a video system (VIS). A summary of the measuring locations is presented in Figure 12.10, from Van Leussen.[5]

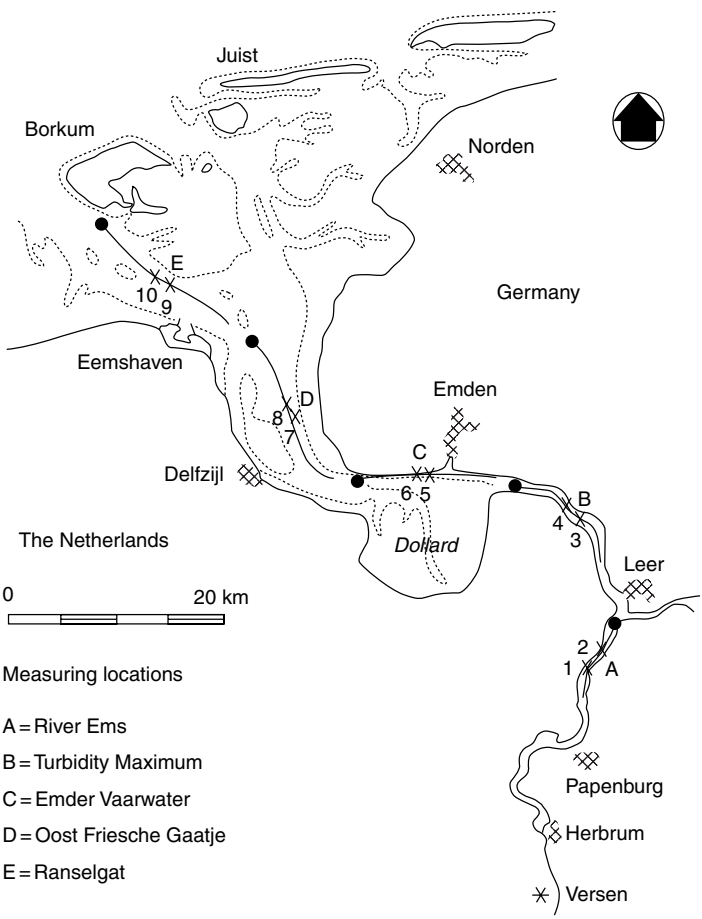

FIGURE 12.10 Locations of field measurements in the Ems estuary. (After Van Leussen, PhD thesis, University of Utrecht, The Netherlands, 1994.)

The river discharge during these measurements was about 10 to 25 m^3/sec, which is very low for the Ems river. As a result, the turbidity maximum is located around stretch B, about 15 km upstream of its usual location in the Emder Fahrwasser. Because of this low river discharge, vertical salinity gradients were virtually absent during the entire measuring campaign. Moreover, the salinity at Station 1 and 2 remains almost constant at $S \approx 0.2$ ppt.

The water level and flow velocity at Stations 1 and 2 were almost identical, and h and U at both stations were also almost in phase. The suspended sediment concentration c at Station 1 was also almost identical to that at Station 2, though during maximum flow velocity, the measured values at Station 1 were somewhat larger than at Station 2. This indicates that, though advection certainly played a role, horizontal gradients in sediment concentration were small. Hence these data are suitable for analysis with a 1DV-model. Maximum values of the depth-mean concentration C varied from about 0.7 to 1.0 g/l during maximum flood and maximum ebb velocity (MEV) down to about 0.3 g/l during slack water, for example, Van Leussen[5] and Winterwerp.[9] Figure 12.11, presenting the measurements in the form of isolutals (i.e. lines of equal suspended sediment concentration), shows that during flood, the sediment was almost homogeneously mixed over the water depth, whereas during ebb, more stratified conditions occurred. Around high water slack (HWS), the suspended sediment concentration dropped rapidly. The very large concentrations around $t = 1000$ min are attributed to instabilities of the steep mud banks, supplying large amounts of mud to the river (Van Leussen[23]), and will be ignored.

The measurements in Station 1 and 2 have been simulated with a 1DV-model, including the effects of sediment-induced buoyancy effects and turbulence-induced flocculation (Winterwerp[9,20]). The measured variation in water level and depth-mean flow velocity is prescribed, and the measured depth-mean suspended sediment concentration is set at $C_0 = 0.61$ g/l, according to the data. All sediment remains in

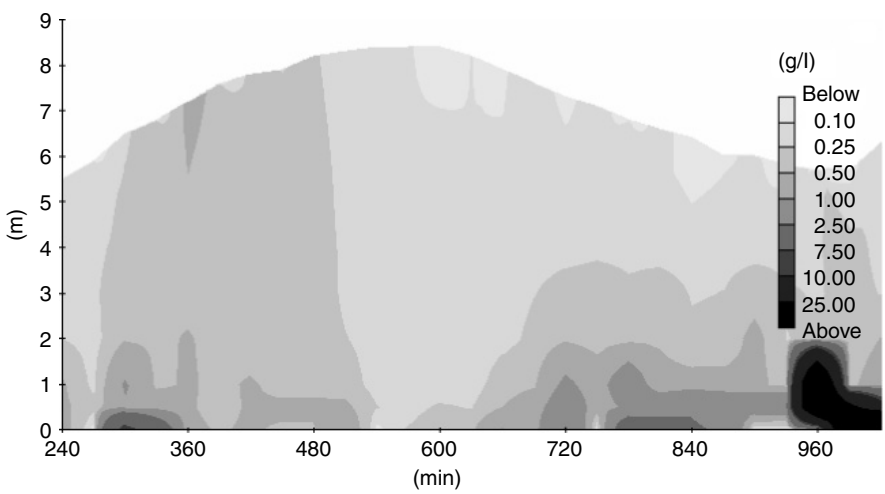

FIGURE 12.11 Isolutals from measurements at Station 2.

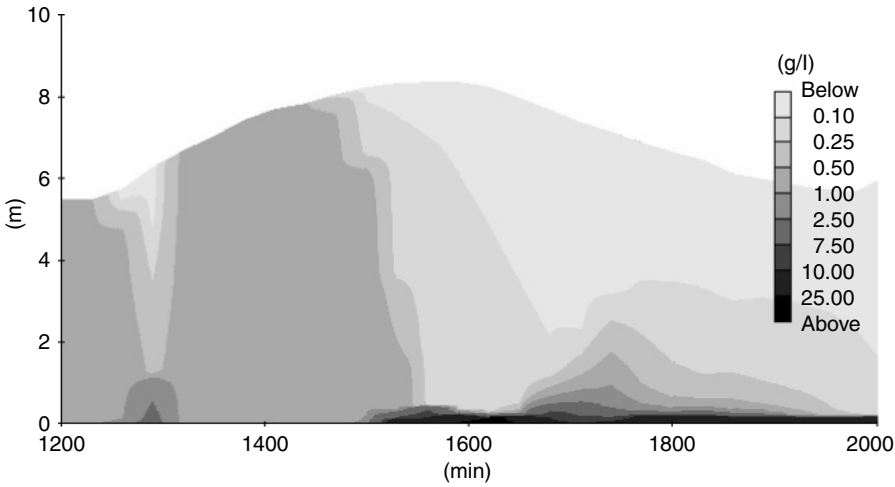

FIGURE 12.12 Isolutals computed with 1DV model with flocculation model. (Subtract 1000 min from time axis to compare with Figure 12.11.)

the computational domain, that is, neither sedimentation nor erosion is modeled. The results of the computations are shown in Figure 12.12 in the form of isolutals and as vertical concentration profiles at $t = 1420$ and 1780 min in Figure 12.13. Note that the model is first run for 1000 min to mediate for spin-up effects; these 1000 min have to be subtracted from the horizontal axes.

The computational results reproduce the vertical structure of the measured concentration distribution, including the characteristic rapid settling around HWS. It is noted that it was not possible to reproduce the character of the measured data with 1DV-computations with a constant settling velocity (no flocculation) or with a constant fluid density (no sediment–fluid interaction), for example, Winterwerp.[9]

During flood, at $t = 1420$ min, the sediment is almost homogeneously distributed over the water column, whereas at $t = 1780$ min, around MEV, the concentration profile is highly stratified.

As the turbulence intensities vary over the tidal cycle, floc size, hence settling velocity, is expected to vary over the tidal cycle. This is indeed the case, as depicted in Figure 12.1, showing the time variation in settling velocity, measured by Van Leussen.[5] Such a variation in floc size, hence settling velocity, was also computed with the 1DV-model, as shown in Figure 12.14, though the time phase of w_s does not match the measured pattern exactly. The absolute value of the computed settling velocity, however, agrees very well with the measurements. The large value of w_s around slack water explains the rapid settling of the sediment around slack water ($t = 1500$ min), as observed during the measuring campaign and predicted with the 1DV-model. The values of w_s around slack water are limited (i.e., much smaller than the equilibrium values) by the large flocculation time T_f around slack water, as shown in Figure 12.15: T_f increases to many hours around slack water, as a result of which equilibrium floc sizes cannot be achieved. The very large flocculation time

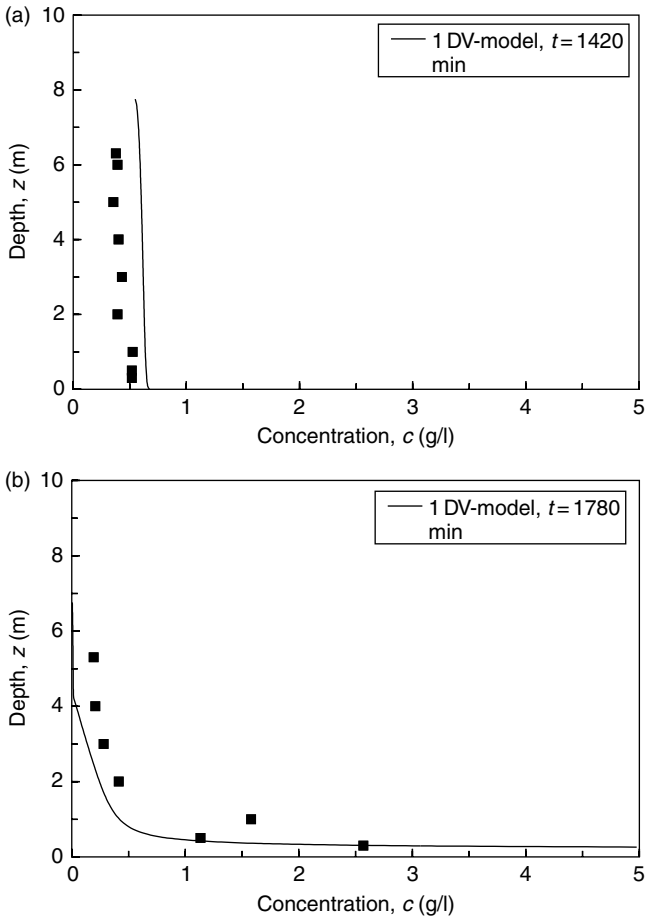

FIGURE 12.13 Computed and measured vertical concentration profiles at (a) t = 1420 minutes and (b) t = 1780 minutes. (Subtract 1000 min from time axis to compare with Figure 12.11.)

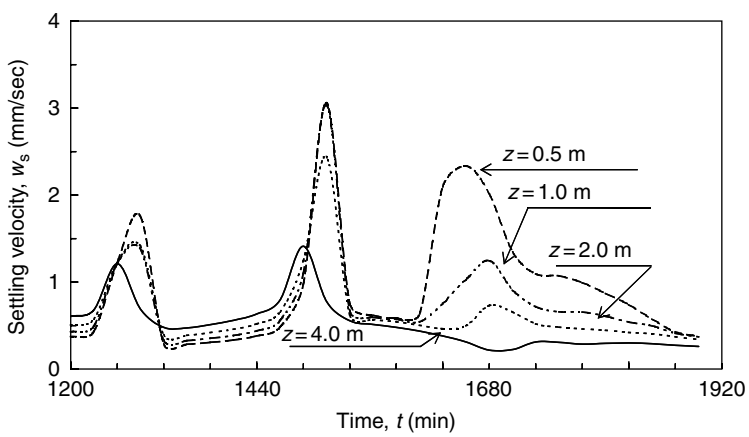

FIGURE 12.14 Computed variation in settling velocity. (Subtract 1000 min from time axis to compare with Figure 12.11.)

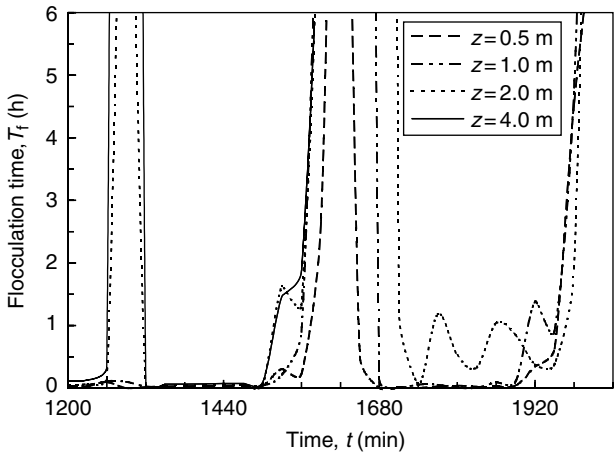

FIGURE 12.15 Computed variation in flocculation time. (Subtract 1000 min from time axis to compare with Figure 12.11.)

around LWS is probably due to the large stratification at that time. Only during MFV equilibrium floc sizes are predicted.

Further, it is important to note that during rising tide (flood), larger settling velocities are found in the upper part of the water column, whereas during falling tide (ebb), larger settling velocities are found near the bed. This results in a destabilizing effect on the vertical concentration profile during flood. The stabilizing effect during ebb enhances the sediment-induced buoyancy effects, resulting in the stratified conditions during ebb. The floc size, hence settling velocity, is governed by the turbulence intensity, parameterized by G and the suspended sediment concentration c (Equation (12.8)). Apparently for the current conditions, the effect of turbulence ("G-effect") is dominant during flood, whereas the effect of concentration ("c-effect") is dominant during ebb.

12.5 SEDIMENT CONCENTRATIONS IN FLUID MUD LAYERS

When mud flocs settle on the bed, they form a space-filling network structure, referred to as a gel, and a measurable strength builds up. The concentration at which this happens is referred to as the gelling point. The volumetric concentration ϕ_f then becomes unity, see Equation (12.4). If we assume that the flocculation model is also valid for these conditions, we can establish the gelling concentration c_{gel} for equilibrium conditions ($dD_f/dt = 0$) as a function of shear rate parameter G for various values of the fractal dimension n_f from the relation (12.4) and the Lagrangian flocculation model (12.7). We assume that $D_p \ll D_f$, and that the sediment concentration is constant, yielding

$$c_{gel} = \left(\frac{a e_b}{k'_A} \sqrt{\frac{\mu}{F_y}} \right)^{(3-n_f)/(4-n_f)} D_p^{(3-n_f)/(4-n_f)} \rho_s G^{(3-n_f)/(2(4-n_f))} \qquad (12.20)$$

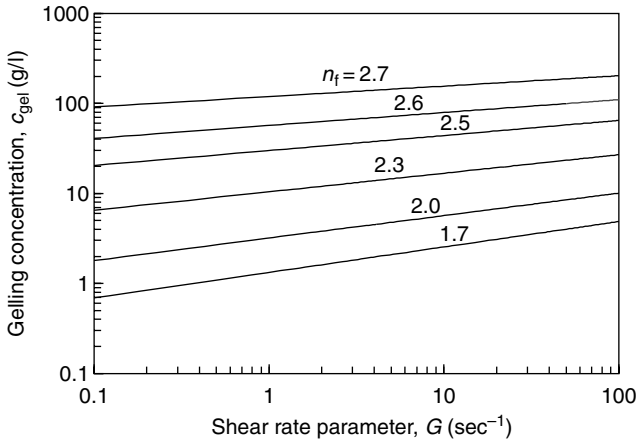

FIGURE 12.16 Variation of gelling concentration c_{gel} with n_f and G for equilibrium conditions. (Equation (12.20).)

Using the various model parameters assessed in Section 12.2, $c_{gel}(G, n_f)$ can be established for equilibrium conditions. The results are presented in Figure 12.16, showing the high sensitivity of c_{gel} to n_f at larger values of n_f. For $n_f = 3$, we obtain the trivial result that $c_{gel} = \rho_s$. We observe that for $n_f = 2.6$ to 2.7, we find $c_{gel} \approx 100$ g/l, which is a characteristic concentration for fluid mud occurrences. However, these n_f values are unrealistically large.

It appears impossible to obtain c_{gel} values of the order of 100 g/l by modifying the other parameters of the flocculation model within reasonable limits. Hence, by applying the flocculation model for equilibrium conditions, fluid mud concentrations of about 100 g/l can only be obtained with fractal dimensions substantially larger than the average n_f values encountered for the mud flocs in the water column. This is an important conclusion, which is explained by the response time of the flocs to a variation in hydrodynamic conditions. Apparently, the fluid mud forming flocs are much smaller than the equilibrium values to be expected within the fluid mud layer because the flocs (settling from the upper part of the water column) get insufficient time to grow. Again, the residence time is the limiting factor here.

Next, 1DV-simulations for Station 3 of Figure 12.10 in the turbidity maximum are discussed. As the horizontal gradients in concentration are fairly large in this area (Van Leussen[5]), such simulations can only be indicative to predict qualitative trends. Again, the measured variation in water-depth and depth-mean velocity are prescribed, and the depth-mean suspended sediment concentration is set at the measured value of $C_0 = 5$ g/l.

The computed vertical concentration distribution at three times is compared with the measurements in Figure 12.17, showing that the near-bed concentrations (fluid mud) are reasonably predicted. It is noted that the observed near-bed concentrations depicted in Figure 12.17 can only be reproduced when the full flocculation model is

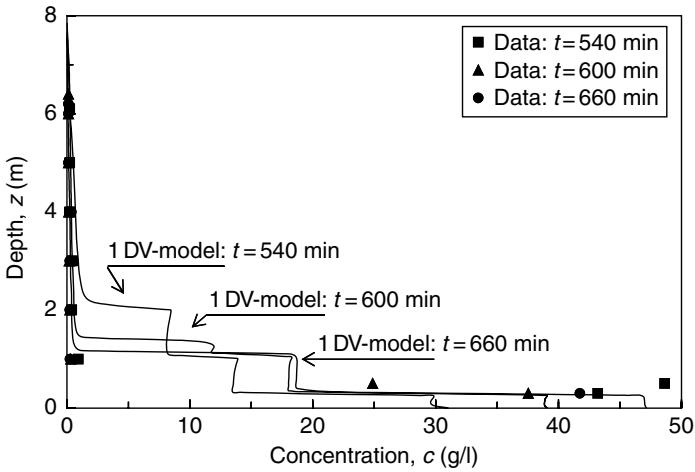

FIGURE 12.17 Comparison of computed and measured concentration distributions and formation of fluid mud at Station 3, turbidity maximum.

TABLE 12.1
Typical Fluid Mud Concentrations (c_{gel}) in Estuaries

Location	Reference	Fluid Mud Concentration (g/l)	Remarks
Severn	Crickmore[24] Kiby and Parker[25]	Appr. 10	
Parret	Odd et al.[26]	40–80	Above cons. bed
Ems Estuary	Van Leussen[5]	Appr. 40	0.35 m from bed
Amazon	Kineke et al.[27,28]	40–250	0–2 m from bed
Loire	Le Hir[29]	Appr. 40	1 m thick layers
Jiaojiang River	Guan et al.[30]	Appr. 40	0.35 m from bed

included in the 1DV-computations. If relaxation effects are omitted, the computed fluid mud concentrations would be much smaller (e.g. the values of Figure 12.16 at $n_f = 2$) because the floc size would become unrealistically large.

It is further noted that the computed values are also in the range of fluid mud concentrations encountered in estuaries and coastal areas, as reported in the literature, and presented in Table 12.1. These values show a considerable scatter, however. The large values on the Amazon shelf may be attributed to the large flow-induced shear stresses, reducing the floc size significantly, yielding large fluid mud concentrations.

We have shown that the suspended sediment behavior in/near the turbidity maximum in the Ems estuary is characterized by a rapid settling around slack water and

a highly stratified concentration profile during ebb. Our analysis of the data with a 1DV-model reveals that this behavior is governed by two processes:

1. Sediment-induced buoyancy effects (not treated here).
2. Flocculation:
   (a) The large growth in floc size, hence settling velocity, causes rapid settling around slack water.
   (b) The stable floc size, hence settling velocity profile during ebb enhances the effects of stratification.

The flocculation time, in relation to the time scale of the driving forces, is important in limiting the growth of the flocs, hence the settling velocity around low-turbulent slack water conditions. Moreover, these relaxation effects result in fluid mud concentration (gelling concentration) of a few tens of grams per liter.

12.6 DISCUSSION AND CONCLUSIONS

We have developed a simple model for turbulence-induced flocculation of cohesive sediment. This model predicts floc sizes, settling velocities, and fluid mud concentrations in agreement with observations in natural systems. We predict large flocculation times, that is, of the order of many hours and more, at low sediment concentration and low turbulence intensity (turbulent shear stresses). These large flocculation times explain the evolution of floc size as a function of shear stress, as hypothesized by Dyer[6] (e.g. Figure 12.2): at low shear stress, the cohesive sediment particles have insufficient time to form large flocs.

This implies that for field conditions at low concentration, as met in many rivers and coastal areas, the floc size is governed by near-bed hydrodynamic processes only. Only at higher concentrations, as often encountered in estuaries, variations in floc size over the water depth, as sketched in Figure 12.3, are expected.

Under such high concentrations, large temporal variations in floc size are also expected (e.g. Figure 12.1 and Figure 12.14). In particular, during slack water, floc size and settling velocity are expected to grow significantly. This growth explains the rapid settling around slack water as often observed in turbid environments (e.g. Figure 12.11). However, their growth is limited by a limited residence time of these flocs in the turbulent water column. In other words, around slack water, no equilibrium conditions are to be expected, contrary to the conditions around MFV (and MEV), when flocculation times are small and equilibrium can be attained.

Sediment concentrations in fluid mud layers are also affected by history effects. The fluid mud forming flocs settling from the upper part of the water column have insufficient time to grow to the equilibrium values that might be expected within the fluid mud layer. Moreover, the vertical density gradients induced by the settling sediment decrease turbulence intensity, augmenting the effect of flocculation time. The large sediment-induced stratification observed in the Ems River is probably responsible for the very large flocculation times predicted around slack water.

These conclusions imply that at low concentrations, floc sizes throughout the water column are in equilibrium with the near-bed processes. Under high concentrations, equilibrium is expected only around MFV and MEV. Around slack water, the flocs can have almost any size, depending on the local hydrodynamic conditions and history effects. This means that measurements of floc size, for example, settling velocity can only be interpreted properly if the hydro-sedimentological conditions and their history are measured as well.

REFERENCES

1. Krone, R.B., Flume studies of the transport of sediment in estuarial shoaling processes, Final Report *Hydraulic Engineering Laboratory and Sanitary Engineering Research Laboratory*, University of California, Berkeley, USA, 1962.
2. Krone, R.B., The significance of aggregate properties to transport processes, in *Lecture Notes on Coastal and Estuarine Studies*, 14, Estuarine and Cohesive Sediment Dynamics, Springer Verlag, 66–84, 1986.
3. Argaman, Y. and Kaufman, W.J., Turbulence and flocculation, *J. Sanit. Eng. Div*, 96, SA2, 223–241, 1970.
4. Parker, D.S., Kaufman, W.J., and Jenkins, D., Floc breakup in turbulent flocculation processes, *J. Sanit. Eng. Div.*, 98, SA1, 79–97, 1972.
5. Van Leussen, W., Estuarine macroflocs and their role in fine-grained sediment transport, PhD thesis, *University of Utrecht*, The Netherlands, 1994.
6. Dyer, K.R., Sediment processes in estuaries: future research requirements, *J. Geoph. Res.*, 94(C10), 14327–14339, 1989.
7. Van Leussen, W., Aggregation of particles, settling velocity of mud flocs — a review, in *Physical Processes in Estuaries*, ed. J. Dronkers and W. van Leussen, Springer-Verlag, Heidelberg, 348–403, 1988.
8. Winterwerp, J.C., A simple model for turbulence induced flocculation of cohesive sediment, *J. Hydr. Eng.*, 36(3), 309–326, 1998.
9. Winterwerp, J.C., On the flocculation and settling velocity of estuarine mud, *Continetal Shelf Res.*, 22, 1339–1360, 2002.
10. Hogg, R., Klimpel, R.C., and Ray, D.T., Structural aspects of floc formation and growth, in *Flocculation, Sedimentation and Consolidation*, ed. B.M. Moudgil and P. Somasundaran, University of Florida, Gainesville, USA, 217–227, 1985.
11. McAnally, W.H. and Mehta, A.J., Significance of aggregation of fine sediment particles in their deposition, *Est., Coast. Shelf Sci.*, 54, 643–653, 2002.
12. McCave, I.N., Size spectra and aggregation of suspended particles in the deep ocean, *Deep Sea Res.*, 31(4) 329–352, 1984.
13. Wacholder, E. and Sather, N.F., The hydrodynamic interaction of two unequal spheres moving under gravity through quiescent viscous fluid, *J. Fluid Mech.*, 5, 417–437, 1974.
14. Stolzenbach, K.D. and Elimelech, M., The effect of density on collisions between sinking particles: implications for particle aggregation in the ocean, *J. Deep Sea Res.* I, 41(3), 469–483, 1994.
15. Kranenburg, C., On the fractal structure of cohesive sediment aggregates, *Est., Coast. Shelf Sci.*, 39, 451–460, 1994.
16. Vicsek, T., *Fractal Growth Phenomena*, World Scientific, Singapore, 1992.
17. Gibbs, R.J., Estuarine flocs: their size, settling velocity and density, *J. Geoph. Res.*, 90(C2), 3249–3251, 1985.

18. Fennessy, M.J., Dyer, K.R., and Huntley, D.A., INSSEV: an instrument to measure the size and settling velocity of flocs in situ, *Mar. Geol.*, 117, 107–117, 1994.
19. Hawley, N., Settling velocity distribution of natural aggregates, *J. Geoph. Res.*, 87(C12), 9489–9498, 1982.
20. Winterwerp, J.C., Stratification effects by cohesive and non-cohesive sediment, *J. Geoph. Res.*, 106(C10), 22,559–22,574, 2001.
21. Nezu, I. and Nakagawa, H., *Turbulence in Open-Channel Flows*, International Association for Hydraulic Research, Monograph Series, Balkema, Rotterdam, 1993.
22. Kranck, K. and Milligan, T.G., Characteristics of suspended particles at an 11-hour anchor station in San Francisco Bay, California, *J. Geoph. Res.*, 97(C7), 11373–11382, 1992.
23. Van Leussen, W., 1999, personal communication.
24. Crickmore, M.J., Data collection — tides, tidal currents and suspended sediment, *The Dock Harbour Auth.*, LXIII, 742, 183–186, 1982.
25. Kirby, R. and Parker, W.R., Distribution and behavior of fine sediment in the Severn estuary and inner Bristol Channel, UK, *Can. J. Fish. Aquat. Sci.*, 40, 83–95, 1983.
26. Odd, N.V.M., Bentley, M.A., and Waters, C.B., Observations and analysis of the movement of fluid mud in an estuary, in *Coastal and Estuarine Studies*, Vol. 42, American Geophysical Union, 430–446, 1993.
27. Kineke, G.C. and Sternberg, R.W., Distribution of fluid muds on the Amazon continental shelf, *Mar. Geol.*, 125, 193–233, 1995.
28. Kineke, G.C., Sternberg, R.W., Trowbridge, J.H., and Geyer, W.R., Fluid mud processes on the Amazon continental shelf, *Continental Shelf Res.*, 16(5/6), 667–696, 1996.
29. Le Hir, P., Fluid and sediment "integrated" modelling application to fluid mud flows in estuaries, in *Proceedings of the 4th Nearshore and Estuarine Cohesive Sediment Transport Conference, INTERCOH'94*, Wallingford, UK, July 1994, ed. N. Burt, R. Parker, and J. Watts, John Wiley & Sons, 417–428, 1997.
30. Guan, W.B., Wolanski, E., and Dong, L.X., Cohesive sediment transport in the Jiaojiang River Estuary, China, *Est. Coast. Shelf Sci.*, 46, 861–871, 1998.

13 Coagulation Theory and Models of Oceanic Plankton Aggregation

George A. Jackson

CONTENTS

13.1 INTRODUCTION

Two of the most fundamental properties of any particle, inert or living, are its length and its mass. These two properties determine how a particle interacts with planktonic organisms as food or habitat, how it affects light, and how fast it sinks. Because organisms are discrete entities, particle processes affect them as well as nonliving material.

Life in the ocean coexists with two competing physical processes favoring surface and bottom of the ocean: light from above provides the energy to fuel the system;

1-56670-615-7/05/$0.00+$1.50

gravity from below collects essential materials encapsulated in particles. Coagulation is the formation of single, larger, particles by the collision and union of two smaller particles; very large particles can be made from smaller particles by multiple collisions. Coagulation makes bigger particles, enhances sinking rates, and accelerates the removal of photosynthate. One result is that coagulation can limit the maximum phytoplankton concentration in the euphotic zone.

Particle size distributions have been measured since the advent of the Coulter Counter in the early 1970s, when Sheldon et al.[1] reported on size distributions predominantly from surface waters around the world. They reported values for particles ostensibly between 1 and 1000 μm, although sampling and instrumental consideration suggest that the range was significantly smaller.[2] There were approximately equal amounts of matter in equal logarithmic size intervals,[1] a distribution that is characteristic of a particle number size spectrum $n \sim r^{-4}$, where r is the particle radius and n is defined in Equation (13.1), and has inspired theoretical models of planktonic systems. Platt and Denman[3] explained the spectral shape using an ecologically motivated model in which mass cascade energy from one organism to its larger consumer. While the emphasis on organism interactions neglected the interactions of nonliving particles, it stimulated the study of organism size–abundance relationships.[4–7] Hunt[8,9] was the first to argue that coagulation theory could explain the spectral slope in the ocean.

The use of coagulation theory to explain planktonic processes in the ocean is more recent and was inspired by observations of large aggregates of algae and other material that were named "marine snow."[10–13] Among the first observations relating marine snow length and mass were the field and laboratory observations of Alldredge and Gotshalk,[14] who fit particle settling rate to power-law relationships of particle length and mass. These observations were later interpreted by Logan and Wilkinson[15] as resulting from a fractal relationship between mass and length.

While there has been an extensive history of applying coagulation theory to explain the removal of particulate matter from surface waters, most early work emphasized coagulation as a removal process in lakes and esuaries.[16–19] Hunt[9] argued that particle size distributions in the ocean were characteristic of coagulation processes, using a dimensional argument that had been made to explain characteristic shapes of atmosphere particle distributions.[20] The influential review of McCave[21] examined the mechanisms and rates of coagulation in the ocean, but purposely passed over particle interactions in the surface layer because of the belief that biological processes would overwhelm coagulation there.

The early models of planktonic systems[22–24] showed that coagulation could occur at rates comparable to those of more biological processes and helped to focus observations on the role of coagulation in marine systems. The physical mechanisms used to describe interactions between inorganic particles in coagulation theory have also been modified to describe the interactions between different types of planktonic organisms, with feeding replacing particle sticking.[25–30]

This chapter is a survey that highlights some of the evolution and usage of coagulation theory to describe dynamics of planktonic systems. The emphasis is on the physical aspect of coagulation theory, describing collision rates, rather than on the chemical aspect, describing the probability of colliding particles sticking together.

As the theory has evolved, the range of formulations applied to plankton models has increased, with no one formulation becoming standard. The divergence between the evolving sophistication of the models and their usage with observational data is symptomatic of this lack of consensus in models. More attention needs to paid to developing simple diagnostic indices that can be used to interpret field observations.

13.2 PRIMER ON PARTICLE DISTRIBUTION AND DYNAMICS

13.2.1 Particle Properties

A case in which the source particles are of one size allows the description of the mass of a particle in terms of the number of monomers present in it (e.g., using the index i), as well as the number concentration (C_i) of such particles. For more typical situations, the distribution in particle size is usually given in terms of the cumulative particle size spectrum $N(s)$, the number of particles smaller than size s, or the differential size spectrum $n(s)$

$$n = -\frac{\mathrm{d}N}{\mathrm{d}s} \tag{13.1}$$

(Note that symbols are also defined in Table 13.1.) Aggregates are not solid spheres that conserve volume when they combine. Theoretical studies[31,32] and observations[15,33–35] have shown that the density declines as aggregate size increases. This increase is usually described using fractal scaling between mass and length:

$$m \sim r^{D_\mathrm{f}} \tag{13.2}$$

where m is the particle mass, r is the particle radius, often identified with the radius of gyration, and D_f is the fractal dimension. If volume were conserved, D_f would equal 3. Observations on aggregated systems yield values of D_f ranging from 1.3 to 2.3.[15,33–36]

13.2.2 Particle Collision Rates

The description of collision rates between particles is the foundation of physical coagulation theory. The rate of collision between two different size particles present at number concentrations of C_i and C_j is

$$\text{Collision rate} = \beta_{ij} C_i C_j \tag{13.3}$$

where β_{ij} is the particle size-dependent rate parameter known as the coagulation kernel. The three different mechanisms used to describe particle collision rates and their rate constants are Brownian motion, $\beta_{ij,\mathrm{Br}}$; shear, $\beta_{ij,\mathrm{sh}}$; and differential sedimentation, $\beta_{ij,\mathrm{ds}}$. The total β_{ij} is usually assumed to be the sum of these three.[20,37] The *rectilinear* formulations are the simplest expressions for these terms and are calculated

TABLE 13.1
Notation: Dimensions are Given in Terms of Length *L*, Mass *M*, and Time *T*

Symbol	Description	Dimensions
C_i	Number concentration of ith particle type	$\#\,L^{-3}$
C_{cr}	Critical particle number concentration	$\#\,L^{-3}$
$C_{V,i}$	Volume concentration of ith particle type	—
$C_{V,cr}$	Critical particle volume concentration	—
D_i	Diffusivity of ith particle type	L^2T^{-1}
D_f	Fractal dimension	—
M	Particle mass	M
n	Particle differential number spectrum	$\#\,L^{-4}$
N	Particle cumulative number spectrum	$\#\,L^{-3}$
r, r_i	Particle radius	L
s	Particle size (mass, length, ...)	—
v_i	Settling velocity of ith particle type	
V, V_i	Particle volume	L^3
Z	Mixed layer depth	L
α	Particle stickiness	—
α'	Stickiness estimated in polydisperse systems	—
β	Coagulation kernel	L^3T^{-1}
γ	Average shear	T^{-1}
λ	Ratio of particle radii, r_1/r_2	—
η	Ratio of particle concentrations, C_1/C_2	—
μ	Algal specific growth rate	T^{-1}

assuming that the particles are impermeable spheres whose presence does not affect water motion, and that chemical attraction or repulsion has negligible effect:

$$\beta_{ij,\mathrm{Br}} = 4\pi(D_i + D_j)(r_i + r_j) \tag{13.4}$$

$$\beta_{ij,\mathrm{sh}} = 1.3\gamma(r_i + r_j)^3 \tag{13.5}$$

$$\beta_{ij,\mathrm{ds}} = \pi(r_i + r_j)^2|v_i - v_j| \tag{13.6}$$

where i and j are the particle indices, r_i is the radius of the ith particle, v_i is its fall velocity, D_i its diffusivity, and γ the average fluid shear.[37]

There are adjustments to these equations that account for fluid flow around the larger particle for the shear[24] and differential sedimentation[38] terms in what I will call the *curvilinear* approximation, as well as higher order terms that include greater hydrodynamic detail as well as attractive forces.[39,40] For example, considering the flow field around a larger particle when considering the rate of collision with a smaller for differential sedimentation leads to[24]

$$\beta_{ij,\mathrm{ds}} = 0.5\pi r_i^2|v_j - v_i| \tag{13.7}$$

where $r_j > r_i$. Similarly, the shear kernel becomes[38]

$$\beta_{ij,\mathrm{sh}} = 9.8\frac{p^2}{(1+2p)^2}\gamma\,(r_i + r_j)^3 \tag{13.8}$$

where $p = r_i/r_j$ and $r_j > r_i$.

The coagulation equations describe the rate of change of each size fraction in terms of the processes which change particle concentration.

$$\frac{\mathrm{d}C_j}{\mathrm{d}t} = \frac{\alpha}{2}\sum_{i=1}^{j-1}\beta_{i,j-i}C_{j-i}C_i - \alpha\sum_{i=1}^{\infty}\beta_{ij}C_jC_i + \text{sources} - \text{sinks} \tag{13.9}$$

where sinks can include loss from settling out of a mixed layer and sources can include algal growth and division.

The equations are modified when considering continuous distributions described with a particle size spectrum:

$$\frac{\partial n(m,\,t)}{\partial t} = \frac{\alpha}{2}\int_0^m n(m-m',\,t)n(m',\,t)\beta(m-m',\,m')\mathrm{d}m' - \alpha\int_0^\infty n(m,\,t)n(m',\,t)\beta(m,\,m')\mathrm{d}m' + \text{sources} - \text{sinks} \tag{13.10}$$

where m is the particle mass.

The integro-differential equations that result from using the number spectra require approximations to solve. Approaches include solving analytically after assuming that $n = ar^{-b}$ (the Jungian spectrum) and solving numerically after separating the spectrum into particle size regions in which the shape as a function of size is constant but the total mass in the region varies (the sectional approach of Gelbard et al.[41]).

One implication of fractal scaling is that aggregates are porous, a property which affects the flow through and around an aggregate. Li and Logan[42,43] have documented the effect of this porosity on particle capture. Their results have been used to modify the coagulation kernels.[44]

The simple fractal relationship presupposes that a system is initially monodisperse (all particles the same). Jackson[45] proposed that a consequence of fractal scaling is that r^{D_f} is conserved in a two-particle collision, in the same way that mass is. This was used to develop two-dimensional particle spectra that describe particle concentrations as functions of particle mass and r^{D_f}.

An important factor in determining whether two colliding particles combine is the stickiness α. Considering the probability of a contact causing two particles to combine, α is usually empirically determined or used as a fitting parameter (see below).

Observations on algal cultures have shown that it can vary with species and with nutritional status for any species with observed values ranging from 10^{-4} to 0.2 (see ref. 46).

Other issues which can affect net coagulation rates are the effect of non-spherical shape,[24,47] and the breakup, or disaggregation, of larger aggregates from fluid forces that exceed the particle strength.[48,49]

13.3 EXAMPLES OF SIMPLE MODELS RELEVANT TO PLANKTONIC SYSTEMS

13.3.1 Rectilinear, Monodisperse, and Volume Conserving

13.3.1.1 Phytoplankton and the Critical Concentration

The original model of Jackson[22] considered an algal population in the surface mixed layer as consisting of single cells whose number concentration C_1 increased as the cells divided with a specific growth rate μ and which disappeared as they fell out of a mixed layer and as they collided to form aggregates:

$$\frac{dC_1}{dt} = \mu C_1 - \alpha \sum_{i=1}^{\infty} \beta_{1i} C_1 C_i - \frac{v_1}{Z} C_1 \tag{13.11}$$

where α is the stickiness, Z is the mixed layer thickness, and v_1 is the settling velocity of a particle composed of one algal cell. Concentrations of aggregates containing j algal cells increased and decreased with aggregation and sinking:

$$\frac{dC_j}{dt} = \frac{\alpha}{2} \sum_{i=1}^{j-1} \beta_{i,j-i} C_{j-i} C_i - \alpha \sum_{i=1}^{\infty} \beta_{ij} C_j C_i - \frac{v_j}{Z} C_j \tag{13.12}$$

for $j > 1$. Note that the index $(j-i)$ is used to indicate that a particle with j monomers requires that the second particle in a collision have $(j-i)$ monomers if the first particle has i monomers. The original model used rectilinear kernels, initially monodisperse particle sources and mass–length relationships akin to fractal scaling.

Simulation results of such a system show that this is essentially a two-state system (Figure 13.1; parameter values in figure caption). For the first 3 days, the only particle size class to change is that of single algal cells, which increases exponentially (linear in a logarithmic axis); larger particles have essentially constant concentrations. With time, ever large particles have their concentrations changed. For the particles composed of 30 monomers, there is an increase in concentration of about 10 orders of magnitude between days 6 and 9. After day 9, there is essentially no change in concentration. The difference in the first 3 days and the period after day 6 can be understood as resulting from very few formation of aggregates at low algal concentrations, but formation of aggregates at a rate that matches algal division at higher monomer concentrations. The rapid aggregate formation blocks any further increase in algal numbers despite continued cell production.

The limitation can be understood by simplifying Equation (13.11) and assuming that the most important loss for single cells is to collision and subsequent coagulation

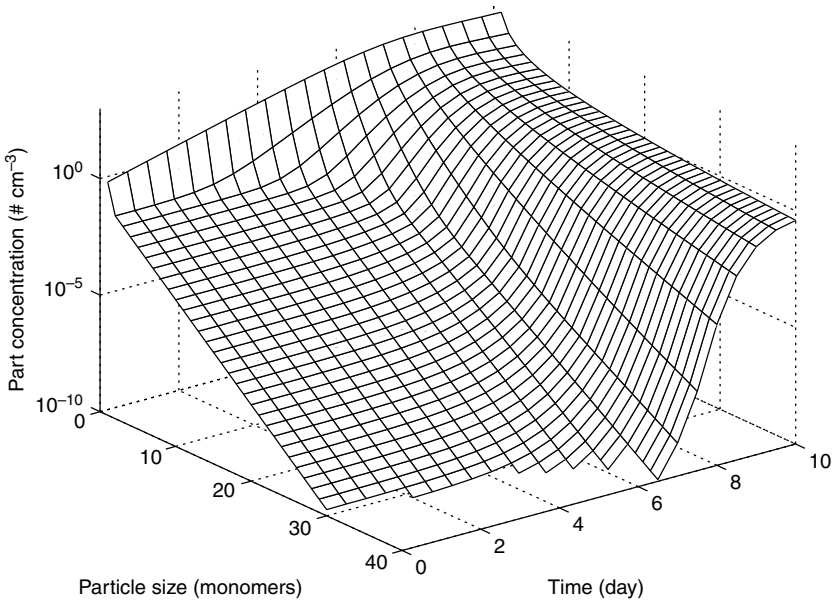

FIGURE 13.1 Number concentration of particles for an exponentially growing algal population as a function of number of algal cells in a particle and time. The single algal cell with a radius of $r_1 = 10$ μm and stickiness of $\alpha = 1$ grows exponentially at $\mu = 1$ per days in a $Z = 30$ m thick mixed layer having a shear of $\gamma = 1$ sec^1. Particle fall velocity is calculated using a particle density of 1.036 g cm^{-3} and fluid density of 1.0 g cm^{-3}. The calculation uses the summation formulation of Equations (13.11 and 13.12) and a rectilinear coagulation kernel.

with other single cells:

$$\frac{dC_1}{dt} = \mu C_1 - \alpha\beta_{11} C_1^2 \tag{13.13}$$

where $\beta_{11} = 1.3\gamma\ (r_1 + r_1)^3$ (the rectilinear shear kernel). Note that the differential sedimentation kernel for collisions between two particles of the same size is zero because they fall at the same rate, and that the Brownian kernel is considerably smaller than that for shear for particles larger than 1 μm. At steady state, the generation of new algal cells by division balances the loss to coagulation. The resulting concentration for the cells is

$$C_{cr} = \frac{\mu}{\alpha\beta_{11}} = \frac{\mu}{1.3\alpha\gamma 8 r_1^3} \tag{13.14}$$

Expressed as a volume concentration for spherical particles, this is:

$$C_{V,cr} = \frac{4}{3}\pi r_1^3 \frac{\mu}{1.3\alpha\gamma 8 r_1^3} \approx \frac{\pi\mu}{\alpha\gamma 8} \tag{13.15}$$

TABLE 13.2
Tests of Critical Concentration in Algal Blooms

Citation	Test	Result	Comment
Kiørboe et al.[50]	C_{cr} for spring bloom	Successfully predict maximum concentration	Measure α
Riebesell[51,52]	C_{cr} for N. Sea bloom	Prediction $10 \times$ high	Assume $\alpha = 0.1$
Olesen[53]	Maximum algal concentration	Unclear. Chl higher than expected	No actual cell concentration or α measured
Prieto et al.[54]	C_{cr} in mesocosm	Successful	Conversion of data required
Boyd et al.[55]	C_{cr} for Fe fertilization experiment SOIREE	Successfully predict non-coagulation	Assume $\alpha = 1$
Boyd et al.[55]	C_{cr} for Fe fertilization experiment IronEx 2	Successfully predict timing of export	Assume $\alpha = 1$
Boyd et al. unpublished results	C_{cr} to Fe fertilization experiment SERIES	Successfully predict maximum concentration	Assume $\alpha = 1$

The critical concentration provides a simple estimate of the maximum concentration that algal population can attain during a bloom situation. It has been remarkably successful when tested against bloom situations (Table 13.2). Its use to predict the effect of ocean fertilization experiments is particularly striking.[55] The stickiness parameter α provides an important tuning parameter. Note that Riebesell[51,52] would have successfully predicted the maximum bloom concentration in the North Sea with $\alpha = 1$ rather than the 0.1 he assumed.

13.3.1.2 Coagulation in a Stirred Container

One well-studied system is a vessel with an imposed (known) shear rate and an initially uniform (monodisperse) particle population.[56,57] In the initial stages of coagulation, interactions among single particles dominate coagulation and, hence, the change in total particle concentration C_T. For small changes in particle number in C_1, C_T decreases by coagulation from collision of monomers:

$$\begin{aligned}\frac{dC_T}{dt} &= -\frac{1}{2}\alpha\beta_{11}C_1^2 = -\frac{1}{2}\alpha\left(\frac{4}{3}\gamma(2r_1)^3\right)C_1^2 \\ &= -\frac{4\alpha\gamma}{\pi}\left(\frac{4}{3}\pi r_1^3 C_1\right)C_1 = -\frac{4\alpha\gamma}{\pi}C_{V,1}C_1\end{aligned} \tag{13.16}$$

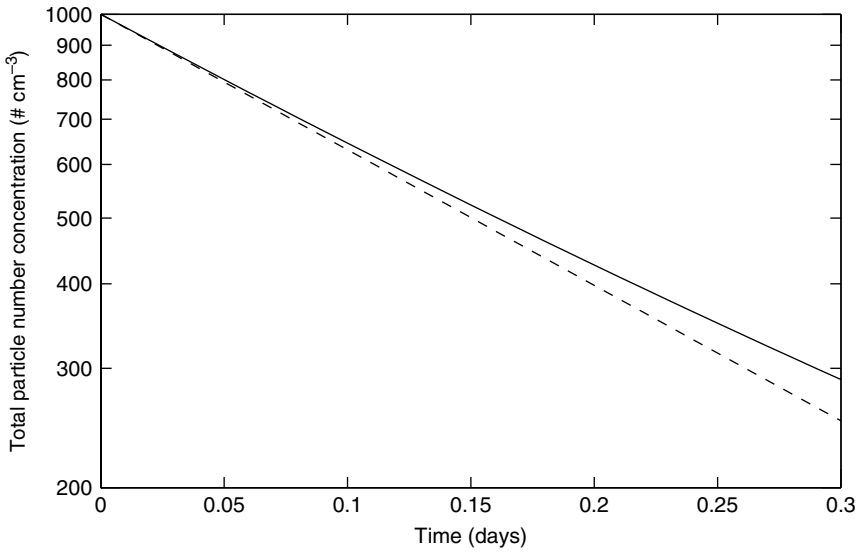

FIGURE 13.2 Total particle concentration through time for an initially monodisperse system. Solid line: solution calculated numerically using Equation (13.9); dashed line: approximate solution calculated using Equation (13.17). Calculation conditions: $\gamma = 10\ \text{sec}^{-1}; r_1 = 10\ \mu\text{m}; \alpha = 1$. Aggregate sizes in the calculation ranged from $i = 1$ to 100 monomers. There was little loss of particle mass from the system within the first 0.3 days. The divergence between the approximate and simulated solutions increases with decreasing particle numbers.

Further simplifying by assuming that $C_{V,1}$ is constant, the model predicts that

$$C_T = C_0 \exp\left(-\frac{4\alpha\gamma C_{V,1} t}{\pi}\right) \tag{13.17}$$

where C_0 is the initial particle concentration. The simplicity of this result has led to its use to determine the value of α as a fitting parameter.[46,57,58]

A numerical calculation of the coagulation in this system shows how the total particle concentration changes in time (Figure 13.2). The rate of change does diverge with time.

13.3.1.3 Steady-State Size Spectra

Hunt[8,9] applied the scaling techniques of Friedlander[20] to estimate the expected shape of particle size spectra in aquatic systems. He predicted that the spectrum should be proportional to the $r^{-2.5}$, r^{-4}, and $r^{-4.5}$ in the size ranges where Brownian motion, shear, and differential sedimentation dominate. This calculation was based on a scaling argument that assumes that particles are continually produced, that coagulation moves mass to ever larger particles until they sediment out, and that only one coagulation mechanism dominates at a given particle size.

Burd and Jackson[59] calculated the spectra numerically and compared them to the results from scaling analysis (Table 13.3). Their results showed that the processes

TABLE 13.3
Particle Size Spectral Slopes for Different Calculations

	Brownian Region	Shear Region	Differential Sedimentation Region
Dimensional analysis	−2.5	−4.0	−4.5
Numerical Base case	−2.5	−5.0	−14.5
No settling	−2.5	−6.3	−2.9
No settling, only 1 mechanism in size range	−2.5	−4.0	−4.6

Note: The base case is a numerical simulation using the sectional approach with all coagulation mechanisms and particle settling possible for all particles. The "no settling" cases result when there is no loss of particles by settling out of a layer.
Source: From Burd and Jackson, *Environ. Sci. Technol.*, 36, 323, 2002.

could not be considered separately. They were able to reproduce the scaling results only when they omitted particle settling and imposed only one coagulation mechanism in a given size range. Thus, the simple analysis is not necessarily correct.

13.3.2 Rectilinear and Heterodisperse

Many of the simple relationships derived from coagulation theory implicitly assume that the systems are initially monodisperse. It is made when assuming that particle number is proportional to volume for all particles or, more basically, in the linearizations that are made to derive the simplified equations. The effect of the monodisperse assumption can be tested by assuming that there are initially two particle sizes and making similar simplifications.

13.3.2.1 Critical Concentration

The simplicity of the formulation and its lack of dependence on particle radius suggest that it could be used to predict a critical concentration for mixed assemblages of phytoplankton, where no one particle type dominates. An expanded version of Equation (13.13) for two particles is

$$\begin{aligned}\frac{dC_a}{dt} &= \mu_a C_a - \alpha\beta_{aa} C_a^2 - \alpha\beta_{ab} C_a C_b \\ \frac{dC_b}{dt} &= \mu_b C_b - \alpha\beta_{bb} C_b^2 - \alpha\beta_{ab} C_a C_b\end{aligned} \tag{13.18}$$

where the subscripts “a” and “b” are used to distinguish the two particles.

At steady state, $dC_a/dt = 0$ and the first part of Equation (13.18) reduces to

$$C_a = \frac{\mu_a}{\alpha\beta_{aa}} - \frac{\beta_{ab}C_b}{\beta_{aa}} = C_{a,cr} - \frac{(r_a + r_b)^3}{(r_a + r_a)^3}C_b$$
$$= C_{a,cr} - \frac{(r_a/r_b + 1)^3 r_b^3}{8r_a^3}C_b = C_{a,cr} - \frac{(\lambda + 1)^3 V_b}{8V_a}C_b$$

where $\lambda = r_a/r_b, V_a = \frac{4}{3}\pi r_a^3$, and $V_b = \frac{4}{3}\pi r_b^3$. Expressing the concentrations in terms of volumes and performing similar manipulations for C_b yields:

$$C_{Va} = C_{V,cr} - \frac{(1 + \lambda)^3}{8}C_{Vb}$$
$$C_{Vb} = C_{V,cr} - \frac{(1 + \lambda^{-1})^3}{8}C_{Va} \tag{13.19}$$

where $C_{Va} = V_a C_a$ and $C_{Vb} = V_b C_b$ represent the volumetric concentrations of the two particles, and $C_{V,cr}$ is the critical concentration for homogeneous distributions if $\mu_a = \mu_b$ (Equation 13.15). The problem is that if $r_a \neq r_b, C_{Va}$ and C_{Vb} cannot both be at steady state and have positive values: a larger particle is more likely to collide with a smaller particle than vice versa. Thus, prediction for the simple monodisperse system is not appropriate for the polydisperse system. It does, however, provide a simple estimate.

13.3.2.2 Estimating Stickiness

The problem of using relationships derived for monodisperse systems to describe the fate of heterodisperse systems extends to the method used to estimate stickiness.

A modified version of Equation (13.16) to describe the effect of collisions between particles with two different sizes is then:

$$\frac{dC_T}{dt} = -\frac{1}{2}\alpha\beta_{aa}C_a^2 - \frac{1}{2}\alpha\beta_{bb}C_b^2 - \alpha\beta_{ab}C_aC_b$$
$$= -\frac{1}{2}\alpha\left(\frac{4}{3}\gamma 8r_a^3 C_aC_a + \frac{4}{3}\gamma 8r_a^3 C_aC_a\right) - \alpha\frac{4}{3}\gamma\ (r_a + r_b)^3 C_aC_b$$
$$= -\frac{4\alpha\gamma}{\pi}(C_{V,a}C_a + C_{V,b}C_b) - \frac{\alpha\gamma}{\pi}\left(\frac{4}{3}\pi r_b^3\right)(1 + \lambda)^3 C_aC_b$$
$$= -\frac{4\alpha\gamma}{\pi}\left(C_{V,a}C_a + C_{V,b}C_b + \frac{(1 + \lambda)^3}{4}C_aC_{V,b}\right) \tag{13.20}$$

where $\lambda = r_a/r_b$, $C_{V,a} = 4/3\pi r_a^3 C_a$, and $C_{V,b} = 4/3\pi r_b^3 C_b$. We would like to put this into the form of Equation (13.16) in order to compare the heterodisperse and monodisperse cases. Noting that the total volumetric concentration is related to the volumetric concentrations of the components by

$$\begin{aligned} C_{V,T}C_T &= (C_{V,a} + C_{V,b})(C_a + C_b) \\ &= C_{V,a}C_a + C_{V,b}C_a + C_{V,a}C_b + C_{V,b}C_b \\ C_{V,a}C_a + C_{V,b}C_b &= C_{V,T}C_T - C_{V,b}C_a - C_{V,a}C_b \end{aligned} \tag{13.21}$$

Substituting the results from Equation (13.21) into Equation (13.20) yields

$$\begin{aligned} \frac{dC_T}{dt} &= -\frac{4\alpha\gamma}{\pi}\left(C_{V,T}C_T - C_{V,b}C_a - C_{V,a}C_b + \frac{(1+\lambda)^3}{4}C_aC_{V,b}\right) \\ &= -\frac{4\gamma\alpha}{\pi}C_{V,T}C_T\left(1 - \frac{C_{V,b}C_a + C_{V,a}C_b - ((1+\lambda)^3/4)C_aC_{V,b}}{C_{V,T}C_T}\right) \\ &= -\frac{4\gamma\alpha}{\pi}C_{V,T}C_T\left(1 - \frac{r_b^3C_bC_a + r_a^3C_aC_b - ((1+\lambda)^3/4)C_ar_b^3C_b}{r_a^3C_a^2 + r_b^3C_bC_a + r_a^3C_aC_b + r_b^3C_b^2}\right) \\ &= -\frac{4\gamma\alpha}{\pi}C_{V,T}C_T\left(1 - \frac{1 + (r_a/r_b)^3 - ((1+\lambda)^3/4)}{(r_a/r_b)^3(C_a/C_b) + 1 + (r_a/r_b)^3 + (C_b/C_a)}\right) \\ &= -\frac{4\gamma\alpha'}{\pi}C_{V,T}C_T \end{aligned} \tag{13.22}$$

where $\alpha' = \alpha(1 - \frac{3}{4}(1 - \lambda - \lambda^2 + \lambda^3)/(\lambda^3\eta + \lambda^3 + 1 + \eta^{-1}))$, $\eta = C_a/C_b$, and $\lambda = r_a/r_b$. α' is the stickiness coefficient that would be estimated by using the procedure for the monodisperse system. The value of α' depends on the relative sizes and concentrations of the two particles (Figure 13.3).

13.3.3 Curvilinear

Models of coagulation in planktonic systems have expanded in their use of both ecological and coagulation descriptions. Recent models use more sophisticated coagulation kernels, calculation schemes, fractal scaling on mass and ecological dynamics (Table 13.4). The kernels in Equations (13.7) and (13.8) are used in the following calculations.

13.3.3.1 Simple Algal Growth

The effect of changing the coagulation kernel on model results can be seen by comparing the results from a simple model of exponential algal growth run with

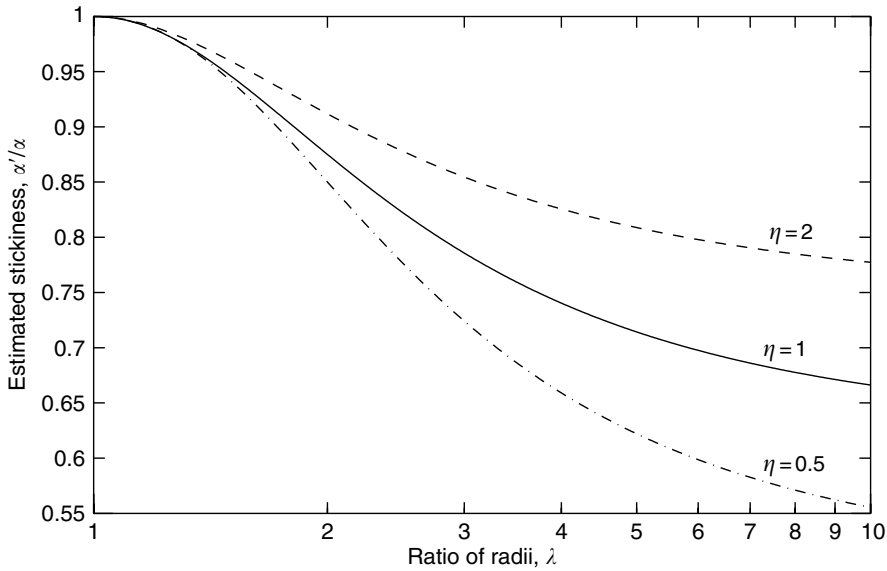

FIGURE 13.3 Estimated stickiness α' relative to the actual stickiness α as a function of the ratio of the radii λ for a polydisperse system. There are initially two distinct particles. Solid line: $\eta = 1$; dashed line: $\eta = 2$; dash-dot: $\eta = 0.5$.

rectilinear and curvilinear kernels (Figure 13.4). These calculations use a sectional approximation for the integral forms of the coagulation equations.[41] The results show significant differences in steady-state particle concentrations (Figure 13.4a), timing and magnitude of particle flux (Figure 13.4b), and average particle settling velocity (Figure 13.4c).

The maximum particle concentration is higher for the curvilinear kernels than for rectilinear, as should be expected from the more rapid rates of coagulation (Figure 13.4). The steady-state concentrations of single algae for the rectilinear and curvilinear kernels are 0.17 and 2.0 times the critical concentration calculated using Equation (13.3) This higher value for the curvilinear kernel reflects the slower rates of collision when using it.

Another difference is in the maximum total particle volumetric flux rate out of the surface mixed layer, 49 and 488 $cm^3\ m^{-2}$ per day for the rectilinear and curvilinear kernels, respectively. This dramatic increase for the curvilinear calculation is a result of the larger particle concentrations available for removal when the coagulation begins to dominate the growth. The peak average settling velocity is larger for the rectilinear kernel, 20 vs 12 m per day. The lower average settling velocity is a reflection of the smaller average particle size in the curvilinear case.

The implication of this comparison is that the form of the coagulation kernel can have a profound effect on properties that are ecologically significant, including particle concentration and, even more dramatically, particle flux. Developers of models need

TABLE 13.4
Features of Dynamic Models for the Marine Ecological Systems Involving Coagulation

Citation	Kernel	Particle distribution	M–L Scale	Comments
Jackson[22]	R	Number of monomers	O	
Hill[24]	C	Sectional equivalent	F	Impose background spectrum
Jackson and Lochmann[23]	C	Sectional	F	
Riebesell and Wolf-Gladrow[60]	C	Number of monomers	O	
Jackson[47]	C	Sectional	F	Compare to expt
Ackleh and Fitzpatrick[61]	R	Sectional equivalent	V	Explore math properties
Ruiz[62]	C		O	Diel turbulence
Mari and Burd[63]	C	Sectional	F	TEP and phyto
Boehm and Grant[64]	R	Jungian spectrum	V	
Kriest and Evans[65]	R	2-parameter spectrum	V	
Ackleh and Forward[66]	R	Sectional equivalent	V	Adds self-shading
Jackson[44]	P	2-D sectional	F	Multiple sources
Dadou et al.[67]	E	Two sizes	O	Vertical profile
Kriest[68]	R	2-parameter spectrum	V	
Ruiz et al.[69]	E	2 to 7 size classes	—	Fit expt results
Stemmann et al.[70,71]	P	Sectional	F	Compare to midwater observations

Note: Kernels: R — rectilinear; C — curvilinear; P — porous correction; E — empirical fit; Mass–length (M–L) scale: V — volume conserved ($m \sim r^3$); F — fractal ($m \sim r^{Df}$); O — other.

to discuss the implications of the formulations that they choose when publishing their results.

13.3.3.2 Plankton Food Web Model

An example of the incorporation of coagulation into a more elaborate food web model is the use of coagulation dynamics to describe the interactions of phytoplankton with colloidal particles and fecal pellets in a food web model (as in Jackson[44]). By incorporating the multidimensional particle size spectra, the model includes aggregates formed from the interaction of multiple particle types (Figure 13.5).

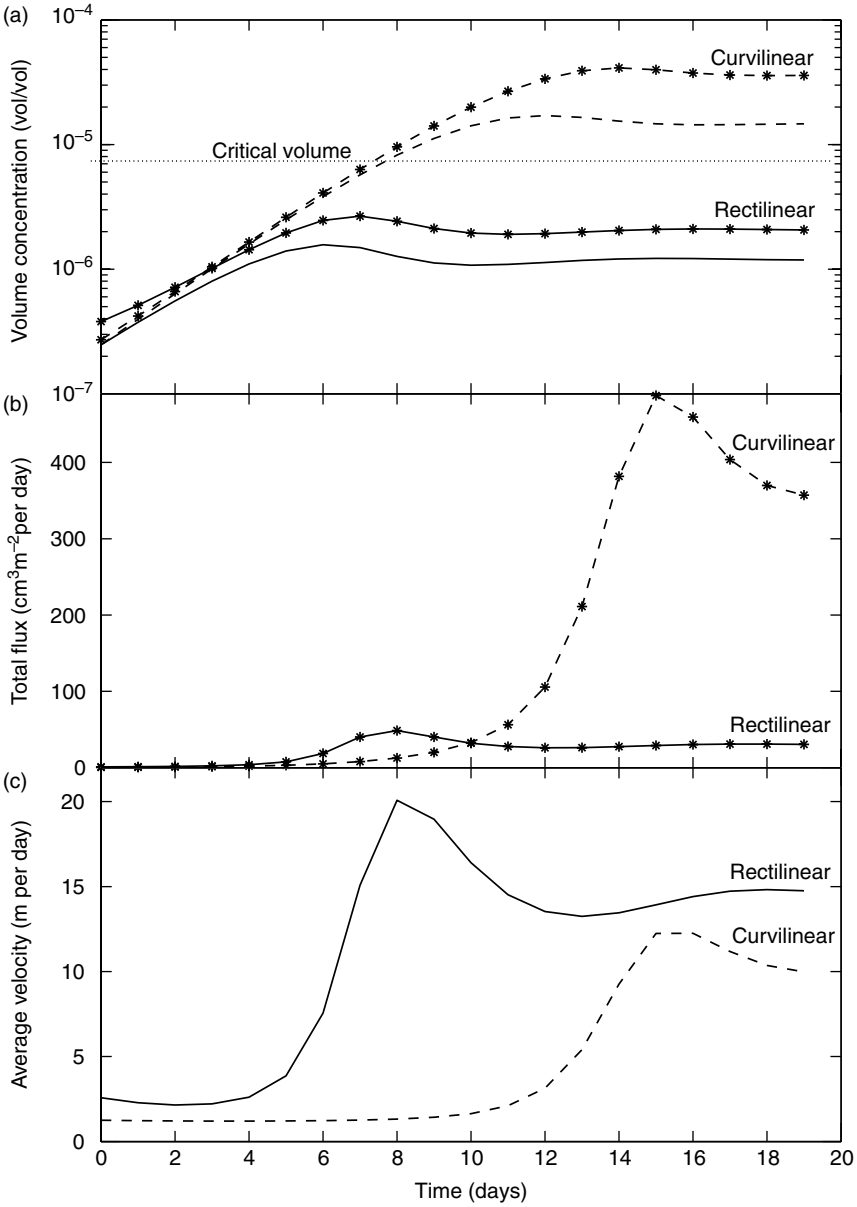

FIGURE 13.4 Comparison of particle properties for a simple model with rectilinear and curvilinear coagulation kernels. Calculations use a simple sectional model[55] for 50 m mixed layer thickness, algal radius $= 5\ \mu$m, specific growth rate $\mu = 0.5$ per day, shear $\gamma = 0.1\ \text{sec}^{-1}$, and stickiness $\alpha = 1$. Solid line indicates a rectilinear kernel; dashed line indicates a curvilinear kernel. (a) Volumetric concentration. Lines with asterisks indicate total particle concentrations; plain lines indicate the volumetric concentration of single algae; the critical concentration is indicated with the dotted horizontal line. (b) Total particle flux at base of mixed layer. (c) Average particle velocity = total flux/total particle concentration.

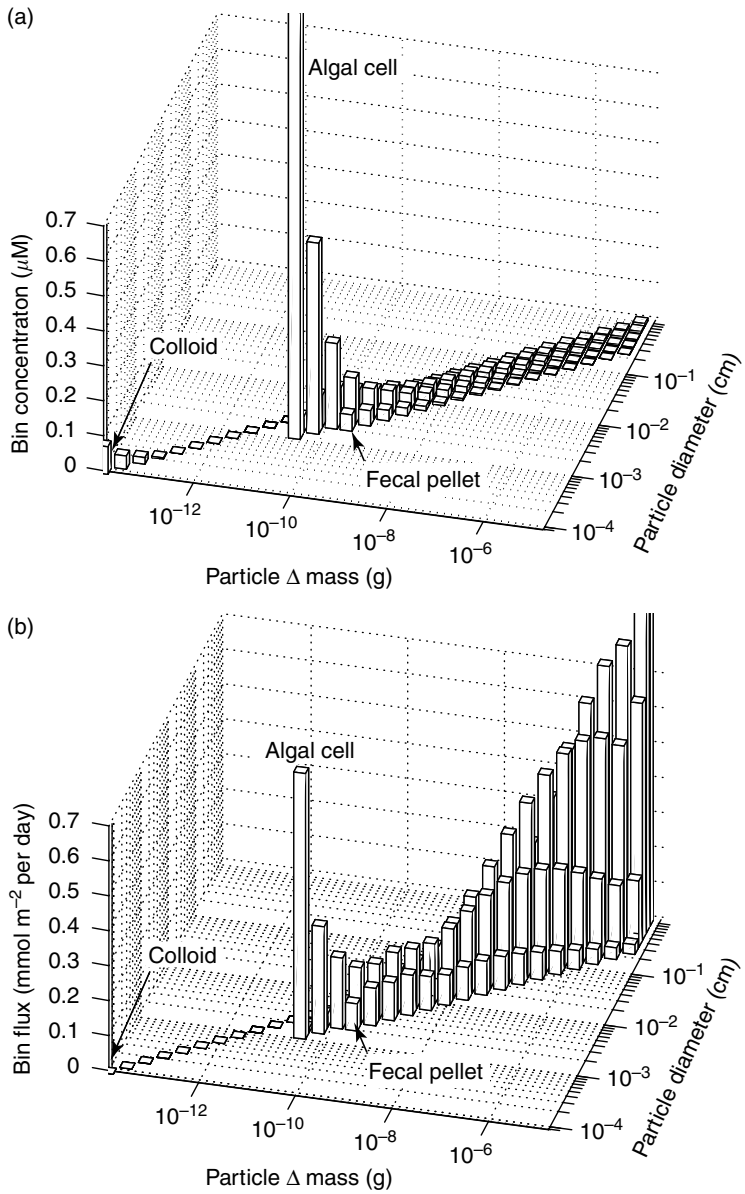

FIGURE 13.5 Results from a model incorporating two-dimensional particle size spectra, fractal kernel, and a planktonic food web. This is similar to the model of Jackson[44] but for conditions more typical of the North Atlantic. Concentrations and fluxes for "bins," size ranges whose upper masses are twice their lower and whose upper value of r^{Df} are twice their lower. (a) Concentration in each bin; (b) flux out of mixed layer for particles in the bin. There are three particle sources: colloids, algae, and fecal pellets. The results are an example of using multidimensional particle size spectra to incorporate multiple particle types.

13.4 DISCUSSION

Simple coagulation models, such as those for the critical concentration and for determining particle stickiness, have proven remarkably useful by providing simple relationships that can be easily applied to interpret environmental data. Unfortunately, the simple relationships do not work as well when applied to more realistic conditions or accurate coagulation mechanisms.[72,73] As a result, the simple mechanisms should be considered semi-quantitative at best.

The number of models of planktonic systems that incorporate coagulation is surprisingly large (Table 13.4). Unfortunately, the range in their formulations is so large that it is difficult to compare and interpret their results. Given the differences resulting from different coagulation kernels, as illustrated above, it is difficult to interpret them together. One response has been to abandon the theoretical structure and instead use values for the interaction kernels determined by fitting results from laboratory experiments.[69] While such an approach does fit the laboratory system, it is unclear how to extrapolate the results to different environmental conditions. Despite the importance that the choice of model formulation can have, there has been remarkably little discussion or consensus on the best one to use.

Finding the best way to incorporate disaggregation into coagulation models for marine systems remains an outstanding problem. There have been attempts to do so,[34,62,74] but more needs to be done. Among the factors that need to be included are the potential roles of zooplankton[75] and any other organisms[29] in weakening and sundering marine aggregates.

One of the outstanding questions in aquatic systems is what is the precise role of transparent exopolymeric particles (TEPs). These are organic particles that have been associated with marine particle coagulation.[76–78] There have been several different roles assigned to them: extra particles to participate in collisions,[63] agents for the changing of particle stickiness,[79] and a separate system of coagulating particles.[76] Unfortunately for the resolution of the role of TEP on coagulation in natural waters, most TEP studies have focused on the ecological aspects of the material and have not accompanied them with the size spectral and stickiness measurements that could be used to test the various possibilities. In future studies, measurements of particle size spectra in conjunction with observations of TEP concentrations would make it easier to test the role of TEP in coagulation.

Stemmann et al.[70,71] have developed a promising approach to test the importance of coagulation, as well as biological processes, in determining particle distributions and fates. The method compares the particle size spectra measured through the water column over time with those expected from different particle transformation processes. This approach would be improved if there were a better quantitative understanding of how organisms, including bacteria and other microorganisms, change the particle properties.

The particle size spectra are probably the most useful measurements that could be made in systems where coagulation is believed to be important. Such measurements should use multiple techniques in order to cover the range of important reactions.[34,35] In addition, multiple measurements on the same particles that could be used to test models that invoke multidimensional particle size spectra would also help.[44,45]

13.5 CONCLUSIONS

The use of coagulation theory to describe particles in planktonic ecosystems is in a transition phase. Simple models have provided simple, useable formulae to describe marine systems. As the underlying models have been modified to improve the mechanistic descriptions, the simplicity is necessarily being left behind. Unfortunately, there is no consensus on how the newer models should be formulated. Furthermore, field observations tend to omit the collection of data that can be used to test the models. Progress in the field will depend on the ability of modeling and field programs to interact.

ACKNOWLEDGMENTS

This chapter incorporates work with my various colleagues, including Steve Lochmann, Lars Stemmann, Thomas Kiørboe, and, most particularly, Adrian Burd. It has been supported by grants, OCE-0097296 and OCE-998765, from the US National Science Foundation.

REFERENCES

1. Sheldon, R.W., Prakash, A., and Sutcliffe, W.H., The size distribution of particles in the ocean. *Limnol. Oceanogr.* 17, 327, 1972.
2. Gardner, W.D., Incomplete extraction of rapidly settling particles from water samplers. *Limnol. Oceanogr.* 22, 764, 1977.
3. Platt, T., and Denman, K., Organization in the pelagic ecosystem. *Helgoland Wiss. Meer.* 30, 575, 1977.
4. Silvert, W., and Platt, T., Energy flux in the pelagic ecosystem: a time dependence equation. *Limnol. Oceanogr*. 23, 813, 1978.
5. Rodriquez, J., and Mullin, M.M., Relation between biomass and body weight of plankton in a steady state oceanic ecosystem. *Limnol. Oceanogr*. 31, 361, 1986.
6. Kiefer, D.A., and Berwald, J., A random encounter model for the microbial planktonic community. *Limnol. Oceanogr*. 37, 457, 1992.
7. Zhou M., and Huntley, M.E., Population dynamics theory of plankton based on biomass spectra. *Mar. Ecol. Prog. Ser.* 159, 61, 1997.
8. Hunt, J.R., Particle dynamics in seawater: implication for predicting the fate of discharged particles. *Environ. Sci. Technol.* 16, 303, 1982.
9. Hunt, J.R., Prediction of oceanic particles size distributions from coagulation and sedimentation mechanisms, in *Particulates in water*, Kavanaugh, M.C., and Leckie, J.O., Eds., American Chemical Society, Washington, DC, p.243, 1980.
10. Trent, J.D., Shanks, A.L., and Silver, M.W., In situ and laboratory measurements on macroscopic aggregates in Monterey Bay, California. *Limnol. Oceanogr.* 23, 626, 1978.
11. Kranck, K., and Milligan, T., Macroflocs: production of marine snow in the laboratory. *Mar. Ecol. Prog. Ser.* 3, 19, 1980.
12. Kranck, K., and Milligan, T., Macroflocs from diatoms: in situ photography of particles in Bedford Basin, Nova Scotia. *Mar. Ecol. Prog. Ser*. 4, 183, 1988.
13. Alldredge, A.L., and Silver, M.W., Characteristics, dynamics, and significance of marine snow. *Prog. Oceanogr.* 20, 41, 1988.

14. Alldredge, A.L., and Gotschalk, C., In situ settling behavior of marine snow. *Limnol. Oceanogr*. 33, 339, 1988.
15. Logan, B.E., and Wilkinson, D.B., Fractal geometry of marine snow and other biological aggregates. *Limnol. Oceanogr*. 35, 130, 1990.
16. O'Melia, C.R., An approach to modeling of lakes. *Schweiz. Zeitsch. Hydrol*. 34, 1, 1972.
17. Edzwald, J.K., Upchurch, J.B., and O'Melia, C.O., Coagulation in estuaries. *Environ. Sci. Technol*. 8, 58, 1974.
18. O'Melia, C.R., and Bowman, K.S., Origins and effects of coagulation in lakes. *Schweiz. Zeitsch. Hydrol*. 46, 64, 1984.
19. Weilenmann, U., O'Melia, C.R., and Stumm, W., Particle transport in lakes: models and measurement. *Limnol. Oceanogr.* 34, 1, 1989.
20. Friedlander, S.K., *Smoke, dust and haze*, Wiley, New York, 317 pp., 1977.
21. McCave, I., Size spectra and aggregation of suspended particles in the deep ocean. *Deep Sea Res.* 31, 329, 1984.
22. Jackson, G.A., A model of the formation of marine algal flocs by physical coagulation processes. *Deep Sea Res*. 37, 1197, 1990.
23. Jackson, G.A., and Lochmann, S.E., Effect of coagulation on nutrient and light limitation of an algal bloom. *Limnol. Oceanogr*. 37, 77, 1992.
24. Hill, P., Reconciling aggregation theory with observed vertical fluxes following phytoplankton blooms. *J. Geophys. Res*. 97, 2295, 1992.
25. Fenchel, T., Suspended bacteria as a food source, in *Flows of energy and materials in marine ecosystems*, Fasham, M.J.R., Ed., Plenum Press, New York, p. 301, 1984.
26. Rothschild, B.J., and Osborn, T.R., Small-scale turbulence and plankton contact rates. *J. Plankton Res.*, 10, 465, 1988.
27. Shimeta, J., and Jumars, P.A., Physical mechanism and rates of particle capture by suspension-feeders. *Oceanogr. Mar. Biol. Ann. Rev.* 29, 191, 1991.
28. Murray, A.G., and Jackson, G.A., Viral dynamics: a model of the effects of size, shape, motion and abundance of single-celled planktonic organisms and other particles. *Mar. Ecol. Prog. Ser*. 89, 103, 1992.
29. Kiørboe, T. Colonization of marine snow aggregates by invertebrate zooplankton: abundance, scaling and possible role. *Limnol. Oceanogr.* 45, 479, 2000.
30. Kiørboe T., and Thygesen, U.H., Fluid motion and solute distribution around sinking aggregates. II. Implications for remote detection by colonizing zooplankters. *Mar. Ecol. Prog. Ser.* 211, 15, 2001.
31. Falconer, K.J., *Fractal geometry: mathematical foundations and applications*, Wiley, New York, 1990.
32. Vicsek, T., *Fractal growth phenomena*, 2nd ed., World Scientific, NJ, 1992.
33. Li, X., and Logan, B.E., Size distributions and fractal properties of particles during a simulated phytoplankton bloom in a mesocosm. *Deep Sea Res. II*, 42, 125, 1995.
34. Jackson, G.A., et al., Combining particle size spectra from a mesocosm experiment measured using photographic and aperture impedance (Coulter and Elzone) techniques. *Deep Sea Res. II,* 42, 139, 1995.
35. Jackson, G.A., et al. Particle size spectra between 1 μm and 1 cm at Monterey Bay determined using multiple instruments. *Deep Sea Res. I*, 44, 1739, 1997.
36. Klips, J.R., Logan, B.E., and Alldredge, A.L., Fractal dimensions of marine snow determined from image analysis of *in situ* photographs. *Deep Sea Res*. 41, 1159, 1994.

37. Pruppacher, H.R., and Klett, J.D., *Microphysics of clouds and precipitation*, Reidel, Boston, MA, 1980.
38. Adler, P.M., Streamlines in and around porous particles. *J. Colloid Interface Sci*. 81, 531, 1981.
39. Han, M., and Lawler, D.F., The (relative) insignificance of G in flocculation. *J. Am. Water Works Assoc.* 84, 79, 1992.
40. Jackson, G.A., and Lochmann, S.E., Modeling coagulation in marine ecosystems, in *Environmental particles, volume 2*, Buffle, J., and van Leeuwen, H.P., Eds., Lewis Publishers, Boca Raton, FL, p. 387, 1993.
41. Gelbard, F., Tambour, Y., and Seinfeld, J.H., Sectional representations for simulating aerosol dynamics. *J. Colloid Interface Sci.* 76, 541, 1980.
42. Li, X., and Logan, B.E., Collision frequencies of fractal particles with small particles by differential sedimentation. *Environ. Sci. Technol.* 31, 1229, 1997.
43. Li, X., and Logan, B.E., Collision frequencies of fractal aggregates and small particles in a turbulently sheared fluid. *Environ. Sci. Technol.* 31, 1237, 1997.
44. Jackson, G.A., Effect of coagulation on a model planktonic food web. *Deep Sea Res. I*, 48, 95, 2001.
45. Jackson, G.A., Using fractal scaling and two dimensional particle size spectra to calculate coagulation rates for heterogeneous systems. *J. Colloid Interface Sci.* 202, 20, 1998.
46. Kiørboe, T. Anderson, K., and Dam, H., Coagulation efficiency and aggregate formation in marine phytoplankton. *Mar. Biol.* 107, 235, 1990.
47. Jackson, G.A., Comparing observed changes in particle size spectra with those predicted using coagulation theory. *Deep Sea Res. II* 42, 159, 1995.
48. Alldredge, A.L., et al., The physical strength of marine show and its implications for particle disaggregation in the ocean. *Limnol. Oceanogr.* 35, 1415, 1990.
49. Al-Ani, S., Dyer, K.R., and Huntley, D.A., Measurement of the influence of salinity on floc density and strength. *Geo-Marine Lett.*, 11, 154, 1991.
50. Kiørboe, T.P. et al., Aggregation and sedimentation processes during a spring phytoplankton bloom: a field experiment to test coagulation theory. *J. Mar. Res.* 52, 297, 1994.
51. Riebesell, U., Particle aggregation during a diatom bloom. I. Physical aspects. *Mar. Ecol. Prog. Ser.* 69, 273, 1991.
52. Riebesell, U., Particle aggregation during a diatom bloom. II. Biological aspects. *Mar. Ecol. Prog. Ser.* 69, 281, 1991.
53. Olesen, M., Sedimentation in Mariager Fjord, Denmark: the impact of sinking velocity on system productivity. *Ophelia* 55, 11, 2001.
54. Prieto, L. et al., Scales and processes in the aggregation of diatom blooms: high time resolution and wide size range records in a mesocosm study. *Deep Sea Res. I,* 49, 1233, 2002.
55. Boyd, P.W., Jackson, G.A., and Waite, A.M., Are mesoscale perturbation experiments in polar waters prone to physical artefacts? Evidence from algal aggregation modelling studies. *Geophys. Res. Let.* 29, 10.1029/2001GL014210, 2002.
56. Camp, T.R., and Stein, P.C., Velocity gradients and internal work in fluid motion. *J. Boston Soc. Civil Engrs.* 30, 219, 1943.
57. Birkner, F.B., and Morgan, J.J., Polymer flocculation kinetics of dilute colloidal suspensions. *J. Am. Water Works Assoc.* 60, 175, 1968.
58. Engel, A., The role of transparent exopolymer particles (TEP) in the increase in apparent particle stickiness (α) during the decline of a diatom bloom. *J. Plankton Res.* 22, 485, 2000.

59. Burd, A.B., and Jackson, G.A., Modeling steady state particle size spectra. *Environ. Sci. Technol.* 36, 323, 2002.
60. Riebesell, U., and Wolf-Gladrow, D.F., The relationship between physical aggregation of phytoplankton and particle flux: a numerical model. *Deep Sea Res*. 39, 1085, 1992.
61. Ackleh, A.S., and Fitzpatrick, B.G., Modeling aggregation and growth processes in an algal population model: analysis and computations. *J. Math. Biol.* 35, 480, 1997.
62. Ruiz, J., What generates daily cycles of marine snow? *Deep Sea Res. I*, 44, 1105, 1997.
63. Mari, X., and Burd, A., Seasonal size spectra of transparent exopolymeric particles (TEP) in a coastal sea and comparison with those predicted using coagulation theory. *Mar. Ecol. Prog. Ser.* 163, 63, 1998.
64. Boehm, A.B., and Grant, S.B., Influence of coagulation, sedimentation, grazing by zooplankton on phytoplankton aggregate distributions in aquatic systems. *J. Geophys. Res.* 103, 15601, 1998.
65. Kriest, I., and Evans, G., Representing phytoplankton aggregates in biogeochemical models. *Deep Sea Res. I* 46, 1841, 1999.
66. Ackleh, A.S., and Forward, R.R., A nonlinear phytoplankton aggregation model with light shading. *SIAM J. Appl. Math.* 60, 316, 1999.
67. Dadou, I. et al., An integrated biological pump model form the euphotic zone to the sediment: a 1-D application in the Northeast tropical Atlantic. *Deep Sea Res. II*, 48, 2345, 2001.
68. Kriest, I., Different parameterizations of marine snow in a 1D-model and their influence on representation of marine snow, nitrogen budget and sedimentation. *Deep Sea Res. I*, 49, 2133, 2002.
69. Ruiz, J., Prieto, L., and Ortegón, F., Diatom aggregate formation and fluxes: a modeling analysis under different size-resolution schemes and with empirically determined aggregation kernels. *Deep Sea Res. I*, 49, 495, 2002.
70. Stemmann, L., Jackson, G.A., and Ianson, D., A vertical model of particle size distributions and fluxes in the midwater column that includes biological and physical processes. I. Model formulation. *Deep Sea Res. I*, 51, 865, 2004.
71. Stemmann, L., Jackson, G.A., and Gorsky, G., A vertical model of particle size distributions and fluxes in the midwater column that includes biological and physical processes. II. Application to a three year survey in the NW Mediterranean Sea. *Deep Sea Res. I*, 51, 885, 2004.
72. Farley, K.J., and Morel, F.M.M., Role of coagulation in the kinetics of sedimentation. *Environ. Sci. Technol.* 20, 187, 1986.
73. Burd, A., and Jackson, G.A., The evolution of particle size spectra. I: pulsed input. *J. Geophys. Res.* 102, 10545, 1997.
74. Hill, P.S., Sectional and discrete representations of floc breakage in agitated suspensions. *Deep Sea Res. I*, 43, 679, 1996.
75. Dilling, L., and Alldredge, A.L., Fragmentation of marine snow by swimming macrozooplankton: a new process impacting carbon cycling in the sea. *Deep Sea Res. I*, 47, 1227, 2000.
76. Alldredge, A.L., Passow, U., and Logan, B.E., The abundance and significance of a class of large, transparent organic particles in the ocean. *Deep Sea Res.* 40, 1131, 1993.
77. Passow, U., Transparent exopolymer particles (TEP) in aquatic environments. *Prog. Oceanogr.* 55, 287, 2002.

78. Logan, B.E., et al., Rapid formation and sedimentation of large aggregates is predictable from coagulation rates (half-lives) of transparent exopolymer particles (TEP). *Deep Sea Res. II*, 42, 203, 1995.
79. Kiørboe, T.P., and Hansen, J.L.S., Phytoplankton aggregate formation: observations of patterns and mechanisms of cell sticking and the significance of exopolymeric material. *J. Plankton Res.* 15, 993, 1993.

III

Engineered Systems

14 Extracellular Enzymes Associated with Microbial Flocs from Activated Sludge of Wastewater Treatment Systems

Gill G. Geesey and Fintan Van Ommen Kloeke

CONTENTS

14.1 INTRODUCTION

The tendency to aggregate is a common trait among microbial cells in contrived experimental laboratory environments, controlled industrial processes, and in nature.[1–3] When aggregation takes place on a surface, it often leads to the formation of biofilms,[4,5] while aggregation of cells in aqueous suspensions results in the formation of flocs.[6] Flocs formed in the water column of the ocean have been termed "marine

1-56670-615-7/05/$0.00+$1.50

snow."[7] Regardless of what form the aggregation process takes, cells engaged in this behavior become physically associated with each other through extracellular polymeric substances (EPS) secreted by at least a portion of the aggregated microbial community. Some of the cells secrete EPS that contributes to the structure of the floc or biofilm, which promotes the formation of close, stable, physical associations between cells of the same and different populations.[8] The physical associations lead to cooperation among cells of the populations present and the formation of consortia.[9,10] EPS also form matrices that function as diffusion barriers between the cells and the external environment,[11,12] which in some instances, protect the cells from insults of the surrounding environment.[13] Extracellular enzymes secreted by floc-encapsulated microorganisms represent another class of EPS that participate in the transformation of toxic chemical species in the environment to nontoxic products,[14] as well as the transformation of nutritionally valuable chemical species in the environment for uptake and utilization by members of the floc-associated microbial community.[15]

In this chapter, we will describe the exoenzymes involved in the degradation of polymeric organic compounds in the activated sludge process of wastewater treatment. Specifically we will describe the distribution of phosphatase (PO_4ase) exoenzymes within flocs produced during the activated sludge process, and the floc-associated microbial populations that synthesize and secrete this important class of enzymes.

14.2 MICROBIAL FLOCS IN WASTEWATER TREATMENT

Floc formation and associated chemical and biological reactions are an important part of many industrial processes.[16–18] Floc formation provides a means of separating solids from the liquid phase in process streams. In wastewater treatment that utilizes the activated sludge process, the quality of the effluent is highly dependent on the efficiency of the solid–liquid separation processes. Flocs play a key role in this regard, and an understanding of floc properties and behavior has led to significant advances in biological C, N, and P removal and in the sludge dewatering process. Floc properties control the efficiency of phase separation.

Floc properties are controlled by the nature of the wastewater. The chemistry of the wastewater controls the types of microorganisms that grow in the system as well as the quality and quantity of EPS elaborated by the microbial community. EPS composition and form depend on process conditions. EPS in activated sludge can be found in two forms: directly associated with microbial cell biomass or physically separated from the biomass as free colloids or slimes.[19,20] Floc properties and behavior directly reflect EPS properties. Bulking and foaming reduce the efficiency of the separation process. Bulking occurs when aggregates do not form dense, compact flocs — a direct consequence of EPS production and composition by the microorganisms in the system. Recently, Sponza[21] provided evidence that EPS composition depends more on waste stream composition than on process operating conditions. Thus, an understanding of microbial EPS production offers new opportunities to control the flocculation process and overall efficiency of wastewater treatment. This chapter will focus on the fraction of EPS comprised of extracellular enzymes.

14.3 EXTRACELLULAR ENZYMES

Hydrolysis of polymeric substances is the first and rate-limiting step in the process of wastewater treatment.[22,23] Due to their large size, organic polymers such as proteins, polysaccharides, and lipids must be hydrolyzed to their subunit molecules before microorganisms can oxidize or recycle them back to inorganic C, N, S, and P. The microbial enzymes responsible for these extracellular hydrolysis reactions are referred to as extracellular enzymes or exoenzymes. Microbial metabolism of complex organic matter begins with reactions catalyzed by extracellular enzymes. Consequently, extracellular enzymes are essential components of many biochemical pathways utilized by microorganisms for growth. Microbial polysaccharases, esterases, lipases, and proteases are examples of extracellular enzymes that play an important role in the biodegradation of polysaccharides, lipids, and proteins, respectively.[15,24] Exoenzymes also liberate inorganic phosphate (P_i), N, and S from organic molecules. Phosphatases (PO_4ases) are a class of enzyme that liberates P_i from phosphate-containing organic compounds. PO_4ases occur as intracellular enzymes where they control intracellular P_i concentrations needed for energy yielding phosphorylation reactions. They also occur in the cell envelope and as extracellular enzymes where they scavenge P_i from polymeric phosphorylated organic compounds to meet their inorganic phosphate requirements.

14.3.1 Forms of Phosphorus in Wastewater

Phosphorus removal from wastewater has become an important part of the overall treatment process. Enhanced biological P removal can achieve 90% to 95% reduction.[25] Some of the steps in the biochemical pathway of enhanced P removal are known, but others remain to be elucidated,[26] and the microorganisms responsible for some of the steps are still not known.[27] Phosphorus entering the activated sludge process exists in both organic and inorganic forms (Table 14.1). These data suggest that one-third to one-half of the total P in the system exists as detrital organic-P. While much attention has been directed toward the microbial populations that accumulate poly-P_i, little attention has been directed to those populations in the activated sludge

TABLE 14.1
Forms of Phosphorus in Activated Sludge

Form	Percent of total *P*
Nucleotide-P, lipid-P, nucleic acid-P, protein-P	31[28]
Trichloroacetic acid-insoluble-P	13
poly-P (inorganic)[29]	
RNA and protein (organic)[30]	
Inorganic-P	
PO_4^{3-} (P_i)	14[28]
poly-phosphate (poly-P_i)	32–44[28]

that process detrital organic-P or those involved in P regeneration (production of P_i from organic-P outside the cell). Little is known, for example, of the processes that depolymerize high molecular weight detrital organic-P compounds in wastewater or those that hydrolyze the phosphomonoesters to the organic subunits and P_i. These processes, however, are likely to influence overall P removal from wastewater streams.

14.3.2 Phosphatase Enzymes

PO_4ase enzymes hydrolyze the P–O bond of phosphomonoesters. PO_4ases are subdivided into alkaline and acid PO_4ases, based on the pH at which optimum activity occurs. Alkaline PO_4 function in the neutral and basic pH range, are induced at low external P_i concentrations, are localized at or near the cell surface, and hydrolyze phosphomonoester-containing organic compounds to provide cells with an alternative source of P_i. Alkaline PO_4ases may also be induced under P_i-sufficient but carbon-limited conditions to meet metabolic requirements of bacterial cells. Acid PO_4ases display maximum activity over the pH range of 4 to 6, are typically intracellular, and are not repressed by P_i. Alkaline PO_4ase has been reported to hydrolyze inorganic poly-P_i, a P-containing storage product that accumulates in a variety of bacteria found in activated sludge.[26,28,31–33] Alkaline PO_4ases have been implicated in P_i release from intact bacterial cells containing poly-P storage products in anaerobic lake sediments.[34] Alkaline PO_4ases may participate in the degradation of cell-surface-associated poly-P, which represents a more transient but significant portion of the total poly-P_i accumulated by cells of *Acinetobacter lwoffii* JW11.[35] Since poly-P_i formation and degradation exerts significant control over enhanced P removal from wastewater,[25,26] a better understanding of the role of extracellular bacterial PO_4ases in poly-P_i degradation and detrital organic-P regeneration should lead to better control over and more efficient P removal in the activated sludge process of wastewater treatment systems.

14.4 QUANTIFYING EXTRACELLULAR ENZYME ACTIVITY ASSOCIATED WITH MICROBIAL FLOCS

Goel et al.[36] used *p*-nitrophenolphosphate as the surrogate substrate for quantifying alkaline and acid PO_4ase activity, *p*-nitrophenol α-D-glucopyranoside as the surrogate substrate for α-glucosidase activity, and azocasein as the model substrate for protease activity in activated sludge. After an appropriate incubation period to allow enzymatic release of P_i, glucose, or peptide from the substrate, the activated sludge samples were centrifuged and the absorbance of the supernatant fraction was measured spectrophotometrically at 410 nm for *p*-nitrophenol (alkaline and acid PO_4ases, α-glucosidase), and at 440 nm, for trichloroacetic acid (TCA) soluble peptides (protease activity). Whiteley et al.[37] used the same substrates to measure exoprotease and extracellular alkaline PO_4ase activity in samples from two large-scale stirred tank laboratory reactors operated in series: the first seeded with a mixed culture of methanogenic bacteria from a standing digester at a sewage works, and the second seeded with a mixed culture of sulfate-reducing bacteria.

Cadoret et al.[12] assayed L-Leu-aminopeptidase, α-glucosidase, protease, and α-amylase activities in whole and dispersed activated sludges, as well as activities associated specifically with the floc EPS fraction. Enzyme activities were based on the rate of release of a chromogenic enzyme substrate following hydrolysis of synthetic substrates over an appropriate incubation period. L-Leu-*p*-nitroanilide, *p*-nitrophenyl-α-D-glucopyranoside, azocasein, and amylose azure were used as substrates for L-Leu-aminopeptidase, α-glucosidase, protease, and α-amylase, respectively. Nitroanaline and *p*-nitrophenol hydrolysis were quantified spectrophotometrically at 410 nm. Azocasein hydrolysis was determined by measuring the amount of cold TCA soluble material produced at 340 nm using a spectrophotometer. α-Amylase hydrolysis was determined by the amount of brilliant blue recovered in the cold TCA soluble material following release from amylose azure and treatment with cold TCA.

Pletschke et al.[38] monitored adenosine triphosphate sulfurylase (ATPS) in methanogenic and sulfidogenic stirred tank reactors operated in series using primary sludge from an anaerobic digester at a sewage works. ATPS catalyzes the first step in dissimilatory sulfate reduction: the formation of adenosine 5′-phosphosulfate (APS) and inorganic pyrophosphate (PP_i). ATPS activity was assayed by measuring ATP produced by reaction of APS with PP_i. The rate of ATP production was measured in the coupled spectrophotometric assay involving phosphorylation of glucose and the subsequent oxidation of glucose-6-phosphate to D-6-P-glucono-δ-lactone coupled to the reduction of NADP.

Boczar et al.[15] assayed esterase activity in the supernatant (cell free) fraction of filtered activated sludge. Esterase activity was determined by measuring the release of fluorescein from fluorescein diesters of acetate, butyrate, caproate, and caprylate, or the release of *p*-nitrophenol or α-napthol from *p*-nitrophenol or α-napthol esters of acetate, butyrate, capriate, caprylate caprate, laurate, myristate, palmitate, and stearate. The amount of *p*-nitrophenol and α-napthol produced was determined spectrophotometrically at 400 nm, and the amount of fluorescein produced was determined spectrophotometrically at 495 nm. Frolund et al.[39] monitored sludge bulk extracellular esterase activity using fluorescein diacetate as an enzyme substrate. A spectrofluorimeter was used to quantify the fluorescence resulting from the formation of fluorescein.

Whiteley et al.[40] monitored lipase activity in methanogenic and sulfidogenic stirred tank reactors operated in series using primary sludge from an anaerobic digester at a sewage works. The assay measured enzymatic cleavage of glycerol from the lipid triacetin. Sludge samples from the reactors were sonicated to release enzymes from the particulate fraction and then centrifuged to separate the enzymes from the particulate material. Triacetin was added to the supernatant fraction, and following an incubation period, the enzyme reaction was terminated by addition of sulfuric acid and sodium periodate. Following addition of $NaHSO_3$ and chromotropic acid reagent and heating, the reaction mixture was cooled and the glycerol released was quantified spectrophotometrically at 570 nm, Since particulate matter interfered with the lipase assay, the sample had to be sonicated and the particulate fraction removed by centrifugation prior to assaying for enzyme activity. As a result, it was not possible to determine whether the lipases were free in solution, bound to the floc matrix, or associated with the cells.

14.5 MEASUREMENT OF PHOSPHATASE ACTIVITY IN ACTIVATED SLUDGE USING FLUOROGENIC SUBSTRATES

Van Ommen Kloeke and Geesey[41] measured PO_4ase activity in activated sludge samples using the soluble, artificial, fluorogenic enzyme substrate methylumbelliferyl phosphate (MUFP) (Figure 14.1). MUFP has been used to monitor phosphomonoesterase activity in lakes.[42,43] MUF substrates are likely hydrolyzed by PO_4ases either at or near the surface of intact cells or by PO_4ases released into the environment by cells.[31] After an appropriate incubation period, the reaction mixture was centrifuged to remove interfering particulate material and the supernatant fraction assayed for fluorescence intensity using a spectrofluorometer at an excitation wavelength of 360 nm and emission wavelength at 430 nm. This substrate yielded quantitative PO_4ase activity in various activated sludge fractions at relatively high sensitivity. Using freshly collected activated sludge samples from the wastewater treatment plant in Bozeman, MT, which contained 2.9 ± 0.3 g l^{-1} total solids and 7 to 14 mg l^{-1} P_i (Table 14.2), it was determined that the particulate fraction (operationally defined as that which sedimented by centrifugation at $27,000 \times g$ for 15 min) exhibited linear PO_4ase activity at pH 7.0 of 7.9 μmol l^{-1} h^{-1}, or 91% of the total activity in "as collected" samples at MUFP final concentrations of 100 μM over a 3 to 4-h period (Figure 14.2). At a final MUFP concentration of 500 μM, the PO_4ase activity was approximately twice that observed at the 100 μM final MUFP concentration, and the activity associated with the particulate fraction was slightly greater than that associated with the "as collected" sample. A Lineweaver Burke plot of reaction rates over a range of added

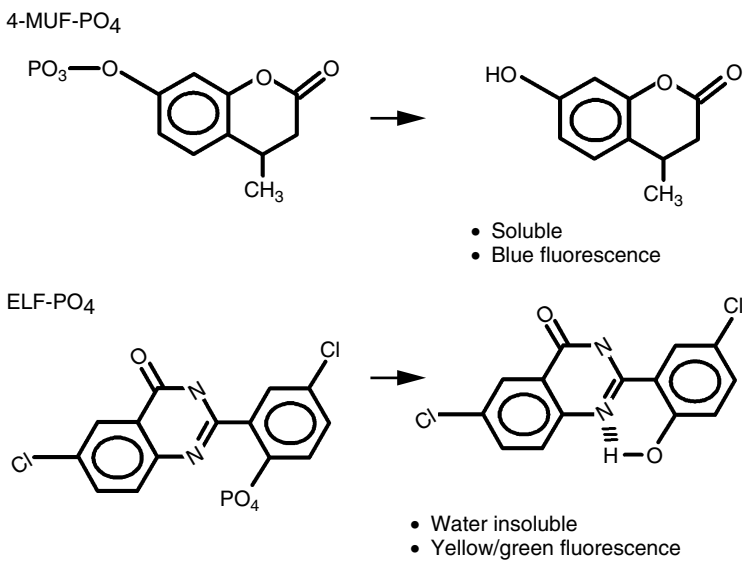

FIGURE 14.1 MUF-PO_4 and ELF-PO_4 fluorogenic substrates for measuring activity and localizing extracellular PO_4ase.

TABLE 14.2
Chemical Constituents of Activated Sludge Solids and Liquid Phases

Sample	Total Solids g l^{-1}	Volatile Solids (g l^{-1})	Protein (mg l^{-1})	Humics (mg l^{-1})	Carbohydrate (mg l^{-1})	Uronic Acids (mg l^{-1})	pH
Solids	2.9 ± 0.03	1.9 ± 0.1	871 ± 21	324 ± 9	339 ± 2	11.7 ± 2	ND[a]
Liquid	ND[a]	ND[a]	2.0 ± 1.0	BD[b]	1.0 ± 1.0	BD[b]	7.2

[a] Not determined.
[b] Below detection.

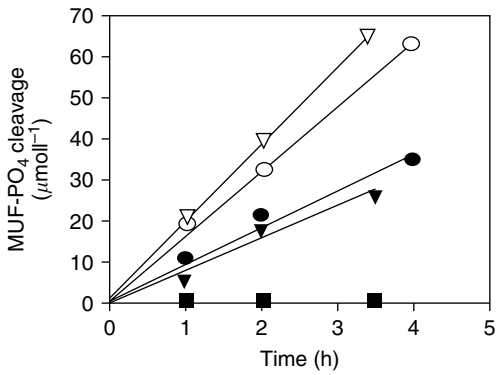

FIGURE 14.2 PO_4ase activity in activated sludge fractions. Samples assayed at 500 μM MUF-PO_4: (◯) "as collected" activated sludge, 15.2 μmol l^{-1} h^{-1}; (▽) resuspended floc, 18.4 μmol l^{-1} h^{-1}; (■) activated sludge supernatant, 0.1 μmol l^{-1} h^{-1}; and samples assayed at 100 μM MUF-PO_4: (●)"as collected" activated sludge, 8.7 μmol l^{-1} h^{-1}; (▼) resuspended floc, 7.9 μmol l^{-1} h^{-1}.

MUFP concentrations yielded a V_{max} of 2×10^4 μmol l^{-1} h^{-1} and Km of 133 μM with respect to MUFP (Figure 14.3). Conversion of MUFP to MUF was not the result of abiotic reactions since autoclave sterilization of the activated sludge samples before addition of the MUFP yielded no fluorescent product.

Additional evidence for the enzymatic release of P_i from detrital organic-P in activated sludge was obtained by following the concentration of P_i in samples of activated sludge under different conditions. Autoclave-sterilized activated sludge showed no change in P_i concentration over a 24-h period (Figure 14.4). Treatment of activated sludge with benzene to arrest growth of microorganisms present, but to allow PO_4ases present to remain active, resulted in an increase in P_i from 13.6 to 18.8 μg ml^{-1} over a 24-h period (Figure 14.4), suggesting the production of new P_i from polyphosphate (poly-P) or organic-P sources present in the activated sludge. That benzene arrested the growth of the microorganisms in the activated sludge was demonstrated by recovering the same number of colony-forming units (cfus) at the end of the

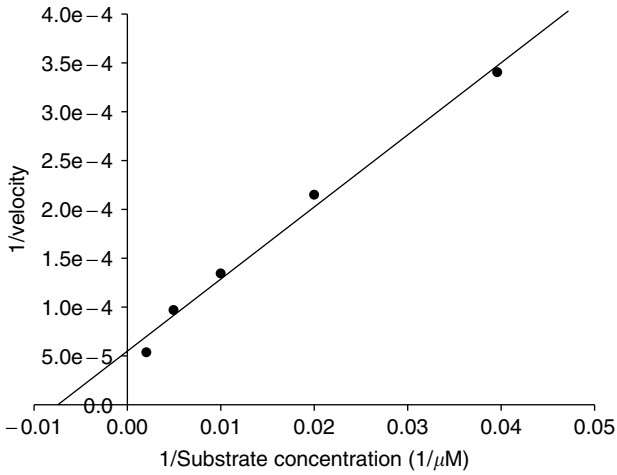

FIGURE 14.3 Lineweaver Burke plot of PO_4ase activity in "as collected" activated sludge using MUF-PO_4 as substrate.

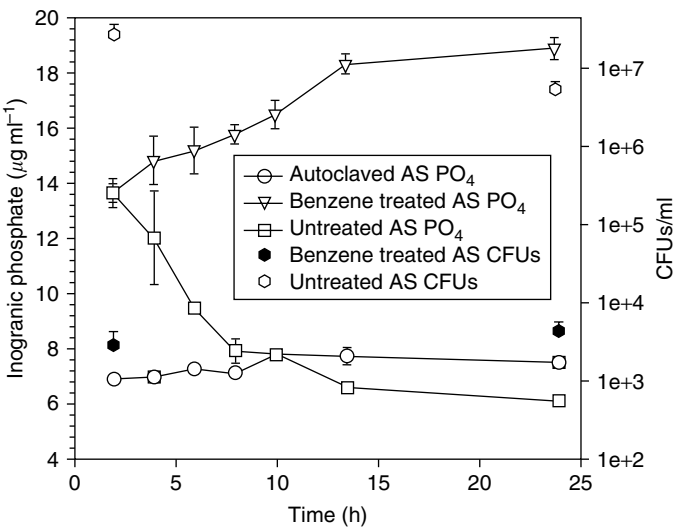

FIGURE 14.4 Effect of extracellular PO_4ase activity on the release of P_i from organic-P.

24-h incubation period as recovered at the beginning of the incubation (Figure 14.4). In contrast, untreated samples showed a decrease in P_i concentration from 13.6 to 6.0 μg ml^{-1}. The data indicate that the majority of the P_i initially present in the activated sludge as well as that produced during the 24-h incubation is converted to poly-P or organic-P by the active microbial populations present in the activated sludge. These results suggest that more P_i is being incorporated into microbial biomass in the form of poly-P and organic-P than is accounted for by the net loss of P_i from the system.

The difference is likely due to the release of "new" P_i from the detrital organic-P pool by PO_4ase exoenzymes.

14.6 LOCALIZING EXTRACELLULAR ENZYME ACTIVITY ASSOCIATED WITH MICROBIAL FLOCS

A number of the studies, including those cited above suggest that the majority of exoenzyme activity detected in the activated sludge process of various wastewater treatment plants is associated with the organic particulate fraction, comprised primarily of flocs derived from the activated sludge process. Protease, PO_4ase, lipase, and esterase activities partition strongly with the particulate phase.[15,37,41] By separating activated sludge into different fractions using centrifugation, filtration, and sonication, Goel et al.[36] determined the activity for alkaline and acid PO_4ase, α-glucosidase, and protease that was associated with bacterial cells, free in the bulk solution, and loosely associated with cells or entrapped in the flocs. A major fraction of the total enzyme activity was found to be associated with the flocs. Richards et al.[44] and Frolund et al.[39] also found that exoenzymes were immobilized in the sludge floc matrix.

Cadoret et al.[12] measured extracellular enzyme activities in whole sludge, in dispersed activated sludges, as well as that associated specifically with the floc EPS. The activated sludge from a treatment plant was treated as follows before being assayed as "whole" sludge for enzyme activities: sludge was allowed to settle, then resuspended in deionized water, then homogenized, and the process repeated. Dispersed activated sludge was first prepared as "whole" sludge before subjecting to sonication or cation exchange resin (Dowex-Na^+ 50 × 8). EPS was recovered from the supernatant fraction of the centrifuged aqueous phase following removal of the cation exchange resin and associated adsorbed material. They found that 17% of the L-Leu-aminopeptidase, 5% of α-glucosidase, 23% of protease, and 44% of α-amylase activity of sludge dispersed by sonication or cation exchange resin were recovered in the EPS fraction. Most of the enzymes remained associated either to tightly bound EPS or directly bound to the bacterial cell surfaces.

Whiteley et al.[37] determined the PO_4ases and protease activity in the supernatant fraction of liquor recovered from methanogenic and sulfidogenic sewage sludge reactors following incubation with substrates selective for these enzymes, sonication, and centrifugation. The majority of the exoprotease and PO_4ase activity was found associated with the particulate fraction that was released upon sonication. Most enzyme activity was therefore found either associated with or immobilized within the particulate matter.

Pletschke et al.[38] determine ATPS activity in the supernatant fraction of liquor recovered from methanogenic and sulfidogenic sewage sludge reactors following sonication and centrifugation. Since >90% of the enzyme activity was released into the supernatant after sonication, it was suggested that the ATPS enzymes were located either intracellularly or immobilized in or on the floc material.

Boczar et al.[15] assayed esterase activity in the particulate fraction of activated sludge using substrates of different chain lengths. C_4-ester yielded the highest activity of the different substrates tested, with activity decreasing with increasing chain length above C_4. The *p*-nitrophenol esters were hydrolyzed at higher rates than fluorescein esters. Esterase activities determined after freeze–thaw treatment suggested that a significant portion of the fluorescein esters was hydrolyzed by enzymes located on the cell surface or within the cell envelope. In general, the bulk of the esterase activity was associated with the particulate flocs with no significant amount of activity detectable in the bulk solution. Similar results were reported by Teuber and Brodish[45] who found that 75% to 99% of the PO_4ase, glucosidase, and aminopeptidase activity was associated with sludge material that pelleted upon centrifugation at $3000 \times g$.

Van Ommen Kloeke and Geesey[41] used a precipitating fluorogenic enzyme substrate ELF-PO_4 (Figure 14.1) to localize PO_4ase activity in the activated sludge liquor. Since this substrate is converted to a water-insoluble, crystalline, yellow, fluorescent product at the site of organic-P hydrolysis, the position of the resulting fluorescent objects identifies the site of active PO_4ase enzymes when viewed by fluorescence microscopy (Figure 14.5). It is evident from the distribution of fluorescence that the PO_4ase activity is localized in discrete locations throughout the matrix of the floc particles, possibly reflecting the distribution of PO_4ase-producing microorganisms. Some areas are as large as 40 μm in diameter (Figure 14.5, inset), although most are on the order of 5 μm in diameter. The intensity of the fluorescence emanating from these local regions in the floc particles increased linearly over a 40-min period (Figure 14.6). Incubations of 60 min allowed the development of maximum density of ELF crystals before increasing crystal size, and fluorescence intensity caused the fluorescent image of adjacent crystals to merge into a single fluorescent object. Sixty-minute incubations were thus used to determine the density and distribution of PO_4ase activity in the flocs.

Frolund et al.[39] showed that a large portion of various classes of exoenzymes present in activated sludge were adsorbed to the EPS matrix. When the EPS was treated with a cation exchanger, large quantities of enzyme were released into the bulk aqueous solution. Since the activities of these extracellular enzymes strongly partition with the floc-containing fraction, these enzymes likely have evolved to remain associated with the cell surface or the floc matrix (Figure 14.7). Flocs provide a conditioned environment conducive for extracellular enzyme accumulation and activity outside the cell. Goel et al.[36] showed that the floc-bound nature of extracellular alkaline PO_4ase, acid PO_4ase, α-glucosidase, and protease enabled the enzymes to remain active under anaerobic as well as aerobic phases of operation. Recently, it has been shown that the EPS of activated sludge aggregates inhibited the diffusion of high molecular weight substrates of extracellular enzymes, limiting their availability to the enzymes and the rate of catalysis.[12] These results challenge the idea that hydrolysis of the organic polymers is the first and rate-limiting step in the activated sludge process, and support the suggestion by Guellil et al.[46] that sorption or uptake of the organic polymers by the exoenzyme-containing floc is a rate-limiting step that precedes hydrolysis (Figure 14.7). Thus, the benefits provided to exoenzymes by EPS

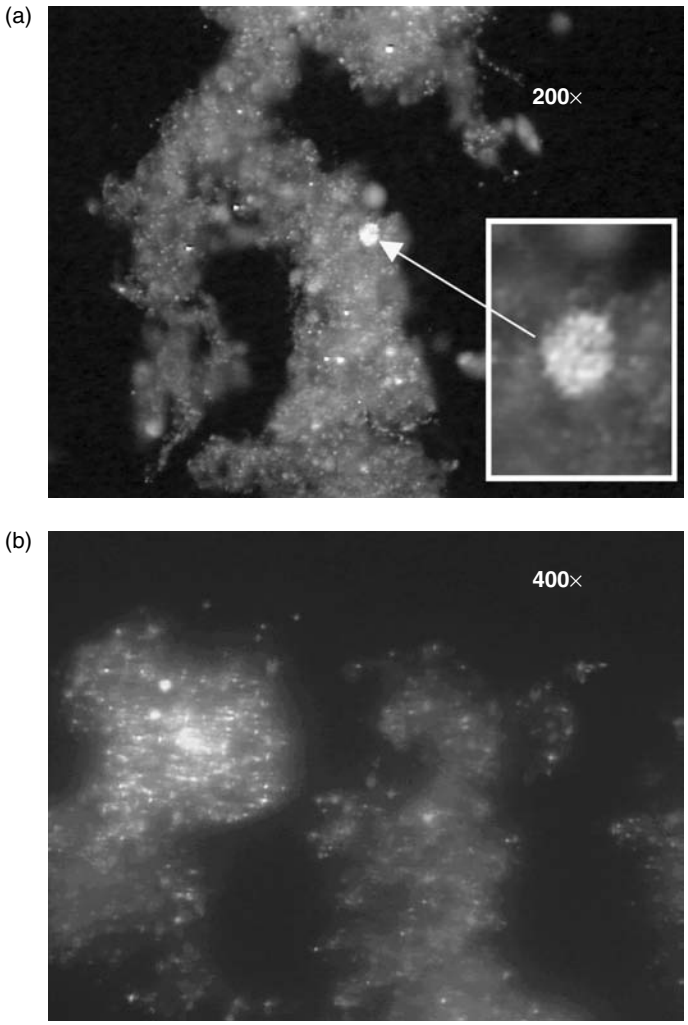

FIGURE 14.5 Epifluorescence microscopic image of ELF crystals precipitated in floc particles recovered from activated sludge and incubated with 100 μM ELF-P for 60 min. (a) Crystals distributed throughout floc matrix. Arrow shows crystal with diameter of approximately 40 μm. (b) Crystals concentrated in one floc particle at densities higher than in adjacent particles.

are, to some extent, offset by the added diffusion resistance the EPS exerts on the enzyme substrates.

Floc formation requires expenditure of energy generated by the bacteria in the system. The main source of this energy is the polymeric organic material in the wastewater aqueous phase that can only be accessed by the microorganisms if first degraded into useable subunits by exoenzymes (Figure 14.8). Since even the smallest

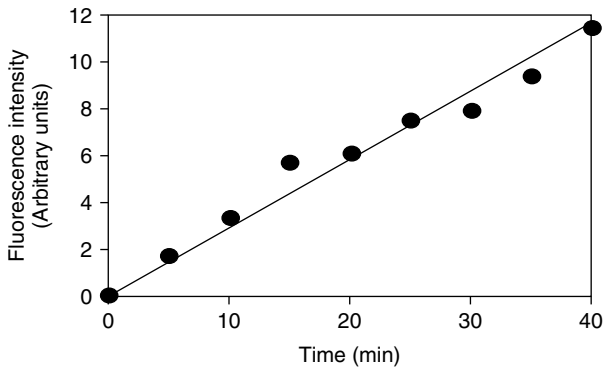

FIGURE 14.6 Increase in fluorescence intensity of area of floc particle as a function of time during which ELF-PO_4 is being hydrolyzed to ELF by extracellular PO_4ase enzymes.

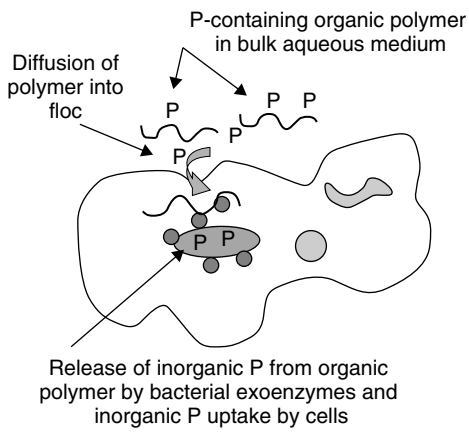

FIGURE 14.7 Schematic representation of detrital, polymeric, organic-PO_4 diffusion from bulk liquid phase into floc matrix containing extracellular PO_4ase-producing bacteria. P_i released at cell surface is taken up by the cells and transformed into biomass-P.

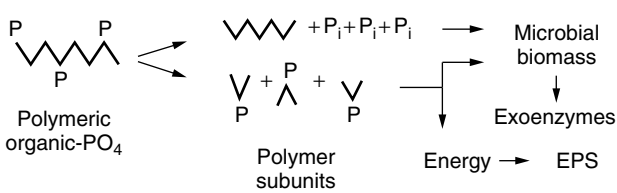

FIGURE 14.8 Schematic diagram of pathway of formation of microbial biomass, exoenzymes, and EPS. Polymer subunit intermediate products have different properties than original polymeric compounds. Production of intermediate products may affect P removal efficiency.

floc particles resolved by light microscopy contained regions of ELF fluorescence, exoenzyme production and secretion likely occurs during or possibly even prior to floc formation in the system.

When floc material was homogenized in a tissue homogenizer to disperse bacterial cells, and the preparation incubated with ELF-P, approximately 9% of the cells that were visualized after staining with the nucleic acid stain acridine orange had ELF crystals precipitated in their immediate vicinity.[41] PO_4ase activity was thus contributed by a small fraction of the floc-associated bacterial community. Of the total area of fluorescence produced by all crystals of ELF evaluated in homogenized floc preparations, approximately 80% was contributed by crystals associated with cells that also reacted positively with SYTO9, a fluorochrome that is taken up by cells with a membrane potential, and thus considered viable.[41] The other ELF crystals could not be associated with any other objects in the floc. PO_4ase activity was therefore primarily associated with active bacterial cells in the floc.

14.7 IDENTIFICATION OF POPULATIONS OF CELLS RESPONSIBLE FOR EXTRACELLULAR PO_4ASE ACTIVITIES WITHIN FLOC-ASSOCIATED MICROBIAL COMMUNITIES

Considerable progress has been made in recent years in identifying the types of bacteria present in activated sludge systems. Besides the poly-P-accumulating bacteria of the genus *Acinetobacter*, those aligning with the cytophaga-flavobacteria group have also been widely reported in activated sludge systems in different parts of the world.[28,47–49] Snaidr et al.[50] reported that the cytophaga-flavobacteria group contributed 12% of the DAPI-stained bacterial community of an activated sludge system. Manz et al.[47] found a similar fraction of the bacteria present in activated sludge that hybridized with the *Bacteria*-specific probe EUB338 probed positive with a cytophaga-flavobacter-specific 16S rRNA oligonucleotide probe. The extent to which these groups of bacteria are responsible for extracellular enzymatic activities measured in activated sludge floc has only recently been assessed.[41,51]

The detection of the cultivable bacterial populations in homogenized activated sludge floc preparations that exhibit extracellular PO_4ase activity was facilitated by the development of a new screening technique.[51] Adding the precipitating fluorogenic substrate 2-(5′-chloro-2′-phosphoryloxyphenyl)-4-[3H]-quinazolinone (CPQ-PO_4) to a bacterial cultivation medium, after medium sterilization but prior to solidification, offered the opportunity to detect PO_4ase active colonies following inoculation and incubation of samples of homogenized activated sludge floc preparations plated on this medium (Figure 14.9). Upon enzymatic cleavage, this molecule yields the stable, highly fluorescent precipitate 2-(5′-chloro-2′-hydroxyphenyl)-4-[3H]-quinazolinone (CPQ)[52] (Figure 14.9). CPQ excites at 345 nm and fluoresces at 530 nm.[51] Phosphatase activity can then be monitored as the colonies grow by viewing the plates under UV light. Another benefit of

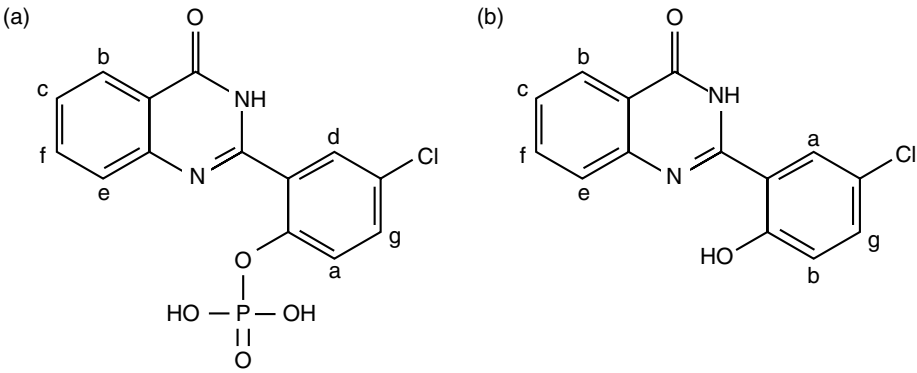

FIGURE 14.9 Fluorogenic substrate (a) 2-(5′-chloro-2′-phosphoryloxyphenyl)-4-[3H]-quinazolinone is hydrolyzed to (b) 2-(5′-chloro-2′-hydroxyphenyl)-4-[3H]-quinazolinone to produce a water-insoluble fluorescent precipitate.

this approach is that it distinguishes between activity of secreted (bacteria-free) and cell-associated PO_4ase activity, due to the precipitating nature of the probe. Colonies actively secreting PO_4ase enzyme into their environment have a fluorescent halo, whereas those PO_4ase-positive colonies which have only cell-associated activity do not produce a halo.[51] Using this approach, these investigators found that 35% of the cfus that grew on LB/HEPES/CPQP agar medium yielded an intense yellow–green fluorescence, indicating the presence of phosphatase-positive clones (Figure 14.10).

The PO_4ase-positive colonies from the homogenized activated sludge preparations displayed two types of fluorescence when plated on the above medium. Some colonies displayed fluorescence that was limited to the area occupied by the colony, whereas, fluorescence displayed by other colonies extended into the surrounding medium producing halos around the colonies. Of all fluorescent colonies obtained on the plates, 36% displayed halos. Isolates displaying these different forms of PO_4ase activity on solid medium are shown in Figures 14.11 and Figure 14.12. Isolate A produced a fluorescent halo around its colony (Figure 14.11), whereas Isolate J produced fluorescence that was restricted to the colony (Figure 14.12). Isolates A and J were further evaluated for the distribution of PO_4ase activity in suspended batch cultures without added agar. Whereas 36% of the total PO_4ase activity produced by Isolate A was recovered with the cell fraction, with the remainder free in the culture menstruum, 99% of the total PO_4ase activity produced by Isolate J was recovered with the cell fraction.[51] PO_4ase activity was induced when cultures of both isolates entered the late exponential growth phase.

Selective identification of PO_4ase-positive colonies of bacterial populations in complex microbial communities makes it feasible to sequence the 16S rDNA gene to establish a phylogenetic affiliation for the population. When the DNA of cells from several of the fluorescent colonies recovered from plates inoculated with

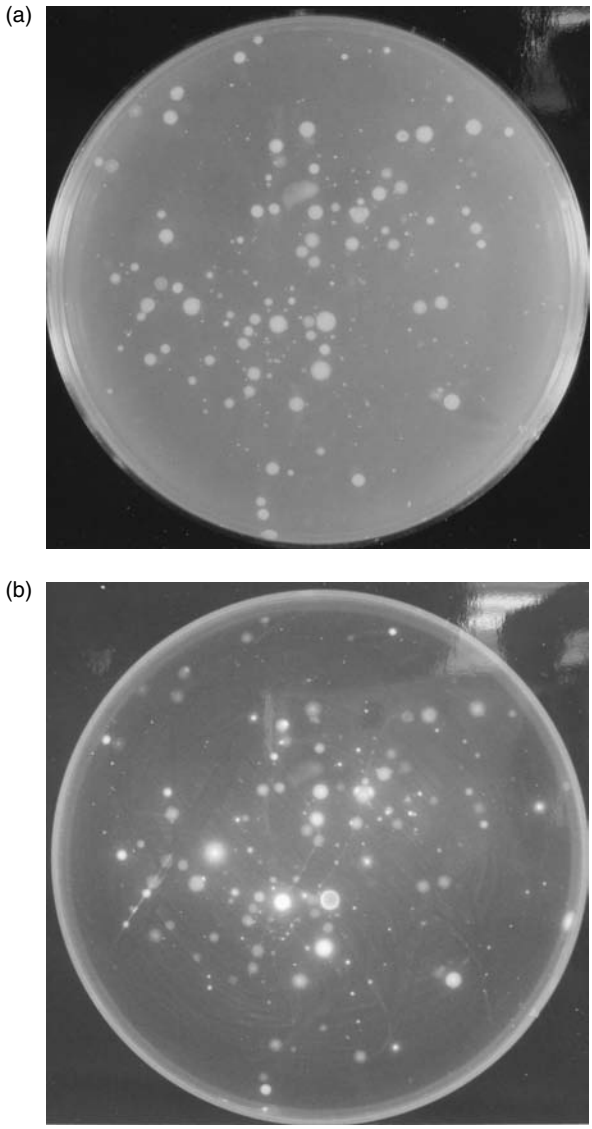

FIGURE 14.10 Colonies formed on LB/HEPES/CPQ-PO_4 solid medium after inoculation with activated sludge from a wastewater treatment plant. (a) Colonies under normal white light and (b) CPQ fluorescent, PO_4ase-producing colonies.

homogenized activated sludge was extracted and a portion of their 16S rDNA amplified by polymerase chain reaction (PCR) using primer set 1056F/1392R, the resulting amplicons, when sequenced, grouped with the cytophaga-flavobacteria in the phylum cytophaga-flavobacter-bacteroides.[41] Three of the isolates reacted positively with the cytophaga-flavobacteria group-specific rRNA probe CF319a. The

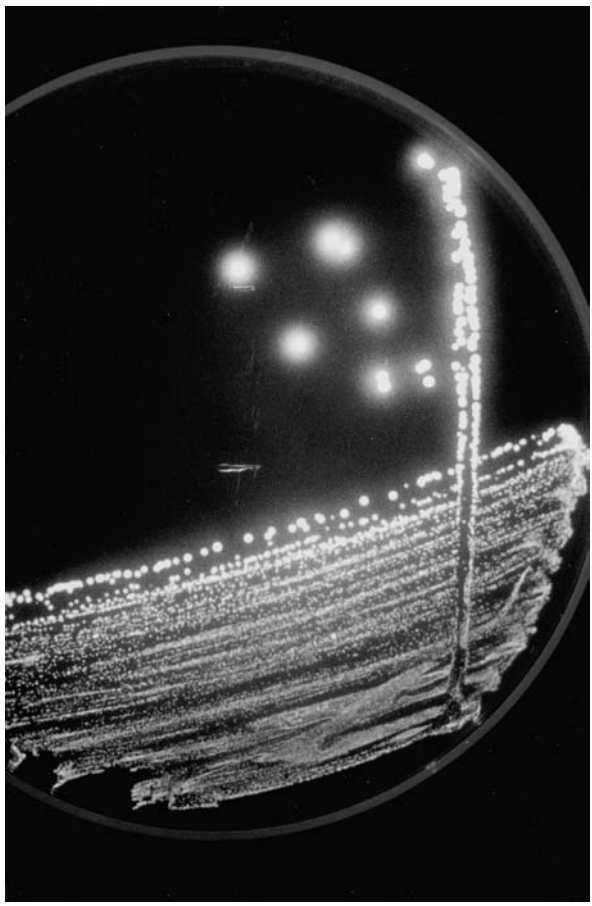

FIGURE 14.11 (**Color Figure 4.11 appears following page 236.**) Colonies of Isolate A growing on LB/HEPES/CPQ-PO_4 solid medium. Note halo of fluorescent CPQ that has precipitated some distance away from the colonies reflecting diffusion of PO_4ase away from the cells and the colony.

CF319a probe reacted positively with approximately 10% of the DAPI-stained bacteria and 17% to 20% of the ELF-precipitating bacteria associated with homogenized floc material from activated sludge samples.[41] These results suggest that although the cytophaga-flavobacteria group resists efforts to cultivate in the laboratory, it is an important contributor of PO_4ase activity in activated sludge. Using a combination of molecular approaches, it is possible to establish structure–function relationships among uncultivated members of complex microbial communities such as those established in flocs of the activate sludge process of wastewater treatment.

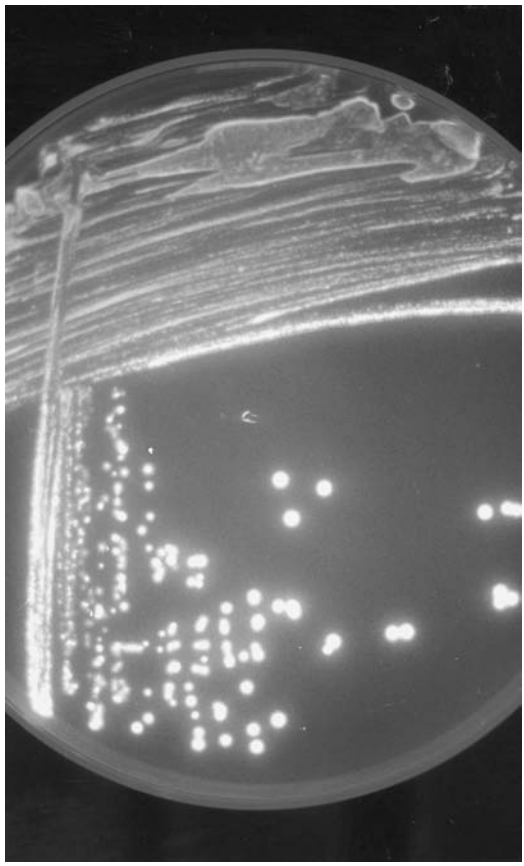

FIGURE 14.12 (**Color Figure 4.11 appears following page 236.**) Colonies of Isolate J growing on LB/HEPES/CPQ-PO_4 solid medium. Note the fluorescent CPQ that has precipitated remains close to the perimeter of the colonies indicating that the PO_4ase enzymes remain closely associated with the cells in the colonies.

14.8 CONCLUSIONS

Floc formation and associated microbial populations play a key role in the degradation of complex detrital organic matter in the activated sludge process of wastewater treatment. Extracellular enzymes represent an important class of EPS associated with the activated sludge floc particles. The extracellular proteases, lipases, and glucosidases hydrolyze large organic molecules too large to be taken up by bacterial cells to smaller subunits that are readily transported into the cell and metabolized. The floc matrix offers a conditioned environment outside the bacterial cells for these enzymes to carry out their function. Other extracellular enzymes such as PO_4ase regenerate the inorganic forms of non-conservative elements such as phosphorus. This represents the

initial step in removal of detrital polymeric organic-P from wastewater streams. Since one-third to one-half of the total P in wastewater exists as detrital polymeric organic P, the bacterial populations that produce active PO_4ase play a key role in P removal from wastewater in the activated sludge process. Members of the cytophaga-flavobacteria group appear to be particularly important in this regard since they account for 17% to 20% of the total PO_4ase-active cells in the system.

ACKNOWLEDGMENTS

This research was supported by the National Science Foundation grant OCE-9720151.

REFERENCES

1. Geesey, G. G., Microbial exopolymers: ecological and economic considerations, *ASM News*, *48*, 14 (1982).
2. Lewis, D.L., and Gattie, D.K., Effects of cellular aggregation on the ecology of microorganisms, *ASM News*, *56*, 263 (1990).
3. Friedman, B.A., Dugan, P.R., Pfister, R.M., and Remsen, C.C., Structure of exocellular polymers and their relationship to bacterial flocculation, *J. Bacteriol.*, *98*, 1328 (1969).
4. ZoBell, C.E., and Allen, E.C., The significance of marine bacteria in the fouling of submerged surfaces, *J. Bacteriol.*, *29*, 239 (1935).
5. ZoBell, C.E., The effect of solid surfaces upon bacterial activity, *J. Bacteriol.*, *46*, 39 (1943).
6. Unz, R.F., and Farrah, S.R., Exopolymer production and flocculation by *Zoogloea* MP6, *Appl. Environ. Microbiol.*, *31*, 623 (1976).
7. Silver, M.W., Shanks, A.L., and Trent, J.D., Marine snow: microplankton habitat and source of small-scale patchiness in pelagic populations, *Science*, *201*, 371 (1978).
8. Jorand, F., Zartarian, F., Thomas, F., Block, J.-C., Bottero, J.Y., Villemin, G., Urbain, V., and Manem, J., Chemical and structural (2D) linkage between bacteria within activated sludge flocs, *Water Res.*, *29*, 1639 (1995).
9. Moller, S., Sternberg, C., Andersen, J.B., Christensen, B.B., Ramos, J. L., Givskov, M., and Molin, S., In situ gene expression in mixed-culture biofilms: evidence of metabolic interactions between community members, *Appl. Environ. Microbiol.*, *64*, 721 (1998).
10. Baty, A.M., Eastburn, C., Diwu, Z., Techkarnjanaruk, S., Goodman, A. E., and Geesey, G.G., Differentiation of chitinase-active and non-chitinase-active subpopulations of a marine bacterium during chitin degradation, *Appl. Environ. Microbiol.*, *66*, 3566 (2000).
11. Abrahamson, M., Lewandowski, Z., Geesey, G.G., Sjak-Braek, G., Strand, W., and Christensen, B.E., Development of an artificial biofilm to study the effects of a single microcolony on mass transport, *J. Microbiol. Methods*, *26*, 161 (1996).
12. Cadoret, A., Conrad, A., and Block, J.-C., Availability of low and high molecular weight substrates to extracellular enzymes in whole and dispersed activated sludges, *Enzyme Microb. Technol.*, *31*, 179 (2002).
13. Suci, P.A., Vrany, J.D., and Mittelman, M.W., Investigation of interactions between antimicrobial agents and bacterial biofilms using attenuated total reflection Fourier transform infrared spectroscopy, *Biomaterials*, *19*, 327 (1998).

14. Fattorini, I., Scardaci, G., Jin, H., Amicosante, G., Franceschini, N., Oratore, A., and Orefici, G., B-lactamase of *Mycobacterium fortuitium*: kinetics of production and relationship with resistance to B-lactam antibiotics, *Antimicrob. Agents Chemother.*, *35*, 1760 (1991).
15. Boczar, B.A., Forney, L.J., Begley, W.M., Larson, R.J., and Federle, T.W., Characterization and distribution of esterase activity in activated sludge, *Water Res.*, *35*, 4208 (2001).
16. van Hamersveld, E.H., van der Lans, R.G. J.M., Caulet, P.J. C., and Luyben, K.C. A.M., Modeling brewersapos yeast flocculation, *Biotechnol. Bioeng.*, *57*, 330 (1998).
17. Kosakai, Y., Soo Park, Y., and Okabe, M., Enhancement of L(+)-lactic acid production using mycelial flocs of *Rhizopus oryzae, Biotechnol. Bioeng.*, *55*, 461 (1997).
18. Lenter, C.M., McDonald, J.L. M., Skousen, J.G., and Ziemkiewicz, P. F., The effects of sulfate on the physical and chemical properties of actively treated acid mine drainage floc, *Mineral Water Environ.*, *21*, 114 (2002).
19. Laspidou, C.S., and Bruce, E.R., A unifying theory for extracellular polymeric substances, soluble microbial products, active and inert biomass, *Water Res.*, *11*, 2711 (2002).
20. Hsieh, K.M., Murgel, G.A., Lion, L., and Shuler, M.L., Interactions of microbial biofilms with toxic trace metals. Observation and modeling of cell growth, attachment, and production of extracellular protein, *Biotechnol. Bioeng.*, *44,* 219–231 (1994).
21. Sponza, D.T., Investigation of extracellular polymer substances (EPS) and physicochemical properties of different activated sludge flocs under steady-state conditions, *Enzyme Microb. Technol., 32*, 375 (2003).
22. Dueholm, T.E., Andreasen, K.H., and Nielsen, P.H., Conceptual model for the transformation of long chain fatty acids and triglycerides in activated sludge, *Water Sci. Technol.*, *43*, 165 (2000).
23. Gessesse, A., Dueholm, T.E., Petersen, S.B., and Nielsen, P.H., Lipase and protease extraction from activated sludge, *Water Res.*, *37*, 3652 (2003).
24. Sutherland, I.W., Polysaccharases for microbial exopolysaccharides, *Carbohydr. Res.*, *38*, 319 (1999).
25. Toerien, D.F., Gerber, A., Lotter, L.H., and Cloete, T.E., Enhanced biological phosphorus removal in activated sludge systems, *Adv. Microb. Ecol.*, *11*, 173 (1990).
26. Christensson, M., Blackall, L.L., and Welander, T., Metabolic transformations and characterization of the sludge community in an enhanced biological phosphorus removal system, *Appl. Microbiol. Biotechnol.*, *49*, 226 (1998).
27. Van Niel, E.W.J., Appeldoom, K.J., Zehnder, A.J.B., and Kortstee, G.J.J. Inhibition of anaerobic phosphate release by nitric oxide in activated sludge, *Appl. Environ. Microbiol.*, *64*, 2925 (1998).
28. Fuhs, G.W., and Chen, M., Microbiological basis of phosphate removal in the activated sludge process for the treatment of wastewater, *Microb. Ecol.*, *2*, 119 (1975).
29. Kulaev, I.S., and Vagabov, V.M., Polyphosphate metabolism in micro-organisms, *Adv. Microb. Physiol.*, *24*, 83 (1983).
30. Rao, N.N., Roberts, M.F., and Torriani-Gorini, A., Polyphosphate accumulation and metabolism in *Escherichia coli*, in *Phosphate metabolism and cellular regulation in microorganisms*, Yagil, E., Ed., American Society for Microbiology, Washington, DC, p. 213 (1987).
31. Chrost, R.J., Environmental control of the synthesis and activity of aquatic microbial ectoenzymes, in *Microbial enzymes in aquatic environments*, Chrost, R.J., Ed., Springer-Verlag, New York, p. 29 (1991).

32. Streichan, M., Golecki, J.R., and Schon, G., Polyphosphate-accumulating bacteria from sewage plants with different processes for biological phosphorus removal, *FEMS Microb. Ecol.*, *73*, 113 (1990).
33. Wagner, M., Erhart, R., Manz, W., Amann, R., Lemmer, H., Wedi, D., and Schleifer, K.H., Development of an rRNA-targeted oligonucleotide probe specific for the genus *Acinetobacter* and its application for *in situ* monitoring in activated sludge, *Appl. Environ. Microbiol.*, *60*, 792 (1994).
34. Gachter, R., Meyer, J.S., and Mares, A., Contribution of bacteria to release and fixation of phosphorus in lake sediments, *Limnol. Oceanogr.*, *33*, 1542 (1998).
35. Halvorson, H.O., Suresh, N., Roberts, M.F., Coccia, M., and Chikarmane, H.M., Metabolically active surface polyphosphate pool in *Acinetobacter Iwoffi*, in *Phosphate metabolism and cellular regulation in microorganisms*, Yagil, E., Ed., American Society for Microbiology, Washington, D.C., p. 220 (1987).
36. Goel, R., Takashi, M., Satoh, H., and Matsuo, T., Comparison of hydrolytic enzyme systems in pure culture and activated sludge under different electron acceptor conditions, *Water Sci. Tech.*, *37*, 335 (1998).
37. Whiteley, C.G., Heron, P., Pletschke, B., Rose, P.D., Tshivhunge, S., and Van Jaarsveld, F.P., The enzymology of sludge solubilization utilizing sulfate reducing systems. Properties of proteases and phosphatases, *Enzyme Microb. Technol.*, *31*, 419 (2002).
38. Pletschke, B.I., Rose, P.D., and Whiteley, C.G., The enzymology of sludge solubilization utilizing sulfate reducing systems. Identification and properties of ATP-sulfurylases, *Enzyme Microbial. Technol.*, *31*, 329 (2002).
39. Frolund, B., Griebe, T., and Nielsen, P.H., Enzymatic activity in the activated-sludge floc matrix, *Appl. Microbiol. Biotechnol.*, *43*, 755 (1995).
40. Whiteley, C.G., Burgess, J.E., Melamane, X., Pletschke, B., and Rose, P.D., The enzymology of sludge solubilization utilizing sulfate-reducing systems: the properties of lipases, *Water Res.*, *37*, 289 (2003).
41. Van Ommen Kloeke, F., and Geesey, G.G., Localization and identification of populations of phosphatase-active bacterial cells associated with activated sludge, *Microb. Ecol.*, *38*, 201 (1999).
42. Chrost, R.J., and Overbeck, J., Kinetics of alkaline phosphatase activity and phosphorous availability for phytoplankton and bacterioplankton in Lake Plubsee (north German eutrophic lake), *Microb. Ecol.*, *13*, 229 (1987).
43. Ollson, H., Phosphatase activity in an acid, limed Swedish lake, in *Microbial enzymes in aquatic environments*, Chrost, R.J., Ed., Springer-Verlag, New York, p. 206 (1991).
44. Richards, S.R., Hastwell, C., and Davies, M., The comparative examination of 14 activated-sludge plants using enzymatic techniques, *J. Water Pollut. Control Fed.*, *83*, 300 (1984).
45. Teuber, M., and Brodish, K.E. U., Enzymatic activities of activated sludge, *Eur. J. Appl. Microbiol.*, *4*, 185 (1977).
46. Guellil, A., Thomas, F., Block, J.-C., Bersillon, J.-L., and Ginestet, P., Transfer of organic matter between wastewater and activated sludge flocs, *Water Res.*, *35*, 143 (2001).
47. Manz, W., Amann, R., Ludwig, W., Vancanney, M., and Schleifer, K.-H., Application of a suite of 16S rRNA-specific oligonucleotide probes designed to investigate bacteria of the phylum cytophaga-flavobacter-bacteroides in the natural environment, *Microbiology*, *142*, 1097 (1996).
48. Gude, H., Occurrence of Cytophagas in sewage plants, *Appl. Environ. Microbiol.*, *39*, 756 (1980).

49. Bond, P.L., Hugenholtz, P., Keller, J., and Blackall, L.L., Bacterial community structures of phosphate-removing and non-phosphate-removing activated sludges from sequencing batch reactors, *Appl. Environ. Microbiol.*, *61*, 1910 (1995).
50. Snaidr, J., Amann, R., Huber, I., Ludwig, W., and Schleifer, K.-H., Phylogenetic analysis and in situ identification of bacteria in activated sludge, *Appl. Environ. Microbiol.*, *63*, 2884 (1997).
51. Van Ommen Kloeke, F., Baty, A.M., Eastburn, C., Diwu, Z., and Geesey, G.G., A novel method for screening bacterial colonies for phosphatase activity, *J. Microbiol. Methods*, *38*, 25 (1999).
52. Haugland, R.P., Zhang, Y.-Z., Yue, S.T., Terpetschnig, E., Olson, N. A., Naleway, J.J., Larison, K.D., and Huang, Z.M., Enzymatic analysis using substrates that yield fluorescent precipitates, *US Patent 748 860* (1994).

15 Molecular Analyses of Microbial Community Structure and Function of Flocs

Holger Daims

CONTENTS

15.1 INTRODUCTION

Microbial flocs, which occur in most freshwater and marine environments, are built by numerous bacterial species that grow as single cells, filaments, or cell aggregates. Flocs also contain extracellular polymeric substances (EPS), which are synthesized by the microorganisms, as well as particulate organic and inorganic matter and cavities between these components. Flocculation is advantageous for microorganisms: the matrix of dense flocs provides some protection from grazing protozoa. Floc bacteria involved in mutualistic symbiotic interactions benefit from the close proximity to their partners. Changes of the environmental conditions outside of flocs may have attenuated effects inside of flocs, where microorganisms to a certain degree create and maintain their own microenvironments. Concentration gradients of soluble nutrients, waste compounds, and gases form within flocs due to diffusion barriers

1-56670-615-7/05/$0.00+$1.50

and microbial metabolic activity. The combination of a complex physical structure with chemical gradients creates in the same floc microhabitats for different functional groups of microorganisms, which may be involved in essential nutrient recycling processes. Flocs also provide niches for species that would otherwise not survive in a particular environment. For example, in aerobic habitats, oxygen is consumed by aerobic organisms, which are located in the outer layers of flocs. Therefore, the central floc regions are depleted in oxygen and can be colonized by microaerophilic or even obligately anaerobic bacteria, which are sensitive to oxygen and do not occur in the same habitat outside of flocs or biofilms.[1] Consequently, flocculation promotes a higher microbial biodiversity in ecosystems.

Any attempt to determine how flocculation influences the performance and stability of ecosystems requires a detailed knowledge of the structure and function of the microbial communities in flocs. Traditional microbiological methods, which are based on the isolation and cultivation of bacteria, fail to provide such insight because most microorganisms in nature are recalcitrant to cultivation.[2] The following text explains how cultivation-independent molecular techniques can be applied to study complex microbial communities in flocs. Since an encompassing description of all available molecular tools would be beyond the scope of this chapter, special emphasis is given to the rRNA approach[2] and to commonly used *in situ* methods, which allow monitoring microorganisms directly in their habitats. The section on methods is followed by a case study, which deals with the discovery and functional analysis of uncultured *Nitrospira*-like bacteria. These organisms are important nitrite oxidizers in natural habitats and in wastewater treatment plants — engineered systems where flocculation plays a critical role.

15.2 MOLECULAR METHODS FOR ANALYZING UNCULTURED BACTERIA

15.2.1 Phylogenetic Analysis of 16S Ribosomal RNA Gene Sequences

The phylogenetic analysis of 16S ribosomal RNA (rRNA) gene sequences[3,4] is the most widely used method for cultivation-independent microbiological surveys of environmental samples. DNA is extracted from a sample and is used as template for the specific amplification, by polymerase chain reaction (PCR) with appropriate primer sets, of bacterial 16S rRNA genes. The amplified 16S rRNA genes are cloned and sequenced. The obtained sequences are compared, by phylogenetic methods, with known reference rRNA sequences in order to infer the phylogenetic affiliations of the different bacteria in the environmental sample. Thousands of suitable reference sequences have already been deposited in public databases. This approach is invaluable for microbial ecology and has not only provided insight into the microbial diversity of many different habitats, but has also led to the discovery of novel, yet uncultured prokaryotic lineages.[5]

However, the analysis of 16S rRNA gene libraries has some pitfalls, which must be considered in order to avoid misinterpretations of the results. A library that consists

of amplified and cloned 16S rRNA genes does not often correctly represent the real bacterial biodiversity in an environmental sample. Inefficient extraction of DNA and biases of PCR and of cloning can cause pronounced differences between the frequencies of specific 16S rRNA genes in the library and the frequencies of the corresponding organisms in the sample.[6–8] These problems can hamper even the detection of those ecological key players, which are highly abundant in a habitat.[9] Therefore, it is recommended to apply different DNA extraction methods on the same sample, to pool the DNA that was isolated by these methods prior to the amplification of 16S rRNA genes, to use different 16S rRNA gene-specific primer sets in parallel PCR experiments, and to use different vectors for cloning.[10] Despite these precautions, in most cases, it will not be feasible to obtain the 16S rRNA gene sequences of all bacterial species living in a complex environmental sample. Already a single library established from such a sample can contain thousands of different 16S rRNA genes. The random selection of clones for sequencing is a simple approach to analyze such libraries, which has the disadvantage that the less frequent 16S rRNA genes may not be encountered while the more frequent 16S rRNA genes are sequenced repeatedly. Alternatively, one could use membrane hybridization with specific rRNA-targeted nucleic acid probes or PCR with highly specific primers to screen rRNA gene libraries for members of different phylogenetic lineages. Nucleic acid fingerprinting techniques, as for example restriction fragment length polymorphism (RFLP) analysis[11] and denaturing gradient gel electrophoresis (DGGE),[12] are other useful tools for systematic analyses of 16S rRNA genes in environmental samples. RFLP analysis can reduce the sequencing effort needed to retrieve a high number of different, already cloned rRNA genes from a library. Genes with identical RFLP patterns are collected in groups, and then only a few representatives of each group are sequenced and further analyzed. DGGE separates different PCR-amplified rRNA gene fragments in polyacrylamide gels with increasing denaturing gradients. In the ideal case, each band in the gel represents one organism in the environmental sample. Single bands can be excised, re-amplified by PCR, and sequenced for phylogenetic analysis. DGGE has the disadvantage that it can separate only fragments of 16S rRNA genes with a maximum size of approximately 500 base pairs. Partial 16S rRNA sequences of this length are of limited use for phylogeny and for the design of rRNA-targeted nucleic acid probes.

Due to the biases of DNA extraction, PCR, and cloning, the quantitative composition of bacterial communities cannot be inferred from the frequencies of different 16S rRNA genes in clone libraries. For the same reason, the intensities of the bands in fingerprints of PCR-amplified rRNA genes do not necessarily correlate with the *in situ* abundance of the corresponding bacteria. Recently developed quantitative variants of PCR (real-time PCR[13,14] and competitive PCR[15–17]), or PCR-independent methods like quantitative dot blot[18,19] and fluorescence *in situ* hybridization (FISH) (discussed in the next section), should be applied for quantitative analyses of microbial communities.

15.2.2 Fluorescence *In Situ* Hybridization

Fluorescence *in situ* hybridization (FISH) with rRNA-targeted probes is a cultivation-independent method to identify microorganisms and to visualize microbial cells

directly in their habitats.[2,20] The ribosomal RNAs are optimal targets for *in situ* hybridization. These ubiquitous molecules have a highly conserved structure and are essential components of the ribosomes in all living cells. The high number of ribosomes in a microbial cell causes a natural amplification of the probe-conferred fluorescence. A specific rRNA-targeted oligonucleotide probe must be sequence complementary to a short base sequence, which exists only on the ribosomal RNA of the probe target organisms. The nontarget organisms should have a different base sequence at the probe-binding site and in all other regions of the ribosomal RNAs. Functions to automatically design new rRNA-targeted probes and to match probes against known rRNA sequences are offered, for example, by the ARB software package[21] and by the Ribosomal Database Project.[22] A comprehensive collection of available rRNA-targeted probes is provided by the ProbeBase database.[23]

FISH with rRNA-targeted probes and phylogenetic analyses complement each other. In the first step, rRNA gene sequences are retrieved from an environmental sample and are analyzed in order to determine the phylogenetic affiliations of the corresponding organisms. In the second step, probes targeting these sequences are designed and are applied in FISH experiments to visualize their target organisms in the original sample. The detection of the probe target cells by FISH confirms that the analyzed rRNA genes belong to organisms, which are really present in the environmental sample, and not to contaminating naked DNA.[2]

Organisms in environmental samples can be identified with a high degree of certainty by FISH with hierarchically nested rRNA-targeted probes. A nested probe set may contain, for example, one species-specific (probe I), one genus-specific (probe II), and one phylum-specific probe (probe III), which are labeled with different fluorescent dyes. Provided that the target species of probe I belongs to the genus and phylum that is targeted by probes II and III, respectively, all target organisms of probe I must also be detected by the other two probes. Accordingly, all target organisms that are stained by probe II must also be stained by probe III. Cells that are detected only by probe I or II are most likely nontarget organisms of these probes and have been stained due to unspecific hybridization. Nested probes make it possible to detect up to seven related phylogenetic groups in the same FISH experiment.[24]

FISH has been applied to study the microbial community structures of activated sludge flocs[25–28] and to monitor important functional groups of bacteria in wastewater treatment plants, as for example organisms involved in nitrification,[9,29–32] in floc formation[33–39] or in enhanced biological phosphorus removal.[40–44]

Sometimes an organism cannot be detected by FISH even if it is clearly detectable by other methods in the same environmental sample. Possible reasons for such failure of FISH are: (i) the abundance of the probe target organism in the sample is below the detection limit of FISH, which is between 10^3 and 10^4 cells per ml,[9] (ii) the probe-conferred fluorescence is too weak due to a low ribosome content of the probe target cells; (iii) the cell wall of the probe target organism is impermeable for oligonucleotide probes and requires special treatment prior to FISH; (iv) the probe-binding site is blocked by secondary structures of the rRNA or by ribosomal proteins; and (v) the hybridization conditions are too stringent for the applied probe. Furthermore, FISH is severely hampered if a sample contains many autofluorescent or DNA-binding particles. Since ribosomal RNA is a phylogenetic and not a physiological marker,

rRNA-targeted FISH alone does not provide insight into the ecophysiology of the detected organisms. An overview of approaches to overcome some limitations of FISH is provided by Wagner et al.[45] Extensions of FISH that allow monitoring metabolic activities of uncultured microorganisms are described later in this chapter.

15.2.3 Quantification and 3D Visualization of Microorganisms by Confocal Laser Scanning Microscopy and Digital Image Analysis

The quantification of uncultured bacteria in environmental samples is a frequently encountered task in microbial ecology. Microbial cells can be stained, for example, by FISH with rRNA-targeted probes, and can then be counted "manually" in an epifluorescence microscope. However, this technique is tedious and yields reliable results only when applied on planktonic bacteria, which do not form larger cell aggregates. Manual counting of cells, which are embedded in aggregates, flocs, or biofilms, is difficult and tends to underestimate the cell numbers.[26] Bacterial cell clusters are often packed very tightly (Figure 15.1) and cannot be broken up prior to counting.[26] Difficulties with the dispersion of cell aggregates also hamper the use of flow cytometry to quantify bacteria in flocs.[46,47]

Semi-automated quantification techniques, which combine FISH or other fluorescence staining methods with digital image analysis, are less tedious than manual cell counting and can accurately quantify planktonic cells as well as clustered bacteria in flocs and biofilms. Epifluorescence microscopes equipped with digital cameras and confocal laser scanning microscopes are used to acquire images of fluorescing bacterial cells. Sharp confocal images, which contain only objects located in the current

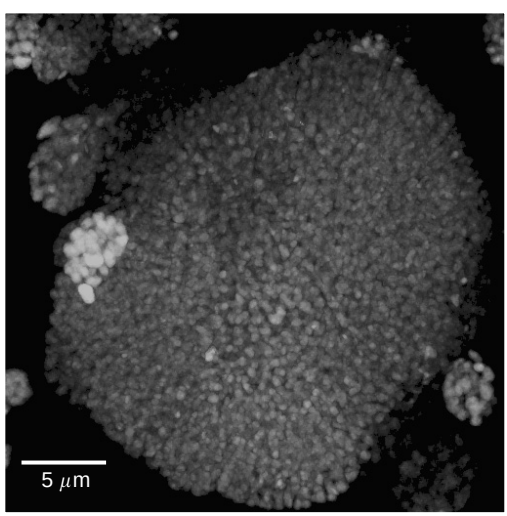

FIGURE 15.1 Confocal micrograph of aggregated ammonia-oxidizing bacteria (*Nitrosomonas* sp.) detected in a nitrifying biofilm by FISH with probe S-*-Nsm-0651-a-A-18.[30]

focal plane, are better input data for image analysis software than pictures recorded by conventional microscopes. Digital image analysis has been applied to quantify soil bacteria, which were labeled by protein staining,[48] and to enumerate planktonic cells that were stained by FISH with rRNA-targeted probes.[49,50] Shopov et al.[51] used image analysis to count planktonic bacteria and cells, which were attached to detritus. Unfortunately, no published image analysis routine is capable of counting the individual cells in dense cell aggregates. These tightly packed cells (Figure 15.1) are not recognized and separated by the algorithms even if the input data are high-quality confocal images. However, aggregated bacteria can be quantified by a stereological method, which does not require single cell recognition. This method determines the volume fraction of a "phase of interest," which is part of a larger reference volume.[52] Any microbial population, which has been stained by FISH with a specific rRNA-targeted probe or by another specific fluorescence labeling technique, can be the phase of interest. The reference volume is either the total volume of all *Bacteria* or the total volume of all microorganisms (*Bacteria*, archaea, and eukaryotes) in the sample. Most known *Bacteria* can be labeled by FISH with the EUB338 probe mix.[53,54] Unspecific labeling of all microbial cells is achieved by nucleic acid stains like 4′,6-diamidino-2-phenylindole (DAPI).[55] The biovolume fraction of the specifically labeled population can be manually determined by using an epifluorescence microscope and a grid ocular. In the current microscope field, all grid points that touch the specifically stained population (point set A) and all grid points that touch the total bacterial or microbial biomass (including the specifically stained population, point set B) are counted. Then the ratio of the number of points in set A to the number of points in set B is calculated (this is the fraction of point set A). This procedure is repeated at random positions within the specimen. Finally, the fractions of point set A that were obtained in the evaluated microscope fields are averaged. Provided that enough microscope fields have been processed, this mean fraction of point set A is equivalent to the biovolume fraction of the specifically stained population. This technique works with solitary and with aggregated microbial cells and can be applied without modifications on all kinds of bacterial morphotypes. A software implementation of this method has been combined with FISH and confocal laser scanning microscopy to quantify bacteria in flocs and biofilms.[56,57] Recently, Juretschko et al.[28] used rRNA sequence analysis, FISH, and the stereological estimation of biovolume fractions to identify, detect, and quantify most bacterial populations in activated sludge from a full-sized industrial wastewater treatment plant. In another recent study, Schmid et al.[39] applied the same quantification method to analyze the bacterial communities in poor-settling activated sludge flocs, and correlated the results with physical floc properties. An extension of this stereological approach allows measuring not only biovolume fractions, but also absolute cell concentrations of clustered and of planktonic bacteria by spiking environmental samples with known amounts of reference cells or fluorescent beads ("Spike-FISH"[58]). Absolute cell concentrations are needed, for example, to compare the abundance of a bacterial population in different environmental samples with different biomass content. Another stereological approach has been applied to quantify the biovolume of filamentous bacteria by image analysis.[59]

Microbial ecology has numerous other applications for digital image analysis. Bacterial cells can be classified by software into morphotypes.[49,60,61] The optimal

hybridization conditions for FISH with new rRNA-targeted oligonucleotide probes are determined by measuring the probe-conferred fluorescence.[54,62] The fluorescence intensity after FISH is also quantified in order to estimate the ribosome content of microbial cells.[63]

Two-dimensional image analysis does not exploit the full potential of confocal laser scanning microscopy. Confocal microscopes allow peeking into complex samples without mechanical sectioning, which could distort three-dimensional structures. Modern confocal microscopes can adjust the *z*-position of the focal plane with high precision in sub-micrometer intervals and can automatically record vertically stacked "optical sections" through a sample. Such image stacks contain 3D information, which is extracted and quantified by 3D image analysis routines. This approach has proven highly useful to quantify key features of biofilms like the total volume of the biomass, the biofilm roughness, and the substratum coverage.[64–66] We are currently developing 3D image analysis algorithms that scan stacks of confocal images and evaluate spatial relationships between probe-defined bacterial populations. This approach could help in discovering ecologically important relationships between uncultured bacteria. For example, the statistically confirmed spatial co-localization of two populations may be used as an indicator for a putative mutualistic symbiosis between these organisms.

Confocal image stacks of probe-stained bacteria are well suited for 3D visualization, which can reveal interesting features like the networks of cavities within the cell clusters of *Nitrospira*-like bacteria[31] (Figure 15.2). Visualization programs should provide high-speed interactive rendering with arbitrary viewing perspectives.

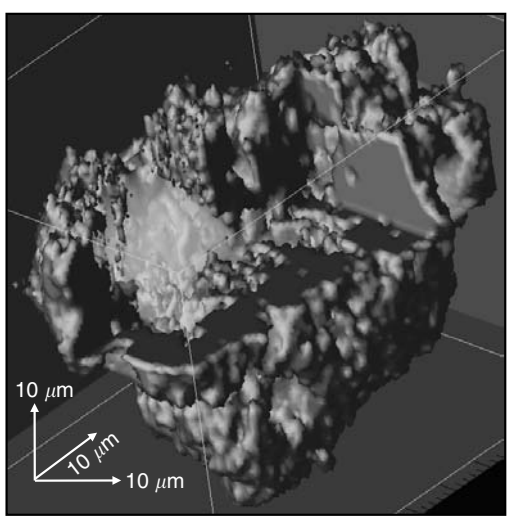

FIGURE 15.2 Three-dimensional reconstruction of a cell aggregate of *Nitrospira*-like bacteria, which were stained by FISH with probe S-G-Ntspa-662-a-A-18.[31] A part of the cell cluster has been removed by software in order to visualize a network of cavities within the microcolony.

Functions for lighting and shading can significantly improve the 3D impression of the rendered images. The quality and information content of 3D visualization is strongly influenced by the applied rendering algorithm. The surfaces of objects can be mathematically transformed to 3D meshes of polygons.[67] The polygons are projected to 2D space, are drawn by the program in a color defined by the user, and are shaded according to the directions of their surface normal vectors and according to the position of a virtual light source. Algorithms based on this approach are relatively simple and fast because only the vertices and the surface normal vectors of the polygons are stored and processed. In contrast, volume rendering uses the whole content of an image stack (the empty space as well as the surfaces and the inner parts of objects) for 3D visualization. Such programs can produce very detailed 3D reconstructions, but interactive volume rendering requires fast computers and sophisticated software implementations. The increasing performance of commodity computers makes 3D visualization by volume rendering cheaper and easier to use as a routine tool in floc and biofilm research.

15.2.4 Methods to Determine Ecological Functions of Uncultured Bacteria

The traditional and well-proven methods to study physiological properties of bacterial pure cultures cannot be used to investigate the ecophysiology of yet uncultured microorganisms in environmental samples. This goal can be achieved only by using cultivation-independent molecular tools.

Microautoradiography (MAR)[68] detects the uptake and incorporation of substrates by microbial cells without the need to cultivate the organisms. An environmental sample is incubated with a radioactively labeled substrate under defined conditions, as for example temperature, pH, and concentrations of electron donors and acceptors. After the incubation, the microbial cells in the sample are chemically fixed and excess radioactivity is removed by washing the sample with appropriate buffer solutions. Samples containing flocs or biofilm are then sectioned by using a microtome or a cryotome. The sections are applied onto microscope slides or cover slips and are covered with a film emulsion, which solidifies at lower temperatures. During the following exposition, which may last several days or weeks, silver grain formation occurs in the film above radioactively labeled cells. In contrast, the film remains clear above cells that do not contain the radioactive tracer. The MAR experiments are evaluated by bright field and phase contrast microscopy. Microautoradiography offers unique possibilities to monitor, with a single cell resolution, the use of specified substrates by bacteria in environmental samples. However, this technique is not able to identify the radioactively labeled cells. This limitation is overcome by the combination of MAR and FISH with rRNA-targeted probes (FISH-MAR)[69,70]: The microbial cells are identified by FISH, and the incorporation of radioactively labeled substrates is detected by MAR (Figure 15.3). The high specificity of FISH and the single cell resolution of both FISH and MAR make FISH–MAR a powerful tool for determining the substrate usage spectra of bacteria in environmental samples, which must be amenable to FISH (this requirement hampers the application of FISH–MAR on many soils and sediments).

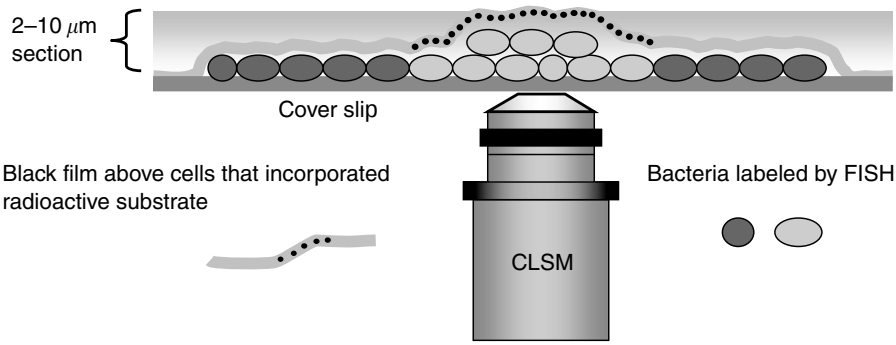

FIGURE 15.3 Schematic illustration of combined FISH and microautoradiography. Refer to text for explanation.

For FISH–MAR, a sample is incubated with a radioactive tracer as described above, but the fixed and sectioned sample is hybridized to fluorescent rRNA-targeted probes before the film emulsion is applied. The *in situ* hybridization requires that the sample is dehydrated with ethanol in order to make the cytoplasmic membranes of microbial cells permeable for the oligonucleotide probes. During the hybridization and the subsequent washing steps, soluble radioactive tracer that has been imported into the cells without incorporation into macromolecules is washed out of the cells through the perforated cytoplasmic membranes and is therefore not detectable by MAR. Therefore, FISH–MAR is restricted to substrates that are incorporated into biomass. Labeled substrate molecules, which adhere to the outer surfaces of microbial cells although they are not used by the microorganisms, can lead to false-positive results of FISH–MAR. The misinterpretation of MAR signals, which are caused by adhesion and not by the uptake and incorporation of a substrate, can be avoided by negative control experiments with pasteurized sample material.[70]

FISH–MAR has been used to study, for example, the *in situ* physiology of *Thiothrix* species involved in activated sludge bulking,[71] the uptake of lipids by the filamentous organism *Microthrix parvicella*,[72] and the use of inorganic and organic carbon sources by uncultured *Nitrospira*-like nitrite-oxidizing bacteria in activated sludge and biofilm.[31] FISH–MAR has also revealed that marine planktonic archaea take up amino acids from ocean water.[73] A recently developed extension of FISH–MAR allows quantifying the incorporated amount of labeled substrate and has been applied to measure the kinetics of acetate incorporation by filamentous bacteria in activated sludge.[74]

Stable-isotope probing (SIP) of DNA[75,76] uses stable isotope tracers to investigate the substrate usage of environmental microorganisms. The rationale of this approach is that bacteria, which can use a particular ^{13}C-labeled carbon source, will incorporate a fraction of the imported ^{13}C atoms into nucleic acids. An environmental sample is incubated with a ^{13}C-labeled substrate and DNA is extracted from the sample afterwards. The ^{13}C-labeled DNA ("heavy DNA") is separated from unlabeled ^{12}C ("light") DNA by density gradient centrifugation. The heavy DNA

fraction is used as template for 16S rRNA-specific PCR, and the amplified 16S rRNA genes are cloned and sequenced. The obtained sequences are subjected to phylogenetic analyses in order to identify the organisms that used the labeled substrate. This technique is applicable on a wide spectrum of environmental samples, but relatively long incubation times and high tracer concentrations are required for sufficient stable-isotope labeling of DNA. During the incubation, bacteria that can use the ^{13}C-labeled substrate will most likely incorporate a fraction of the ^{13}C label into waste compounds, which are excreted and may be metabolized by other bacteria that could not directly use the original labeled substrate ("cross-feeding"). The addition of relatively large amounts of labeled substrates may cause an enrichment of organisms that can use these substrates. Cross-feeding between different bacterial populations and shifts of the microbial population structure become more likely during prolonged incubation periods and can falsify the results of SIP. Manefield et al.[77] demonstrated that shorter incubation times are possible if ribosomal RNA instead of DNA is extracted and analyzed. The stable isotope is incorporated into rRNA whenever the cell produces new ribosomes, while DNA is labeled only during genome replication prior to cell division. However, both variants of SIP require PCR-amplification and cloning of rRNA genes. If the heavy nucleic acid fraction is contaminated prior to PCR with light nucleic acid, the rRNA genes of bacteria that used the labeled substrate are amplified together with the rRNA genes of bacteria that did not use it. These genes cannot be distinguished during the following phylogenetic analyses. Unfortunately, such contamination can never be ruled out. We have in collaboration with Linda Blackall at the University of Queensland demonstrated that SIP can be combined with FISH–MAR in order to overcome some drawbacks of these techniques.[78] In the first step of the combined approach, SIP is applied on an environmental sample. New, highly specific rRNA-targeted probes are then designed based on 16S rRNA gene sequences, which were retrieved from the heavy nucleic acid fraction. These new probes are used to identify their target organisms in FISH–MAR experiments with the same sample and substrate that was used for SIP, but for FISH–MAR the substrate is radioactively labeled. This combination of methods is particularly useful for studying phylogenetically heterogeneous microbial guilds. Such functional groups of organisms are difficult to analyze by FISH–MAR if one has no clue which of their members occur in an environmental sample, and which rRNA-targeted probes should be used to detect these organisms *in situ*. The combined approach solves this problem because candidate organisms that may use the offered substrates are identified by SIP. Therefore, one must perform only a few FISH–MAR experiments with specific probes that target these organisms. FISH–MAR is independent from PCR, works with shorter incubation times than SIP, and therefore is used to verify the results that were obtained by SIP. However, this combination of SIP and FISH–MAR is restricted to environmental samples that are amenable to FISH.

Recently, the high sensitivity and substrate specificity of isotope techniques have been combined with the high degree of parallelization, which is offered by DNA microarrays. The isotope array.[79] contains specific rRNA-targeted probes. Following the incubation of an environmental sample with a radioactive substrate, rRNA is extracted from the sample and is labeled with a fluorescent dye. The rRNA

is then hybridized to the microarray, which afterward is scanned for fluorescence and for radioactivity. The pattern of fluorescing spots on the array shows which probe-target organisms are present in the sample, while radioactive probe spots indicate which of these organisms incorporated the radioactive tracer into their ribosomal RNA.

DNA microarrays that target functional genes are promising tools for monitoring specific physiological groups of microorganisms. In a pioneering study, Wu et al.[80] designed and evaluated a microarray, which detected some functional genes of nitrification, denitrification, and methane oxidation. Dennis et al.[81] applied another functional gene array to monitor the induction of genes coding for the degradation of resin acid. Further development of DNA microarray technology will most likely improve the specificity and the sensitivity of microarrays, and will eventually make it possible to quantitatively analyze, with the efficiency of a high-throughput technique, the expression patterns of numerous functional genes in complex environmental samples.

One could assume that combining certain fluorescent life stains and FISH with rRNA-targeted probes makes it possible to detect and identify metabolically active cells *in situ* in environmental samples. Tetrazolium dyes, for example, are reduced and form insoluble formazan crystals in living cells. Staining with the tetrazolium dye 5-cyano-2,3-tolyl-tetrazolium chloride (CTC)[82] can be combined with FISH because the fluorescent formazan crystals remain in the cells during the fixation and hybridization steps.[83] Unfortunately, CTC and other life stains fail to detect all active bacterial cells in environmental samples.[83,84]

The ribosome content of microbial cells can also act as an indicator for metabolic activity. Fluctuations of the cellular ribosome content are detected by measuring and comparing the fluorescence intensity of cells stained by FISH with rRNA-targeted probes. This method is suitable for monitoring the physiological state of bacterial species like *Escherichia coli*, which show a correlation of ribosome content and growth rate.[85] However, in marine *Synechococcus* cells, such a correlation exists only at medium growth rates.[86] Interestingly, at the highest growth rates, the *Synechococcus* cells contained fewer ribosomes than at lower growth rates. Chemolithoautotrophic ammonia-oxidizing bacteria maintain a high ribosome content even during starvation and when ammonia oxidation is chemically inhibited.[29,63] Thus, the ribosome content should not be used to measure metabolic activity unless a clear correlation between activity and ribosome content has been demonstrated for the organisms being studied. This can be achieved by using FISH–MAR, which allows monitoring activity and ribosome content simultaneously. However, for this purpose, at least one substrate must be known that will be incorporated by most active cells of the investigated bacterial population.

Primary transcripts (precursors) of ribosomal RNA, which are transient intermediates of ribosome synthesis, seem to be better indicators for bacterial metabolic activity than mature ribosomes. The bacterial 16S, 23S, and 5S rRNA genes are separated by intergenic spacer regions. These spacers are transcribed together with the rRNA genes, but are degraded when the primary transcript is processed during ribosome maturation. Cangelosi and Brabant[87] designed oligonucleotide probes, which targeted the spacer regions between the rRNA genes of *Escherichia coli*, and applied

these probes in FISH experiments with pure cultures of *E. coli*. Probe-conferred fluorescence after FISH with the spacer-targeted probes indicated that the stained cells contained rRNA precursors and had been producing new ribosomes prior to fixation for FISH. The fluorescence intensity mirrored the intracellular concentration of rRNA precursors and the degree of ribosome-producing activity. These experiments with *E. coli* showed that fluctuations of the precursor rRNA level correlated better with changes of the growth phase than the less pronounced shifts of the mature ribosome content. However, the magnitude of the fluctuations in the precursor rRNA pool depended on the kind of the applied growth-limiting conditions.[87] Thus, the results of FISH with spacer-targeted probes must be carefully interpreted in order to determine how different stress factors affect the metabolic activity of bacteria.

Spacer-targeted probes do not stain inactive bacterial cells because the rRNA precursors have been degraded when the cells fall into dormancy. These probes also allow observing relatively rapid activity changes. Schmid et al.[88] monitored, by using spacer-targeted probes, a rapid decrease of the activity of anaerobic ammonium-oxidizing bacteria while these organisms were being exposed to oxygen. Oerther et al.[89] designed spacer-targeted probes specific for *Acinetobacter* and observed that the activity of *Acinetobacter* cells in activated sludge increased while the sludge was being mixed with wastewater that was high in nutrients. Probes targeting the ribosomal RNA can be used together with spacer-targeted probes in the same FISH experiment, and the same image analysis methods can be applied to quantify cells detected by spacer-targeted probes and cells detected by rRNA-targeted probes. However, the design of spacer-targeted probes, which cover larger phylogenetic groups, is more difficult because the nucleotide sequences of the intergenic spacers are less conserved than the sequences of the ribosomal RNAs. A spacer-targeted probe may already fail to detect some strains of one target species due to strain-specific sequence differences at the probe-binding site. On the other hand, the lower degree of sequence conservation in the spacer regions allows developing strain-specific probes, which make it possible to monitor the activity of very closely related bacteria in the same environmental sample.

15.3 DISCOVERY AND INVESTIGATION OF *NITROSPIRA*-LIKE BACTERIA IN WASTEWATER TREATMENT PLANTS

Aerobic nitrification is a two-stage process driven by chemolithoautotrophic bacteria: ammonia oxidizers like *Nitrosomonas* species convert ammonia to nitrite, and nitrite oxidizers like *Nitrobacter* species oxidize nitrite further to nitrate. According to textbook knowledge, *Nitrosomonas* and *Nitrobacter* species catalyze aerobic nitrification in wastewater treatment plants.[90,91] The widespread opinion that *Nitrobacter* species are the predominant nitrite oxidizers in wastewater treatment arose because these bacteria can be isolated from most nitrifying activated sludge samples. However, this concept was challenged when molecular techniques were applied on nitrite-oxidizing bacteria in nitrifying bioreactors. Quantitative dot blot or FISH with

rRNA-targeted probes failed to detect *Nitrobacter* in nitrifying aquarium filters[92] or in activated sludge,[93] respectively. These findings launched a hunt for the real nitrite oxidizers in such habitats. Two years later, bacteria related to the genus *Nitrospira* were detected by 16S rRNA sequence analysis in a nitrite-oxidizing, laboratory-scale bioreactor.[94] At approximately the same time, Hovanec et al.[95] found 16S rRNA sequences of *Nitrospira*-like bacteria in biofilms from freshwater aquaria and confirmed, by quantitative dot blot with *Nitrospira*-specific oligonucleotide probes, that these organisms were highly abundant in the biofilms. The genus *Nitrospira* contains only two cultured species, *Nitrospira marina*,[96] and *Nitrospira moscoviensis*,[97] which are chemolithoautotrophic nitrite oxidizers. These organisms belong to a deep-branching bacterial lineage (the phylum *Nitrospirae*), which is not related to the genus *Nitrobacter*.[97] The detection of uncultured *Nitrospira*-like bacteria in nitrifying bioreactors was a surprise because the two cultured *Nitrospira* species had never been found in similar habitats. However, it was still unclear whether the *Nitrospira*-like bacteria, which had been detected in laboratory-scale reactors and in aquaria, were also key nitrite oxidizers in full-scale wastewater treatment plants. The importance of these organisms for wastewater treatment was confirmed when FISH with a *Nitrospira*-specific, rRNA-targeted probe revealed great abundance of *Nitrospira*-like bacteria in a large industrial wastewater treatment plant.[9] All attempts to isolate and culture these *Nitrospira*-like bacteria were unsuccessful. Interestingly, a *Nitrobacter* strain could be isolated from the same activated sludge although FISH failed to detect *Nitrobacter* cells *in situ*, indicating that the cell density of *Nitrobacter* in the sludge was much lower than the density of *Nitrospira*-like bacteria. This discovery made clear that the apparent importance of *Nitrobacter* for wastewater treatment was merely an artifact of cultivation-dependent methods to detect bacteria in environmental samples. The key role of *Nitrospira*-like bacteria for nitrite oxidation in wastewater treatment was confirmed by later studies, which used FISH and microelectrodes in order to correlate local abundance of *Nitrospira*-like bacteria with zones of active nitrite oxidation in biofilms.[32,98,99]

The kinetics of nitrification was studied decades ago with pure cultures of *Nitrosomonas* and *Nitrobacter* species. The results have influenced the design and operation of nitrifying bioreactors in all industrialized countries. In particular, industrial wastewater treatment plants often suffer from unpredictable irregularities or even total breakdowns of nitrification performance. Many of these problems may be caused by yet unknown biological differences between *Nitrobacter*, the model organism for bioreactor design, and *Nitrospira*-like bacteria, which are the real nitrite oxidizers in the bioreactors. The physiology of these *Nitrospira*-like bacteria is difficult to investigate because pure cultures are not available and the only cultured *Nitrospira* species live in habitats that are markedly different from wastewater treatment plants. However, molecular methods have provided first insight into the biology of *Nitrospira*-like bacteria. A set of new rRNA-targeted probes, which covers the genus *Nitrospira* and all other lineages of the phylum *Nitrospirae*, was used to detect and quantify *Nitrospira*-like bacteria in nitrifying bioreactors[9,31,32] (Figure 15.4). These probes were also applied in FISH–MAR experiments, which revealed that the *Nitrospira*-like bacteria found in wastewater

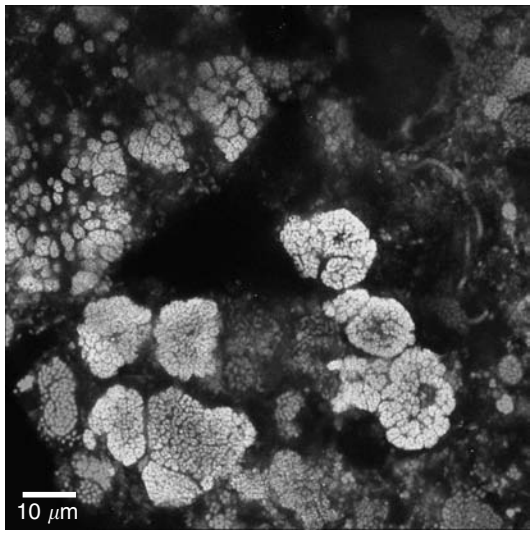

FIGURE 15.4 **(Color Figure 15.4 appears following page 236.)** Detection of *Nitrospira*-like bacteria in a nitrifying biofilm by FISH with probe S-G-Ntspa-662-a-A-18[31] and the EUB probe mix, which targets most *Bacteria*.[54] *Nitrospira*-like bacteria (eightgray) are simultaneously stained by probes S-G-Ntspa-662-a-A-18 and EUB338-I.

treatment plants fix CO_2 under aerobic conditions, but can also use pyruvate as additional carbon source.[31] Based on results obtained with FISH and microelectrodes, Schramm et al.[98] proposed that *Nitrospira*-like bacteria could be K-strategists with a high affinity for nitrite and lower growth rates, while *Nitrobacter* species could be r-strategists with a lower affinity for nitrite and higher growth rates. This means that *Nitrospira*-like bacteria could reach high cell densities when the nitrite concentration is particularly low, and that *Nitrobacter* species could not grow under such conditions. This hypothesis could explain why *Nitrospira*-like bacteria outcompete *Nitrobacter* in wastewater treatment plants, where nitrite is continuously available in low concentrations. We have hitherto detected coexistence of *Nitrobacter* and *Nitrospira*-like bacteria in only one pilot-scale sequencing batch biofilm reactor receiving high loads of ammonia (Figure 15.5). The activity of ammonia-oxidizing bacteria caused a pronounced nitrite peak during each operational cycle of the reactor.[100] The temporal shifts of the nitrite concentration created ecological niches for *Nitrospira*-like bacteria and for *Nitrobacter* in the biofilm.[31,101]

Measurements with microelectrodes have revealed that *Nitrospira*-like bacteria living in biofilms can cope with relatively low partial pressures of oxygen.[102] Interestingly, the cultured species *N. moscoviensis* is able to transfer electrons from H_2 to nitrate in the absence of oxygen.[97] The uncultured *Nitrospira*-like bacteria may have similar capabilities, which would confer high physiological and ecological flexibility.

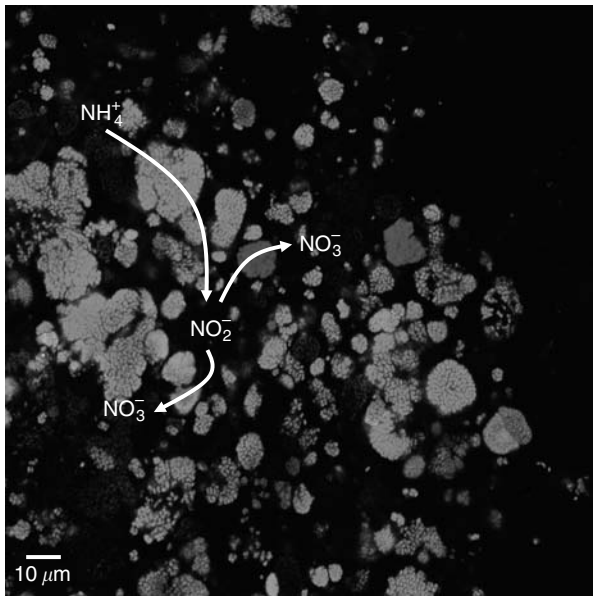

FIGURE 15.5 **(Color Figure 15.5 appears following page 236.)** Simultaneous detection of ammonia-oxidizing bacteria (*Nitrosomonas* sp.) and two different populations of nitrite-oxidizing bacteria (*Nitrospira* sp. and *Nitrobacter* sp.) in a nitrifying sequencing batch biofilm reactor. *Nitrosomonas* cells were stained by FISH with probe S-*-Nsm-0651-a-A-18,[30] *Nitrospira* cells with probe S-G-Ntspa-662-a-A-18,[31] and *Nitrobacter* cells with probe S-G-Nbac-1035-a-A-18.[93]

15.4 OUTLOOK

Cultivation-independent molecular methods have opened new windows into the microbial world. Microbial ecologists can now investigate elusive bacteria, which are abundant in many ecosystems but have so far resisted all attempts of isolation and cultivation. However, many currently used molecular methods are too slow and labor-intensive for broad ecological studies, which require comparative analyses of many environmental samples. Recent technical progress includes the development of DNA microarrays that detect particular phylogenetic groups of bacteria in the environment (so-called "PhyloChips").[103–106] PhyloChips, isotope arrays, and functional gene arrays make it possible to analyze the structure and function of microbial communities faster and in more samples than achievable with nonparallelized techniques.

What else can be done to investigate uncultured bacteria? The term "environmental genomics" comprises methods to clone and analyze genome fragments, or even whole genomes, of yet uncultured microbes.[107–111] Genes found by this approach may encode ecologically important or even completely novel physiological properties. Methods like the isotope array and FISH–MAR can be used to link the genetic data to the phenotype of the corresponding organisms. In addition, transkriptomics and proteomics will offer a wide range of possibilities to study the responses of

uncultured bacteria to changing environmental conditions, and to discover the details of novel biochemical pathways.

Insight into the ecology of uncultured bacteria has many practical applications. For example, the biodiversity of nitrifying bacteria in wastewater treatment plants may have significant impact on the stability and performance of these systems. A high diversity of nitrifiers could guarantee that nitrification does not collapse during shifts of environmental conditions. The more the different populations of ammonia and nitrite oxidizers, the higher the chance that at least one population of each group will adapt to new conditions and will continue oxidizing ammonia or nitrite, respectively. Strategies to influence the diversity of nitrifiers and of other microbial guilds in engineered and agricultural habitats could be developed. Detailed insight into the ecology and physiology of the involved microorganisms is needed to achieve this goal.

Biological, chemical, and physical processes influence the formation and stability of flocs. In order to understand flocculation, physical, chemical, and microbiological approaches must be integrated. A task for the near future of flocculation research is to bring the methods and views of these disciplines together, and to strengthen the role of microbial ecology in this fascinating and promising field.

REFERENCES

1. Schramm, A. et al., On the occurrence of anoxic microniches, denitrification, and sulfate reduction in aerated activated sludge, *Appl. Environ. Microbiol.*, 65, 4189, 1999.
2. Amann, R.I., Ludwig, W., and Schleifer, K.-H., Phylogenetic identification and *in situ* detection of individual microbial cells without cultivation, *Microbiol. Rev.*, 59, 143, 1995.
3. Woese, C.R., Bacterial evolution, *Microbiol. Rev.*, 51, 221, 1987.
4. Ludwig, W. et al., Bacterial phylogeny based on comparative sequence analysis, *Electrophoresis*, 19, 554, 1998.
5. Hugenholtz, P., Goebel, B.M., and Pace, N.R., Impact of culture-independent studies on the emerging phylogenetic view of bacterial diversity, *J. Bacteriol.*, 180, 4765, 1998.
6. Suzuki, M.T. and Giovannoni, S.J., Bias caused by template annealing in the amplification of mixtures of 16S rRNA genes by PCR, *Appl. Environ. Microbiol.*, 62, 625, 1996.
7. Suzuki, M., Rappe, M.S., and Giovannoni, S.J., Kinetic bias in estimates of coastal picoplankton community structure obtained by measurements of small-subunit rRNA gene PCR amplicon length heterogeneity, *Appl. Environ. Microbiol.*, 64, 4522, 1998.
8. Meyerhans, A., Vartanian, J.P., and Wain-Hobson, S., DNA recombination during PCR, *Nucleic Acids Res.*, 18, 1687, 1990.
9. Juretschko, S. et al., Combined molecular and conventional analyses of nitrifying bacterium diversity in activated sludge: *Nitrosococcus mobilis* and *Nitrospira*-like bacteria as dominant populations, *Appl. Environ. Microbiol.*, 64, 3042, 1998.
10. Loy, A., Daims, H., and Wagner, M., Activated sludge: molecular techniques for determining community composition, in *The Encyclopedia of Environmental Microbiology*, Bitton, G., Ed., Wiley, New York, pp. 26, 2002.

11. Moyer, C.L., Dobbs, F.C., and Karl, D.M., Estimation of diversity and community structure through restriction fragment length polymorphism distribution analysis of bacterial 16S rRNA genes from a microbial mat at an active, hydrothermal vent system, Loihi Seamount, Hawaii, *Appl. Environ. Microbiol.*, 60, 871, 1994.
12. Muyzer, G., de Waal, E.C., and Uitterlinden, A.G., Profiling of complex microbial populations by denaturing gradient gel electrophoresis analysis of polymerase chain reaction-amplified genes coding for 16S rRNA, *Appl. Environ. Microbiol.*, 59, 695, 1993.
13. Holland, P.M. et al., Detection of specific polymerase chain reaction product by utilizing the $5' \rightarrow 3'$ exonuclease activity of *Thermus aquaticus* DNA polymerase, *Proc. Natl. Acad. Sci. USA*, 88, 7276, 1991.
14. Heid, C.A. et al., Real time quantitative PCR, *Genome Res.*, 6, 986, 1996.
15. Diviacco, S. et al., A novel procedure for quantitative polymerase chain reaction by coamplification of competitive templates, *Gene*, 122, 313, 1992.
16. Bjerrum, L., Kjaer, T., and Ramsing, N.B., Enumerating ammonia-oxidizing bacteria in environmental samples using competitive PCR, *J. Microbiol. Methods*, 51, 227, 2002.
17. Gilliland, G. et al., Analysis of cytokine mRNA and DNA: detection and quantitation by competitive polymerase chain reaction, *Proc. Natl. Acad. Sci. USA*, 87, 2725, 1990.
18. Stahl, D.A. et al., Use of phylogenetically based hybridization probes for studies of ruminal microbial ecology, *Appl. Environ. Microbiol.*, 54, 1079, 1988.
19. Raskin, L. et al., Quantification of methanogenic groups in anaerobic biological reactors by oligonucleotide probe hybridization, *Appl. Environ. Microbiol.*, 60, 1241, 1994.
20. DeLong, E.F., Wickham, G.S., and Pace, N.R., Phylogenetic stains: ribosomal RNA based probes for the identification of single cells, *Science*, 243, 1360, 1989.
21. Ludwig, W. et al., ARB: a software environment for sequence data, *Nucleic Acids Res.*, 32, 1363, 2004.
22. Cole, J.R. et al., The Ribosomal Database Project (RDP-II): previewing a new autoaligner that allows regular updates and the new prokaryotic taxonomy, *Nucleic Acids Res.*, 31, 442, 2003.
23. Loy, A., Horn, M., and Wagner, M., probeBase: an online resource for rRNA-targeted oligonucleotide probes, *Nucleic Acids Res.*, 31, 514, 2003.
24. Amann, R. et al., *In situ* visualization of high genetic diversity in a natural microbial community, *J. Bacteriol.*, 178, 3496, 1996.
25. Wagner, M. et al., Probing activated sludge with oligonucleotides specific for *Proteobacteria*: inadequacy of culture-dependent methods for describing microbial community structure, *Appl. Environ. Microbiol.*, 59, 1520, 1993.
26. Manz, W. et al., *In situ* characterization of the microbial consortia active in two wastewater treatment plants, *Water Res.*, 28, 1715, 1994.
27. Snaidr, J. et al., Phylogenetic analysis and *in situ* identification of bacteria in activated sludge, *Appl. Environ. Microbiol.*, 63, 2884, 1997.
28. Juretschko, S. et al., The microbial community composition of a nitrifying-denitrifying activated sludge from an industrial sewage treatment plant analyzed by the full-cycle rRNA approach, *Sys. Appl. Microbiol.*, 25, 84, 2002.
29. Wagner, M. et al., *In situ* identification of ammonia-oxidizing bacteria, *Syst. Appl. Microbiol.*, 18, 251, 1995.
30. Mobarry, B.K. et al., Phylogenetic probes for analyzing abundance and spatial organization of nitrifying bacteria, *Appl. Environ. Microbiol.*, 62, 2156, 1996.
31. Daims, H. et al., *In situ* characterization of *Nitrospira*-like nitrite-oxidizing bacteria active in wastewater treatment plants, *Appl. Environ. Microbiol.*, 67, 5273, 2001.

32. Schramm, A. et al., Identification and activities *in situ* of *Nitrosospira* and *Nitrospira* spp. as dominant populations in a nitrifying fluidized bed reactor, *Appl. Environ. Microbiol.*, 64, 3480, 1998.
33. Wagner, M. et al., Identification and *in situ* detection of gram-negative filamentous bacteria in activated sludge, *Syst. Appl. Microbiol.*, 17, 405, 1994.
34. Rosselló-Mora, R.A. et al., The abundance of *Zoogloea ramigera* in sewage treatment plants, *Appl. Environ. Microbiol.*, 61, 702, 1995.
35. Erhart, R. et al., Development and use of fluorescent *in situ* hybridization probes for the detection and identification of "*Microthrix parvicella*" in activated sludge, *Syst. Appl. Microbiol.*, 20, 310, 1997.
36. Kanagawa, T. et al., Phylogenetic analysis of and oligonucleotide probe development for eikelboom type 021N filamentous bacteria isolated from bulking activated sludge, *Appl. Environ. Microbiol.*, 66, 5043, 2000.
37. van der Waarde, J. et al., Molecular monitoring of bulking sludge in industrial wastewater treatment plants, *Water Sci. Technol.*, 46, 551, 2002.
38. Thomsen, T.R. et al., *In situ* studies of the phylogeny and physiology of filamentous bacteria with attached growth, *Environ. Microbiol.*, 4, 383, 2002.
39. Schmid, M. et al., Characterization of activated sludge flocs by confocal laser scanning microscopy and image analysis, *Water Res.*, 37, 2043, 2003.
40. Hesselmann, R.P.X. et al., Enrichment, phylogenetic analysis and detection of a bacterium that performs enhanced biological phosphate removal in activated sludge, *Syst. Appl. Microbiol.*, 22, 454, 1999.
41. Crocetti, G.R. et al., Identification of polyphosphate-accumulating organisms and design of 16S rRNA-directed probes for their detection and quantitation, *Appl. Environ. Microbiol.*, 66, 1175, 2000.
42. Levantesi, C. et al., Analysis of the microbial community structure and function of a laboratory scale enhanced biological phosphorus removal reactor, *Environ. Microbiol.*, 4, 559, 2002.
43. Lee, N. et al., Population dynamics and *in situ* physiology of phosphorus-accumulating bacteria in wastewater treatment plants with enhanced biological phosphorus removal operated with and without nitrogen removal, in *3rd IWA International Specialized Conference on Microorganisms in Activated Sludge and Biofilm Processes*, Rome, p. 114, 2001.
44. Liu, W.T. et al., *In situ* identification of polyphosphate- and polyhydroxyalkanoate-accumulating traits for microbial populations in a biological phosphorus removal process, *Environ. Microbiol.*, 3, 110, 2001.
45. Wagner, M., Horn, M., and Daims, H., Fluorescence *in situ* hybridization for the identification of prokaryotes, *Curr. Opin. Microbiol.*, 6, 302, 2003.
46. Wallner, G., Erhart, R., and Amann, R., Flow cytometric analysis of activated sludge with rRNA-targeted probes, *Appl. Environ. Microbiol.*, 61, 1859, 1995.
47. Wallner, G. et al., Flow sorting of microorganisms for molecular analysis, *Appl. Environ. Microbiol.*, 63, 4223, 1997.
48. Bloem, J., Veninga, M., and Shepherd, J., Fully automatic determination of soil bacterium numbers, cell volumes, and frequencies of dividing cells by confocal laser scanning microscopy and image analysis, *Appl. Environ. Microbiol.*, 61, 926, 1995.
49. Ramsing, N.B. et al., Distribution of bacterial populations in a stratified fjord (Mariager Fjord, Denmark) quantified by *in situ* hybridization and related to chemical gradients in the water column, *Appl. Environ. Microbiol.*, 62, 1391, 1996.
50. Pernthaler, J., Pernthaler, A., and Amann, R., Automated enumeration of groups of marine picoplankton after fluorescence *in situ* hybridization, *Appl. Environ. Microbiol.*, 69, 2631, 2003.

51. Shopov, A., Williams, S.C., and Verity, P.G., Improvements in image analysis and fluorescence microscopy to discriminate and enumerate bacteria and viruses in aquatic samples, *Aquat. Microb. Ecol.*, 22, 103, 2000.
52. Thompson, E., Quantitative microscopic analysis, *J. Geol.*, 38, 193, 1930.
53. Amann, R.I. et al., Combination of 16S rRNA-targeted oligonucleotide probes with flow cytometry for analyzing mixed microbial populations, *Appl. Environ. Microbiol.*, 56, 1919, 1990.
54. Daims, H. et al., The domain-specific probe EUB338 is insufficient for the detection of all *Bacteria*: development and evaluation of a more comprehensive probe set, *Syst. Appl. Microbiol.*, 22, 434, 1999.
55. Hicks, R.E., Amann, R.I., and Stahl, D.A., Dual staining of natural bacterioplankton with 4′,6-diamidino-2-phenylindole and fluorescent oligonucleotide probes targeting kingdom-level 16S rRNA sequences, *Appl. Environ. Microbiol.*, 58, 2158, 1992.
56. Bouchez, T. et al., Ecological study of a bioaugmentation failure, *Environ. Microbiol.*, 2, 179, 2000.
57. Schmid, M. et al., Molecular evidence for a genus-level diversity of bacteria capable of catalyzing anaerobic ammonium oxidation, *Syst. Appl. Microbiol.*, 23, 93, 2000.
58. Daims, H. et al., Cultivation-independent, semiautomatic determination of absolute bacterial cell numbers in environmental samples by fluorescence *in situ* hybridization, *Appl. Environ. Microbiol.*, 67, 5810, 2001.
59. Nedoma, J. et al., Quantification of pelagic filamentous microorganisms in aquatic environments using the line-intercept method, *FEMS Microbiol. Ecol.*, 38, 81, 2001.
60. Pernthaler, J. et al., *In situ* classification and image cytometry of pelagic bacteria from a high mountain lake (Gossenköllesee, Austria), *Appl. Environ. Microbiol.*, 63, 4778, 1997.
61. Blackburn, N. et al., Rapid determination of bacterial abundance, biovolume, morphology, and growth by neural network-based image analysis, *Appl. Environ. Microbiol.*, 64, 3246, 1998.
62. Manz, W. et al., Phylogenetic oligodeoxynucleotide probes for the major subclasses of proteobacteria: problems and solutions, *Syst. Appl. Microbiol.*, 15, 593, 1992.
63. Morgenroth, E. et al., Effect of long-term idle periods on the performance of sequencing batch reactors, *Water Sci. Tech.*, 41, 105, 2000.
64. Heydorn, A. et al., Quantification of biofilm structures by the novel computer program COMSTAT, *Microbiology*, 146, 2395, 2000.
65. Xavier, J.B. et al., Objective threshold selection procedure (OTS) for segmentation of scanning laser confocal microscope images, *J. Microbiol. Methods*, 47, 169, 2001.
66. Kuehn, M. et al., Automated confocal laser scanning microscopy and semiautomated image processing for analysis of biofilms, *Appl. Environ. Microbiol.*, 64, 4115, 1998.
67. Guéziec, A. and Hummel, R., Exploiting triangulated surface extraction using tetrahedral decomposition, *IEEE Trans. Vis. Comput. Graph.*, 1, 328, 1995.
68. Brock, T.D. and Brock, M.L., Autoradiography as a tool in microbial ecology, *Nature*, 209, 734, 1968.
69. Ouverney, C.C. and Fuhrman, J.A., Combined microautoradiography-16S rRNA probe technique for determination of radioisotope uptake by specific microbial cell types *in situ, Appl. Environ. Microbiol.*, 65, 1746, 1999.
70. Lee, N. et al., Combination of fluorescent *in situ* hybridization and microautoradiography — a new tool for structure-function analyses in microbial ecology, *Appl. Environ. Microbiol.*, 65, 1289, 1999.

71. Nielsen, P.H., de Muro, M.A., and Nielsen, J.L., Studies on the *in situ* physiology of *Thiothrix* spp. present in activated sludge, *Environ. Microbiol.*, 2, 389, 2000.
72. Nielsen, P.H. et al., *Microthrix parvicella*, a specialized lipid consumer in anaerobic-aerobic activated sludge plants, *Water Sci. Technol.*, 46, 73, 2002.
73. Ouverney, C.C. and Fuhrman, J.A., Marine planktonic archaea take up amino acids, *Appl. Environ. Microbiol.*, 66, 4829, 2000.
74. Nielsen, J.L. et al., Quantification of cell-specific substrate uptake by probe-defined bacteria under *in situ* conditions by microautoradiography and fluorescence *in situ* hybridization, *Environ. Microbiol.*, 5, 202, 2003.
75. Radajewski, S. et al., Stable-isotope probing as a tool in microbial ecology, *Nature*, 403, 646, 2000.
76. Whitby, C.B. et al., (13)C incorporation into DNA as a means of identifying the active components of ammonia-oxidizer populations, *Lett. Appl. Microbiol.*, 32, 398, 2001.
77. Manefield, M. et al., RNA stable isotope probing, a novel means of linking microbial community function to phylogeny, *Appl. Environ. Microbiol.*, 68, 5367, 2002.
78. Ginige, M.P. et al., Use of stable-isotope probing, full-cycle rRNA analysis, and fluorescence *in situ* hybridization-microautoradiography to study a methanol-fed denitrifying microbial community, *Appl. Environ. Microbiol.*, 70, 588, 2004.
79. Adamczyk, J. et al., The isotope array, a new tool that employs substrate-mediated labeling of rRNA for determination of microbial community structure and function, *Appl. Environ. Microbiol.*, 69, 6875, 2003.
80. Wu, L. et al., Development and evaluation of functional gene arrays for detection of selected genes in the environment, *Appl. Environ. Microbiol.*, 67, 5780, 2001.
81. Dennis, P. et al., Monitoring gene expression in mixed microbial communities by using DNA microarrays, *Appl. Environ. Microbiol.*, 69, 769, 2003.
82. Rodriguez, G.G. et al., Use of a fluorescent redox probe for direct visualization of actively respiring bacteria, *Appl. Environ. Microbiol.*, 58, 1801, 1992.
83. Karner, M. and Fuhrman, J.A., Determination of active marine bacterioplankton: a comparison of universal 16S rRNA probes, autoradiography, and nucleoid staining, *Appl. Environ. Microbiol.*, 63, 1208, 1997.
84. Nielsen, J.L., Aquino de Muro, M., and Nielsen, P.H., Evaluation of the redox dye 5-cyano-2,3-tolyl-tetrazolium chloride for activity studies by simultaneous use of microautoradiography and fluorescence *in situ* hybridization, *Appl. Environ. Microbiol.*, 69, 641, 2003.
85. Bremer, H. and Dennis, P.P., Modulation of chemical composition and other parameters of the cell by growth rate, in *Escherichia coli and Salmonella: Cellular and Molecular Biology*, 2nd ed., Neidhardt, F.C. et al., Eds., ASM Press, Washington, DC, p. 1553, 1996.
86. Binder, B.J. and Liu, Y.C., Growth rate regulation of rRNA content of a marine *Synechococcus* (Cyanobacterium) strain, *Appl. Environ. Microbiol.*, 64, 3346, 1998.
87. Cangelosi, G.A. and Brabant, W.H., Depletion of pre-16S rRNA in starved *Escherichia coli* cells, *J. Bacteriol.*, 179, 4457, 1997.
88. Schmid, M. et al., 16S-23S rDNA intergenic spacer and 23S rDNA of anaerobic ammonium-oxidizing bacteria: implications for phylogeny and *in situ* detection, *Environ. Microbiol.*, 3, 450, 2001.
89. Oerther, D.B. et al., Monitoring precursor 16S rRNAs of *Acinetobacter* spp. in activated sludge wastewater treatment systems, *Appl. Environ. Microbiol.*, 66, 2154, 2000.

90. Bever, J., Stein, A., and Teichmann, H., *Weitergehende Abwasserreinigung*, R. Oldenbourg Verlag, München, 1995.
91. Henze, M. et al., *Wastewater Treatment*, 2nd ed., Springer-Verlag, Berlin, 1997.
92. Hovanec, T.A. and DeLong, E.F., Comparative analysis of nitrifying bacteria associated with freshwater and marine aquaria, *Appl. Environ. Microbiol.*, 62, 2888, 1996.
93. Wagner, M. et al., *In situ* analysis of nitrifying bacteria in sewage treatment plants, *Water Sci. Technol.*, 34, 237, 1996.
94. Burrell, P.C., Keller, J., and Blackall, L.L., Microbiology of a nitrite-oxidizing bioreactor, *Appl. Environ. Microbiol.*, 64, 1878, 1998.
95. Hovanec, T.A. et al., *Nitrospira*-like bacteria associated with nitrite oxidation in freshwater aquaria, *Appl. Environ. Microbiol.*, 64, 258, 1998.
96. Watson, S.W. et al., *Nitrospira marina* gen. nov. sp. nov.: a chemolithotrophic nitrite-oxidizing bacterium, *Arch. Microbiol.*, 144, 1, 1986.
97. Ehrich, S. et al., A new obligately chemolithoautotrophic, nitrite-oxidizing bacterium, *Nitrospira moscoviensis* sp. nov. and its phylogenetic relationship, *Arch. Microbiol.*, 164, 16, 1995.
98. Schramm, A. et al., Microscale distribution of populations and activities of *Nitrosospira* and *Nitrospira* spp. along a macroscale gradient in a nitrifying bioreactor: quantification by *in situ* hybridization and the use of microsensors, *Appl. Environ. Microbiol.*, 65, 3690, 1999.
99. Okabe, S., Satoh, H., and Watanabe, Y., *In situ* analysis of nitrifying biofilms as determined by *in situ* hybridization and the use of microelectrodes, *Appl. Environ. Microbiol.*, 65, 3182, 1999.
100. Arnold, E., Böhm, B., and Wilderer, P.A., Application of activated sludge and biofilm sequencing batch reactor technology to treat reject water from sludge dewatering systems: a comparison, *Water Sci. Technol.*, 41, 115, 2000.
101. Gieseke, A. et al., Structure and activity of multiple nitrifying bacterial populations co-existing in a biofilm, *Environ. Microbiol.*, 5, 355, 2003.
102. Schramm, A. et al., Microenvironments and distribution of nitrifying bacteria in a membrane-bound biofilm, *Environ. Microbiol.*, 2, 680, 2000.
103. Loy, A. et al., Oligonucleotide microarray for 16S rRNA gene-based detection of all recognized lineages of sulfate-reducing prokaryotes in the environment, *Appl. Environ. Microbiol.*, 68, 5064, 2002.
104. Guschin, D.Y. et al., Oligonucleotide microchips as genosensors for determinative and environmental studies in microbiology, *Appl. Environ. Microbiol.*, 63, 2397, 1997.
105. Small, J. et al., Direct detection of 16S rRNA in soil extracts by using oligonucleotide microarrays, *Appl. Environ. Microbiol.*, 67, 4708, 2001.
106. Urakawa, H. et al., Single-base-pair discrimination of terminal mismatches by using oligonucleotide microarrays and neural network analyses, *Appl. Environ. Microbiol.*, 68, 235, 2002.
107. Rondon, M.R. et al., Cloning the soil metagenome: a strategy for accessing the genetic and functional diversity of uncultured microorganisms, *Appl. Environ. Microbiol.*, 66, 2541, 2000.
108. Beja, O. et al., Bacterial rhodopsin: evidence for a new type of phototrophy in the sea, *Science*, 289, 1902, 2000.
109. Tyson, G.W. et al., Community structure and metabolism through reconstruction of microbial genomes from the environment, *Nature*, 428, 37, 2004.

110. Schleper, C. et al., Genomic analysis reveals chromosomal variation in natural populations of the uncultured psychrophilic archaeon *Cenarchaeum symbiosum*, *J. Bacteriol.*, 180, 5003, 1998.
111. Venter, J.C. et al., Environmental genome shotgun sequencing of the Sargasso Sea, *Science*, 304, 66, 2004.

16 Using Atomic Force Microscopy to Study Factors Affecting Bioadhesion at Molecular to Nanoscale Levels

Bruce E. Logan

CONTENTS

16.1 INTRODUCTION

Understanding the fate of particles (individual cells as well as flocculated material) is important for describing the flux of organic matter to sediments in lakes and oceans. Coagulation can play an important role in the fate of these particles as it can result in the production of larger particles that either can serve as food for particle-feeding animals, or can settle out and be lost to deep marine sediments. Understanding the chemical and physical factors that affect adhesion and, therefore, coagulation rates has not been easy. There are a variety of particle types and sizes in aquatic systems that affect both the collision rate and the collision efficiency. Here, we consider factors affecting the success of the initial adhesion event with a focus on molecular-scale effects.

Most particles (both biotic and abiotic) in freshwater and marine systems carry a net negative charge. Conventional DLVO theory has been used to understand the

1-56670-615-7/05/$0.00+$1.50

collision and adhesion of these like-charged particles. According to this theory, the forces governing the approach of two colloidal particles (or surfaces) are described in terms of Lifshitz–van der Waals (LW) attractive forces and electrostatic (EL) repulsive forces between like-charged particles.[1] Particle charge is typically measured in terms of zeta potential based on the velocity of a particle suspended in water between two plates set at a fixed potential. Because of the high salinity of seawater, we expect that the repulsive layer thickness around a particle will be small (less than 1 nm) and, therefore, that electrostatic forces play a small role in particle adhesion (except where salinity undergoes changes from fresh to saline conditions). The reduction in electrostatic repulsion between particles at seawater salinities means that particles could come close to each other without being repelled. Two particles that get close to each other would, therefore, be attracted to each other due to LW forces, but this is clearly not the only force active as not all particles are "sticky" in seawater. Biotic particles, such as bacteria and phytoplankton that form aggregates as large as marine snow in the ocean, can even change their relative stickiness as a function of growth cycle or, for example, the stage of a phytoplankton bloom.[2] Thus, it is clear that other factors must be relevant to colloidal and particle coagulation processes in marine systems.

Extended DLVO (XDLVO) theory has been used to describe the interactions of molecules at the surfaces of two particles. XDLVO theory adds additional short-range force due to acid-based (AB) interactions due to electron donor and electron acceptor interactions that affect hydrogen bonding between two surfaces immersed in a polar solvent such as water.[3] The AB force can be calculated based on contact angles measured on layers of particles, typically using polar solutions such as glycerol and water, and a nonpolar solution such as diiodomethane.[4] The inclusion of this new force has increased our understanding of interactions of particles, but additional factors have yet to be included in these models. These factors include the effect of steric interactions on particle approach and adhesion, and the impact of a small number of molecules at the surface of a particle that may not be detectable using bulk property measurements. For example, Feick and Velegol[5] have shown, using a novel rotational electrophoresis technique, that charge density is not constant on some colloidal particles.

Researchers have turned to using techniques that directly measure interaction forces such as the surface force apparatus (SFA) and atomic force microscopy (AFM).[6] SFA is more useful for examining properties of different materials as a material or chemical must be placed onto atomically flat surfaces such as mica during measurement. AFM is better suited for examining particle–particle and particle–surface interactions. The AFM tip can be used to probe the topography of a surface, either through direct contact of the tip with the surface (contact mode) or by intermittent tapping of the tip on the surface (tapping mode). Forces can be measured by holding the tip fixed at a specific location in an x–y plane, and then lowering the tip toward the surface (or retracting the tip), measuring the bending of the tip in terms of tip attraction (bending down) or repulsion (bending up). The interaction of the tip with an inorganic surface can be understood as a function of pH and ionic strength using DLVO theory if the tip is assumed to be a sphere of a much larger radius (100s of nm) than the true curvature of the tip at the end (10s of nm).[7] Some researchers who have examined bacterial adhesion have bound bacteria onto a tip in order to probe

cell interactions with a specific surface.[8,9] The disadvantage of this technique is that the geometry of two surfaces (bacteria spread nonuniformly on a pyramid-shaped tip) during the measured interaction is not well defined. Another approach to probe a surface is to bind a colloid to the tip to better define the geometry of the system.[10] This latter configuration allows surfaces or colloids to be coated with chemicals, greatly extending the range of interactions that can be examined using the AFM approach.

While the operation of an AFM is quite simple, it can be difficult to interpret the data and extract information on interaction forces. It is not the intent here to provide extensive background on the operation of the AFM or to review the AFM literature, as there are many excellent reviews available.[6,11,12] The purpose of this chapter is to briefly review a few findings by my own research group in the area of using AFM to understand bacterial adhesion, and to point out the limitations and future challenges of this new and powerful approach.

16.2 METHODS

AFM images presented in this study were all obtained with an AFM mounted on an inverted microscope (Bioscope; Digital Instruments) with samples analyzed either in air or in water using a fluid cantilever holder (as indicated). Force curves were conducted in water using DNP-S silicon nitride cantilevers (Digital Instruments) with the force constants measured for individual tips determined using a correlation based on the Cleveland method[13] contained in the DI software (v. 4.32). For more details on specific experiments, the reader should consult the indicated references.

Results are presented here for bacteria that include: *Pseudomonas putida* KT2442, a bacterium that can degrade substituted aromatic compounds; *Pseudomonas stutzeri* KC, capable of reductively dehalogenating chlorinated aliphatic compounds; and three strains of *Escherichia coli* that differ in the length of the lipopolysaccharide (LPS) on the cell surface.[8,14,15] Two *E. coli* strains had progressively truncated LPS chain lengths. *E. coli* strain D21 (wild type) expresses an LPS that extends from the lipid to the outer core region, while mutant strain D21f2 has an LPS chain that is truncated just after the KDO carboxyl group.[8] *E. coli* K-23 strain JM-109 contains these two parts of the LPS plus an O-antigen, and therefore this strain has a full LPS layer.[16]

Bacteria were anchored to glass slides for AFM imaging using two different techniques. In the first approach, carboxyl groups on the surface of the bacterium were covalently bonded to amino groups of amino-silane compounds on the surface of a glass slide.[17] In the second approach, bacteria were placed onto polyethylenimine (PEI; 750,000 Da) coated slides.[16,18]

16.3 RESULTS AND DISCUSSION

16.3.1 Bacterial Topography

AFM imaging occurs by rastering the tip back and forth across a surface. The AFM software converts the position of the tip to location, and the plane and a height above a plane so that the image can be presented either as a series of lines in three dimensions,

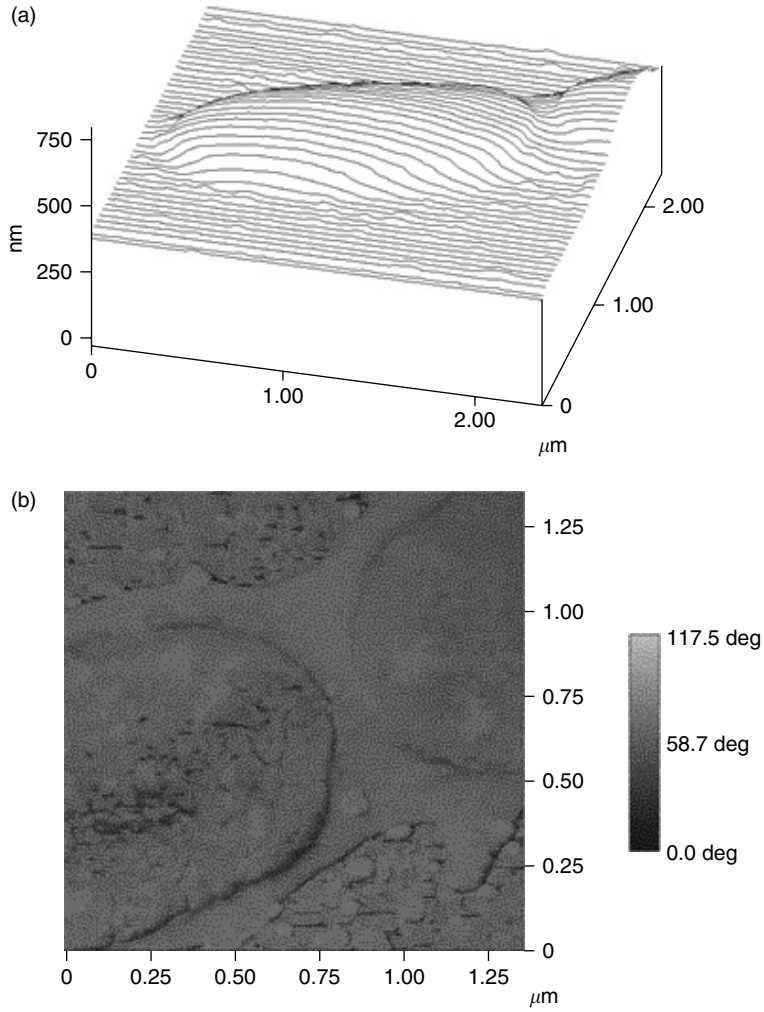

FIGURE 16.1 (**Color Figure 16.1 appears following page 236.**) Topographic AFM images of individual cells of *P. stutzeri* KC imaged in air showing the bacteria using (a) line plot and (b) phase imaging techniques. (Bacteria were prepared in MOPS buffer and covalently bonded to the glass surface.) (Modified from figure 2 and figure 6 in Camesano et al., *Langmuir*, 16, 4563–4572, 2000. With permission.)

or as two- or three-dimensional images with color variations (different colors or shading). A line plot of a single *P. stutzeri* KC bacterium is shown in Figure 16.1a. The image was taken using tapping mode in air of a bacterium originally prepared in MOPS buffer; the cell was covalently bound to the surface to prevent it from moving during imaging. The tapping of the tip was driven by a piezo at a set frequency, but as the tip contacted the surface, it shifted out of phase with the driving frequency. This phase shift was monitored and graphed as shown in Figure 16.1b (phase image) for

the same bacterium. Changes in the phase shift indicate differences in the chemical and physical properties of the surface, making it easier to distinguish the boundaries of the bacterium (a soft surface) from the hard glass surface. The phase image also provides evidence of heterogeneity of structure of the bacterial surface itself.

The height and elasticity of bacteria can introduce artifacts in the images produced with the AFM.[19] Shown in Figure 16.2 is a false-color image of a single *E. coli* cell (strain D21, fixed with 2.5% glutaraldehyde) obtained using tapping mode (Figure 16.2a) along with the corresponding phase image (Figure 16.2b). The cells in this image were anchored to the surface with PEI and imaged in 100 mM NaCl and 1 mM Tris buffer. It looks as if there is material that is adjacent to the bacterium (upper right of Figure 16.2a) that could represent material pulled off the cell or attached to the cell. However, the apparent presence of that material is an imaging artifact. The

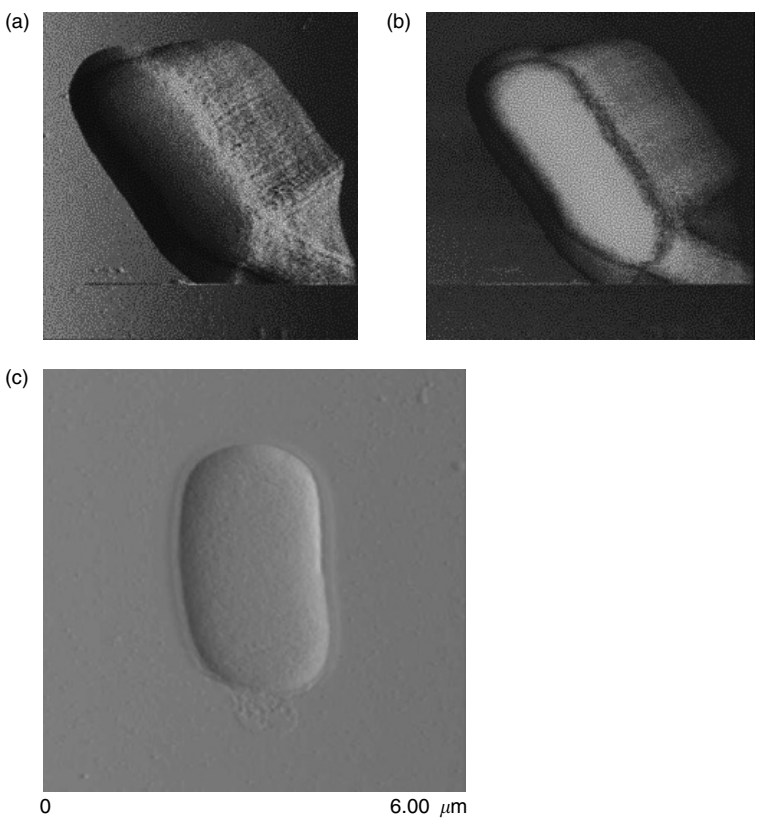

FIGURE 16.2 (**Color Figure 16.2 appears following page 236.**) A single *E. coli* (strain D21) imaged in water that apparently shows some "material" off to the right side of the bacterium: (a) false color height image and (b) phase image. (c) Imaging the bacterium under air reduces the height of the cell, and the absence of any "material" off to the right side of the cell indicates that the "material" is an imaging artifact. (Adapted from figure 2 and figure 4 in Velegol et al., *Langmuir*, 19, 851–857, 2003. With permission.)

height of the bacterium is large enough that the side of the pyramid-shaped tip, which is angled ~10° from the surface, hits the side of the cell making it appear as if there is some material that the bottom of the tip is hitting. The key factors in identifying the material as an artifact are that the material appears on only one side of the cell (it has a ~30° offset to the horizontal line during rastering of the tip across the surface), and that the location of the material relative to the cell and tip orientation is always on the same side.[18] When the water was removed for imaging, the cell dried and the height of the cell decreased due to desiccation of the bacterium, and the artifact disappeared (Figure 16.2c).

16.3.2 Surface Roughness

When particles attach to surfaces, the properties of both the particles and the surfaces will be important. Chemical factors such as surface hydrophobicity and energy are known to be important, but physical factors such as roughness can also be important. Shellenberger and Logan[20] examined the attachment of inorganic colloids (latex microspheres) and bacteria to two surfaces (glass beads) having different average roughnesses. One surface had an average roughness of 15 ± 2 nm, as measured by contact mode AFM, while the other surface had a roughness of 38 ± 4 nm. The rougher surface, shown in Figure 16.3, has many large asperities that served to interact with the surface of the bacteria and other particles. These asperities reached heights

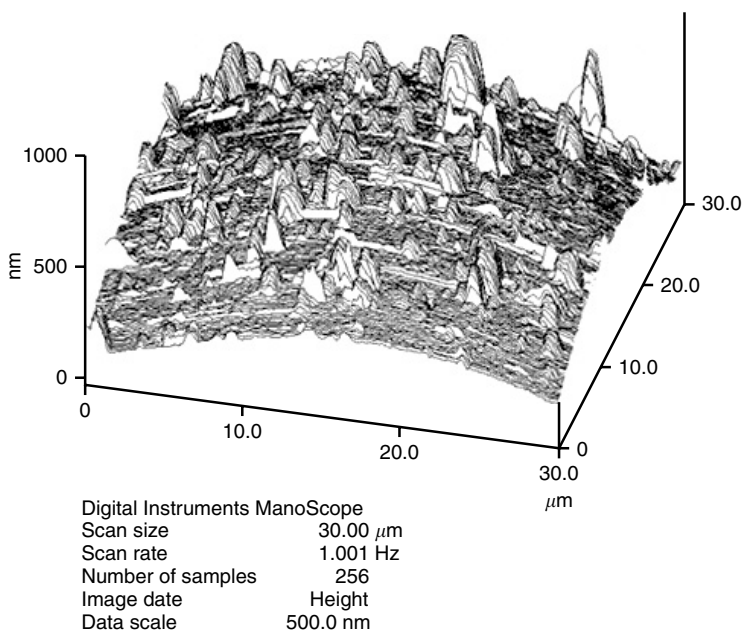

FIGURE 16.3 The surface of a glass bead roughened using chromic acid shows asperities on the glass surface that average 38 ± 4 nm and can reach over 50 nm. (From Shellenberger and Logan, *Environ. Sci. Technol.*, 36, 184–189, 2002. With permission.)

of over 50 nm and therefore extended well outside the conventional electrostatic repulsion layer of colloids and larger particles. The researchers found that attachment of bacteria and latex microspheres was greater to the rougher surface than to the smoother surface. The extent that surface roughness is important to adhesion efficiencies between different types of biological and inorganic particles in marine systems is an issue that should be further explored.

16.3.3 Interaction Forces

One of the most interesting aspects of probing surfaces with AFM is the ability to measure interaction forces between the AFM tip (or a colloid on the tip) and a surface or particle. Camesano and Logan[21] examined the interaction between a silicon nitride (SiN_4) tip and individual cells of *P. putida* KT2442. During the approach of the tip to the surface, they observed repulsion of the tip by the bacterial surface at pHs ranging from 2.2 to 8.7 (Figure 16.4a). The magnitude of the force measured at

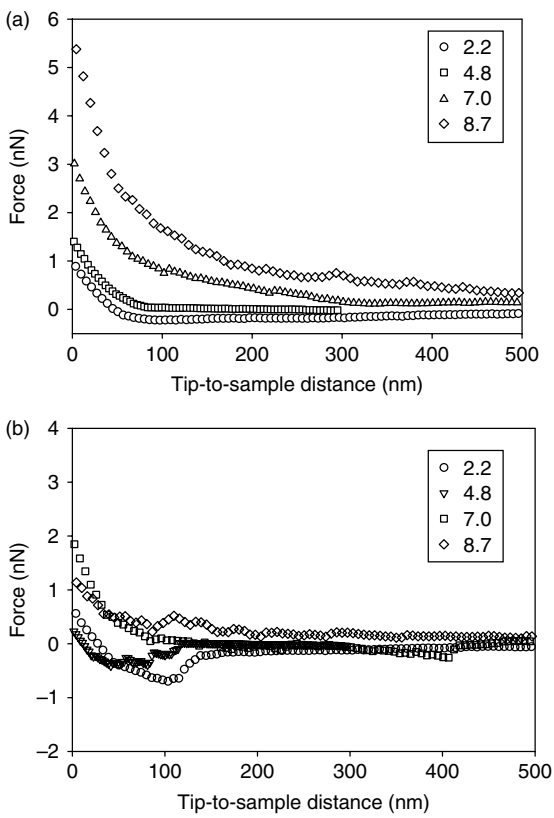

FIGURE 16.4 Force curves obtained on individual bacteria of *P. putida* strain KT2442 in water at different pH values: (a) approach curves and (b) retraction curves. (Adapted from Camesano and Logan, *Environ. Sci. Technol.*, 34, 3354–3362, 2000. With permission.)

the "origin" decreased with pH, suggesting that electrostatic effects were important because decreasing the pH decreased the repulsive layer thickness of the bacterial surface. That is, a reduction in pH brought the net surface charge of the bacterium closer to its isoelectric point (2.3 for strain KT2442; typically around a pH of 2 to 3 for bacteria). The "origin" shown in Figure 16.4a was not a fixed point during force curve imaging. During the approach of the tip to the surface, both the tip and surface can be deflected by electrostatic repulsion between the tip and molecules as well as by small numbers of molecules on the surface.[18] Thus, the surface deflected downward during imaging and was lower than its original point by the time the tip and surface were in complete contact.

During the retraction of the tip from the bacterial surface, there were adhesion forces measured between the tip and the surface at the two lowest pH values (Figure 16.4b). However, there were repulsive forces measured between the tip and surface at the two higher pH values (7.0 and 8.7). Attractive forces could be due to covalent and electrostatic bonds between the tip and surface, but capillary forces could be important in this system as well.

Solution ionic strength, as well as pH, can be an important effect in determining bacterial interactions with surfaces. As solution ionic strength is decreased, it is expected from DLVO theory that the electrostatic repulsion layer thickness will increase. It has been observed that the repulsion between an AFM tip and a bacterial surface increases as ionic strength is decreased in accordance with this theory (Fig. 16.5). However, the interaction distances (100s of nanometers) are much larger than those predicted from electrostatic interactions alone (10s of nanometers). Thus, it is likely that these interactions result from changes in orientation of large molecules on the surface of the bacteria in response to changes in ionic strength as well as to changes in pH.

The finding that interaction distances between bacteria and AFM tips are large has prompted extensive studies into measurements of molecular interactions at bacterial surfaces. Razatos and coworkers[8,9] first worked with two strains of *E. coli* that had different lengths of LPS (strains D21 and D21f2). In their experiments, the AFM tip was coated with bacteria and this coated tip brought down near a glass surface. They found that the AFM tip coated with D21f2 was repelled by the glass surface but that coated with strain D21 was attracted to the surface. They hypothesized that the extra polysaccharide on outer layer of D21 shielded the charge of the highly negatively charged keto group (that was exposed on D21f2) because this outer polysaccharide layer was attracted to the surface. They therefore concluded that adhesion increased with an increase in the length of the LPS.

The conclusion that the presence or absence of an O-antigen affects adhesion has been postulated in other studies.[22] However, findings by Razatos[8,9] that the LPS layer length determines the adhesion properties of these *E. coli* strains has not been confirmed by others.[16] AFM measurements were made between AFM tips and individual bacteria for the two strains used by the Razatos group, and a third strain of *E. coli* that contained a full LPS layer (keto group, core polysaccharide, and O-antigen). For all three strains, AFM force curves between a bare silicon nitride tip and the bacterial surface were found to be identical (Figure 16.6). In addition, sticking coefficients measured in column tests between the bacteria and glass beads showed that the adhesion of D21 was larger than that of D21f2 only for conditions of low ionic strength

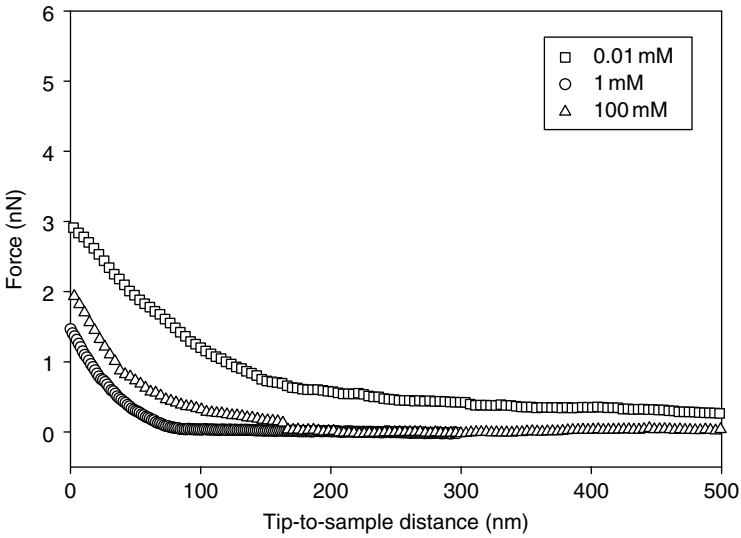

FIGURE 16.5 Approach force curves obtained on individual bacteria of *P. putida* strain KT2442 in different ionic strength solutions. (Adapted from Camesano and Logan, *Environ. Sci. Technol.*, 34, 3354–3362, 2000. With permission.)

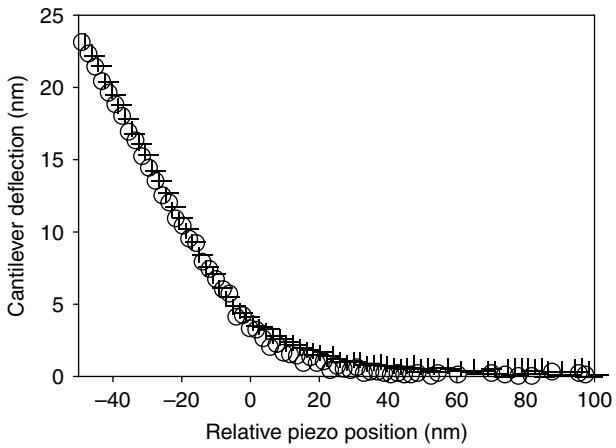

FIGURE 16.6 Approach force curves as a function of the relative piezo movement when silicon nitride tip interacts with *E. coli* strains D21(◯), D21f2 (−), and JM109 (|). Cells were prepared in 1 mM Tris and attached to glass slides using PEI. (From Burks et al., *Langmuir*, 19(6), 2366–2371. With permission.)

and for non-glutaraldehyde-treated cells.[16] When bacteria were placed in a solution of higher ionic strength, or were treated with glutaraldehyde (all bacteria used by Razatos were fixed with glutaraldehyde), the sticking coefficient was larger for D21f2 than D21. Thus, trends between cell adhesion and the molecular composition

of the bacteria observed with AFM techniques were not always correlated to conditions observed in macroscopic adhesion tests. Additional research is needed to understand how these chemical treatment and solution changes affect the adhesion of these bacteria to glass surfaces.

16.3.4 Outlook for Using AFM to Study Attachment Processes

There have been many successes using AFM to study the topography of colloids, flocs, and surfaces, and forces between molecules, colloids, and surfaces. The AFM remains one of the most useful tools to study such systems, but additional work will be needed to understand how molecular interactions affect the binding of bacteria, and other particles, to surfaces. The flexibility of the AFM in terms of different methods of operation (contact, tapping, phase, and forces imaging), as well as the ability to chemically modify tips or colloids on the AFM cantilever, make AFM an exceptional tool for further investigations of molecular and nanoscale interactions that affect particle adhesion.

ACKNOWLEDGMENTS

The support of the National Science Foundation (NFS) CRAEMS program grant CHE-0089156 and the Penn State Biogeochemical Research Initiative for Education (BRIE) (NSF IGERT grant DGE-9972759) are gratefully acknowledged.

REFERENCES

1. Logan, B.E., *Environmental Transport Processes*. John Wiley & Sons, New York, 1999.
2. Dam, H.G. and Drapeau, D.T., Coagulation efficiency, organic-matter glues and the dynamics of particles during a phytoplankton bloom in a mesocosm study, *Deep Sea Res. II*, 42, 111–123, 1995.
3. Van Oss, C.J., Hydrophobicity of biosurfaces — origin, quantitative determination and interaction energies, *Colloid Surf. B: Biointerfaces*, 5, 91–110, 1995.
4. Holm, R.E., Nielsen, P.H., Albrechtsen, H., and Christensen, T.H., Importance of unattached bacteria and bacteria attached to sediment in determining potentials for degradation of xenobiotic organic contaminants in an aerobic aquifer, *Appl. Environ. Microbiol.*, 58, 3020–3026, 1992.
5. Feick, J.D. and Velegol, D., Electrophoresis of spheroidal particles having a random distribution of zeta potential, *Langmuir*, 16, 10315–10321, 2000.
6. Claesson, P.M., Ederth, T., Bergeron, V., and Rutland, M.W., Techniques for measuring surface forces, *Adv. Colloid Interface Sci.*, 67, 119–183, 1996.
7. Senden, T.J. and Drummond, C.J., Surface chemistry and tip–sample interactions in atomic force microscopy, *Colloids Surf. A: Physicochem. Eng. Aspects*, 94, 29–51, 1995.
8. Razatos, A., Ong, Y.-L., Sharma, M.M., and Georgiou, G., Molecular determinants of bacterial adhesion monitored by atomic force microscopy, *Proc. Natl. Acad. Sci., USA*, 95, 11059–11064, 1998.

9. Ong, Y.-L., Razatos, A., Georgiou, G., and Sharma, M.M., Adhesion forces between *E. coli* bacteria and biomaterial surfaces, *Langmuir*, 15, 2719–2725, 1999.
10. Bowen, W.R., Hilan, N., Lovitt, R.W., and Wright, C.J., An atomic force microscopy study of the adhesion of a silica sphere to a silica surface — effects of surface cleaning, *Colloids Surf. A: Physicochem. Eng. Aspects*, 157, 117–125, 1999.
11. Maurice, P., Applications of atomic-force microscopy in environmental colloid and surface chemistry, *Colloids Surf. A: Physicochem. Eng. Aspects*, 107, 57–75, 1996.
12. García, R. and Pérez, R., Dynamic atomic force microscopy methods, *Surf. Sci. Rep.*, 47, 197–301, 2002.
13. Cleveland, J.P., Manne, S., Bocek, D., and Hansma, P.K., A nondestructive method for determining the spring constant of cantilevers for scanning force microscopy, *Rev. Sci. Instr.*, 64, 403–405, 1993.
14. Nusslein, K., Maris, D., Timmis, K., and Dwyer, D.F., Expression and transfer of engineered catabolic pathways harbored by Pseudomonas spp. introduced into activated sludge microcosms, *Appl. Environ. Microbiol*., 58, 3380–3386, 1992.
15. Criddle, C.S., DeWitt, J.T., Grbic-Galic, D., and McCarty, P.L., Transformation of carbon tetrachloride by *Pseudomonas* sp. strain KC under denitrification conditions. *Appl. Environ. Microbiol*., 56, 3240–3246, 1996.
16. Burks, G.A., Velegol, S.B., Paramanova, E.U., Lindenmuth, B.E., Feick, J.D., and Logan, B.E., Macroscopic and nanoscale measurements of the adhesion of bacteria with varying outer layer surface composition, *Langmuir*, 19, 2366–2371, 2003.
17. Camesano, T.A., Nataon, M.J., and Logan, B.E., Observation of changes in bacterial cell morphology using tapping mode atomic force microscopy, *Langmuir*, 16, 4563–4572, 2000.
18. Velegol, S.,B., Pardi, S., Li, X., Velegol, D., and Logan, B.E., AFM imaging artifacts due to bacterial cell height and AFM tip geometry, *Langmuir*, 19, 851–857, 2003.
19. Velegol. S.B. and Logan, B.E., Contributions of bacterial surface polymers, electrostatics and cell elasticity to the shape of AFM force curves, *Langmuir*, 18, 5256–5262, 2002.
20. Shellenberger, K. and Logan, B.E., Effect of molecular scale roughness of glass beads on colloidal and bacterial deposition, *Environ. Sci. Technol.*, 36, 184–189, 2002.
21. Camesano, T.A. and Logan, B.E., Probing electrostatic interactions using atomic force microscopy, *Environ. Sci. Technol.*, 34, 3354–3362, 2000.
22. DeFlaun, M.F., Oppenheimer, S.R., Streger, S., Condee, C.W., and Fletcher, M., Alterations in adhesion, transport, and membrane characteristics in an adhesion-deficient Pseudomonad, *Appl. Environ. Microbiol.*, 65, 759–765, 1999.

17 Impact of Stresses or Transient Conditions on Deflocculation in Engineered Microbial Systems

Fernando Morgan-Sagastume and D. Grant Allen

CONTENTS

1-56670-615-7/05/$0.00+$1.50

Biological systems are subject to transient conditions. For instance, natural and designed microbial systems commonly undergo variations in the environmental conditions to which microbial biomass is exposed. Engineered biological treatment systems, although generally designed to operate under steady-state or stable conditions, experience environmental transients that can compromise their performance. Loss of the microbial aggregate structure and disintegration of bioaggregates appear to be common responses of suspended biomass to transient operating conditions and environmental stresses. These changes can be related to inhibition of metabolism, to physiological stress responses, and to physico-chemical abiotic effects.

This chapter reviews common transient conditions and stresses in microbial systems engineered for the treatment of wastewater, including aerobic and anaerobic wastewater treatment processes. Emphasis is given to technologies with biomass in suspension where bioaggregate disintegration, that is, sludge deflocculation, has been identified to occur under microbial physiological stresses and transient conditions, and where biomass deflocculation poses challenges to the operation of the systems. Special attention is given to activated sludge deflocculation under mesophilic–thermophilic temperature transients, as part of recent work in our research group. Mechanisms leading to biomass deflocculation or weak bioaggregate structure are reported, and proposed for the case of mesophilic–thermophilic temperature upshifts in order to explain experimental observations.

17.1 INTRODUCTION

17.1.1 Definition of Terms

For the purpose of this chapter, transient conditions or transients refer to dynamic, variable, or shifting conditions. The term deflocculation is used to describe the process of disintegration of microbial mass aggregates. Biomass aggregates or flocs are terms used to describe the physical entities formed by the gathering together of microorganisms under physiological conditions[1] in engineered systems. Therefore, for the purpose of this chapter, the term flocs encompasses other terms generally applied to similar structures: pellets, granules, clusters, agglomerates, with or without the prefix bio. Deflocculation is defined as the coming apart of the constitutive elements of a microbial aggregate that renders it smaller or disperses it into solution. The terms deflocculation, floc disintegration, and disaggregation are synonymous in this work. Nonetheless, it is important to differentiate the specific processes whereby deflocculation may occur.

The overall term of deflocculation can be understood as the process of sludge floc destruction and size reduction involving floc fragmentation or floc erosion. Floc fragmentation is the fracture of flocs into smaller pieces that lead to more exposed floc surface area, and floc erosion is the detachment of small particles or components from flocs under hydrodynamic, shear stress.[2,3] The term sludge deflocculation has been more widely used in the literature on biological wastewater treatment to account for both floc fragmentation and erosion. Floc erosion appears to govern the generation of colloidal particles causing increased effluent turbidity and suspended solids under shear stress.[2,4] The preference to use deflocculation in the literature may arise from

the inability to separate the distinct phenomena of floc fragmentation and floc erosion, especially when studying floc stress that is not due to hydrodynamic shear.

Overall, the processes of biomass aggregation and disaggregation are considered a dynamic equilibrium. Sludge flocs appear to be under a dynamic equilibrium between flocculation (aggregation) and deflocculation (disintegration),[2,4,5] and also more specifically under an equilibrium between adhesion and erosion.[2,3]

17.1.2 Objectives and Scope of the Chapter

Although transients are not always linked to stresses, this chapter focuses on common transients that disturb the operation of engineered microbial systems designed and intended to deliver a steady-state performance. The chapter is aimed at compiling the available literature on the effects of transients in biological wastewater treatment systems, both aerobic and anaerobic, where deleterious effects from transient conditions are commonly encountered. More specifically, the chapter identifies the different types of transient conditions that act as physico-chemical or physiological stresses impairing proper biological wastewater treatment performance due to biomass deflocculation. This chapter also focuses on deflocculation of bacterial- or microbial-community aggregates, resulting from reduced floc stability or weakened floc structure.

Hydrodynamic stress leading to biomass disaggregation is not reviewed in this work. Although some types of stresses and transients may directly lead to microbial floc disaggregation, other types may only impair floc stability or weaken bioaggregate structures. It is the hydrodynamic stress to which the bioflocs are normally exposed that erodes and fragments the weakened microbial aggregates. The impacts of hydrodynamic stresses on deflocculation are better understood, and have been studied in nonbiological aggregates[6,7] and in some microbial aggregates, such as activated sludge flocs.[2–4] The effects of hydrodynamic stresses like extensional deformation, rotation, and translation on microbial flocs are not considered in this work, but remain an area where comprehensive understanding may still be required.[8,9]

The impact of transient conditions on the deflocculation of aggregates of filamentous fungi, cellular slime moulds, algae, or eukaryotic microbes are not covered since this has not been reported to pose a problem in the operation of engineered microbial processes. Deflocculation of yeast aggregates has been reviewed elsewhere as part of yeast flocculation reviews.[1]

17.1.3 Why Should Biomass Deflocculation under Transient Conditions Be Studied?

The interest in identifying and understanding the factors causing microbial disaggregation and the mechanisms of deflocculation has arisen from the need to operate biological processes more robustly, that is, with constant outputs that comply with stringent quality requirements. Biomass deflocculation poses a complex challenge to biological treatment since it leads to the loss of biocatalyst used in pollutant degradation, to solids discharges, and to the discharge of bioactive compounds adsorbed onto biomass. A better understanding of what causes deflocculation and how different

factors affect this process will permit its control. These ideas have motivated a great deal of research in the area of microbial aggregation and adhesion, for which there have been many reviews.[1,10–12] Nevertheless, the process of microbial disaggregation in biological treatment processes has received little attention. The literature on microbial deflocculation in biological treatment under different stresses is relatively recent (1995 to the present), with some sporadic studies before 1995, especially in aerobic treatment. The increase in the number of more recent studies in this area responds to the increasing necessity to control reliably biological treatment systems as they are pushed to their limits.

17.2 TRANSIENT CONDITIONS AND STRESSES IN ENGINEERED BIOLOGICAL TREATMENT SYSTEMS

Various biological wastewater treatment processes operate with inherent dynamic conditions due to system configuration and operation; however, these processes tend to reach stable treatment performance and, therefore, are considered as controlled unsteady-state processes.[13] Examples of these systems are sequencing batch reactors (SBRs); contact stabilization processes; activated sludge processes with selectors, subjecting biomass to different substrate concentrations along the treatment train; nutrient removal processes exposing biomass to alternating anaerobic, anoxic, or aerobic environments; and deep-shaft activated sludge processes. Most biotreatment processes strive to operate at steady state in order to provide constant effluent concentrations of pollutants within regulatory limits; however, common system variations may lead to uncontrolled unsteady-state operation that can violate effluent discharge limits.

The microbial response of a biological treatment process to variable operating conditions is of a transient nature, and has been related to poor treatment performance. Generally, these transient, dynamic conditions in biological wastewater treatment are caused by changes in substrate and nutrient characteristics and concentrations, and by changes in the environmental conditions to which biomass is exposed (e.g., dissolved oxygen (DO), pH, temperature).

Overall, the impact of transient conditions on the treatment performance of anaerobic reactors has been studied more extensively and under more controlled conditions than in aerobic reactors treating wastewater, as reviewed in the following sections.

17.2.1 Carbon Substrate Transients

Transient substrate conditions are related to variations in substrate concentration or type and have been more extensively studied than other transients, especially in activated sludge systems.[14] Most of the work on substrate transients has been on input concentration transients (or loading rates) conducted in pure and mixed cultures after growth and acclimation in lab- or pilot-scale systems with defined substrates. A few respirometric batch experiments with spikes of a single readily degradable substrate have been conducted with activated sludge from full-scale plants.

Two main physiological responses occur under unbalanced microbial growth due to substrate concentration increases: internal storage of available substrate as poly-β-hydroxyalkanoates (PHAs) or glycogen[14,15] and increased growth rate.[15–17] Substrate storage is rapid, requiring little physiological adaptation because synthesis of storage polymers is simpler than that of other cell constituents, and polymers stored internally can be utilized for growth under substrate limited conditions. Substrate storage in mixed cultures has been studied under anaerobic, aerobic, anoxic, and mixed conditions.[18] The increased growth rate response to substrate spikes is slower than polymer storage since it requires protein synthesis.[14] Nevertheless, when microorganisms are still adapting to a specific environment and a substrate spike occurs, microorganisms are believed to almost immediately increase their specific growth rate.[15]

Additional mechanisms of response to high substrate concentrations include the release of soluble metabolites and of extracellular polymeric substances (EPS),[14,19] and the accumulation[20] and sorption of substrate. Accumulation refers to the transport of substrate into the cell where it is stored in an almost unchanged form or transformed into low molecular weight metabolic intermediates. Release of EPS may be relevant in biofilm systems where extreme extracellular polymeric release was observed to take place.[21]

In activated sludge microbial communities, feast and famine substrate dynamic conditions or substrate concentration gradients select for specific microbial populations with different physiological characteristics. This selection occurs due to the different maximum growth rates of microorganisms, for example, selection of floc-forming bacteria against filamentous bacteria in selectors or SBRs.[13,14,22–24] It has been hypothesized that floc-forming bacteria have a greater ability for polymer storage under substrate transients than filamentous bacteria.[24] For intermittently and continuously fed activated sludge, polymer storage is the main response to changes in substrate concentrations over time.

The effects of organic and hydraulic overloads on the treatment performance of anaerobic reactors have been broadly covered in stability studies, likely due to the greater sensitivity of anaerobic processes to disturbances compared to aerobic processes. Poor treatment performance, characterized by high concentrations of volatile fatty acids (VFAs), chemical oxygen demand (COD), and suspended solids in the effluent, and high sludge volume index (SVI), has been observed due to these types of transients, as reported elsewhere.[25,26] These reports have been briefly reviewed by Nachaiyasit and Stuckey (1997) and Xing et al. (1997).[27–29]

Shifts in substrate types and increase in loading rates have been reported to disturb treatment performance and select for microorganisms with different phenotypes within anaerobic granules. Under thermophilic conditions, a feed rich in acetate or volatile fatty acids was observed to select for acetoclastic methanogens over acidogenic and hydrogenotrophic methanogens, whereas a sugar-based feed selected for a symbiotic community of acidogenic and hydrogenotrophic methanogens in an upflow anaerobic sludge blanket (UASB) reactor.[30] The transitions between feeds were characterized by variations in methanogenic activity, COD removals, and changes in the granule properties. Compact and surface-homogeneous granules were formed with a sucrose feed, but not with an acetate feed, which promoted poor

granulation.[30] Increased loading rates of linoleic acid deterred methanogenic activity on different substrates, which was accompanied by granule disintegration and the release of free filamentous organisms in an expanded granular sludge bed (EGSB) reactor.[31]

Several studies report that anaerobic processes, although sensitive to substrate transients, can develop robustness against perturbations in substrate concentrations. High biomass concentrations in anaerobic baffled reactors have helped in the fast recovery of system performance from short-term substrate concentration and hydraulic transients.[27] Nachaiyasit and Stuckey[27,28] (1997) have argued that a high biomass concentration in anaerobic reactors can be used to increase reactor stability, since a significant amount of biomass remains after washout from imposing low hydraulic retention times (HRT). Xing et al.[29] (1997) observed the adaptation of an anaerobic microbial community and a new steady-state performance in a completely stirred tank reactor (CSTR) under long-term (>400 days) periodic glucose concentration changes. Increasing sulfate concentrations in an UASB reactor also showed gradual assimilation of the shock loads with overall good treatment performance over a period of 266 days.[32] Some studies even report no impact on treatment performance of increasing COD loading rates in a pilot-scale anaerobic hybrid reactor [33] and full-scale UASB reactor followed by trickling filters.[34]

Previous studies on cell decay and death, defined as the inability of cells to reproduce and respire further,[35] have shown that cell death due to lack of substrate hardly ever occurs.[36] Sporulating bacteria form spores when exposed to starvation whereas non-sporulating bacteria become dormant, and can be reactivated in the presence of specific extracellular compounds. Internal decay leading to a loss in microbial weight and activity, but not necessarily in the number of microorganisms, is active in all microbial systems exposed to starvation.[35]

17.2.2 Periodic Substrate Oscillations

The studies on substrate oscillations in biological treatment of wastewater indicate that microbial acclimation leading to stable treatment is achievable. The stable operation of a chemostat resulting from periodic substrate variations due to the establishment of a mixed culture of competing microbial populations or in pure cultures is well reported in the literature.[37–39]

Long-term periodic changes in substrate concentration have also shown to induce stable treatment in anaerobic processes. Xing et al.[29] (1997) observed the adaptation of an anaerobic microbial community and CSTR steady-state performance under long-term (400 days) periodic substrate perturbations. An anaerobic microbial consortium is sensitive to short-term perturbations due to complex symbiotic microbial interactions and slow growth rates of acetoclastic methanogens. However, the diversity in populations within the consortium can also give an advantage to anaerobic communities under long-term perturbations since they can adapt selectively, as studies on changes on community structure suggest.[40,41] For example, hydrogen-utilizing methanogens can quickly adapt to changes in environmental conditions.[29]

17.2.3 Environmental Transients

The most common environmental transients in biological treatment systems are with respect to DO concentrations, toxic compounds, pH, and temperature. Although transient conditions have been studied in anaerobic systems for more than two decades, the impact of these transients in aerobic treatment has received more attention only relatively recently.

17.2.3.1 Dissolved Oxygen (DO) Transients

The literature on DO transients in biological wastewater treatment systems is limited. Most of the studies have addressed the impact of low DO levels or anaerobic conditions as stresses on activated sludge. This literature is reviewed in Section 17.3 as stress conditions leading to deflocculation.

The few studies on DO transients tend to agree in that variable or low DO levels select for microorganisms that thrive under these conditions. However, a thorough characterization of the physiology and metabolism of the microorganisms selected by these transients has not been conducted. Sharp decreases in DO levels associated with sudden substrate overloads in activated sludge have been shown to favor the growth of filamentous bacteria.[42] Pernelle et al.[42] (2001) showed experimentally that the continuous proliferation of filamentous bacteria (Type 021N, *Thiothrix*, *Nostocoida limilicola II*, and especially *Haliscomenobacter hydrossis*) in an activated sludge pilot plant leading to sludge bulking was triggered by the combined transient of a substrate overload (meat and vegetable extracts and sugar) with an imposed DO deficit. Separately, the DO deficiency and the increase in substrate caused transitory, small-scale proliferation of some of the filaments. Similarly, but on a positive side, alternating aerobic and anaerobic conditions in an activated sludge plant promoted a microbial community shift toward facultative organisms without affecting COD removals or settling, as SVI.[43]

The effects of periodic DO oscillations resulting in the selection of a mixed community of nitrifiers, aerobic heterotrophs, and denitrifiers in activated sludge have only been simulated using the AQUASIM model,[44] but experimental validation is required.

17.2.3.2 Toxicity and pH Transients

Phenol and hydrogen peroxide (H_2O_2) have been used to study toxic transient effects on microbial metabolism. Sudden increases in these toxic compounds have been shown to cause deleterious effects on biological wastewater treatment. Phenol spikes and shock loadings have been shown to cause activated sludge deflocculation and the immediate reduction in sludge oxygen uptake rates (OURs),[45] and to decrease the sludge substrate removal capacity in respirometric assays.[46] Phenol is known to inhibit growth rate kinetics in activated sludge systems, but it is degraded after sludge acclimation.[45] Similarly, Larisch and Duff[47] (1997) observed that sudden H_2O_2 increases in the influent (5 to 50 mg/l influent) to lab-scale activated sludge reactors led to decreased mixed liquor volatile suspended solids (MLVSS) levels, weakly bonded flocs, and high effluent suspended solids (ESS).

If microbial metabolism is not completely eliminated by high toxic concentrations, microbial communities are known to undergo adaptive changes in structure and function capability in order to tolerate and degrade xenobiotic compounds.[48] Preacclimation of activated sludge to toxic compounds tends to buffer the impacts of toxic spikes, as shown for increased phenol shock loading spikes[45] and increased H_2O_2 concentrations[47] in activated sludge.

Some studies have reported decreased OUR and settleability in activated sludge respirometric assays due to the toxicity of chemicals used in the manufacturing of paper and pulp.[49–51] These studies, however, have not been able to provide conclusive mechanistic explanations of the observed effects. Chemicals that have inhibited microbial activity, assessed as reduced OURs,[49,50] include a cleaning solvent, turpentine, microbiocides containing 2,2-dibromo-3-nitrilopropionamide (20%), methylenebisthiocyanate (9%), and carbamate, several paper dyes (e.g., Orange 3, Violet 5, Red B), monochloro acetic acid (80% in water) and soft soap. In batch experiments,[50] the same biocides decreased the OURs and the dissolved organic carbon removal efficiencies; acrylic latex increased sludge settleability probably by adsorbing onto flocs, while aluminum sulfate and an optical brightener decreased sludge settleability probably due to floc charge instability. A simulated black-liquor spill into a lab-scale activated sludge decreased the biological oxygen demand (BOD) and COD removals, the sludge-specific adenosine triphosphate (ATP) concentration, and increased ESS and effluent toxicity.[51]

The impacts of chemicals on activated sludge are dose- and type-dependent.[52] Some chemicals have no effect on the OUR or on settleability[49,50] and others even increase the OUR.[49,50,53] The chelating nature of chemicals, such as that of diethylene triamine pentaacetic acid (DTPA), has decreased the OURs in a dose-dependent fashion in batch experiments and lab-scale continuous activated sludge reactors treating bleached kraft mill effluent.[47] DTPA has also decreased the BOD removal (39%) and caused sludge floc disintegration.[47]

Depending on the nature of the compound, chemical transients can be associated with pH stresses. Overall, bacteria seem to be more sensitive to low pH than to high pH values.[36,54,55] Bacteria in activated sludge flocs appear more resistant to chemical and pH stresses than microorganisms in more dispersed biomass (i.e., from lagoons) due to the high-biomass-density structure of activated sludge flocs.[55] Both acid and basic shocks decrease activated sludge metabolism,[36,55] and decrease specific ATP concentrations,[36] which is a measurement of decreased microbial metabolic activity.

Toxicity in anaerobic systems is generally related to the inhibition of methanogens by the increase in concentration of VFA, particularly, butyrate and acetate, but it can also be associated with sulfide and heavy metals, as reviewed in refs 56 and 57. The inhibitory effect of VFA is related to the lowering of pH. Since substrate concentration and temperature transients can lead to the accumulation of VFA, the effect of these transients can be compounded by a pH inhibitory effect on methanogens.

17.2.3.3 Temperature Transients

Temperature transients in biological wastewater treatment can result from seasonal variations and from the operation of batch units and shutdowns/start-ups in

upstream industrial processes. Industrial treatment systems may be subjected to frequent and drastic temperature transients that affect treatment performance. On the contrary, sewage treatment systems may experience mainly seasonal transients of which winter may represent the most challenging due to reduced microbial activity.

Temperature transients have been identified in activated sludge plants treating pulp and paper mill effluents during the summer.[58] Deterioration of activated sludge metabolic activity was detected by respirometry in several pulp and paper mills at temperatures exceeding 38°C, and effluent cooling towers were installed to counteract these effects.[58,59] Cocci and McCarthy[60] (1998) also reported the installation of wastewater cooling towers prior to SBRs treating pulp and paper mill effluents in Canada. The cooling towers in these systems generally reduced the raw wastewater temperature by approximately 10°C. The reported mean winter and summer operating temperatures of the SBR systems were 28°C and 37°C, respectively. Several mills, probably those without or with undersized cooling systems, were reported to operate with temperatures over 40°C, but with concerns about system performance.[60]

Similarly, temperature increases in full-scale anaerobic reactors treating industrial wastewater have been reported.[61,62] An accidental increase in temperature from 36°C to 50°C in a full-scale anaerobic filter reduced the COD removal efficiency from 85% to 45% over a seven-hour exposure at 50°C.[61]

In anaerobic treatment processes, a better understanding has been achieved of the effects of temperature shifts on reactor performance, granule characteristics, and microbial community structure from conducting systematic studies.[25,62–65]

In general, poor treatment performance has been reported due to temperature shifts in anaerobic reactors. Short-term (8–9 and 5–24 h) temperature shifts from mesophilic (30°C and 37°C to 39°C) to thermophilic (46°C, 55°C, 61°C, and 65°C) conditions have decreased the removal efficiencies of volatile fatty acids and biomass methanogenic activity in UASB reactors treating a sulfate-containing wastewater,[62] VFA, and vinasse.[64,66,67] Thermophilic temperature shifts from 55°C to 65°C have increased the concentration of total organic carbon in the effluent in association with granule disintegration in an UASB reactor,[63] and have increased the effluent VFA concentrations and decreased the methanogenic activity in an anaerobic digester.[65] Short-term (6 and 12 h) temperature downshifts from 35°C to 25°C and 15°C increased the concentrations of COD, VFA, and ESS in an anaerobic fluidized bed reactor treating ice-cream wastewater.[68] Interestingly, temperature shifts from mesophilic temperatures (30°C and 37°C to 39°C) to 45°C[62,64] or from 35°C to 42°C[67] have had no significant effect on the treatment performance of UASB reactors.

The literature on temperature shifts in anaerobic treatment indicates that the recovery of anaerobic reactors from short-term mesophilic–thermophilic temperature shifts is possible and is dependent on the growth rate of microorganisms. For instance, methanogens are more sensitive than sulfate-reducing bacteria to shifts from 30°C to 55°C and 65°C due to relatively slower growth rates.[62] Exposure of mesophilic anaerobic granules to temperatures above 60°C may completely eliminate methanogenic and acetogenic activity.[64] However, even after a drastic temperature increase

from 38°C to 75°C that almost eliminated anaerobic digestion in an UASB reactor, the system began to recover after 12 days.[67] Anaerobic digestion has also recovered from a thermophilic temperature shift from 55°C to 65°C, in which the activity of methanogens and acidogens was reduced, but not that of hydrolytic and fermentative populations.[65]

There is agreement in the literature that temperature upshifts from mesophilic to thermophilic or within thermophilic conditions cause granule disintegration in anaerobic treatment systems. Disintegration of anaerobic granules has been reported under a six-h thermophilic shift from 55°C to 65°C in an UASB reactor treating a sucrose-containing wastewater,[63] and under temperature shifts from mesophilic to thermophilic conditions during UASB startups.[66,67] Anaerobic granular disintegration under the thermophilic temperature upshift seems to be gradual, and takes place long after the temperature has been increased (80 days). A gradual increase in effluent VSS and decrease in the reactor's VSS was observed over a period of 80 days at 65°C in an UASB,[63] and complete granule disintegration was observed 2 to 3 months after subjecting mesophilic granules to temperatures above 45°C during the startup of thermophilic UASB reactors.[66] It is probable that some level of biomass detachment occurs from biomass carriers in an anaerobic fluidized bed reactor due to temperature downshifts from 35°C to 25°C and 15°C, as indicated by an increase in effluent suspended solids.[68]

Although observed in practice, the effects of temperature transitions on activated sludge metabolism, microbial community structure, settling characteristics, and bioflocculation are not well understood. Table 17.1 summarizes different types of studies where temperature transients have been reported in aerobic treatment of wastewater. The transitional conditions from an initial to a final stage of a temperature shift have received little attention in aerobic treatment of wastewater. Until very recently, little work had been conducted on the effects of temperature disturbances on the response and overall performance of wastewater aerobic biological treatment processes. Most of the studies reporting temperature transients in aerobic wastewater treatment are not systematic and tend to be anecdotal as part of experiments at different temperatures, but under steady-state conditions (e.g., see ref. [69,75,77] as per Table 17.1). Most of these experiments have not addressed temperature transients in long-term experiments or have not been able to show reproducibility of the effects (e.g., see ref. [36,51,70,72,74] as per Table 17.1).

In general, microbial growth rate and cellular metabolism increase with increasing temperature within a survival temperature range (e.g., from 10°C to 40°C for mesophiles) up to a maximum value.[54,78] Beyond this maximum value, growth rate and metabolism decrease. Therefore, a temperature shift over the optimal temperature limits, for example, from a mesophilic to a thermophilic range, is likely to lead to decreased microbial activity and represents a disturbance leading to poor treatment performance. The effects of temperature shift in the upper limit of mesophilic treatment or between mesophilic and thermophilic treatment remain to be fully characterized and fundamentally understood. Recent work in our group has focused on understanding how these transients affect aerobic treatment.

TABLE 17.1
Overview of Literature on the Effects of Temperature Transients on Wastewater Biological Treatment

Reference	System	Temperature shifts	Effect on treatment performance
Lee et al. (1975)[69]	Lab-scale aerated lagoon treating bleached kraft mill effluent	Reduction from a steady temperature of 60°C to 35°C. Increase from 35°C to 45°C (5°C/day)	No significant impact or improved treatment performance
Prensner et al. (1976)[70]	Heated rotating biological discs treating synthetic wastewater	Increase from 30°C to 32.2°C. Further increases from 32.2°C to 38°C and to 43°C within 2 days. On the subsequent 2 days, increase to 49°C and 55°C	Deterioration in treatment performance Slight improvement at the highest temperatures
Sakka et al. (1980)[71]	Culture of flocs from isolates of *Pseudomonas sp.* C-120 from activated sludge	Incubation for 5 min, at 35°C, 40°C, 45°C, 50°C, 55°C, and 65°C	Flocs began to deflocculate at temperatures higher than 40°C Complete deflocculation occurred above 55°C
Barr et al. (1996)[72]	Lab-scale activated sludge treating primary clarified bleached kraft mill effluent	Decreases in 7°C, 16.5°C, 32°C, and 40.5°C from 50°C for approximately 8 to 10 h	Deterioration proportional to the magnitude of the temperature decrease. The smallest temperature shocks (7°C, 16.5°C) had no impact
Rinkus et al. (1996)[73]	Test tubes containing oil–water emulsions (esters, oleic acid, triethanol amine)	Heating from 50°C to 70°C, 80°C, and 90°C during 10, 20, 30, 40, and 50 min at each *T*	Survival of microorganisms below 70°C only
Kriebitzsch et al. (1998)[74]	Bench-scale SBRs treating synthetic wastewater containing lignin	Increases from 30°C to 40°C, from 20°C to 30°C, and from 40°C to 50°C	Deterioration in microbial activity
Tripathi and Allen (1999)[75]	Four parallel SBRs treating bleached kraft pulp mill effluent operated at 35°C, 45°C, 55°C, and 60°C	Unsteady-state operation after increases from 35°C to 45°C, from 45°C to 55°C, and from 55°C to 65°C. From 35°C to 45°C: in 2.5°C steps, with 6 to 7 days of acclimation after each shift. From 45°C to 55°C: over 2 weeks, 3 to 4 days in between 2°C increases. From 55°C to 60°C: slow increase over 1 week	Variable and, on average, deterioration in treatment performance

TABLE 17.1 Continued

Reference	System	Temperature shifts	Effect on treatment performance
Norris et al. (2000)[76]	Bench-scale SBR treating paper mill wastewater with high organic acid levels	Increase from 25°C to 56°C over a 76-day period. Increase from 23°C to 40°C and to 45°C in 1 day	Deterioration in treatment performance
Bergeron and Paice (2001)[51]	Lab-scale activated sludge	Increase from 25°C to 40°C in 1 day; operation at 40°C for 3 days; decrease from 40°C to 25°C in 1 day	No impact on treatment performance. Increase in metabolic rates
Vogelaar et al. (2002)[77]	Lab-scale activated sludge plug flow reactor	Decrease from 55°C to 20°C within 1 day	Deterioration in treatment performance
Archibald and Young (2002)[36]	Short-term (5 min) respirometric tests with activated sludge samples	Mixed liquor samples (3 ml) adapted to 30°C to 35°C subjected for 5 min at 30°C, 40°C, 45°C, 50°C, and 55°C	Increased substrate removal capacity up to 50°C Substrate removal capacity eliminated at 55°C

17.3 BIOMASS DEFLOCCULATION UNDER TRANSIENTS OR STRESSES IN BIOLOGICAL TREATMENT SYSTEMS

17.3.1 Transients Leading to Biomass Deflocculation

Perturbations or stress conditions are known causes of biomass deflocculation, such as sudden variations in toxic compound concentrations, DO levels, pH, ionic strength, and temperature. Increases in the effluent turbidity have been related to deflocculation and weak flocculation due to several stress conditions: oxygen-supply disruption[79–81] or anaerobic storage[82]; 1000-mg/l phenol spikes [45,83]; the addition of metabolic inhibitors and decrease of temperature from 20°C to 4°C[84]; decreased[19] and increased[85] substrate loadings; low[86] or high[87] ionic strength; glucose spikes[45]; Hg (30 to 1000 mg/l), Cd (30 to 1000 mg/l), and Zn (100 to 1000 mg/l) shock doses[88]; temperature increases[71], and Cr(VI) shock doses (0.5 to 5 mg/l).[89] Activated sludge deflocculation has also been reported due to the chemical reduction of Fe(III) to FeS by the presence of sulfide,[90] and the activity of the external addition of polymer-degrading enzymes, such as deoxyribonuclease[71] and pronase.[91]

Toxic shocks have been reported to cause activated sludge deflocculation, poor treatment performance, and increased effluent turbidity. Batch shocks of aluminum sulfate and paper optical brightener concentrations were reported to decrease activated

sludge settleability, and increase discharges of effluent suspended solids.[50] Similarly, continuous exposure to Orange 3 dye in a pilot activated sludge plant resulted in decreased SOURs, increased effluent solids losses, and dispersed, pin-point growth.[49] Sludge deflocculation has been reported due to a pH shock (up to 9 for 9 h) caused by a spill of 50% sodium hydroxide solution into an activated sludge plant treating pulp and paper mill effluent,[50] due to sudden increases in hydrogen peroxide concentrations,[47] and increases in potassium concentrations (0.5 to 1 g/l influent).[92] Increased sludge supernatant turbidity due to cell detachment from flocs was also observed due to increasing surfactant concentrations (i.e., decreasing water surface tension) in batch experiments.[93]

Sludge deflocculation has been characterized by turbidity, polymeric, and suspended solids measurements in the supernatant of settled activated sludge mixed liquor, and by microscopic quantification and observation of pin-point flocs.[2,19,94] Turbidity has been correlated to the number of cells in the supernatant, and the concentrations of proteins, carbohydrates, and humic substances.[81,84] Total polysaccharides or carbohydrates have also been measured in the supernatant of deflocculated sludge.[45,83,86]

Few researchers have isolated bacteria from activated sludge and studied their flocculating characteristics via deflocculation experiments. One example is the work of Sakka et al.[71] (1981), in which deflocculation of aggregates of *Pseudomonas* sp. was caused by washings with distilled water, guanidine-HCl, and NaCl, and temperatures above 40°C. Reflocculation occurred when solutions of KCl and $MgCl_2$ were added, and the temperature was decreased to approximately 4°C.[71]

Changes in substrate types and loading rates have been observed to change the diversity of bacterial populations in anaerobic granules and render them more susceptible to disintegration. Acetoclastic methanogens have been selected over hydrogenotrophic methanogens and acetogenic bacteria due to the shift from a sugar-rich feed (alcohol distillery wastewater) to an acetate feed in a thermophilic UASB reactor.[30] Anaerobic granules with a predominant population of acetate-utilizing methanogens (*Methanosaeta* sp.) developed a porous surface and were prone to disintegration, whereas anaerobic granules with a predominant symbiotic community of acetogens and hydrogenotrophic methanogens developed smoother surfaces and compact granules.[30] Increased loading rates of oleic acid, one of the toxic long-chain fatty acids (LCFAs) to acidogens and methanogens, in an expanded granular sludge bed (EGSB) reactor have been associated with granule disintegration.[31] Anaerobic granule disintegration was related to the surfactant effect of LCFA lowering water surface tension and hindering aggregation, and to the washout of acetogenic bacteria in the granules.[31] However, the specific mechanisms of deflocculation were not identified.

17.3.2 Mechanisms of Biomass Deflocculation

Overall, the mechanisms whereby deflocculation under transients or stresses occurs are not well understood; however, these mechanisms can be divided into abiotic or biotic. Deflocculation via abiotic mechanisms proceeds via physical interactions

or chemical reactions. Conversely, microbial metabolism or physiology mediates deflocculation via biotic mechanisms.

The abiotic mechanisms of sludge deflocculation are better understood than the microbially mediated ones. Deflocculation via physical means has been shown to occur due to anaerobic reduction of Fe(III) by the presence of Fe(III)-reducing bacteria and sulfide-producing bacteria[84,86,95]; low[86] and high[87] ionic strength; the imbalance between divalent (Ca^{2+}, Mg^{2+}) and monovalent (Na^{+}) cations,[91] and the removal of Ca^{2+} from sludge flocs[86] or ionic exchange of Ca^{2+} by H^{+}, Na^{+}, K^{+}, or Mg^{2+}.[96] Sludge deflocculation has been observed to increase with increasing solids concentration and turbulent shear rates.[2] These effects have been described by an adhesion–erosion equilibrium model based on thermodynamic considerations.[2,3] The process of sludge floc deflocculation and reflocculation or reaggregation appears to be somewhat reversible[97] involving floc constituent exchange, at least under variable shear stress.[5]

Microbially mediated sludge deflocculation has been explained hypothetically under different conditions: anaerobic conditions,[81,98] phenol spikes,[83] cadmium spikes,[99] decreased metabolic activity,[84] decreased substrate loadings,[19] and due to adverse environmental conditions, such as drastic shifts in pH, temperature, and concentration of toxic compounds.[35] Deflocculation of activated sludge has been shown to occur due to the activity of exocellular proteases (pronase)[91]; however, it remains to be demonstrated that this occurs under physiological conditions.

Sludge deflocculation has been related to a reduction in microbial metabolic activity.[84] Wilén et al.[84] (2000) showed that improved sludge bioflocculation (stronger flocs) or less deflocculation (measured as less supernatant turbidity) was attained only if the microorganisms were metabolically active under aerobic conditions or in the presence of an electron acceptor, such as oxygen or nitrate under anoxic conditions. The lack of aerobic metabolic activity by the addition of azide and chloramphenicol, by anaerobic conditions, and by the reduction in temperature from 20°C to 4°C caused deflocculation. Similarly, phenol shocks were found to lower sludge ATP levels and reduce the oxygen uptake rates and cause deflocculation simultaneously.[45,83] These results suggest that microbial floc stability is directly maintained by microbial metabolism.

Transient conditions in biological treatment processes represent stresses or perturbations that seem to have similar impacts as in suspended-growth systems, that is, deflocculation and decreased activity. The mechanisms leading to these effects, however, appear to be different depending on the stress. Although the same response mechanisms may result from different transients, such as microbial cell lysis, the causes leading to these mechanisms could be different (e.g., membrane damage under phenol spikes vs death of strictly aerobic bacteria under anaerobic conditions), and are not well identified.

The poor understanding of the mechanisms of sludge deflocculation is reflected in the many hypotheses explaining its causes. Deflocculation has been explained in association with EPS, microbial community shifts, bacterial physiological responses, microbial metabolism, and abiotic processes, as outlined in Table 17.2.

Little work has been done in linking microbial physiological stress responses with the effects of stress or transient conditions on biological treatment performance.

TABLE 17.2
Hypotheses Explaining the Causes of Activated Sludge Deflocculation

Factors associated with sludge deflocculation	Hypothetical mechanisms
Extracellular polymeric substances (EPS)	Physiological inhibition of EPS production[79,83] Production of EPS degrading enzymes[101] Depletion of EPS and PHB due to substrate deficiency[19]; EPS degradation under anaerobic storage with microbial reduction of ferric iron and sulfate[98]
Microbial community shifts	Death of floc-forming bacteria with a narrow range of temperature tolerance; death of aerobic floc-forming bacteria due to anaerobic conditions; outbreak of non-flocculating populations due to phenolic step loadings causing effluent turbidity[102] Bacterial and protozoan–metazoan lysis, which deactivates bacterial flocculating properties and changes physico-chemical interactions among flocs
Bacterial physiological responses	Active movement due to signaling or chemotaxis[103] Release of proteins involved in physiological protection/detoxification mechanisms leading to deflocculation[99] Cell lysis leading to biomass reduction[35]; lysis due to cell membrane damage under phenolic shocks[83] Anaerobically mediated reduced hydrophobicity[104] Microbial death from a temperature downshift from 50°C to 9.5°C[72]
Microbial metabolism	Lack of terminal electron acceptors: oxygen under anaerobic conditions; nitrate under anoxic conditions[84] Increased feed toxicity to microorganisms due to a temperature downshift from 50°C to 9.5°C[72]
Abiotic processes	Decrease in surface hydrophobicity and change in physico-chemical properties,[105] and decrease in hydrophobic interactions.[77] Decreased sludge hydrophobicity, as measured under phenolic shocks,[83] probably due to the effect of lysed microbial products and the amphiphatic properties of phenol Contraction and expansion of adhesive polymers[87] Solubilization of EPS, such as of bound lipids by specific solvents (methanol, n-butanol) in yeast aggregates[106] Reduced solution ionic strength in sludge whose structure is dependent in double-layer electrostatic interactions or ionic bridging[5] Ion exchange of Ca^{2+} by K^{+} and Mg^{2+} released by polyphosphate accumulating bacteria under anaerobic storage[82] Decreased sludge adsorption capacity of contaminants due to anaerobic conditions[80]

Only recently, Love and Bott[100] (2002) hypothesized how different microbial stress responses to oxidative chemicals lead to decreased BOD removals, increased colloidal suspended solids, and affected sludge bioflocculation. Love and Bott[100] (2002) suggested that *cis–trans* isomerization of unsaturated fatty acids (i) decreases substrate active transport through the membrane and increases effluent BOD due to decreased membrane fluidity; (ii) changes the membrane surface chemistry, affecting bioflocculation; and (iii) alters the transport rate of extracellular hydrolytic enzymes, decreasing colloidal material biodegradation. Love and Bott[100] (2002) also hypothesized that decreased COD removals are related to redirecting energy from growth to stress protein synthesis, but this hypothesis was discarded when the induction of the stress protein GroEL was not correlated to poor COD removals in sludge deflocculation experiments. Nevertheless, deflocculation due to electrophilic stressors has been correlated to K^+ efflux from activated sludge flocs into bulk liquid. Potassium-ions efflux may increase local K^+ concentrations inside flocs and increase the monovalent to divalent cation ratio, causing weak floc structure and deflocculation. Potassium-ions efflux is a possible stress response mechanism that directly relates to deflocculation.[100]

Only hypotheses have been put forward for explaining anaerobic granule disintegration. Under a thermophilic temperature shift from 55°C to 65°C, Uemura et al.[63] (1995) explained anaerobic granule disintegration by digestion of EPS and microbial cells, and by the selective lysis of acidogens due to the temperature shift. Under a temperature shift from 38°C to 75°C in an UASB reactor, biomass granulation was hindered by the growth in suspension of active methanogens that were eventually washed out.[67] Van Lier et al.[67] (1992) explained granule disintegration due to a temperature increase from 38°C to 55°C in an UASB reactor by the absence of acidifying bacteria and their metabolites. The anaerobic granules at 55°C showed a spongy appearance both in the core or medulla and the surrounding cortex 4 months after increasing the temperature from 38°C to 55°C, and were observed to eventually wash out from the reactor. The formation of these spongy granules may have been favored by the VFA-based substrate (without sugars).[67]

The understanding of the mechanisms governing the flocculation of some industrially significant yeast systems is much more advanced than that of bacterial or microbial-community flocs in biotreatment. This derives from the longer history of brewing processes and also the homogeneity of these types of aggregates; yeast flocs are generally formed by yeast cells from the same flocculating species. An extensive and detailed review has been conducted by Calleja,[1] who also reports the many reviews on the topic before 1981. Reports on deflocculation of aggregates from brewer's yeast date from 1896, and yeast deflocculation has been experimentally investigated under gravity sedimentation, sugar spikes, heating, low ionic strength, removal of Ca^{2+}, and protein denaturation due to proteases, alkali, or urea. Flocculation of yeast is so well understood that the nature of the binding forces that keep yeast cells together are known, and the effect of physico-chemical parameters have been well characterized.[1] For example, flocculating and non-flocculating yeast strains are known, yeast flocculation is known to depend on wall–wall interactions involving proteins and glycoproteins on the protein-manan layer, hydrogen bonds are the principal forces involved in yeast flocculation, and deflocculation is reversible as long

as protein denaturation does not occur. The experience and knowledge accumulated through the study of yeast aggregates can likely find parallels in the study of bacterial and mixed community flocs in biotreatment.

Finally, one important aspect that must be remembered when studying deflocculation is that there is a wide range of floc strength values within activated sludge or anaerobic granules, as work on activated sludge sonication suggests.[107] Deflocculation may be related to the fraction of flocs with low floc strength.

17.4 MECHANISMS OF ACTIVATED SLUDGE DEFLOCCULATION UNDER MESOPHILIC–THERMOPHILIC TEMPERATURE TRANSIENTS

Recent research in our laboratory has been focused on assessing the impacts of temperature shifts from 30°C or 35°C to 45°C on the treatment performance of activated sludge.[108] As part of this research, activated sludge deflocculation under such temperature shifts has been identified and studied.[109] The impacts of these temperature transients with respect to deflocculation mechanisms are discussed in the following sections.

17.4.1 Sludge Floc Responses to the Temperature Shifts

The temperature shift stress from 30°C or 35°C to 45°C caused three major responses in activated sludge flocs, as assessed in continuous sequencing batch reactors (SBRs) treating pulp and paper mill effluent, and in batch experiments with fresh municipal sludge. The three responses were decreased or more negative sludge surface charge,[108] increased maintenance respiration rates, and sublethal inhibition of metabolism or decreased substrate removal capacity. Figure 17.1 and Figure 17.2 show the effects of the temperature shift from 30°C to 45°C on increasing maintenance respiration rates and inhibiting metabolism of activated sludge in batch and continuous experiments, respectively.

Figure 17.1 and Figure 17.2 present measurements of three specific oxygen uptake rates (SOURs) conducted to assess the sludge substrate removal capacity: the mixed liquor standard SOUR, the SOUR of mixed liquor diluted by 10% with raw wastewater ($SOUR_{10\%}$), and the SOUR of mixed liquor diluted by 50% with raw wastewater ($SOUR_{50\%}$). The measurement of SOURs in samples that are diluted with raw wastewater ($SOUR_{10\%}$ and $SOUR_{50\%}$) is comparable with traditional respirometric assays with substrate addition, and has been proposed by Archibald et al.[46] (2001) and Archibald and Young[36] (2002) to monitor sludge activity under different stresses. These measurements allow for a comparative assessment of sludge oxygen consumption rates associated with the endogenous respiration phase and with substrate uptake rates under transients and stresses. Details of this are explained elsewhere.[46,51]

The decrease in the sludge substrate removal capacity is demonstrated by the significant decrease in the three sets of SOURs after the temperature shift. The

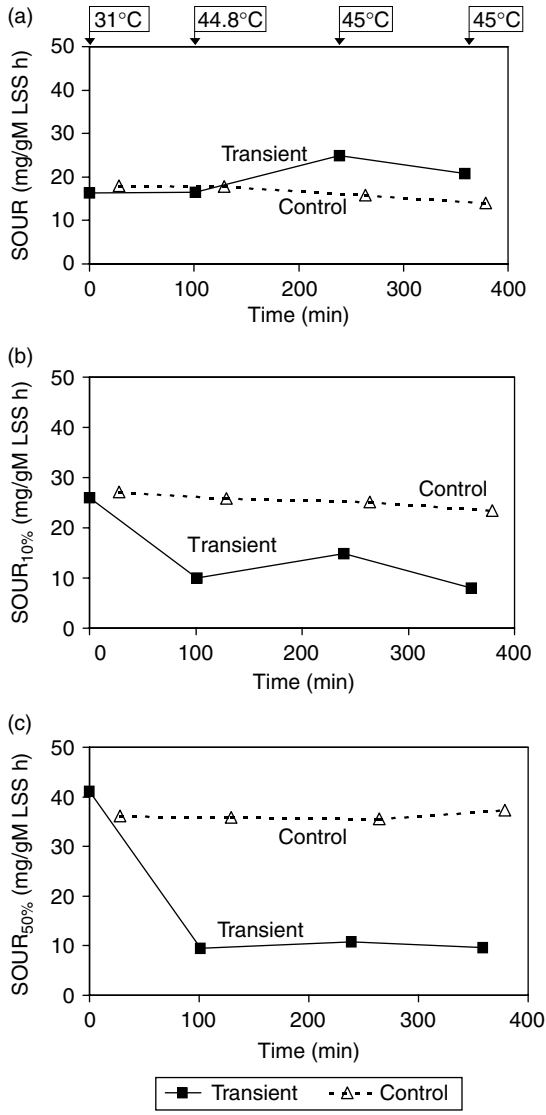

FIGURE 17.1 Profiles of (a) standard specific oxygen uptake rates (SOUR), (b) SOUR with 10% feed dilution ($SOUR_{10\%}$), and (c) SOUR with 50% feed dilution ($SOUR_{50\%}$) from the control reactor at 31°C and the transient reactor under a shift from 31°C to 45°C. The temperatures in the transient reactor at the moment of sampling are indicated at the top of the figure. Time = 0 corresponds to the time when the temperature was changed in the water bath.

$SOUR_{10\%}$ and $SOUR_{50\%}$ after the temperature shift were significantly lower compared with the $SOUR_{10\%}$ and the $SOUR_{50\%}$ from the control reactor and before the shift (Figure 17.1b,c and Figure 17.2b,c). The standard SOURs (without feed dilution) after the shift during the first hours of the reaction phase (Figure 17.2a) were also

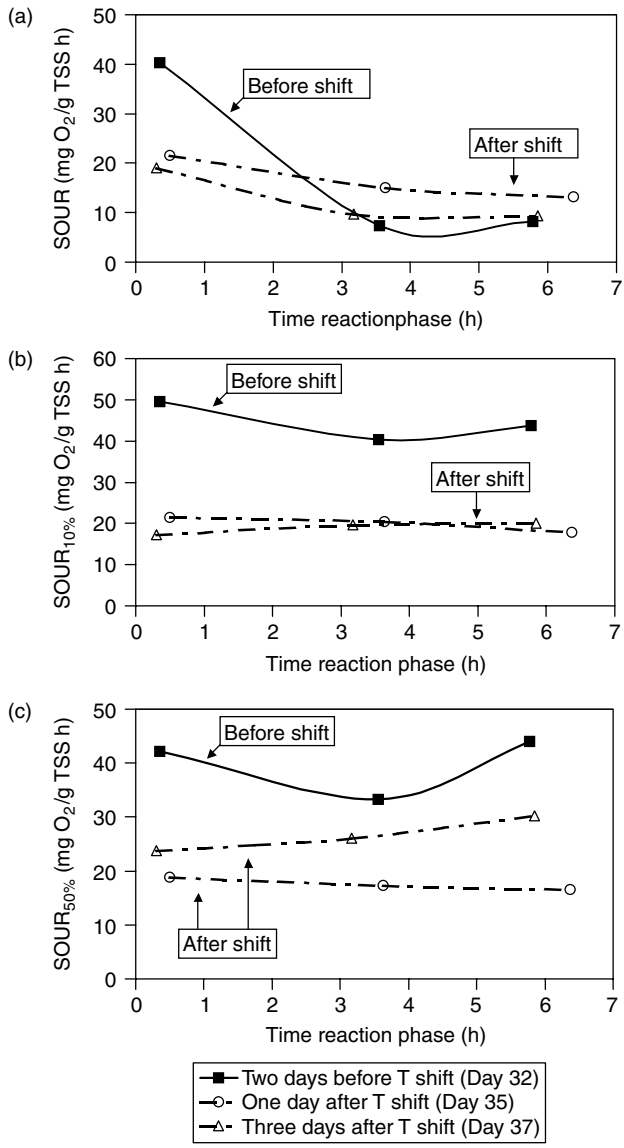

FIGURE 17.2 Typical SOUR profiles during the reaction phase of an operating cycle of an SBR before and after a temperature shift from 30°C to 45°C. (a) SOURs without feed addition; (b) SOURs with 10% dilution with feed ($SOUR_{10\%}$); (c) SOURs with 50% dilution with feed ($SOUR_{50\%}$). The 30°C to 45°C temperature shift took place on Day 34.

lower than the SOUR before the shift. In the control reactor, at a constant temperature of 30°C, the standard SOUR, the $SOUR_{10\%}$, and the $SOUR_{50\%}$ remained constant during the experiments. This was consistent with a healthy sludge under limited substrate conditions with a high substrate removal capacity in the control reactor. The

control reactor's $SOUR_{10\%}$ and the $SOUR_{50\%}$ were greater than the standard SOUR, indicating that the sludge biomass was under starvation and had a higher substrate removal capacity.

The SOUR profiles during the reaction phase indicate substrate utilization at the beginning (<3 h) and starvation at the end (hours 3 to 6 of the reaction phase before the temperature shift; Figure 17.2). The substrate uptake profiles during the reaction phase of the SBRs prior to the temperature shifts were consistent with the standard SOUR profiles. During the reaction phase before the shift, the $SOURs_{10\%}$ and $SOURs_{50\%}$ were higher than the standard SOURs consistent with higher oxygen requirements associated with increased feed. Higher $SOURs_{10\%}$ and $SOURs_{50\%}$ than SOURs describe a healthy sludge able to utilize substrate to which it is acclimated. At the end of the reaction phase, the $SOURs_{10\%}$ tended to decrease slightly (Figure 17.2b); however, the $SOURs_{50\%}$ increased significantly (Figure 17.2c), indicating a high substrate removal capacity by starving sludge. Starving conditions are inherent to SBR operation[13] and microbial internal decay or endogenous respiration is associated with these conditions.[35]

The set of three SOURs measured during the reaction phase of the SBRs under the temperature transient showed the inhibition of the sludge substrate removal capacity and increased respiration rates during the endogenous respiration phase. The temperature stress caused the SOUR to decrease at the beginning of the reaction phase and to increase at the end of the reaction phase, relative to the control (Figure 17.2a). This suggests that increased respiration rates are a stress response of the microorganisms to the shift from 30°C to 45°C. These increased respiration rates are not indicative of higher substrate uptake rates, as demonstrated by the reduced $SOUR_{10\%}$ and $SOUR_{50\%}$. The increased respiration rates relative to the control occurred only at the end of the reaction phase when part of the available substrate had been utilized, and the sludge is not at its highest substrate removal capacity. This is in agreement with the higher standard SOUR measured after the temperature shift in the transient reactor compared to the standard SOURs in the control in batch experiments (Figure 17.1a).

The activated sludge floc responses and how they could relate to sludge deflocculation and impaired treatment performance are presented in Figure 17.3. The link between increased maintenance respiration rates, more negative sludge surface charge, and sublethal metabolic inhibition, and sludge deflocculation and treatment performance can only be hypothesized, and remains a research area in need of further investigation.

Increased maintenance respiration rates can be explained by increased microbial maintenance requirements as a sublethal–inhibition stress response to the temperature shifts. High maintenance requirements and intense metabolism (high biochemical activity) have been associated with thermophilic organisms.[110–112] It is probable that microorganisms under a heat shock stress may induce an active metabolism to be able to repair damage by heat.[111] Misfolded protein detection is considered to be a mechanism of heat shock response initiating protein folding, degradation, and resynthesis,[113] processes which are known to be maintenance functions.[114] Variations in microbial energy maintenance requirements occur via energy loss mechanisms; energy spilling is a mechanism considered to protect cells from toxicity resulting from sudden sugar

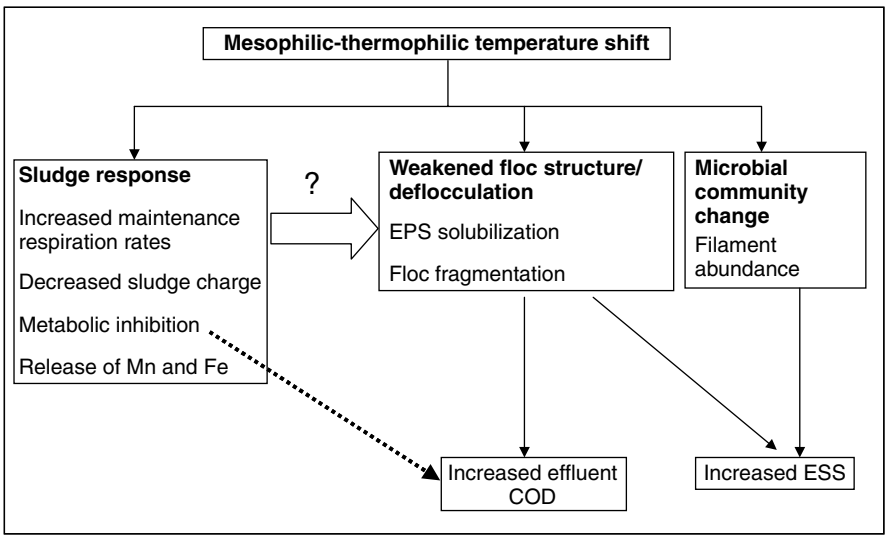

FIGURE 17.3 Sludge floc responses, sludge deflocculation, and treatment performance effects of a temperature shift from 30°C to 35°C to 45°C, as identified in research.[109]

metabolism (as from glucose pulse doses).[114] The actual mechanisms of this extra energy spilling remain unclear and similar microbial energetic mechanisms could be triggered by heat stress.

The generation of negative sludge charge due to the temperature shift[108,109] can have different causes. The adsorption of solubilized EPS or lysed soluble microbial products bearing negative charges (e.g., sulfate-, hydroxyl-, and carboxyl-containing polysaccharides, polypeptides, and humic substances) onto remaining sludge flocs could have rendered the sludge more negatively charged. EPS biopolymers with anionic functional groups tend to decrease the sludge surface charge, as experimentally shown by Mikkelsen et al.[115] (1996) using an anionic detergent. This adsorption process is suspected to be collateral to a major cause driving the more negatively charged sludge. The decrease in sludge surface charge is not an immediate response and it takes from 1–2 to 8 days to manifest itself.[108]

The decrease in sludge surface charge may arise from bacterial physiological stress responses. The degree of unsaturation of fatty acids in the cytoplasmic membrane is thought to control the cellular stress response to temperature changes.[116] Heat shocks could increase cytoplasmic membrane flexibility, which could trigger microorganisms to increase the levels of saturated fatty acids in the membrane phospholipids to decrease membrane fluidity and cope with increasing membrane fluidity. Saturation of phospholipids could be achieved by negatively charged groups that render the cell surface more negatively charged. An increase in saturated fatty acids in the cytoplasmic membrane, as a primary heat shock sensor, has been correlated to the heat shock induction of messenger RNA (mRNA) transcripts in yeasts.[117] Gaughran[110] (1947) reported experiments showing the occurrence of more saturated fatty acids in bacteria (*Bacillus subtilis*) and moulds (*Aspergillus niger*) at higher

temperatures (e.g., from 14°C to 38°C), even above optimal-growth temperatures. A decrease in cytoplasmic membrane fluidity, transforming the liquid crystalline membrane into a gel-phase state, results from cold shocks and induces the increase in membrane unsaturated fatty acids that lower the membrane phospholipid melting point and add membrane flexibility.[116]

The so-called "compatible solutes" are known to be synthesized or taken up from the environment due to hyperosmotic environmental stress, but also due to cold shocks, desiccation, and heating.[118] Although compatible solutes are generally polar and neutral at physiological pH, negatively charged organic osmolytes (e.g., sulfotrehalose, diglycerolphosphate) are used by thermophilic Archaea.[118] It is possible that such compounds accumulate in the sludge flocs when released from some cells under heat stress and promote more negatively charged flocs. Increased transport of osmolytes and polymerization reactions are energy demanding cellular processes that would increase respiration rates due to increased energy maintenance.[114]

17.4.2 Proposed Mechanisms of Sludge Deflocculation

The recent research in our group has identified that temperature shifts from 30°C or 35°C to 45°C cause activated sludge deflocculation, which occurs via polymer solubilization and floc fragmentation, leading to poor treatment performance.[109] In this section, several mechanisms that could link the occurrence of sludge deflocculation with decreased metabolic activity, more negatively charged sludge and increased maintenance respiration rates are discussed. A summary is presented in Figure 17.4.

Sludge deflocculation resulting from a temperature shift from 30°C or 35°C to 45°C could be explained by the abiotic change of the physico-chemical characteristics of the sludge flocs and by microbially mediated mechanisms that reduce microbial substrate removal capacity, increase respiration rates, and decrease sludge surface charge. Metabolic inhibition leading to decreased sludge substrate removal capacity could directly induce deflocculation due to a "flocculating-ability shut-off mechanism." This would be similar to negative cellular control mechanisms. Other physiologically mediated mechanisms could render the sludge surface more negatively charged, lead to EPS solubilization, and to the release of soluble products from the cells.

Microbial metabolism could be an indispensable requirement for sludge floc stability; therefore, a significant reduction in sludge substrate uptake would dissipate the sludge flocculating ability. Whatever the actual cellular mechanisms of metabolic inhibition in deflocculation be, the results from the present study agree with the findings of Schwartz-Mittelmann and Galil[83] (2000) and Wilén et al.[81,84] (2000), in that suppression of metabolism leads to deflocculation. Sludge deflocculation, however, may be governed by different mechanisms under different stress conditions.

The temperature shifts could also increase the cytoplasmic membrane permeability. Elevated temperatures may increase the cell membrane proton permeability and uncouple oxidative phosphorylation, as reviewed by Low and Chase[119] (1999).

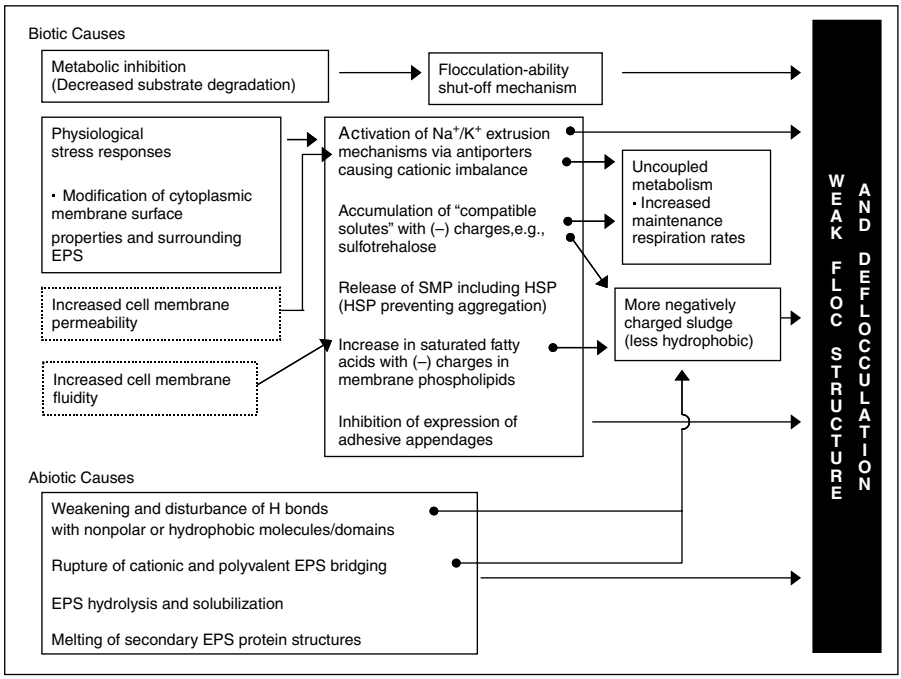

FIGURE 17.4 Proposed mechanisms of activated sludge deflocculation under a temperature shift from 30°C to 45°C. SMP — soluble microbial products, HSP — heat shock proteins, EPS — extracellular polymeric substances.

Increased membrane permeability could cause Na^+ stress due to high internal cellular Na^+ concentrations, leading to the activation of Na^+ (and even K^+) extrusion mechanisms via antiporters, known to be involved in bacterial Na^+ and pH stress responses.[120,121] This would cause an increase in the local levels of monovalent cations in the EPS, as also proposed by Love and Bott[100] (2002) under oxidative stress, and cause sludge floc instability and deflocculation. The activation of respiration-coupled Na^+ extrusion mechanisms[121] or futile ion cycles would cause an increase in respiration rates providing for increased maintenance energy requirements.[114,119] This would explain the higher maintenance respiration rates observed after the temperature shifts during endogenous metabolism.

The accumulation of compatible solutes with negative charges on the flocs and the increase in saturated fatty acids in membrane phospholipids with negative charges have been discussed in Section 17.4.1 above as physiological stress responses of bacteria explaining the decrease in surface charge under the temperature shifts (Figure 17.4). Also, the temperature upshift may inhibit the expression of adhesive appendages in cells (pili and fimbriae) that are responsible for cell attachment and are regulated by several environmental factors, including temperature.[122,123] At this point in time, the connecting mechanisms between physiological stress responses to mesophilic–thermophilic temperature shifts and sludge deflocculation remain unknown.

The response of the sludge flocs to the mesophilic–thermophilic temperature shifts could also be abiotic. Sludge physico-chemical changes triggered by the temperature shifts could include the melting of secondary structures of proteins present in EPS and in the cellular membrane, and temperature-induced EPS hydrolysis, destroying the aggregating properties of a fraction of these biopolymers and solubilizing them. Also, EPS bridging could be compromised by the weakening of hydrogen bonds that keep EPS flocculated via bridging, and the weakening and rupture of cationic and polyvalent EPS bridging (e.g., by Mn(II) and Fe(II)). The release of cations from the rupture of cationic EPS bridging could also promote an increase in the relative abundance of adsorbed anionic functional groups onto floc EPS, rendering the sludge more negatively charged. Therefore, the decrease in surface charge could also be a result of a pure abiotic process. More negatively charged cells could cause further desorption of EPS due to high electrostatic repulsion, as suggested by Erdincler and Vesilind [124] (2000). Another abiotic explanation is that increased temperature disturbs the orientation of water molecules interacting via hydrogen bonds with nonpolar or hydrophobic molecules or domains, as suggested by Vogelaar et al.[77] (2002), which would agree with the decreased hydrophobicity of the sludge.

The relative extent of deflocculation due to biotic and abiotic mechanisms is unknown. Nevertheless, the temperature shifts can be postulated to have a greater impact on deflocculation as EPS solubilization via abiotic mechanisms than biotic mechanisms governed by active metabolism. This idea is supported by the relatively large amount of organic biomass detached from sludge flocs due to the temperature shift from 30°C to 45°C vs that detached due to suppression of aerobic metabolism reported by Wilén et al. (2000).[81] Whereas the 30°C to 45°C temperature shift caused an approximate 11% reduction in the total organic biomass (in batch experiments), only 1% to 2% of the total amount of organic sludge matter detached under suppressed aerobic metabolism.[81] The abiotic mechanisms of the temperature shifts seem predominant vs those regulated by active metabolism, considering that cell viability was not significantly affected[109] and that a low percentage of viable cells is present in activated sludge at high SRTs (10% to 15% of MLSS).[125]

In general, under microbial stress conditions, sludge bacterial lysis may be involved in the mechanisms of sludge deflocculation as a consequence of inactivation of cell metabolism and cell death, and as a source of biopolymers that decrease sludge stability. Although sludge lysis occurred due to the temperature shift from 30°C to 45°C, it was marginal[109] and would minimally affect deflocculation significantly. Under other stress conditions (e.g., toxic shocks or drastic temperature shifts over 55°C to 60°C), however, cell death and lysis may weaken the sludge floc structure and cause deflocculation by directly affecting cell metabolism.[126,127]

17.5 SUMMARY AND FUTURE PERSPECTIVES

Engineered microbial systems frequently encounter transient or dynamic conditions. Microbial systems where biomass form aggregates, flocs, or granules are sensitive to transients, as is the case of anaerobic and aerobic biological processes treating wastewater. Weakening of microbial aggregate structure and

disintegration of bioaggregates, that is, deflocculation, appear to be common responses of suspended biomass to transient operating conditions and environmental stresses.

Transient conditions leading to poor treatment performance represent a challenge in biological wastewater treatment due to poor pollutant removal efficiency, high effluent suspended solids (ESS), and variable overall performance. Some of the impacts of transients in biological wastewater treatment systems have been identified in this chapter. For example, substrate and toxic compound perturbations have been related to high ESS, poor pollutant removal efficiencies, poor sludge settling, and sludge deflocculation. Biomass deflocculation is of particular interest because it leads to the loss of biocatalyst, the discharge of suspended solids and of solids-associated bioactive compounds. Biomass deflocculation in aerobic and anaerobic processes treating wastewater has been identified to occur under shocks of toxic compounds, low dissolved oxygen concentrations, and temperature.

Although deflocculation under different transients and stresses in biological treatment systems is becoming a well-characterized phenomenon, the actual mechanisms whereby deflocculation occurs remain little understood. Some abiotic processes leading to activated sludge deflocculation have been reported in the literature, such as the removal of Ca^{2+} from flocs and Fe(III) reduction to Fe(II) by the presence of sulfide or iron-reducing bacteria. Many microbially mediated mechanisms have been proposed to explain biomass deflocculation both in aerobic and anaerobic processes. These mechanisms are diverse: decreased microbial metabolism, degradation of EPS, physiological stress responses, and modified floc physico-chemical properties. However, the biotic mechanisms of sludge deflocculation remain to be proven.

Recent research in our group has shown that activated sludge deflocculation occurs due to temperature shifts in the upper limit of mesophilic treatment due to temperature shifts from 30°C to 45°C. Activated sludge deflocculation was identified to take place by the solubilization of extracellular polymeric substances (EPS) and floc fragmentation, which impaired overall treatment performance. Several mechanisms that could link the occurrence of sludge deflocculation with inhibition of metabolic activity, more negatively charged sludge, and increased maintenance respiration rates were proposed. However, the responses of aggregates of microbial communities, like that of activated sludge, to transient conditions and deflocculation need to be better understood. Important areas of future research, where work has already begun, are the link of microbial physiological stress responses with biomass deflocculation and poor treatment performance, the characterization of the chemical nature and adhesive properties of EPS in microbial aggregates under transient conditions, and the characterization of the microbial community structure of flocculent and non-flocculent biomass.

A better understanding of mixed-culture and bacterial flocculation and deflocculation can be achieved by learning from the experience on yeast flocculation. The more fundamental understanding of how yeast aggregate and the experimental approaches used to identify the governing forces in maintaining yeast cells flocculated can serve as guidelines for improving the understanding of other microbial aggregation phenomena.

REFERENCES

1. Calleja, G.B., Cell aggregation, in *The Yeasts*, A.H. Rose and J.S. Harrison, Eds, Academic Press Inc., London, UK, pp. 165–237, 1987.
2. Mikkelsen, L.H. and Keiding, K., Equilibrium aspects of the effects of shear and solids content on aggregate deflocculation, *Adv. Colloid Interface Sci.*, 80, 151–182, 1999.
3. Mikkelsen, L.H. and Keiding, K., The shear of activated sludge: an evaluation of the possibility for a standardised floc strength test, *Water Res.*, 36, 2931–2940, 2002.
4. Biggs, C.A. and Lant, P.A., Activated sludge flocculation: on-line determination of floc size and the effect of shear, *Water Res.*, 34(9), 2542–2550, 2000.
5. Chaignon, V., Lartiges, B.S., El Samrani, A., and Mustin, C., Evolution of size distribution and transfer of mineral particles between flocs in activated sludge: an insight into floc exchanges dynamics, *Water Res.*, 36, 676–684, 2002.
6. Glasgow, L.A. and Luecke, R.H., Mechanisms of deaggregation for clay-polymer flocs in turbulent systems, *Ind. Eng. Chem. Fundam.*, 19, 148–156, 1980.
7. Liu, S.X. and Glasgow, L.A., Aggregate disintegration in turbulent jets, *Water Air Soil Pollut.*, 95, 257–275, 1997.
8. Ellis, C.E. and Glasgow, L.A., Deformability and breakage of flocs, *Adv. Environ. Res.*, 3(1), U2–27, 1999.
9. Glasgow, L.A., Deformation of individual aggregates and flocs, *J. Disper. Sci. Technol.*, 24(5), 715–720, 2003.
10. Berkeley, R.C.W., Lynch, J.M., Melling, J., Rutter, P.R., and Vincent, B., Eds., *Microbial Adhesion onto Surfaces*, Ellis Horwood Ltd., Chichester, West Sussex, England, 1980.
11. Fletcher, M., Bacterial attachment in aquatic environments: a diversity of surfaces and adhesion strategies, in *Bacterial Adhesion: Molecular and Ecological Diversity*, M. Fletcher, Ed., Wiley-Liss, Inc., New York, pp. 1–24, 1996.
12. Marshall, K.C., Ed., *Report on the Dahlem Workshop on Microbial Adhesion and Aggregation*, Life Sciences Research Reports, S. Bernhard, Ed., Springer-Verlag, Berlin, Germany, 1984.
13. Irvine, R.L., Wilderer, P.A., and Flemming, H.-C., Controlled unsteady state processes and technologies — An overview, *Water Sci. Technol.*, 35(1), 1–10, 1997.
14. Majone, M., Dircks, K., and Beun, J.J., Aerobic storage under dynamic conditions in an activated sludge processes. The state of the art, *Water Sci. Technol.*, 39(1), 61–73, 1999.
15. Daigger, G.T. and Grady, C.P.L.J., The dynamics of microbial growth on soluble substrates. A unifying theory, *Water Res.*, 16(4), 365–382, 1982.
16. Lishman, L.A., Legge, R.L., and Farquhar, G.J., Temperature effects on wastewater treatment under aerobic and anoxic conditions, *Water Res.*, 34(8), 2263–2276, 2000.
17. Neubauer, P., Häggström, L., and Enfors, S.-O., Influence of substrate oscillations on acetate formation and growth yield in *Escherichia coli* glucose limited fed-batch cultivations, *Biotechnol. Bioeng.*, 47(2), 139–146, 1995.
18. Majone, M., Massanisso, P., and Ramadori, R., Comparison of carbon storage under aerobic and anoxic conditions, *Water Sci. Technol.*, 38(8–9), 77–84, 1998.
19. Barbusinski, K. and Koscielniak, H., Influence of substrate loading intensity on the floc size in activated sludge process, *Water Res.*, 29(7), 1703–1710, 1995.
20. Grau, P., Chudoba, J., and Dohanyos, M., Theory and practice of accumulation-regeneration approach to the control of activated sludge filamentous bulking, in *Bulking of Activated Sludge: Preventative and Remedial Methods*, B. Chambers and

E.J. Tomlinson, Eds, Ellis Horwood Limited, Chichester, West Sussex, England, pp. 111–122, 1982.
21. Farrugia, V.M., The development and properties of biofilms in biofilters, Master of Applied Science thesis, Department of Chemical Engineering and Applied Chemistry, University of Toronto, Ontario, Canada, 1999.
22. LeBlanc, M.-A., Control of filamentous bulking and oxygen transfer in a pulp and paper sequential batch reactor (SBR), in *Proc. Int. Environ. Conf. Exhibit*, TAPPI Press, Vancouver, British Columbia, 1998.
23. Krishna, C. and Van Loosdrecht, M.C.M., Effect of temperature on storage polymers and settleability of activated sludge, *Water Res.*, 33(10), 2374–2382, 1999.
24. Thompson, G., Swain, J., Kay, M., and Forster, C.F., The treatment of pulp and paper mill effluent: a review, *Bioresour. Technol.*, 77, 275–286, 2001.
25. Borja, R. and Banks, C.J., Response of an anaerobic fluidized bed reactor treating ice-cream wastewater to organic, hydraulic, temperature and pH shocks, *J. Biotechnol.*, 39, 251–259, 1995.
26. Paula Jr., D.R. and Foresti, E., Kinetic studies on a UASB reactor subjected to increasing COD concentration, *Water Sci. Technol.*, 25(7), 103–111, 1992.
27. Nachaiyasit, S. and Stuckey, D.C., The effect of shock loads on the performance of an anaerobic baffled reactor (ABR). 1. Step changes in feed concentration at constant retention time, *Water Res.*, 31(11), 2737–2746, 1997.
28. Nachaiyasit, S. and Stuckey, D.C., The effect of shock loads on the performance of an anaerobic baffled reactor (ABR). 2. Step and transient hydraulic shocks at constant feed strength, *Water Res.*, 31(11), 2747–2754, 1997.
29. Xing, J., Criddle, C., and Hickey, R., Effects of a long-term periodic substrate perturbation on an anaerobic community, *Water Res.*, 31(9), 2195–2204, 1997.
30. Syutsubo, K., Sinthurat, N., Ohashi, A., and Harada, H., Population dynamics of anaerobic microbial consortia in thermophilic granular sludge in response to feed composition change, *Water Sci. Technol.*, 43(1), 59–66, 2001.
31. Pereira, M.A., Roest, K., Stams, A.J.M., Akkermans, A.D.L., Amaral, A.L., Pons, M.-N., Ferreira, E.C., Mota, M., and Alves, M.M., Image analysis, methanogenic activity measurements, and molecular biological techniques to monitor granular sludge from an EGSB reactor fed with oleic acid, *Water Sci. Technol.*, 47(5), 181–188, 2003.
32. Henriques Callado, N. and Foresti, E., Response of an upflow anaerobic sludge blanket reactor to increasing sulfate concentrations, in *Proc. 47th Industr. Waste Conf.*, Lewis Publishers, Purdue University, West Lafayette, IN, 1992.
33. Hall, E.R., Melcer, H., Cornacchio, L.-A., and Jones, R.M., Anaerobic treatment for pulp and paper wastewaters, in *Anaerobic Treatment of Industrial Wastewaters*, M.F. Torpy, Ed., Noyes Data Corporation, Park Ridge, NJ, pp. 15–22, 1988.
34. Gross, R.L. and Lanting, J., Anaerobic wastewater treatment of a fuel ethanol facility, in *Anaerobic Treatment of Industrial Wastewaters*, M.F. Torpy, Ed., Noyes Data Corporation, Park Ridge, NJ, pp. 23–34, 1988.
35. Van Loosdrecht, M.C.M. and Henze, M., Maintenance, endogenous respiration, lysis, decay and predation, *Water Sci. Technol.*, 39(1), 107–117, 1999.
36. Archibald, F. and Young, F. Common stresses affecting activated sludge health and performance — What the four-assay set can tell us, in *Proc. Int. Environ. Conf. Exhibit*, TAPPI Press, Montreal, Quebec, Canada, 2002.
37. Dikshitulu, S., Baltzis, B.C., and Lewandowski, G.A., Competition between two microbial populations in a sequencing fed-batch reactor: theory, experimental

verification, and implications for waste treatment applications, *Biotechnol. Bioeng.*, 42(5), 643–656, 1993.
38. Lenas, P., Baltzis, B.C., Lewandowski, G.A., and Ko, Y.-F., Biodegradation of wastes in a cyclically operated reactor: theory, experimental verification and optimization studies, *Chem. Eng. Sci.*, 49(24A), 4547–4561, 1994.
39. Stephanopoulos, G., Fredrickson, A.G., and Aris, R., The growth of competing microbial populations in a CSTR with periodically varying inputs, *AIChE J.*, 25(5), 863–872, 1979.
40. Fernandez, A.S., Hashsham, S.A., Dollhopf, S.L., Raskin, L., Glagoleva, O., Dazzo, F.B., Hickey, R.F., Criddle, C.S., and Tiedje, J.M., Flexible community structure correlates with stable community function in methanogenic bioreactor communities perturbed by glucose, *Appl. Environ. Microbiol.*, 66(9), 4058–4067, 2000.
41. Hashsham, S.A., Fernandez, A.S., Dollhopf, S.L., Dazzo, F.B., Hickey, R.F., Tiedje, J.M., and Criddle, C.S., Parallel processing of substrate correlates with greater function stability in methanogenic bioreactor communities perturbed by glucose, *Appl. Environ. Microbiol.*, 66(9), 4050–4057, 2000.
42. Pernelle, J.-J., Gaval, G., Cotteux, É., and Duchène, P., Influence of transient substrate overloads on the proliferation of filamentous bacterial populations in an activated sludge pilot plant, *Water Res.*, 35(1), 129–134, 2001.
43. González-Martínez, S., Staud, R., Wilderer, P.A., Hartman, L., and Norouzian, M., Alternating aerobic and anaerobic operation of an activated sludge plant, *J. WPCF*, 59(2), 65–71, 1987.
44. Horntvedt, B.R., Rambekk, M., and Bakke, R., Oscillating conditions for influencing the composition of mixed biological cultures, *Water Sci. Technol.*, 37(4–5), 259–262, 1998.
45. Galil, N.I., Schwartz-Mittelman, A., and Saroussi-Zohar, O., Biomass deflocculation and process disturbances exerted by phenol induced transient load conditions, *Water Sci. Technol.*, 38(8–9), 105–112, 1998.
46. Archibald, F., Méthot, M., Young, F., and Paice, M.G., A simple system to rapidly monitor activated sludge health and performance, *Water Res.*, 35(10), 2543–2553, 2001.
47. Larisch, B.C. and Duff, S.J.B., Effect of H_2O_2 and DTPA on the characteristics and treatment of TCF (totally chlorine-free) and ECF (elementally chlorine-free) kraft pulping effluents, *Water Sci. Technol.*, 35(2–3), 163–171, 1997.
48. Karthikeyan, S., Wolfaardt, G.M., Korber, D.R., and Caldwell, D.E., Functional and structural responses of a degradative microbial community to substrates with varying degrees of complexity in chemical structure, *Microb. Ecol.*, 38, 215–224, 1999.
49. Keech, G.W., Whiting, P., and Allen, D.G., Effect of paper machine additives on the health of activated sludge, *TAPPI J.*, 83(3), 86–93, 2000.
50. Sarlin, T., Halttunen, S., Vuoriranta, P., and Puhakka, J., Effects of chemical spills on activated sludge treatment performance in pulp and paper mills, *Water Sci. Technol.*, 40(11–12), 319–325, 1999.
51. Bergeron, J. and Paice, M., Monitoring of activated sludge systems using a combination of specific oxygen uptake rates and specific adenosine triphosphate measurements, *Water Qual. Res. J. Canada*, 36(4), 659–685, 2001.
52. Dalzell, D.J.B., Alte, S., Aspichueta, E., de la Sota, A., Etxebarria, J., Gutierrez, M., Hoffmann, C.C., Sales, D., Obst, U., and Christofi, N., A comparison of five rapid

direct toxicity assessment methods to determine toxicity of pollutants to activated sludge, *Chemosphere*, 47, 535–545, 2002.
53. Carvalho, G., Paul, E., Novais, J.M., and Pinheiro, H.M., Studies on activated sludge response to variations in the composition of a synthetic surfactant-containing feed effluent, *Water Sci. Technol.*, 42(5–6), 135–143, 2000.
54. Madigan, M.T., Martinko, J.M., and Parker, J., *Brock Biology of Microorganisms*, 8th ed., Prentice-Hall Inc., Upper Saddle River, NJ, 1997.
55. Yu, Z. and Mohn, W.W., Bioaugmentation with the resin acid-degrading bacterium *Zoogloea resiniphila* DhA-35 to counteract pH stress in an aerated lagoon treating pulp and paper mill effluent, *Water Res.*, 36, 2793–2801, 2002.
56. Pohland, F.G., Anaerobic treatment: fundamental concepts, applications, and new horizons, in *Design of Anaerobic Process for the Treatment of Industrial and Municipal Wastes*, J.F. Malina and F.G. Pohland, Eds, Technomic Publishing Company, Inc., Lancaster, Pennsylvania, pp. 1–40, 1992.
57. Hall, E.R., Anaerobic treatment of wastewaters in suspended growth and fixed film processes, in *Design of Anaerobic Processes for the Treatment of Industrial and Municipal Waste*, J.F. Malina and F.G. Pohland, Eds, Technomic Publishing Company, Inc., Lancaster, Pennsylvania, pp. 41–118, 1992.
58. Carpenter, W.L., Vamvakias, J.G., and Gellman, I., Temperature relationships in aerobic treatment and disposal of pulp and paper wastes, *J. WP*CF. 40(5), 733–741, 1968.
59. Flippin, T.H. and Eckenfelder, W.W., Effects of elevated temperature on the activated sludge process, in *Proc. Int. Environ. Conf. Exhibit*, TAPPI Press, Portland, Oregon, 1994.
60. Cocci, A.A. and McCarthy, P.J. Sequencing batch reactors in the pulp and paper industry. A bench-marking study, in *Proc. Int. Envir. Conf. Exhibit*,TAPPI Press, Vancouver, British Columbia, 1998.
61. Lescure, J.P., Delannoy, D., Verrier, D., and Albgnac, G. Consequence of a thermal accident on the microbial activity of an industrial anaerobic filter, in *Proc. Fifth Int. Symp. Anaerobic Digest.*, Bologna, Italy, 1988.
62. Visser, A., Gao, Y., and Lettinga, G., Effects of short-term temperature increases on the mesophilic anaerobic breakdown of sulfate containing synthetic wastewater, *Water Res.*, 27(4), 541–550, 1993.
63. Uemura, S., Tseng, I.-C., and Harada, H., Effect of temperature elevation from 55°C to 65°C on the performance of a thermophilic UASB reactor and characteristics of methanogenic granular sludge, *Environ. Technol.* 16, 987–994, 1995.
64. Van Lier, J.B., Rintala, J., Sanz Martin, J.L., and Lettinga, G., Effect of short-term temperature increase on the performance of a mesophilic UASB reactor, *Water Sci. Technol.*, 22(9), 183–190, 1990.
65. Ahring, B.K., Ibrahim, A.A., and Mladenovska, Z., Effect of temperature increase from 55°C to 65°C on performance and microbial population dynamics of anaerobic reactor treating cattle manure, *Water Res.*, 35(10), 2446–2452, 2001.
66. van Lier, J.B., Grolle, K.C.F., Stams, A.J.M., de Macario, E.C., and Lettinga, G., Start-up of a thermophilic upflow anaerobic sludge bed (UASB) reactor with mesophilic granular sludge, *Appl. Microbiol. Biotech.*, 37, 130–135, 1992.
67. van Lier, J.B., Lettinga, G., Macario, A.J.L., and de Macario, E.C., Permanent increase of the process temperature of mesophilic upflow anaerobic sludge bed (UASB) reactors to 46, 55, 64 and 75°C, in *Proc. 47th Industrial Waste Conf.*, R.F. Wukasch, Ed., Lewis Publishers, Purdue University, West Lafayette, IN, 1992.

68. Borja, R. and Banks, C.J., Response of an anaerobic fluidized bed reactor treating ice-cream wastewater to organic, hydraulic, temperature, and pH shocks, *J. Biotechnol.*, 39, 251–259, 1995.
69. Lee, E.G.-H., Mueller, J.C., and Walden, C.C., Effect of temperature and sludge loading on BOD_5 removal and sludge settleability in activated sludge systems treating bleached kraft effluent, *TAPPI J.*, 58(6), 100–103, 1975.
70. Prensner, D.S., Muchmore, C.B., Gilmore, R.A., and Qazi, A.N., Wastewater treatment by heated rotating biological discs, *Biotechnol. Bioeng.*, 28, 1615–1621, 1976.
71. Sakka, K., Endo, T., and Watanabe, M., Deoxyribonuclease-susceptible floc forming *Pseudomonas sp.*, *Agric. Biol. Chem.*, 45(2), 497–504, 1981.
72. Barr, T.A., Taylor, J.M., and Duff, S.J.B., Effect of HRT, SRT and temperature on the performance of activated sludge reactors treating bleached kraft mill effluent, *Water Res.*, 30(4), 799–810, 1996.
73. Rinkus, K.M., Lin, W., Jha, A., and Reed, B.E., Investigation of microbial temperature sensitivity and effect of microorganisms on the integrity of a commercial metalworking fluid, in *Proc. Hazard. Ind. Wastes 29th Mid-Atlantic Ind. Hazard. Waste Conf.*, 1997.
74. Kriebitzsch, K., Adamietz, E., Schiegl, C., Helmreich, B., Wilderer, P.A., and Wuertz, S., Assessment of biological activity during temperature changes in a bench-scale sequencing batch reactor fed with synthetic medium containing lignin, *Water Sci. Technol.*, 37(4–5), 251–254, 1998.
75. Tripathi, C., Thermophilic aerobic biological treatment of bleached kraft pulp mill effluent and its effects on floc formation and settleability, Ph.D. thesis, Department of Chemical Engineering and Applied Chemistry, University of Toronto, Ontario, Canada, 1999.
76. Norris, P., Marshall, R., and Richard, M., High temperature effects on activated sludge treatment performance and sludge quality in a recycle mill, in *Proc. TAPPI Int. Environ. Conf. Exhibit*, TAPPI Press, Denver, CO, 2000.
77. Vogelaar, J.C.T., Bouwhuis, E., Klapwijk, A., Spanjers, H., and van Lier, J.B., Mesophilic and thermophilic activated sludge post-treatment of paper mill process water, *Water Res.*, 36, 1869–1879, 2002.
78. Fernández-Galiano, D., The ammoniacal silver carbonate method as a general procedure in the study of protozoa from sewage (and other) waters,*Water Res.*, 28(2), 495–496, 1994.
79. Starkey, J.E. and Karr, J.E., Effect of low dissolved oxygen concentration on effluent turbidity, *J. Water Pollut. Control. Fed.*, 56(7), 837–843, 1984.
80. Wilén, B.-M. and Balmér, P., Short-term effects of dissolved oxygen concentration on the turbidity of the supernatant of activated sludge, *Water Sci. Technol.*, 38(3), 25–33, 1998.
81. Wilén, B.-M., Keiding, K., and Nielsen, P.H., Anaerobic deflocculation and aerobic reflocculation of activated sludge, *Water Res.*, 34(16), 3933–3942, 2000.
82. Rasmussen, H., Bruus, J.H., Keiding, K., and Nielsen, P.H., Observations on dewaterability and physical, chemical and microbiological changes in anaerobically stored activated sludge from a nutrient removal plant, *Water Res.*, 28(2), 417–425, 1994.
83. Schwartz-Mittelmann, A. and Galil, N.I., Biological mechanisms involved in bioflocculation disturbances caused by phenol, *Water Sci. Technol.*, 42(1–2), 105–110, 2000.

84. Wilén, B.-M., Nielsen, J.L., Keiding, K., and Nielsen, P.H., Influence of microbial activity on the stability of activated sludge flocs, *Colloid Surf. B: Biointerfaces,* 18, 145–156, 2000.
85. Chudoba, P. and Pujol, R., Activated sludge plant facing grape harvest period — a case study, *Water Sci. Technol.*, 34(11), 25–32, 1996.
86. Keiding, K. and Nielsen, P.H., Desorption of organic macromolecules from activated sludge: effect of ionic composition, *Water Res.*, 31(7), 1665–1672, 1997.
87. Zita, A. and Hermansson, M., Effects of ionic strength on bacterial adhesion and stability of flocs in a wastewater activated sludge system, *Appl. Environ. Microbiol.*, 60(9), 3041–3048, 1994.
88. Neufeld, R.D., Heavy metals-induced deflocculation of activated sludge, *J. WPCF*, 48(8), 1940–1947, 1976.
89. Stasinakis, A.S., Thomaidis, N.S., Mamais, D., Papanikolaou, E.C., Tsakon, A., and Lekkas, T.D., Effects of chromium (VI) addition on the activated sludge process, *Water Res.*, 37(9), 2140–2148, 2003.
90. Nielsen, P.H. and Keiding, K., Disintegration of activated sludge flocs in presence of sulfide, *Water Res.*, 32(2), 313–320, 1998.
91. Higgins, M.J. and Novak, J.T., Characterization of exocellular protein and its role in bioflocculation, *J. Environ. Eng.*, May, 479–485, 1997.
92. Müller, E., Kriebitzsch, K., Wilderer, P.A., and Wuertz, S., Community structure of micro- and macroflocs in pin-point sludge and the influence of sludge age and potassium addition on microfloc formation, *Water Sci. Technol.*, 46(1–2), 405–412, 2002.
93. Olofsson, A.-C., Zita, A., and Hermansson, M., Floc stability and adhesion of green-fluorescent-protein-marked bacteria to flocs in activated sludge, *Microbiology*, 144, 519–528, 1998.
94. Heine, W., Sekoulov, I., Burkhardt, H., Bergen, L., and Behrendt, J., Early warning system for operation failures in biological stages of WWTPs by on-line image analysis, *Water Sci. Technol.*, 46(4–5), 117–124, 2002.
95. Caccavo, F.J., Frolund, B., Kloeke, F.v.O., and Nielsen, P.H., Deflocculation of activated sludge by the dissimilatory Fe(II)-reducing bacterium *Shewanella alga* BrY, *Appl. Environ. Microbiol.*, 62(4), 1487–1490, 1996.
96. Bruus, J.H., Nielsen, P.H., and Keiding, K., On the stability of activated sludge flocs with implications to dewatering, *Water Res.*, 26(12), 1597–1604, 1992.
97. Govoreanu, R., Seghers, D., Nopens, I., De Clercq, B., Saveyn, H., Capalozza, C., Va der Meeren, P., Verstraete, W., Top, E., and Vanrolleghem, P.A., Linking floc structure and settling properties to activated sludge population dynamics in an SBR, *Water Sci. Technol.*, 47(12), 9–18, 2003.
98. Nielsen, P.H., Frølund, B., and Keiding, K., Changes in the composition of extracellular polymeric substances in activated sludge during anaerobic storage, *Appl. Microbiol. Biotechnol.*, 44, 823–830, 1996.
99. Bott, C.B. and Love, N.G., The immunochemical detection of stress proteins in activated sludge exposed to toxic chemicals, *Water Res.*, 35(1), 91–100, 2001.
100. Love, N.G. and Bott, C.B., Evaluating the role of microbial stress response mechanisms in causing biological treatment system upset, *Water Sci. Technol.*, 46(1–2), 11–18, 2002.
101. Boyd, A. and Chakrabarty, A.M., Role of alginate lyase in cell detachment of *Pseudomonas aeruginosa, App. Environ. Microbiol.*, 60(7), 2355–2359, 1994.

102. Watanabe, K., Teramoto, M., and Harayama, S., An outbreak of nonflocculating catabolic populations caused the breakdown of a phenol-digesting activated sludge process, *Appl. Environ. Microbiol.*, 65(7), 2813–2819, 1999.
103. Belas, R., Sensing, response, and adaptation to surfaces: swarmer cell differentiation and behavior, in *Bacterial Adhesion, Molecular and Ecological Diversity*, M. Fletcher, Ed., Wiley-Liss, New york, pp. 281–331, 1996.
104. Palmgren, R., Jorand, F., Nielsen, P.H., and Block, J.C., Influence of oxygen limitation on the cell surface properties of bacteria from activated sludge, *Water Sci. Technol.*, 37(4–5), 349–352, 1998.
105. Marshall, K.C., Adhesion as a strategy for access to nutrients, in *Bacterial Adhesion. Molecular and Ecological Diversity*, M. Fletcher, Ed., Wiley-Liss, Inc., New York, pp. 59–87, 1996.
106. Lycette, R.M. and Hedrick, L.R., Action of deflocculating agents on *Saccharomyces cerevisiae* Class III brewer's yeast, *Appl. Microbiol.*, 10, 428–430, 1962.
107. King, R.O. and Forster, C.F., Effects of sonication on activated sludge, *Enzyme Microb. Technol.*, 12(February), 109–115, 1990.
108. Morgan-Sagastume, F. and Allen, D.G., Effects of temperature transient conditions on aerobic biological treatment of wastewater, *Water Res.*, 37(15), 3590–3601, 2003.
109. Morgan-Sagastume, F., Effect of mesophilic-thermophilic temperature transients on aerobic biological treatment of wastewater, Ph.D. thesis, Department of Chemical Engineering and Applied Chemistry, University of Toronto, Ontario, Canada, 2003.
110. Gaughran, E.R.L., The thermophilic microorganisms, *Bact. Revs.*, 11, 189–225, 1947.
111. Allen, M.B., The thermophilic aerobic sporeforming bacteria, *Bact. Revs.*, 17, 125–173, 1953.
112. LaPara, T.M. and Alleman, J.E., Thermophilic aerobic biological wastewater treatment, *Water Res.*, 33(4), 895–908, 1999.
113. Yura, T., Kanemori, M., and Morita, M.T., The heat shock response: regulation and function, in *Bacterial Stress Responses*, R.G. Storz and Hengge-Aronis, Eds, ASM Press, Washington, DC, pp. 3–18, 2000.
114. Russell, J.B. and Cook, G.M., Energetics of bacterial growth: balance of anabolic and catabolic reactions, *Microbiol. Rev.*, Mar, 48–62, 1995.
115. Mikkelsen, L.H., Gotfredsen, A.K., Agerbæk, M.L., Nielsen, P.H., and Keiding, K., Effects of colloidal stability on clarification and dewatering of activated sludge, *Water Sci. Technol.*, 34(3–4), 449–457, 1996.
116. Phadtare, S., Yamanaka, K., and Inouye, M., The cold shock response,in *Bacterial Stress Responses*, G.S.a.R. Hengge-Aronis, Ed., ASM Press, Washington, DC, 2000, 33–45.
117. Carratù, L., Franceschelli, S., Pardini, C.L., Kobayashi, G.S., Horvath, I., Vigh, L., and Maresca, B., Membrane lipid perturbation modifies the set point of the temperature of heat shock response in yeast, *Proc. Natl. Acad. Sci. USA,* 93(April), 3870–3875, 1996.
118. Bremer, E. and Krämer, R., Coping with osmotic challenges: osmoregulation through accumulation and release of compatible solutes in bacteria, in *Bacterial Stress Responses*, G.S.a.R. Hengge-Aronis, Ed., ASM Press, Washington, DC, pp. 79–97, 2000.
119. Low, E.W. and Chase, H.A., Reducing production of excess biomass during wastewater treatment, *Water Res.*, 33(5), 1119–1132, 1999.
120. Foster, J.W., Microbial responses to acid stress, in *Bacterial Stress Responses*, G.S.a.R. Hengge-Aronis, Ed., ASM Press, Washington, DC, pp. 99–115, 2000.

121. Padan, E. and Krulwich, T.A., Sodium stress, in *Bacterial Stress Response*, G.S.a.R.Hengge-Aronis, Ed., ASM Press, Washington, DC, pp. 117–130, 2000.
122. Krabbe, M., Weyand, N., and Low, D., Environmental control of pilus gene expression, in *Bacterial Stress Responses*, G.S.a.R. Hengge-Aronis, Ed., ASM Press, Washington, DC, pp. 305–321, 2000.
123. Silverman, M., Belas, R., and Simon, M., Genetic control of bacterial adhesion, in *Microbial Adhesion and Aggregation*, K.C. Marshall, Ed., Springer-Verlag, Berlin, Heidelber, New York, Tokyo, pp. 95–107, 1984.
124. Erdincler, A. and Vesilind, P.A., Effect of sludge cell disruption on compactibility of biological sludges, *Water. Sci. Technol.*, 42(9), 119–126, 2000.
125. Jørgensen, P.E., Eriksen, T., and Jensen, B.K., Estimation of viable biomass in wastewater and activated sludge by determination of ATP, oxygen utilization rate and FDA hydrolysis, *Water. Res.*, 26(11), 1495–1501, 1992.
126. Häner, A., Mason, C.A., and Hamer, G., Death and lysis during aerobic thermophilic sludge treatment: characterization of recalcitrant products, *Water Res.*, 28(4), 863–869, 1994.
127. Rocher, M., Goma, G., Pilas-Begue, A., Louvel, L., and Rols, J.L., Towards a reduction in excess sludge production in activated sludge processes: biomass physicochemical treatment and biodegradation, *Appl. Microbiol. Biotechnol.*, 51, 883–890, 1999.

18 Flocs and Ultraviolet Disinfection

Ramin Farnood

CONTENTS

18.1 INTRODUCTION

The presence of pathogenic bacteria, viruses, and parasites in recreation waters is a potential source for the spread of diseases. To protect the public health and the quality of water resources, wastewater is often disinfected by chemical or physical means prior to discharge to the receiving water.

Waterborne pathogens might exist as dispersed (or free) organisms or could be embedded within microbial flocs. In a typical wastewater, microbial flocs vary in size from several microns up to hundreds of microns. The floc structure acts as a barrier to the penetration of chemical and physical disinfectants and therefore reduces the disinfection efficiency. Flocs also provide a vehicle for the transport and spreading of pathogens in the environment. In this chapter we focus our attention on the ultraviolet (UV) disinfection and the effect of flocs on this process.

The antimicrobial effects of ultraviolet light were discovered in early 1900s.[1] Ultraviolet light is part of the electromagnetic spectrum and is often divided into four regions, UVA (315 to 400 nm), UVB (280 to 315 nm), UVC (200 to 280 nm), and vacuum UV (<200 nm).[2] It is the high energy UVC photons that are responsible for the germicidal action of light, for example the photon energy at 253.7 nm is 7.8×10^{-19} J or 4.9 eV with a high germicidal efficiency.

1-56670-615-7/05/$0.00+$1.50

Disinfection of water with UV light is considered to be a photochemical process that results in the alteration of DNA and RNA and therefore prevents microorganisms from reproduction.[3] In this process, the main mechanism for the microbial inactivation is believed to be the formation of pyrimidine dimers (thymine dimers in the case of DNA). Insufficient irradiation results in partial damage to the nucleic acid that may be either repaired by cellular repair mechanisms or cause mutant progeny.[4]

The germicidal effectiveness of inactivation of pathogens exhibits a peak at around 264 nm (Figure 18.1).[5] Protein and DNA also absorb strongly in the UVC region.[6,7] Therefore, the disinfection of floc-associated pathogens can be adversely affected by the shielding effect of adjacent microbes and by the UV absorption of extracellular polymeric substances (EPS) present within the floc matrix. Additionally, flocs can alter the light intensity field by absorption and scattering of UV light. Thus, the presence of flocs not only reduces the average ultraviolet dose in the sample but also modifies the apparent kinetics of disinfection. Figure 18.2 shows the schematic diagram of such interactions.[8]

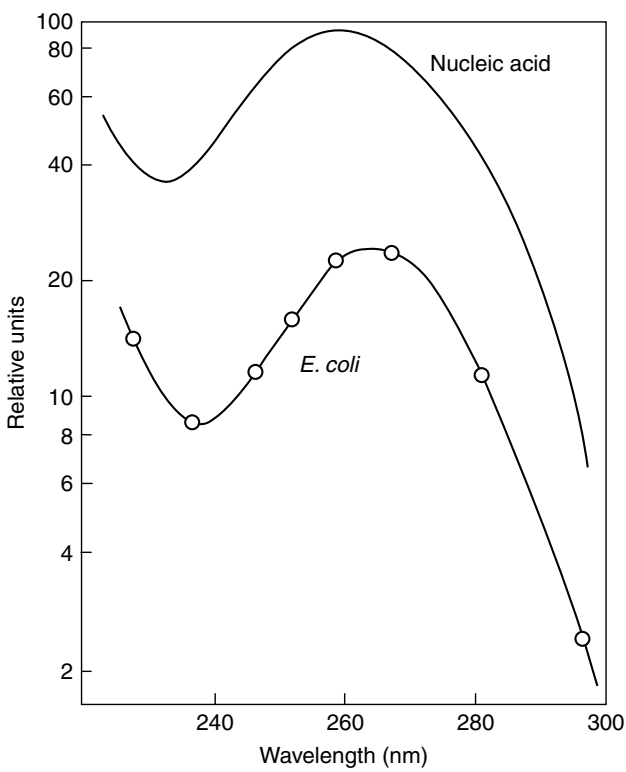

FIGURE 18.1 Action spectrum of *E. coli* and DNA absorbance. (From Harm, W., *Biological Effects of Ultraviolet Radiation*. Cambridge University Press, New York, 1980.)

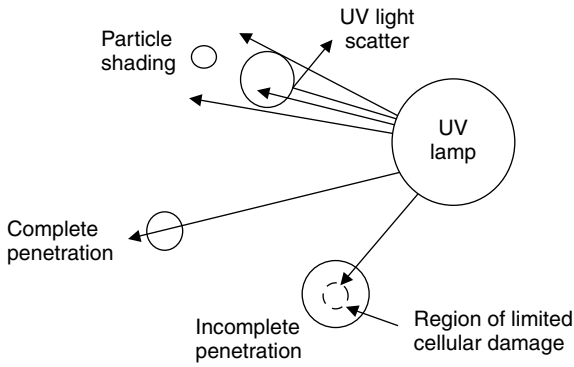

FIGURE 18.2 Interaction of suspended particles with light. (From Snider, K., Tchobanoglous, G.G., and Darby, J., *Evaluation of Ultraviolet Disinfection for Wastewater Reuse Applications in California.* University of California, Davis, 1991.)

18.2 KINETICS OF ULTRAVIOLET DISINFECTION OF MICROBIAL FLOCS

The kinetics of ultraviolet disinfection governs the scale and the operation of UV reactors. Therefore, an understanding of disinfection kinetics will help to improve the design and performance of disinfection processes.

18.2.1 Dose–Response Curves

The kinetics of ultraviolet disinfection is quantified by exposing the sample to various doses (= U*V intensity* × time) of UV light and enumerating the survived colonies. The sample is a stirred liquid suspension and the irradiation is carried out using a collimated beam apparatus. The purpose of collimating the UV beam is to provide a parallel beam of light perpendicular to the surface of the sample.

In the case of wastewater disinfection, a common technique for the enumeration of survived organisms is the *membrane filtration* method.[9] In this method, the irradiated sample is filtered, cultured in an appropriate medium, and the number of colonies is counted after an incubation period. A plot of the log of number of colony forming units (CFU) per 100 ml of the sample versus the applied dose of UV light is called the *dose–response curve*. This plot represents the kinetics of inactivation and quantifies the UV demand of wastewater to achieve a certain level of disinfection.

The shapes of dose–response curves that typically occur are given in Figure 18.3. The inactivation of dispersed or free organisms usually follows first order kinetics (curve 1). However, in some cases, the inactivation of free microbes results in an apparent lag or a *shoulder* at low doses (curve 2). This phenomenon may be explained by the clumping of microbes to form flocs[10] or by the action of cellular repair mechanisms.[3] The most common kinetics for municipal wastewaters is shown schematically by curve 3. At low doses, the shape of the curve is governed by the UV response of free microbes. However, at higher doses, the curve exhibits a *plateau* or a *tailing* effect. There is strong evidence that the tailing phenomenon is primarily due to

the presence of microbial flocs.[11] Curve 4 illustrates a case for which the disinfection kinetics exhibits both an initial shoulder and a subsequent tailing phenomenon.[12]

Response of wastewater to UV radiation depends on the type of target organism. The most common indicator organisms used for wastewater disinfection are total and fecal coliform, *E. coli*, and enterococci.[13] In the present study, all dose–response data are based on the enumeration of the surviving fecal coliforms unless it is stated otherwise.

18.2.2 Mathematical Models for UV Disinfection

Kinetic models are often used for estimating the impact of wastewater quality on the reactor performance and for effective reactor design. A summary of kinetic models that are published in the literature is given in Table 18.1.

The *one-hit* model assumes that a single harmful event (hit) is sufficient to inactivate a biological unit.[14] This model represents a Poisson process where the mean

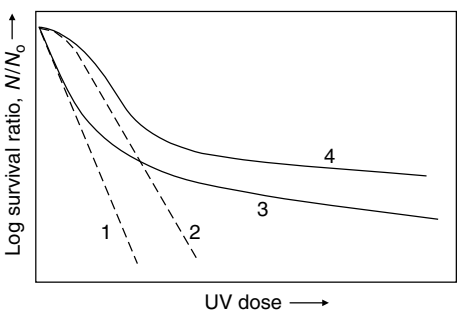

FIGURE 18.3 Schematic survival curves showing the kinetics of UV disinfection with and without the presence of microbial flocs.

TABLE 18.1
Kinetic Models for UV Disinfection

Model	Equation	Reference
One-hit	$\frac{N}{N_o} = e^{-kD}$	[14]
Multi-target	$\frac{N}{N_o} = 1 - (1 - e^{-kD})^m$	[14]
Multi-hit	$\frac{N}{N_o} = e^{-kD} \sum_{i=0}^{m-1} \frac{(kD)^i}{i!}$	[14]
Double-exponential	$\frac{N}{N_o} = (1-\beta)e^{-k_1 D} + \beta e^{-k_2 D}$	[3]
Modified two population	$\frac{N}{N_o} = (1-\beta)(1 - (1 - e^{-kD})^m) + \beta e^{-k_2 D}$	
Cairns et al.	$\frac{N}{N_o} = (1-\beta)e^{-kD} + \sum \beta_r e^{-kT_\mu^r D}$	[15]
Emerick et al.	$\frac{N}{N_o} = (1-\beta)e^{-kD} + \frac{\beta}{kD}(1 - e^{-kD})$	[16]

probability of the survival of a microorganism corresponds to the probability that the effective cross-section of the organism (a) escapes the incident photons. If N is the total number of incident photons over area A, then:

$$\text{Probability of survival} = N/N_o = e^{-aN/A} \tag{18.1}$$

Or simply:

$$N/N_o = e^{-kD} \tag{18.2}$$

This corresponds to first order kinetics and is a typical representation of free microbe inactivation, where k is the inactivation constant and D is the ultraviolet dose.

An alternative picture for modeling the microbial inactivation is based on the presence of multiple "targets" in an organism. In this case, that is known as the *multi-target* model, all such targets must receive at least one hit for inactivation.[14] Similar to the one-hit model, the inactivation of each target follows the negative exponential rule, therefore the probability of the inactivation of such an organism is:

$$\begin{aligned}\Pr[\text{inactivation}] &= \Pr[1\text{st target is hit}] \times \Pr[2\text{nd target is hit}] \\ &\quad \times \cdots \times \Pr[m\text{th target is hit}] \\ &= (1 - e^{-kD})(1 - e^{-kD}) \cdots (1 - e^{-kD})\end{aligned} \tag{18.3}$$

The probability of the survival of the organism in the multi-target model is:

$$N/N_o = 1 - (1 - e^{-kD})^m \tag{18.4}$$

In an alternative approach, the organism contains a single "target" that has to receive multiple "hits" before it is inactivated. This model is known as the *multi-hit* model[14] or the *series-event* model.[10] Both multi-target and multi-hit models successfully account for shouldered survival curves, but they do not predict the tailing phenomenon observed in wastewater disinfection processes.

A simple method to account for the tailing of dose–response curve is to consider the microbial population to consist of two subgroups.[3] Both subgroups are inactivated in a one-hit fashion, but one is more resistant to ultraviolet irradiation than the other:

$$N/N_o = (1 - \beta)e^{-k_1 D} + \beta e^{-k_2 D} \tag{18.5}$$

where β is the fraction of UV-resistant organisms (e.g., floc-associated microbes), and k_1 and $k_2 (< k_1)$ are the inactivation constants. This approach, known as the *double-exponential* model, predicts the tailing of dose-response curves, but it cannot create any "shoulder." To address this shortcoming, a simple variation of this model is suggested here, where the UV-sensitive subpopulation follows the multi-target model while the UV-resistant subgroup obeys the one-hit model:

$$N/N_o = (1 - \beta)(1 - (1 - e^{-k_1 D})^m) + \beta e^{-k_2 D} \tag{18.6}$$

A rigorous model to account for effects of flocs on the UV disinfection was proposed by Cairns et al.[15] This approach considers the interaction of light with free microbes, floc size distribution, total number of microbial counts associated with flocs, and transmittance of the flocs to UV. Application of this model requires knowledge of size distribution of viable flocs. However, since such information is rarely available, this model has found limited use.

Most recently, Emerick et al.[16] proposed that the inactivation of a microbial floc is controlled by the inactivation of a "critical" organism, and that the fraction of dose received by this organism is uniformly distributed. According to Emerick et al., flocs larger than a threshold diameter (about 20 microns) are not inactivated by ultraviolet irradiation. This model predicts that the survival rate at high doses of UV ($D > 20$) is inversely proportional to the UV dose, and cannot account for the shoulder.

18.3 EFFECT OF FLOC CHARACTERISTICS ON DISINFECTION KINETICS

18.3.1 The Role of Floc Size

To systematically investigate the effect of floc size on disinfection, UV disinfection of model samples with narrow floc size distributions was studied.[17] Wastewater samples were collected from the main treatment plant of the city of Toronto located at Ashbridges Bay and fractionated using 150, 125, 90, 75, 53, and 45 μm sieves. Three size fractions were chosen for further study with nominal ranges of 150/125, 90/75, and 53/45. Each size fraction was prepared by continuous washing of sieved particles with distilled water for at least 15 min or until a narrow size distribution is achieved. A Coulter particle size analyzer, Multisizer 3 (Beckman Coulter, Miami, FL), was used to count the number concentration of particles and to ensure the effectiveness of the fractionation process. Figure 18.4 shows the floc size distribution of the three fractions obtained using this technique. Each fraction was diluted with distilled water and 20 ml of diluted sample was transferred into a petri dish for exposure to UV light. For accurate estimation of UV dose, an IL 1700 radiometer (International Lights Co., Newburyport, MA) was used to measure the intensity at 33 points within the region irradiated by the lamp. To correct for the UV absorption of sample, the absorbance of each sample was determined using Lambda 35 UV/Vis spectrometer (Perkin Elmer, Boston, MA) at 253.7 nm. Based on these measurements, the exposure times were determined using the Beer–Lambert law. The sample was irradiated using a low-pressure collimated beam system (Trojan Technologies Inc., London, Ontario). The irradiated sample was filtered using a 0.45 μm filter paper and was cultured for a day in the dark. The number of colony forming units was then counted for each sample. In addition, a blank sample (nonirradiated) from each fraction was cultured to determine the concentration of viable microorganisms in the original sample. All experiments were conducted in replicates.

Figure 18.5 shows the dose–response curves for the three floc size fractions. Although there is a considerable variability in the results, a distinct increase in the average UV dose demand with increased floc size is observed. For comparison, the

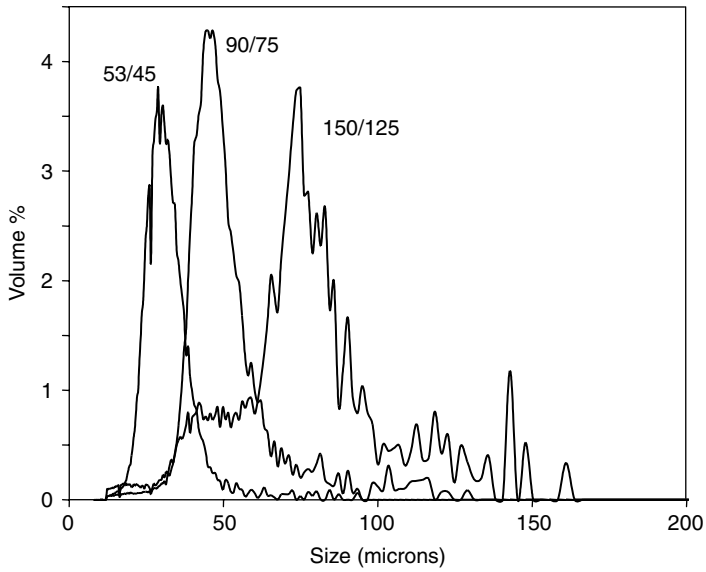

FIGURE 18.4 Size distribution of various sieve fractions used for disinfection studies.

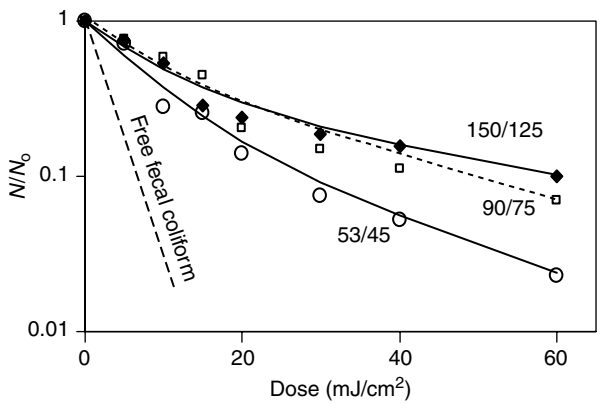

FIGURE 18.5 Dose–response curve for various sieve fractions.

dose–response curve for free fecal coliforms is also shown in this figure. The initial slope for flocs is significantly smaller than that of free coliforms. This indicates that there are very few, if any, free microbes in the sieved samples. At higher UV doses, the slope of dose–response curve decreases as the floc size increases, indicating an increase in the UV resistance of the larger flocs in the sample. Using nonlinear regression analysis (Mathematica, v5.1), the double-exponential model parameters were estimated for the three sieve fractions (see Table 18.2). By increasing the particle size, both the fraction of resistant flocs (β) and their resilience to the ultraviolet light

TABLE 18.2
Parameters of Double-Exponential Model (Equation (18.5)) and the Fraction of Colony Forming Flocs for Various Sieve Fractions

Sieve fraction[a]	Floc size[b] (microns)	β	k_1 (cm^2/mJ)	k_2 (cm^2/mJ)	% Viable (±std.)
150/125	74	0.350	0.115	0.021	11.0 (±0.2)
90/75	45	0.321	0.086	0.026	9.1 (±0.8)
53/45	28	0.235	0.128	0.038	7.0 (±0.4)

[a] Sieve size in microns.
[b] Mode of particle size distribution from Coulter particle size analyzer.

increases (i.e., the inactivation rate constant, k_2, decreases), emphasizing that larger particles are harder to disinfect.

For any given size fraction, the ratio of the number of colony forming units obtained prior to the UV irradiation and the number concentration of particles obtained from the Coulter analyzer will provide an estimation of the percentage of viable flocs (Table 18.2). Based on this result, the percentage of colony forming flocs increased from 7% to 11%, when comparing 53/45 to 150/125 μm sieve fraction. This observation emphasizes the importance of larger flocs in UV disinfection, that is although there is smaller number of large flocs in a typical wastewater compared to small flocs, a larger fraction of them are viable and they are harder to disinfect.

18.3.2 The Role of Floc Composition

Microbes that are embedded in flocs are shielded and receive reduced doses of UV light. The UV light intensity within a floc depends on the size and composition of floc. To understand better, the potential effect of floc composition and particularly the role of EPS on the light penetration into flocs, EPS was extracted from pure cultures of *Klebsiella* sp. and its UV absorbance was measured.[18]

Klebsiella cultures were grown to allow for the formation of flocs. Ethanolic extraction[19] was used to extract EPS from the cultured samples. The broth samples were collected and the mixed liquor suspended solids (MLSS) was separated by centrifugation at 9000 rcf and 4°C for 15 min. The supernatant was decanted and the sludge pellet was dissolved in ethanol. These solutions were left in parafilm-sealed containers at ambient conditions for several days for extraction. The solution was then filtered using Whatman Microfibre GF/A filters and the filtrate was rotary evaporated under vacuum to remove ethanol. The remaining EPS was weighed and dissolved in a known amount of ethanol and the UV absorbance of EPS solution was measured at 253.7 nm using a UV–Vis spectrometer. This measurement was repeated for five concentrations of EPS.

To investigate the effect of carbon source on the UV absorbance of EPS, the above procedure was repeated for two different carbon sources, a lactose-fed culture and a

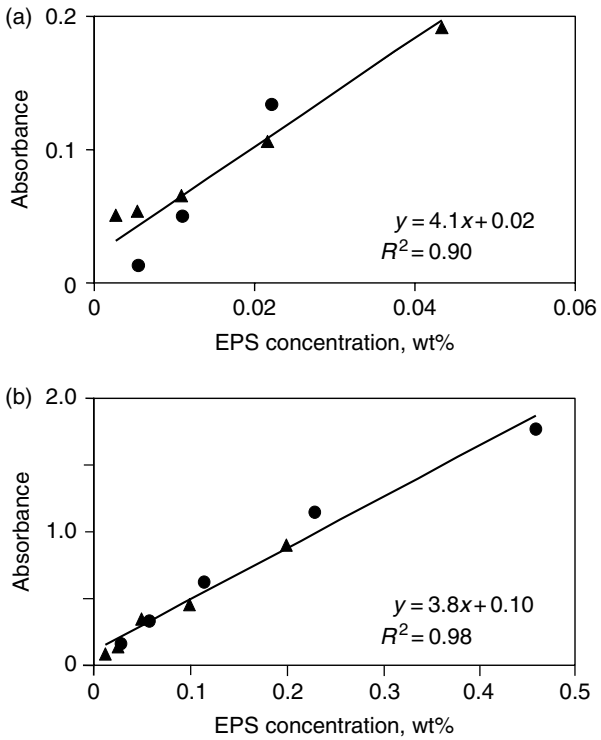

FIGURE 18.6 UV absorbance of EPS for (a) glucose-fed samples, (b) lactose-fed samples.

glucose-fed culture. Each test was conducted in replicates. Figure 18.6(a) and 18.6(b) show the plot of absorbance versus EPS concentration for all runs. The slope of both curves is about 4 wt%, indicating a strong UV absorptivity for EPS. For comparison, the UV absorbance of protein (bovine serum albumin) and DNA (calf thymus) at 253 nm are 4.1 and 155 wt%, respectively (estimated based on data reported by Harm[5]). The results also indicate that the carbon source has a minimal impact on the absorbance of EPS produced by *Klebsiella* sp. as measured by this method.

The effect of EPS on the UV penetration into microbial flocs depends on its spatial distribution. To illustrate this point, we take the three idealized cases presented in Figure 18.7. We consider a 100 μm spherical floc with a density of 1 g/cm^3 and a porosity of 90%. Assuming an EPS concentration of 50 mg/g MLSS with an absorbance of 400 cm^{-1}, and assuming that EPS accumulates around a single target organism within the floc (Figure 18.7a), 55% of the incident UV light would be absorbed by the EPS before reaching the shielded microbe. On the other hand, if EPS was assumed to be uniformly adsorbed on the surface of the floc while forming a thin film around it (Figure 18.7c), only 1% of the UV light will be attenuated in the EPS layer. Finally, if EPS was homogeneously distributed within the floc volume (Figure 18.7b), 3% of the UV light will be absorbed by EPS before reaching the center of the floc. The above models are oversimplifications of the actual distribution of EPS

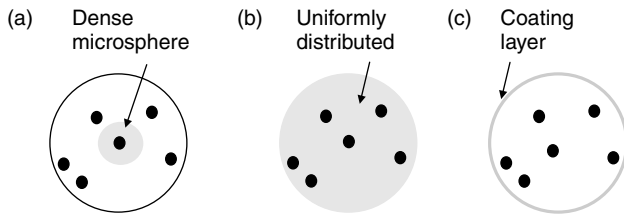

FIGURE 18.7 Schematic diagram showing the spatial distribution of EPS in a spherical floc: (a) shielding a single organism in the center of the floc, (b) uniformly distributed within the floc volume, and (c) coating the surface of the floc. The black circles represent target microbes and the gray areas represent EPS containing zones.

within microbial flocs, but they emphasize on the importance of the EPS distribution in the disinfection of flocs.

18.4 CONCLUSIONS

Analysis of microbial flocs collected from a municipal wastewater treatment plant shows that by increasing the floc size fraction from 53/45 μm to 150/125 μm, the percentage of viable flocs increases from 7% to 11%. At the same time, the dose demand of samples to achieve one log inactivation more than doubled, increasing from ~25 to ~60 mJ/cm^2 with increased floc size. Analysis of EPS extracted from pure cultures of a *Klebsiella* sp. shows that EPS is a strong absorber of ultraviolet light with absorbance of about 400 cm^{-1}; however, the reduction in the UV light intensity within the floc due to the presence of EPS could vary from less than 1% up to ~55%, depending on whether the EPS was all surface associated (an extreme) or forming a dense microsphere within the floc (another extreme).

ACKNOWLEDGMENTS

Support from Natural Sciences and Engineering Research Council of Canada and the University of Toronto is greatly acknowledged.

REFERENCES

1. Wolfe, R.L., Ultraviolet Disinfection of Potable Water, *Environ. Sci. Technol*. 24, 768, 1990.
2. Meulemans, C.C.E., The Basic Principles of UV-Disinfection of Water, *Ozone Sci. & Eng*. 9, 299–314, 1987.
3. Jagger, J., *Introduction to Research in Ultraviolet Photobiology*. Prentice-Hall, Englewood Cliffs, New Jersey, 1977.
4. USEPA, *Ultraviolet Light Disinfection Technology in Drinking Water Application — An Overview*. EPA 811-R-96-002, Office of Ground Water and Drinking Water, USEPA, Washington, D.C., 1996.
5. Harm, W., *Biological Effects of Ultraviolet Radiation*. Cambridge University Press, New York, 1980.

6. Philips, R., *Sources and Application of Ultraviolet Light*. Academic Press, New York, 1983.
7. Calvert, J.G. and Pitts, J.N., *Photochemistry*. Wiley, New York, 1966.
8. Snider, K., Tchobanoglous, G.G., and Darby, J., *Evaluation of Ultraviolet Disinfection for Wastewater Reuse Applications in California.* University of California, Davis, 1991.
9. Clesceri, L.S., Greenberg, A.E., and Eaton, A.D., eds, *Standard Methods for the Examination of Water and Wastewater*, 20th Ed., American Public Health Association, Washington, D.C., 1998.
10. Severin, B.F., Suidan, M.T., and Engelbrecht, R.S., Kinetic Modeling of UV Disinfection of Water, *Water Res*. 17, 1669, 1983.
11. Qualls, R.G., Flynn, M.P., and Johnson, J.D., The Role of Suspended Particles in Ultraviolet Disinfection, *J. Water Pollut. Control Fed*. 55, 1280, 1983.
12. Harris, G.D., Dean Adams, V., Sorensen, D.L., and Curtis, M.S., Ultraviolet Inactivation of Selected Bacteria and Viruses with Photoreactivation of the Bacteria. *Water Res*. 21, 687, 1987.
13. Oppenheimer, J.A. et al. Microbial Inactivation and Characterization of Toxicity and By-Products Occurring in Reclaimed Wastewater Disinfected with UV Radiation, in *Planning, Design and Overview of Effluent Disinfection Systems, Specialty Conference Series*, Whippany, New Jersey, 1993, 13.
14. Zimmer, K.G., *Studies on Quantitative Radiation Biology*. Hafner Publishing Co., New York, 1961.
15. Cairns, W.L., Sakamoto, G., Comair, C.B., and Gehr, R., Assessing UV Disinfection of a Physico-Chemical Effluent by Medium Pressure Lamps Using a Collimated Beam and Pilot Plant, in *WEF Specialty Conference Series*, Whippany, Water Environment Federation, Alexandria, 1993, 433.
16. Emerick, R.W., Loge, F.J., Ginn, T., and Darby, J.L., Modeling the Inactivation of Particle Associated Coliform Bacteria, *Water Environ. Res.* 72, 432, 2000.
17. Mahabir, R., *The Effect of Particle Size on the Efficiency of Ultraviolet Reactors*. B.A.Sc. Thesis, University of Toronto, 2003.
18. Luh, J., *Analysis of the Physicochemical Properties of Extracellular Polymeric Substances*. B.A.Sc. Thesis, University of Toronto, 2003.
19. Forster, C.F. and Clarke, A.R., The Production of Polymer from Activated Sludge by Ethanolic Extraction and its Relation to Treatment Plant Operation. *Water Pollut. Control*, 121, 430, 1983.

19 Surface Thermodynamics and Hydrophobic Properties of Microbial Flocs

B.Q. Liao, Gary G. Leppard, D. Grant Allen, Ian G. Droppo, and Steven N. Liss

CONTENTS

19.1 INTRODUCTION

The flocculating ability of activated sludge and adhesion of dispersed cell or fine flocs to large floc surfaces influence the level of effluent suspended solids (ESS), or non-settleable fine particles, in the final effluent of biologically treated wastewaters.[1–8] Proposed mechanisms for floc formation, including charge neutralization, and polymer- and salt-bridging emphasize the importance of surface properties in floc interactions.[2–5,9–12] Increasing attention has been given to the hydrophobic nature of sludge floc and its role in bioflocculation. A more hydrophobic surface has been related to a lower level of ESS.[6,13–16] The composition and the properties of extracellular polymeric substances (EPS), particularly proteins, have been shown to be major determinants of the physicochemical properties of flocs, including the hydrophobicity.[12,15,17,18]

1-56670-615-7/05/$0.00+$1.50

Microbial flocs are naturally hydrated, due to the presence of large numbers of hydroxyl, carboxyl, and phosphate groups. Side chains in amino acids, the methyl groups in polysaccharides, and the long-chain carbon groups in lipids all contribute to the hydrophobic properties of sludge flocs. Flocs are negatively charged under neutral pH conditions. The presence of ionizable groups such as carboxyl, phosphate, and amino groups in the EPS and cell surfaces is responsible for the density of surface charge. The zeta potential of sludge flocs is usually in the range of -10 to -30 mV.[2,13,19] Simple measures of the physicochemical properties, including hydrophobicity and surface charge, may be reliable indicators for predicting bioflocculation in the operation of biological wastewater treatment processes.[15]

The purposes of this study were to evaluate the surface tension of sludge flocs by using contact angle measurement and Neumann's equation-of-state, to investigate the influence of sludge retention time (SRT) on the surface tension of sludge flocs, and to test the feasibility of using surface thermodynamic concept to predict bioflocculation.

19.2 EXPERIMENTS

19.2.1 Activated Sludge Samples

Activated sludge samples were taken from the laboratory-controlled sequencing batch reactors (SBRs) fed a synthetic wastewater containing glucose and inorganic salts. The SBRs were operated at different SRTs (4 to 20 days). Details of the SBR system are given by Liao et al.[15]

19.2.2 Contact Angle Measurement

Sludge samples collected from the SBRs were first washed with deionized distilled water twice using a centrifuge at $2000 \times g$ for 5 min each time. Then the washed sludge samples were dispersed by a Vortex mixer and deposited on a membrane filter (Black MSI Microsep*, 0.45 μm) under 400 mmHg vacuum. The sludge cake was filtered until moist and there were no signs of excess water that could be sucked. Contact angle of deionized distilled water on sludge cakes was measured on a partially hydrated sludge cake using the axisymmetric drop shape analysis-contact diameter (ADSA-CD) technique.[20,21]

19.2.3 Liquid Surface Tension

Surface tension of the treated effluent was determined by a CENCO tension-meter (Sigma Chemical Co., MO) equipped with a 6 cm diameter platinum ring at ambient temperature (21 ± 2°C). Prior to surface tension measurement, the effluent was centrifuged at $15,000 \times g$ for 15 min at 4°C to remove colloidal particles.

19.2.4 Effluent Suspended Solids

The flocculating ability of activated sludge was evaluated by determining the ESS after 40 min settling of mixed liquor in the SBRs. The mixed liquor suspended solids at different SRTs were maintained at the same level (2000 ± 150 mg/l). The measurement of ESS was in accordance with Standard Methods.[22]

19.3 SURFACE THERMODYNAMIC MODEL

The surface thermodynamic model predicts that the system free energy is minimized at equilibrium and adhesion between two surfaces will occur.[23,24] Consequently, bioflocculation will be thermodynamically favored if the process itself causes the system free energy to decrease. Ignoring electrostatic interactions and other specific binding, two hydrophobic surfaces approaching at short distances will result in the surrounding bound water layers to overlap with the eventual displacement of the bound water into the bulk water. This would lead to a decrease in the interfacial free energy and thus bioflocculation.

The interfacial free energy of the interaction between two identical bacterial cells (B), immersed in liquid (L) can be described as follows:

$$\Delta G_{\text{flocculation}} = -2\gamma_{\text{BL}} \tag{19.1}$$

where $\Delta G_{\text{flocculation}}$ is the interfacial free energy of floc formation and γ_{BL} is the interfacial tension for the bacteria (B)–liquid (L) interface. If the total free energy of a system is reduced ($\Delta G_{\text{flocculation}} < 0$) by cell interactions, then bioflocculation will be thermodynamically favored.[23,25,26] Neumann et al.[26] have demonstrated that γ_{BL} is a function of γ_{BV} and γ_{LV} (where γ_{BV} and γ_{LV} stand for the interfacial tension of bacteria–vapor and liquid–vapor, respectively), and developed an equation-of-state to describe the relationship among γ_{BL}, γ_{BV}, and γ_{LV}:

$$\gamma_{\text{BL}} = (\sqrt{\gamma_{\text{BV}}} - \sqrt{\gamma_{\text{LV}}})^2/(1 - 0.015\sqrt{\gamma_{\text{BV}}}\sqrt{\gamma_{\text{LV}}}) \tag{19.2}$$

In conjunction with Young's equation:

$$\gamma_{\text{BV}} - \gamma_{\text{BL}} = \gamma_{\text{LV}}\cos(\theta) \tag{19.3}$$

A third equation is yielded as:

$$\cos(\theta) = \frac{[(0.015\gamma_{\text{BV}} - 2.00)\sqrt{(\gamma_{\text{BV}} + \gamma_{\text{LV}})} + \gamma_{\text{LV}}]}{[\gamma_{\text{LV}}(0.015\sqrt{\gamma_{\text{BV}}}\sqrt{\gamma_{\text{LV}}} - 1)]} \tag{19.4}$$

Based on Equation (19.4), the surface tension (γ_{BV}) of sludge flocs is determined by measuring the contact angle of a liquid with known surface tension (γ_{LV}). The change in the interfacial free energy of the system, $\Delta G_{\text{flocculation}}$, is then calculated from Equations (19.1) to (19.4).[27]

19.4 RESULTS AND DISCUSSION

Table 19.1 shows the changes in surface tensions of sludge flocs and effluent, and the $\Delta G_{\text{flocculation}}$ with respect to SRTs. The surface tension of the effluent at different SRTs was similar and the values were quite close to the theoretical value (72 ± 1 ergs/cm^2) of deionized distilled water at ambient temperature. This is perhaps not surprising, as the effluent, after centrifugation, contained only water and a

TABLE 19.1
Contact Angles, Surface Tensions, Interfacial Tensions Associated with Bioflocculation of Sludges at Different Solids Retention Times (SRTs)

SRT (days)	Contact angle[a] (degrees)	γ_{BV} (ergs/cm^2)	γ_{LV} (ergs/cm^2)	γ_{BL} (ergs/cm^2)	$\Delta G_{bioflocculation}$ (ergs/cm^2)
4	20–29 (25 ± 3)	64.50–68.40	72 ± 1	0.28–1.07	−0.56 to −2.14
9	15–23 (17 ± 4)	67.20–70.12	72 ± 1	0.47–0.09	−0.18 to −0.94
12	29–31 (30 ± 1)	63.50–64.50	72 ± 1	1.07–1.35	−2.14 to −2.70
16	30–47 (36 ± 7)	54.70–64.00	72 ± 1	1.2–5.27	−2.40 to −10.54
20	31–45 (37 ± 6)	55.90–63.50	72 ± 1	1.35–4.61	−2.70 to −9.22

[a] 6–8 independent contact angle measurements were conducted at different experimental times at each SRT.

small amount of soluble chemical oxygen demand (COD) and inorganic salts with a lower ionic strength (1.5×10^{-4} mol/l).[15] The presence of small amount of soluble COD[28] and inorganic salts[29] has only limited influence on the surface tension of water.

On the other hand, surface tensions of sludge flocs were significantly different with respect to SRTs. A lower surface tension was associated with sludge flocs at the higher SRTs (16 and 20 days), as compared to that at the lower SRTs (4 and 9 days) (Analysis of Variances [ANOVA], $p < 0.05$). It appeared that a transit range of SRT (about 12 days) existed for a significant change in surface tension of sludge surfaces. This was the same for the interfacial tension between sludge surfaces and treated effluent, as shown in Table 19.1. These results suggest that the surface tension of sludge flocs and the interfacial tension between sludge surfaces and effluent can be biologically manipulated through the control of physiological status at a microbial community level.

A plot of ESS against the $\Delta G_{flocculation}$ is shown in Figure 19.1. There is a strong positive correlation between the $\Delta G_{flocculation}$ values and the effluent suspended solids (Spearman's coefficient, $r_s = 0.85$, $p < 0.01$). A higher ESS is associated with a higher level of $\Delta G_{flocculation}$, which is close to 0, particularly for sludge at lower SRTs. This is consistent with the prediction of the surface thermodynamic approach in that dispersed cells and fine flocs will aggregate to form settleable large flocs driven by the decrease in interfacial free energy (more negative). The large variation of the ESS for a given value of $\Delta G_{flocculation}$, particularly for the higher level of $\Delta G_{flocculation}$, indicates that electrostatic interactions might also be involved in governing bioflocculation except for hydrophobic interactions.

The results from this study provide firsthand information on the surface tension of sludge flocs and its relationship to bioflocculation in a well-controlled laboratory activated sludge system. A higher SRT produces a sludge surface with a lower surface tension. A strong positive correlation was found between the interfacial free energy of bioflocculation and the level of ESS, indicating the importance of surface

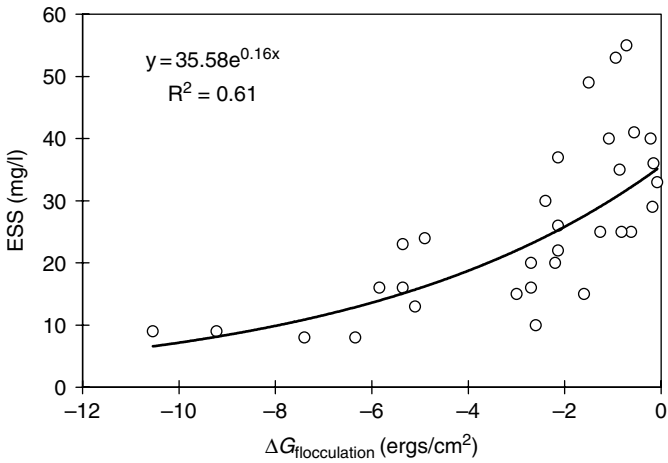

FIGURE 19.1 Relationship between the surface free energy of bioflocculation ($\Delta G_{\text{flocculation}}$(ergs/cm^2) and the level of ESS (mg/l).

thermodynamics in explaining sludge floc formation. To date the characterization of the physicochemical properties of microbial floc, particularly hydrophobicity and surface charge, has been an academic activity. Given the relative ease of measuring hydrophobic properties (e.g., microbial adhesion to hydrocarbon and contact angle measurement) and surface charge (e.g., colloidal titration) of flocs, properties that can be correlated to bioflocculation and floc structure,[15,16,30] such determinations may be of greater value in assessing sludge separation properties than the emphasis given to the role of filamentous bacteria.[31]

19.5 CONCLUSIONS

The surface tension of sludge flocs can be influenced by changes in SRT. A higher SRT produces a sludge surface with a lower surface tension. A strongly positive correlation was found between the $\Delta G_{\text{flocculation}}$ and the level of ESS, implying the importance of surface thermodynamics in explaining sludge floc formation.

ACKNOWLEDGMENTS

The project was funded by the Natural Sciences and Engineering Research Council (NSERC) of Canada through the strategic grants to SNL, IGD, and GGL (STR0167324) and SNL, DGA, GGL, and IGD (STPGP201976-97). The assistance of Z. Policova, Applied Surface Thermodynamics Laboratory at the University of Toronto, in using the ADSA-CA technique for contact angle measurement is highly appreciated.

REFERENCES

1. Chao, A.C. and Keinath, T.M. (1979) Influence of process loading intensity on sludge clarification and thickening characteristics. *Water Res*., 13(12), 1213–1220.
2. Forster, C.F. (1971) Activated sludge surfaces in relation to the sludge volume index. *Water Res*., 5, 861–870.
3. Forster, C.F. (1985) Factors involved in the settlement of activated sludge-I: nutrients and surface polymers. *Water Res*., 19(10), 1259–1264.
4. Eriksson, L. and Alm, B. (1991) Study of flocculation mechanisms by observing effects of a complexing agent on activated sludge properties. *Water Sci. Technol*., 24(7), 21–28.
5. Zita, A. and Hermansson, M. (1994) Effect of ionic strength on bacterial adhesion and stability of flocs in a wastewater activated sludge system. *Appl. Environ. Microbiol*., 60(9), 3041–3048.
6. Zita, A. and Hermansson, M. (1997) Effects of bacterial cell surface structure and hydrophobicity on attachment to activated sludge flocs. *Appl. Environ. Microbiol*., 63(3), 1168–1170.
7. Mikkelsen, L.H., Gotfredsen, A.K., Agerbk, M.L., Nielsen, P.H., and Keiding, K. (1996) Effect of colloidal stability on clarification and dewatering of activated sludge. *Water Sci. Technol*., 34(3–4), 449–457.
8. Mikkelsen, L.H. and Keiding, K. (1999) Equilibrium aspects of the effects of shear and solids content on aggregate deflocculation. *Adv. Colloid Interface Sci*., 80, 151–182.
9. Campbell, L.A. (1972) The initiation of bioflocculation. *Water Pollut. Control*, 14–17.
10. Pavoni, J.L., Tenney, M.W., and Echelberger, W.F. Jr. (1972) Bacterial extracellular polymers and biological flocculation. *J. Water Pollut. Control Fed*., 44(3), 414–431.
11. Higgins, M.J. and Novak, J.T. (1997) The effect of cations on the compression and dewatering of activated sludges. *Water Environ. Res*., 69, 225–232.
12. Higgins, M.J. and Novak, J.T. (1998) Characterization of extracellular protein and its role in bioflocculation. *J. Environ. Eng*., ASCE, 123(50), 479–485.
13. Valin, S.D. and Sutherland, D.J. (1982) Predicting bioflocculation: new developments in the application of flocculation theory. *Environ. Technol. Lett*., 3, 363–374.
14. Daffonchio, D., Thaveesri, J., and Verstraete, W. (1995) Contact angle measurement and cell hydrophobicity of granular sludge from upflow anaerobic sludge bed reactors. *Appl. Environ. Microbiol*., 61(10), 3676–3680.
15. Liao, B.Q., Allen, D.G., Droppo, I.G., Leppard, G.G., and Liss, S.N. (2001) Surface properties of sludge and their role in bioflocculation and settleability. *Water Res*., 35(2), 339–350.
16. Liss, S.N. (2002) Microbial Flocs Suspended Biofilms In: *Encyclopaedia of Environmental Microbiology*, Volume 4. G. Bitton (editor). John Wiley and Sons, New York, NY pp 2000–2012.
17. Jorand, F., Guicherd, P., Urbain, V., Manem, J., and Block, J.C. (1994) Hydrophobicity of activated sludge flocs and laboratory-grown bacteria. *Water Sci. Technol*., 30(11), 211–218.
18. Jorand, F., Boue-Bigne, F., Block, J.C., and Urbain, V. (1998) Hydrophobic/ hydrophilic properties of activated sludge exopolymeric substances. *Water Sci. Technol*., 37(4–5), 307–316
19. Forster, C.F. (1968) The surface of activated sludge particles in relation to their settling characteristics. *Water Res*., 2, 767–776.

20. Duncan-Hewitt, W.C., Policova, Z., Cheng, P., Vargha-Butler, E.I., and Neumann, A.W. (1989) Semiautomatic measurement of contact angles on cell layers by a modified axisymmetric drop shape analysis. *Colloids Surf*., 42, 391–403.
21. Neumann, A.W., Li, D., Spelt, G., and Cheng, P. (1996) *Applied Surface Thermodynamics*. Marcel Dekker, New York.
22. APHA (1992) *Standard Methods for the Examination of Water and Wastewater*, 18th edn. American Public Health Association, American Water Works Association, Water Environmental Federation, Washington.
23. Absolom, D.R., Lamberti, F.V., Policova, Z., Zingg, W., van Oss, C.J., and Neumann, A.W. (1983) Surface thermodynamics of bacterial adhesion. *Appl. Environ. Microbiol*., 46(1), 90–97.
24. Thaveesri, J., Daffonchio, D., Liessens, B., Vandermeren, P., and Verstraete, W. (1995) Granulation and sludge bed stability in upflow anaerobic sludge bed reactors in relation to surface thermodynamics. *Appl. Environ. Microbiol*., 61(10), 3681–3686.
25. Neumann, A.W., Gillman, C.F., and van Oss, C.J. (1974a) Phagocytosis and surface free energies. *Electroanalytical Chem. Interfacial Electrochem.*, 49, 393–400.
26. Neumann, A.W., Good, R.J., Hope, C.J., and Sejpal, M. (1974b) An equation-of-state approach to determine surface tensions of low-energy solids from contact angles. *J. Colloid Interface Sci*., 49, 291–304.
27. Neumann, A.W., Absolom, D.R., Francis, D.W., and van Oss, C.J. (1980) Conversion tables of contact angles to surface tensions. *Sep. Purif. Methods*., 9(1), 69–163.
28. Bura, R. (2000) Effect of extracellular polymeric substances on the chemistry of effluent. M.A.Sc. thesis, Department of Chemical Engineering & Applied Chemistry, University of Toronto, Toronto, ON, Canada.
29. Facchini, P.J., Neumann, A.W., and DiCosmo, F. (1989) Adhesion of suspension-cultured *Catharanthus roseus* cells to surfaces: effect of pH, ionic strength, and cation valency. *Biomaterials*, 10, 318–324.
30. Liao, B.Q., Allen, D.G., Leppard, G.G., Droppo, I.G., and Liss, S.N. (2002) Interparticle interactions affecting the stability of sludge flocs. *J. Colloid Interface Sci*., 249, 372–380.
31. Krhutkova, O., Ruzikova, I., and Wanner, J. (2002) Microbial evaluation of activated sludge and filamentous populations at eight Czech nutrient removal activated sludge plants during year 2000. *Water Sci. Technol*., 46 (1–2), 471–488.

IV

Summary

20 Opportunities, Needs, and Strategic Direction for Research on Flocculation in Natural and Engineered Systems

Ian G. Droppo, Gary G. Leppard, Steven N. Liss, and Timothy G. Milligan

CONTENTS

1-56670-615-7/05/$0.00+$1.50

20.1 INTRODUCTION

The workshop, *Flocculation in Natural and Engineered Systems*, held in September, 2003 at the Canada Centre for Inland Waters provided a unique perspective of flocculation processes through the integration of current knowledge obtained from natural and engineered systems. This multidisciplinary workshop incorporated scientists who work in freshwater and saltwater environments, and engineered systems. This allowed for a cross communication of ideas from disciplines that have largely remained isolated in their study of flocculation processes. This integration of ideas and methods provides researchers from different disciplines and work environments with different motivations in their effort to answer the very different questions dictated by the environment of investigation. The different approaches to the study of flocculation presented in this chapter allow individuals to look at it from an alternative perspective. With an integrated approach, new opportunities arise for flocculation research within all three environments.

As can be seen from the preceding chapters, flocculation plays an essential role in mediating the physical, chemical, and biological properties of not only the suspended flocs themselves, but also of the aquatic or engineered system as a whole. As such, the flocculation process has significant environmental and socioeconomic implications. For example, flocculation plays an important role in sediment associated contaminant fate and effect, reduces reservoir capacity and fisheries habitat due to increased sedimentation, is used as a remediation strategy for oil spills and toxic algal blooms, and dictates the efficiency of wastewater treatment systems. While untold billions of dollars are spent each year on issues for which flocculation is the key process, our understanding of the underlying mechanisms is still developing. The goal of this workshop was to improve our knowledge of flocculation and its role in what appear at first glance to be very different environments. The free exchange of methods, models, and ideas between researchers has identified areas of convergence and divergence within the study of flocculation. The workshop demonstrated that, in general, the important variables in the flocculation process are the same regardless of environmental constraints (freshwater, saltwater, or engineered systems). Apparent differences lie in the perceived relative importance of these variables and in the specific approach used for their assessment.

It is clear that there are three basic principles and one emerging issue which are supported in all three environments. The principles are (1) that flocculation is agreed, at its most simplistic level, to be the aggregating together of smaller particles to form larger particles; (2) that successful aggregation occurs through mechanisms described

by the basic coagulation theory; and (3) that the substantive physical behavioral impact of flocculation is the modification (generally increasing) of the downward flux of sediments. The biology of flocculated sediment, particularly the microbial activity, is quickly emerging as an important issue; bacterial activities modify much of the physical, chemical, and biological behavior of the sediment particles and the system as a whole. The biological aspects of flocculation have, of course, always been an important issue in engineered systems (e.g., wastewater treatment) but are only in the last few decades being explored within the freshwater and saltwater environments as a significant mechanism influencing the flocculation process. Beyond these three principles and the emergence of biological activity as an important aspect of flocculation, all other aspects of this complex phenomenon were generally agreed to be ruled by site-specific parameters culminating in unique structures and chemical and biological behaviors within the medium of transport. This chapter summarizes the outcomes of the workshop and guides us toward a better understanding of the unifying principles of flocculation.

20.2 UNIFYING PRINCIPLES OF FLOCCULATION

The workshop was structured so that three focus areas were addressed for each environment of study. They were modeling, physicochemical, and biological aspects of flocculation. Based on specialty, delegates were divided into three breakout sessions to address one of these focus areas. Each focus group contained researchers from the freshwater, saltwater, and engineered systems to ensure a cross communication of ideas between environments and to facilitate an understanding of the unifying principles of flocculation. Each focus group was provided the following five common questions to ensure continuity for the final plenary session:

1. What are the common and different theories and principles used in each environment of study to address the focus topic?
2. What methods of parameter analysis are common and different between each environment of study to address the focus topic? What are the important parameters to be addressed?
3. How have field and laboratory studies been employed to address the focus topic and what are the similarities and differences between the environments of study?
4. Is there latitude to employ theories, methods, analysis, etc. not commonly used in one environment of study to another?
5. Are there emerging issues?

The following sections summarize the discussions focused on these five questions during the plenary session.

20.2.1 Common or Different Issues and Principles

Given the environmental and disciplinary differences of the researchers working in each system, it is not surprising to see that there are many different issues or principles considered by each. This section discusses those principles or issues for which

there was agreement on their significance within flocculation research within all three environments.

20.2.1.1 Definition of a Floc

While the simplistic definition of flocculation provided earlier is agreed upon, the expansion from this basic level to more complex structures is driven by system specific conditions including the dominant particle types or the constituent particle of focus. A wide range of constituent particles enter into flocculation and these are summarized in Chapter 2. Many of these were discussed within the workshop with differences evident between systems of focus. While not always the case, generally freshwater researchers were concerned more with the inorganic fraction of the floc particles due to the need to assess mass transport within rivers and lakes. The saltwater researchers dealing with estuaries, continental shelf, and open-ocean settings tended to focus on both the inorganic and organic fractions, while the engineering researchers were almost exclusively concerned with the biological fraction due to the focus of wastewater treatment. Examples of floc differences with regard to environments are aggregates delivered to rivers via overland flow or eroded from the bed (Chapters 3 and 4), marine snow (Chapter 11), estuarine turbidity maxima (Chapter 10), and engineered microbial flocs (Chapters 14, 17, and 19). All researchers from all environments of study, however, realize the importance of organic and inorganic colloids and microbial activity within their flocculation studies.

20.2.1.2 Coagulation Theory and Floc Kinetics

Coagulation theory is fundamental to the study of flocculation in all environments. The principle of small individual particles adhering and forming larger faster sinking particles underlies the study of sedimentation in all three disciplines. Within the workshop, it was obvious that the initial starting point of coagulation had been refined within each of the different environments to enable researchers to understand better the process they were studying. Much of the work being carried out in freshwater and saltwater ignores the initial onset of coagulation and concentrates more on the behavior of established floc kernels. Most of the attention in those fields lies within the realm of physics (particle transport and collision) rather than chemistry (destabilization of particles to make them sticky). In contrast, the initiation and control of coagulation is an essential part of engineered systems.

20.2.1.3 Modeling within the Smoluchowski Framework

The majority of the modeling efforts for flocculation are centered on the Smoluchowski framework. The principles captured within the Smoluchowski framework appear to be universal, and the major emphasis within the workshop was on further development and application of these principles within respective disciplines. It was evident, however, that within engineering systems, modeling of the flocculation process is not extensively applied. This divergence from natural system modeling is due to the

process-oriented nature of engineered treatment systems (e.g., wastewater). Modeling which is performed in this environment tends to be based on the plant operation rather than on flocculation specifically.

The freshwater and saltwater disciplines share a common interest in modeling the formation of flocs in suspension (Chapters 8 and 12). Both disciplines require floc models to determine the subsequent transport and deposition of suspended material. Due in part to the somewhat recent realization that flocculation is an essential factor in freshwater, the majority of the modeling work has been carried out in marine environments. The roots for model development in the saltwater discipline are found in the classic case of flocculation at the saltwater interface of rivers. This simple, chemical-based aggregation was well suited to application of the Smoluchowski framework, hence significant advances were made. The need to reconcile the rapid vertical transport of carbon in the open ocean and the presence of abundant flocs in freshwater has forced researchers in both areas to consider biologically mediated aggregation in their models (Chapter 13).

20.2.1.4 Settling Dynamics

Research from all environments places a strong emphasis on the understanding of floc settling dynamics. This is based on the knowledge that the ostensible effect of flocculation is the modification of the downward flux of sediments. Understanding, modeling, and controlling settling dynamics has environmental, social, and economic benefits. Examples stemming from the workshop include the removal of sediments and contaminants from engineered systems (Chapter 19), the development of estuarine turbidity maxima (Chapter 10), and infilling of reservoirs and destruction of habitat due to increased sedimentation (Chapter 4).

20.2.1.5 Hindered Settling

Hindered settling is a principle that applies mostly to the engineered system; however, it is also an issue within saltwater systems that have high sediment load. In the engineered system, microbial floc formation and gravity sedimentation of the synthesized biomass in secondary clarifiers of activated sludge plants are considered to determine the overall efficiency of this secondary wastewater treatment process. Hindered settling has plagued the activated sludge process since its inception and is related to solids separation problems, such as microbial bulking and foaming, settling difficulties of microbial flocs, and difficult dewatering of the sediment sludge. Hindered settling in engineered systems is most often reflective of a buoyant property due mostly to the trapping of water, bubbles, and filamentous microorganisms (e.g., algae and bacteria) between and within floc particles.

Hindered settling within saltwater systems occurs when at high concentrations the return flow of water around settling particles creates an upward drag on neighboring particles. At sufficiently high concentrations, hindered settling can keep sediment fluidized and prevent settling. In saltwater systems, hindered settling can lead to the development of extremely high concentrations, near bottom sediment layers, that can reduce boundary layer turbulence.

20.2.1.6 Suspended Solids Concentration

While agreed to be an important issue in all environments, it takes on different significance within each. Within the natural systems, suspended solids concentration is important in the modeling of flocculation due to its impact on collision frequency, maintenance of maximal floc size, loading of receiving water bodies, and burial rates among others. Within engineering facilities such as those of wastewater treatment, suspended solids concentration is a critical parameter related to the maintenance of a specific sludge volume (important for effective operation), to an optimization of sludge dewatering properties, and to an optimization of settling characteristics within clarifiers. See Chapter 19 for further discussion.

20.2.1.7 Emphasis on Gross Morphology

The reflection of gross morphology on an individual basis or through grain size distributions is employed more within flocculation research from the freshwater and saltwater systems. This is attributed to the needs for assessing particle transport and as such a need to understand how floc structure influences floc transport. In the engineered systems, the gross structure of flocs tends to be less important than the overall mass characteristics of sediment within, for example, activated sludge systems. The exception to this is, however, seen in research efforts centered on the development of a "designer" floc which will have specific physical, chemical, and biological characteristics and which will optimize a given engineering requirement. For example, the formation of a population of more compact flocs with good settling characteristics and low water content will improve dewatering performance (Chapters 2, 3, 4, and 5).

20.2.1.8 Microbial Activities

The speciation of the microbial component, the microbial optimization of their own environment and EPS (extracellular polymeric substance) production are all related to microbial activities within the floc. Within the majority of wastewater engineering applications, the activity of the microbial component is paramount to the development and behavior of flocs within the system (Chapters 14 and 15). The principle of the great importance of microbial activity within natural flocs has only more recently been explored (Chapters 2 and 6) with the saltwater research being more advanced in this regard than the freshwater systems, due largely to the microbial research involved in marine snow investigations. Microbial activity is fast becoming the dominant phenomenon of interest within flocculation research in both natural systems because of its strong influence on the physical, chemical, and biological activity of the sediments and system as a whole (Chapters 2 and 6).

20.2.1.9 Floc Stability

Stability is a critical principle within flocculation research in all environments due to its obvious influence on particle transport, erosion, and engineered system performance. While floc formation is fairly well constrained, floc breakup under applied stress is not well understood. As such, it was agreed that one of the greatest needs

in flocculation research is the need to develop methods to measure properly this floc characteristic (see Section 20.2.2.5). Such characterization would aid greatly in the effective modeling of flocculation processes within all three environments (Chapter 16).

20.2.1.10 Response to Stressors — Function and Structure

In essence this is the heart of all flocculation research regardless of environment. Traditionally within the natural environments, research is centered on a sediment's response to an applied or changing shear stress with concomitant influence on floc development and transport (Chapter 5). This is particularly true for the modeling aspect of flocculation research (Chapter 8). From the engineered system, however, the stressors are often related more to nutrient or contaminant fluxes which can modify the performance of a system by influencing floc structure and biological activity (Chapter 17) (physical shear is obviously also an issue). The use of a stressor such as ultraviolet radiation has been used successfully in disinfection (Chapter 18). More recently, researchers studying natural systems are beginning to assess the interaction of contaminants with flocs. This is an emerging issue within floc models which require additional parameters to predict spatial and temporal contaminant changes within sediment systems.

20.2.1.11 Chemical Gradients

The realization that chemical gradients may be set up within a floc via diffusional or advective processes is primarily restricted to engineered systems where contamination interaction is a large and expanding area of research. Analysis of gradients within natural systems stems largely from biofilm research (Chapter 6) where such issues are important at sediment water interfaces. It is now understood that many of the processes occurring in biofilms also occur in flocs. In essence flocs can often be considered suspended biofilms (Chapters 2, 6, and 14).

20.2.2 Common or Different Parameters and the Methods Used to Investigate Them

There are numerous parameters that are measured in the study of flocculation. The majority of these are common among all three environments of study. As expected, because of the very different physical, chemical, and biological constraints within these environments, there is disagreement on the relative importance of these parameters. There is a movement away from relying on bulk measurements to assess sediment characteristics, to that of assessing individual flocs within a population to gain a much more in-depth understanding of how floc structure will influence floc behavior or system performance as a whole.

Following are the most important floc parameters influencing flocculation, as agreed upon by the delegates, and the relative importance of each parameter to each environment. There are some standard methods for the assessment of these parameters; however, different approaches are often taken by researchers who are driven by

constraints imposed by external variables and by the accessibility of state-of-the-art technologies. Often location, concentration, and size differences (e.g., colloid versus particulate) lead to a requirement for different methods. Rather than provide in-depth discussion on the various methods for the measurement of these variables, the reader is referred to Chapter 1 for an overview and insight into the methods applied to the study of flocculation.

20.2.2.1 Floc Size

Floc size is the most common parameter which is used within all environments and is often manifested as a distribution (by volume or number) or as a statistical representation of a distribution such as median size or maximal floc size. Complicating the parameter of floc size is that measuring or even defining it is problematical and not uniform between disciplines and researchers. Different physical properties (e.g., equivalent spherical diameter, longest dimension) are often used to reflect floc size distributions. In addition different instruments measure a physical property differently, resulting in potentially dissimilar results. Caution must also be taken when characterizing flocs by volume distributions only, due to the overriding influence that a few large particles can have on the distribution. Often an insignificant number of particles (relative to the total number) can represent significant volumes of the total sample. Nonetheless, floc size is a key component of any model for the prediction of sediment transport, deposition, and erosion. Floc size will also have an impact on filter feeding organisms and on the trapping efficiency of gravel beds; it will also have a bearing on sludge volume within wastewater treatment systems. Chapters 3, 4, 5, 9, 17, and 18 all utilize floc size as in important part of the research investigations.

20.2.2.2 Settling Velocity

While floc size is the most common physical characteristic measured, settling velocity is the most common behavioral characteristic measured. It is also the most critical parameter for transport models and is generally measured using *in situ* or laboratory settling columns. It is acknowledged that older methods such as Owens tubes, which determine settling velocity from clearance rate, must be used with caution since they are based on the derivation of Stokes' equation that assumes solid spherical units. Flocs, as amply demonstrated in this book, are not solid spherical units. Differences between settling velocities derived from settling columns can vary from *in situ* velocities by an order of magnitude. The critical role of settling velocity in modeling sediment transport and the assessment of an engineered system's efficiency can be seen in Chapters 4, 5, 8, 10, and 11.

20.2.2.3 Density and Porosity

Density and porosity are two variables which are highly related and which will have an effect on the transport characteristics of the sediment (Chapters 3, 4, and 5). As porosity increases, density decreases primarily due to an increase in pore water. Engineers are very much aware of this parameter as it will dictate the dewatering

efficiencies for sludge removal. Particle density is also a critical variable for most modeling efforts regardless of environment. There is no standard direct measurement of these two parameters. Generally they are estimated, based on measuring the settling velocity of known size particles and then using Stokes' equation (or a derivation thereof with a correction factor) from which the density is derived. Porosity has been derived by a mass balance between the dry floc density, wet floc density, and the water density (Chapter 1). Direct measurements of porosity are irrelevant due to the tortuous nature of pores as dictated by the extracellular polymeric substances (EPS) matrix within flocs (Chapter 2).

20.2.2.4 Shape (Fractals)

The shape of a floc is often used to help explain the settling and transport behavior of flocs. Most often this is done by using a shape factor such as roundness or sphericity as a correction factor for data from settling equations such as Stokes' law. Fractal dimensions are also used and these are believed to be a more sensitive assessment of particle shape and roughness. There are many variants on assessing fractal dimension, with the majority based on the slope of the line between surface area and perimeter for a population, or individually as the change in perimeter with incremental increases in measurement steps around the floc. There are many more variations for which the reader is referred to Chapters 4 and 5.

20.2.2.5 Strength

This parameter relates back to the stability issue from Section 20.2.1.9. There is no defined standard method for the measurement of floc strength or a standard unit of measurement. Atomic force microscopy (AFM) is one technique which demonstrates promise in this regard (Chapter 16); however, other means for the characterization of stability are needed. The majority of stability work performed to date has been based on the correlation between measures of shear and floc size (Chapter 5). This relationship has been restricted to laboratory studies where often unrealistic shears are applied. A field method of assessing floc stability is critical. It must, however, not be based on the assessment of changes in volume distributions as these are severely biased toward larger flocs and will provide erroneous relationships (Chapter 1).

20.2.2.6 Stickiness

This parameter is similar to strength in that there is no standard unit of measurement or method of measurement. Once again AFM is fast becoming the method for its assessment (Chapter 16); however, it is not ideal as it can be very expensive to use. Occasionally, carbohydrates, uronic acids, or other EPS components are used as a surrogate variable to suggest a degree of stickiness within a population of flocs. Assessment of individual floc stickiness is still, however, an elusive, but highly sought after, variable. Stickiness and a tendency to flocculate are related. In this regard, some progress has been made to show relationships between flocculation, system free energy, and the physicochemical properties of floc. The level of

effluent suspended solids in biologically treated wastewaters is a strong indicator of flocculation and is related to the physicochemical properties of microbial floc formed in the aeration tank of wastewater treatment systems. Increasing experimental evidence indicates that hydrophobic interactions play an important role in flocculation (Chapter 19).

20.2.2.7 Microbial Ecology

Microbial ecology is currently receiving a great impetus from environmental genomics and the use of specific probes in conjunction with analytical microscopy (Chapters 1, 6, and 15). Environmental genomics is a genetics-based, interdisciplinary field of research that seeks to understand external factors affecting organisms when they are exposed to environmental stresses, such as contaminants and pathogens. Host responses to these stresses include changes in gene expression and genetic products, changes that culminate with alterations in host phenotype, including host EPS composition.

Until recently it has been very difficult to determine the true level of diversity of microorganisms in both natural and engineered ecosystems. However, advances in molecular biology have now made it possible for microbiologists to use novel tools in studies of the ecology, diversity and evolution of microbes. The advantage of using molecular techniques is that bacterial cells present in a complex microbial community can be detected and classified without any necessity for their cultivation. Thus, comparative sequence analysis either provides researchers with the phylogenetic framework for unequivocally placing unknown bacteria, or allows the development of tools such as fluorescent *in situ* hybridization (FISH) DNA probes to identify the large number of uncultured bacteria seen under the microscope in natural environments. However, the limited number of probes that can be applied in one hybridization experiment becomes a distinct bottleneck when this technique is used for community analysis where a high level of phylogenetic resolution is required. The fact that many of the molecular methods described are not widely accessible to all, as well as the difficulties in mastering these methods, presents challenges to floc researchers wishing to fully employ these in their studies.

20.2.2.8 Surface Properties

More emphasis is being placed on the structure, composition, and the physicochemical properties (e.g., surface properties) of flocs and the suspending medium as these may strongly influence the behavior (e.g., bioflocculation, settling properties, biosolids management, or contaminant removal) of biomass. The role of surface properties in floc interactions is particularly important in understanding microbial floc formation (Chapter 19). The proposed mechanisms for microbial floc formation can be classified into five types: (1) charge neutralization; (2) hydrophobic interaction; (3) polymer bridging; (4) salt bridging; and (5) the surface thermodynamic approach. The polymer bridging mechanism has received the greatest attention (Chapters 7 and 9); it involves the entanglement and adsorption of microorganisms and other particles by

the EPS. The differences between these models lie in which of the surface properties is considered to be most important, and how a particular parameter is affected by nutritional and environmental conditions.

A wide variety of methods have been applied to examine the gross morphological properties of flocs, their ultrastructure and physicochemical properties (including hydrophobicity and surface charge), and the composition of their EPS (Chapter 1). Greater emphasis in the future should be directed to applying these methods across all floc types, as well as to increasing the standardization of methods and techniques, for permitting comparative analysis of different properties among different floc types. The desired outcome will be to have reliable tools and a comprehensive knowledge of floc that can enhance cost and energy efficiencies, optimize processes and sustainability, and manage better the risks related to important flocculation-mediated environmental processes in environmental and engineered systems.

20.2.2.9 Large Number of Common Variables

There are a host of common standard variables for the three environments of study. These typically are pH, temperature, DOC, POC, BOD, COD, and ionic strength and do not need elaboration in this chapter.

20.2.3 Field and Laboratory Studies

A discussion on the similarities and differences of field and laboratory studies between environments demonstrated a strong split in needs. Generally within the engineered systems, research into flocculation is exclusively lab based, given the nature of the requirements. Within the natural systems (freshwater, saltwater), there tends to be an emphasis on field work; however, there is still some important experimental laboratory work oriented ostensibly around modeling issues. Laboratory experiments often take the form of flume work (Chapter 5) or shear related experiments (Chapter 8). Of course any modeling efforts generated from laboratory experiments will need to be validated within the field. The greatest difficulty in using laboratory studies to represent the "real world" is in scaling the findings from the laboratory to the field. This difficulty in transferability is likely to be related to scaling differences in turbulence intensity between the two environments (laboratory versus field) and the impossibility of accounting for the myriad of uncontrolled variables within the field. Nonetheless, natural and engineered laboratory experiments do allow for the assessment of the dominant mechanisms influencing flocculation.

The single most difficult issue, regardless of a field or laboratory approach, is the sampling of flocs for investigation. The issue lies around maintaining the integrity of the flocs during sampling, transport, and analysis. It was interesting to note differences in the focus of the groups studying natural systems and those studying engineered systems. While natural systems studies concentrated more on *in situ* studies, engineered systems were far advanced in the study of individual flocs. The difference in emphasis may reflect the difference in the stability of the flocs in natural and engineered

systems. While flocs from batch reactors and other controlled and recirculating systems are relatively robust, flocs in both marine and freshwater systems are ephemeral, making transport to the lab extremely problematic. Generally, flocs are presumed to be inherently unstable and prone to break up. Floc stability changes, and changes to resulting morphological correlates of stability, can occur quickly during storage of a sample prior to analysis; no bulk storage prior to analysis is recommended. Methods are now available which transplant laboratory stabilization techniques (common to microscopy) to the field, thus allowing minimal perturbations and prolonged sample storage prior to analysis. Stabilization is, however, only feasible for small sample populations. Sampling of flocs in the natural systems is made more difficult due to uncontrollable external variables such as weather and spatial and temporal variations.

Through the preceding chapters, this book provides an extensive cross-section of both field- and laboratory-based work. It is evident that both approaches are required and need to be integrated in order to more fully understand the complex issues of flocculation in natural and engineered systems.

20.2.4 Latitude for Linkage of Freshwater, Saltwater, and Engineering Principles, Methods, and Analysis

From the workshop and from the preceding chapters, it is evident that there is significant latitude for overlap in the use of principles, methods, and analysis between the freshwater, saltwater, and engineered systems. The greatest potential for the transfer of technology is with regard to microbiology. As stated earlier, it was agreed that the microbial consortia play a large role in controlling floc structure and behavior. The engineered system has been the leader in the assessment of floc microbiology and, as such, lends great potential to assist the freshwater and saltwater environments in developing methods and indices that would provide further insight into flocculation processes for these environments. Specifically, areas that could be developed are genomics, molecular, and microscopic methods within freshwater and saltwater systems.

Further, it was also agreed that there was scope for integrating the rapidly evolving approaches of nanotechnology, and surface and materials science into all systems. Scanning transmission x-ray microscopy, using synchrotron radiation, has shown great potential to map floc architecture and chemistry at high resolution in three dimensions. Atomic force microscopy is a promising new tool for measuring the interaction forces between one colloidal particle and another. Advanced optical microscopies, including confocal laser scanning microscopy, are permitting the integration of topographical, chemical, and three-dimensional structural information, with molecular and ecological determinants that determine floc characteristics.

Often models have remained somewhat mutually exclusive to the environment or issue that they were used to investigate. Many if not all of these models have at least some common components or assumptions. Given this realization, it was discussed that a base-line sediment transport model with a common modeling framework would be of great advantage for the investigation of floc related issues. Such a base model would greatly improve cross linkages between environments and allow for transfer of technology between environments for expanded and improved assessment

capabilities. Such an approach would also make it easier to integrate models for a more holistic look at the greater environment. For example, it was agreed that great utility would be achieved if models of rivers, estuaries, continental shelves, and open oceans could be linked given their real world connection.

Finally, it was agreed that the natural systems have traditionally dominated the floc research approach which uses *in situ* technology to investigate floc form and behavior. *In situ* methods for measuring particle sizing and settling velocity are becoming common place (see Chapter 1) and often use direct observation (video) or indirect (laser particle sizing) methods to make assessments in a temporal or spatial context. It was agreed that the potential exists to implement similar systems in-line or in-tank for many engineered systems such as wastewater and drinking water treatment.

20.2.5 Emerging Issues and Challenges

While microbiology is an area of commonality, it is still an emerging issue, particularly within the freshwater and saltwater environments. Issues which will require further development reside in the efforts to deal with heterogeneity and diversity of the floc microbial population and their impact on floc behavior. In particular, we must ascertain which bacterial species play the most important roles in creating floc architecture, and which environmental signals modulate their efforts. Within the engineering field there is the need to optimize particle specific conditions toward the development of the "designer floc." The designer floc will be the product of a bioengineered system for promoting the formation of flocs which are functionally adept at achieving a desired result such as specific contaminant removal or effective settling.

Contaminant interactions with sediments and flocculated particles, in particular, are poorly understood. This was effectively born out of the traditional bulk sample approach to contaminant concentration assessments. The effective microscale biogeochemical pathways and mechanisms which mediate the uptake, transformation and fate of contaminants in aquatic and engineered system flocs remain largely unknown. In order to develop and initiate effective contaminated sediment remediation strategies, it is essential that the microscale processes of contaminant interaction be ascertained. Further, little is known about the interactions of pathogens and hosts within flocs and how the floc influences pathogen viability, proliferation, and activation within sediment water systems.

Further emerging issues relate to source area identification of sediments and the role that flocs formed in the water column versus aggregates formed in the terrestrial environment (water stable soil aggregates) play in the transport of sediment and associated contaminants. Further, there is a lack of knowledge on how a floc's biogeochemical characteristics influence bed sediment development and biogeochemical characteristics, particularly in terms of biofilm development, contaminant assimilation and transformations, and bed stability.

The advancement of floc research in all environments will continue to benefit from the development of *in-situ* techniques, as these methods allow for the unobtrusive real-time assessment of changes in floc population characteristics. In so doing, water managers can adjust protocols to provide for a more effective management of water

resources. Such management could pertain to sediment remediation efforts or to wastewater treatment system operations.

Contaminated sediment and aquatic remediation are increasingly employing flocculation principles. For example, promoting flocculation of oil with clay has been successfully used for oil spill remediation, thus adding it to a list of available strategies for environmental clean up. Other technologies are emerging which also embody flocculation as an integral part of the technology, such as the addition of clay to toxic algal blooms to promote flocculation and thereby reduce their impact on commercial fisheries. There is great potential for flocculation research to aid in the development of other remediation technologies in the future.

Finally floc strength is realized to be a critical characteristic in relation to sediment and contaminant transport; however, there is no suitable method of measuring it. This in conjunction with the microbial activity of flocs was viewed as the most urgent challenge facing flocculation researchers.

20.3 CONCLUSION

Sediments within both natural (freshwater and saltwater) environments and engineered facilities play significant environmental, economic, and public health roles in society. The majority of priority pollutants including heavy metals and organic contaminants (such as PAHs) are associated with sediment particles. The beneficial use impairment of many aquatic environments, including every area of concern as defined within Remedial Action Plans of the Great Lakes basin of North America and elsewhere internationally, is related to contaminated sediments. These beneficial use impairments include swimming, boating, fishing, esthetics, odor, and benthic community impacts. Substantial sums of money are invested each year in the remediation of contaminated sites in an attempt to increase beneficial uses. Within engineered systems such as drinking water and wastewater treatment facilities, the removal of solids is the key aspect of treatment and, as such, here too significant sums of money are invested to provide the most efficient operating system possible.

Within both natural and engineered systems, when sediment issues are in question it is inevitable that flocculation will be a dominant process that will contribute to, or control the issue. This is because the majority of cohesive sediments within natural systems are transported and eroded within a flocculated state and the floc is the model form of solids for most engineered systems. Given that the structure of a floc will influence its physical (transport), chemical (uptake and transformation of contaminants), and biological (community dynamics and biochemical activities) behavior, it is not surprising that flocculation plays a dominant role in influencing the environmental, economic, and public health impacts of sediments. While this is widely accepted, there is still a fundamental lack of knowledge related to many aspects of the flocculation process and the resultant floc and as such our abilities to manage water resources are impaired.

Through the sharing of information between researchers of different disciplines and environments, the workshop has contributed to improving our knowledge of

the greater flocculation process and impact within the freshwater, saltwater, and engineered systems. The workshop has demonstrated the strengths and weaknesses within floc research in the three environments and has pointed to the need for continued collaboration between researchers. Of particular note is that cross-environment multidisciplinary studies would be of great benefit in ascertaining the universality of flocculation processes and impacts. Presently such cross-environment studies are very limited in scope. Continued development of new and innovative methods which can be effectively used between environments will be essential to the advancement of flocculation research.

The contributors to the *Workshop on Flocculation in Natural and Engineered Systems* have provided herein some integral elements to advancing our understanding of flocculation processes; however, the work has only just begun. By integrating resources, expertise, and ideas, researchers will continue to advance our knowledge in this vitally important environmental, economic, and public health issue.

ACKNOWLEDGMENTS

The authors would like to thank the participants of the *Workshop on Flocculation in Natural and Engineered Systems*. This chapter represents a perspective derived from the chapter contributions and the discussions with all participants of the workshop during breakout and plenary sessions.